

UNIVERSITÄT
BAYREUTH



Nanostructured Earth-abundant Metal Catalysts for Hydrogenation Reactions in Complex Organic Synthesis

DISSERTATION

zur Erlangung des akademischen Grades eines
Doktors der Naturwissenschaften (Dr. rer. nat.)
an der Bayreuther Graduiertenschule für Mathematik und
Naturwissenschaften (BayNAT)

vorgelegt von

Christof Bauer, M. Sc.

geboren am 25.01.1996 in Kötzting j. Bad Kötzting

Bayreuth, 06.08.2025

Die vorliegende Arbeit wurde in der Zeit von Mai 2021 bis November 2024 in Bayreuth am Lehrstuhl Anorganische Chemie II – Katalysatordesign, Sustainable Chemistry Centre unter der Betreuung von Herrn Prof. Dr. Rhett Kempe angefertigt.

Vollständiger Abdruck der von der Bayreuther Graduiertenschule für Mathematik und Naturwissenschaften (BayNAT) der Universität Bayreuth genehmigten Dissertation zur Erlangung des akademischen Grades eines Doktors der Naturwissenschaften (Dr. rer. nat.).

Form der Dissertation: Kumulative Dissertation

Dissertation eingereicht am: 08.01.2025

Zulassung durch das Leitungsgremium: 13.01.2025

Wissenschaftliches Kolloquium: 15.07.2025

Amtierender Direktor: Prof. Dr. Jürgen Köhler

Prüfungsausschuss:

Prof. Dr. Rhett Kempe (Gutachter)

Prof. Dr. Günter Motz (Gutachter)

Prof. Dr. Markus Retsch (Vorsitz)

Prof. Dr. Rainer Schobert

*Für meine großartige Familie,
die mich immer unterstützt und meine Neugier und Begeisterung geweckt hat.*

*Mehr als die Vergangenheit interessiert mich die Zukunft,
denn in ihr gedenke ich zu leben.*

Albert Einstein

Table of Contents

Abbreviations	VIII
1 Summary/Zusammenfassung	10
1.1 Summary	10
1.2 Zusammenfassung	13
2 Introduction	16
2.1 Sustainable Chemistry with Respect to Heterogeneous Earth-abundant Metal Catalysis	16
2.2 N-doped Support Materials for Heterogeneous Catalysts	18
2.3 Polymer Derived Ceramics as Support Materials for Heterogeneous Catalysts	20
2.4 Aromatic Heterocycles in Chemistry	23
2.4.1 Synthesis Approaches to N-Heterocycles	23
2.4.2 Selective Hydrogenation of Aromatic Heterocycles	25
2.5 Synthesis Methods towards Amines	26
2.5.1 Reductive Amination of Carbonyl Compounds	26
2.5.2 Borrowing Hydrogen/Hydrogen Autotransfer Concept	27
2.6 References	29
3 Overview of Thesis Results	37
3.1 Synopsis	37
3.2 Individual Contributions to Joint Publications	54
4 A Highly Active Cobalt Catalyst for the General and Selective Hydrogenation of Aromatic Heterocycles	56
5 The Synthesis of Hydroquinolines from Nitroaldehydes and Ketones by Hydrogenation Sequences and Condensations	163

6	General Synthesis of Alkyl Amines via Borrowing Hydrogen and Reductive Amination	266
7	List of Publications and Conference Contributions	415
7.1	Publications	415
7.2	Conference Contributions.....	416
8	Acknowledgement/Danksagung	417
8.1	Acknowledgement.....	417
8.2	Danksagung	419
9	(Eidesstattliche) Versicherungen und Erklärungen.....	421

Abbreviations

AIBN	<i>azobis(isobutyronitrile)</i>
BH	<i>Borrowing Hydrogen</i>
EDX.....	<i>Energy Dispersive X-ray Spectroscopy</i>
EELS	<i>Electron Energy Loss Spectroscopy</i>
fcc	<i>face-centered cubic</i>
FFT	<i>Fast Fourier Transformation</i>
HA	<i>Hydrogen Autotransfer</i>
HAADF	<i>High-Angle Annular Dark Field</i>
HR	<i>High Resolution</i>
ICP-OES.....	<i>Inductively Coupled Plasma Optical Emission Spectrometry</i>
M/N	<i>metal to N/C</i>
N/C	<i>nitrogen/carbon</i>
N-doping.....	<i>nitrogen-doping</i>
PDC	<i>Polymer Derived Ceramic</i>
PDF.....	<i>Pair Distribution Function</i>
PXRD	<i>Powder X-ray Diffraction</i>
salen.....	<i>Bis(salicyliden)ethylenediamin</i>
SEM.....	<i>Scanning Electron Microscopy</i>
SiBCN	<i>silicon boron carbonitride</i>
SiC	<i>silicon carbide</i>
SiCN	<i>silicon carbonitride</i>
SiOC	<i>silicon oxycarbide</i>
SiOCN	<i>silicon oxycarbonitride</i>
SMP-10.....	<i>polycarbosilane precursor</i>
STEM	<i>Scanning Transmission Electron Microscopy</i>
TGA.....	<i>Thermogravimetric Analysis</i>
THQ.....	<i>1,2,3,4-Tetrahydroquinoline</i>
XPS.....	<i>X-ray Photoelectron Spectroscopy</i>

1 Summary/Zusammenfassung

1.1 Summary

This thesis addresses the development of heterogeneous, nanostructured catalysts based on earth-abundant metals and their application in thermal catalytic processes for complex organic synthesis, with a particular emphasis on the production of amines, including tetrahydroquinolines, as well as primary, secondary, and tertiary alkyl amines.

The first part of the thesis focuses on designing a novel synthesis protocol for a nanostructured cobalt catalyst and its application in the selective hydrogenation of aromatic heterocycles. This approach aimed at decoupling the metal and N/C sources, allowing for their independent optimization for improved catalytic performance. Three components, an inexpensive metal precursor $[\text{Co}(\text{OAc})_2 \cdot 4 \text{H}_2\text{O}]$, an easy-to-synthesize N/C precursor (meso-octamethylcalix[4]pyrrole), and a commercially available porous support material (SiO_2) are pyrolyzed at 800 °C under nitrogen atmosphere to form the Co/ SiO_2 catalyst in a simple, single synthesis step. Various parameters, including pyrolysis temperature, support materials, metal precursors, and M/N ratios, were investigated to optimize catalyst activity. By varying the M/N ratio from 1:1 to 1:10, it was found that a specific M/N ratio of 1:4 is optimal. This is due to the microporous N/C structure or the optimal thickness of the embedding N/C layer, which balances educt access and catalyst stability. Too thick a layer impedes access, while too thin a layer risks cobalt leaching due to nanoparticle detachment. The catalyst with 1.81 wt% cobalt loading showed the best activity, confirmed by ICP-OES. In summary, the reaction proceeds efficiently and selectively with 5.0 mol% Co, 2.0 MPa H_2 , 70 °C, and 20 h reaction time. HAADF-STEM showed homogeneous distribution of cobalt nanoparticles (4.8 nm). The surface area of the support (194 m^2/g) and corresponding catalyst (217 m^2/g) was determined by N_2 physisorption, with an increase in surface area and additional microporosity due to carbon black entrapment. HAADF-STEM combined with EDX and EELS, SEM-EDX, XPS, PXRD, and PDF confirm that the particles are composed of metallic cobalt with cobalt oxide on their surface. A total of 31 N-, O-, and S-heterocycles were selectively hydrogenated, with increased conditions required for O- and S-heterocycles.

The second part of the thesis presents a new catalytic pathway for synthesizing hydroquinolines directly from nitroaldehydes and ketones, given their importance in drug molecules and precursors. The challenge of quinoline substrate synthesis is addressed by the *Friedländer* synthesis, which requires 2-aminoaldehydes that are challenging to prepare. This work solves

the issue using a reusable Ni/N-SiC catalyst, enabling efficient 2-aminoaldehyde synthesis from 2-nitrobenzaldehyde, followed by the *Friedländer* reaction and hydrogenation to hydroquinolines. The N-SiC support is prepared by crosslinking the commercial polycarbosilane SMP-10 and acrylonitrile with AIBN, followed by pyrolysis at 1000 °C under nitrogen and base treatment to remove the Si-rich phase. Active nickel nanoparticles are obtained on the N-SiC support by wet impregnation with $\text{Ni}(\text{NO}_3)_2 \cdot 6 \text{H}_2\text{O}$ followed by pyrolysis and reduction. SEM-EDX and HAADF-STEM show a homogeneous distribution of nickel nanoparticles (8.5 nm). HAADF-STEM with EDX, HR-TEM with EELS and FFT, XPS, and PXRD confirm metallic nickel nanoparticles with nickel oxide on their surface. Argon physisorption shows a slight decrease in surface area from 580 m²/g (N-SiC) to 563 m²/g (Ni/N-SiC). ICP-OES and CHN analysis confirm a nickel content of 4.0 wt%, with 83.3 % C, 5.7 % N, and 7.0 % Si. Several parameters were screened in the one-pot reaction of 2-nitrobenzaldehyde with acetophenone to obtain 2-phenyl-1,2,3,4-tetrahydroquinoline, divided into three steps: (A) selective hydrogenation of 2-nitrobenzaldehyde to 2-aminobenzaldehyde with Ni/N-SiC, (B) *Friedländer* synthesis with LiOH, and (C) hydrogenation of 2-phenylquinoline to 2-phenyl-1,2,3,4-tetrahydroquinoline using the Ni/N-SiC catalyst from (A). For step A, 4.0 mol% Ni, 0.5 mmol nitrobenzaldehyde, 0.5 mmol acetophenone, 3 mL ethanol, 3.0 MPa H₂, 40 °C for 20 h are the best conditions. For step B, 0.3 mmol LiOH are added for 20 h at 60 °C. For step, C 5.0 MPa H₂, 120 °C for 48 h are aligned. Step C is the most challenging, limiting step with a maximum yield of 91 % 2-phenyl-1,2,3,4-tetrahydroquinoline in the benchmark synthesis. Using optimal conditions, 16 aldehyde-derived and 21 ketone-derived substrates were synthesized along with three highly functionalized substrates and four precursors for bioactive drug molecules.

The third part of the thesis focuses on the synthesis of primary, secondary, and tertiary alkyl amines, inspired by the hydroquinoline synthesis work. In addition to heterocyclic amines, the synthesis of substituted alkyl amines is crucial for the synthesis of bioactive molecules. To achieve this, a synthetic approach combining reductive amination and BH/HA using ammonia, alcohols, aldehydes, ketones, and hydrogen with a CoSc/N-SiC catalyst is developed. The catalyst is synthesized using N-SiC, $\text{Co}(\text{NO}_3)_2 \cdot 6 \text{H}_2\text{O}$ and $\text{Sc}(\text{NO}_3)_3 \cdot 5 \text{H}_2\text{O}$ as described in the second part. HAADF-STEM shows a homogeneous distribution of Co nanoparticles (13.9 nm), with orders of magnitude smaller Sc particles finely dispersed over the support, as confirmed by EELS. XPS analysis shows that the Sc fraction is ten times higher than the Co fraction, although the same concentration is expected. This indicates that Sc is finely dispersed on the outer layer, while Co is present in the form of large particles, consistent with STEM-

EELS results. ICP-OES (2.0 wt% Co, 2.0 wt% Sc) and SEM-EDX further confirm this. Using the catalyst, 13 primary amines, 24 secondary amines, and 8 tertiary amines, including five novel compounds, are synthesized.

1.2 Zusammenfassung

Die Dissertation beschäftigt sich mit der Entwicklung heterogener, nanostrukturierter 3d-Metallkatalysatoren und deren Anwendung in thermisch-katalytischen Prozessen für komplexe organische Synthesen. Ein besonderer Schwerpunkt liegt auf der Herstellung von Tetrahydrochinolinen sowie primären, sekundären und tertiären Alkylaminen.

Der erste Teil der Arbeit konzentriert sich auf die Entwicklung eines neuartigen Syntheseprotokolls für einen nanostrukturierten Kobaltkatalysator und dessen Anwendung für die selektive Hydrierung von aromatischen Heterocyclen. Ziel war es, die Metall- und N/C-Quellen zu entkoppeln, um eine unabhängige Optimierung zur Verbesserung der katalytischen Aktivität zu ermöglichen. Drei Komponenten, eine kostengünstige Metallvorstufe $[\text{Co}(\text{OAc})_2 \cdot 4 \text{H}_2\text{O}]$, eine leicht herstellbare N/C-Vorstufe (meso-Octamethylcalix[4]pyrrol) und ein poröses Trägermaterial (SiO_2) wurden bei 800 °C in Stickstoffatmosphäre pyrolysiert, um den Co/ SiO_2 -Katalysator in einem einfachen, einstufigen Syntheseschritt herzustellen. Verschiedene Parameter wie Pyrolysetemperatur, Trägermaterialien, Metall-Präkursoren und M/N-Verhältnisse wurden untersucht, um die katalytische Aktivität zu optimieren. Ein M/N-Verhältnis von 1:4 erwies sich als optimal, da die mikroporöse N/C-Struktur bzw. die optimale Dicke der eingebetteten N/C-Schicht den Zugang der Edukte und die Stabilität des Katalysators begünstigt. Eine zu dicke Schicht behindert die Zugänglichkeit, eine zu dünne Schicht begünstigt die Auswaschung von Kobalt durch Ablösung der Nanopartikel. Der Katalysator mit 1,81 wt% Kobalt zeigte die beste Aktivität, was durch ICP-OES bestätigt wurde. Zusammenfassend läuft die Reaktion bei 5,0 mol% Co, 2,0 MPa H_2 , 70 °C und einer Reaktionszeit von 20 Stunden effizient und selektiv ab. HAADF-STEM zeigte eine homogene Verteilung der Kobalt-Nanopartikel (4,8 nm). Die spezifische Oberfläche des Trägers (194 m^2/g) und des entsprechenden Katalysators (217 m^2/g) wurde durch N_2 -Physisorption bestimmt. Die Zunahme der Oberfläche und der Mikroporosität ist auf die Generierung von Aktivkohle zurückzuführen. HAADF-STEM in Kombination mit EDX und EELS, SEM-EDX, XPS, PXRD und PDF zeigen, dass die Partikel aus metallischem Kobalt bestehen und von einer Kobaltoxidschicht umgeben sind. Insgesamt wurden 31 N-, O- und S-Heterocyclen selektiv hydriert, wobei für O- und S-Heterocyclen erhöhte Reaktionsbedingungen erforderlich waren.

Im zweiten Teil der Arbeit wird ein neuer katalytischer Weg zur direkten Synthese von Hydrochinolinen aus Nitroaldehyden und Ketonen vorgestellt, die für Arzneimittel und deren Vorstufen von Bedeutung sind. Das Problem der Chinolin-Synthese wird durch die *Friedländer*-Synthese gelöst, die schwer zugängliche 2-Aminoaldehyde erfordert. Diese

Schwierigkeit wird durch die Verwendung eines wiederverwendbaren Ni/N-SiC-Katalysators gelöst, der eine effiziente Synthese von 2-Aminoaldehyden aus 2-Nitrobenzaldehyden ermöglicht, gefolgt von der *Friedländer*-Reaktion und der Hydrierung zu Hydrochinolinen. Das N-SiC Trägermaterial wird durch Vernetzung des Polycarbosilans SMP-10 mit Acrylnitril mittels AIBN, anschließender Pyrolyse bei 1000 °C unter Stickstoffatmosphäre und Basenbehandlung zur Entfernung der Si-reichen Phase hergestellt. Aktive Nickel-Nanopartikel werden durch Nassimprägnierung des N-SiC Trägermaterials mit $\text{Ni}(\text{NO}_3)_2 \cdot 6 \text{H}_2\text{O}$, gefolgt von Pyrolyse und Reduktion, synthetisiert. SEM-EDX und HAADF-STEM Aufnahmen zeigen eine homogene Verteilung der Nickel-Nanopartikel (8,5 nm). HAADF-STEM mit EDX, HR-TEM mit EELS und FFT, XPS und PXRD Messungen bestätigen metallische Nickel-Nanopartikel mit einer Nickeloxidoberfläche. Die Ar-Physisorption zeigt eine leichte Abnahme der spezifischen Oberfläche von 580 m²/g (N-SiC) auf 563 m²/g (Ni/N-SiC). ICP-OES und CHN-Analyse bestätigen einen Nickelgehalt von 4,0 wt% mit 83,3 % C, 5,7 % N und 7,0 % Si. Bei der One-Pot-Reaktion von 2-Nitrobenzaldehyd mit Acetophenon, zur Herstellung von 2-Phenyl-1,2,3,4-tetrahydrochinolin, wurden verschiedene Parameter untersucht und optimiert. Die Reaktion besteht aus drei Schritten: (A) selektive Hydrierung von 2-Nitrobenzaldehyd zu 2-Aminobenzaldehyd mit Ni/N-SiC, (B) *Friedländer* Synthese mit LiOH und (C) Hydrierung von 2-Phenylchinolin zu 2-Phenyl-1,2,3,4-tetrahydrochinolin mit dem Katalysator aus (A). Für Schritt A sind 4,0 mol% Ni, 0,5 mmol 2-Nitrobenzaldehyd, 0,5 mmol Acetophenon, 3 mL Ethanol, 3,0 MPa H₂ und 40 °C für 20 h optimal. Für Schritt B werden 0,3 mmol LiOH bei 60 °C für 20 h zugegeben. Schritt C wird bei 5,0 MPa H₂ und 120 °C für 48 h durchgeführt. Schritt C ist der anspruchsvollste und limitierende Schritt, mit einer maximalen Ausbeute von 91 % 2-Phenyl-1,2,3,4-tetrahydrochinolin in der Referenzsynthese. Unter optimalen Bedingungen wurden 16 Aldehyd- und 21 Keton-Derivate sowie drei hochfunktionalisierte Substrate und vier Vorstufen für bioaktive Wirkstoffe synthetisiert.

Der dritte Teil der Arbeit konzentriert sich auf die Synthese von primären, sekundären und tertiären Alkylaminen, inspiriert von der Hydrochinolin-Synthese. Neben heterocyclischen Aminen ist die Synthese substituierter Alkylamine für die Herstellung bioaktiver Moleküle von entscheidender Bedeutung. Zu diesem Zweck wurde ein Syntheseansatz entwickelt, der die reduktive Aminierung und das BH/HA Konzept kombiniert und Ammoniak, Alkohole, Aldehyde, Ketone und Wasserstoff mit einem CoSc/N-SiC-Katalysator verknüpft. Der Katalysator wird unter Verwendung von N-SiC, $\text{Co}(\text{NO}_3)_2 \cdot 6 \text{H}_2\text{O}$ und $\text{Sc}(\text{NO}_3)_3 \cdot 5 \text{H}_2\text{O}$, wie im zweiten Teil der Dissertation dargestellt, synthetisiert. Die HAADF-STEM Aufnahmen zeigen eine homogene Verteilung der Co-Nanopartikel (13,9 nm) mit deutlich kleineren

Sc-Partikeln, die fein über den Träger verteilt sind, wie durch EELS-Aufnahmen bestätigt wird. XPS-Analysen zeigen, dass der Sc-Anteil zehnmal höher ist als der Co-Anteil, obwohl gleiche Konzentrationen erwartet werden. Dies deutet darauf hin, dass Sc in der äußeren Schicht fein verteilt ist, während Co in Form von großen Partikeln vorliegt, was mit den STEM-EELS Ergebnissen übereinstimmt. ICP-OES Messungen (2,0 wt% Co, 2,0 wt% Sc) und SEM-EDX Aufnahmen bestätigen dies ebenfalls. Mit dem Katalysator wurden erfolgreich 13 primäre, 24 sekundäre und 8 tertiäre Amine synthetisiert, darunter fünf neue Verbindungen.

2 Introduction

2.1 Sustainable Chemistry with Respect to Heterogeneous Earth-abundant Metal Catalysis

The mathematician and physicist Jean Baptiste Joseph Fourier first formulated and established the principle of the greenhouse effect in the atmosphere in 1824. He reported that the Earth is much warmer than it would be without an atmosphere, which is good in principle. The reason for this is that the atmosphere is very transparent to short-wave solar radiation. This is not the case with infrared radiation. It is emitted from the Earth's heated ground, and some of it reflects back to the Earth. This is called the greenhouse effect.^[1] This effect has increased massively since industrialization and its pollution. Society, industry, and policymakers have long ignored this phenomenon until it has long since affected everyone on the planet. The climate crisis is undoubtedly one of the most pressing challenges of our time. Its consequences are far-reaching and imminent. Extreme weather events such as heat waves, droughts and floods are increasing, polar ice caps and glaciers are melting at an alarming rate, and sea levels are rising at an extraordinary speed.^[2] Today, society is more aware of this phenomenon as well as industrial pollution and of its own responsibilities. Research is also shifting its focus to a science-based approach to environmental protection.^[3] By developing a sustainable approach to the chemical industry, society could enjoy the benefits of everyday products such as pharmaceuticals and polymer-based materials, while conserving fossil resources and reducing climate change. In 1998, to address the sustainability aspect of chemical research, *Anastas* and *Warner* presented the 12 Principles of Green Chemistry.^[4] This includes the design, development, and implementation of chemical processes and products for the reduction or elimination of substances hazardous to human health and the environment.^[5] A chemical reaction must meet the 12 principles to be classified as green. This was later simplified by the acronym PRODUCTIVELY.^[6] Catalysts play a key role in green chemistry by reducing energy requirements, providing catalysts instead of stoichiometric amounts of materials, improving selectivity, and using less toxic materials.^[7] Supported metal catalysts are used in a wide range of critical processes in the modern chemical industry including petrochemicals, energy storage, and pollution control. Many modern products are synthesized with the help of catalysts. These include high-temperature lubricants, high-performance polymers, and pharmaceuticals.^[8] Depending on the aggregate state of the reactant and catalyst, a difference is made between homogeneous and heterogeneous catalysis. Homogeneous catalysts are in the same phase as the substrates being catalyzed, whereas heterogeneous catalysts are in a different phase.^[9] Because

heterogeneous catalysts are easier to separate from the reaction solution, and thus more recyclable and robust than their homogeneous counterparts, the class of heterogeneous catalysts plays an important role in industry.^[10] However, many of the catalysts used are precious metal catalysts. A promising approach is to replace them with earth-abundant metal catalysts, as they are much more abundant in the earth's crust, which directly translates into a lower price. For example, 3d metal catalysts consist of essential elements of living bodies with relatively low toxicity. Another advantage is that catalysts based on these abundant metals have a completely different selectivity pattern than known precious metal systems, allowing new synthetic pathways and reactions with a wider substrate range.^[11] Therefore, the use of reusable nanostructured earth-abundant metal catalysts for a broad applicability in complex organic synthesis as well as electrical and chemical storage applications is highly desirable.

In recent years, the *Kempe* group has established many fundamental works according to heterogeneous catalysis used in organic synthesis. For example, the selective hydrogenolysis of aryl ethers using a nickel catalyst^[12] and the hydrogenation of lignin with rhodium nanoclusters have been carried out using a sustainable feedstock for important chemical materials.^[13] In addition, the synthesis of pyrroles, a very important class of compounds in medicinal chemistry via acceptorless dehydrogenative condensation of secondary alcohols and 1,2-aminoalcohols mediated by an iridium catalyst has been introduced.^[14] In addition, several Fe, Co, and Ni catalysts that promote the selective and highly efficient hydrogenation of nitro compounds to the corresponding amines have been published.^[15,16,17] Follow-up chemistry has also been performed using the hydrogenation of nitro compounds and further chemical reaction sequences to synthesize imines, benzimidazoles, 1*H*-perimidines, 3,4-dihydro-2*H*-pyrroles and quinoxalines.^[16,17,18] Moreover, the concept of reductive amination with aqueous ammonia using Fe, Co, Ni, and a bimetallic catalyst (Co and Sc) was introduced for the synthesis of primary, secondary, and tertiary amines.^[19–23] This concept was transferred to the reductive alkylation of nitrile compounds by aldehydes and ketones.^[24] Since heterocycles play a key role in the synthesis of biologically active molecules, synthesis concepts were introduced as well as the selective hydrogenation of these compounds using Co, Pd, Ru, and Ir catalysts.^[25,26] Additionally, a cobalt-cerium deoxygenation catalyst was published for the use of late-stage modification of biomass-derived molecules into fuels and chemicals.^[27] Simple, chemoselective hydrogenation of olefines has been investigated using a Ni catalyst with a tremendous tolerance in functional groups.^[28] It has also been shown that reversible hydrogen storage using a bimetallic palladium and ruthenium catalyst for both hydrogenation and dehydrogenation of *N*-ethylcarbazole is possible.^[29]

2.2 N-doped Support Materials for Heterogeneous Catalysts

Most heterogeneous catalysts used in chemistry and industry are supported catalysts, where the active component is carried by a support material. Porous solids such as γ - Al_2O_3 , SiO_2 , TiO_2 , CeO_2 , zeolites, or activated carbon are suitable as support materials in many applications.^[30] Since the interactions between the active phase and the support phase play an important role for the activity in catalysis, the choice of a suitable support is of great importance for heterogeneous catalysts. The properties required from the support material are diverse. They range from chemical inertness, stability under reaction and regeneration conditions, and a high surface area to highly oxidation and thermal shock resistant materials. The properties of the support material should be individually tunable for each catalytic process. Moreover, carbon-based carriers are widely used because of their microporous structures and excellent electrical conductivity, which improve the catalytic activity drastically.^[30,31] In this regard, substitutional heteroatom doping of the carbon-matrix is a suitable way to optimize the intrinsic reactivity of the active sites. Between the different dopants (e.g. B, P, F or S), N is the most intensively studied element, which had already been investigated in the early 1960s.^[32] Over the past decade, N-doping of carbon materials has enabled advances in many industrially important processes, including oxidation, reduction, Fischer-Tropsch synthesis, and hydrogen evolution reaction.^[33]

Metal or metal oxide nanoparticles supported on N-doped carbon materials are promising heterogeneous catalyst materials. The most common bonding forms of N-dopants in a given carbon matrix are pyridine, pyrrole, graphitic (quaternary) and pyridine N-oxide forms (Figure 1a).^[34,35] Pyridine N atoms are mainly found at the edges or defects of graphitic carbon layers. On the other hand, pyrrole N atoms are part of the five-membered ring. Graphitic (quaternary) N atoms refer to N atoms that have replaced C atoms in the carbon backbone. The inclusion of

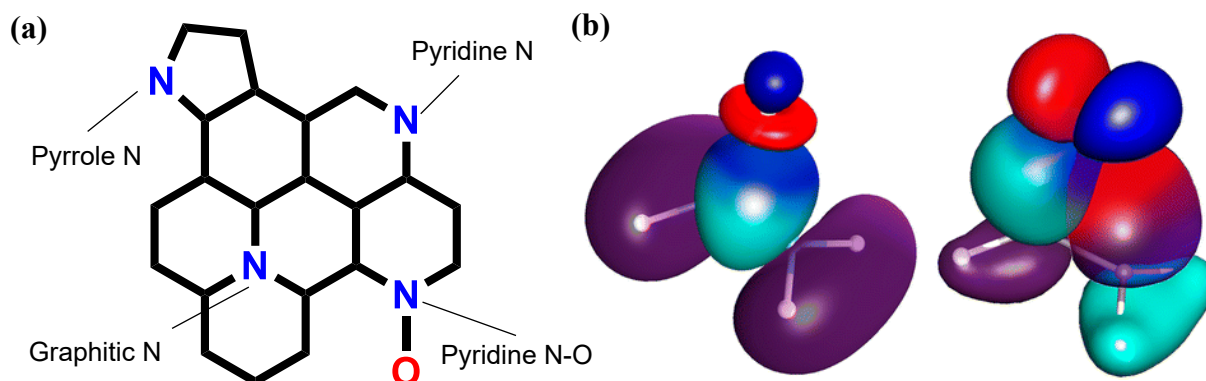


Figure 1: (a) Common bonding situations of N atoms in carbon matrices. (b) Proposed metal-nitrogen interaction: σ -bonding between an empty metal d-orbital (negative: blue, positive: red) and a filled π -orbital (negative: pale blue, positive: violet) of the support; π -backbonding between filled metal d-orbital and empty π^* -antibonding orbital of the support.

N-dopants results in defects or other imperfections in the graphite lattice. To describe the effect of N-dopants, it is important to understand the atomic structure and electron delocalization of N-dopants with neighboring C atoms. The incorporation of N into the graphite plane is energetically favored because native point defects and N-dopants attract each other. In addition, N-dopants lead to point defects with lower formation energy resulting in noticeable bond disorder and latent strain. The two different electronic states of C and N generate permanent dipoles that can be modulated by their defect types with different configurations.^[36] Once N atoms are introduced into the lattice, they influence the properties of the original carbon matrix and thus, the metal (oxide) nanoparticles are attached to the support in several ways. Among other things, defective CN positions, and N inclusions provide active centers for nucleation and growth of metal nanoparticles.^[37] Furthermore, in most cases, the binding energy for the formation of metal species is high for N-doped carbon materials. This leads to a high stability of the synthesized catalysts. An explanation can be given by the interaction of an N species with a metal center, which involves hybrid formation of the π -orbitals of N with the d-orbitals of the transition metal (Figure 1b).^[34,38] In addition, an enhanced metal-carrier interaction can result from close contact with the N-induced defects.^[39] This interpretation allows the view that N-doped carbon materials can be considered as “solid ligands”.^[34,40] The interfacial charge transfer at the metal-support binding site and the tunable acid-base character of the support surface play an important role in the unique mode of interaction between metal, support, and reactant in catalysis. As a result, there is an increase in the performance of the catalytic activity of metal nanoparticles on N-doped carbon compared to the undoped analogues.^[41]

The N-doping of carbon can be achieved by treatment with ammonia at high temperatures,^[42] by gas-phase deposition of nitrogen-containing compounds,^[43] or by liquid-phase polymerization of various compounds.^[44] If N-doped carbon supports are already available, methods for subsequent loading, such as impregnation and deposition/precipitation, offer simple fabrication options for carrier-fixed metal catalysts.^[45] Metal catalysts on N-modified carbon supports can also be obtained by pyrolysis processes.^[46] Nitrogen-rich motifs and their metal complexes are suitable precursors for this purpose.^[47] In the pyrolysis process, the structure of the nitrogen-rich motif is partially or completely decomposed, allowing the formation of metal nanoparticles. Similar N-doped carbon-fixed metal nanocatalysts can be prepared by pyrolyzing carbon with metal salts and nitrogen sources, which are cheap and readily available (e.g. inorganic metal salts). The most used nitrogen sources are melamine, 1,10-phenanthroline, dicyanidamide or triazine. Depending on the materials used, a clearly distinguishable catalytic behavior can be observed.^[48]

2.3 Polymer Derived Ceramics as Support Materials for Heterogeneous Catalysts

Polymer derived ceramics (PDCs) have attracted considerable interest in the last 50 years due to their excellent properties, and are used in a wide variety of applications.^[49] Unlike traditional high-temperature ceramic manufacturing, PDC processing is a relatively new technology that offers several advantages over conventional methods. In PDCs, the polymer is first generated, then crosslinked or gelled, and finally converted into a ceramic component by pyrolysis at suitable temperatures. The removal of organic components during pyrolysis by cleavage of C-H bonds, releasing H₂, CH₄, or other volatile compounds, leads to the formation of an inorganic material. The ceramic material is obtained through a complex microstructural evolution that depends on the thermal process and the heating temperature. The resulting nanoscale crystalline phase is embedded in an amorphous matrix containing a free carbon phase.^[50] By using different educts and different reaction types, the chemical and physical properties of the preceramic polymer, such as elemental composition, solubility, fusibility, and viscosity, can be adjusted. Special functional groups allow further modification of the polymer to create completely new ceramic materials with high purity and homogeneous distribution of elements. On the other hand, they provide 3-dimensional cross-linking to an unmeltable polymer, the so-called greenbody, which is the prerequisite for ceramization. The transformation from thermoset to the ceramic takes place at relatively low temperatures (< 1000 °C). Further, the polymeric nanostructure has an influence on the structure of the ceramic, and can be therefore tailored to the desired properties. Due to the different properties of the preceramic polymers and the resulting ceramics, various applications have been established, such as ceramic fibers, porous ceramics, polymer, and ceramic coatings, and as ceramic matrices.^[51] Because of these applications, combined with versatile forming methods, precursors such as polycarbosilanes have led to the synthesis and commercialization of various Si- or B-based polymeric precursors, such as polysiloxane, polysilazane, polyborazylene, and pure polycarbosilanes. These materials allow a range of ceramic materials with different compositions such as silicon oxycarbide (SiOC), silicon oxycarbonitride (SiOCN), silicon carbonitride (SiCN), silicon boron carbonitride (SiBCN), and silicon carbide (SiC).^[52] Therefore, PDCs can be categorized into oxide ceramics, which contain an oxygen moiety, and non-oxide ceramics, which do not contain any oxygen. These materials have advantageous properties in terms of oxidation resistance, refractoriness, low creep rate, chemical and thermal durability, and stability, or even functional properties such as piezo resistivity, that cannot be achieved by conventional ceramic synthesis processes.^[53] Such materials have a wide range of applications, including high-performance

coatings, sensors, nanocomposites, and fibers. The potential of these and other applications, such as energy technologies and catalysis, can be enhanced by the incorporation of metallic or intermetallic nanoparticles or phases.^[54]

There are several strategies to synthesize metal enhanced polymer derived non-oxide ceramics. A chemical approach is to mix the preceramic polymers with metal or metal oxide powders prior to crosslinking and pyrolysis. The molecular route involves the synthesis of metallopolymers and the chemical modification of precursors using coordination compounds. Further, PDCs can be used as support materials. The metal precursor is introduced to the support by wet impregnation of metal salts or complexes. Subsequent pyrolysis results in the formation of active catalyst species on the material, mostly nanoparticles. In this method, the active catalyst species is generated only on the surface of the material. In contrast, the chemical method also generates active species directly in the nanocomposite matrix. Therefore, it is very important to have a high porosity to access the active metal centers in the nanocomposite matrix for catalytic approaches.^[54,55]

Our group established several works using a PDC support material denoted as N-SiC for the synthesis of Fe/N-SiC and Co/N-SiC as well as CoSc/N-SiC nanostructured catalysts.^[20,22–24] *Bäumler et al.* synthesized at first the N-SiC material according to a modified procedure and the corresponding Fe/N-SiC catalyst (Figure 2).^[23,56] For this, the commercially available polycarbosilane SMP-10 and acrylonitrile are crosslinked to give the greenbody, which is subsequent pyrolyzed at 1000 °C in a nitrogen atmosphere. The resulting ceramic is then

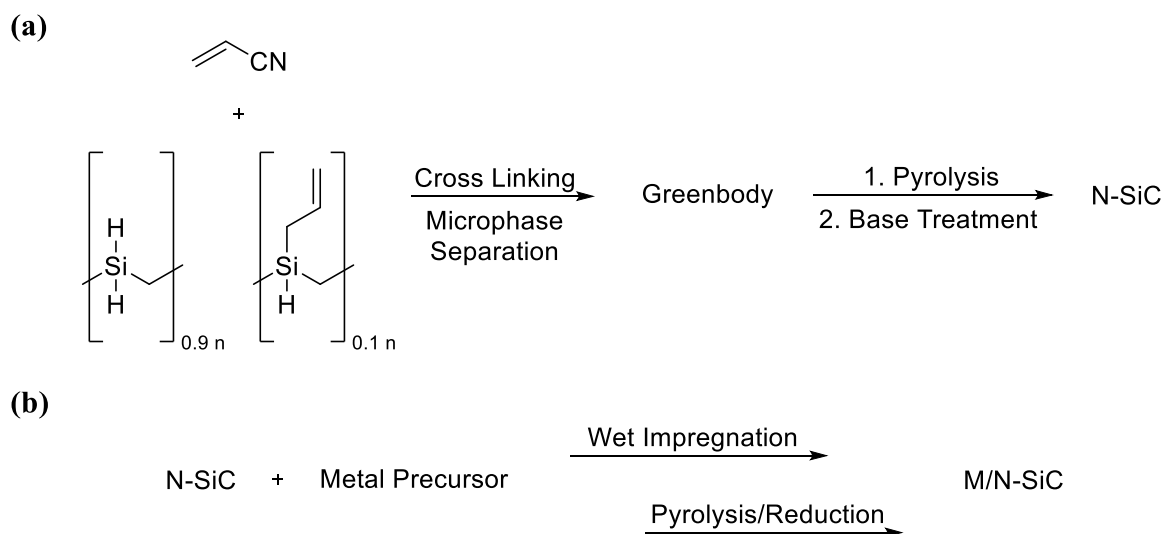


Figure 2: (a) Synthesis pathway of N-SiC starting from the cross linking of acrylonitrile and the polycarbosilane SMP-10 to the greenbody with subsequent pyrolysis and base treatment. (b) Catalyst synthesis by wet impregnation of a metal precursor and N-SiC followed by pyrolysis and reduction to obtain the active catalyst species (M/N-SiC).

washed in NaOH to leach out the silicon-rich domains from the material to obtain a high surface area with porosity (Figure 2a). For catalyst synthesis, the resulting N-SiC support is wet impregnated with a metal precursor and the solvent is removed. The material is then pyrolyzed and reduced to yield the active catalyst (Figure 2b). With the prepared catalysts Fe/N-SiC and Co/N-SiC, the synthesis of primary amines via reductive amination of carbonyl compounds with NH_3 was applied.^[22,23] The concept was transferred to the reductive alkylation of nitriles by aldehydes and ketones to receive secondary amines with a Co/N-SiC catalyst.^[24] Furthermore, it is shown that a bimetallic CoSc/N-SiC catalyst can promote the general synthesis of alkyl amines mediating two reactions, the BH/HA mechanism and reductive amination with hydrogen to obtain primary, secondary, and tertiary amines, which is also part of this dissertation.^[20]

2.4 Aromatic Heterocycles in Chemistry

2.4.1 Synthesis Approaches to N-Heterocycles

Heterocycles are essential structural elements in chemistry, found in many natural products, pharmaceuticals, and organic materials. They consist of rings containing at least one atom other than carbon, such as nitrogen, oxygen, or sulfur, which gives them unique properties.^[57] The synthesis of N-heterocycles has attracted much attention due to their prevalence in natural products and drugs.^[58] There are many aromatic heterocycles that vary in structure, ring size, and number of nitrogen atoms in the ring motif. Common N-heterocycles include pyrrole, imidazole, pyridine, pyrimidine, pyrazine, triazine, quinoline, isoquinoline, indole, or acridine are well known and many synthesis protocols have been reported.^[59] For example, the quinoline motif is present in many bioactive natural products, and various quinolines are known to exhibit a wide range of pharmacological properties. Quinoline derivatives, for instance, can be used as anti-cancer,^[60] anti-HIV,^[61] anti-hypertensive,^[62] anti-tuberculosis,^[63] and anti-alzheimer^[64] drugs (Figure 3).

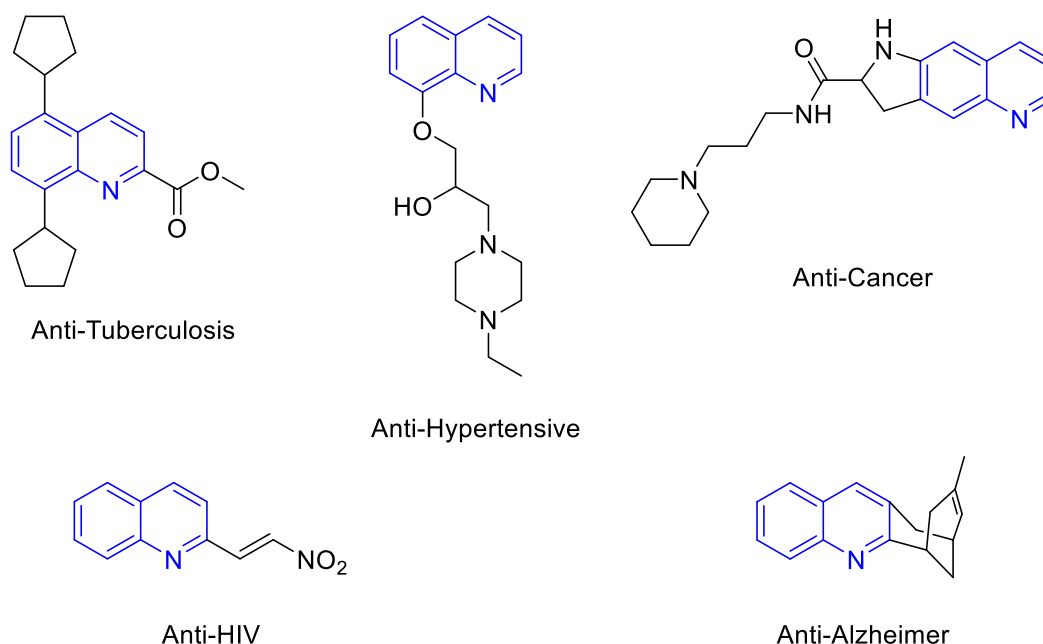


Figure 3: Pharmacologically active molecules with a quinoline motif (motif shown in blue). The drugs can be used as anti-tuberculosis, anti-hypertensive, anti-cancer, anti-HIV, and anti-alzheimer agents.

Quinoline was first synthesized by *Koenigs* in 1879 by passing allyl aniline over lead oxide.^[65] After, the *Skraup* synthesis, first published by *Skraup* in 1880 is the second synthetic approach to quinoline. It is based on aniline, which is converted to quinoline in the presence of glycerol,

sulphuric acid, and an oxidizing agent. Glycerol is first dehydrated to acrolein, which is required as an α,β -unsaturated carbonyl compound for cyclization.^[66] Among many other methods available for constructing the quinoline ring, the *Friedländer* quinoline synthesis first published by *Friedländer* in 1882 has proven to be a very powerful tool for the synthesis of quinolines.^[67] The condensation of 2-aminobenzaldehyde with acetophenone bearing a reactive methylene group in the α -position is, for example, base-catalyzed to the product 2-phenylquinoline. The reaction consists of two distinct steps. The condensation between the amino group and the carbonyl group of the aldehyde, and the irreversible intramolecular condensation of the methylene group or methyl group, and the carbonyl group in *ortho*-position in the aromatic ring. Based on this, it is assumed that an aldol-type condensation is involved in the entire condensation at a certain reaction stage. Thus, both acids and bases can catalyze this reaction.^[68] Figure 4 shows the mechanism of the *Friedländer* synthesis with 2-aminobenzaldehyde and acetophenone base catalyzed with LiOH.

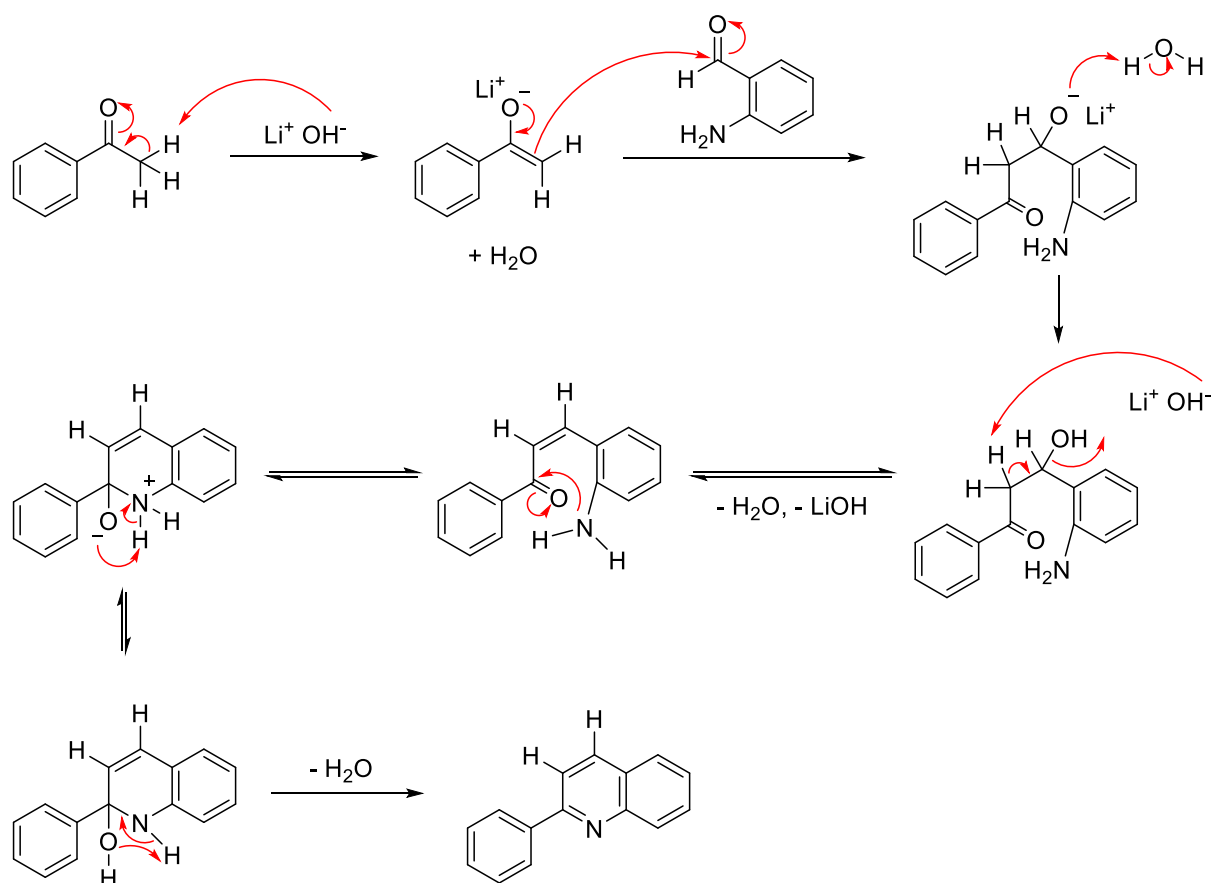


Figure 4: Reaction mechanism of the *Friedländer* synthesis on the example with 2-aminobenzaldehyde and acetophenone catalyzed by LiOH.

2.4.2 Selective Hydrogenation of Aromatic Heterocycles

The reduction of arenes to saturated cyclic compounds is of great interest for the production of bulk and fine chemicals as well as for the synthesis of pharmaceuticals, and agrochemicals.^[69] Hydrogenation is a particularly attractive reduction protocol because hydrogen is cheap, abundant, atom-efficient, and sustainable.^[70] Furthermore, arene hydrogenation is an elegant way to chemically store hydrogen. Here, nanostructured and reusable catalysts are of particular interest.^[71] The reduction of N-heterocycles to the corresponding partially or fully saturated derivatives has gained considerable importance due to their immense utility as biologically active building blocks and important intermediates in the production of pharmaceuticals, agrochemicals, and other fine chemicals.^[72] Selective hydrogenation of the aromatic ring is extremely attractive to produce complex molecules. The generation of catalysts for this step is therefore highly desirable. With respect to the quinoline motif, the selective hydrogenation to 1,2,3,4-tetrahydroquinoline (THQ), which is a component of various natural products and synthetic bioactive compounds, leads to a high demand in synthetic pathways. Well known drugs and natural products based on the THQ-motif are used as anti-bacterial,^[73] tubulin polymerization inhibitor,^[74] 5-HT₃ receptor antagonist,^[75] anti malaria,^[76] anti-fungal,^[77] and anti-tumor^[78] reagents (Figure 5). Many nanostructured 3d metal catalysts have been developed for the selective hydrogenation of quinolines to THQs, mainly cobalt^[26,79,80] and nickel^[79,81] catalysts, and only a few iron^[79,82] catalysts are known in the literature.

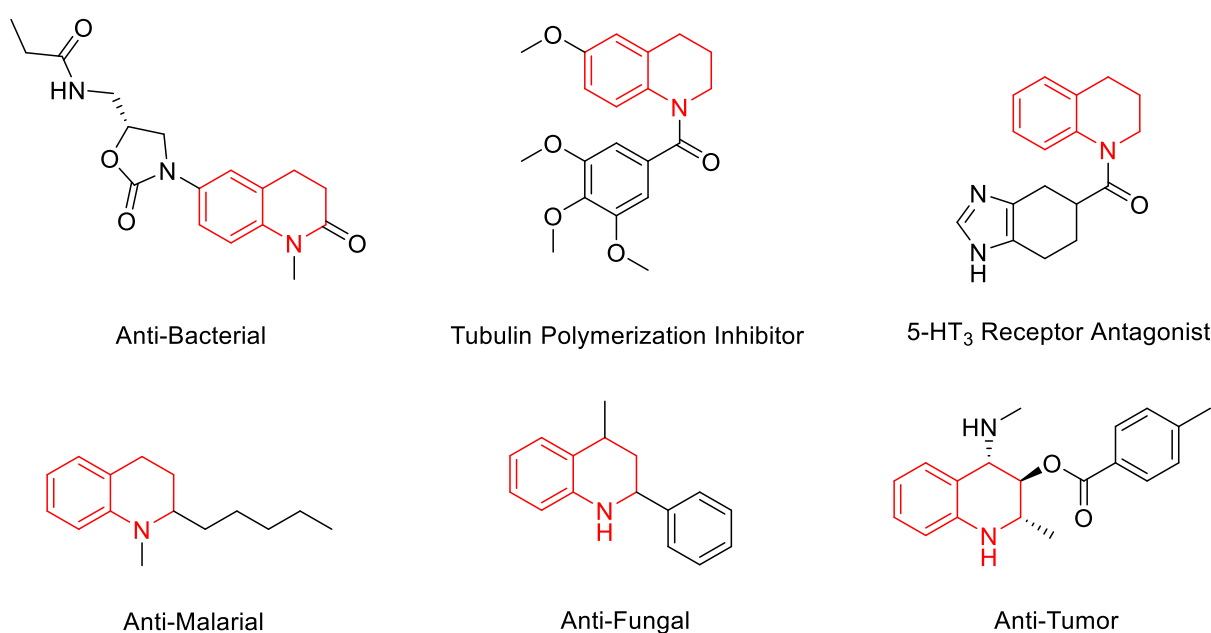


Figure 5: Pharmaceutical and drug molecules with a 1,2,3,4-tetrahydroquinoline motif (shown in red). The drugs are active in several areas and often used in medicine.

2.5 Synthesis Methods towards Amines

Amines represent a significant class of substrates with a wide range of applications across numerous industrial sectors, including the pharmaceutical, polymer, agrochemical, dye, surfactant, and fine chemical industries. The selective synthesis of differently substituted primary, secondary, and tertiary alkylamines is particularly challenging because the alkylated product amine is a better nucleophile and more reactive than the amine or ammonia starting material.^[69,83] There is a wide range of name reactions, such as the *Gabriel* synthesis, the *Hoffmann* degradation, the *Leuckart-Wallach* reaction, or the *Staudinger* reaction to produce amines. In addition, amination of alcohols, hydroamination, hydrogenation of nitro or cyano compounds, or reductive amination allow the synthesis of amines. For all these reactions, efficient catalytic and atom-efficient synthetic routes with few by-products are of great interest.^[84]

2.5.1 Reductive Amination of Carbonyl Compounds

The reductive amination of carbonyl compounds was introduced by *Mignonac* in 1921, using a nickel catalyst and dry ammonia as nitrogen source.^[85] It is an important amine synthesis and has been intensively studied in academia and industry for a century. In addition to aldehydes, ketones, or amines, starting materials have been used that can be converted to carbonyl or amine compounds in the presence of the same reducing agent and catalyst, such as carboxylic acids, organic carbonates, nitriles, or nitro compounds. The reaction pathway for the reductive amination of carbonyl compounds is shown in Figure 6.

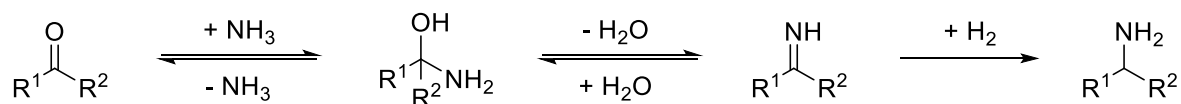


Figure 6: Reaction mechanism of the reductive amination of carbonyls to give amines introduced by *Mignonac* in 1921.

Aldehydes and ketones usually react with ammonia or amines by condensation to form a hemiaminal (carbinolamine). Further elimination of H₂O gives a Schiff base (imine). The following reduction to the amine takes place in the presence of a reducing agent such as formic acid, metal hydrides and molecular hydrogen, and/or a catalyst. The imine, as a reactive intermediate, or the primary amine, due to its enhanced nucleophilicity, can act as an amination

agent, and secondary and tertiary amines are often formed in parallel with the primary amine. Selectivity control is therefore important and this is where catalysts play an essential role. On the other hand, reductive amination is impressive in terms of product scope, as primary, secondary, and tertiary alkyl amines are accessible, and hydrogen is the most attractive reducing agent, especially when large scale product formation is an issue, as hydrogen is cheap and abundant. Therefore, reductive amination is characterized by cheap and abundant starting materials and a wide variety of substrates that can be converted and much effort has been put into research and development of catalysts over the past decades.^[86] A large number of applications for Raney Ni have been reported in the literature.^[87] However, in recent years, nanostructured 3d metal catalysts based on Fe,^[23,88] Co,^[89] and Ni^[19,90] have been successfully developed to provide reusability and facile handling of catalysts, as well as excellent selectivity.

2.5.2 Borrowing Hydrogen/Hydrogen Autotransfer Concept

The Borrowing Hydrogen/Hydrogen Autotransfer (BH/HA) concept was introduced by *Winans* and *Adkins* in 1932, using a heterogeneous nickel catalyst for the alkylation of amines by alcohols (Figure 7).^[91]

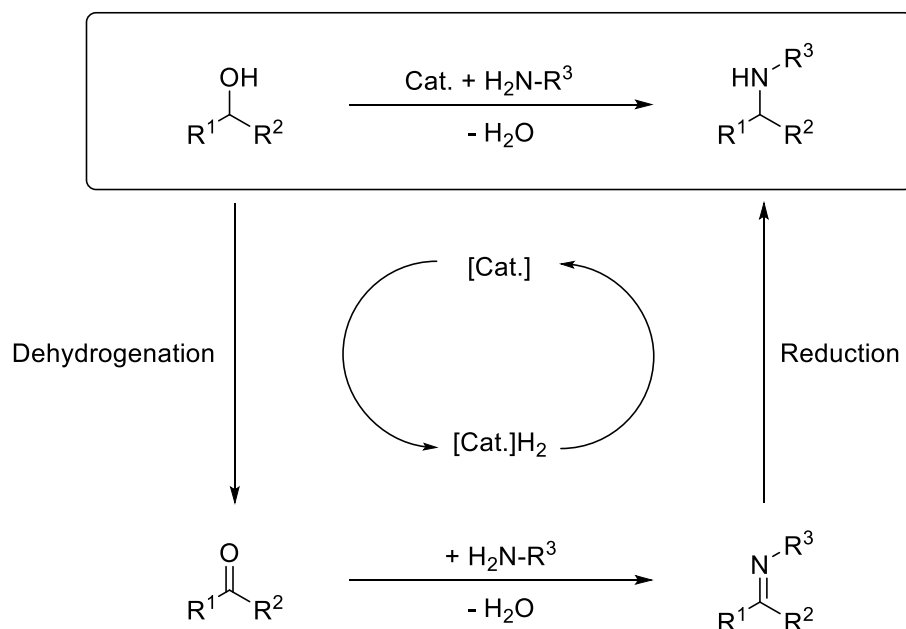


Figure 7: Alkylation of amines by alcohols following the Borrowing Hydrogen/Hydrogen Autotransfer concept.

This reaction is an important example of an alcohol refunctionalization reaction. It is highly atom-efficient and sustainable because alcohols can be used and no additional hydrogen is required. Alcohols can be produced from sustainable resources such as biomass. Lignocellulose, an underutilized, indigestible, and abundantly available waste material, is perfect for this purpose because it can be processed into alcohols.^[92] The alcohol starting material is first oxidized by dehydrogenation. The two hydrogen atoms are removed from the alcohol and the catalyst stores the hydrogen. The carbonyl compound formed can undergo a Schiff base reaction (condensation reaction) to form an imine intermediate, which can be reduced using the hydrogen atom equivalents gained in the dehydrogenation step to yield an alkylated amine (Figure 7). If ammonia is used as the nucleophile, as first demonstrated by the *Baiker* group using a heterogeneous cobalt catalyst, the hydroxy group of the alcohol is directly converted into an NH₂ group or a primary aliphatic amine.^[93]

Grigg^[94], *Watanabe*^[95] and co-workers introduced the first homogeneous catalysts for the BH/HA concept in 1981. Since then, numerous homogeneous transition metal catalyst systems have been developed to provide an elegant and broadly applicable method for the selective N-alkylation of amines by alcohols, as evidenced by numerous publications.^[96] Heterogeneous transition metal catalysts remain underrepresented in the literature, although reports have been published on catalysts with Fe,^[97] Co,^[20,98] Ni,^[99] and Cu,^[100] and are therefore of significant interest due to their enhanced stability and reusability as well as their greater sustainability.

2.6 References

- [1] J. Fourier, *Theorie du mouvement de la chaleur dans les corps solides*, **1824**.
- [2] a) *The Global Climate 2011-2020: A Decade of Accelerating Climate Change*, United Nations, **2023**; b) Copernicus Climate Change Service (C3S), *European State of the Climate 2023*, Copernicus Climate Change Service (C3S), **2024**.
- [3] M. Poliakoff, J. M. Fitzpatrick, T. R. Farren, P. T. Anastas, *Science* **2002**, *297*, 807–810.
- [4] P. T. Anastas, J. C. Warner, *Green chemistry. Theory and practice*, Oxford University Press, Oxford, **1998**.
- [5] P. T. Anastas, M. M. Kirchhoff, T. C. Williamson, *Appl. Catal. A: Gen.* **2001**, *221*, 3–13.
- [6] S. L. Y. Tang, R. L. Smith, M. Poliakoff, *Green Chem.* **2005**, *7*, 761.
- [7] P. T. Anastas, L. B. Bartlett, M. M. Kirchhoff, T. C. Williamson, *Catal. Today* **2000**, *55*, 11–22.
- [8] a) E. Antolini, *Appl. Catal. B: Environ.* **2010**, *100*, 413–426; b) S. Chen, C. Pei, J. Gong, *Energy Environ. Sci.* **2019**, *12*, 3473–3495; c) A. K. Datye, M. Votsmeier, *Nat. Mater.* **2021**, *20*, 1049–1059; d) L. Piccolo, *Catal. Today* **2021**, *373*, 80–97.
- [9] M. Binnewies, M. Jäckel, *Allgemeine und anorganische Chemie*, Spektrum Akademischer Verlag, Heidelberg, **2004**.
- [10] J. H. Clark, D. J. Macquarrie, *Org. Process Res. Dev.* **1997**, *1*, 149–162.
- [11] R. M. Bullock, *Science* **2013**, *342*, 1054–1055.
- [12] M. Zaheer, J. Hermannsdörfer, W. P. Kretschmer, G. Motz, R. Kempe, *ChemCatChem* **2014**, *6*, 91–95.
- [13] S. Fehn, M. Zaheer, C. E. Denner, M. Friedrich, R. Kempe, *New J. Chem.* **2016**, *40*, 9252–9256.
- [14] D. Forberg, J. Obenauf, M. Friedrich, S.-M. Hühne, W. Mader, G. Motz, R. Kempe, *Catal. Sci. Technol.* **2014**, *4*, 4188–4192.
- [15] a) G. Hahn, J.-K. Ewert, C. Denner, D. Tilgner, R. Kempe, *ChemCatChem* **2016**, *8*, 2461–2465; b) M. Eckardt, M. Zaheer, R. Kempe, *Sci. Rep.* **2018**, *8*, 2567; c) B. Klausfelder, R. Kempe, *Z. Anorg. Allg. Chem.* **2023**, 649.
- [16] T. Schwob, R. Kempe, *Angew. Chem. Int. Ed.* **2016**, *55*, 15175–15179.
- [17] C. Bäumler, R. Kempe, *Chem. Eur. J.* **2018**, *24*, 8989–8993.
- [18] a) B. Klausfelder, P. Blach, N. de Jonge, R. Kempe, *Chem. Eur. J.* **2022**, e202201307; b) T. Schwob, M. Ade, R. Kempe, *ChemSusChem* **2019**, *12*, 3013–3017.
- [19] G. Hahn, P. Kunnas, N. de Jonge, R. Kempe, *Nat. Catal.* **2019**, *2*, 71–77.

-
- [20] M. Elfinger, C. Bauer, J. Schmauch, M. Moritz, C. Wichmann, C. Papp, R. Kempe, *Adv. Synth. Catal.* **2023**.
- [21] R. Kempe, M. Klarner, P. Blach, H. Wittkaemper, N. de Jong, C. Papp, *ChemCatChem* **2021**.
- [22] M. Elfinger, T. Schönauer, S. L. J. Thomä, R. Stäglich, M. Drechsler, M. Zobel, J. Senker, R. Kempe, *ChemSusChem* **2021**, *14*, 2360–2366.
- [23] C. Bäuml, C. Bauer, R. Kempe, *ChemSusChem* **2020**, *13*, 3110–3114.
- [24] T. Schönauer, S. L. J. Thomä, L. Kaiser, M. Zobel, R. Kempe, *Chem. Eur. J.* **2020**, 1609–1614.
- [25] a) D. Forberg, T. Schwob, R. Kempe, *Nat. Commun.* **2018**, 1751; b) D. Forberg, F. Kallmeier, R. Kempe, *Inorganics* **2019**, *7*, 97.
- [26] C. Bauer, F. Müller, S. Keskin, M. Zobel, R. Kempe, *Chem. Eur. J.* **2023**, *29*, e202300561.
- [27] T. Schwob, P. Kunnas, N. de Jonge, C. Papp, H.-P. Steinrück, R. Kempe, *Sci. Adv.* **2019**, *5*, eaav3680.
- [28] M. Klarner, S. Bieger, M. Drechsler, R. Kempe, *Z. Anorg. Allg. Chem.* **2021**.
- [29] D. Forberg, T. Schwob, M. Zaheer, M. Friedrich, N. Miyajima, R. Kempe, *Nat. Commun.* **2016**, *7*, 13201.
- [30] W. Reschetilowski, *Einführung in die Heterogene Katalyse*, Springer Spektrum, Berlin, **2015**.
- [31] a) H. Marsh, F. Rodríguez-Reinoso, *Activated carbon*, **2006**; b) M. C. Román-Martínez, D. Cazorla-Amorós, A. Linares-Solano, C.-M. de Lecea, H. Yamashita, M. Anpo, *Carbon* **1995**, *33*, 3–13.
- [32] J. L. Figueiredo, P. Serp, *Carbon materials for catalysis*, John Wiley & Sons, Hoboken, **2009**.
- [33] a) P. Ayala, R. Arenal, M. Rümmele, A. Rubio, T. Pichler, *Carbon* **2010**, *48*, 575–586; b) M. Li, F. Xu, H. Li, Y. Wang, *Catal. Sci. Technol.* **2016**, *6*, 3670–3693; c) J.-Q. Yan, W. Peng, S.-S. Zhang, D.-P. Lei, J.-H. Huang, *Int. J. Hydrog. Energy* **2020**, *45*, 16094–16104.
- [34] R. Arrigo, M. E. Schuster, Z. Xie, Y. Yi, G. Wowsnick, L. L. Sun, K. E. Hermann, M. Friedrich, P. Kast, M. Hävecker et al., *ACS Catal.* **2015**, *5*, 2740–2753.
- [35] S. P. Jiang, P. K. Shen, *Nanostructured and advanced materials for fuel cells*, CRC Press, Boca Raton, **2014**.
- [36] W. J. Lee, J. Lim, S. O. Kim, *Small Methods* **2017**, *1*.

- [37] a) B. Choi, H. Yoon, I.-S. Park, J. Jang, Y.-E. Sung, *Carbon* **2007**, *45*, 2496–2501; b) Y.-H. Li, T.-H. Hung, C.-W. Chen, *Carbon* **2009**, *47*, 850–855.
- [38] W. Xia, *Catal. Sci. Technol.* **2016**, *6*, 630–644.
- [39] M. N. Groves, A. Chan, C. Malardier-Jugroot, M. Jugroot, *Chem. Phys. Lett.* **2009**, *481*, 214–219.
- [40] L. Zhang, A. Wang, W. Wang, Y. Huang, X. Liu, S. Miao, J. Liu, T. Zhang, *ACS Catal.* **2015**, *5*, 6563–6572.
- [41] a) D. S. Su, S. Perathoner, G. Centi, *Chem. Rev.* **2013**, *113*, 5782–5816; b) L. He, F. Weniger, H. Neumann, M. Beller, *Angew. Chem. Int. Ed.* **2016**, *55*, 12582–12594.
- [42] J. Przepiórski, M. Skrodzewicz, A. Morawski, *Appl. Surf. Sci.* **2004**, *225*, 235–242.
- [43] Z. Jin, J. Yao, C. Kittrell, J. M. Tour, *ACS Nano* **2011**, *5*, 4112–4117.
- [44] J. S. Lee, X. Wang, H. Luo, G. A. Baker, S. Dai, *J. Am. Chem. Soc.* **2009**, *131*, 4596–4597.
- [45] a) E. Castillejos, R. Chico, R. Bacsá, S. Coco, P. Espinet, M. Pérez-Cadenas, A. Guerrero-Ruiz, I. Rodríguez-Ramos, P. Serp, *Eur. J. Inorg. Chem.* **2010**, *2010*, 5096–5102; b) P. Chen, L. M. Chew, W. Xia, *J. Catal.* **2013**, *307*, 84–93.
- [46] E. Castillejos, B. Bachiller-Baeza, E. Asedegbega-Nieto, A. Guerrero-Ruiz, I. Rodríguez-Ramos, *RSC Adv.* **2015**, *5*, 81583–81598.
- [47] Z. Chen, D. Higgins, A. Yu, L. Zhang, J. Zhang, *Energy Environ. Sci.* **2011**, *4*, 3167.
- [48] K. N. Wood, R. O'Hayre, S. Pylypenko, *Energy Environ. Sci.* **2014**, *7*, 1212–1249.
- [49] R. Sujith, S. Jothi, A. Zimmermann, F. Aldinger, R. Kumar, *Int. Mater. Rev.* **2021**, *66*, 426–449.
- [50] P. Colombo, G. Mera, R. Riedel, G. D. Sorarù, *J. Am. Chem. Soc.* **2010**.
- [51] a) R. Riedel, G. Mera, R. Hauser, A. Klonczynski, *J. Ceram. Soc. Jpn.* **2006**, *114*, 425–444; b) A. S. Abd-El-Aziz, C. E. Carraher, C. U. Pittman, M. Zeldin, *Macromolecules Containing Metal and Metal-Like Elements. Boron-Containing Particles*, John Wiley & Sons Inc, Hoboken, **2007**; c) P. Miele, S. Bernard, D. Cornu, B. Toury, *Soft Mater.* **2007**, *4*, 249–286; d) P. Miele, S. Bernard in *Macromolecules Containing Metal and Metal-Like*, pp. 103–120; e) H. Schmidt, *Soft Mater.* **2007**, *4*, 143–164.
- [52] a) S. Yajima, J. Hayashi, M. Omori, K. Okamura, *Nature* **1976**, *261*, 683–685; b) S. Yajima, K. Okamura, J. Hayashi, M. Omori, *J. Am. Ceram. Soc.* **1976**, *59*, 324–327.
- [53] P. Colombo, E. Bernardo, G. Parciannello, *J. Eur. Ceram.* **2013**, *33*, 453–469.
- [54] M. Zaheer, T. Schmalz, G. Motz, R. Kempe, *Chem. Soc. Rev.* **2012**, *41*, 5102–5116.

- [55] G. Glatz, T. Schmalz, T. Kraus, F. Haarmann, G. Motz, R. Kempe, *Chem. Eur. J.* **2010**, *16*, 4231–4238.
- [56] L. F. B. Ribeiro, O. Flores, P. Furtat, C. Gervais, R. Kempe, R. A. F. Machado, G. Motz, *J. Mater. Chem. A* **2017**, *5*, 720–729.
- [57] B. P. Nandeshwarappa, S. S. O., *Heterocycles. Synthesis and biological activities*, IntechOpen, London, **2020**.
- [58] J. A. Joule, K. Mills, G. F. Smith, *Heterocyclic chemistry*, CRC Press; Taylor & Francis, London, Abingdon, **2020**.
- [59] J. A. Joule, *Heterocyclic chemistry at a glance*, John Wiley & Sons, Chichester, West Sussex, Hoboken, **2013**.
- [60] A. Tsotinis, M. Vlachou, S. Zouroudis, A. Jeney, F. Timar, D. Thurston, C. Roussakis, *LDDD* **2005**, *2*, 189–192.
- [61] X. Franck, A. Fournet, E. Prina, R. Mahieux, R. Hocquemiller, B. Figadère, *Bioorg. Med. Chem. Lett.* **2004**, *14*, 3635–3638.
- [62] N. Muruganantham, R. Sivakumar, N. Anbalagan, V. Gunasekaran, J. T. Leonard, *Biol. Pharm. Bull.* **2004**, *27*, 1683–1687.
- [63] A. Nayyar, A. Malde, R. Jain, E. Coutinho, *Bioorg. Med. Chem* **2006**, *14*, 847–856.
- [64] P. Camps, E. Gómez, D. Muñoz-Torrero, A. Badia, N. M. Vivas, X. Barril, M. Orozco, F. J. Luque, *J. Med. Chem.* **2001**, *44*, 4733–4736.
- [65] W. Koenigs, *Ber. Dtsch. Chem. Ges.* **1879**, *12*, 453.
- [66] Z. H. Skraup, *Ber. Dtsch. Chem. Ges.* **1880**, *13*, 2073–2097.
- [67] a) P. Friedlaender, *Ber. Dtsch. Chem. Ges.* **1882**, *15*, 2572–2575; b) P. Friedländer, C. F. Gohring, *Ber. Dtsch. Chem. Ges.* **1883**, *16*, 1833–1839; c) J. J. Li, *Name Reactions*, Springer Berlin Heidelberg, Berlin, Heidelberg, **2009**.
- [68] Z. Wang, *Comprehensive organic name reactions and reagents*, Wiley, Chichester, **2010**.
- [69] K. Weissermel, H.-J. Arpe, *Industrial Organic Chemistry*, Wiley-VCH, Weinheim, **2008**.
- [70] P. G. Andersson, *Modern Reduction Methods*, John Wiley & Sons Incorporated, Weinheim, **2008**.
- [71] a) K. C. Tan, T. He, Y. S. Chua, P. Chen, *J. Phys. Chem. C* **2021**, *125*, 18553–18566; b) Y. Jo, J. Oh, D. Kim, J. H. Park, J. H. Baik, Y.-W. Suh, *Korean J. Chem. Eng.* **2022**, *39*, 20–37; c) M. S. Salman, N. Rambhujun, C. Pratthana, K. Srivastava, K.-F. Aguey-Zinsou, *Ind. Eng. Chem. Res.* **2022**, *61*, 6067–6105.
- [72] a) T. J. Donohoe, R. Garg, C. A. Stevenson, *Tetrahedron Asymmetry* **1996**, *7*, 317–344; b) A. Gualandi, D. Savoia, *RSC Adv.* **2016**, *6*, 18419–18451.

- [73] D. K. Hutchinson, *Curr. Top. Med. Chem.* **2003**, *3*, 1021–1042.
- [74] J.-P. Liou, Z.-Y. Wu, C.-C. Kuo, C.-Y. Chang, P.-Y. Lu, C.-M. Chen, H.-P. Hsieh, J.-Y. Chang, *J. Med. Chem.* **2008**, *51*, 4351–4355.
- [75] V. Sridharan, P. A. Suryavanshi, J. C. Menéndez, *Chem. Rev.* **2011**, *111*, 7157–7259.
- [76] I. Jacquemond-Collet, F. Benoit-Vical, A. Valentin, E. Stanislas, M. Mallié, I. Fourasté, *Planta Med.* **2002**, *68*, 68–69.
- [77] L. Y. Vargas M, M. V. Castelli, V. V. Kouznetsov, J. M. Urbina G, S. N. López, M. Sortino, R. D. Enriz, J. C. Ribas, S. Zacchino, *Bioorg. Med. Chem.* **2003**, *11*, 1531–1550.
- [78] R. Hiessböck, C. Wolf, E. Richter, M. Hitzler, P. Chiba, M. Kratzel, G. Ecker, *J. Med. Chem.* **1999**, *42*, 1921–1926.
- [79] J. E. Shaw, P. R. Stapp, *J. Heterocycl. Chem.* **1987**, *24*, 1477–1483.
- [80] a) F. Chen, A.-E. Surkus, L. He, M.-M. Pohl, J. Radnik, C. Topf, K. Junge, M. Beller, *J. Am. Chem. Soc.* **2015**, *137*, 11718–11724; b) P. Ji, K. Manna, Z. Lin, A. Urban, F. X. Greene, G. Lan, W. Lin, *J. Am. Chem. Soc.* **2016**, *138*, 12234–12242; c) Z. Wei, Y. Chen, J. Wang, D. Su, M. Tang, S. Mao, Y. Wang, *ACS Catal.* **2016**, *6*, 5816–5822; d) J. Li, G. Liu, X. Long, G. Gao, J. Wu, F. Li, *J. Catal.* **2017**, *355*, 53–62; e) I. Sorribes, L. Liu, A. Doménech-Carbó, A. Corma, *ACS Catal.* **2018**, *8*, 4545–4557; f) W. Gong, Q. Yuan, C. Chen, Y. Lv, Y. Lin, C. Liang, G. Wang, H. Zhang, H. Zhao, *Adv. Mater.* **2019**, *31*, e1906051; g) G. Jaiswal, M. Subaramanian, M. K. Sahoo, E. Balaraman, *ChemCatChem* **2019**, *11*, 2449–2457; h) Z.-H. He, Y.-C. Sun, K. Wang, Z.-Y. Wang, P.-P. Guo, C.-S. Jiang, M.-Q. Yao, Z.-H. Li, Z.-T. Liu, *Mol. Catal.* **2020**, *496*, 111192; i) J. Hervochon, V. Dorcet, K. Junge, M. Beller, C. Fischmeister, *Catal. Sci. Technol.* **2020**, *10*, 4820–4826; j) R. Huang, C. Cao, J. Liu, L. Zheng, Q. Zhang, L. Gu, L. Jiang, W. Song, *ACS Appl. Mater. Interfaces.* **2020**, *12*, 17651–17658; k) K. Murugesan, V. G. Chandrashekar, C. Kreyenschulte, M. Beller, R. V. Jagadeesh, *Angew. Chem. Int. Ed.* **2020**, *132*, 17561–17565; l) V. M. Asaula, V. V. Buryanov, B. Y. Solod, D. M. Tryus, O. O. Pariiska, I. E. Kotenko, Y. M. Volovenko, D. M. Volochnyuk, S. V. Ryabukhin, S. V. Kolotilov, *Justus Liebigs Ann. Chem.* **2021**, *2021*, 6616–6625; m) N. Antil, A. Kumar, N. Akhtar, W. Begum, M. Chauhan, R. Newar, M. S. Rawat, K. Manna, *Inorg. Chem.* **2022**, *61*, 1031–1040; n) M. Puche, L. Liu, P. Concepción, I. Sorribes, A. Corma, *ACS Catal.* **2021**, *11*, 8197–8210; o) F. Tang, G. Zhang, L. Wang, J. Huang, Y.-N. Liu, *J. Catal.* **2022**, *414*, 101–108; p) F. Tang, G. Zhang, L. Wang, J. Huang, Y.-N. Liu, *J. Catal.* **2022**, *414*, 101–108; q) O. O. Pariiska, D. O. Mazur, V. M. Asaula, V. V. Buryanov, R. Socha, Y. Kurys, S. V. Kolotilov, V. G. Koshechko, v. d. Pokhodenko, *Theor. Exp. Chem.*

- 2023**, 58, 417–426; r) H. Yang, M. Xu, L. Zhang, W. Fang, E. Liu, H. Zhang, *Microporous Mesoporous Mat.* **2023**, 360, 112701; s) Y. Hu, X. Li, M. Liu, S. Bartling, H. Lund, J. Rabeah, P. J. Dyson, M. Beller, R. V. Jagadeesh, *ChemCatChem* **2024**, 16, e202301027; t) X. Rong, H. Li, L. Chen, B. Yuan, A. Guo, Z. Jiang, G. Bai, B. Wang, *New J. Chem.* **2024**, 48, 4880–4885.
- [81] a) H. Adkins, H. R. Billica, *J. Am. Chem. Soc.* **1948**, 70, 695–698; b) F. Alonso, M. Yus, *Adv. Synth. Catal.* **2001**, 343, 188–191; c) F. Alonso, P. Candela, C. Gómez, M. Yus, *Adv. Synth. Catal.* **2003**, 345, 275–279; d) C. Liu, Z. Rong, Z. Sun, Y. Wang, W. Du, Y. Wang, L. Lu, *RSC Adv.* **2013**, 3, 23984–23988; e) H. Jiang, S. Zhang, B. Sun, *Catal. Lett.* **2018**, 148, 1336–1344; f) R. Yun, W. Ma, L. Hong, Y. Hu, F. Zhan, S. Liu, B. Zheng, *Catal. Sci. Technol.* **2019**, 9, 6669–6672; g) L. Niu, Y. An, X. Yang, G. Bian, Q. Wu, Z. Xia, G. Bai, *Mol. Catal.* **2021**, 514, 111855; h) Y. Zhu, J. Gu, Z. Huang, H. Ding, H. Xia, S. Qiu, K. Xie, *J. Alloys Compd.* **2022**, 925, 166703; i) V. V. Subotin, M. O. Ivanytsya, A. V. Terebilenko, P. S. Yaremov, O. O. Pariiska, Y. M. Akimov, I. E. Kotenko, T. M. Sabov, M. M. Kurmach, S. V. Ryabukhin et al., *Catalysts* **2023**, 13, 706; j) Z. Yuan, X. Li, G. Wang, Z. Zhu, Y. Liao, Z. Zhang, B. Liu, *Mol. Catal.* **2023**, 540, 113052.
- [82] B. Sahoo, C. Kreyenschulte, G. Agostini, H. Lund, S. Bachmann, M. Scalone, K. Junge, M. Beller, *Chem. Sci.* **2018**, 9, 8134–8141.
- [83] a) S. A. Lawrence, *Amines. Synthesis, properties, and applications*, Cambridge University Press, Cambridge, **2004**; b) R. Vardanyan, V. Hruby, *Synthesis of best-seller drugs*, Academic Press, London, **2016**.
- [84] a) T. Laue, A. Plagens, *Namen- und Schlagwort-Reaktionen der organischen Chemie*, Vieweg + Teubner, Wiesbaden, **2009**; b) A. Ricci, *Modern Amination Methods*, Wiley-VCH, Weinheim, **2008**.
- [85] G. Mignonac, *Compt. Rend.* **1921**, 172, 223–226.
- [86] T. Irrgang, R. Kempe, *Chem. Rev.* **2020**, 120, 9583–9674.
- [87] a) E. J. Schwoegler, H. Adkins, *J. Am. Chem. Soc.* **1939**, 61, 3499–3502; b) C. F. Winans, *J. Am. Chem. Soc.* **1939**, 61, 3566–3567; c) A. S. Chan, C. Chen, Y. Lin, *Appl. Catal. A: Gen.* **1994**, 119, L1–L5; d) K. A. Pollart, R. E. Miller, *J. Org. Chem.* **1962**, 27, 2392–2394; e) P. Dolezal, O. Machalicky, M. Pavelek, P. Kubec, K. Hradkova, R. Hrdina, R. Sulakova, *Appl. Catal. A: Gen.* **2005**, 286, 202–210.
- [88] a) T. Stemmler, A.-E. Surkus, M.-M. Pohl, K. Junge, M. Beller, *ChemSusChem* **2014**, 7, 3012–3016; b) X. Zhuang, X. Wei, X. Hu, Q. Zhang, X. Zhang, L. Chen, J. Liu, L. Ma,

- Green Chem.* **2023**, *25*, 7109–7125; c) Y. Kita, N. Yanagisawa, M. Arai, K. Kamata, M. Hara, *Catal. Sci. Technol.* **2024**, *14*, 5430–5438.
- [89] a) T. Stemmler, F. A. Westerhaus, A.-E. Surkus, M.-M. Pohl, K. Junge, M. Beller, *Green Chem.* **2014**, *16*, 4535–4540; b) S. Pisiewicz, T. Stemmler, A.-E. Surkus, K. Junge, M. Beller, *ChemCatChem* **2015**, *7*, 62–64; c) F. Mao, D. Sui, Z. Qi, H. Fan, R. Chen, J. Huang, *RSC Adv.* **2016**, *6*, 94068–94073; d) L.-F. Chen, Q. Xu, *Science* **2017**, *358*, 304–305; e) X. Cui, K. Liang, M. Tian, Y. Zhu, J. Ma, Z. Dong, *J. Colloid. Interface Sci.* **2017**, *501*, 231–240; f) R. V. Jagadeesh, K. Murugesan, A. S. Alshammari, H. Neumann, M.-M. Pohl, J. Radnik, M. Beller, *Science* **2017**, *358*, 326–332; g) L. Jiang, P. Zhou, Z. Zhang, Q. Chi, S. Jin, *New J. Chem.* **2017**, *41*, 11991–11997; h) H. Wu, C. Shen, C. Xia, L. He, *Sci. China Mater.* **2017**, *60*, 1269–1271; i) P. Zhou, L. Jiang, F. Wang, K. Deng, K. Lv, Z. Zhang, *Sci. Adv.* **2017**, *3*, e1601945; j) Z. Yuan, B. Liu, P. Zhou, Z. Zhang, Q. Chi, *J. Catal.* **2019**, *370*, 347–356; k) T. Senthamarai, V. G. Chandrashekar, M. B. Gawande, N. V. Kalevaru, R. Zbořil, P. C. J. Kamer, R. V. Jagadeesh, M. Beller, *Chem. Sci.* **2020**, *11*, 2973–2981; l) A. Skita, F. Keil, W. Stühmer, *Ber. Dtsch. Chem. Ges. A/B* **1942**, *75*, 1696–1702; m) M. Sheng, S. Fujita, S. Yamaguchi, J. Yamasaki, K. Nakajima, S. Yamazoe, T. Mizugaki, T. Mitsudome, *JACS Au* **2021**, *1*, 501–507; n) K. Kato, D. Deng, Y. Kita, K. Kamata, M. Hara, *Catal. Sci. Technol.* **2022**, *12*, 5425–5434; o) B. Zheng, J. Xu, J. Song, H. Wu, X. Mei, K. Zhang, W. Han, W. Wu, M. He, B. Han, *Chem. Sci.* **2022**, *13*, 9047–9055.
- [90] a) K. Murugesan, M. Beller, R. V. Jagadeesh, *Angew. Chem. Int. Ed.* **2019**, *58*, 5064–5068; b) Y. V. Popov, V. M. Mokhov, S. E. Latyshova, A. O. Panov, P. M. Shirkhanyan, *Russ. J. Gen. Chem.* **2017**, *87*, 2546–2551; c) W. Chen, Y. Sun, J. Du, Z. Si, X. Tang, X. Zeng, L. Lin, S. Liu, T. Lei, *J. of Chemical Tech. & Biotech.* **2018**, *93*, 3028–3034; d) T. Trégner, *Chem. Biochem. Eng. Q.* **2018**, *31*, 455–470; e) O. I. Afanasyev, E. Kuchuk, D. L. Usanov, D. Chusov, *Chem. Rev.* **2019**, *119*, 11857–11911; f) M. Manzoli, E. C. Gaudino, G. Cravotto, S. Tabasso, R. B. N. Baig, E. Colacino, R. S. Varma, *ACS Sustainable Chem. Eng.* **2019**, *7*, 5963–5974; g) K. Murugesan, M. Beller, R. V. Jagadeesh, *Angew. Chem. Int. Ed.* **2019**, *131*, 5118–5122; h) H. Yuan, J.-P. Li, F. Su, Z. Yan, B. T. Kusema, S. Streiff, Y. Huang, M. Pera-Titus, F. Shi, *ACS Omega* **2019**, *4*, 2510–2516; i) Y. Zhang, H. Yang, Q. Chi, Z. Zhang, *ChemSusChem* **2019**, *12*, 1246–1255.
- [91] C. F. Winans, H. Adkins, *J. Am. Chem. Soc.* **1932**, *54*, 306–312.

-
- [92] a) T. P. Vispute, H. Zhang, A. Sanna, R. Xiao, G. W. Huber, *Science* **2010**, *330*, 1222–1227; b) Z. Sun, G. Bottari, A. Afanassenko, M. C. A. Stuart, P. J. Deuss, B. Fridrich, K. Barta, *Nat. Catal.* **2018**, *1*, 82–92.
- [93] A. Fischer, M. Maciejewski, T. Bürgi, T. Mallat, A. Baiker, *J. Catal.* **1999**, *183*, 373–383.
- [94] R. Grigg, T. R. B. Mitchell, S. Sutthivaiyakit, N. Tongpenyai, *J. Chem. Soc.* **1981**, 611.
- [95] Y. Watanabe, Y. Tsuji, Y. Ohsugi, *Tetrahedron Lett.* **1981**, *22*, 2667–2670.
- [96] T. Irrgang, R. Kempe, *Chem. Rev.* **2019**, *119*, 2524–2549.
- [97] C. Gonzalez-Arellano, K. Yoshida, R. Luque, P. L. Gai, *Green Chem.* **2010**, *12*, 1281.
- [98] Z. Ma, B. Zhou, X. Li, R. G. Kadam, M. B. Gawande, M. Petr, R. Zbořil, M. Beller, R. V. Jagadeesh, *Chem. Sci.* **2021**, *13*, 111–117.
- [99] a) X. Cui, X. Dai, Y. Deng, F. Shi, *Chem. Eur. J.* **2013**, *19*, 3665–3675; b) K. Shimizu, N. Imaiida, K. Kon, S. M. A. Hakim Siddiki, A. Satsuma, *ACS Catal.* **2013**, *3*, 998–1005; c) K. Shimizu, K. Kon, W. Onodera, H. Yamazaki, J. N. Kondo, *ACS Catal.* **2013**, *3*, 112–117; d) A. Tomer, F. Wyrwalski, C. Przybylski, J.-F. Paul, E. Monflier, M. Pera-Titus, A. Ponchel, *J. Catal.* **2017**, *356*, 111–124; e) A. Afanassenko, S. Elangovan, M. C. A. Stuart, G. Bonura, F. Frusteri, K. Barta, *Catal. Sci. Technol.* **2018**, *8*, 5498–5505.
- [100] a) F. Santoro, R. Psaro, N. Ravasio, F. Zaccheria, *ChemCatChem* **2012**, *4*, 1249–1254; b) M. Dixit, M. Mishra, P. A. Joshi, D. O. Shah, *Catal. Commun.* **2013**, *33*, 80–83; c) H. Liu, G.-K. Chuah, S. Jaenicke, *J. Catal.* **2015**, *329*, 262–268; d) S. Pang, Y. Deng, F. Shi, *Chem. Commun.* **2015**, *51*, 9471–9474.

3 Overview of Thesis Results

The thesis consists of three publications, which are presented in chapter 4 to 6. Two of them have been published and one is submitted. The synopsis, chapter 3.1, gives an overview of the individual publications of this thesis and discusses them in an overall context. The individual contributions to the joint publications are described in detail in chapter 3.2.

3.1 Synopsis

Heterogeneous catalysis is a key technology which addresses sustainability in multiple areas and contexts. Precious metals, which are very expensive and not readily available, are commonly used in industrial catalytic systems and processes. Therefore, it is highly desirable to replace precious metals with more abundant and available alternatives. In recent years, the *Kempe* group has focused on the synthesis and design of novel heterogeneous, nanostructured catalysts for complex organic syntheses. Here, the *Kempe* group made a decisive contribution to this topic by introducing several earth-abundant metal catalysts for hydrogenation and dehydrogenation reactions. Heterogeneous, nanostructured metal catalysts supported by porous materials were developed for chemoselective hydrogenation and consecutive organic reactions. The motif of the metal-salen complexes were successfully introduced as precursors for several catalyst systems with different support materials. In addition, highly active nickel, cobalt and iron systems were introduced with a wide product range and different reaction mechanisms.

However, the metal-salen method has the major disadvantage that the metal and nitrogen/carbon (N/C) sources cannot be tuned individually. This makes it impossible to tune the N-doping of the material to obtain materials with higher activity due to the doping and to find an optimum in doping. The first publication of this thesis introduces a synthesis protocol for nanostructured earth-abundant metal catalysts where both the metal and N/C content are individually adjustable. Three components, an inexpensive metal precursor, an easy-to-synthesize N/C precursor and a commercially available porous support material undergo pyrolysis to give the catalyst material in a simple, single synthesis step. First, the N/C precursor meso-octamethylcalix[4]pyrrole was synthesized. The basic motif is an N₄-macrocycle without π - π -stacking and a flat structure; therefore, it is excellent soluble for the wet impregnation process and can be molecularly dispersed easily. For the catalyst synthesis, the N/C precursor and cobalt acetate tetrahydrate are dissolved in methanol together with SiO₂ as support material.

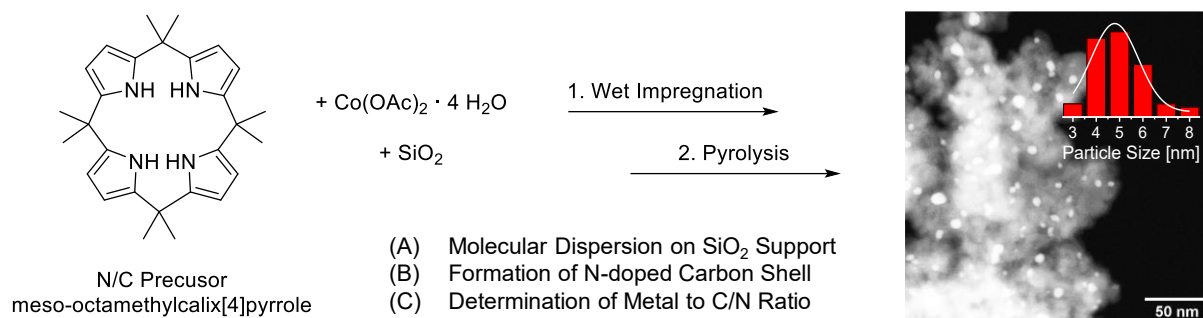


Figure 8: Synthesis procedure of the catalyst material starting with wet impregnation of meso-octamethylcalix[4]pyrrole and $\text{Co}(\text{OAc})_2 \cdot 4 \text{H}_2\text{O}$ with SiO_2 and subsequent pyrolysis. The key is the spatially separated N/C and metal precursor to tune the N-doping of the material on a mesoporous silica support to receive a highly active catalyst.

After the removal of the solvent at 70 °C, the sample was pyrolyzed under nitrogen atmosphere to give the active catalyst material (Figure 8). In order to find the best catalyst, a variation of several parameters was performed by testing the catalysts in the selective hydrogenation of quinoline to 1,2,3,4-tetrahydroquinoline (see Chapter 4). By varying the metal to N/C ratio (M/N ratio) from a ratio of 1:1 to 1:10 the nitrogen doping was increased. The high activity of the Co/SiO_2 catalyst is due to a specific ratio of N/C precursor to cobalt precursor. A certain amount of microporous N/C or a certain thickness of the embedding N/C layer is optimal for educt access and catalyst stability. Too thick a layer may prevent educt access, and too thin a layer may lead to cobalt leaching, as the metal nanoparticles are more easily removed from the support. Maximum activity in the benchmark reaction is observed when a ratio of metal to N/C precursor of 1:4 is used. More N-doping leads to a decrease in product yield to a certain plateau at about 60 % yield. In the catalyst material study, 1.81 wt% cobalt is loaded on the material which shows the best activity in the benchmark reaction with 5.0 mol% cobalt loading in the catalysis. The pyrolysis temperature and different commercial support materials and cobalt precursors were also tested. The best pyrolysis temperature was found to be 800 °C, while SiO_2 as support material showed superior activity over other cobalt catalysts based on $\gamma\text{-Al}_2\text{O}_3$, TiO_2 , and CeO_2 . Using activated carbon as support material only showed little activity in the benchmark reaction. In addition, it is important which metal precursor is used in the wet impregnation and pyrolysis process. Cobalt acetylacetonate, cobalt stearate and cobalt chloride show little to no activity. Cobalt nitrate was able to show some activity. Furthermore, time-conversion studies show that the conversion of quinoline to THQ is achieved after 17 h under the optimal reaction conditions used. To ensure completion, a reaction time of 20 h was chosen. In summary, with 5.0 mol% Co, 2.0 MPa H_2 , 70 °C and 20 h reaction time, the reaction can be carried out smoothly and selectively.

In an attempt to gain more insight into the Co/SiO₂ catalyst, several characterization methods were applied. First, Thermogravimetric Analysis (TGA) revealed the high volatility of the N/C precursor and the decomposition of the metal precursor under catalyst synthesis conditions (see Chapter 4). This ensures the molecular dispersion of the metal precursor on the support material within the formation of N-doped carbon shells embedded nanoparticles and the carbon supply during the pyrolysis process. ICP-OES analysis confirms the cobalt content of 1.81 wt% (see Chapter 4). The surface characterization and pore size distribution of the catalyst were determined via nitrogen physisorption measurements. The catalyst surface area of 217 m²/g showed an increase compared to the support material SiO₂ (194 m²/g). This can be explained by the formation of additional microporosity due to the carbon black formation during the catalyst synthesis (see Chapter 4). Moreover, XPS analysis was conducted. It showed the presence of metallic cobalt and cobalt oxide on the surface of the Co/SiO₂ catalyst (Figure 9f). Three different nitrogen binding modes within the catalyst are suggested by detailed XPS analysis. HAADF-STEM shows that the cobalt nanoparticles are homogeneously distributed throughout the support and have an average particle size of 4.8 nm (Figure 8). This was also confirmed by SEM-EDX measurements (see Chapter 4). To take a closer look at the active

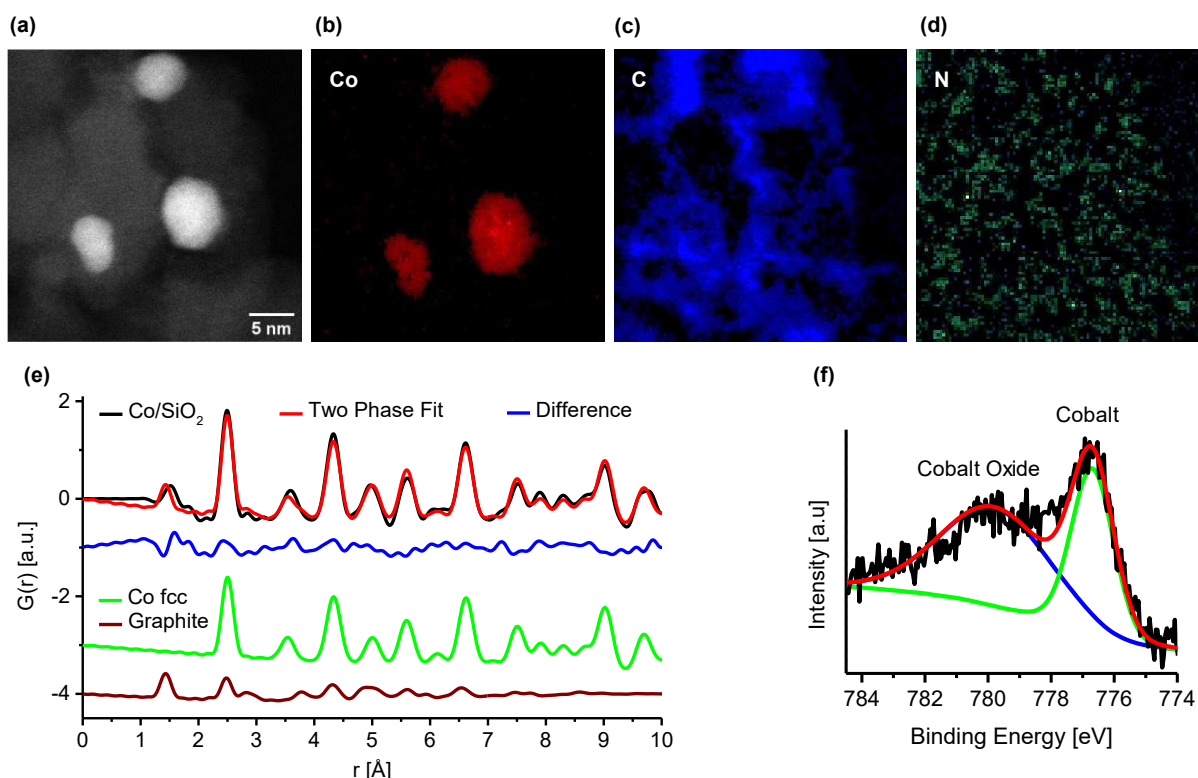


Figure 9: Characterization of the Co/SiO₂ catalyst. (a)-(d) HAADF-STEM images of Co/SiO₂ with representative EELS element maps of cobalt (b), carbon (c) and nitrogen (d). (e) The PDF of Co/SiO₂ was fitted with a Co fcc phase of 3.1 nm particle diameter and a graphitic domain, both contributions shown in the offset. (f) XPS analysis of the surface area of the Co 2p_{3/2} area with an asymmetric fit shows Co metal (61 %) and cobalt oxide (39 %).

catalyst species, HAADF-STEM analysis combined with EDX elemental mapping was performed. Also, high resolution HAADF-STEM with EELS was performed to gain insight into the close environment of the cobalt nanoparticles, consisting out of the interface of the support matrix (carbon and SiO₂), the cobalt nanoparticles and the nitrogen environment (Figure 9a-d). PDF and PXRD studies validate the results and reveal the active species to be crystalline Co fcc structured nanoparticles with a maximum particle size of 3.1 nm (Figure 9e).

With the optimal reaction conditions and catalyst characterization in hand, a substrate scope in the hydrogenation of various N-, O- and S-heterocycles was established (Figure 10). First, several quinoline derivatives were used in the hydrogenation to the corresponding 1,2,3,4-tetrahydroquinolines (Figure 10a). To our delight, fifteen quinoline derivatives were selectively hydrogenated under very mild conditions (5.0 mol% Co, 2.0 MPa H₂, 70 °C, 20 h). Five examples led to an extraordinary yield of 99 % THQ. We were able to show that the nature and position of the substituent is individually eligible. Both, electron-donating methyl substituents and electron-withdrawing halogen substituents have been introduced. Moreover, methoxy, hydroxy, and amine groups can be tolerated. Two functional groups can also be tolerated by our catalyst. Some of the synthesized products above are used as precursors for drug molecules, more specifically, for the synthesis of 5-HT₃ receptor antagonists, anti-trypanosome drugs, and

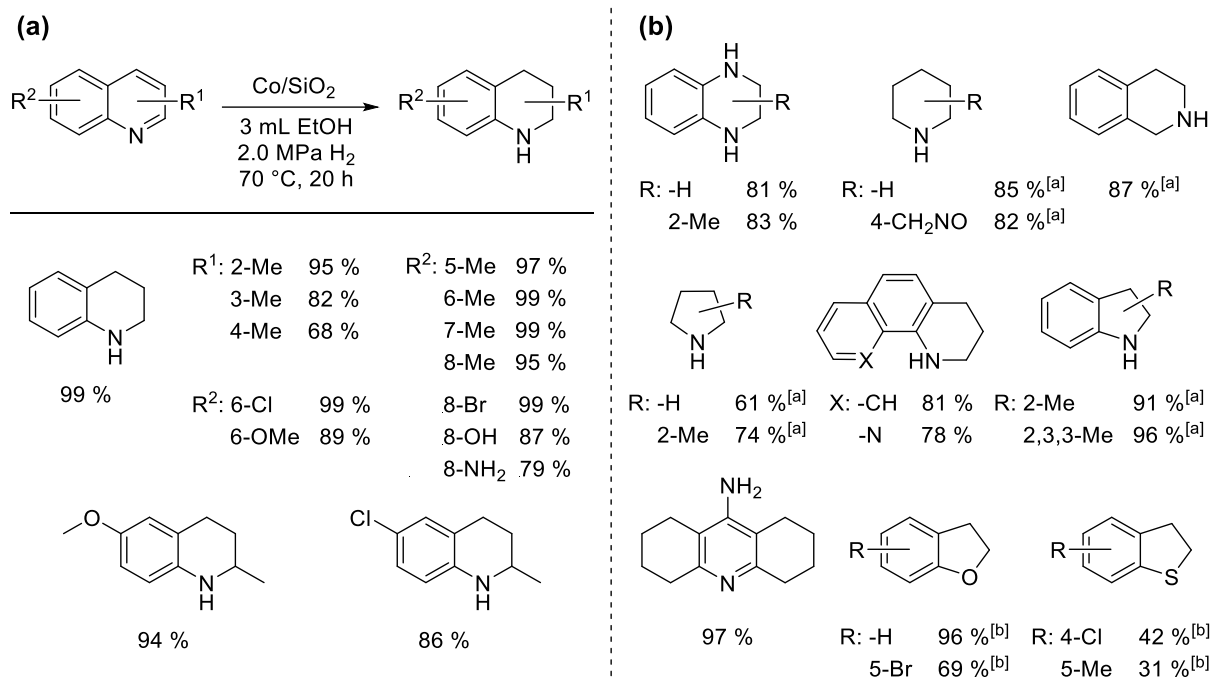


Figure 10: (a) Hydrogenation of quinolines to the corresponding THQs. (b) Products of the hydrogenation of different N-, O- and S-heterocycles. Reaction conditions for (a) and (b): 5.0mol% Co (1.81 wt% Co, 0.01 mmol Co, 0.59 mg Co), 0.2 mmol substrate, 3 mL ethanol, 70 °C, 2.0 MPa H₂, 20 h. [a] 10 mol% Co, 120 °C, 5.0 MPa H₂. [b] 100 °C, 3.0 MPa H₂. [c] 15 mol% Co, 150 °C, 6.0 MPa H₂, 48 h. Isolated yields are given.

tubulin polymerization inhibitors. After the successful hydrogenation of quinoline derivatives, we tried different types of heterocycles (Figure 10b). Here we were able to convert several classes of compounds into the corresponding selectively hydrogenated ones. For example, 2-methyl-1,2,3,4-tetrahydroquinoxaline was obtained for the first time with a nanostructured cobalt catalyst. Simple five- and six-membered N-heterocycles with substituents were also generally applicable. This required a slight increase in the reaction conditions. Of all the products, isonicotinamide stands out as a reversible organic hydrogen storage liquid for potential hydrogen-powered fuel cells in mobile applications, and its hydrogenation is of great interest. In addition, hydrogenation of indoles was possible. Indolines and their scaffold are known as important pharmaceuticals and agrochemicals, and it is particularly useful to have selective and easy access to this class of compounds. Besides that, larger heterocycles such as acridine and phenanthroline-like molecules can be introduced in our protocol. More challenging is the selective hydrogenation of O- and S-heterocycles, where we need to raise the conditions for each class to harsher conditions. Since the associated products are important bioactive compounds, a way to make the hydrogenation mild and smooth is of great importance. With the Co/SiO₂ catalyst we were able to do this with two different benzofurans and two different benzothiophenes. It should be noted that the yield for the sulfur-containing substrates is only moderate. This is due to the strong binding of sulfur to the active metal sites of our catalyst which poisons the catalyst. Therefore, the research so far has focused only on the pure benzothiophene and not on some other derivatives. Here we were able to extend the state of the art to a broader range. To demonstrate the reusability of the Co/SiO₂ catalyst, five consecutive hydrogenation reactions of quinoline to THQ were performed and showed no loss of activity (see Chapter 4). TEM measurements show no agglomeration or growth of nanoparticles in the used catalyst. A particle diameter of 6.2 nm was observed, which is in good agreement with the diameter of the freshly prepared catalyst (see Chapter 4). A hot filtration test was performed to demonstrate that no active homogeneous species are formed during catalysis. No active sites are leached from the catalyst. The leaching of the cobalt catalyst was determined by ICP-OES and was found to be 0.7 % and is attributable to measurement inaccuracies (see Chapter 4). The efficiency and practicality of the Co/SiO₂ catalyst was demonstrated in an upscaling experiment with an overall THQ yield of 90 % (see Chapter 4).

Encouraged by the excellent results in the selective hydrogenation of N-heterocycles, a new catalytic pathway for the direct synthesis of hydroquinolines from nitroaldehydes and ketones was developed with a new nickel-based catalyst system. As mentioned in Chapter 2.4, several N-heterocycles and selectively hydrogenated N-heterocycles are used in a wide range of drug

molecules or as precursors. In particular, hydroquinolines play an important role in this scenario and the most common way is to selectively hydrogenate the unsaturated compounds. However, there is a problem of quinoline substrate synthesis, which can be easily solved by the attractive *Friedländer* synthesis. For this purpose, there is a huge demand for a large number of 2-aminoaldehydes, and their preparation is not very convenient. This problem can be solved by the Ni/N-SiC catalyst presented in this work, which combines the attractive 2-aminoaldehyde synthesis starting from 2-nitrobenzaldehyde with the subsequent *Friedländer* reaction followed by hydrogenation to hydroquinolines. The key in this work is the reusability and high selectivity and activity of the Ni/N-SiC catalyst to allow different reaction conditions for each reaction.

First, the catalyst support N-SiC (a porous N-doped amorphous SiC) was prepared according to previously published procedures based on the crosslinking of the commercial polycarbosilane precursor SMP-10 and acrylonitrile using AIBN as initiator. The resulting greenbody was pyrolyzed at 1000 °C under nitrogen atmosphere and the Si-rich phase was partly removed by base treatment (see Chapter 2.3). By wet impregnation of N-SiC with $\text{Ni}(\text{NO}_3)_2 \cdot 6 \text{H}_2\text{O}$ in water, followed by pyrolysis at 700 °C (N_2 flow), and reduction at 550 °C (H_2/N_2 flow) after evaporation of the solvent at 105 °C, active nickel nanoparticles are obtained on the support surface (Figure 11a-b). SEM-EDX analysis verified a homogeneous distribution of nickel, nitrogen, carbon and silicon throughout the material and confirmed a smooth wet impregnation process with no inadvertent elemental contamination (see Chapter 5). HAADF-STEM imaging shows a homogeneous distribution of nanoparticles with an average diameter of 8.5 nm. The presence of nickel nanoparticles embedded in a N-doped SiC matrix on the support was confirmed using EDX element maps (Figure 11c-d). In addition, the EDX mapping for the HAADF-STEM images of nitrogen, carbon and silicon can be seen in Figure 12a-c. This gives a direct insight into the environment of the particles and the interface of the support matrix

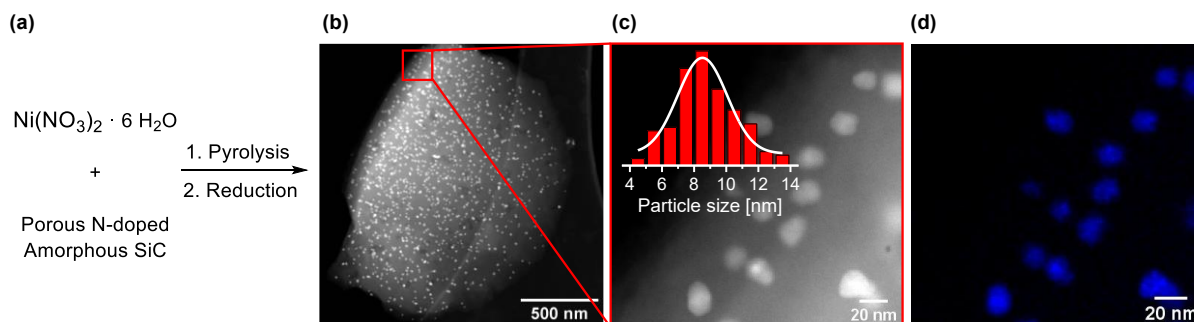


Figure 11: (a) Synthesis of Ni/N-SiC catalyst by wet impregnation of N-SiC and nickel nitrate hexahydrate in aqueous solution followed by pyrolysis and reduction to nickel nanoparticles. (b) HAADF-STEM analysis of the catalyst. (c) Enlargement of the HAADF-STEM image and the corresponding particle distribution centered around 8.5 nm. (d) EDX elemental map of nickel from the HAADF-STEM image in (c).

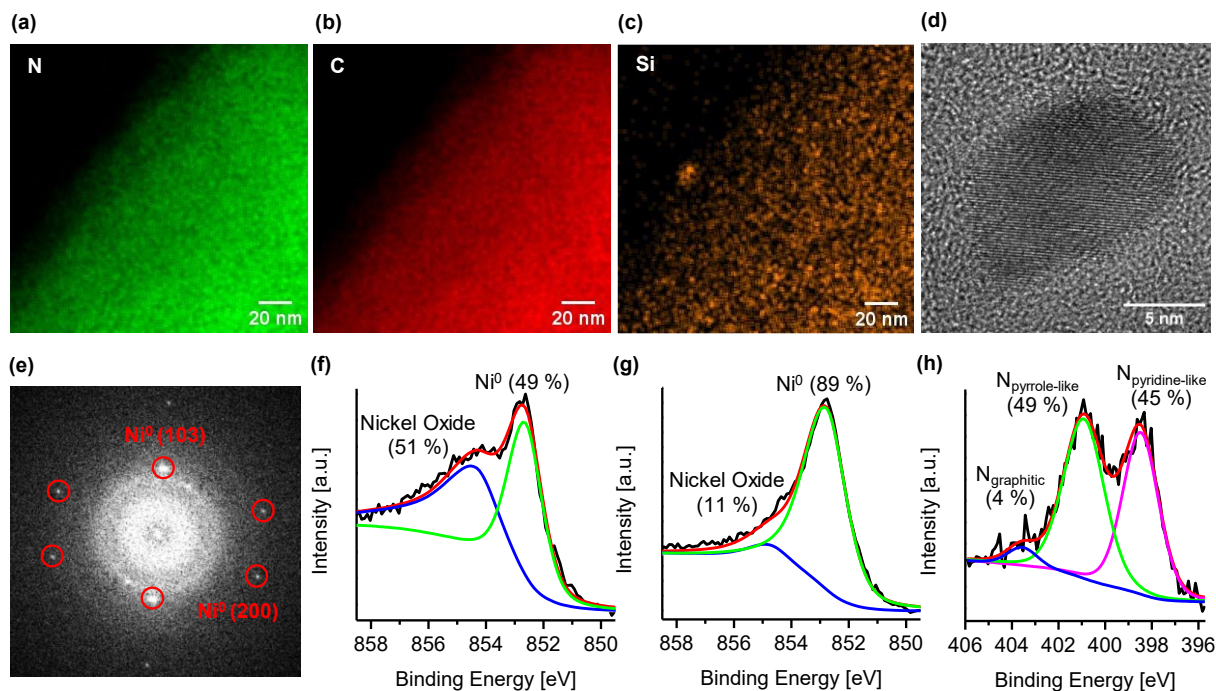


Figure 12: (a)-(c) HAADF-STEM images of Ni/N-SiC with representative EDX element maps for nitrogen (a), carbon (b) and silicon (c). (d) HR-TEM images of a nickel nanoparticle with visible lattice spacings. (e) FFT of the nanoparticle shown in (d). Examination of the diffraction spots revealed two Miller planes (200 and 103) consistent with cubic nickel. (f) XPS analysis of the Ni 2p_{3/2} region with an asymmetric fit before platinum sputtering shows a nickel oxide coating on the cubic nickel nanoparticles. (g) XPS analysis after platinum sputtering shows the degradation of the oxide coating on Ni⁰ nanoparticles. (h) Analysis of the nitrogen region suggests different nitrogen binding models within the catalyst.

and the nickel nanoparticles. The carbon and silicon as well as nitrogen are connected to the nickel nanoparticles and the particles are embedded in an N/C environment. Besides that, HR-TEM combined with EELS with a line scan over a nickel nanoparticle, and placing the Ni(L₃) edge in relation to the Ni(L₂) edge, confirms the presence of Ni⁰. No oxygen edge was detected and therefore, metallic nickel nanoparticles on the N-SiC support are the active catalyst species (see Chapter 5). Moreover, an FFT of a single nanoparticle was performed and one can see the diffraction spots of two Miller planes consistent with cubic nickel (Figure 12d-e). XPS analysis also confirms the presence of nickel oxide on the surface. After sputtering with Pt, the amount of nickel oxide decreases. This indicates that the Ni nanoparticles are surrounded by a very thin layer of nickel oxide on top of the surface (Figure 12f-h). Detailed XPS analysis of the nitrogen region suggests three different bonding modes characteristic of the N-SiC support. In addition, PXRD of the Ni/N-SiC catalyst was performed to gain further insight into the catalytic species. It shows cubic nickel reflections as well as orthorhombic graphite for the support material. The active sites can be assigned to a Ni fcc phase (see Chapter 5). Argon physisorption experiments revealed the surface properties of the catalyst with a slight decrease in surface area from

580 m²/g to 563 m²/g from the N-SiC support to the catalyst. The pore size distribution was calculated by DFT. The pores are in the range of micropores (see Chapter 5). ICP-OES investigations verify the nickel content of 4.0 wt% on the catalyst material. Further, CHN analysis validates the composition of the catalyst material with 83.3 % C, 5.7 % N and 7.0 % Si in addition to Ni (see Chapter 5).

To determine optimal reaction conditions, several parameters were screened in the benchmark reaction of 2-nitrobenzaldehyde with acetophenone to obtain 2-phenyl-1,2,3,4-tetrahydroquinoline (see Chapter 5). Since this is a sequential one-pot reaction, each parameter must be optimized throughout the synthesis. Therefore, the synthesis is divided into three steps. Step A is the selective hydrogenation of 2-nitrobenzaldehyde to 2-aminobenzaldehyde with Ni/N-SiC catalyst. Step B is the *Friedländer* synthesis catalyzed by a catalytic amount of LiOH and step C is the subsequent hydrogenation of the formed quinoline to the corresponding THQ using the Ni/N-SiC catalyst from step A. Overall, the direct synthesis of hydroquinolines is carried out under the following conditions. For step A, 4.0 mol% Ni is used with 0.5 mmol nitrobenzaldehyde, 0.5 mmol ketone, 3 mL ethanol, and 3.0 MPa H₂ pressure for 20 h at 40 °C reaction temperature. Immediately thereafter, step B follows with the addition of 0.6 eq LiOH and 20 h reaction time to obtain the quinoline. Step C is then performed by applying 5.0 MPa H₂ pressure at 120 °C for 48 hours. In the entire reaction sequence, step C is the most challenging step of the process and is the limiting factor for the yield. In the benchmark synthesis, a maximum yield of 91 % 2-phenyl-1,2,3,4-tetrahydroquinoline is obtained.

To demonstrate the versatility and effectiveness of the synthesis protocol, a wide range of substrates was established using the optimal reaction conditions. First, we investigated the introduction of several different aldehyde derivatives into the synthesis protocol (Figure 13a). In total, 16 substrates were synthesized. To our delight, several electron-donating substituents in each position, such as methyl, are obtained in very high yields. This is an indication that the nature and position of the substituents in the catalytic process can be highly variable. In addition, electron-withdrawing substituents can be introduced easily. For example, it is possible to address each substituent position with a chlorine group and even the more demanding bromine group in very good yields. Further halogen substitutions with a fluorine group and a sterically demanding CF₃ group are obtained in excellent yields. The introduction of a methoxy group as well as a bifunctional substrate bearing a bromine and a fluorine group is possible. It is noteworthy that the difficulty of introducing halogen substituents due to the harsh conditions in step C and thus dehalogenation during the synthesis is little or not observed. After the variation of the aldehyde side, we investigated the variation of the ketone substrates in the

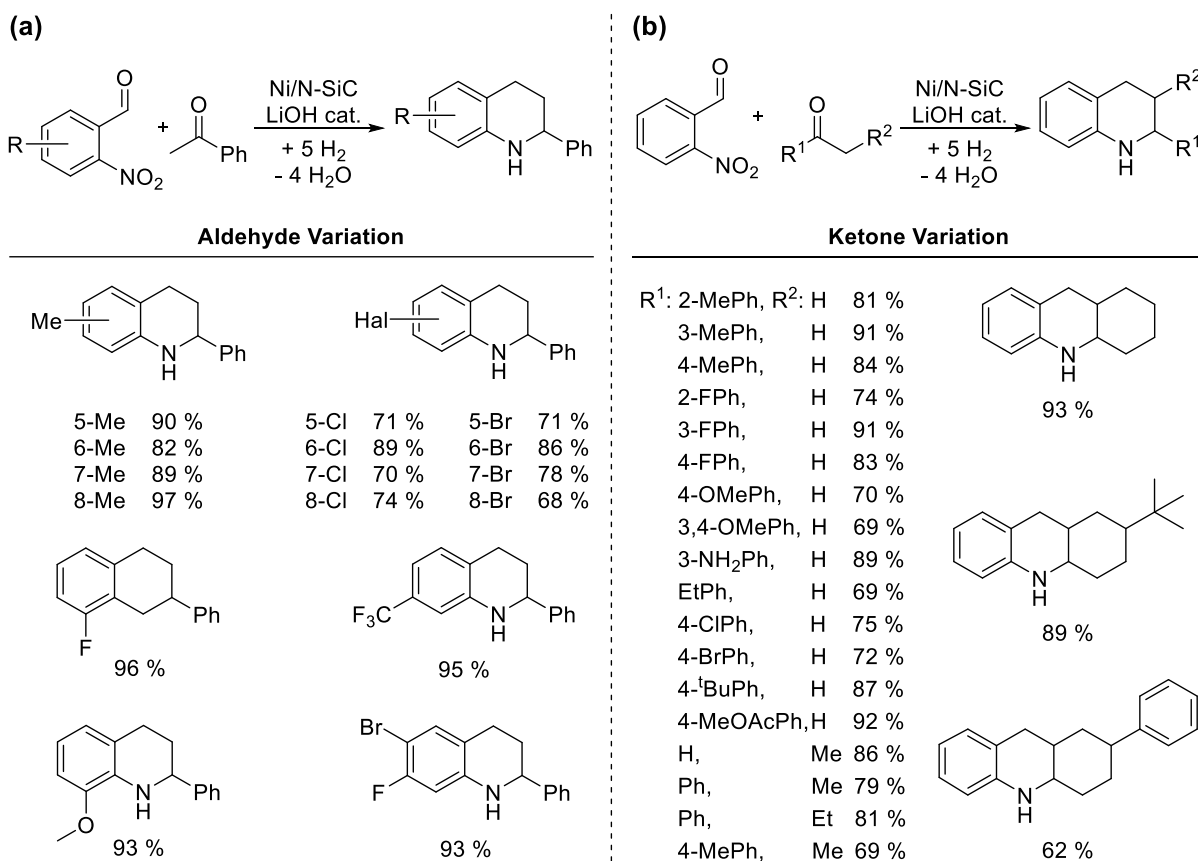


Figure 13: Substrate scope of the direct synthesis of hydroquinolines. (a) Variation of the aldehyde educts. (b) Variation of the ketone educts. Reaction conditions for (a) and (b): Step A: 29.3 mg Ni/N-SiC catalyst (4 mol% Ni, 0.02 mmol Ni, 1.17 mg Ni), 0.5 mmol aldehyde, 0.5 mmol ketone, 3 mL ethanol, 3.0 MPa H₂, 40 °C, 20 h. Step B: Addition of 0.3 mmol LiOH. Then 60 °C, 20 h. Step C: 5.0 MPa H₂, 120 °C, 48 h. Isolated yields are given.

synthesis concept (Figure 13b). In summary, 21 different substrates have been synthesized with good to excellent yields using different ketones. The introduction of electron-donating methyl groups to the 2-phenyl group attached to the THQ in *para*-, *meta*- and *ortho*-position is shown. Moreover, electron-withdrawing groups on the acetophenone motif such as halogen substituents have been introduced. Fluorine groups can be tolerated at any substituent position in good to very good yields. It should be noted that there is a decrease in yield in the 2-position in the phenyl ring due to steric hindrance. Many more halogen substituents such as chlorine and even bromine, besides the harsh conditions in step C, led to product formation and not to the dehalogenated products. More sterically demanding groups such as *tert*-butyl or acetate can also be tolerated in excellent yields. In addition, substrates with methoxy, dimethoxy, and amine groups are synthesized. Overall, it can be suggested that a higher electron withdrawal is better for the overall catalytic performance. Also, more aliphatic compounds, more sophisticated compounds, and the introduction of substituents only at the 3-position of the quinoline using

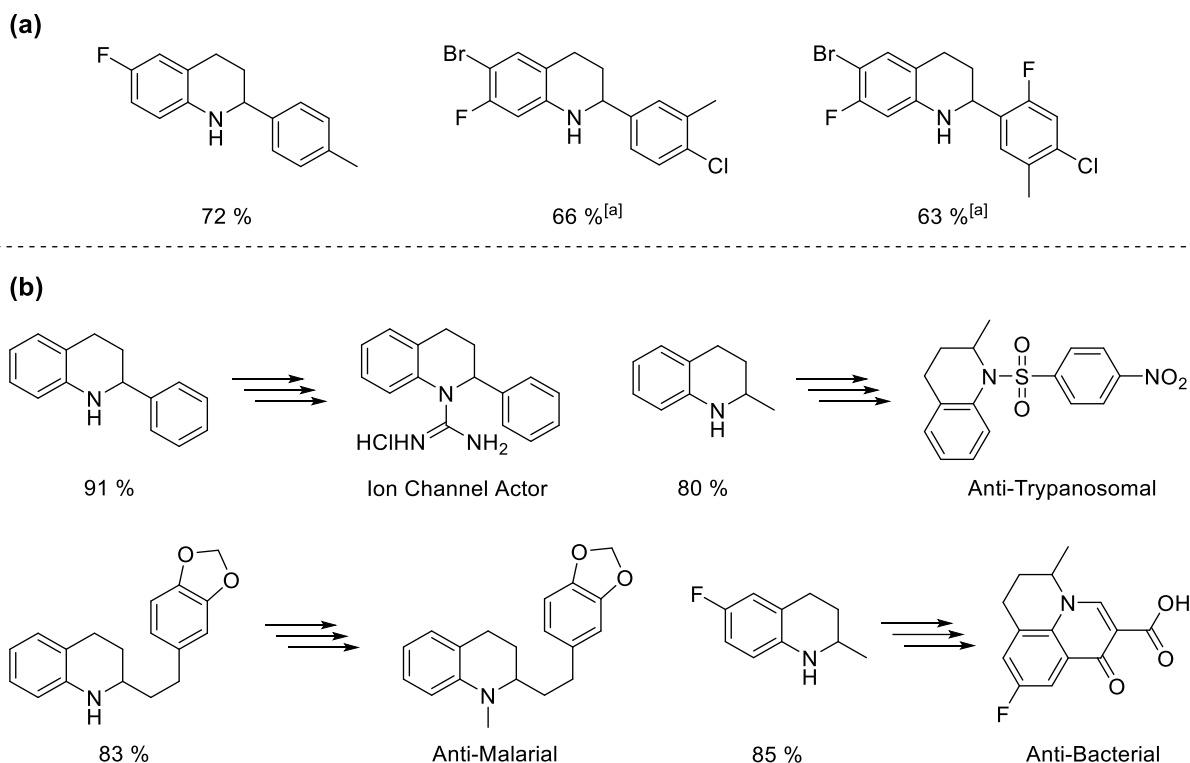


Figure 14: (a) Substrate scope of highly functionalized THQs varying both aldehyde and ketone sides. (b) Application of synthesized THQs as precursor molecules for the synthesis of bioactive molecules. Reaction conditions for (a) and (b): Step A: 29.3 mg Ni/N-SiC catalyst (4 mol% Ni, 0.02 mmol Ni, 1.17 mg Ni), 0.5 mmol aldehyde, 0.5 mmol ketone, 3 mL ethanol, 3.0 MPa H₂, 40 °C, 20 h. Step B: Addition of 0.3 mmol LiOH. Then 60 °C, 20 h. Step C: 5.0 MPa H₂, 120 °C, 48 h. [a] Step B: 1.5 mmol LiOH. Isolated yields are given.

two aldehydes as well as simultaneously at the 2- and 3-positions, varying the ketone substituents, show the versatility and independent approach of the synthesis protocol. To proceed, we have synthesized products where we can vary both sides, aldehyde and ketone, to obtain highly functionalized products. Both electron-withdrawing and electron-donating groups are tolerated at the same time, making the products very interesting for further organic chemistry (Figure 14a). To demonstrate the applicability of the catalyst and the applications of our synthesized products, we synthesized several precursor molecules for the synthesis of bioactive molecules which are used as drug molecules and pharmacologically active compounds (Figure 14b). Furthermore, the synthesis protocol is upscaled easily and the catalyst is reusable (see Chapter 5). After catalysis, no agglomeration of the nanoparticles was observed in TEM images, and no homogeneous catalytically active species is formed during catalysis. No irreversible leaching was observed (see Chapter 5).

As a result of the work to obtain THQs in the above work, the question of how to synthesize primary, secondary, and tertiary alkyl amines arose. Since amines represent a significant class

of compounds, and the synthesis of differently substituted primary, secondary, and tertiary alkyl amines is inherently challenging, a synthesis approach was developed to facilitate the production of these alkyl amines from ammonia, alcohols, aldehydes, ketones, and hydrogen. The approach to the synthesis of amines was pursued following the interesting concept of combining reductive amination (Chapter 2.5.1) and BH/HA (Chapter 2.5.2). The *Kempe* group has made significant contributions to the field of reductive amination, publishing several noteworthy studies on the use of heterogeneous 3d metal catalysts. Additionally, *Kempe* and co-workers have conducted pioneering research on homogeneous 3d metal catalysts for the BH/HA concept. The key to combining both concepts at once is a heterogeneous, nanostructured, bimetallic Co/Sc catalyst capable of mediating both reactions or concepts simultaneously with optimal efficiency.

The synthesis of the catalyst support based on the crosslinking of the polycarbosilane precursor SMP-10 with acrylonitrile using AIBN, followed by pyrolysis and base treatment (see also Chapter 2.3), follows the synthesis of N-SiC described in the work above. The metal nanoparticles were prepared by wet impregnation of the N-SiC support and the two metal salts $\text{Co}(\text{NO}_3)_2 \cdot 6 \text{H}_2\text{O}$ and $\text{Sc}(\text{NO}_3)_3 \cdot 5 \text{H}_2\text{O}$ in water, pyrolysis (700 °C, N_2) and subsequent

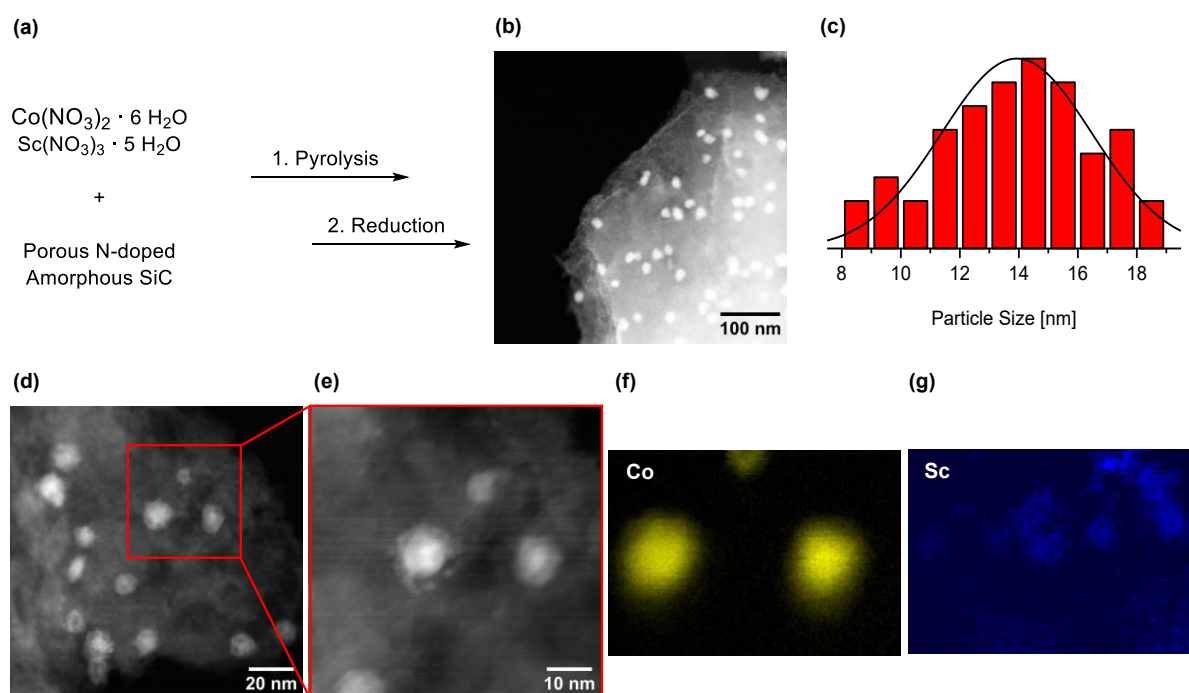


Figure 15: Synthesis and characterization of the CoSc catalyst. (a) Synthesis of the catalyst via wet impregnation, pyrolysis and reduction. (b) HAADF-STEM overview image of the CoSc/N-SiC catalyst. (c) Particle size distribution with a mean particle diameter of 13.9 nm. (d) HAADF-STEM analysis of catalyst nanoparticles and (e) high-resolution image. (f)-(g) STEM-EELS analysis shows that the nanoparticles consist of cobalt and that there is a significant size difference with respect to the scandium particles, the latter being significantly smaller and finely dispersed on the support material.

reduction at 550 °C under forming gas (Figure 15a-b). Several analytical techniques were used to characterize the CoSc/N-SiC catalyst and its active sites. The ICP-OES measurement shows no significant deviation from the theoretical metal content of 2.0 wt% Co and 2.0 wt% Sc (see Chapter 6). HAADF-STEM analysis revealed the presence of homogeneously distributed cobalt nanoparticles with an average particle size of 13.9 nm (Figure 15b-c). In combination with EELS (Figure 15d-g) STEM analysis shows that the scandium particles are orders of magnitude smaller than the cobalt particles, with the former being finely dispersed on the N-SiC support. SEM-EDX also confirmed the homogeneous distribution of cobalt nanoparticles and showed that the remaining silicon, which was not removed from the support material, is distributed in the same way as the scandium particles (see Chapter 6). To further investigate the nature of the catalyst, XPS measurements were performed. Figure 16a shows a wide scan with the expected signals for both the support material (Si 2p, N 1s, C 1s, O 1s) and the supported catalyst particles (Si 2p, C 1s, O 1s, Sc 2p, Co 2p), as well as carbon and oxygen impurities. Additional ghost signals, originating from Ga L α radiation and shifted by 155.7 eV are marked with an asterisk. Figure 16b shows the Co 2p_{3/2} region. As expected, no support signals are visible. For the CoSc catalyst there is a broad signal at 780 eV. Two binding energies at 780.6 eV and 786.4 eV for

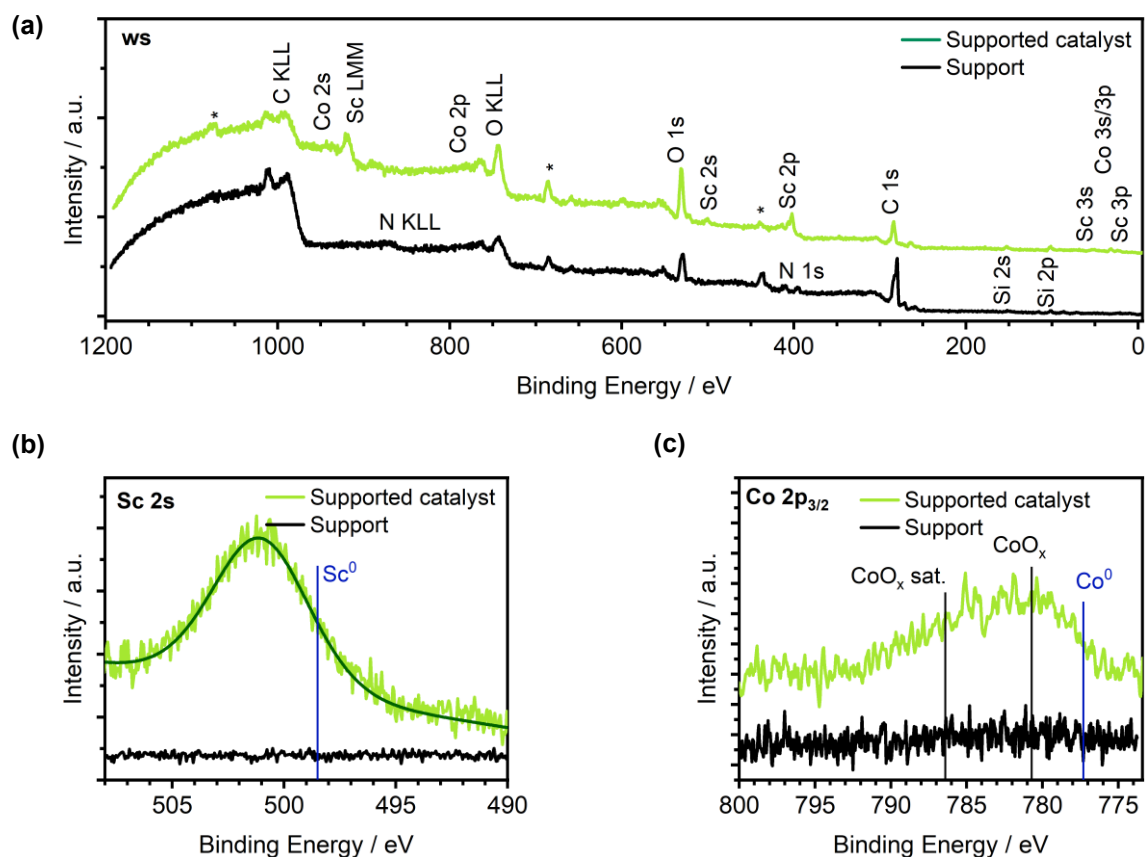


Figure 16: XPS spectra of the CoSc/N-SiC catalyst. (a) Wide scan with ghost peaks from Ga L α excitation (*). (b) Detailed Co 2p region. (c) Detailed Sc 2s region.

the Co oxides and their shake-ups are shown. The splitting is characteristic for Co_2O_3 and/or $\text{Co}(\text{OH})_2$. In addition, a third energy of 777.3 eV is given for metallic Co. The observed binding energies suggest that the surface Co is oxidized. Figure 16c shows the Sc 2s region. A single species with a binding energy of 501.1 eV is found, indicating oxidized Sc considering the literature binding energy for metallic Sc of 499 eV. Comparing the corrected signal areas of the Co 2p and Sc 2s regions, the amount of Sc detected by XPS is 10 times higher than that of Co (9.6:1.3 at%, Sc:Co), although the same concentration would be expected from the ICP-OES results. Based on the high surface sensitivity of XPS and additional information from microscopy, it can be concluded that Sc is finely dispersed on the outer layer, while Co is present as or within larger particles. This suggests that the close proximity of the Co and Sc oxide centers is advantageous for the combination of (de)hydrogenation and condensation steps required in both catalytic reactions - reductive amination and BH/HA.

The BH/HA reaction of benzyl alcohol with gaseous ammonia was used to determine the optimal reaction conditions for the CoSc/N-SiC catalyst (see Chapter 6). Solvent screening revealed toluene as the most suitable solvent with a perfect volume of 2.0 mL for maximum yield of benzyl amine. Potassium hydroxide in equimolar amounts, a temperature of 160 °C and 2.0 MPa ammonia pressure were found to be optimal. For a better comparison of catalyst activities, a variation of rare earth metals has been performed (see Chapter 6). The smaller the rare earth metal used, the higher the selectivity of the catalyst. This resulted in Sc being the most active. Neither Co nor Sc as a monometallic catalyst could provide the outstanding activity of the bimetallic CoSc/N-SiC catalyst. Varying the support material resulted in activated carbon showing only moderate activity, while $\gamma\text{-Al}_2\text{O}_3$, TiO_2 and SiO_2 showed little to no benzyl alcohol conversion. Pure N-SiC showed no activity at all.

To demonstrate the applicability of the CoSc/N-SiC catalyst, a broad range of substrates was synthesized. For clarity, the substrate scope is divided into three parts, one each for primary, secondary, and tertiary amines. First, 13 primary amines were synthesized (Figure 17). Once the aromatic ring of the benzyl alcohol derivative has been substituted, the reaction temperature must be raised from 160 °C to 180 °C. This allowed for multiple electron-donating substituents in different ring positions as well as electron-withdrawing substituents. Unfortunately, when the CF_3 group is in the *ortho*-position, there is too much steric hindrance for the reaction to proceed. Due to side reactions, NO_2 , CN , and CONR_2 groups were not tolerated. A second amine function within the alcohol was not a problem. The catalyst can be used to synthesize two fully aliphatic amines from ketones by reductive amination. Biologically active molecules can also be introduced into the reaction sequence. As can be seen, the bimetallic catalyst could

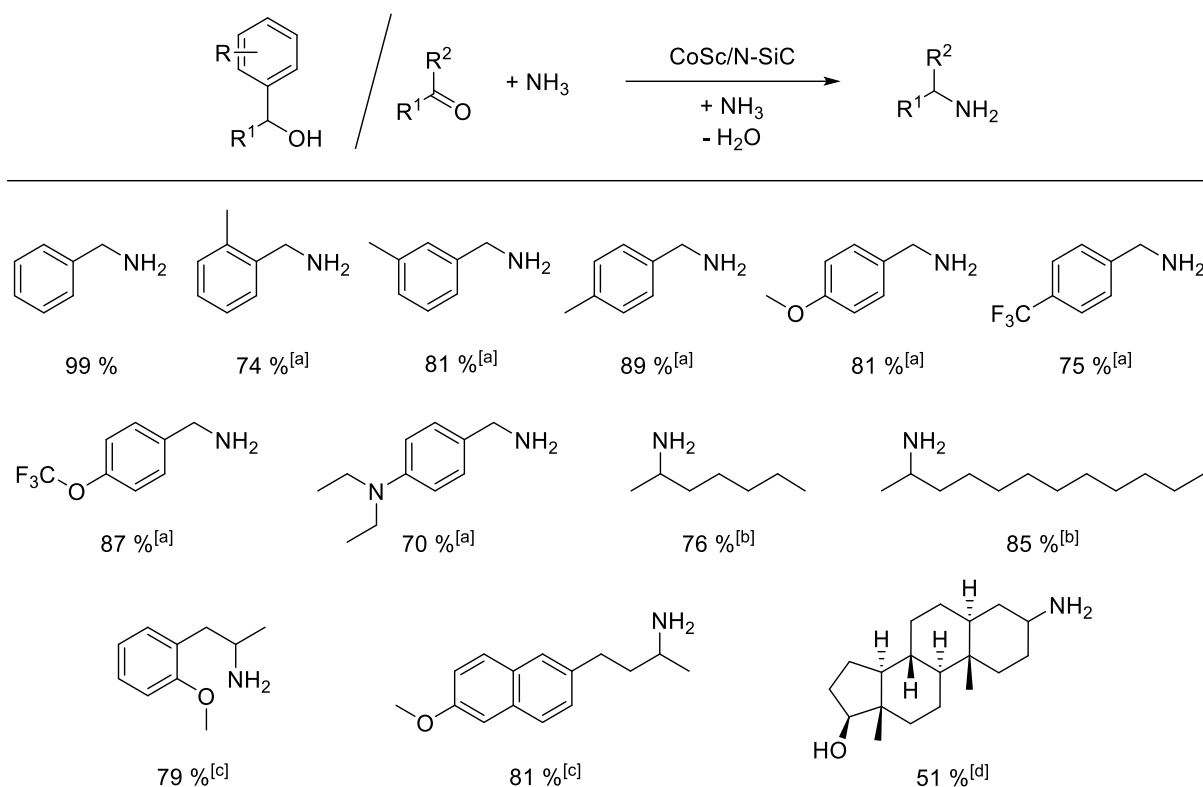


Figure 17: Synthesis of primary amines using CoSc/N-SiC catalyst. Reaction condition: 28.8 mg CoSc/N-SiC catalyst (2.0 wt% Co, 1.5 mol% Co, 0.01 mmol Co, 0.58 mg Co, 2.0 wt% Sc, 0.49 mol% Sc, 0.013 mmol Sc, 0.58 mg Sc), 0.5 mmol alcohol, 2.0 mL toluene, 0.5 mmol KOH, 2.0 MPa NH₃, 160 °C, 44 h. [a] 180 °C. [b] 0.5 mmol ketone, 3.5 mL aq. NH₃-32 %, 1.0 MPa H₂, 50 °C, 20 h. [c] 0.5 mmol ketone, 3.5 mL aq. NH₃-32 %, 1.5 MPa H₂, 60 °C, 20 h. [d] 0.25 mmol ketone, 0.3 mL ethanol, 3.2 mL aq. NH₃-32 %, 1.5 MPa H₂, 65 °C, 20 h. Isolated yields of the converted hydrochloride salts are given.

also mediate the reductive amination of these ketones with aqueous ammonia. The next step was to explore the substrate scope of secondary amines (Figure 18). We have already shown that the catalyst can enable reductive amination of carbonyl compounds. Therefore, we combined this with the BH/HA concept as a sequential reaction to produce more complex amine structures. The same catalyst is reused for the second step, and in addition to neutralization, 0.8 mmol of carbonyl compound is added. The reductive amination part is then carried out at 100 °C and 4.0 MPa H₂ pressure. These conditions allow the synthesis of short, medium, and long aliphatic moieties. Terminal hydroxy groups on the carbonyl compound were not a problem for the catalyst nor were double branched or alicyclic ketones. The combination of an aliphatic moiety with a terminal aromatic ring is possible as is the use of acetophenone and its fluorine-substituted derivative in the reductive amination step. It must be said that the difficulty of introducing halide substituted educts in the BH/HA step due to dehalogenation under these harsh conditions is not a problem. The variation of the benzyl alcohol side of the amine is associated with an increase in temperature to 180 °C and a methyl group in all ring positions as

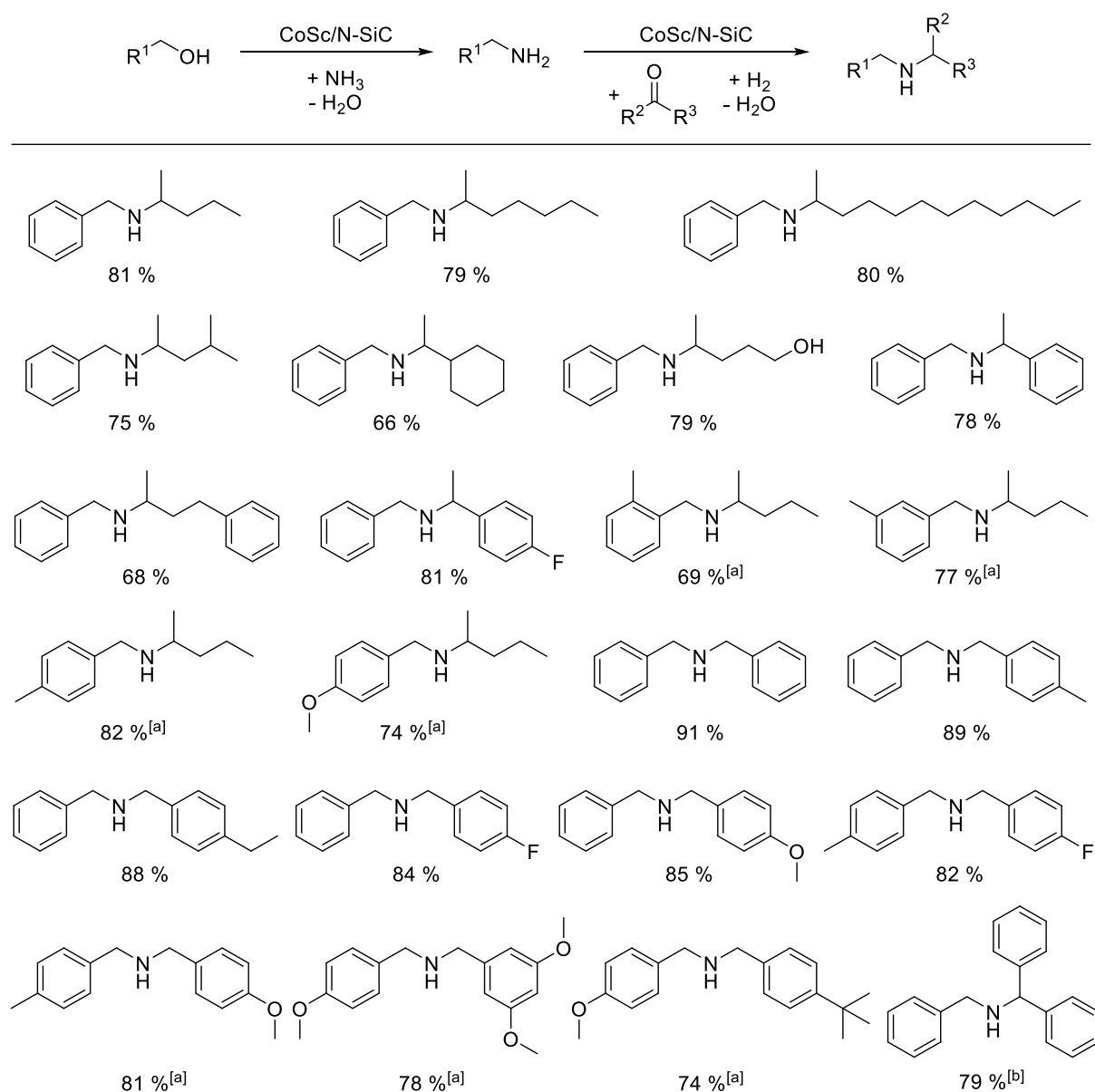


Figure 18: One pot synthesis of secondary amines using CoSc/N-SiC catalyst. Reaction conditions for the first step: 28.8 mg CoSc/N-SiC catalyst (2.0 wt% Co, 1.5 mol% Co, 0.01 mmol Co, 0.58 mg Co, 2.0 wt% Sc, 0.49 mol% Sc, 0.013 mmol Sc, 0.58 mg Sc), 0.5 mmol alcohol, 2.0 mL toluene, 0.5 mmol KOH, 2.0 MPa NH₃, 160 °C, 44 h. [a] 180 °C. Reaction conditions for the second step: 28.8 mg CoSc/N-SiC catalyst (2.0 wt% Co, 1.5 mol% Co, 0.01 mmol Co, 0.58 mg Co, 2.0 wt% Sc, 0.49 mol% Sc, 0.013 mmol Sc, 0.58 mg Sc), 0.8 mmol carbonyl compound, 2.0 mL toluene, 0.05 mL 32 % HCl, 4.0 MPa H₂, 100 °C, 20 h. [b] 150 °C. Isolated yields of the converted hydrochloride salts are given.

well as a methoxy group is tolerated. Switching the carbonyl compound of the reductive amination step from ketones to aldehydes, dibenzyl amine derivatives with electron-withdrawing and electron-donating substituents, and variations on both sides are tolerated. Even benzophenone as an educt is tolerated by raising the temperature to 150 °C in the second step. The biggest challenge was the synthesis of tertiary amines (Figure 19). For the synthesis of

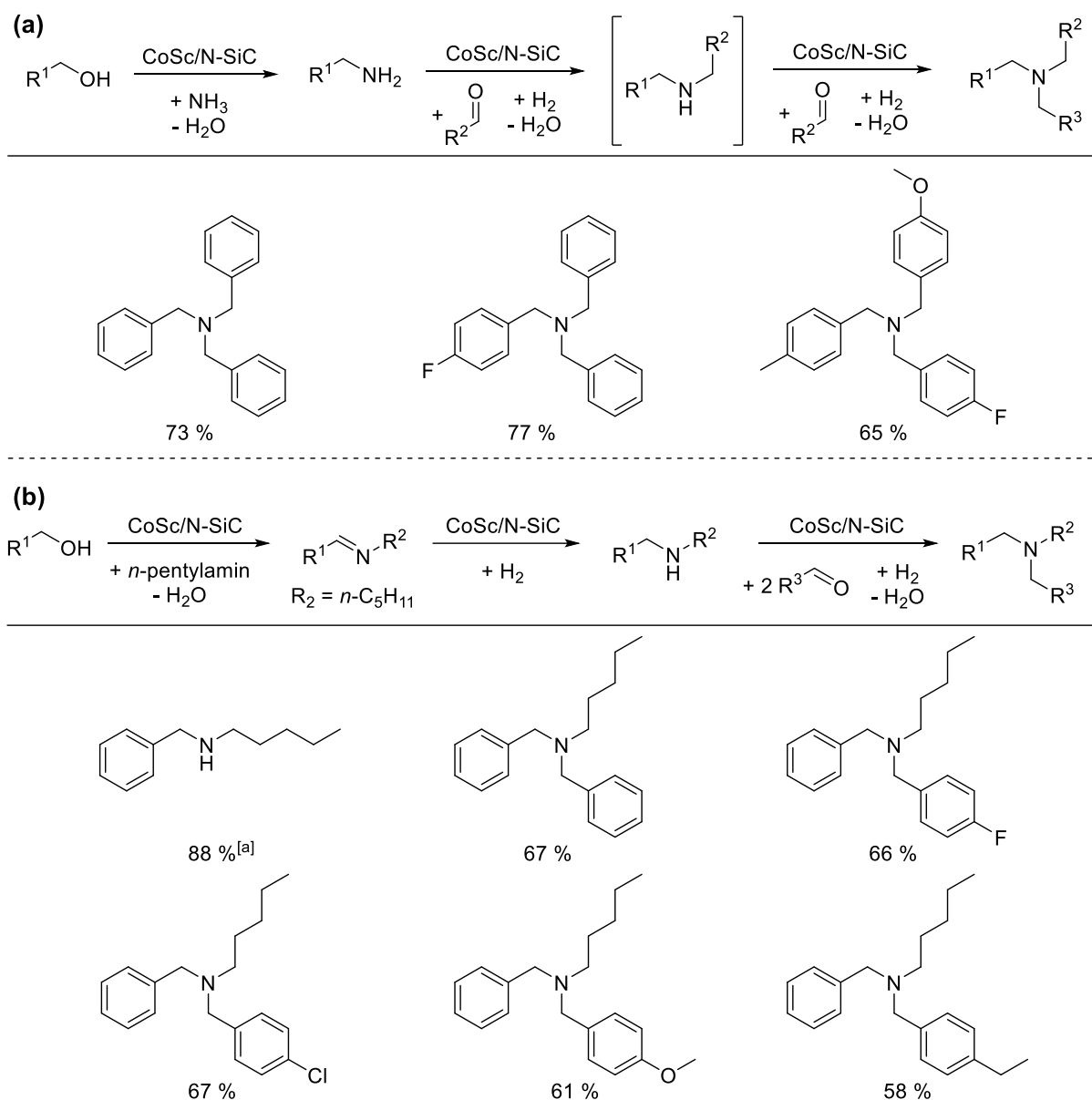


Figure 19: One pot synthesis of tertiary amines using CoSc/N-SiC catalyst. (a) Reaction conditions for the first step: 28.8 mg CoSc/N-SiC catalyst (2.0 wt% Co, 1.5 mol% Co, 0.01 mmol Co, 0.58 mg Co, 2.0 wt% Sc, 0.49 mol% Sc, 0.013 mmol Sc, 0.58 mg Sc), 0.5 mmol alcohol, 2.0 mL toluene, 0.5 mmol KOH, 2.0 MPa NH₃, 160 °C, 44 h. Reaction conditions for the second step: 28.8 mg CoSc/N-SiC catalyst (2.0 wt% Co, 1.5 mol% Co, 0.01 mmol Co, 0.58 mg Co, 2.0 wt% Sc, 0.49 mol% Sc, 0.013 mmol Sc, 0.58 mg Sc), 0.8 mmol aldehyde, 2.0 mL toluene, 0.05 mL 32 % HCl, 4.0 MPa H₂, 100 °C, 20 h. Reaction conditions for the third step: 28.8 mg CoSc/N-SiC catalyst (2.0 wt% Co, 1.5 mol% Co, 0.01 mmol Co, 0.58 mg Co, 2.0 wt% Sc, 0.49 mol% Sc, 0.013 mmol Sc, 0.58 mg Sc), 1.0 mmol aldehyde, 2.0 mL toluene, 0.05 mL 32 % HCl, 4.0 MPa H₂, 140 °C, 20 h. (b) Reaction conditions for the first step: 38.4 mg CoSc/N-SiC, 0.5 mmol alcohol, 0.5 mmol *n*-pentylamine, 2.0 mL toluene, 0.5 mmol KOH, Ar atmosphere, 140 °C, 44 h. Reaction conditions for the second step: 38.4 mg CoSc/N-SiC, 2.0 mL toluene, 4.0 MPa H₂, 100 °C, 20 h. Reaction conditions for the third step: 38.4 mg CoSc/N-SiC, 1.0 mmol aldehyde, 2.0 mL toluene, 0.05 mL 32 % HCl, 2.0 MPa H₂, 150 °C, 20 h. [a] Product isolated after second step. Isolated yields of the converted hydrochloride salts are given.

tertiary amines with three benzylic alkyl substituents, the consecutive synthesis was extended by a third step (Figure 19a). For the synthesis, 1.0 mmol of another aldehyde was added and the temperature was raised to 140 °C. The addition of 0.05 mL of concentrated HCl was necessary to promote the tertiary imine formation of the secondary amine with the aldehyde. The synthesis of three tertiary amines with one, two, and three different moieties is demonstrated. Figure 19b shows a workaround approach for the synthesis of tertiary amines. For the BH/HA step, the gaseous ammonia was replaced with *n*-pentylamine. The catalyst loading was increased to 2.0 mol% Co and the temperature was lowered to 140 °C. Under an argon atmosphere, the catalyst was able to generate the imine but not further hydrogenate it to the corresponding amine. Therefore, an additional hydrogenation step was required to obtain *N*-benzylpentan-1-amine (4.0 MPa H₂ at 100 °C for 20 h). By adding 1.0 mmol of aldehyde and 0.05 mL of concentrated HCl and slightly modifying the reaction conditions (2.0 MPa H₂, 150 °C), five more tertiary amines were isolated. Unfortunately, the synthesis of branched alkyl substituted tertiary alkyl amines derived from a ketone educt failed due to steric hindrance. Despite the reaction protocol itself confirms the reusability of the CoSc/N-SiC catalyst, five more consecutive runs of the first reaction step, the BH/HA reaction with the benchmark substrate benzyl alcohol, were performed without any loss of activity (see Chapter 6). Upscaling the reaction sequence by performing the above reaction with sequential reductive amination to give *N*-benzylpentan-2-amine is not a problem. Using ten times the amount of educts, 76 % yield can be isolated (see Chapter 6). To exclude the formation of homogeneous catalytic active compounds, a hot filtration test was performed. The filtrate showed no activity and no irreversible leaching of the active metal sites was observed (see Chapter 6). In addition, competition experiments for BH/HA and reductive amination were performed to gain more insight into the reaction sequence (see Chapter 6).

3.2 Individual Contributions to Joint Publications

The results published in this thesis were achieved in collaboration with others and are published as indicated below. The contributions of all co-authors to the respective publication is specified. The corresponding author is annotated by an asterisk (*).

Chapter 4

This work is published in *Chem. Eur. J.* **2023**, e202300561 with the title:

A Highly Active Cobalt Catalyst for the General and Selective Hydrogenation of Aromatic Heterocycles

Christof Bauer, Felix Müller, Sercan Keskin, Mirijam Zobel, Rhett Kempe*

I designed the experiments, performed the catalyst synthesis and most of the catalyst characterization. The catalytic reactions and related analyses were carried out by me. Felix Müller and Mirijam Zobel performed the XRD analyses and PDF refinement. Sercan Keskin recorded HAADF-STEM coupled with EDX and EELS measurements. Rhett Kempe and I co-wrote the manuscript and made corrections. Rhett Kempe supervised this work and participated in scientific discussions.

Chapter 5

This work is published in *Chem. Eur. J.* **2025**, e202500462 with the title:

The Synthesis of Hydroquinolines from Nitroaldehydes and Ketones by Hydrogenation Sequences and Condensations

Christof Bauer, Fatemeh Zare, Lisa Nüßlein, Johanna Frank, Maxime Boniface, Thomas Lunkenbein, Rhett Kempe*

I designed the experiments, synthesized the catalyst, and carried out most of the catalyst characterization. Catalytic reactions and associated analytics were carried out by Fatemeh Zare, Lisa Nüßlein and me. Lisa Nüßlein and Johanna Frank performed some preliminary work and catalytic reactions during their bachelor thesis. Maxime Boniface performed together with me the TEM analysis. Thomas Lunkenbein was involved in scientific discussions and evaluation of the TEM analysis. Rhett Kempe and I co-wrote the manuscript and made corrections. Rhett Kempe supervised this work and participated in scientific discussions.

Chapter 6

This work is published in *Adv. Synth. Catal.* **2023**, 365, 4654-4661 with the title:

General Synthesis of Alkyl Amines via Borrowing Hydrogen and Reductive Amination

Matthias Elfinger, Christof Bauer, Jörg Schmauch, Michael Moritz, Christoph Wichmann, Christian Papp, Rhett Kempe*

I revised the manuscript and supporting information, corrected the data and carried out the necessary experiments and catalytic reactions as well as co-wrote the manuscript. Matthias Elfinger carried out the catalyst synthesis, catalytic reactions and parts of the catalyst characterization. Jörg Schmauch performed the STEM-EELS measurements. Michael Moritz measured the XPS samples. Michael Moritz, Christian Papp and Christoph Wichmann performed XPS data analysis and evaluation. Matthias Elfinger and Rhett Kempe co-wrote the manuscript. Rhett Kempe supervised the work and participated in the scientific discussion.

4 A Highly Active Cobalt Catalyst for the General and Selective Hydrogenation of Aromatic Heterocycles

Christof Bauer, Felix Müller, Sercan Keskin, Mirijam Zobel and Rhett Kempe

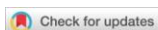
A Highly Active Cobalt Catalyst for the General and Selective Hydrogenation of Aromatic Heterocycles.

Chem. Eur. J. **2023**, e202300561.

Copyright Wiley-VCH GmbH.

Reproduced with permission (<https://creativecommons.org/licenses/by/4.0/>).

DOI: <https://doi.org/10.1002/chem.202300561>



A Highly Active Cobalt Catalyst for the General and Selective Hydrogenation of Aromatic Heterocycles

Christof Bauer,^[a] Felix Müller,^[b] Sercan Keskin,^[c] Mirijam Zobel,^[b] and Rhett Kempe^{*,[a]}

Abstract: Nanostructured earth abundant metal catalysts that mediate important chemical reactions with high efficiency and selectivity are of great interest. This study introduces a synthesis protocol for nanostructured earth abundant metal catalysts. Three components, an inexpensive metal precursor, an easy to synthesize N/C precursor, and a porous support material undergo pyrolysis to give the catalyst material in a simple, single synthesis step. By applying this catalyst synthesis, a highly active cobalt catalyst for the general and

selective hydrogenation of aromatic heterocycles could be generated. The reaction is important with regard to organic synthesis and hydrogen storage. The mild reaction conditions observed for quinolines permit the selective hydrogenation of numerous classes of N-, O- and S-heterocyclic compounds such as: quinoxalines, pyridines, pyrroles, indoles, isoquinoline, acridine amine, phenanthroline, benzofuranes, and benzothiophenes.

Introduction

The reduction of arenes to saturated cyclic compounds is of considerable interest for the production of bulk and fine chemicals as well as the synthesis of pharmaceuticals and agrochemicals.^[1] Hydrogenation is an especially attractive reduction protocol since hydrogen is inexpensive and abundantly available and can be produced sustainably.^[2] Furthermore, arene hydrogenation is an elegant way to store hydrogen chemically. Here, nanostructured and reusable catalysts are especially interesting.^[3] With regard to the selective hydrogenation of N-heterocycles, nanostructured 3d-metal catalysts^[4] and especially cobalt catalysts^[5,6-9] have been developed. Unfortunately, the applicability or scope of nanostructured 3d-metal catalysts for the general and selective hydrogenation of N-, O-, and S-heterocycles is rather limited (see below, section substrate scope). The key here might be novel synthesis

protocols for nanostructured 3d-metal catalysts to permit their operation under mild reaction conditions. We introduce a synthesis protocol for nanostructured earth abundant metal catalysts recently.^[10] Unfortunately, the flexibility with regards to the ratio of the metal species and the N-doped carbon for embedding the metal species (metal-N/C ratio) can only be altered slightly by employing different (salen) ligands. As a consequence, we have been searching for a catalyst synthesis protocol having a high flexibility with regard to the ratio of N-doped carbon to 3d-metal species. Three components, an inexpensive metal precursor, a N/C precursor, and a porous support material undergo pyrolysis to give the catalyst material in a simple single synthesis step. The catalyst synthesis is highly flexible about the earth abundant metal that is used. The metal and the N/C precursors permit an optimization of the metal-N/C ratio to boost catalyst performance. Small and reactive metal nanoparticles embedded in a microporous N-doped carbon matrix are formed during pyrolysis. By applying our catalyst synthesis, a highly active cobalt catalyst for the selective hydrogenation of aromatic N-, O-, and S-heterocycles could be identified.

Results and Discussion

Our catalyst synthesis procedure, with spatially separated nitrogen/carbon and metal precursors and a (mesoporous) support material, is shown in Figure 1a. First, the nitrogen/carbon precursor meso-octamethylcalix[4]pyrrole was synthesized according to an adapted literature procedure (Supporting Information 2.1).^[11] For the catalyst synthesis, silica was impregnated with meso-octamethylcalix[4]pyrrole and the metal precursor cobalt acetate tetrahydrate with a ratio of 4:1 in methanol. After removal of the solvent at 70 °C, the sample was pyrolyzed under a nitrogen atmosphere at 800 °C (Supporting Information 2.2). Thermogravimetric analysis (TGA) shows the

[a] C. Bauer, Prof. Dr. R. Kempe
Inorganic Chemistry II – Catalyst Design
Sustainable Chemistry Centre
University of Bayreuth
95440 Bayreuth (Germany)
E-mail: kempe@uni-bayreuth.de
Homepage: www.sustainable-chemistry-centre.uni-bayreuth.de

[b] F. Müller, Prof. Dr. M. Zobel
Institute of Crystallography
RWTH Aachen University
52066 Aachen (Germany)

[c] Dr. S. Keskin
INM - Leibniz Institute for New Materials
Campus D2.2
66123 Saarbrücken (Germany)

Supporting information for this article is available on the WWW under <https://doi.org/10.1002/chem.202300561>

© 2023 The Authors. Chemistry – A European Journal published by Wiley-VCH GmbH. This is an open access article under the terms of the Creative Commons Attribution License, which permits use, distribution and reproduction in any medium, provided the original work is properly cited.

A Highly Active Cobalt Catalyst for the General and Selective Hydrogenation of Aromatic Heterocycles

Chemistry—A European Journal

Research Article
doi.org/10.1002/chem.202300561

Chemistry
Europe
European Chemical
Societies Publishing

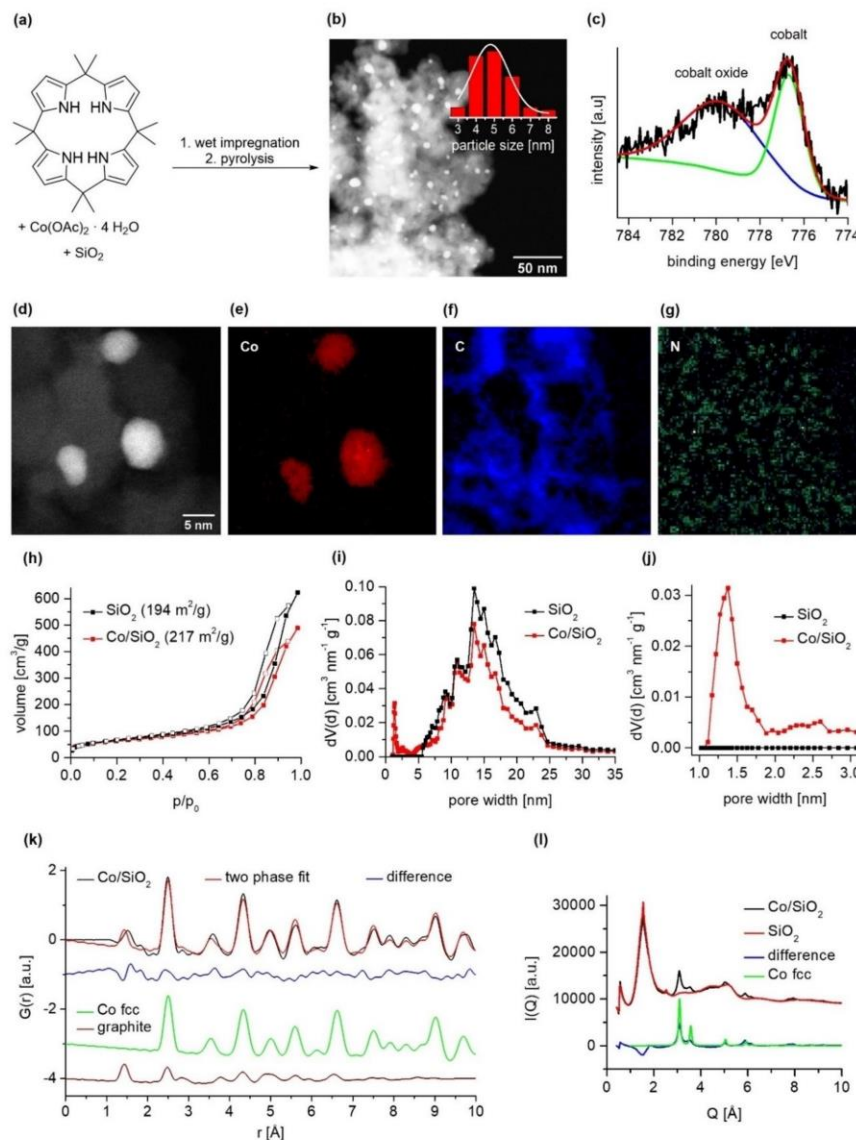


Figure 1. Synthesis and characterization of the Co/SiO₂ catalyst. (a) Synthesis of the cobalt catalyst starting with wet impregnation of meso-octamethylcalix[4]pyrrole and Co(OAc)₂·4 H₂O with SiO₂ and subsequent pyrolysis. (b) HAADF-STEM analysis suggests the presence of homogeneously distributed Co nanoparticles with an average particle size of 4.8 nm. (c) XPS analysis of the surface area of the Co 2p_{3/2} area with an asymmetric fit shows Co metal (61 %) and cobalt oxide (39 %). (d)–(g) HAADF-STEM images of Co/SiO₂ (d), representative EELS element maps of cobalt (e), carbon (f) and nitrogen (g). (h) Surface characterization and (i) pore size distribution of the catalyst via N₂ physisorption measurements (calculation model: N₂ at –196.15 °C: slit/cylindrical pore, NLDFT equilibrium model). The specific surface area showed a slight increase from 194 m²/g of the support material to 217 m²/g of the catalyst. (j) Detailed pore size analysis shows the generation of micropores. (k) The PDF of Co/SiO₂ was fitted with a Co fcc phase of 3.1 nm particle diameter and a graphitic domain, both contributions shown in offset. (l) PXRD data of the catalyst Co/SiO₂ and the support material SiO₂ together with their difference (catalyst-support), which is supposed to be the active catalyst phase. The peaks of the active phase can be assigned to a cobalt fcc phase.

A Highly Active Cobalt Catalyst for the General and Selective Hydrogenation of Aromatic Heterocycles

Chemistry—A European Journal

Research Article
doi.org/10.1002/chem.202300561

Chemistry
Europe
European Chemical
Societies Publishing

volatility of the N/C precursor and the decomposition of cobalt acetate under catalyst synthesis conditions (Supporting Information 3.2). Inductively coupled plasma optical emission spectrometry (ICP-OES) analysis of the catalyst revealed a cobalt content of 1.81 wt. % (Supporting Information 3.1). The specific surface area could be determined by nitrogen physisorption measurements (Figure 1h) and showed an increase in surface area from 194 m²/g for the support material to 217 m²/g for the catalyst. The pore size distribution of the catalyst material (Figure 1i–j) indicates the generation of additional microporosity compared to the pure silica support material, which is mesoporous. The meso-octamethylcalix[4]pyrrole precursor seems to form a microporous N-doped carbon layer, which embeds the cobalt nanoparticles. The applied 800 °C pyrolysis temperature seem to be optimal for this process. A homogeneous distribution of the cobalt nanoparticles over the support material (Figure 1b) and an average particle size of 4.8 nm could be determined via high-angle annular dark field scanning transmission electron microscopy (HAADF-STEM). In addition, X-ray photoelectron spectroscopy (XPS) showed the presence of metallic cobalt and cobalt oxide on the surface of the catalyst material (Figure 1c). Detailed analysis of the nitrogen area suggests different binding modes of nitrogen within the catalyst (Supporting Information 3.3). Scanning electron microscopy (SEM) in combination with energy dispersive X-ray spectroscopy (EDX) confirmed the homogeneous distribution of the cobalt nanoparticles over silica, as well as nitrogen and carbon (Supporting Information 3.4). The presence of cobalt nanoparticles embedded in a N-doped C matrix on the SiO₂ support was again confirmed using HAADF-STEM in combination with EDX element maps (Supporting Information 3.5). To obtain an insight into the direct environment of the nanoparticles, high resolution HAADF-STEM (Figure d) with electron energy loss spectroscopy (EELS) was performed (Figure e–g). It shows the interface of the support matrix and the cobalt nanoparticles. The carbon component (C, blue) is connected to the cobalt nanoparticles (Co, red) and a signal of nitrogen (N, green) is present in the vicinity of the cobalt nanoparticles as well as in the matrix. Pair distribution function (PDF) studies and corresponding fits (Figure 1k) reveal the active species of the catalyst. Crystalline Co face-centered cubic lattice (fcc) nanoparticles with a spherical shape function indicate a maximum particle size of 3.1 nm (Table S1). The first peak occurring below 1.5 Å is not consistent with pure Co fcc, which has a nearest neighbor distance around 2.51 Å.^[12] However, this peak matches very well with a C–C or a C–N bond distance of N-doped graphite, which was formed via pyrolysis.^[13] Figure 1l shows the PXRD data of the SiO₂ support and the Co/SiO₂ catalyst. By subtracting the scattering contribution of the pure support material from the catalyst signal, the cobalt loading can be determined. The active sites can be assigned to a Co fcc phase with slightly shifted Q values (Supporting Information 3.6).

To determine suitable reaction conditions for the hydrogenation of aromatic heterocyclic compounds, the hydrogenation of quinoline to 1,2,3,4-tetrahydroquinoline was chosen as a benchmark reaction. The solvent screening revealed that

ethanol is the most suitable solvent for the model reaction (Table S2–3). Next the reaction temperature (Table S4) and the hydrogen pressure were screened (Table S5). The optimized parameters of 3 mL ethanol, 2.0 MPa H₂ and 70 °C were determined. The pyrolysis temperature was then varied, and different commercially available support materials and cobalt precursors were tested (Table 1). Lowering the pyrolysis temperature to 700 °C leads to a yield in the trace range, at 600 °C no conversion takes place. With the application of a higher temperature (900 °C) only traces of 1,2,3,4-tetrahydroquinoline were found, indicating the superiority of the catalyst, that was pyrolyzed at 800 °C. Pure SiO₂ support showed no conversion of quinoline. The use of activated carbon as a catalyst support material showed some activity in the selective hydrogenation of quinoline, while cobalt catalysts based on other supports, such as γ -Al₂O₃, TiO₂ and CeO₂ are not suitable for this reaction under the given conditions (Table 1). Further, the use of cobalt acetate is important to the activity of the catalyst. The metal precursors cobalt acetylacetonate, cobalt stearate and cobalt chloride show little to no activity. The only metal precursor with some activity of the final catalyst was cobalt nitrate. We continued our investigation by varying metal loadings of the catalyst. The experiments revealed that the catalyst with theoretically 4.0 wt. % (measured 1.81 wt. %) cobalt showed the best activity (Table S6). Moreover, we examined the effect of the catalyst loading upon catalysis. We observed that the best results were obtained at 5.0 mol % catalyst loading (Table S7). Further, the high activity of our catalyst is based on a specific ratio of the N/C precursor to the cobalt precursor. We assume that a certain amount of microporous N-doped carbon or a certain thickness of the embedding N-doped carbon layer is optimal for educt access and catalyst stability. A layer too thick might prevent educt access and a layer too thin might lead to cobalt leaching since the metal nanoparticles can be more easily removed from the support. Maximum activity in our benchmark reaction is observed if a ratio of metal to C/N precursor of 1:4 is used (M/N ratio). More N-doping leads to a decrease of product yield into a certain plateau at around 60 % yield (Table 1). Time conversion studies (Supporting Information 4.2) show that the conversion of quinoline to 1,2,3,4-tetrahydroquinoline is achieved after 17 h under the applied optimal reaction conditions. To ensure completion, a reaction time of 20 h was chosen. In summary, the reaction can be carried out smoothly and selectively with 5 mol % Co, 2.0 MPa H₂, 70 °C and 20 h reaction time. Very mild conditions for the benchmark reaction using nanostructured cobalt catalysts have been disclosed by Beller^[5,6] and Zhao^[7] and co-workers. Reaction conditions for the work of the Beller group were: 4 mol % Co, 2.0 MPa H₂, 100 °C and 48 h^[5] and 9 mol % Co, 1.0 MPa H₂, 70 °C and 24 h.^[6] The Co catalyst developed by the Zhao group operates under the following optimal reaction conditions: 2.0 MPa H₂, 100 °C, 3–6 h.^[7]

With the optimized reaction conditions in hand, we became interested in the substrate scope of our catalyst system. As shown in Scheme 1, a series of substituted and functionalized quinolines underwent selective hydrogenation to produce aliphatic cyclic derivatives in excellent yields under very mild

A Highly Active Cobalt Catalyst for the General and Selective Hydrogenation of Aromatic Heterocycles

Chemistry—A European Journal

Research Article
doi.org/10.1002/chem.202300561

Chemistry
Europe
European Chemical
Societies Publishing

Table 1. Cobalt catalyst comparison.^[a]

Entry	M/N ratio	Metal source	Support material	Pyrolysis temperature [°C]	Yield [%]
1 ^[b]	1:0	Co(OAc) ₂ ·4 H ₂ O	SiO ₂	800	0
2 ^[b]	1:1	Co(OAc) ₂ ·4 H ₂ O	SiO ₂	800	traces
3 ^[b]	1:2	Co(OAc) ₂ ·4 H ₂ O	SiO ₂	800	11
4 ^[b]	1:3	Co(OAc) ₂ ·4 H ₂ O	SiO ₂	800	16
5 ^[b]	1:4	Co(OAc)₂·4 H₂O	SiO₂	800	88
6 ^[b]	1:5	Co(OAc) ₂ ·4 H ₂ O	SiO ₂	800	62
7 ^[b]	1:10	Co(OAc) ₂ ·4 H ₂ O	SiO ₂	800	60
8	1:4	Co(OAc)₂·4 H₂O	SiO₂	800	> 99
9 ^[b]	1:4	Co(OAc) ₂ ·4 H ₂ O	SiO ₂	600	0
10 ^[b]	1:4	Co(OAc) ₂ ·4 H ₂ O	SiO ₂	700	traces
11 ^[b]	1:4	Co(OAc) ₂ ·4 H ₂ O	SiO ₂	800	13
12 ^[b]	1:4	Co(OAc) ₂ ·4 H ₂ O	SiO ₂	900	traces
13	1:4	Co(OAc) ₂ ·4 H ₂ O	activated carbon	800	25
14	1:4	Co(OAc) ₂ ·4 H ₂ O	γ-Al ₂ O ₃	800	0
15	1:4	Co(OAc) ₂ ·4 H ₂ O	TiO ₂	800	0
16	1:4	Co(OAc) ₂ ·4 H ₂ O	CeO ₂	800	0
17	1:4	Co(acac) ₃	SiO ₂	800	0
18	1:4	Co(NO ₃) ₂ ·6 H ₂ O	SiO ₂	800	48
19	1:4	Co(II)stearate	SiO ₂	800	9
20	1:4	CoCl ₂ ·6 H ₂ O	SiO ₂	800	0
21	1:4	—	SiO ₂	800	0

[a] Reaction conditions: 5.0 mol % Co (1.81 wt % Co, 0.01 mmol Co, 0.59 mg Co), 0.2 mmol quinoline, 3 mL ethanol, 70 °C, 2.0 MPa H₂, 20 h. Yields were determined by GC using *n*-dodecane as an internal standard. [b] Same as [a] but 60 °C.

conditions. First, we applied our catalyst for the hydrogenation of pure quinoline and achieved an excellent yield. Subsequent investigations involved fifteen quinoline derivatives, which were hydrogenated also under relatively mild conditions. This led to the formation of 1,2,3,4-tetrahydroquinolines with up to 99% isolated yields (Scheme 1, products **1**, **6**, **7**, **9** and **10**) indicating that the catalytic process is able to proceed with considerable variation in the nature and the position of the substituents. In particular, both electron-donating methyl substituents (Scheme 1, products **2–8**) and electron-withdrawing halogen substituents (Scheme 1, products **9** and **10**) yield the desired product in high yield. Furthermore, the catalyst succeeds when methoxy, hydroxy and amine groups (Scheme 1, products **11–13**) are present. Finally, the catalyst is also able to tolerate two functional groups (Scheme 1, product **14** and **15**) producing the intended 1,2,3,4-tetrahydroquinolines in excellent yields. It is worth mentioning some of the 1,2,3,4-tetrahydroquinolines presented in Scheme 1 serve as precursors or intermediates for the synthesis of bioactive molecules. In particular, products **1**, **2** and **11** can result in 5-HT₃ receptor antagonists, antitrypanosomally drugs and tubulin polymerization inhibitors.^[14] Following the selective hydrogenation of quinolines, we became interested in the hydrogenation of other N-heterocycles. First, quinoxaline could be converted to the corresponding hydrogenated product (Scheme 2, product **16**) under very mild conditions. In addition, 2-methyl-1,2,3,4-tetrahydroquinoxaline (Scheme 2, product **17**) was obtained for the first time with a nanostructured cobalt catalyst in good yield under mild reaction conditions. Next, we were interested in the hydrogenation of pyridines and pyrroles to demonstrate the superior

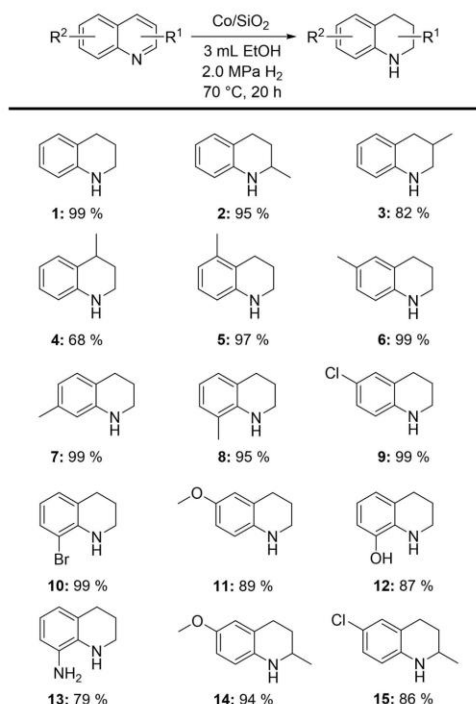
general applicability of our cobalt catalyst. To achieve good yields, the reaction conditions had to be modified and required 5.0 MPa H₂, 120 °C and 10 mol % Co. Under these conditions, we were able to hydrogenate pure pyridine efficiently (Scheme 2, product **18**) as well as isonicotinamide (Scheme 2, product **19**) which is known as a reversible organic hydrogen storage liquid for potential hydrogen-powered fuel cells in mobile applications.^[15] Simple pyrrole and 2-methylpyrrole (Scheme 2, products **20** and **21**) could be also converted to the corresponding hydrogenated products in good yields. We further tested our catalyst in the hydrogenation of indoles. 2-methylindole as well as 2,3,3-trimethylindolenin can be converted to the products in excellent yields (Scheme 2, product **22** and **23**). Indolines and their scaffold are known as important pharmaceuticals and agrochemicals and it is particularly useful to have a selective and simple access to this class of compounds.^[16] As a consequence, hydrogenation catalysis has been used to synthesize indolines.^[17] The reduction of isoquinoline (Scheme 2, product **24**) was also performed. It is noteworthy, that drastic conditions are needed for complete selective hydrogenation compared to quinoline. When our catalyst is used with 9-aminoacridine, we selectively obtain 1,2,3,4,5,6,7,8-octahydro-9-aminoacridine (Scheme 2, product **25**). This is in contrast to the other products, as we were able to selectively hydrogenate the phenyl rings instead of the N-heterocycle. We assume that partial hydrogenation takes place in the N-heterocycle part and subsequent rearrangement. In the case of phenanthroline and benzo[*h*]quinoline, we were also able to selectively reduce the N-heteroarene rings and the corresponding partially reduced products were obtained in up to 81 % yield (Scheme 2, products

A Highly Active Cobalt Catalyst for the General and Selective Hydrogenation of Aromatic Heterocycles

Chemistry – A European Journal

Research Article
doi.org/10.1002/chem.202300561

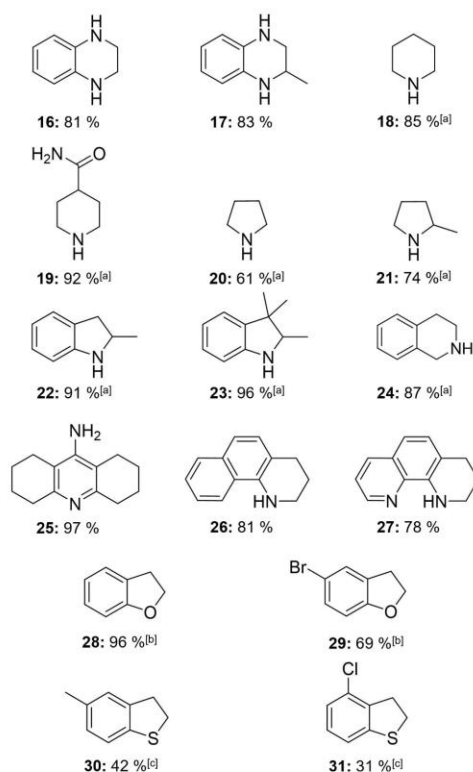
Chemistry
Europe
European Chemical
Societies Publishing



Scheme 1. Hydrogenation of quinolines to the corresponding 1,2,3,4-tetrahydroquinolines. Reaction conditions: 5.0 mol % Co (1.81 wt % Co, 0.01 mmol Co, 0.59 mg Co), 0.2 mmol substrate, 3 mL ethanol, 70 °C, 2.0 MPa H₂, 20 h. Isolated yields are given.

26 and 27). In addition to N-heterocycles, we applied our catalyst to the more challenging hydrogenation of O- and S-heterocycles. The selective hydrogenation of benzofurans is of great interest^[9,18,19] because the associated products are important bio-active molecules. With our catalyst, we are able to selectively hydrogenate benzofuran to 2,3-dihydrobenzofuran (Scheme 2, product **28**). We had to modify the initial conditions slightly i.e. 3.0 MPa H₂ and 100 °C to obtain an excellent yield. Moreover, we could also demonstrate the selective hydrogenation of 5-bromobenzofuran (Scheme 2, product **29**). Having shown the successful hydrogenation of N- and O-heterocycles, the compounds 5-methylbenzothiophene and 4-chlorobenzothiophene were hydrogenated. To achieve a reasonable yield, we had to modify the reaction conditions by using 6.0 MPa H₂, 150 °C, 48 h and 15 mol % Co (Scheme 2, product **30** and **31**). The hydrogenation of benzothiophenes is very challenging and research has focused on benzothiophene.^[19,20] The strong binding of sulfur containing heterocycles to the active metal sites is an additional hurdle.^[21] Very recently and parallel to our work, Beller/Jagadeesh and coworkers introduced an earth abundant metal based heterogeneous catalyst system able to hydrogenate benzofuran derivatives and benzothiophenes.^[22]

Chem. Eur. J. 2023, 29, e202300561 (5 of 7)



Scheme 2. Products of the hydrogenation of different N-, O-, and S-heterocycles. Reaction conditions: 5.0 mol % Co (1.81 wt % Co, 0.01 mmol Co, 0.59 mg Co), 0.2 mmol substrate, 3 mL ethanol, 70 °C, 2.0 MPa H₂, 20 h. Isolated yields are given. [a] 10 mol % Co (1.81 wt % Co, 0.02 mmol Co, 1.18 mg Co), 0.2 mmol substrate, 3 mL ethanol, 120 °C, 5.0 MPa H₂, 20 h. Isolated yields are given. [b] 5 mol % Co (1.81 wt % Co, 0.01 mmol Co, 0.59 mg Co), 0.2 mmol substrate, 3 mL ethanol, 100 °C, 3.0 MPa H₂, 20 h. Isolated yields are given. [c] 15 mol % Co (1.81 wt % Co, 0.03 mmol Co, 1.77 mg Co), 0.2 mmol substrate, 3 mL ethanol, 150 °C, 6.0 MPa H₂, 48 h. Isolated yields are given.

Regarding reusability, five consecutive runs were carried out (Supporting Information 4.3) and the yields and initial rates obtained indicate very good recyclability. As observed by TEM measurements, there is no agglomeration or growing of nanoparticles in the used catalyst during catalysis. Moreover, particle size distribution after catalysis with an average diameter of 6.2 nm has been observed (Supporting Information 4.4.1). In addition, a hot filtration test was performed, and the separated solution showed no activity. This indicates that irreversibly leached cobalt species play no significant role in arene hydrogenation catalysis. The leaching of our catalyst was determined by ICP-OES and found to be 0.7 % (Supporting Information 4.4.3). To demonstrate the efficiency and practicality of our cobalt catalyst, an upscaling of the benchmark reaction was

© 2023 The Authors. Chemistry - A European Journal published by Wiley-VCH GmbH

15213765, 2023, 30, Downloaded from https://chemistry-europe.onlinelibrary.wiley.com/doi/10.1002/chem.202300561 by Universitat Bayreuth, Wiley Online Library on [16/05/2024]. See the Terms and Conditions (https://onlinelibrary.wiley.com/terms-and-conditions) on Wiley Online Library for rules of use; OA articles are governed by the applicable Creative Commons License

A Highly Active Cobalt Catalyst for the General and Selective Hydrogenation of Aromatic Heterocycles

Chemistry—A European Journal

Research Article
doi.org/10.1002/chem.202300561

Chemistry
Europe
European Chemical
Societies Publishing

performed using 10 mmol quinoline. This resulted in the isolated yield of 90% of 1,2,3,4-tetrahydroquinoline (Supporting Information 4.5).

Conclusion

In conclusion, we introduced a protocol to synthesize highly active and selective nano-structured 3d-metal catalysts and succeeded in identifying a selective cobalt hydrogenation catalyst. A variation in the ratio of metal to N/C precursor can be used to boost catalyst performance. Our catalyst can operate under very mild conditions permitting the hydrogenation of numerous classes of N-, O- and S-heterocycles selectively. The discovered catalyst synthesis protocol might assist others to find selective and highly active nanostructured 3d-metal catalysts for arene hydrogenation and other important catalytic transformations.

Experimental Section

Catalyst synthesis: To a suspension of meso-octamethylcalix[4]pyrrole (1.352 mmol, 579.32 mg) in 12 mL MeOH, Co(OAc)₂·4 H₂O (0.338 mmol, 84.16 mg, 4 wt.% ideally) is added to 500 mg SiO₂ and the solvent is evaporated at 70 °C under slow, constant stirring. The active catalyst material is generated by pyrolysis at 800 °C under nitrogen flow, followed by pyrolysis at 550 °C under nitrogen flow.

Catalyst characterization: TEM was carried out by using a JEOL JEM 2200FS (200 kV) device. For the sample preparation, the samples were suspended in chloroform and sonicated for 5 min. For analysis, LC200-Cu grids were used. Scanning transmission electron microscopy (STEM) measurements were performed using a JEM-ARM200F (JEOL) equipped with a cold emission gun, a STEM probe corrector (CEOS GmbH), and an energy filter (GATAN). The microscope was operated at 200 kV with a probe current of 80 pA. The probe convergence semi-angle was 13.4 mrad (20 µm condenser lens aperture). The images were recorded with an annular dark-field (ADF) detector using a detector distance of 8 cm resulting in a collection angle of 68–280 mrad. The image size, pixel size, and pixel dwell time of the STEM images were 1024×1024 pixels, 0.063 nm, and 16 µm, respectively. Electron energy loss spectroscopy (EELS) measurements were performed in STEM mode with the same probe size, condenser lens aperture, and detector distance. The energy dispersion of the spectrometer was set to 0.25 eV. The image collection semi-angle was 20.8 mrad. The image size, pixel size, and pixel dwell time of the EELS spectrum images were 100×100 pixels, 0.33 nm, and 20 ms, respectively. X-ray photoelectron spectroscopy (XPS) was performed using a Physical Electronics Phi 5000 Versa Probe III instrument. As X-ray source a monochromatic Al K α with a spot size of 100 µm (21.1 W) was used. The kinetic pass energy of the photoelectrons was determined with a hemispheric analyzer (45°) set to pass energy of 13 eV for high-resolution spectra. Pore characterizations were carried out via nitrogen physisorption measurements using a Nova2000e (Quantochrome) apparatus. The pore size distribution was computed via DFT calculations (calculation model: N₂ at –196.15 °C: slit/cylindrical pore, NLDFT equilibrium model). The specific surface area was calculated using p/p_0 values from 0.05–0.3 (BET). PXRD and PDF measurements have been taken at the European Synchrotron Radiation Facility (ESRF), beamline ID-15 A, which is equipped with a PILATUS 2 M, S/N 24-0131, X series detector. The powder was

packed in Lindemann special glass capillaries with a diameter of 1 mm. Measurements were made for one minute at a photon energy of 90 keV (30 images each 2 seconds). Distance calibration was done with a CeO₂ NIST 674b standard.

General procedure for the hydrogenation of aromatic heterocycles: A 10 mL glass reaction vial was charged with a magnetic stirring bar, 0.2 mmol substrate, 3 mL EtOH and 32.6 mg catalyst (5.0 mol% Co). The vial was placed in a 300 mL high-pressure autoclave (Parr Instruments). The autoclave was flushed three times with 2.0 MPa hydrogen. Afterwards, 2.0 MPa hydrogen was applied, and the reaction was stirred at 70 °C for 20 h. After completion of the reaction time, the autoclave was cooled to room temperature and the hydrogen was released. The catalyst was removed by filtration. The solvent was removed via rotary evaporation and high vacuum. After purification via column chromatography, the product was analysed by ¹H- and ¹³C NMR spectroscopy. NMR measurements were performed using a Varian INOVA 300 (300 MHz for ¹H, 75 MHz for ¹³C) and a Varian INOVA 400 (400 MHz for ¹H, 100 MHz for ¹³C) instrument at 296 K. For certain substrates, hydrogen pressure, temperature and reaction time as well as catalyst loading have been adapted.

Acknowledgements

We thank the DFG KE 756/34-1 and the Exzellenzcluster 2186, 'The Fuel Science Center' ID: 390919832, for financial support. In addition, the authors thank F. Baier for XPS measurements and Dr. C. Denner for SEM-EDX measurements and the Bavarian Polymer Institute (University of Bayreuth, KeyLab Electron and Optical Microscopy) for assistance with TEM measurements. We acknowledge Stefano Checchia for PDF measurements at ID15, ESRF. We thank E. Arzt for his support through INM. Open Access funding enabled and organized by Projekt DEAL.

Conflict of Interest

The authors declare no conflict of interest.

Data Availability Statement

The data that support the findings of this study are available in the supplementary material of this article.

Keywords: catalyst synthesis · cobalt · heterocycles · heterogeneous catalysis · hydrogenation

- [1] K. Weissmermel, H.-J. Arpe, *Industrial Organic Chemistry*, Wiley-VCH, Weinheim, 2008.
- [2] P. G. Andersson, *Modern Reduction Methods*, John Wiley & Sons Incorporated, Weinheim, 2008.
- [3] a) M. S. Salman, N. Rambhujun, C. Prathana, K. Srivastava, K.-F. Aguey-Zinsou, *Ind. Eng. Chem. Res.* **2022**, 61, 6067–6105; b) Y. Jo, J. Oh, D. Kim, J. H. Park, J. H. Baik, Y.-W. Suh, *Korean J. Chem. Eng.* **2022**, 39, 20–37; c) K. C. Tan, T. He, Y. S. Chua, P. Chen, *J. Phys. Chem. C* **2021**, 125, 18553–18566.
- [4] a) M. El-Shahat, *J. Heterocycl. Chem.* **2022**, 59, 399–421; b) M. P. Wiesenfeldt, Z. Nairoukh, T. Dalton, F. Glorius, *Angew. Chem. Int. Ed.* **2019**, 58, 10460–10476; *Angew. Chem.* **2019**, 131, 10570–10586; c) Z.

A Highly Active Cobalt Catalyst for the General and Selective Hydrogenation of Aromatic Heterocycles

Chemistry—A European Journal

Research Article
doi.org/10.1002/chem.202300561



15313165, 2023, 30, Downloaded from https://onlinelibrary.wiley.com/doi/10.1002/chem.202300561 by Universitat Bayreuth, Wiley Online Library on [16/05/2024]. See the Terms and Conditions (https://onlinelibrary.wiley.com/terms-and-conditions) on Wiley Online Library for rules of use; OA articles are governed by the applicable Creative Commons License

- Wei, F. Shao, J. Wang, *Chin. J. Catal.* **2019**, *40*, 980–1002; d) A. Gualandi, D. Savoia, *RSC Adv.* **2016**, *6*, 18419–18451.
- [5] F. Chen, A.-E. Surkus, L. He, M.-M. Pohl, J. Radnik, C. Topf, K. Junge, M. Beller, *J. Am. Chem. Soc.* **2015**, *137*, 11718–11724.
- [6] K. Murugesan, V. G. Chandrashekhara, C. Kreyenschulte, M. Beller, R. V. Jagadeesh, *Angew. Chem. Int. Ed.* **2020**, *132*, 17561–17565.
- [7] W. Gong, Q. Yuan, C. Chen, Y. Lv, Y. Lin, C. Liang, G. Wang, H. Zhang, H. Zhao, *Adv. Mater.* **2019**, *31*, e1906051.
- [8] a) N. Antil, A. Kumar, N. Akhtar, W. Begum, M. Chauhan, R. Newar, M. S. Rawat, K. Manna, *Inorg. Chem.* **2022**, *61*, 1031–1040; b) F. Tang, G. Zhang, L. Wang, J. Huang, Y.-N. Liu, *J. Catal.* **2022**, *414*, 101–108; c) V. M. Asaula, V. V. Buryanov, B. Y. Solod, D. M. Tryus, O. O. Pariiska, I. E. Kotenko, Y. M. Volovenko, D. M. Volochnyuk, S. V. Ryabukhin, S. V. Kolotilov, *Justus Liebigs Ann. Chem.* **2021**, *2021*, 6616–6625; d) M. Puche, L. Liu, P. Concepción, I. Sorribes, A. Corma, *ACS Catal.* **2021**, *11*, 8197–8210; e) R. Huang, C. Cao, J. Liu, L. Zheng, Q. Zhang, L. Gu, L. Jiang, W. Song, *ACS Appl. Mater. Interfaces.* **2020**, *12*, 17651–17658; f) J. Hervochon, V. Dorcet, K. Junge, M. Beller, C. Fischmeister, *Catal. Sci. Technol.* **2020**, *10*, 4820–4826; g) Z.-H. He, Y.-C. Sun, K. Wang, Z.-Y. Wang, P.-P. Guo, C.-S. Jiang, M.-Q. Yao, Z.-H. Li, Z.-T. Liu, *J. Mol. Catal.* **2020**, *496*, 111192; h) G. Jaiswal, M. Subaramanian, M. K. Sahoo, E. Balaraman, *ChemCatChem* **2019**, *11*, 2449–2457; i) I. Sorribes, L. Liu, A. Doménech-Carbó, A. Corma, *ACS Catal.* **2018**, *8*, 4545–4557; j) J. Li, G. Liu, X. Long, G. Gao, J. Wu, F. Li, *J. Catal.* **2017**, *355*, 53–62; k) Z. Wei, Y. Chen, J. Wang, D. Su, M. Tang, S. Mao, Y. Wang, *ACS Catal.* **2016**, *6*, 5816–5822; l) J. E. Shaw, P. R. Stapp, *J. Heterocycl. Chem.* **1987**, *24*, 1477–1483.
- [9] P. Ji, K. Manna, Z. Lin, A. Urban, F. X. Greene, G. Lan, W. Lin, *J. Am. Chem. Soc.* **2016**, *138*, 12234–12242.
- [10] a) C. Bäuml, C. Bauer, R. Kempe, *ChemSusChem* **2020**, *13*, 3110–3114; b) G. Hahn, P. Kunnas, N. de Jonge, R. Kempe, *Nat. Catal.* **2019**, *2*, 71–77; c) T. Schwob, P. Kunnas, N. de Jonge, C. Papp, H.-P. Steinrück, R. Kempe, *Sci. Adv.* **2019**, *5*, eaav3680.
- [11] J. A. Shriver, S. G. Westphal, *J. Chem. Educ.* **2006**, *83*, 1330–1332.
- [12] A. Khor, S. Roslyakov, P. Loginov, *Nano-Struct. Nano-Objects* **2021**, *26*, 100727.
- [13] F. H. Allen, O. Kennard, D. G. Watson, L. Brammer, A. G. Orpen, R. Taylor, *J. Chem. Soc. Perkin Trans. 1* **1987**, S1.
- [14] a) V. Sridharan, P. A. Suryavanshi, J. C. Menéndez, *Chem. Rev.* **2011**, *111*, 7157–7259; b) R. J. Pagliaro, S. Lusvardi, A. B. Pierini, R. Brun, M. R. Mazzieri, *Bioorg. Med. Chem.* **2010**, *18*, 142–150; c) J.-P. Liou, Z.-Y. Wu, C.-C. Kuo, C.-Y. Chang, P.-Y. Lu, C.-M. Chen, H.-P. Hsieh, J.-Y. Chang, *J. Med. Chem.* **2008**, *51*, 4351–4355.
- [15] Y. Cui, S. Kwok, A. Bucholtz, B. Davis, R. A. Whitney, P. G. Jessop, *New J. Chem.* **2008**, *32*, 1027–1037.
- [16] a) I. V. Ukrainets, N. L. Bereznyakova, *Chem. Heterocycl. Compd.* **2012**, *48*, 155–165; b) Y.-J. Wu in *Topics in Heterocyclic Chemistry*, Vol. 26 (Ed.: G. W. Gribble), Springer, Heidelberg, **2010**, pp. 1–29; c) E. Lacivita, M. Leopoldo, *Curr. Top. Med. Chem.* **2006**, *6*, 1927–1970.
- [17] a) S. Zhang, J. Gan, Z. Xia, X. Chen, Y. Zou, X. Duan, Y. Qu, *Chem* **2020**, *6*, 2994–3006; b) H. Bernas, N. Kumar, A. Aho, R. Leino, D. Y. Murzin, *Catal. Commun.* **2014**, *56*, 41–44; c) H. Cho, F. Török, B. Török, *Org. Biomol. Chem.* **2013**, *11*, 1209–1215; d) D. Clarisse, B. Fenet, F. Fache, *Org. Biomol. Chem.* **2012**, *10*, 6587–6594; e) A. Kulkarni, W. Zhou, B. Török, *Org. Lett.* **2011**, *13*, 5124–5127.
- [18] a) A. Hamza, D. Moock, C. Schlepphorst, J. Schneidewind, W. Baumann, F. Glorius, *Chem. Sci.* **2022**, *13*, 985–995; b) D. Timelthaler, C. Topf, *Synthesis* **2022**, *54*, 629–642; c) D. Moock, T. Wagener, T. Hu, T. Gallagher, F. Glorius, *Angew. Chem. Int. Ed.* **2021**, *60*, 13677–13681; *Angew. Chem.* **2021**, *133*, 13791–13796; d) S. Rengshausen, C. van Stapen, N. Levin, S. Tricard, K. L. Luska, S. DeBeer, B. Chaudret, A. Bordet, W. Leitner, *Small* **2021**, *17*, e2006683; e) Y. Ge, Z. Wang, Z. Han, K. Ding, *Chem. Eur. J.* **2020**, *26*, 15482–15486; f) S. El Sayed, A. Bordet, C. Weidenthaler, W. Hetaba, K. L. Luska, W. Leitner, *ACS Catal.* **2020**, *10*, 2124–2130; g) X. Long, Z. Li, G. Gao, P. Sun, J. Wang, B. Zhang, J. Zhong, Z. Jiang, F. Li, *Nat. Commun.* **2020**, *11*, 4074; h) K. Murugesan, T. Senthamarai, A. S. Alshammari, R. M. Altamimi, C. Kreyenschulte, M.-M. Pohl, H. Lund, R. V. Jagadeesh, M. Beller, *ACS Catal.* **2019**, *9*, 8581–8591; i) P. Ji, Y. Song, T. Drake, S. S. Veroneau, Z. Lin, X. Pan, W. Lin, *J. Am. Chem. Soc.* **2018**, *140*, 433–440; j) A. Karakulina, A. Gopakumar, Z. Fei, P. J. Dyson, *Catal. Sci. Technol.* **2018**, *8*, 5091–5097; k) H. Jiang, J. Xu, B. Sun, *Appl. Organomet. Chem.* **2018**, *32*, e4260; l) T.-N. Ye, J. Li, M. Kitano, H. Hosono, *Green Chem.* **2017**, *19*, 749–756; m) A. Karakulina, A. Gopakumar, I. Akçok, B. L. Roulier, T. LaGrange, S. A. Katsyuba, S. Das, P. J. Dyson, *Angew. Chem. Int. Ed.* **2016**, *128*, 300–304; n) L. Pauli, R. Tannert, R. Scheil, A. Pfaltz, *Chem. Eur. J.* **2015**, *21*, 1482–1487; o) Y. Gong, P. Zhang, X. Xu, Y. Li, H. Li, Y. Wang, *J. Catal.* **2013**, *297*, 272–280; p) C. Liu, Z. Rong, Z. Sun, Y. Wang, W. Du, Y. Wang, L. Lu, *RSC Adv.* **2013**, *3*, 23984–23988; q) N. Ortega, S. Urban, B. Beiring, F. Glorius, *Angew. Chem. Int. Ed.* **2012**, *51*, 1710–1713; *Angew. Chem.* **2012**, *124*, 1742–1745; r) N. Ortega, B. Beiring, S. Urban, F. Glorius, *Tetrahedron* **2012**, *68*, 5185–5192; s) M. Maris, W.-R. Huck, T. Mallat, A. Baiker, *J. Catal.* **2003**, *219*, 52–58.
- [19] H. Jiang, S. Zhang, B. Sun, *Catal. Lett.* **2018**, *148*, 1336–1344.
- [20] a) M. Fang, R. A. Sánchez-Delgado, *J. Catal.* **2014**, *311*, 357–368; b) K. Okamoto, R. Akiyama, S. Kobayashi, *J. Org. Chem.* **2004**, *69*, 2871–2873.
- [21] J. Oudar, *Catal. Rev.* **1980**, *22*, 171–195.
- [22] B. Zhou, V. G. Chandrashekhara, Z. Ma, C. Kreyenschulte, S. Bartling, H. Lund, M. Beller, R. V. Jagadeesh, *Angew. Chem. Int. Ed.* **2023**, e202215699.

Manuscript received: February 20, 2023

Accepted manuscript online: February 24, 2023

Version of record online: March 31, 2023

Chemistry–A European Journal

Supporting Information

A Highly Active Cobalt Catalyst for the General and Selective Hydrogenation of Aromatic Heterocycles

Christof Bauer, Felix Müller, Sercan Keskin, Mirijam Zobel, and Rhett Kempe*

Table of Contents

1	General considerations.....	3
2	Experimental procedures.....	5
2.1	Synthesis of meso-octamethylcalix[4]pyrrole.....	5
2.2	Catalyst synthesis	5
2.3	Catalytic selective hydrogenation of aromatic heterocycles – general procedure	6
3	Characterization of the catalyst.....	7
3.1	ICP-OES	7
3.2	TGA.....	7
3.3	XPS.....	8
3.4	SEM-EDX	9
3.5	HAADF-STEM with EDX.....	10
3.6	PXRD and PDF	11
4	Catalytic studies	13
4.1	Screening of reaction parameters	13
4.2	Time turnover	16
4.3	Reusability.....	17
4.4	Evaluation of the used catalyst.....	18
4.4.1	TEM measurements.....	18
4.4.2	Hot filtration test	18
4.4.3	Leaching test	19
4.5	Upscaling of the reaction.....	19
5	Characterization of isolated products.....	20
6	NMR spectra	36
7	References.....	98

1 General considerations

All air- and moisture sensitive reactions were performed under dry argon or nitrogen atmosphere using standard Schlenk and glove box techniques. Dried solvents were obtained from a solvent purification system (activated alumina cartridges) or purchased from commercial sources. Deuterated solvents were dried via molecular sieves. All chemicals were acquired from commercial sources with purity over 95 % and used without further purification.

Pyrolysis of the catalyst were performed under nitrogen atmosphere in a ChemBET Pulsar TPR/TPD instrument from Quantachrome.

Transmission electron microscopy (TEM) was carried out by using a JEOL JEM 2200FS (200 kV) device. For the sample preparation, the samples were suspended in chloroform and sonicated for 5 min. For analysis, LC200-Cu grids were used. Scanning transmission electron microscopy (STEM) measurements were performed using a JEM-ARM200F (JEOL) equipped with a cold emission gun, a STEM probe corrector (CEOS GmbH), and an energy filter (GATAN). The microscope was operated at 200 kV with a probe current of 80 pA. The probe convergence semi-angle was 13.4 mrad (20 μ m condenser lens aperture). The images were recorded with an annular dark-field (ADF) detector using a detector distance of 8 cm resulting in a collection angle of 68-280 mrad. The image size, pixel size, and pixel dwell time of the STEM images were 1024 x 1024 pixels, 0.063 nm, and 16 μ s, respectively. Electron energy loss spectroscopy (EELS) measurements were performed in STEM mode with the same probe size, condenser lens aperture, and detector distance. The energy dispersion of the spectrometer was set to 0.25 eV. The image collection semi-angle was 20.8 mrad. The image size, pixel size, and pixel dwell time of the EELS spectrum images were 100 x 100 pixels, 0.33 nm, and 20 ms, respectively.

Scanning electron microscopy (SEM) and coupled energy dispersive X-ray spectroscopy (EDX) measurements were carried out by using a Zeiss Ultra plus device. The acceleration voltage was 20 kV. The detection was carried out with an in-lens backscatter detector. For a conductive surface, the samples were sputtered with platinum (layer thickness: 1.3 μ m) with the Sputter Coater 208HR from Cressington.

Pore characterizations were carried out via nitrogen physisorption measurements using a Nova2000e (Quantachrome) apparatus. The pore size distribution was computed via DFT calculations (calculation model: N₂ at -196.15 °C: slit/cylindrical pore, NLDFT equilibrium model). The specific surface area was calculated using p/p_0 values from 0.05-0.3 (BET).

PXRD and PDF measurements have been taken at the European Synchrotron Radiation Facility (ESRF), beamline ID-15A, which is equipped with a PILATUS 2M, S/N 24-0131, X series detector. The powder was packed in Lindemann special glass capillaries with a diameter of 1 mm. Measurements were made for one minute at a photon energy of 90 keV (30 images each 2 seconds). Distance calibration was done with a CeO₂, NIST 674b standard. We use xPDFsuite to calculate the G(r) function, and Diffpy-CMI for fitting.^[1] Theoretical XRD patterns have been created with the Mercury software^[2], using Crystallographic Information Files of Co (database code: ICSD 136039) and graphite (database code: ICSD 18838).^[3]

The cobalt content was determined by ICP-OES. The fusion of the catalyst was carried out in a Berghof Speed Wave 4 microwave, for the ICP-OES measurement an Agilent 5800 was used (standing flame with axial and radial observation).

X-ray photoelectron spectroscopy (XPS) was performed using a Physical Electronics Phi 5000 Versa Probe III instrument. As X-ray source a monochromatic Al K α with a spot size of 100 μ m (21.1 W) was used. The kinetic pass energy of the photoelectrons was determined with a hemispheric analyzer (45°) set to pass energy of 13 eV for high-resolution spectra.

Elemental analyses were carried out on an Elementar UNICUBE® device.

NMR measurements were performed using a Varian INOVA 300 (300 MHz for ¹H, 75 MHz for ¹³C), a Varian INOVA 400 (400 MHz for ¹H, 100 MHz for ¹³C) and a Bruker Avance III HD 500 (500 MHz for ¹H, 125 MHz for ¹³C) instrument at 296 K. Chemical shifts are reported in ppm relative to the residual solvent signal (CDCl₃: 7,26 ppm (¹H), 77,16 ppm (¹³C); DMSO-d₆: 2.50 ppm (¹H), 39.51 ppm (¹³C)), coupling constants (J) are reported in Hz. Estimated ¹H and ¹³C NMR spectra were simulated (DMSO-d₆, 300 MHz) using ChemDraw Professional Version 21.0.0.28.

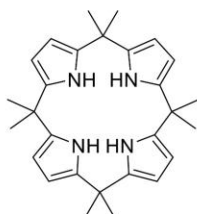
GC analyses were carried out on an Agilent 6850 GC system equipped with an Optima 17 column (30 m x 0.32 mm x 0.25 μ m).

The hydrogenation experiments were carried out with Parr Instrument stainless steel autoclaves N-MT5 300 mL equipped with heating mantles and temperature controller.

2 Experimental procedures

2.1 Synthesis of meso-octamethylcalix[4]pyrrole

Meso-octamethylcalix[4]pyrrole was synthesized according to an adapted literature procedure.^[4] To a solution of 50 mL MeOH with 2.96 mL acetone (40 mmol) and 0.4 mL concentrated H₂SO₄ (0,0075 mmol) were 2.78 mL pyrrole in 10 mL MeOH slowly added. The reaction solution is stirred for 1.5 h at room temperature and then placed in the freezer (-24 °C) overnight. The white precipitate is filtered, washed with cold MeOH, and dried under vacuo.



CHN (C₂₈H₃₆N₄): C 78.1 (78.5), H 8.3 (8.5), N 13.0 (13.1),

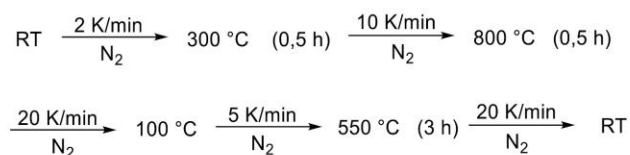
¹H NMR (500 MHz, CDCl₃, 296 K): δ = 7.02 (s, 4H), 5.92-5.91 (d, *J* = 2.7, 8H), 1.53 (s, 24H) ppm.

¹³C NMR (125 MHz, CDCl₃, 296 K): δ = 138.45, 102.84, 35.21, 29.13 ppm.

Yield: 3.99 g (9.3 mmol, 93 %)

2.2 Catalyst synthesis

To a suspension of meso-octamethylcalix[4]pyrrole (1.352 mmol, 579.32 mg) in 12 mL MeOH, Co(OAc)₂ · 4 H₂O (0.338 mmol, 84.16 mg, 4 wt% ideally), respectively Co(acac)₃, Co(NO₃)₂ · 6 H₂O, Co(II)stearate and CoCl₂ · 6 H₂O, is added to 500 mg SiO₂ (respectively activated carbon, γ-Al₂O₃, TiO₂, CeO₂) and the solvent is evaporated at 70 °C under slow, constant stirring. The active catalyst material is generated by pyrolysis at 800 °C under nitrogen flow, followed by pyrolysis at 550 °C under nitrogen flow.



2.3 Catalytic selective hydrogenation of aromatic heterocycles – general procedure

A 10 mL glass reaction vial was charged with a magnetic stirring bar, 0.2 mmol substrate, 3 mL EtOH and 32.6 mg catalyst (Co/SiO₂, M/L = 1:4, 5.0 mol% Co). The vial was placed in a 300 mL high-pressure autoclave (Parr Instruments). The autoclave was flushed at least three times with 2.0 MPa hydrogen. Afterwards, 2.0 MPa hydrogen was applied, and the reaction was stirred at 70 °C for 20 h. After completion of the reaction time, the autoclave was cooled to room temperature and the hydrogen was released. The catalyst was removed by filtration. The solvent was removed via rotary evaporation and high vacuum. After purification via column chromatography, the product was analysed by ¹H- and ¹³C-NMR spectroscopy.

3 Characterization of the catalyst

3.1 ICP-OES

25 mg of the sample were solved in 5 mL HNO_3 (65 % p.a.) and 2 mL HF (40 % supra) and heated in the microwave at 210 °C for 40 min.

Theoretical Co content: 4.00 wt%

Measured Co content: 1.81 wt%

The huge difference is understandable, due to the loss of precursor materials in the nitrogen stream of catalyst synthesis and the high sublimability of the precursor materials.

3.2 TGA

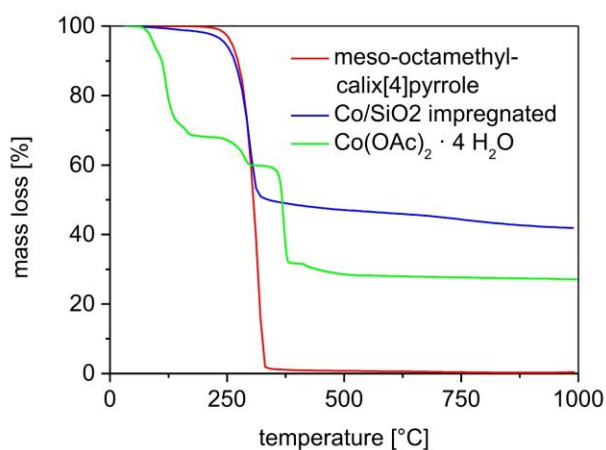


Figure S 1: TGA analysis of meso-octamethylcalix[4]pyrrole (red), the impregnated precursor materials (blue) and $\text{Co}(\text{OAc})_2 \cdot 4 \text{H}_2\text{O}$ (green). Measurements were performed in the range of 30-1000 °C (heating ramp 10 K/min) in constant N_2 flow.

3.3 XPS

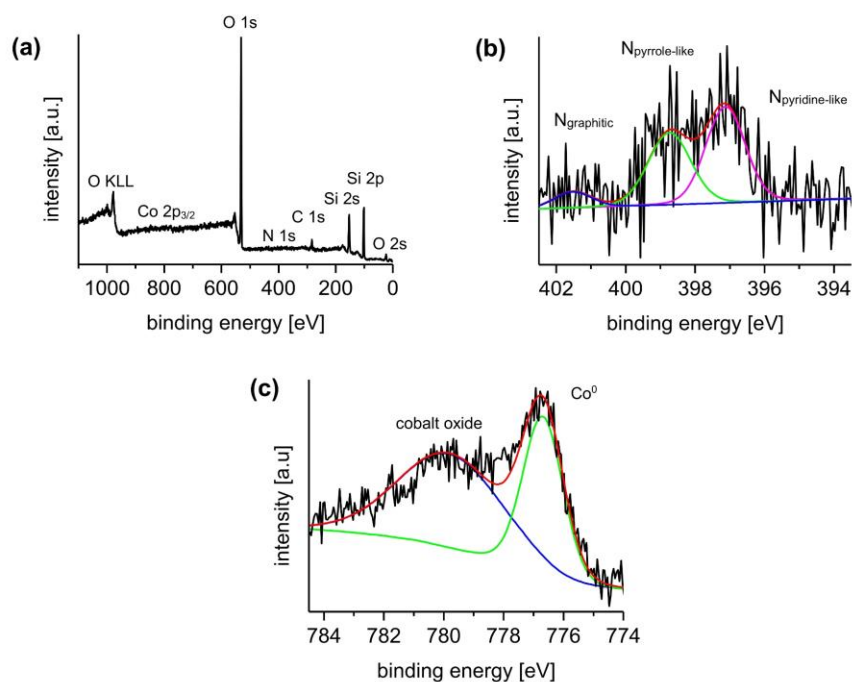


Figure S 2: X-ray photoelectron spectra (XPS) of the surface area of the catalyst Co/SiO₂. (a) XPS survey of Co/SiO₂. The catalyst contains Si, O, C, N and Co. (b) Analysis of the nitrogen area suggests different binding models of nitrogen within the catalyst (graphitic: 8 %, pyrrole-like: 41 %, pyridine-like: 51 %). (c) Analysis of the Co 2p_{3/2} area with an asymmetric fit. It shows Co⁰ (61 %) and cobalt oxide (39 %) on the surface.

3.4 SEM-EDX

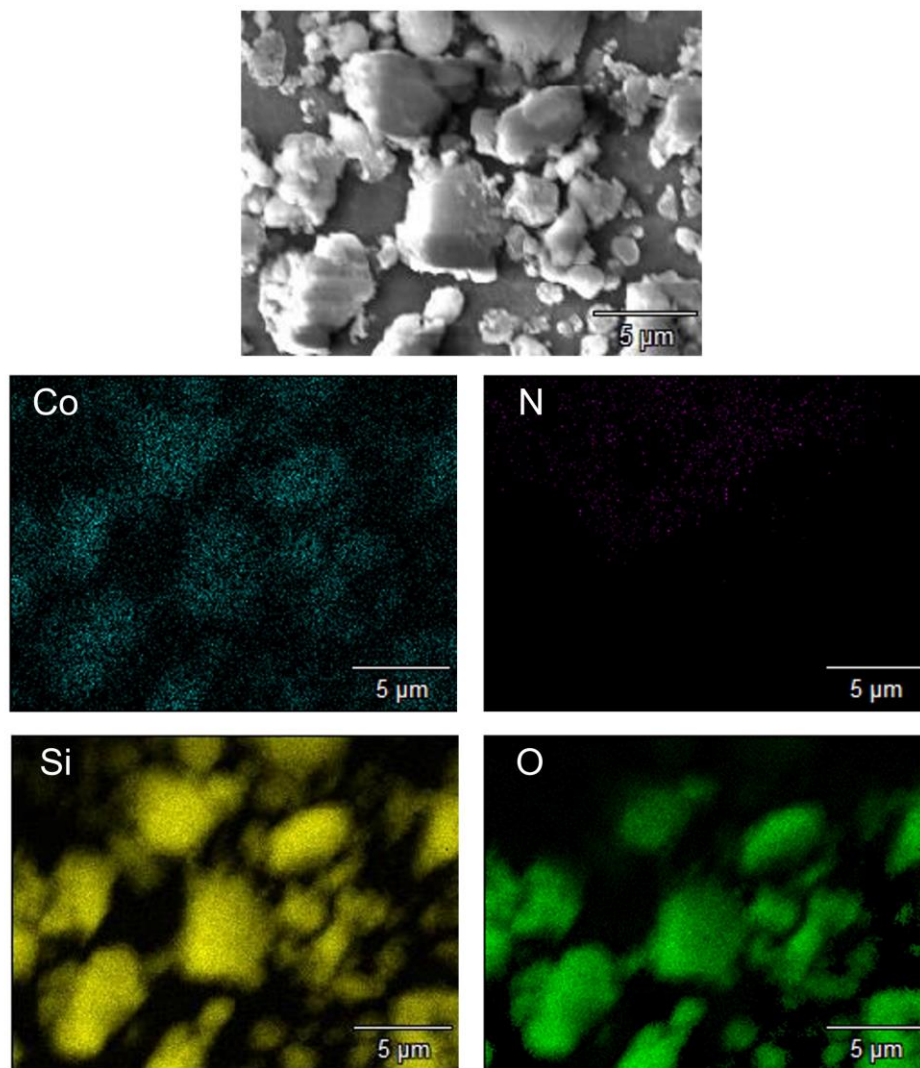


Figure S 3: Scanning electron microscopy (SEM) in combination with energy dispersive X-ray (EDX) mapping of the catalyst. The measurements show a homogeneous distribution of the cobalt nanoparticles over the entire material which indicates a smooth impregnation process. The distribution of N, Si and O verifies a homogeneous surface of the support material.

3.5 HAADF-STEM with EDX

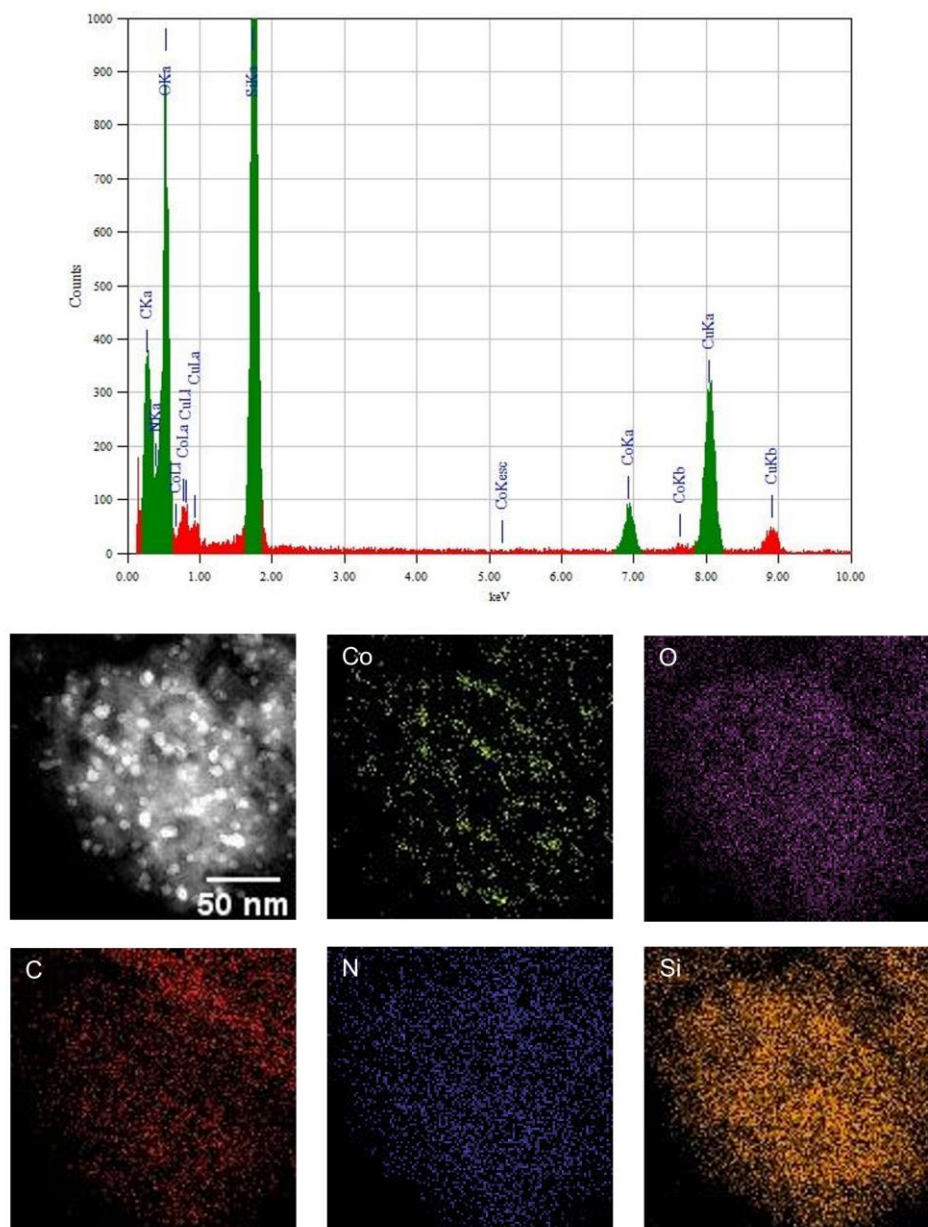


Figure S 4: Characterization of the Co nanoparticles by high-angle annular dark-field scanning TEM (HAADF-STEM) analysis combined with energy-dispersed X-ray (EDX) element mapping. SiO₂ (Si: orange, O: magenta) is covered with homogeneously dispersed Co nanoparticles (Co: green). The nanoparticles are embedded in a nitrogen doped carbon layer (C: red, N: blue).

3.6 PXRD and PDF

Figure S 5 (left) shows the PXRD data of the SiO₂ support (red) and the Co/SiO₂ catalyst (blue), corrected for scattering of air and the capillary. Due to the low signal to noise ratio, as well as the broad diffuse scattering beneath the diffraction peaks, common XRD refinements cannot yield further insight into the nanostructure^[5], known as the "nanostructure problem".^[6] Complementary, the atomic pair distribution function (PDF) technique not only utilizes the sharp Bragg peaks, but also the diffuse scattering, representing the structural information as a histogram of all interatomic distances. Structural models of cobalt and graphite combined with a spherical shape function were used to fit the data. There seems to be no alteration of the support's crystal structure due to the loading since its peaks remain at the same positions and keep their original shape. By subtracting the scattering contribution of the pure support, the signal from the Cobalt loading can be isolated (**Figure S 5**, right). The catalyst data shows several Bragg peaks on top of a broad and continuous intensity distribution, that is primarily related to the crystallite size, as shown by Jiang et al.^[7] The peaks of the active phase, can be assigned to a Co (fcc) phase, i.e. (111), (200), (220) and (311) reflexes, while being slightly shifted to lower Q values.

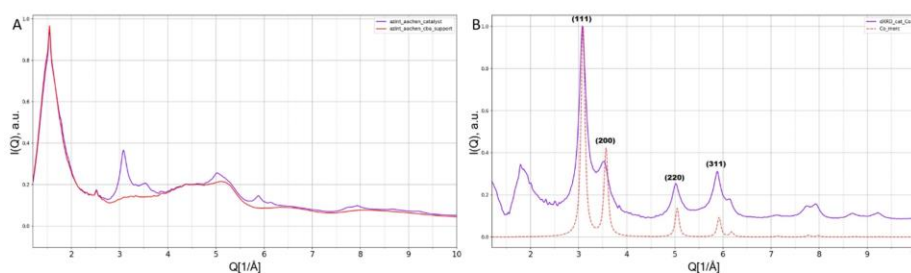


Figure S 5: PXRD of the catalyst (blue) and the support SiO₂ (red) on the left side and the difference PXRD, which is the active phase with the support contribution subtracted (blue) with the Co (fcc) reference phase (orange).

PDF data and their corresponding fits are shown in **Figure S 6**. The active species of the catalyst are best fitted using a fcc structure of pure Cobalt, with a spherical shape function indicating a maximum particle size of 3.1 nm, and a goodness-of-fit value R_w of 0.27, with all but one peak well described. The first peak occurring at 1.52 Å cannot be described by a pure Cobalt (fcc) species, which have their nearest neighbour distance at around 2.51 Å.^[3] However, this peak matches very well a C-C bond distance of 1.54 Å.^[8] It can be fitted by introducing a graphite phase (database code: ICSD 18838).^[9] Even though this phase does not fit to the cobalt phase,

it can be explained because of the pyrolysis step at the catalyst synthesis and the formation of N-doped graphite in the catalyst material.

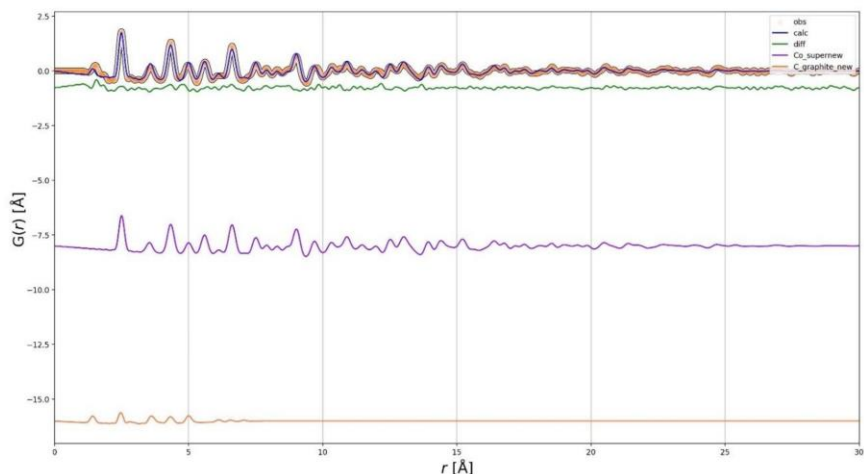


Figure S 6: PDF of the active phase (orange) with its fit (blue) and the corresponding difference curve (green). Contributions of co (purple) and graphite (bottom, orange) can be seen below.

Compared to bulk cobalt, the nanoparticles show a shrinkage of their unit cell and corresponding cell volume by 1.35 % for all numbers (Table S 1). This phenomenon has been observed before for various metal nanoparticles and is attributed to surface tension in particular when crystal sizes become smaller than 5 nm.^[10] Smaller crystals have a higher ratio of the number of surface atoms compared to the total number of atoms, which induces a compression of lattice parameters.

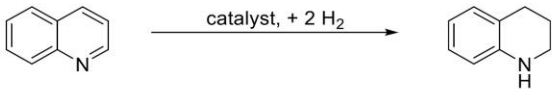
Table S 1: Results of PDF refinement for the cobalt phase. Unit cell parameters (starting values in brackets); B_{iso}: isotropic atomic displacement parameters, delta 2: correlated atomic motion parameter; R_w: goodness of fit value.

Lattice parameter a, b	3.5390 (3.5551)
Lattice parameter c	3.5390 (3.5551)
Cell volume	44.32 (44.93)
Size	3.17
B _{iso}	0.6961
delta 2	3.000
R _w	0.27

4 Catalytic studies

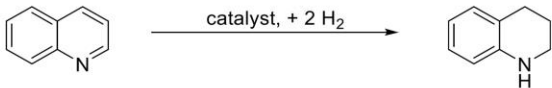
4.1 Screening of reaction parameters

Table S 2: Reaction parameters – solvent.

		
Entry	Solvent	Yield [%]
1	Ethanol	> 99
2	Methanol	54
3	Water	0
4	Tetrahydrofuran	0
5	2-Methyltetrahydrofuran	0
6	Toluene	78
7	Xylene	51
8	Diglyme	0
9	1,4-Dioxane	0
10	Triethylamine	0

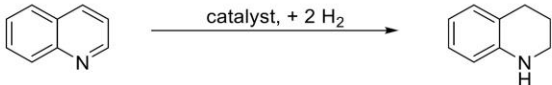
Reaction conditions: 5.0 mol% Co (1.81 wt% Co, 0.01 mmol Co, 0.59 mg Co), 0.2 mmol quinoline, 3 mL solvent, 70 °C, 2.0 MPa H₂, 20 h. Yields were determined by GC using *n*-dodecane as an internal standard.

Table S 3: Reaction parameters – amount of ethanol.

		
Entry	Solvent [mL]	Yield [%]
1	1	24
2	2	97
3	3	> 99
4	4	> 99
5	5	> 99

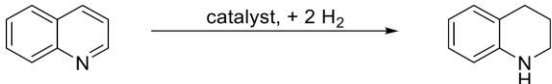
Reaction conditions: 5.0 mol% Co (1.81 wt% Co, 0.01 mmol Co, 0.59 mg Co), 0.2 mmol quinoline, ethanol, 70 °C, 2.0 MPa H₂, 20 h. Yields were determined by GC using *n*-dodecane as an internal standard.

Table S 4: Reaction parameters – reaction temperature.

		
Entry	Temperature [°C]	Yield [%]
1	40	0
2	50	0
3	60	88
4	70	> 99
5	80	> 99
6	90	> 99
7	100	> 99

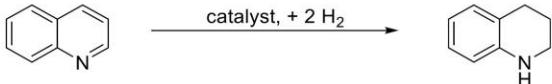
Reaction conditions: 5.0 mol% Co (1.81 wt% Co, 0.01 mmol Co, 0.59 mg Co), 0.2 mmol quinoline, 3 mL ethanol, 2.0 MPa H₂, 20 h. Yields were determined by GC using *n*-dodecane as an internal standard.

Table S 5: Reaction parameters – H₂ pressure.

		
Entry	Pressure [MPa]	Yield [%]
1	1.0	20
2	2.0	> 99
3	3.0	> 99

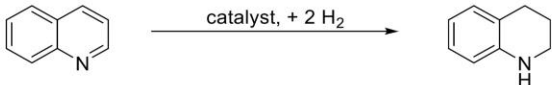
Reaction conditions: 5.0 mol% Co (1.81 wt% Co, 0.01 mmol Co, 0.59 mg Co), 0.2 mmol quinoline, 3 mL ethanol, 70 °C, 20 h. Yields were determined by GC using *n*-dodecane as an internal standard.

Table S 6: Reaction parameters – metal loading on catalyst.

<div style="text-align: center;">  </div>		
Entry	Metal loading [wt%]	Yield [%]
1	1.0	0
2	2.0	0
3	3.0	17
4	4.0 (1.81)	> 99
5	5.0	88

Reaction conditions: 5.0 mol% Co (0.01 mmol Co, 0.59 mg Co), 0.2 mmol quinoline, 3 mL ethanol, 2.0 MPa H₂, 70 °C, 20 h. Yields were determined by GC using *n*-dodecane as an internal standard.

Table S 7: Reaction parameters – catalyst loading in catalysis.

<div style="text-align: center;">  </div>		
Entry	Catalyst loading [mol%]	Yield [%]
1	1.0	0
2	2.0	18
3	3.0	46
4	4.0	81
5	5.0	> 99

Reaction conditions: Catalyst (1.81 wt% Co), 0.2 mmol quinoline, 3 mL ethanol, 2.0 MPa H₂, 70 °C, 20 h. Yields were determined by GC using *n*-dodecane as an internal standard.

4.2 Time turnover

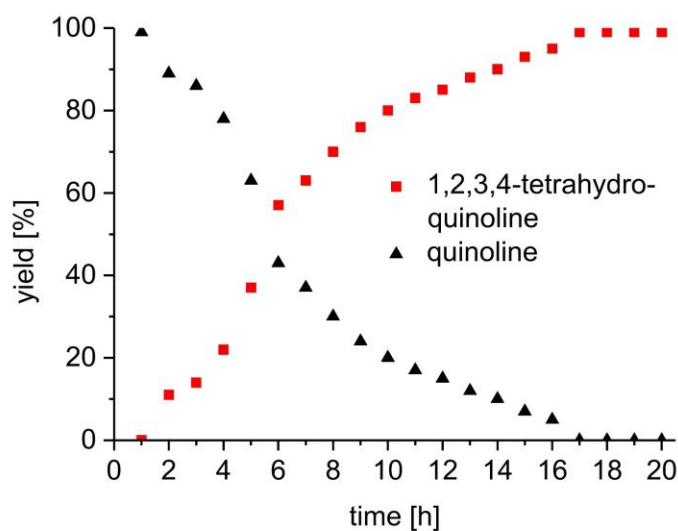


Figure S 7: Reaction progress for the selective hydrogenation of quinoline (black) at different intervals of time to the corresponding 1,2,3,4-tetrahydroquinoline (red). Reaction conditions: 0.2 mmol quinoline, 3 mL ethanol, 32.6 mg catalyst (5 mol%), 70 °C and 2.0 MPa hydrogen. Yields were determined by GC using *n*-dodecane as internal standard.

4.3 Reusability

The hydrogenation of quinoline to 1,2,3,4-tetrahydroquinoline was chosen to investigate the recyclability of the novel Co/SiO₂ catalyst. A 10 mL reaction vial was charged with a magnetic stirring bar, 0.2 mmol quinoline, 3 mL EtOH and 32.6 mg catalyst (5 mol% Co). The vial was placed in a high-pressure autoclave (Parr Instruments) and the autoclave was flushed five times with 2.0 MPa hydrogen. The autoclave was pressured with 2.0 MPa hydrogen and the reaction was carried out for six hours at 70 °C to obtain 60 % yield. After six hours the autoclave was opened and there the catalyst was washed three times with ethanol via centrifugation. Therefore, the catalyst could be completely recovered. The yield of 1,2,3,4-tetrahydroquinoline was determined by GC using *n*-dodecane as an internal standard (Figure S 8).

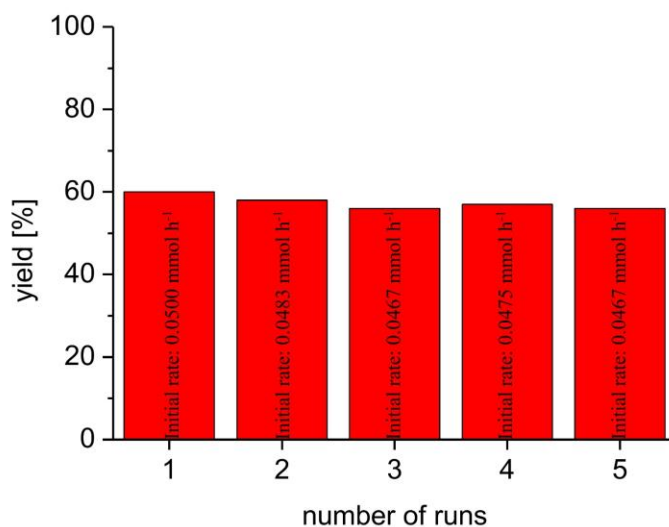


Figure S 8: Results and the initial rates of the recycling experiment. There is no decrease of the catalytic activity in five consecutive runs.

4.4 Evaluation of the used catalyst

4.4.1 TEM measurements

The Co/SiO₂ catalyst was investigated with TEM measurements after the catalysis. The general procedure for the hydrogenation of quinoline was applied in a 10 mL reaction vial. The vial was charged with a magnetic stirring bar, 0.2 mmol quinoline, 3 mL EtOH and 32.6 mg catalyst (5 mol% Co). The vial was placed in a 300 mL high-pressure autoclave (Parr Instruments) and the autoclave was flushed three times with 2.0 MPa hydrogen. Afterwards, 2.0 MPa hydrogen was applied, and the reaction was stirred at 70 °C for 20 h. After completion of the reaction time, the autoclave was cooled down to room temperature and the hydrogen was released. The catalyst was removed by centrifugation and the organic phase was separated. After, the catalyst was washed three times with ethanol and dried in vacuo. The catalyst was characterized via TEM measurements.

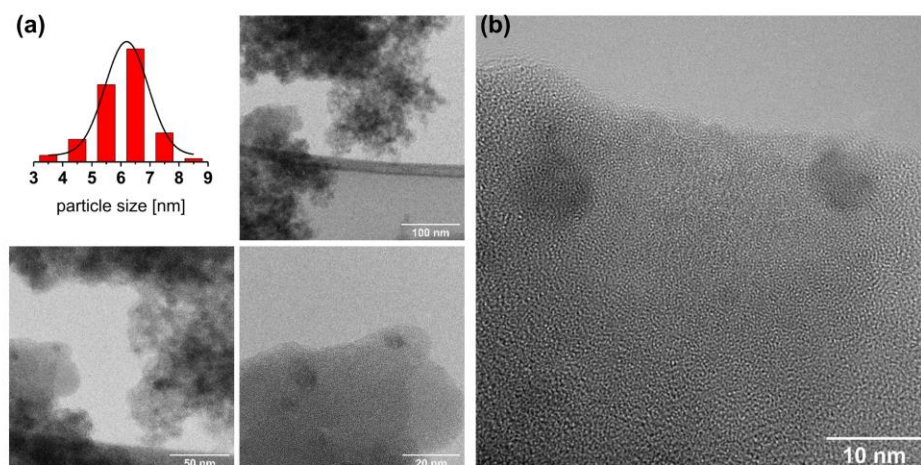


Figure S 9: (a) TEM characterization of the used Co/SiO₂ catalyst. There is no agglomeration or growing of nanoparticles. The particle size distribution is homogeneous with an average diameter of 6.2 nm. (b) HR-TEM measurement of the catalyst. The particles are in good shape with the particles before catalysis.

4.4.2 Hot filtration test

To demonstrate the catalyst stability a hot filtration test was performed. Therefore, a 10 mL reaction vial was charged with a magnetic stirring bar, 0.2 mmol quinoline, 3 mL ethanol and 32.6 mg catalyst (5 mol% Co). The vial was placed in a 300 mL high-pressure autoclave (Parr Instruments) and the autoclave was flushed three times with 2.0 MPa hydrogen. Afterwards,

2.0 MPa hydrogen was applied, and the reaction was stirred at the desired 70 °C. When 15 % yield of 1,2,3,4-tetrahydroquinoline were generated, the hot catalytic mixture was filtered to remove the catalyst. Afterwards, 0.2 mmol quinoline were added to the filtrate and the mixture was stirred at the catalytic conditions mentioned above. The filtrate did not show any activity and the desired product 1,2,3,4-tetrahydroquinoline was not generated. No other product was to be seen either. The yield of 1,2,3,4-tetrahydroquinoline was determined by GC using *n*-dodecane as an internal standard.

4.4.3 Leaching test

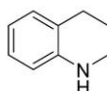
A leaching test was performed to demonstrate, that our catalyst does not form homogeneous cobalt species. A 10 mL reaction vial was charged with a magnetic stirring bar, 0.2 mmol quinoline, 3 mL ethanol and 32.6 mg catalyst (5.0 mol%). The vial was placed in a 300 mL high-pressure autoclave (Parr Instruments) and the autoclave was flushed three times with 2.0 MPa hydrogen. After, 2.0 MPa hydrogen was applied, and the reaction was stirred at 70 °C for 20 h. Upon completion of the reaction time, the autoclave was cooled to room temperature and the hydrogen was released. The reaction mixture was separated from the catalyst and the leaching amount of the Co/SiO₂ catalyst was determined via ICP-OES. The leaching rate of cobalt is 0.7 %.

4.5 Upscaling of the reaction

The benchmark reaction, the selective hydrogenation of quinoline to 1,2,3,4-tetrahydroquinoline, was used to carry out an upscaling experiment. For the reaction, 1630 mg Co/SiO₂ (5 mol%), 10 mmol quinoline and 150 mL EtOH were stirred in a 200 mL glass vial equipped with a magnetic stirring bar. The vial was placed in a 300 mL high-pressure autoclave (Parr Instruments) and the autoclave was flushed three times with 2.0 MPa hydrogen. After pressuring the autoclave with the desired 2.0 MPa hydrogen pressure, the reaction was stirred for 20 h at 70 °C. The autoclave was cooled to room temperature and the hydrogen was released. The reaction mixture was separated from the catalyst and the yield of 1,2,3,4-tetrahydroquinoline was isolated. **Yield:** 90 % (1196 mg) as an oil.

5 Characterization of isolated products

1,2,3,4-Tetrahydroquinoline (1)



MW ($\text{C}_9\text{H}_{11}\text{N}$) = 133.1 g/mol (M)

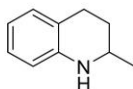
^1H NMR (400 MHz, CDCl_3 , 296 K): δ = 7.05 – 6.92 (m, 2H), 6.63 (td, J = 7.4, 1.2 Hz, 1H), 6.54 - 6.43 (m, 1H), 3.78 (s, 1H), 3.37 - 3.27 (m, 2H), 2.79 (t, J = 6.4 Hz, 2H), 2.04 - 1.89 (m, 2H) ppm.

^{13}C NMR (100 MHz, CDCl_3 , 296 K): δ = 144.87, 129.60, 126.81, 121.52, 117.02, 114.28, 42.08, 27.08, 22.29 ppm.

Yield: 99 % (25.8 mg) as an oil.

The spectroscopic data match those reported in literature.^[11] (CAS Number: 635-46-1)

2-Methyl-1,2,3,4-tetrahydroquinoline (2)



MW ($\text{C}_{10}\text{H}_{13}\text{N}$) = 147.22 g/mol (M)

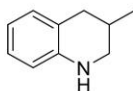
^1H NMR (300 MHz, CDCl_3 , 296 K): δ = 7.10 – 6.89 (m, 2H), 6.63 (td, J = 7.4, 1.0 Hz, 1H), 6.49 (dd, J = 8.3, 0.9 Hz, 1H), 3.71 (s, 1H), 3.49 – 3.34 (m, 1H), 2.93 – 2.70 (m, 2H), 2.00 – 1.90 (m, 1H), 1.61 (dddd, J = 12.8, 11.5, 10.0, 5.5 Hz, 1H), 1.23 (d, J = 6.3 Hz, 3H) ppm.

^{13}C NMR (75 MHz, CDCl_3 , 296 K): δ = 144.90, 129.39, 126.80, 121.21, 117.08, 114.11, 47.27, 30.25, 26.72, 22.74 ppm.

Yield: 95 % (28.0 mg) as an oil.

The spectroscopic data match those reported in literature.^[12] (CAS Number: 1780-19-4)

3-Methyl-1,2,3,4-tetrahydroquinoline (3)



MW (C₁₀H₁₃N) = 147.22 g/mol (M)

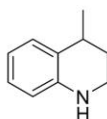
¹H NMR (300 MHz, CDCl₃, 296 K): δ = 6.97 (ddd, J = 7.6, 2.4, 0.7 Hz, 2H), 6.63 (td, J = 7.4, 1.2 Hz, 1H), 6.54 – 6.45 (m, 1H), 3.86 (s, 1H), 3.29 (ddd, J = 11.0, 3.7, 2.0 Hz, 1H), 2.95 – 2.88 (m, 1H), 2.78 (dd, J = 4.8, 2.0 Hz, 1H), 2.17 – 1.73 (m, 2H), 1.07 (d, J = 6.6 Hz, 3H) ppm.

¹³C NMR (75 MHz, CDCl₃, 296 K): δ = 144.39, 129.61, 126.78, 121.18, 116.98, 113.94, 77.16, 48.93, 35.57, 27.27, 19.15 ppm.

Yield: 82 % (24.0 mg) as an oil.

The spectroscopic data match those reported in literature.^[13] (CAS Number: 20668-20-6)

4-Methyl-1,2,3,4-tetrahydroquinoline (4)



MW (C₁₀H₁₃N) = 147.22 g/mol (M)

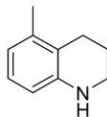
¹H NMR (300 MHz, CDCl₃, 296 K): δ = 7.13 – 6.78 (m, 2H), 6.65 (td, J = 7.4, 1.2 Hz, 1H), 6.48 (dd, J = 8.0, 1.2 Hz, 1H), 3.87 (s, 1H), 3.42 – 3.20 (m, 2H), 2.93 (dd, J = 12.5, 6.3 Hz, 1H), 2.06 – 1.93 (m, 1H), 1.69 (dtd, J = 9.9, 6.3, 3.7 Hz, 1H), 1.31 (d, J = 7.0 Hz, 3H) ppm.

¹³C NMR (75 MHz, CDCl₃, 296 K): δ = 146.29, 128.53, 126.81, 122.67, 117.01, 114.24, 39.09, 30.32, 29.96, 22.76 ppm.

Yield: 68 % (20.0 mg) as an oil.

The spectroscopic data match those reported in literature.^[13] (CAS Number: 19343-78-3)

5-Methyl-1,2,3,4-tetrahydroquinoline (5)



MW (C₁₀H₁₃N) = 147.22 g/mol (M)

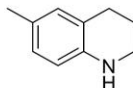
¹H NMR (300 MHz, CDCl₃, 296 K): δ = 7.08 – 6.78 (m, 1H), 6.65 – 6.49 (m, 1H), 6.48 – 6.36 (m, 1H), 3.83 (s, 1H), 3.42 – 3.22 (m, 2H), 2.73 (dt, J = 13.1, 6.4 Hz, 2H), 2.33 – 2.18 (m, 3H), 2.10 – 1.98 (m, 2H) ppm.

¹³C NMR (75 MHz, CDCl₃, 296 K): δ = 145.04, 137.26, 126.24, 120.24, 118.95, 112.51, 41.65, 24.15, 22.63, 19.47 ppm.

Yield: 97 % (28.5 mg) as an oil.

The spectroscopic data match those reported in literature.^[14] (CAS Number: 58960-02-4)

6-Methyl-1,2,3,4-tetrahydroquinoline (6)



MW (C₁₀H₁₃N) = 147.22 g/mol (M)

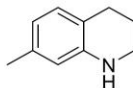
¹H NMR (300 MHz, CDCl₃, 296 K): δ = 6.84 (d, J = 5.0 Hz, 2H), 6.45 (d, J = 8.6 Hz, 1H), 3.68 (s, 1H), 3.36 – 3.26 (m, 2H), 2.79 (t, J = 6.4 Hz, 2H), 2.26 (s, 3H), 2.04 – 1.92 (m, 2H) ppm.

¹³C NMR (75 MHz, CDCl₃, 296 K): δ = 142.50, 130.14, 127.31, 126.27, 121.64, 114.52, 42.25, 27.00, 22.51, 20.50 ppm.

Yield: 99 % (29.0 mg) as an oil.

The spectroscopic data match those reported in literature.^[14] (CAS Number: 91-61-2)

7-Methyl-1,2,3,4-tetrahydroquinoline (7)



MW (C₁₀H₁₃N) = 147.22 g/mol (M)

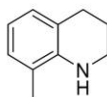
¹H NMR (300 MHz, CDCl₃, 296 K): δ = 6.87 (dd, *J* = 14.0, 5.8 Hz, 1H), 6.47 (t, *J* = 9.3 Hz, 1H), 6.33 (d, *J* = 11.9 Hz, 1H), 4.07 – 3.44 (m, 1H), 3.30 (dd, *J* = 14.3, 8.8 Hz, 2H), 2.84 – 2.68 (m, 2H), 2.34 – 2.18 (m, 3H), 2.04 – 1.88 (m, 2H) ppm.

¹³C NMR (75 MHz, CDCl₃, 296 K): δ = 144.69, 136.41, 129.45, 118.59, 117.96, 114.84, 42.09, 26.69, 22.48, 21.21 ppm.

Yield: 99 % (29.0 mg) as an oil.

The spectroscopic data match those reported in literature.^[14] (CAS Number: 58960-03-5)

8-Methyl-1,2,3,4-tetrahydroquinoline (8)



MW (C₁₀H₁₃N) = 147.22 g/mol (M)

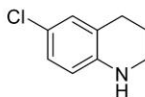
¹H NMR (300 MHz, CDCl₃, 296 K): δ = 6.86 (ddd, *J* = 10.1, 7.7, 0.6 Hz, 2H), 6.56 (t, *J* = 7.4 Hz, 1H), 3.38 (dd, *J* = 6.9, 4.1 Hz, 2H), 2.79 (t, *J* = 6.4 Hz, 2H), 2.08 (s, 3H), 1.97 – 1.89 (m, 2H), 1.59 (s, 1H) ppm.

¹³C NMR (75 MHz, CDCl₃, 296 K): δ = 142.82, 127.97, 127.50, 121.32, 121.01, 116.53, 42.48, 27.42, 22.29, 17.30 ppm.

Yield: 95 % (28.0 mg) as an oil.

The spectroscopic data match those reported in literature.^[14] (CAS Number: 52601-70-4)

6-Chloro-1,2,3,4-tetrahydroquinoline (9)



MW (C₉H₁₀ClN) = 167.64 g/mol (M)

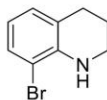
¹H NMR (400 MHz, CDCl₃, 296 K): δ = 7.06 – 6.74 (m, 2H), 6.38 (d, J = 8.0 Hz, 1H), 3.60 (s, 1H), 3.34 – 3.22 (m, 2H), 2.72 (t, J = 6.4 Hz, 2H), 1.99 – 1.83 (m, 2H) ppm.

¹³C NMR (100 MHz, CDCl₃, 296 K): δ = 143.39, 129.14, 126.61, 122.98, 121.27, 115.19, 41.96, 26.98, 21.86 ppm.

Yield: 99 % (33.5 mg) as an oil.

The spectroscopic data match those reported in literature.^[13] (CAS Number: 49716-18-9)

8-Bromo-1,2,3,4-tetrahydroquinoline (10)



MW (C₉H₁₀BrN) = 212.09 g/mol (M)

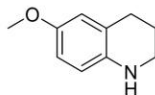
¹H NMR (300 MHz, CDCl₃, 296 K): δ = 7.23 (d, J = 7.9 Hz, 1H), 6.89 (d, J = 7.2 Hz, 1H), 6.45 (t, J = 7.7 Hz, 1H), 4.43 (s, 1H), 3.48 – 3.28 (m, 2H), 2.78 (t, J = 6.3 Hz, 2H), 2.01 – 1.83 (m, 2H) ppm.

¹³C NMR (75 MHz, CDCl₃, 296 K): δ = 141.64, 129.95, 128.33, 122.78, 116.84, 108.65, 41.99, 27.39, 21.64 ppm.

Yield: 99 % (42.4 mg) as an oil.

The spectroscopic data match those reported in literature.^[15] (CAS Number: 937640-02-3)

6-Methoxy-1,2,3,4-tetrahydroquinoline (11)



MW (C₁₀H₁₃NO) = 163.22 g/mol (M)

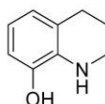
¹H NMR (400 MHz, CDCl₃, 296 K): δ = 6.66 – 6.55 (m, 2H), 6.46 (d, J = 8.5 Hz, 1H), 3.74 (d, J = 0.8 Hz, 3H), 3.50 (s, 1H), 3.30 – 3.22 (m, 2H), 2.77 (t, J = 6.5 Hz, 2H), 2.00 – 1.89 (m, 2H) ppm.

¹³C NMR (100 MHz, CDCl₃, 296 K): δ = 151.86, 138.97, 122.89, 115.60, 114.94, 112.96, 55.85, 42.40, 27.24, 22.52 ppm.

Yield: 89 % (29.1 mg) as a colourless oil.

The spectroscopic data match those reported in literature.^[12] (CAS Number: 120-15-0)

8-Hydroxy-1,2,3,4-tetrahydroquinoline (12)



MW (C₉H₁₁NO) = 149.19 g/mol (M)

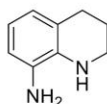
¹H NMR (400 MHz, DMSO-d₆, 296 K): δ = 8.90 (s, 1H), 6.52 – 6.41 (m, 1H), 6.36 (dd, J = 7.5, 0.9 Hz, 1H), 6.27 (t, J = 7.6 Hz, 1H), 4.64 (s, 1H), 3.25 – 3.13 (m, 2H), 2.63 (d, J = 6.4 Hz, 2H), 1.82 – 1.71 (m, 2H) ppm.

¹³C NMR (100 MHz, DMSO-d₆, 296 K): δ = 143.25, 133.86, 120.39, 119.95, 114.76, 111.46, 40.97, 26.55, 21.87 ppm.

Yield: 87 % (25.9 mg) as a colourless oil.

The spectroscopic data match those reported in literature.^[12] (CAS Number: 6640-50-2)

8-Amino-1,2,3,4-tetrahydroquinoline (13)



MW ($\text{C}_9\text{H}_{12}\text{N}_2$) = 148.21 g/mol (M)

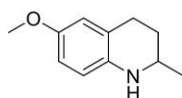
^1H NMR (300 MHz, CDCl_3 , 296 K): δ = 6.68 – 6.45 (m, 3H), 3.46 – 3.06 (m, 5H), 2.77 (t, J = 6.4 Hz, 2H), 1.97 – 1.86 (m, 2H) ppm.

^{13}C NMR (75 MHz, CDCl_3 , 296 K): δ = 134.03, 133.95, 123.34, 121.22, 118.11, 114.16, 42.67, 27.13, 22.50 ppm.

Yield: 79 % (23.4 mg) as an oil.

The spectroscopic data match those reported in literature.^[16] (CAS Number: 54012-92-9)

6-Methoxy-2-methyl-1,2,3,4-tetrahydroquinoline (14)



MW ($\text{C}_9\text{H}_{11}\text{NO}$) = 177.25 g/mol (M)

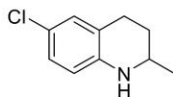
^1H NMR (300 MHz, CDCl_3 , 296 K): δ = 6.62 (d, J = 8.2 Hz, 2H), 6.47 (d, J = 8.1 Hz, 1H), 3.75 (s, 3H), 3.48 (d, J = 18.4 Hz, 1H), 3.35 (ddd, J = 12.2, 6.2, 3.1 Hz, 1H), 2.82 (dtd, J = 15.0, 11.7, 4.5 Hz, 2H), 2.01 – 1.86 (m, 1H), 1.60 (ddd, J = 23.2, 11.8, 5.6 Hz, 1H), 1.22 (d, J = 6.2 Hz, 3H) ppm.

^{13}C NMR (75 MHz, CDCl_3 , 296 K): δ = 151.81, 138.96, 122.46, 115.33, 114.61, 112.83, 55.76, 47.47, 30.34, 26.95, 22.57 ppm.

Yield: 94 % (33.3 mg) as a colourless oil.

The spectroscopic data match those reported in literature.^[16] (CAS Number: 42835-96-1)

6-Chloro-2-methyl-1,2,3,4-tetrahydroquinoline (15)



MW ($\text{C}_{10}\text{H}_{12}\text{ClN}$) = 181.66 g/mol (M)

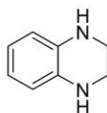
^1H NMR (300 MHz, CDCl_3 , 296 K): δ = 6.90 (dd, J = 11.8, 2.6 Hz, 2H), 6.41 (d, J = 8.3 Hz, 1H), 4.02 (s, 1H), 3.42 – 3.34 (m, 1H), 2.74 (ddd, J = 9.2, 8.3, 4.6 Hz, 2H), 1.96 – 1.88 (m, 1H), 1.56 (dddd, J = 12.9, 11.2, 9.9, 5.6 Hz, 1H), 1.21 (d, J = 6.3 Hz, 3H) ppm.

^{13}C NMR (75 MHz, CDCl_3 , 296 K): δ = 143.03, 128.83, 126.49, 122.85, 121.48, 115.23, 47.26, 29.62, 26.45, 22.39 ppm.

Yield: 86 % (31.2 mg) as a colourless oil.

The spectroscopic data match those reported in literature.^[17] (CAS Number: 28328-97-4)

1,2,3,4-Tetrahydroquinoxaline (16)



MW ($\text{C}_8\text{H}_{10}\text{N}_2$) = 134.18 g/mol (M)

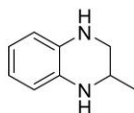
^1H NMR (400 MHz, CDCl_3 , 296 K): δ = 6.63 – 6.43 (m, 2H), 3.65 (s, 1H), 3.42 (s, 2H) ppm.

^{13}C NMR (100 MHz, CDCl_3 , 296 K): δ = 133.79, 118.87, 114.83, 41.51 ppm.

Yield: 81 % (21.7 mg) as a dark red oil.

The spectroscopic data match those reported in literature.^[11] (CAS Number: 3476-89-9)

2-Methyl-1,2,3,4-tetrahydroquinoxaline (17)



MW ($\text{C}_9\text{H}_{12}\text{N}_2$) = 148.21 g/mol (M)

^1H NMR (300 MHz, CDCl_3 , 296 K): δ = 6.64 – 6.54 (m, 2H), 6.54 – 6.45 (m, 2H), 3.52 (dtd, J = 15.3, 6.3, 2.9 Hz, 3H), 3.32 (dd, J = 10.7, 2.9 Hz, 1H), 3.04 (dd, J = 10.7, 8.2 Hz, 1H), 1.19 (d, J = 6.3 Hz, 3H) ppm.

^{13}C NMR (75 MHz, CDCl_3 , 296 K): δ = 133.67, 133.28, 118.81, 118.80, 114.58, 114.54, 110.63, 48.36, 45.83, 20.02 ppm.

Yield: 83 % (24.6 mg) as a brown solid.

The spectroscopic data match those reported in literature.^[18] (CAS Number: 6640-55-7)

Piperidine (18)



MW ($\text{C}_5\text{H}_{11}\text{N}$) = 85.15 g/mol (M)

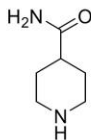
^1H NMR (300 MHz, CDCl_3 , 296 K): δ = 2.82 – 2.70 (m, 4H), 1.59 – 1.43 (m, 6H), 1.39 (s, 1H) ppm.

^{13}C NMR (75 MHz, CDCl_3 , 296 K): δ = 47.55, 27.30, 25.21 ppm.

Yield: 85 % (14.5 mg) as a transparent liquid.

The spectroscopic data match those reported in literature.^[19] (CAS Number: 110-89-4)

Piperidine-4-carboxamide (19)



MW (C₆H₁₂N₂O) = 128.18 g/mol (M)

¹H NMR (300 MHz, CDCl₃, 296 K): δ = 7.17 (s, 1H), 6.67 (s, 1H), 2.90 (d, J = 12.1 Hz, 3H), 2.40 (t, J = 11.9 Hz, 2H), 2.11 (ddd, J = 15.0, 7.9, 3.4 Hz, 1H), 1.64 – 1.48 (m, 2H), 1.37 (qd, J = 12.1, 3.9 Hz, 2H) ppm.

¹³C NMR (75 MHz, CDCl₃, 296 K): δ = 176.91, 45.71, 42.50, 29.54 ppm.

Yield: 92 % (23.6 mg) as a white solid.

The spectroscopic data match those reported in literature.^[20] (CAS Number: 39546-32-2)

Pyrrolidine (20)



MW (C₄H₉N) = 71.12 g/mol (M)

¹H NMR (300 MHz, CDCl₃, 296 K): δ = 2.79 (t, J = 5.0 Hz, 4H), 1.70 – 1.52 (m, 4H), 1.45 (s, 1H) ppm.

¹³C NMR (75 MHz, CDCl₃, 296 K): δ = 47.21, 25.60 ppm.

Yield: 61 % (8.7 mg) as a transparent fluid.

The spectroscopic data match those reported in literature.^[21] (CAS Number: 123-75-1)

2-Methylpyrrolidine (21)



MW (C₅H₁₁N) = 85.15 g/mol (M)

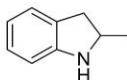
¹H NMR (300 MHz, CDCl₃, 296 K): δ = 3.06 – 2.95 (m, 2H), 2.77 (ddd, J = 10.7, 8.1, 7.0 Hz, 1H), 1.90 – 1.60 (m, 4H), 1.59 (s, 1H), 1.10 (d, J = 6.2 Hz, 3H) ppm.

¹³C NMR (75 MHz, CDCl₃, 296 K): δ = 54.63, 46.86, 33.80, 25.82, 21.32 ppm.

Yield: 74 % (12.6 mg) as a transparent fluid.

The spectroscopic data match those reported in literature.^[22] (CAS Number: 765-38-8)

2-Methylindoline (22)



MW (C₉H₁₁N) = 133.19 g/mol (M)

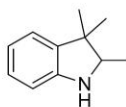
¹H NMR (300 MHz, CDCl₃, 296 K): δ = 7.12 (dd, J = 4.1, 3.7 Hz, 1H), 7.05 (td, J = 7.6, 0.6 Hz, 1H), 6.73 (td, J = 7.4, 0.9 Hz, 1H), 6.63 (d, J = 7.7 Hz, 1H), 4.02 (ddq, J = 8.4, 7.9, 6.2 Hz, 1H), 3.77 (s, 1H), 3.18 (dd, J = 15.4, 8.5 Hz, 1H), 2.67 (dd, J = 15.4, 7.8 Hz, 1H), 1.35 – 1.29 (m, 3H) ppm.

¹³C NMR (75 MHz, CDCl₃, 296 K): δ = 151.04, 128.95, 127.30, 124.78, 118.57, 109.22, 55.28, 37.84, 22.35 ppm.

Yield: 94 % (25.0 mg) as a transparent fluid.

The spectroscopic data match those reported in literature.^[23] (CAS Number: 6872-06-6)

2,3,3-Trimethylindoline (23)



MW (C₁₁H₁₅N) = 161.25 g/mol (M)

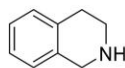
¹H NMR (300 MHz, CDCl₃, 296 K): δ = 7.05 – 7.00 (m, 2H), 6.74 (dd, J = 10.6, 4.1 Hz, 1H), 6.63 (dd, J = 7.3, 0.8 Hz, 1H), 3.72 (s, 1H), 3.52 (q, J = 6.5 Hz, 1H), 1.29 (s, 3H), 1.18 (d, J = 6.5 Hz, 3H), 1.05 (s, 3H) ppm.

¹³C NMR (75 MHz, CDCl₃, 296 K): δ = 149.41, 139.25, 127.26, 122.37, 118.99, 109.53, 65.26, 43.49, 26.28, 22.48, 15.26 ppm.

Yield: 96 % (31.0 mg) as a yellow oil.

The spectroscopic data match those reported in literature.^[24] (CAS Number: 18781-58-3)

1,2,3,4-Tetrahydroisoquinoline (24)



MW (C₉H₁₁N) = 133.19 g/mol (M)

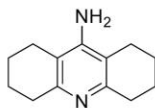
¹H NMR (400 MHz, CDCl₃, 296 K): δ = 7.19 – 6.88 (m, 4H), 4.01 (s, 2H), 3.20 – 3.04 (m, 2H), 2.79 (t, J = 5.9 Hz, 2H), 1.67 (s, 1H) ppm.

¹³C NMR (100 MHz, CDCl₃, 296 K): δ = 136.10, 134.87, 129.38, 126.26, 126.03, 125.75, 48.44, 44.01, 29.29 ppm.

Yield: 87 % (25.9 mg) as a colourless oil.

The spectroscopic data match those reported in literature.^[16] (CAS Number: 91-21-4)

1,2,3,4,5,6,7,8-Octahydroacridine-9-amine (25)



MW (C₁₃H₁₈N₂) = 202.30 g/mol (M)

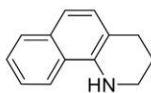
¹H NMR (300 MHz, CDCl₃, 296 K): δ = 5.18 (s, 1H), 2.55 (d, *J* = 5.5 Hz, 4H), 2.32 (d, *J* = 5.6 Hz, 4H), 1.78 – 1.61 (m, 8H) ppm.

¹³C NMR (75 MHz, CDCl₃, 296 K): δ = 152.27, 150.17, 112.21, 32.73, 23.48, 23.24, 23.01 ppm.

Yield: 97 % (39.2 mg) as a white solid.

The spectroscopic data match those reported in literature.^[25] (CAS Number: 13415-07-1)

1,2,3,4-Tetrahydrobenzo[*h*]quinoline (26)



MW (C₁₃H₁₃N) = 183.25 g/mol (M)

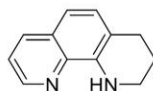
¹H NMR (300 MHz, DMSO-*d*₆, 296 K): δ = 8.66 (dd, *J* = 4.1, 1.7 Hz, 1H), 8.11 (dd, *J* = 8.3, 1.5 Hz, 1H), 7.41 – 7.36 (m, 1H), 7.04 (dd, *J* = 53.7, 8.2 Hz, 3H), 6.40 (s, 1H), 3.41 (s, 2H), 2.82 (d, *J* = 6.3 Hz, 2H), 1.93 – 1.89 (m, 2H) ppm.

¹³C NMR (75 MHz, DMSO-*d*₆, 296 K): δ = 146.73, 140.70, 136.77, 135.70, 128.98, 127.03, 120.75, 115.46, 112.11, 109.53, 40.67, 26.69, 21.19 ppm.

Yield: 78 % (28.6 mg).

The spectroscopic data match those reported in literature.^[13] (CAS Number: 5223-80-3)

1,2,3,4-Tetrahydro-1,10-phenanthroline (27)



MW ($C_{12}H_{12}N_2$) = 184.24 g/mol (M)

1H NMR (300 MHz, DMSO- d_6 , 296 K): δ = 8.66 (dd, J = 4.1, 1.7 Hz, 1H), 8.11 (dd, J = 8.3, 1.5 Hz, 1H), 7.38 (dd, J = 8.2, 4.1 Hz, 1H), 7.12 (d, J = 8.2 Hz, 1H), 6.94 (d, J = 8.2 Hz, 1H), 6.39 (s, 1H), 3.44 – 3.38 (m, 2H), 2.83 (t, J = 6.3 Hz, 2H), 1.97 – 1.82 (m, 2H) ppm.

^{13}C NMR (75 MHz, DMSO- d_6 , 296 K): δ = 146.73, 140.70, 136.77, 135.70, 128.98, 127.03, 120.75, 115.46, 112.11, 40.67, 26.69, 21.19 ppm.

Yield: 81 % (29.8 mg).

The spectroscopic data match those reported in literature.^[11] (CAS Number: 3188-84-9)

2,3-Dihydrobenzofuran (28)



MW (C_8H_8O) = 120.15 g/mol (M)

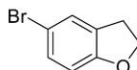
1H NMR (300 MHz, $CDCl_3$, 296 K): δ = 7.22 (d, J = 7.3 Hz, 1H), 7.14 (t, J = 7.7 Hz, 1H), 6.85 (dd, J = 17.5, 7.7 Hz, 2H), 4.58 (dd, J = 12.5, 4.9 Hz, 2H), 3.23 (t, J = 8.7 Hz, 2H) ppm.

^{13}C NMR (75 MHz, $CDCl_3$, 296 K): δ = 160.09, 128.01, 126.96, 124.99, 120.41, 109.44, 71.09, 29.84 ppm.

Yield: 96 % (23.1 mg) as a colourless liquid.

The spectroscopic data match those reported in literature.^[26] (CAS Number: 496-16-2)

5-Bromo-2,3-Dihydrobenzofuran (29)



MW (C_8H_7BrO) = 199.05 g/mol (M)

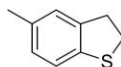
1H NMR (300 MHz, $CDCl_3$, 296 K): δ = 7.17 (dd, J = 8.4, 2.3 Hz, 2H), 6.67 (d, J = 3.2 Hz, 1H), 4.57 (t, J = 8.7 Hz, 2H), 3.20 (t, J = 8.7 Hz, 2H) ppm.

^{13}C NMR (75 MHz, $CDCl_3$, 296 K): δ = 160.52, 128.44, 127.39, 125.42, 120.84, 109.87, 71.52, 30.27 ppm.

Yield: 69 % (27.6 mg) as a white solid.

The spectroscopic data match those reported in literature.^[27] (CAS Number: 66826-78-6)

5-Methyl-2,3-Dihydrobenzothiophene (30)



MW ($C_9H_{10}S$) = 150.24 g/mol (M)

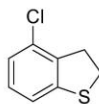
1H NMR (300 MHz, $CDCl_3$, 296 K): δ = 7.10 (d, J = 7.8 Hz, 1H), 7.02 (s, 1H), 6.96 – 6.90 (m, 1H), 3.39 – 3.29 (m, 2H), 3.24 (t, J = 7.2 Hz, 2H), 2.28 (s, 3H) ppm.

^{13}C NMR (75 MHz, $CDCl_3$, 296 K): δ = 140.35, 138.05, 133.95, 128.16, 125.46, 121.96, 36.33, 33.65, 21.07 ppm.

Yield: 42 % (12.6 mg) as a colourless liquid.

The spectroscopic data match those reported in literature.^[28] (CAS Number: 14450-23-8)

4-Chloro-2,3-Dihydrobenzothiophene (31)



MW ($\text{C}_8\text{H}_7\text{ClS}$) = 170.65 g/mol (M)

^1H NMR (300 MHz, CDCl_3 , 296 K): δ = 7.07 (m, 1H), 6.82 – 6.74 (m, 2H), 3.13 (d, J = 1.4 Hz, 4H) ppm.

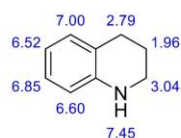
^{13}C NMR (75 MHz, CDCl_3 , 296 K): δ = 138.21, 130.96, 128.79, 125.03, 124.57, 124.30, 35.69, 32.30 ppm.

Yield: 31 % (10.6 mg) as a colourless liquid.

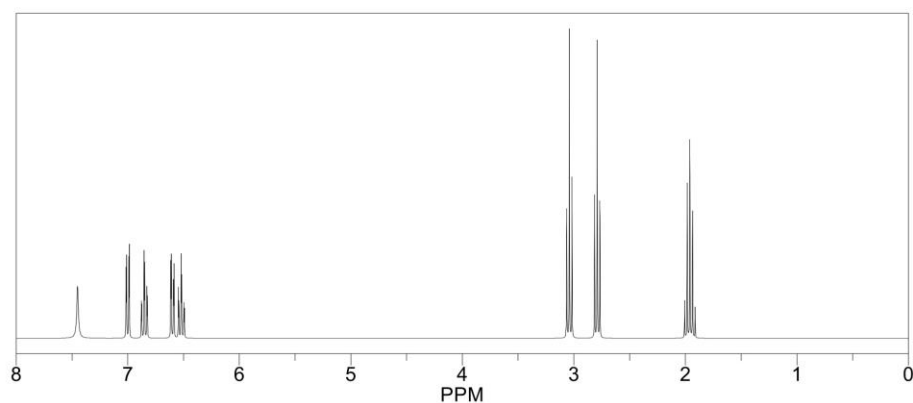
The spectroscopic data match those reported in literature.^[29] (CAS Number: 1309361-57-6)

6 NMR spectra

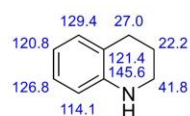
ChemNMR ^1H Estimation



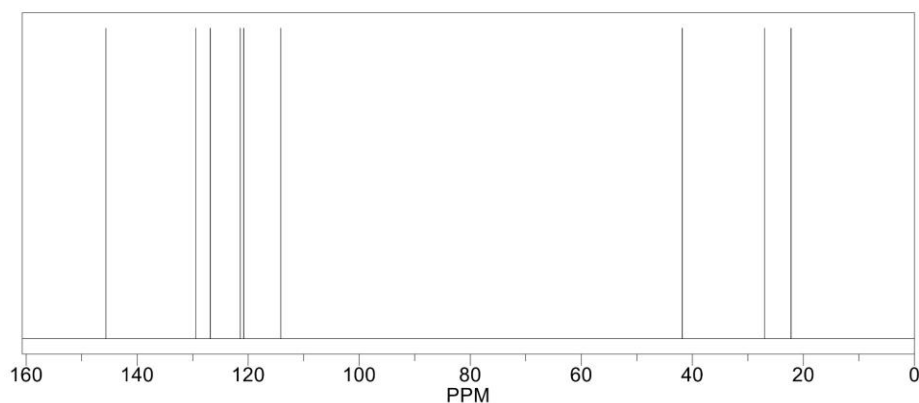
Estimation quality is indicated by color: good, medium, rough



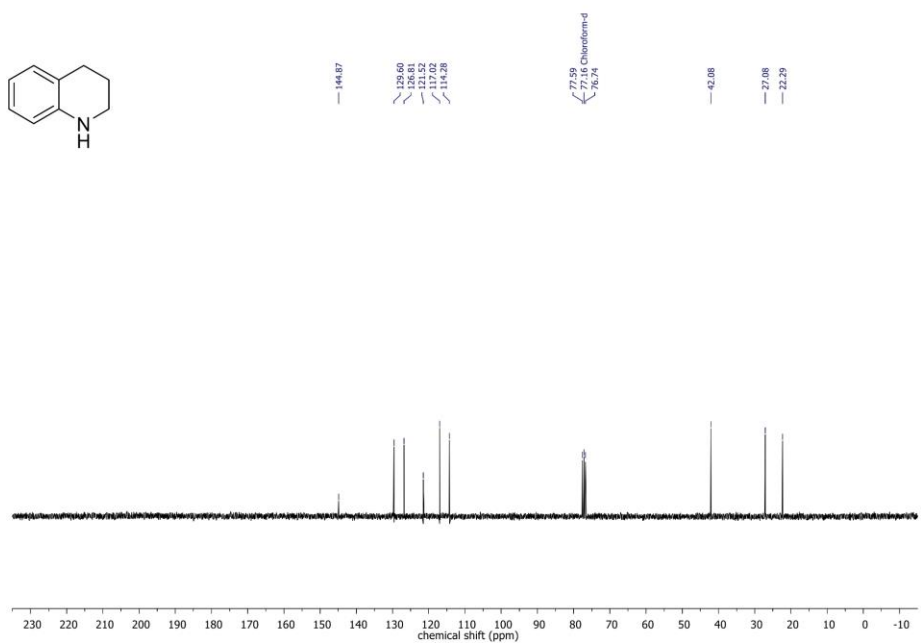
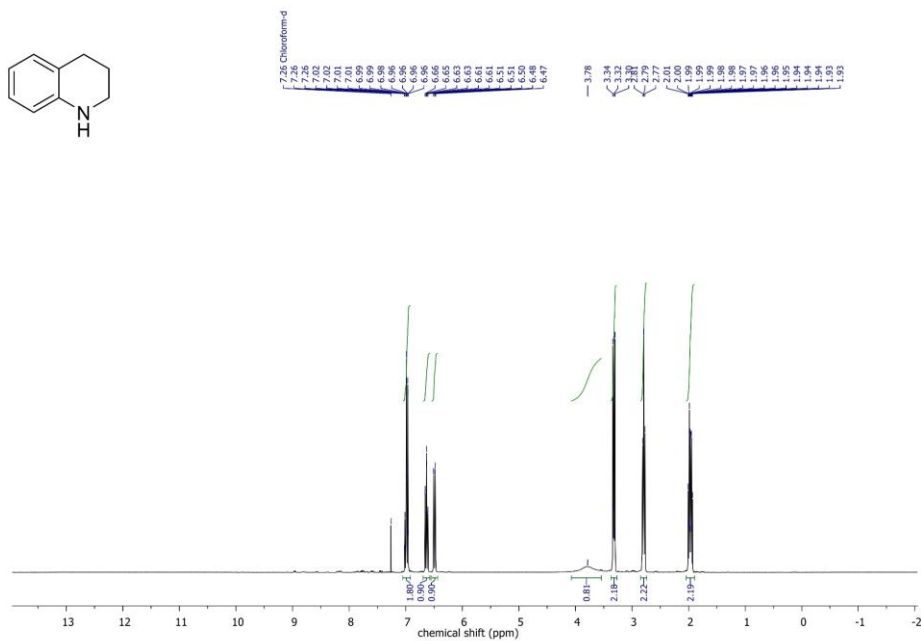
ChemNMR ^{13}C Estimation



Estimation quality is indicated by color: good, medium, rough



A Highly Active Cobalt Catalyst for the General and Selective Hydrogenation of Aromatic Heterocycles

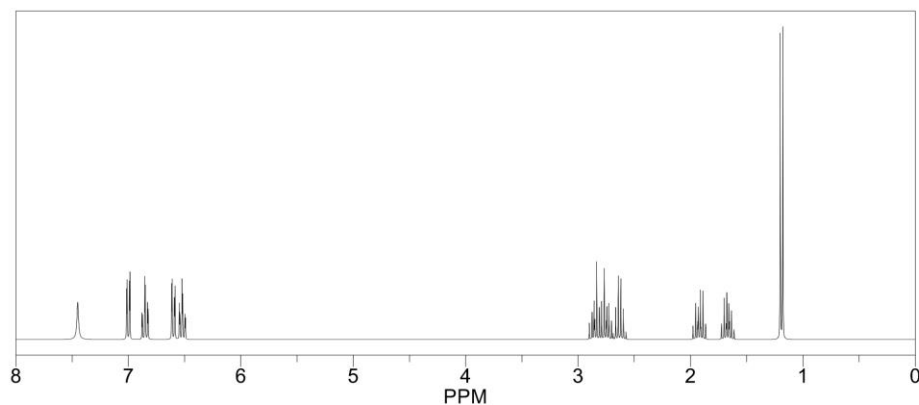


A Highly Active Cobalt Catalyst for the General and Selective Hydrogenation of Aromatic Heterocycles

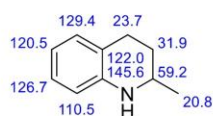
ChemNMR ^1H Estimation



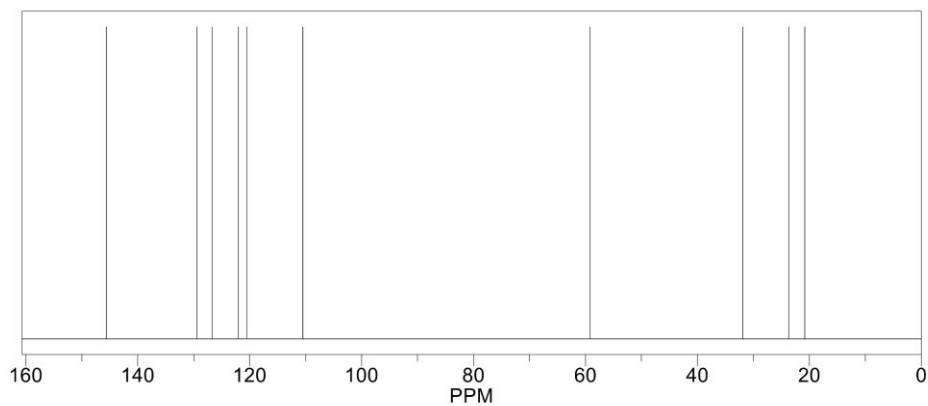
Estimation quality is indicated by color: good, medium, rough



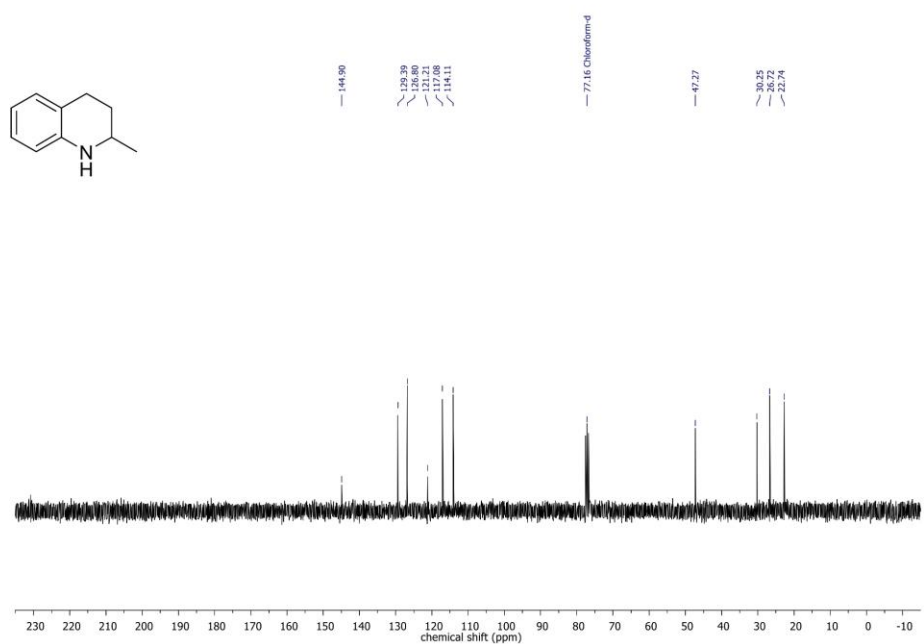
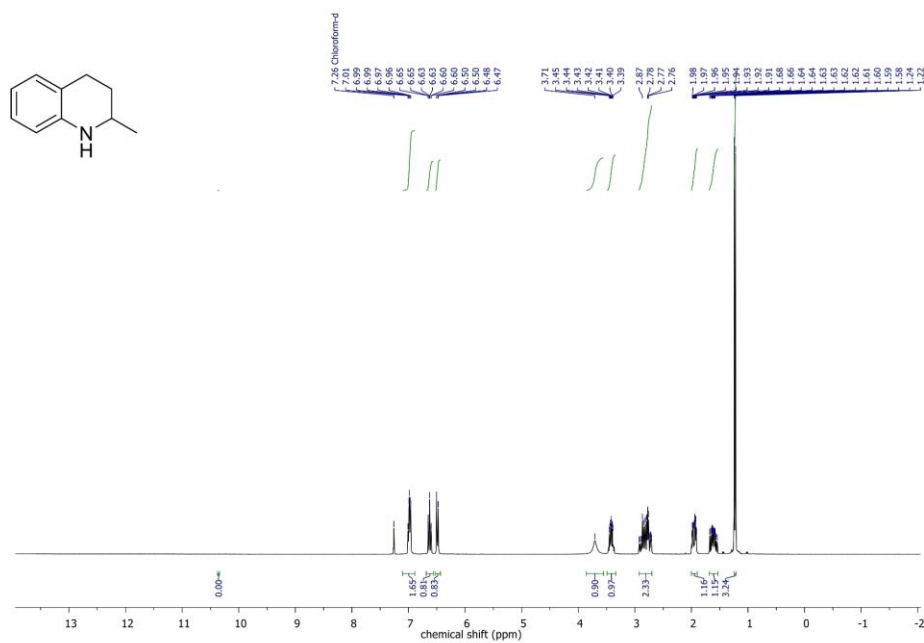
ChemNMR ^{13}C Estimation



Estimation quality is indicated by color: good, medium, rough



A Highly Active Cobalt Catalyst for the General and Selective Hydrogenation of Aromatic Heterocycles

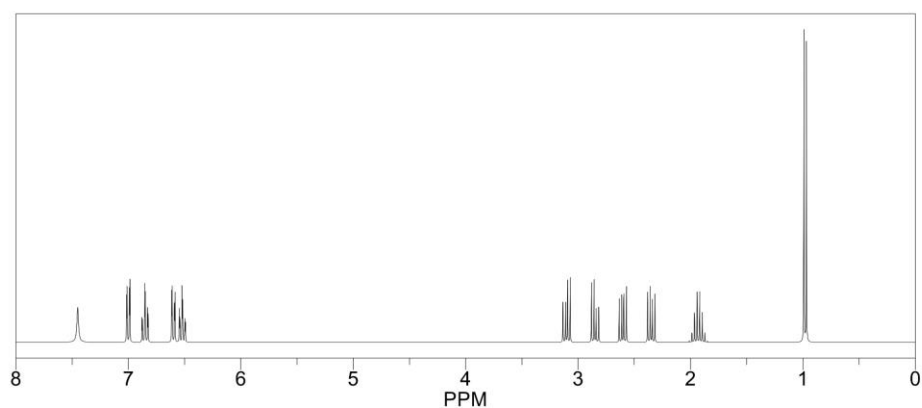


A Highly Active Cobalt Catalyst for the General and Selective Hydrogenation of Aromatic Heterocycles

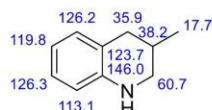
ChemNMR ^1H Estimation



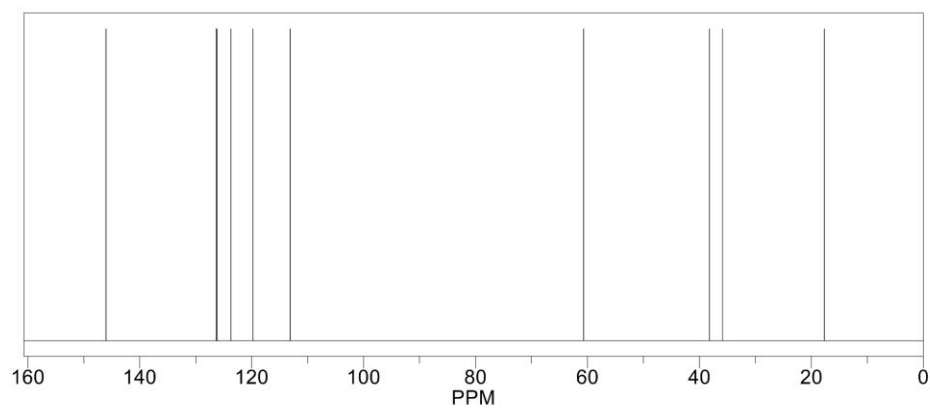
Estimation quality is indicated by color: good, medium, rough



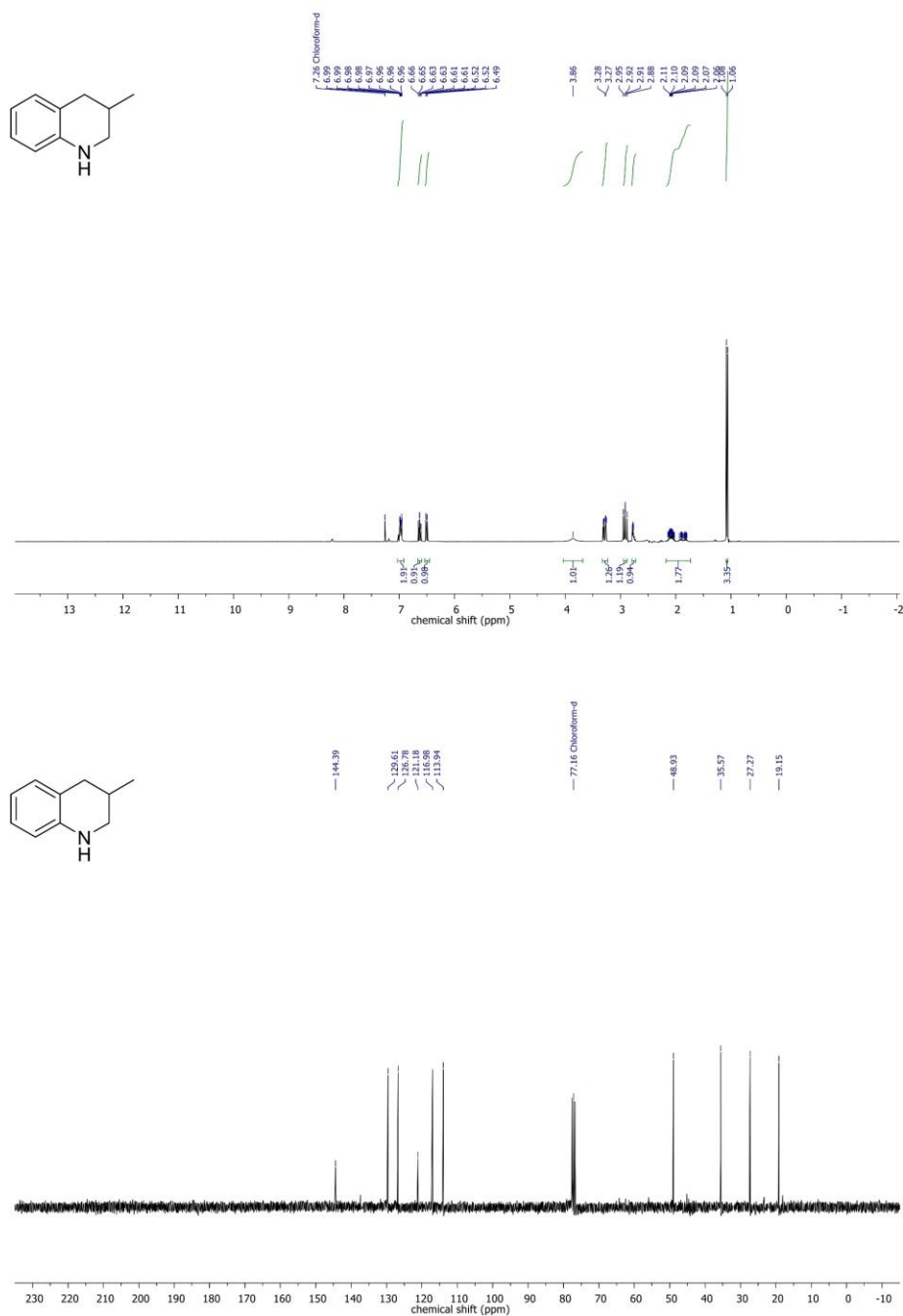
ChemNMR ^{13}C Estimation



Estimation quality is indicated by color: good, medium, rough

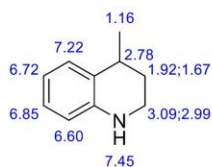


A Highly Active Cobalt Catalyst for the General and Selective Hydrogenation of Aromatic Heterocycles

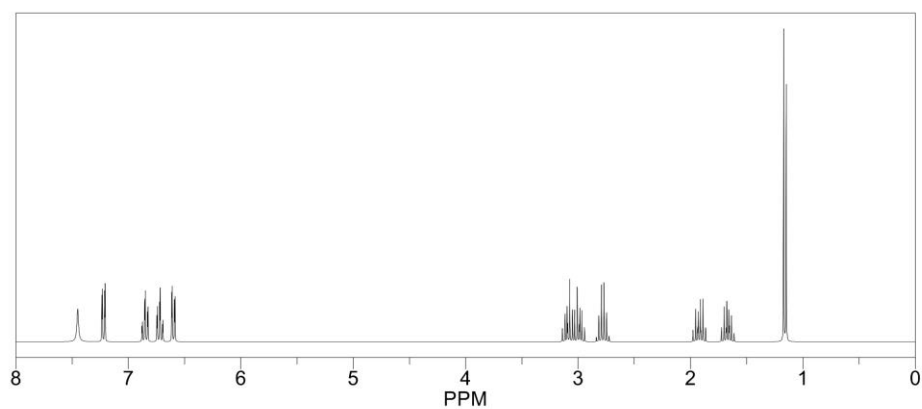


A Highly Active Cobalt Catalyst for the General and Selective Hydrogenation of Aromatic Heterocycles

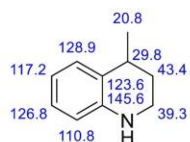
ChemNMR ^1H Estimation



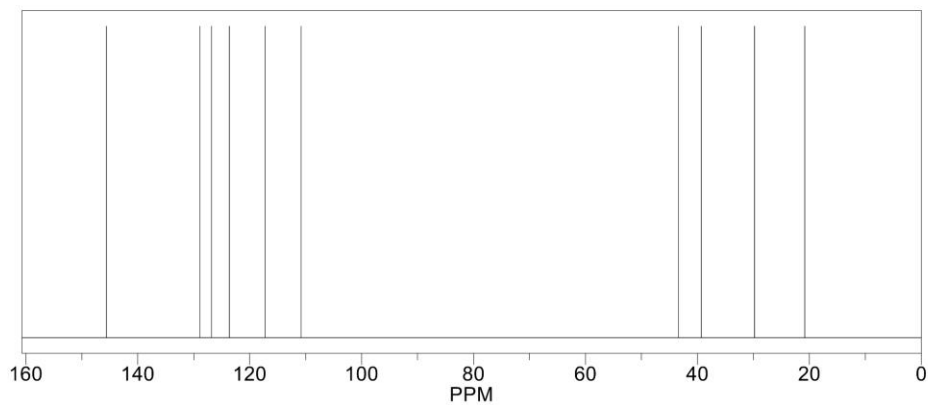
Estimation quality is indicated by color: good, medium, rough



ChemNMR ^{13}C Estimation



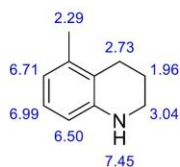
Estimation quality is indicated by color: good, medium, rough



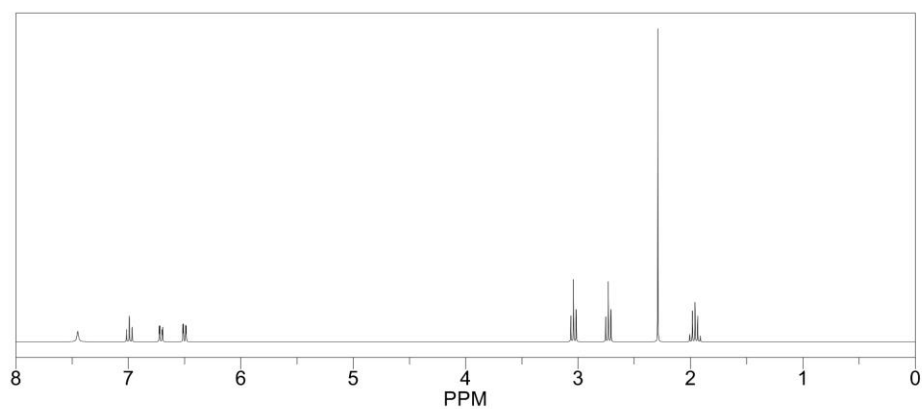


A Highly Active Cobalt Catalyst for the General and Selective Hydrogenation of Aromatic Heterocycles

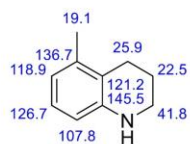
ChemNMR ^1H Estimation



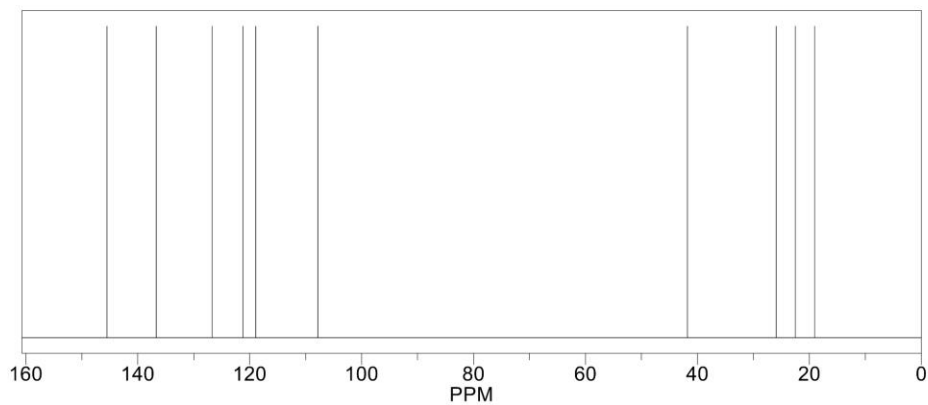
Estimation quality is indicated by color: good, medium, rough



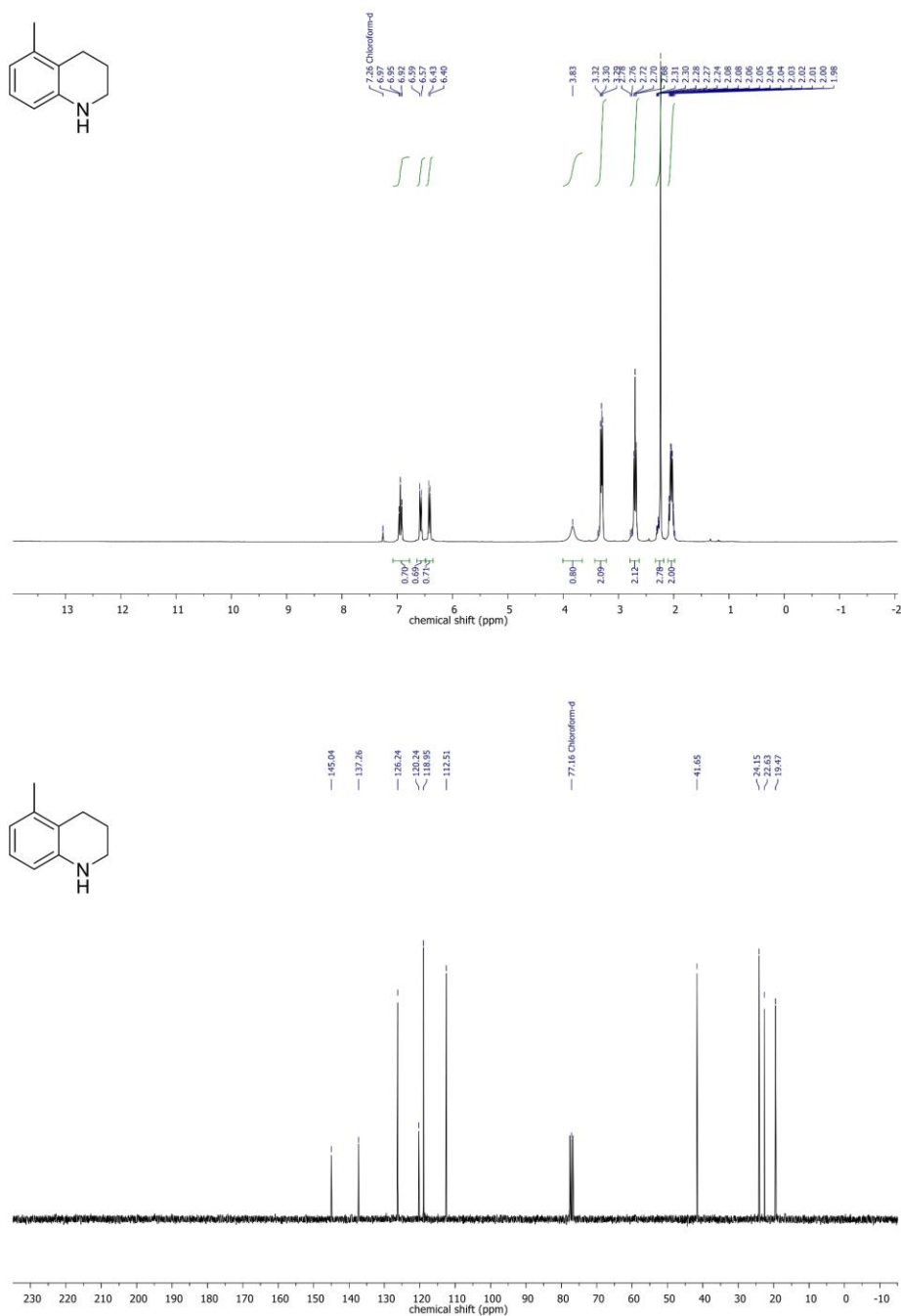
ChemNMR ^{13}C Estimation



Estimation quality is indicated by color: good, medium, rough



A Highly Active Cobalt Catalyst for the General and Selective Hydrogenation of Aromatic Heterocycles

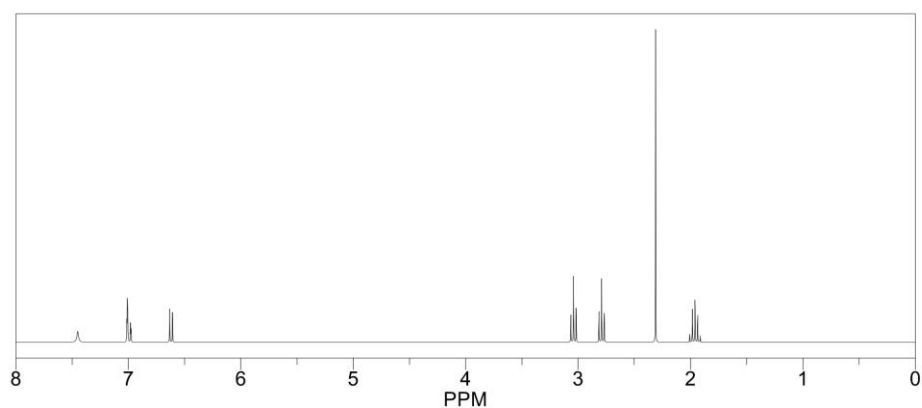


A Highly Active Cobalt Catalyst for the General and Selective Hydrogenation of Aromatic Heterocycles

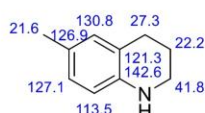
ChemNMR ^1H Estimation



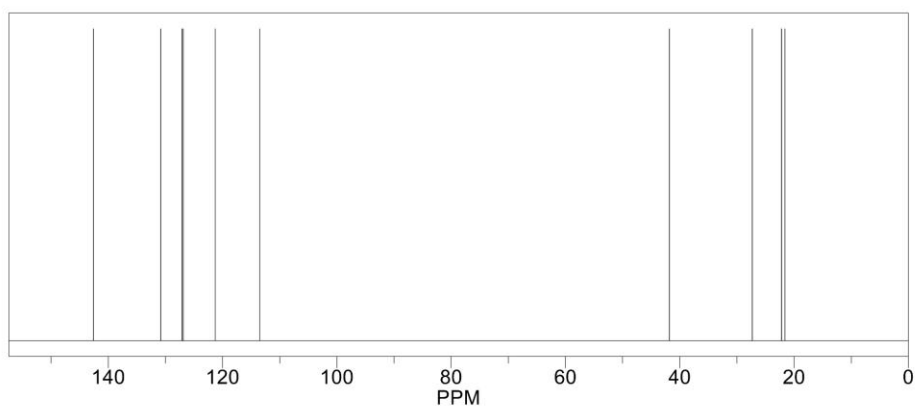
Estimation quality is indicated by color: good, medium, rough



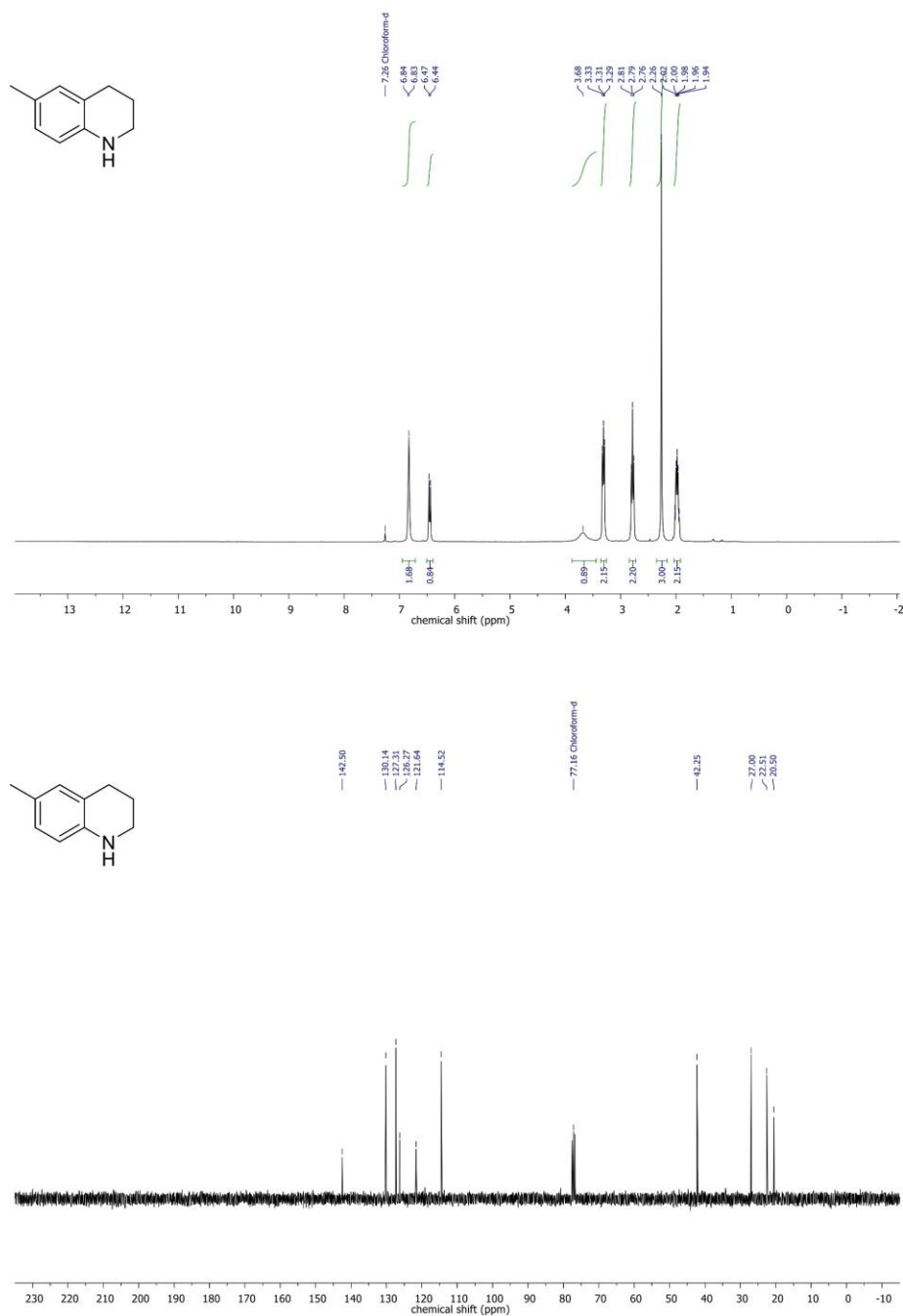
ChemNMR ^{13}C Estimation



Estimation quality is indicated by color: good, medium, rough

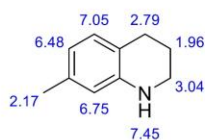


A Highly Active Cobalt Catalyst for the General and Selective Hydrogenation of Aromatic Heterocycles

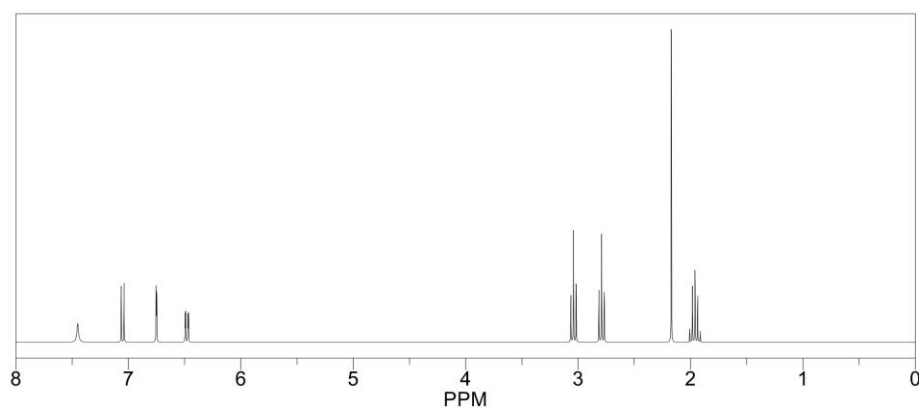


A Highly Active Cobalt Catalyst for the General and Selective Hydrogenation of Aromatic Heterocycles

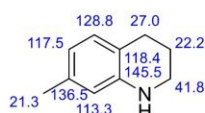
ChemNMR ^1H Estimation



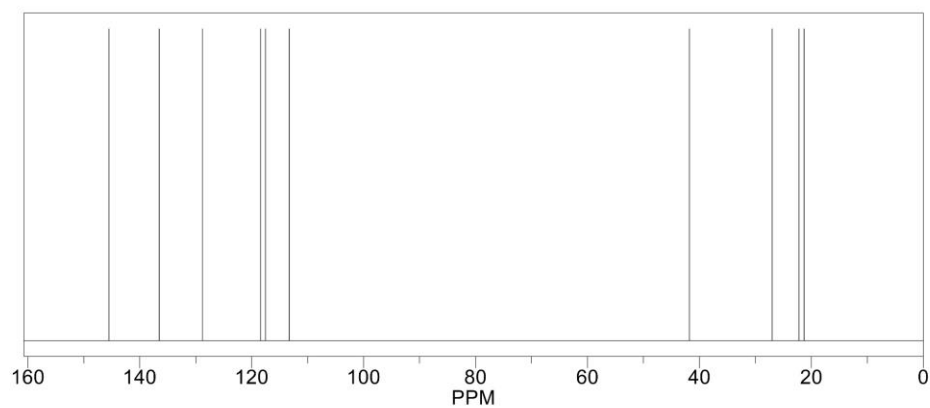
Estimation quality is indicated by color: good, medium, rough



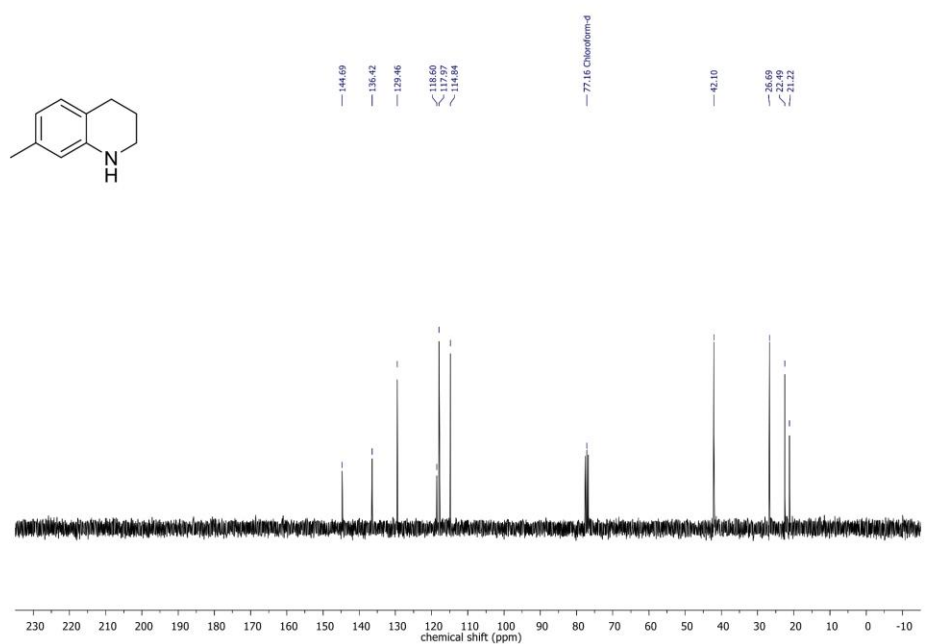
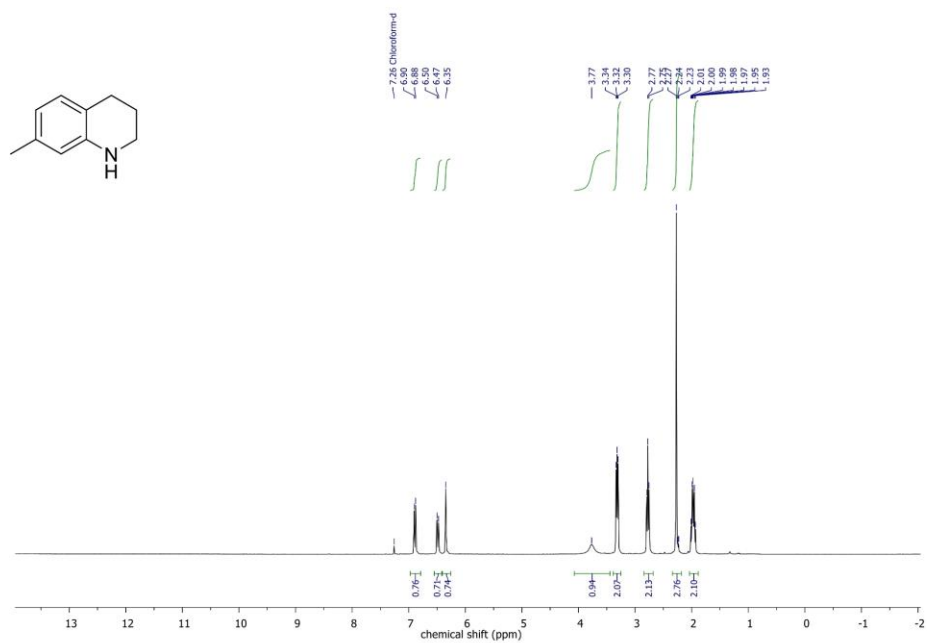
ChemNMR ^{13}C Estimation



Estimation quality is indicated by color: good, medium, rough

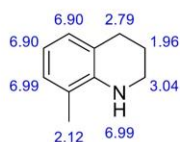


A Highly Active Cobalt Catalyst for the General and Selective Hydrogenation of Aromatic Heterocycles

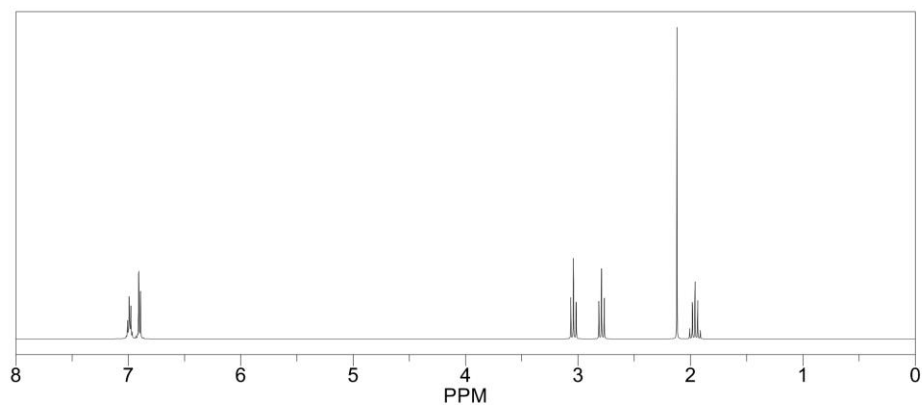


A Highly Active Cobalt Catalyst for the General and Selective Hydrogenation of Aromatic Heterocycles

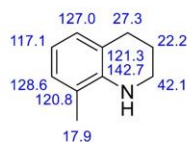
ChemNMR ^1H Estimation



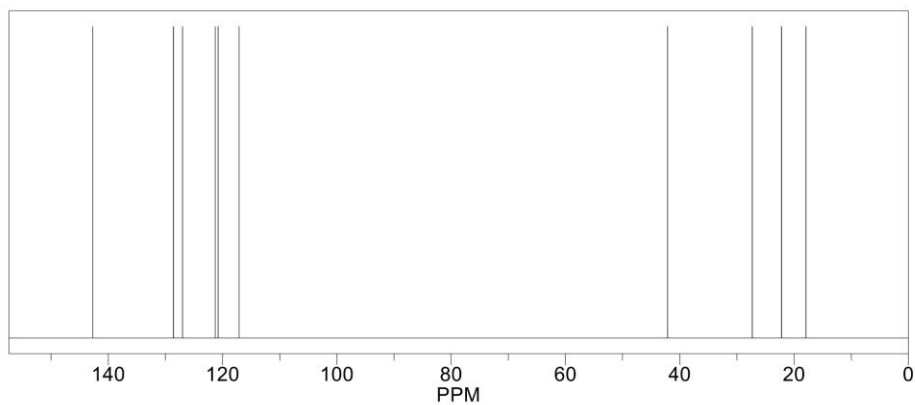
Estimation quality is indicated by color: good, medium, rough



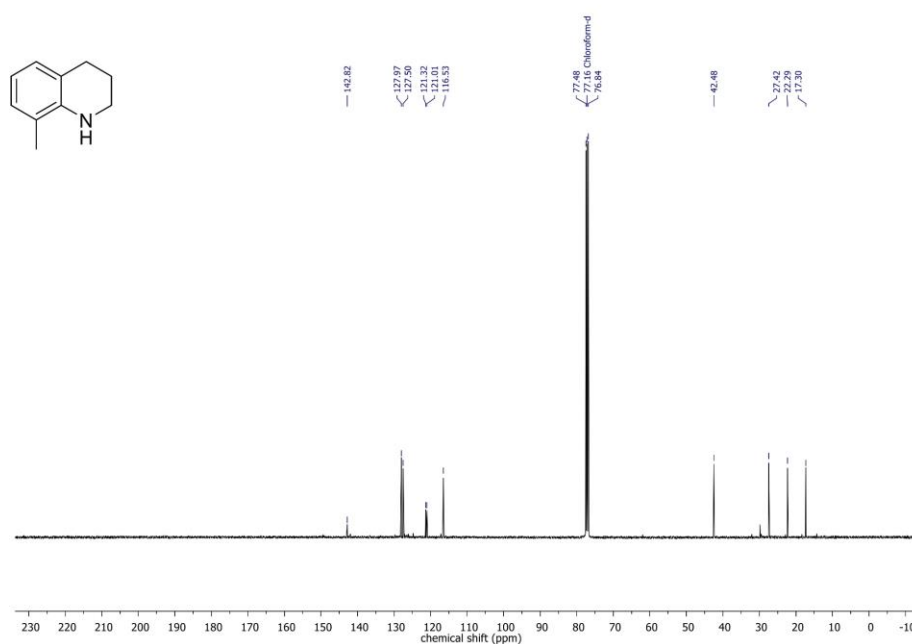
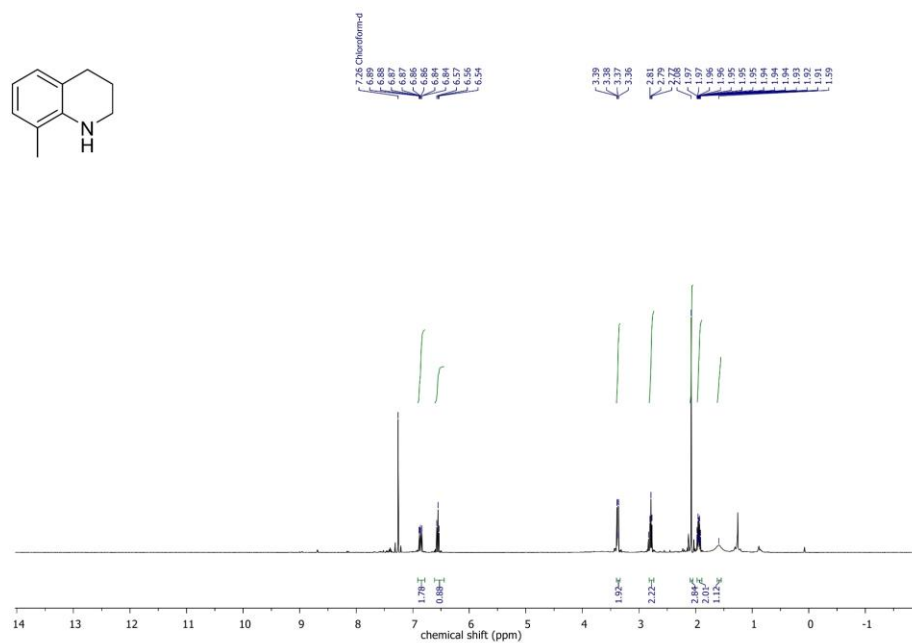
ChemNMR ^{13}C Estimation



Estimation quality is indicated by color: good, medium, rough

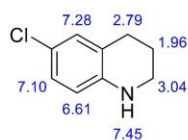


A Highly Active Cobalt Catalyst for the General and Selective Hydrogenation of Aromatic Heterocycles

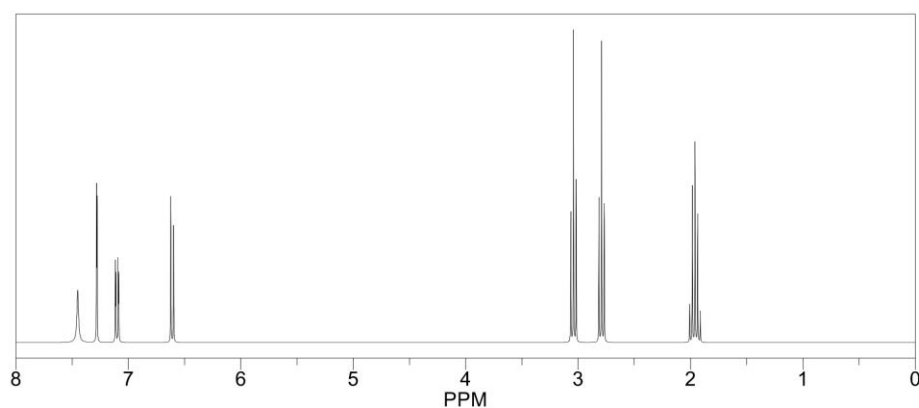


A Highly Active Cobalt Catalyst for the General and Selective Hydrogenation of Aromatic Heterocycles

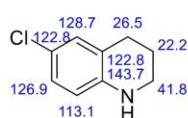
ChemNMR ^1H Estimation



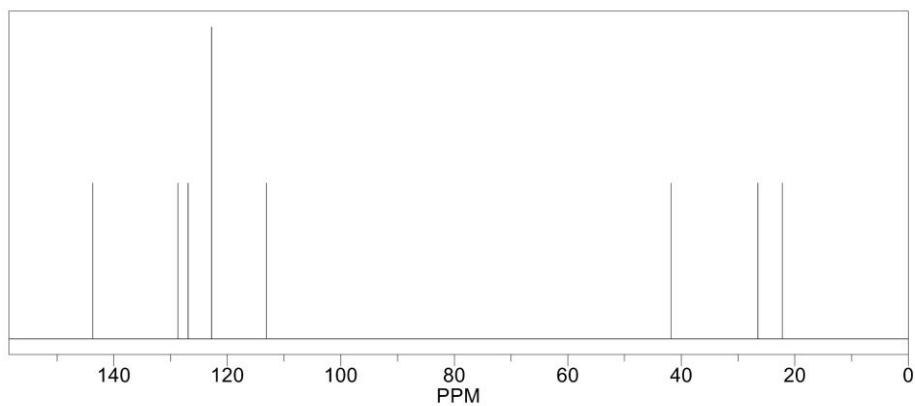
Estimation quality is indicated by color: good, medium, rough



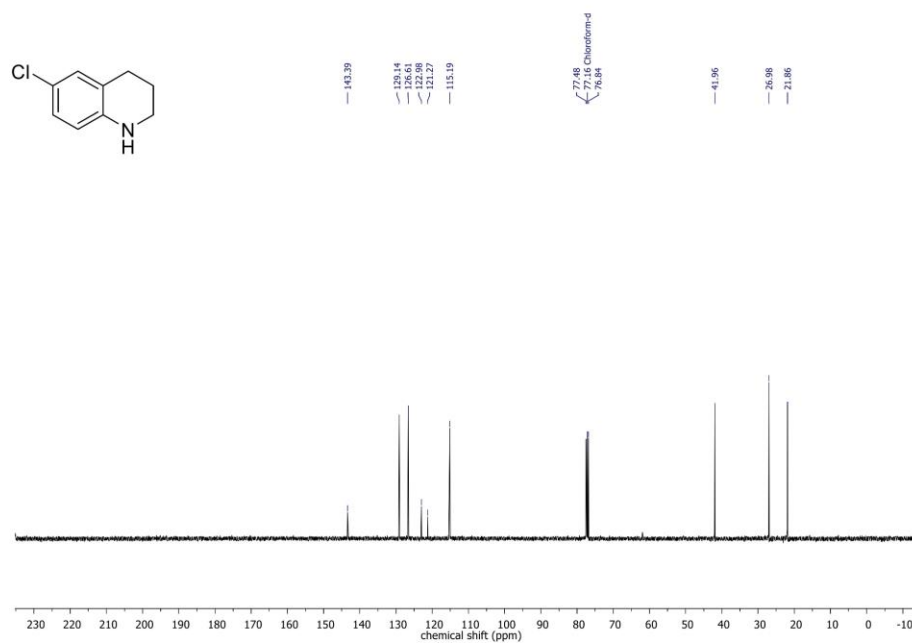
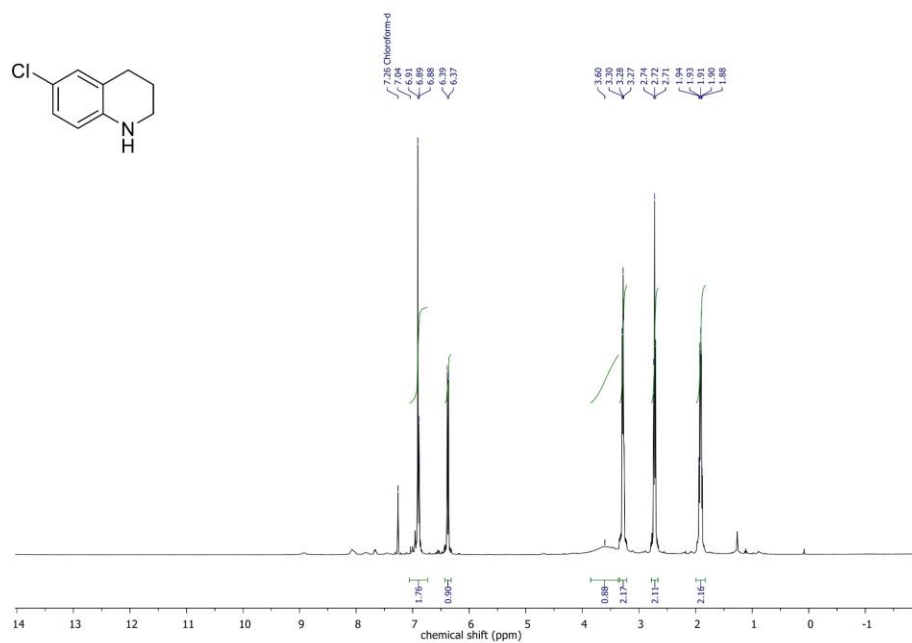
ChemNMR ^{13}C Estimation



Estimation quality is indicated by color: good, medium, rough



A Highly Active Cobalt Catalyst for the General and Selective Hydrogenation of Aromatic Heterocycles

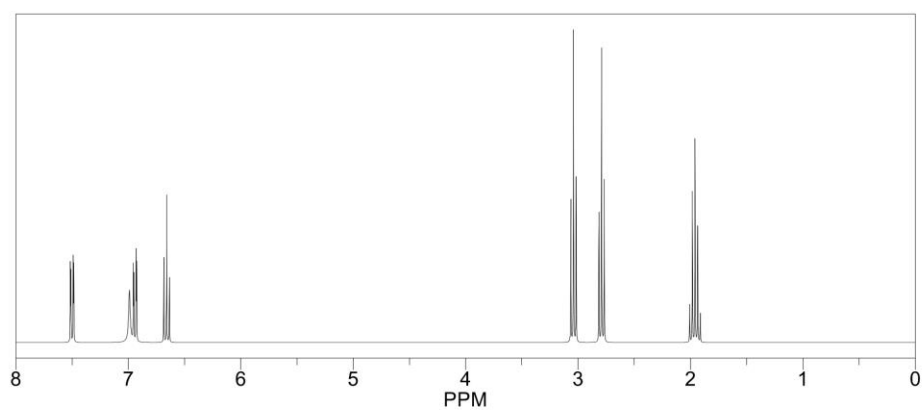


A Highly Active Cobalt Catalyst for the General and Selective Hydrogenation of Aromatic Heterocycles

ChemNMR ^1H Estimation



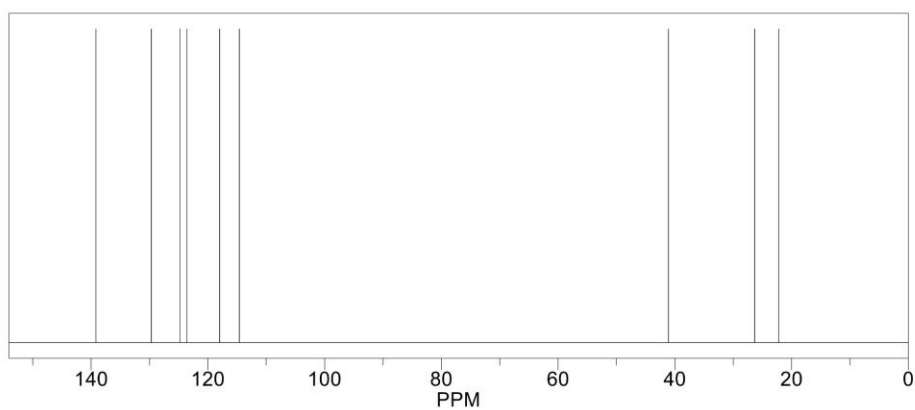
Estimation quality is indicated by color: good, medium, rough



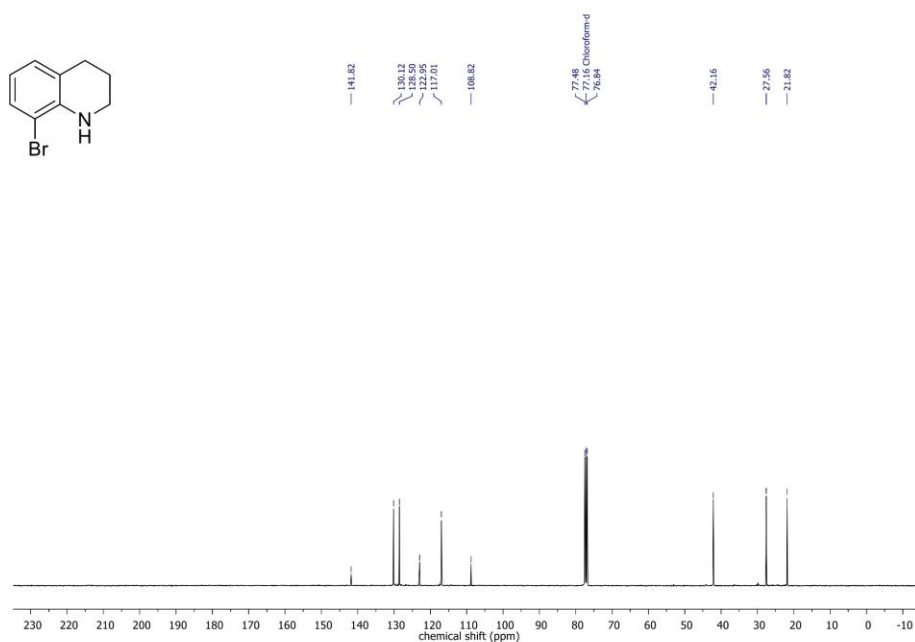
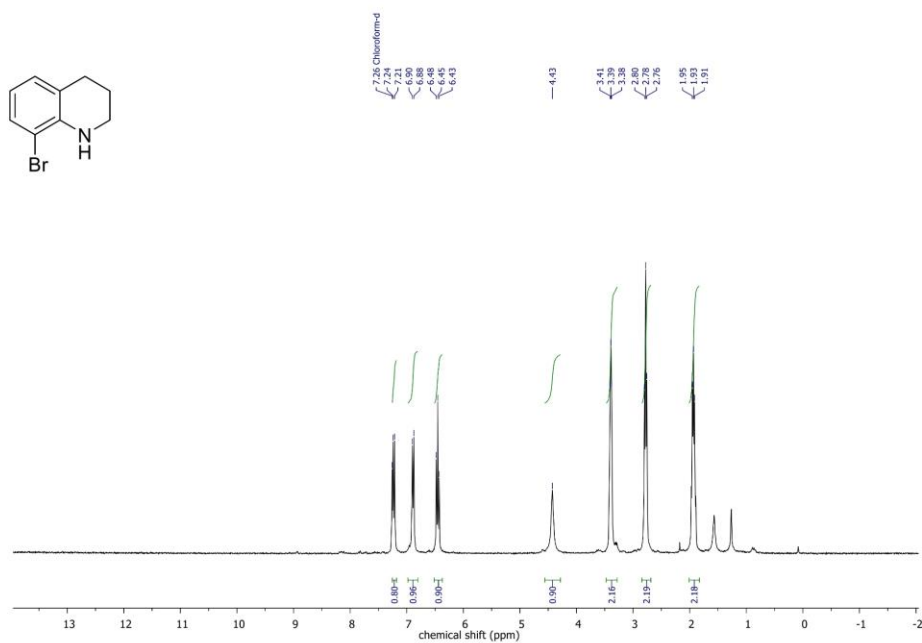
ChemNMR ^{13}C Estimation



Estimation quality is indicated by color: good, medium, rough

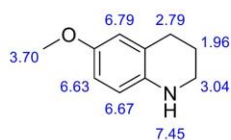


A Highly Active Cobalt Catalyst for the General and Selective Hydrogenation of Aromatic Heterocycles

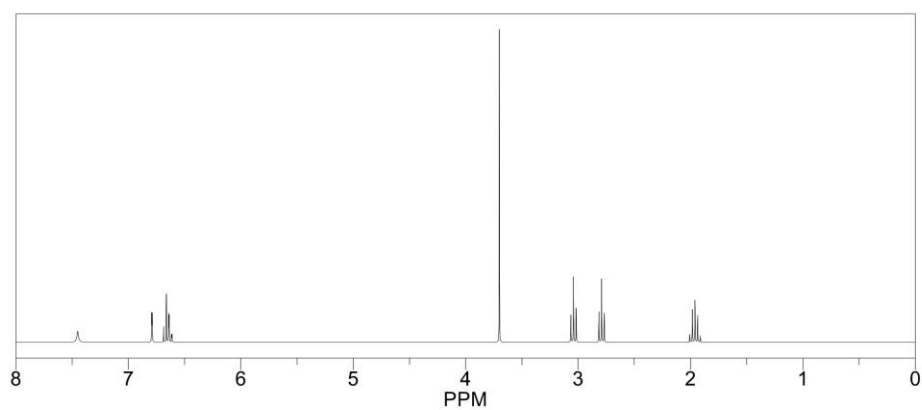


A Highly Active Cobalt Catalyst for the General and Selective Hydrogenation of Aromatic Heterocycles

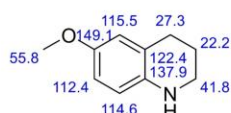
ChemNMR ^1H Estimation



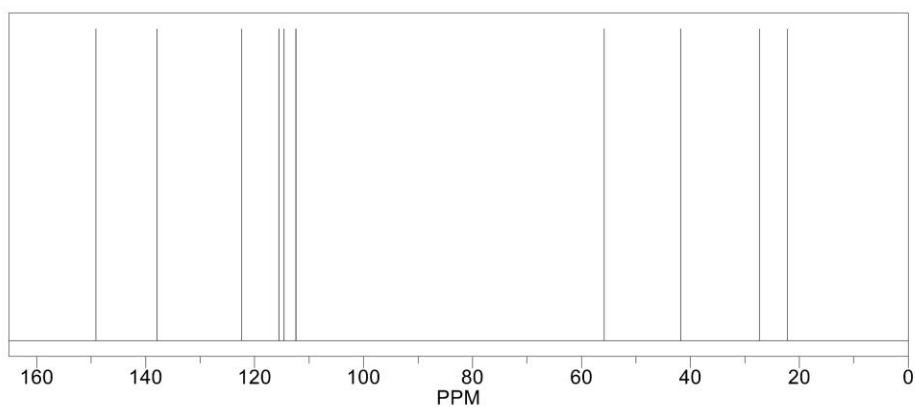
Estimation quality is indicated by color: good, medium, rough



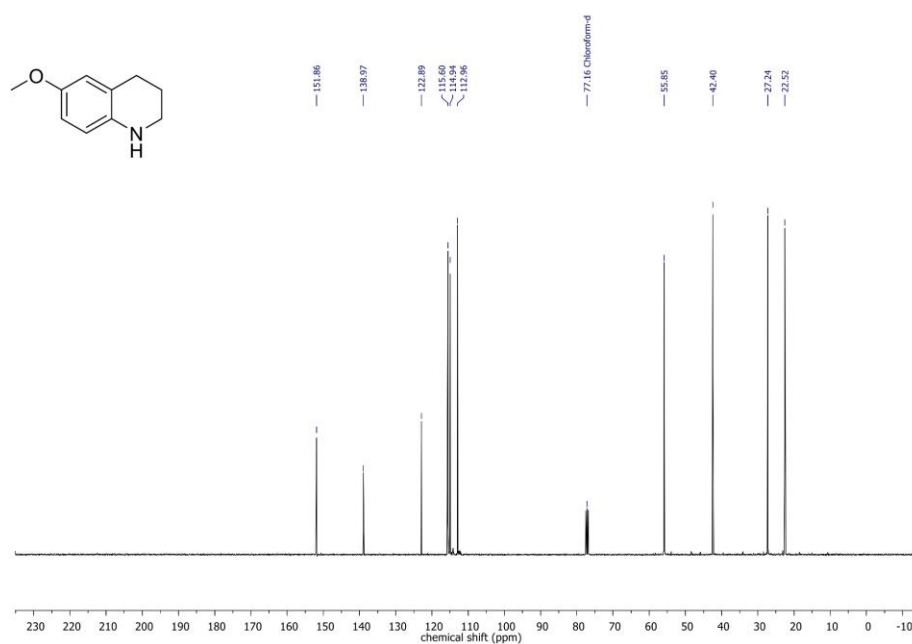
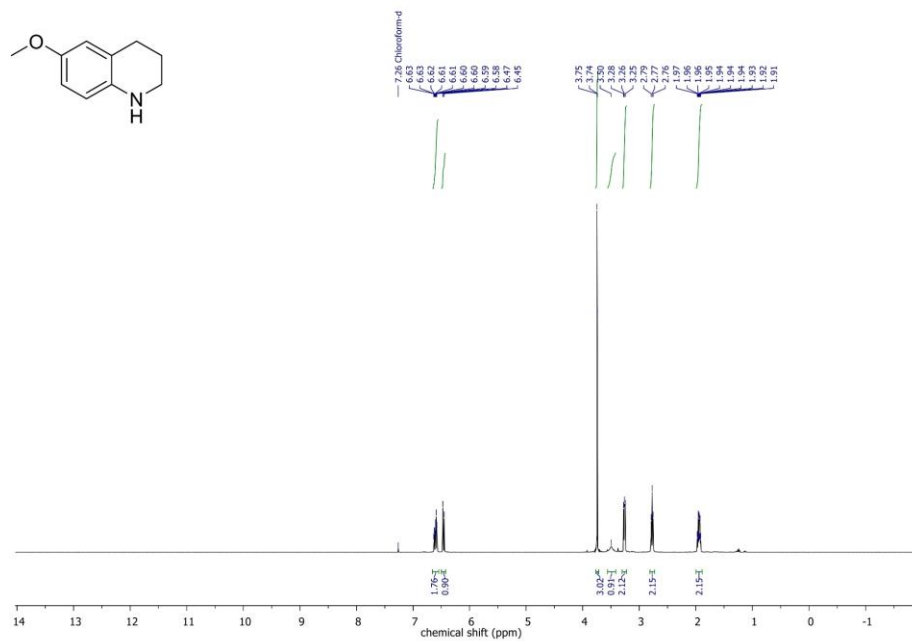
ChemNMR ^{13}C Estimation



Estimation quality is indicated by color: good, medium, rough



A Highly Active Cobalt Catalyst for the General and Selective Hydrogenation of Aromatic Heterocycles

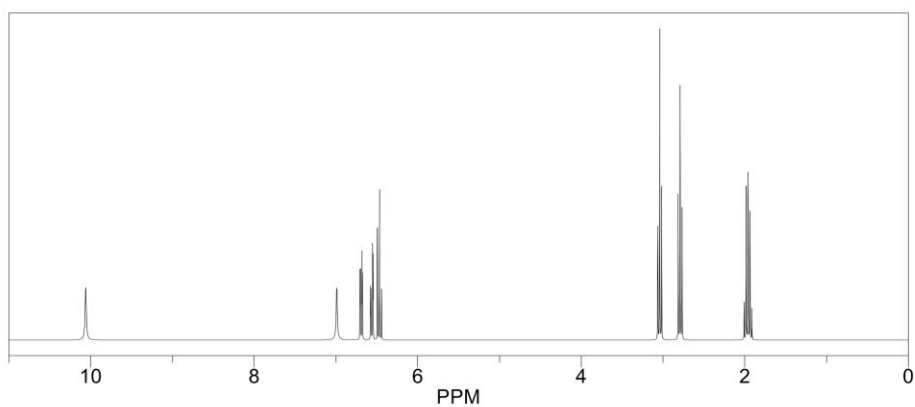


A Highly Active Cobalt Catalyst for the General and Selective Hydrogenation of Aromatic Heterocycles

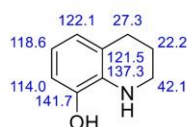
ChemNMR ^1H Estimation



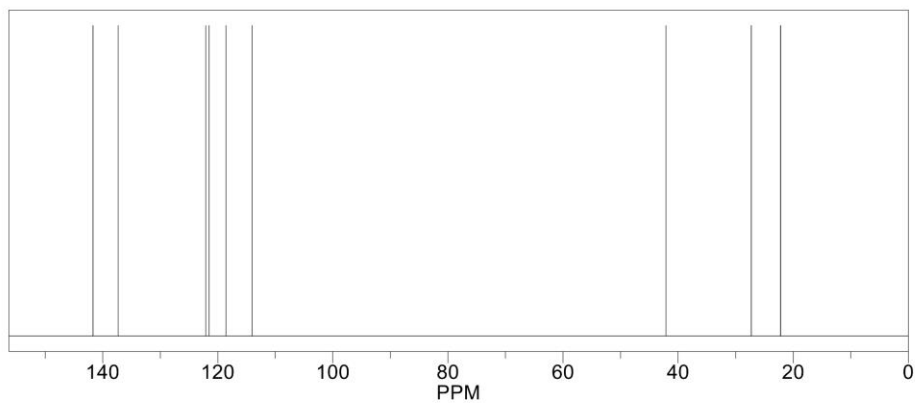
Estimation quality is indicated by color: good, medium, rough



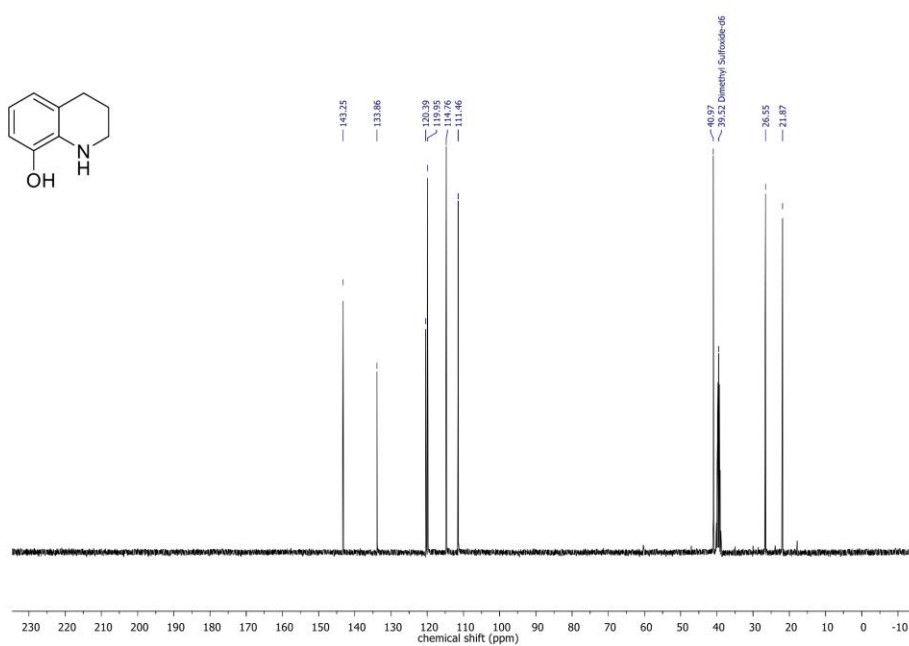
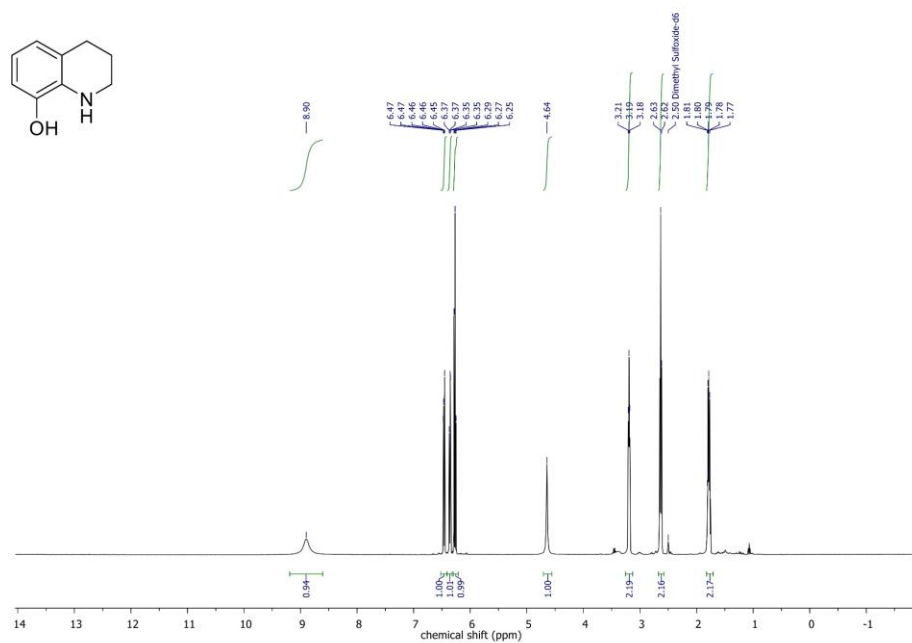
ChemNMR ^{13}C Estimation



Estimation quality is indicated by color: good, medium, rough



A Highly Active Cobalt Catalyst for the General and Selective Hydrogenation of Aromatic Heterocycles

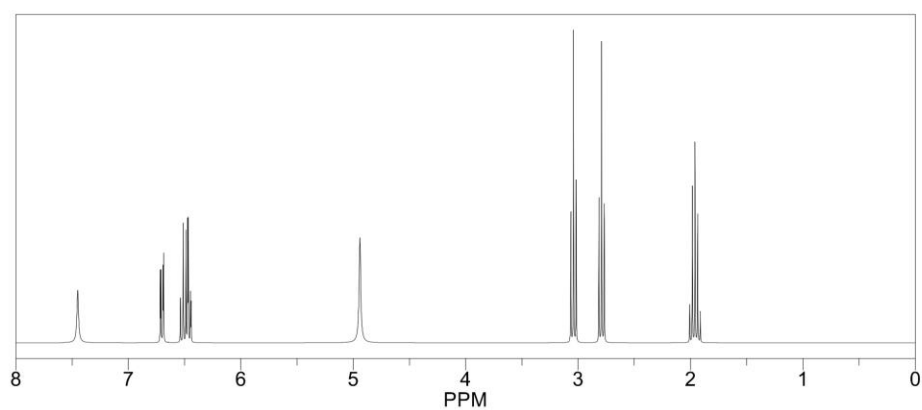


A Highly Active Cobalt Catalyst for the General and Selective Hydrogenation of Aromatic Heterocycles

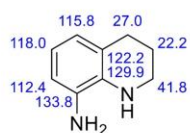
ChemNMR ^1H Estimation



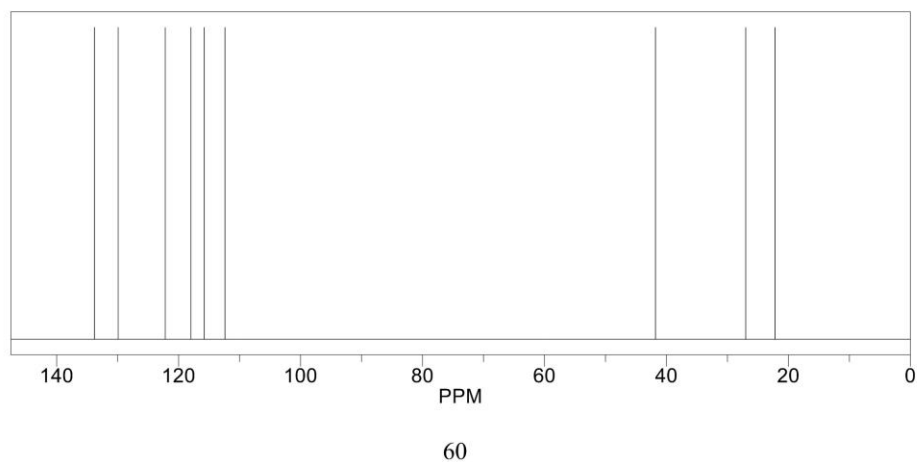
Estimation quality is indicated by color: good, medium, rough



ChemNMR ^{13}C Estimation



Estimation quality is indicated by color: good, medium, rough



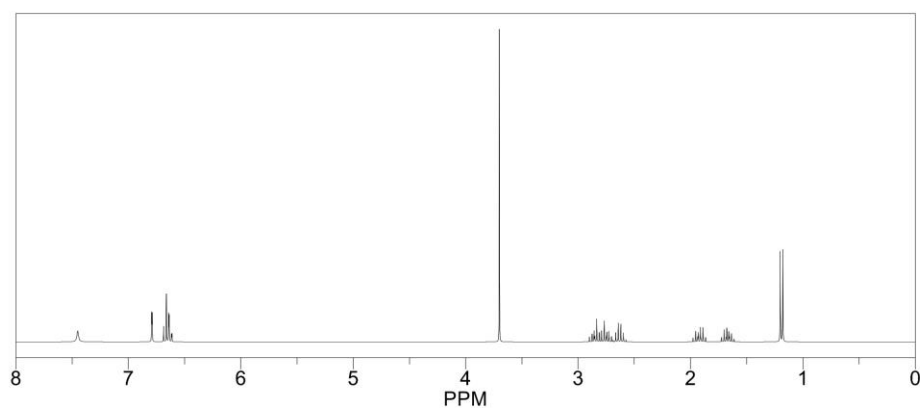


A Highly Active Cobalt Catalyst for the General and Selective Hydrogenation of Aromatic Heterocycles

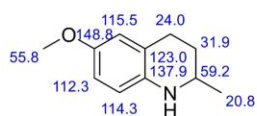
ChemNMR ^1H Estimation



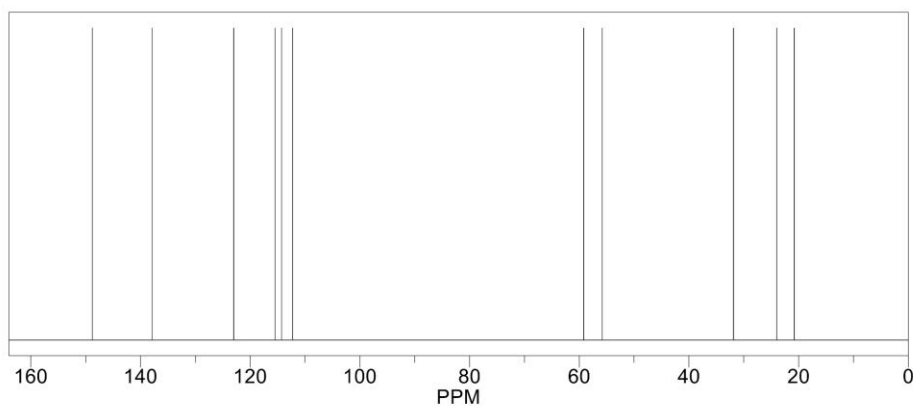
Estimation quality is indicated by color: good, medium, rough



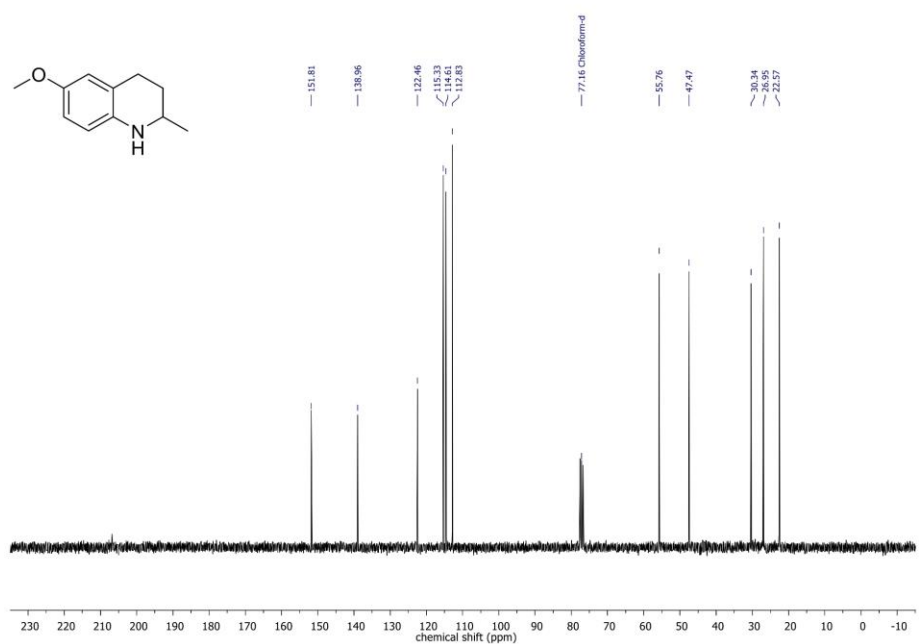
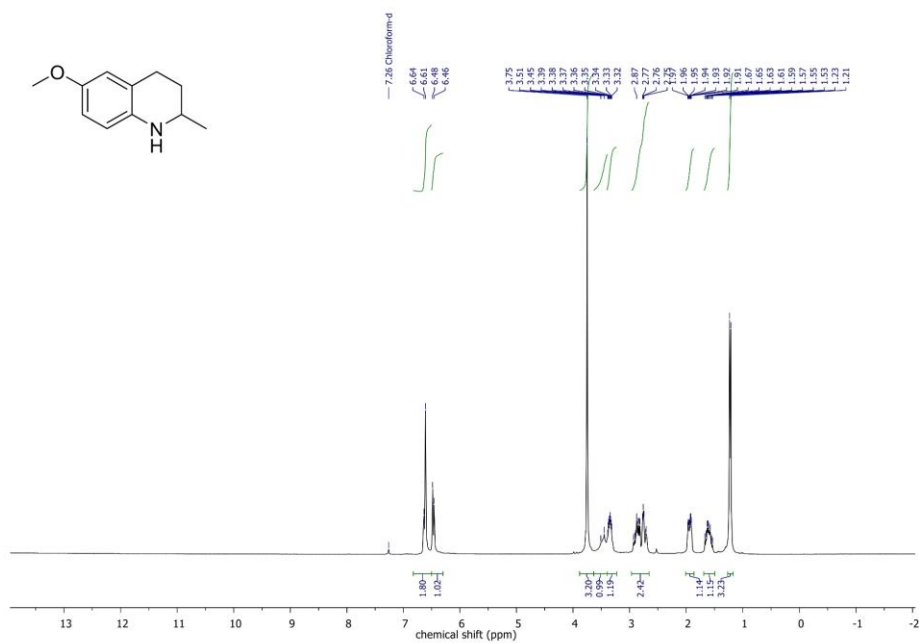
ChemNMR ^{13}C Estimation



Estimation quality is indicated by color: good, medium, rough



A Highly Active Cobalt Catalyst for the General and Selective Hydrogenation of Aromatic Heterocycles

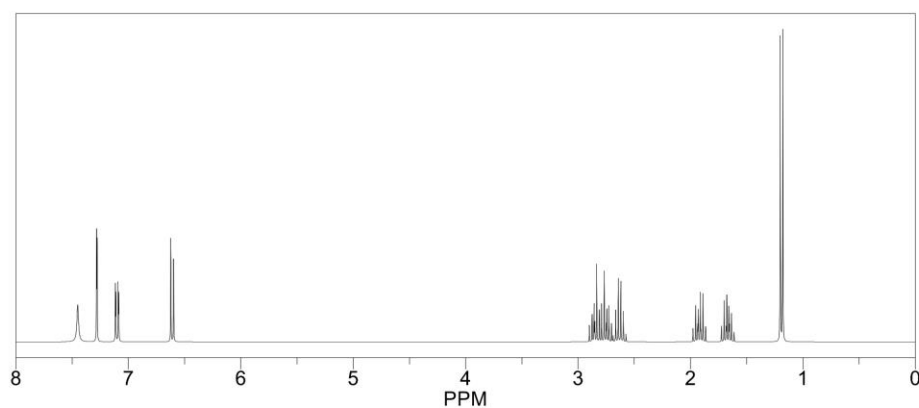


A Highly Active Cobalt Catalyst for the General and Selective Hydrogenation of Aromatic Heterocycles

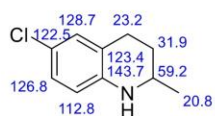
ChemNMR ^1H Estimation



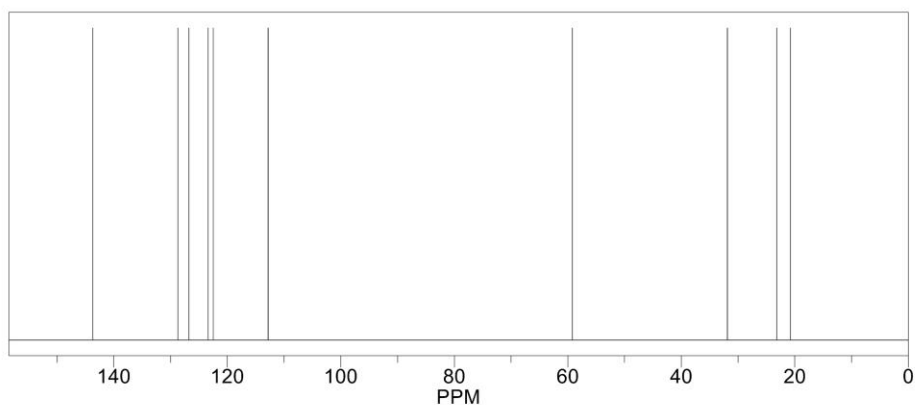
Estimation quality is indicated by color: good, medium, rough



ChemNMR ^{13}C Estimation



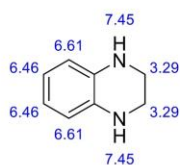
Estimation quality is indicated by color: good, medium, rough



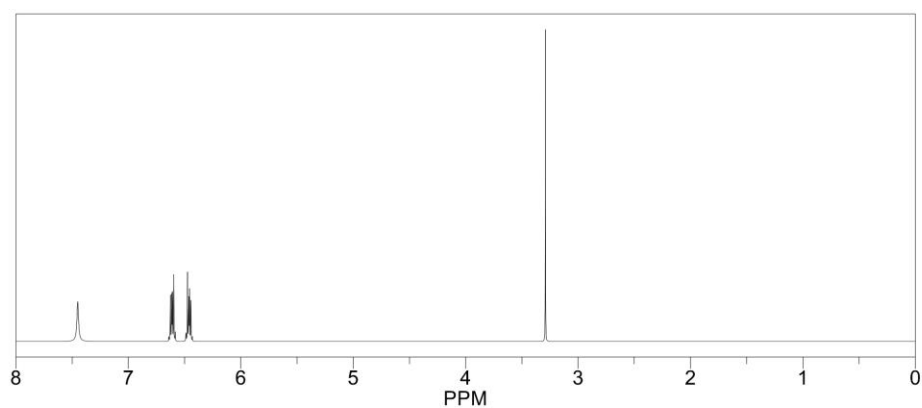


A Highly Active Cobalt Catalyst for the General and Selective Hydrogenation of Aromatic Heterocycles

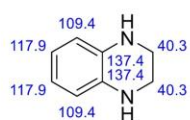
ChemNMR ^1H Estimation



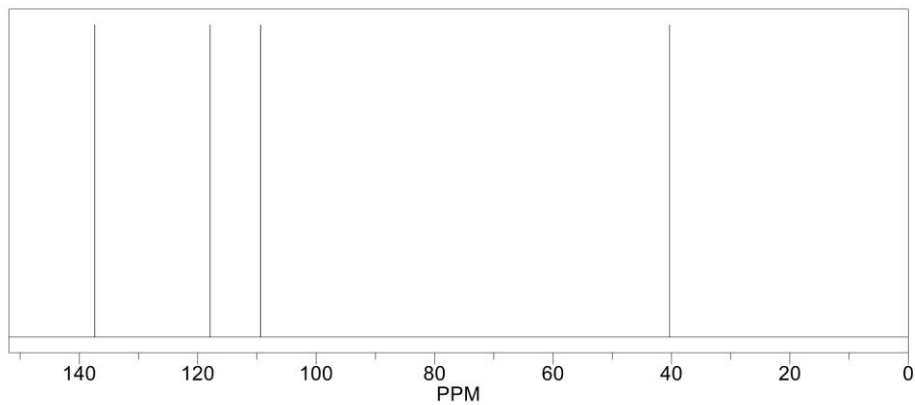
Estimation quality is indicated by color: good, medium, rough



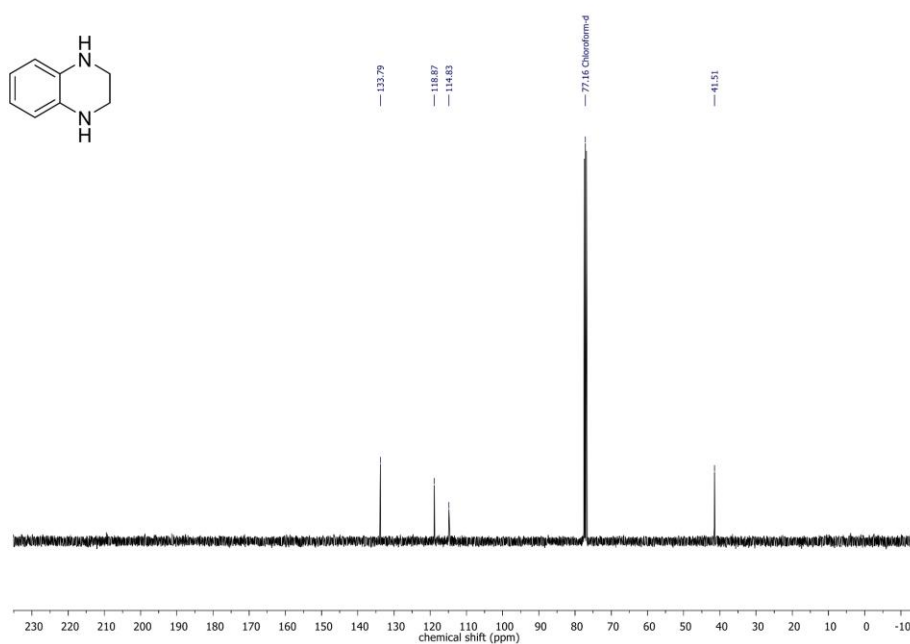
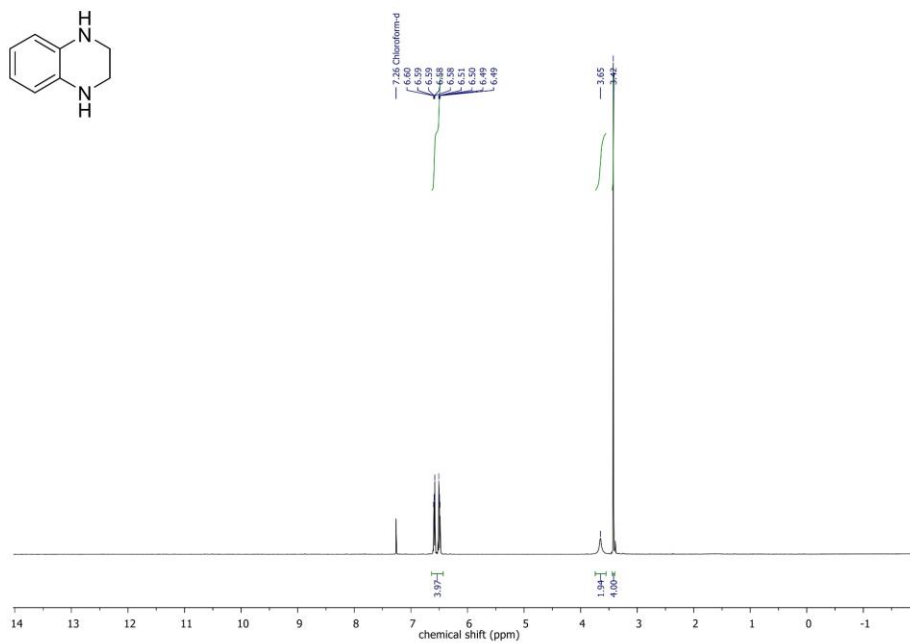
ChemNMR ^{13}C Estimation



Estimation quality is indicated by color: good, medium, rough

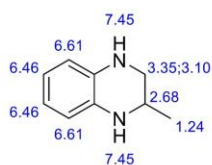


A Highly Active Cobalt Catalyst for the General and Selective Hydrogenation of Aromatic Heterocycles

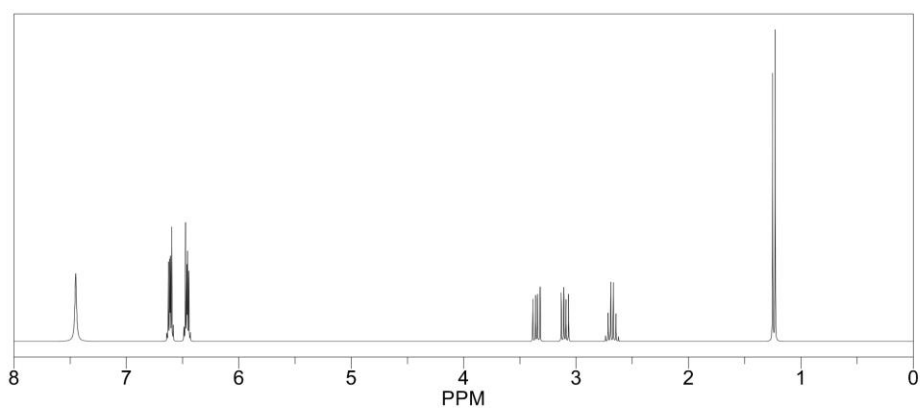


A Highly Active Cobalt Catalyst for the General and Selective Hydrogenation of Aromatic Heterocycles

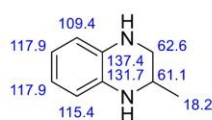
ChemNMR ^1H Estimation



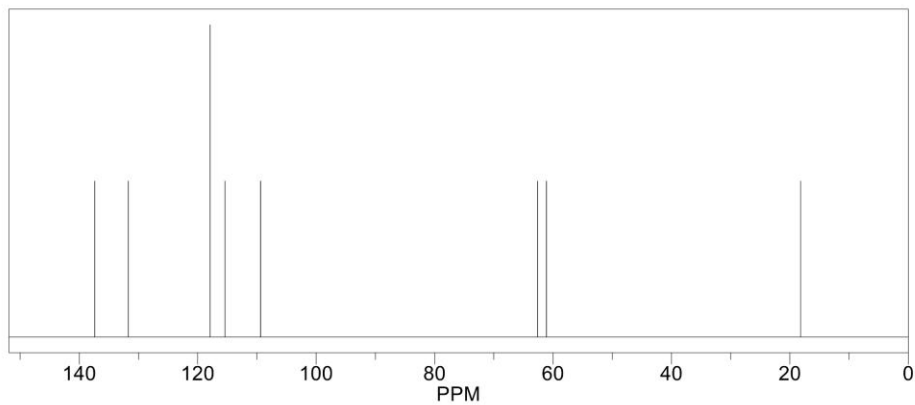
Estimation quality is indicated by color: good, medium, rough



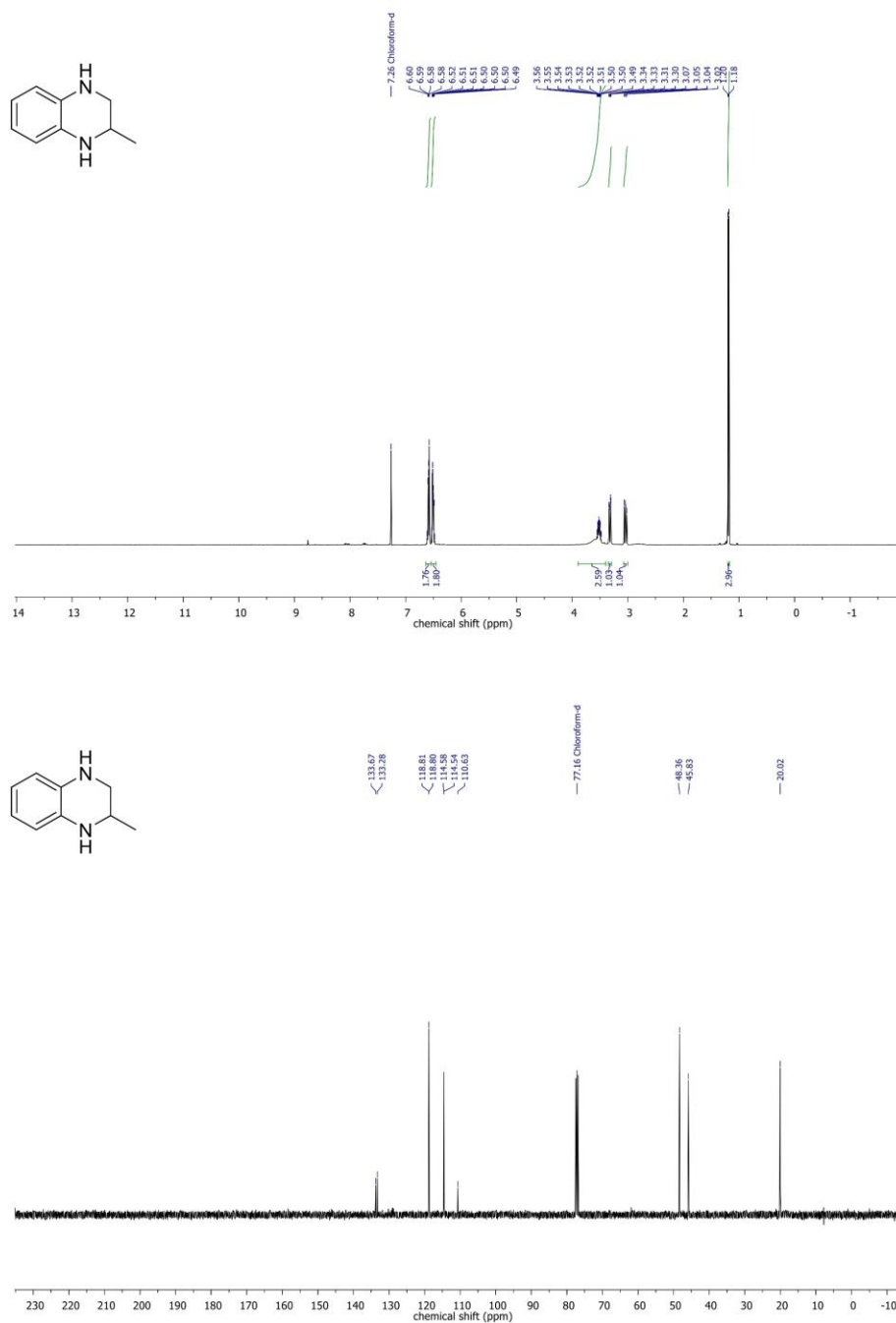
ChemNMR ^{13}C Estimation



Estimation quality is indicated by color: good, medium, rough

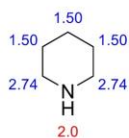


A Highly Active Cobalt Catalyst for the General and Selective Hydrogenation of Aromatic Heterocycles

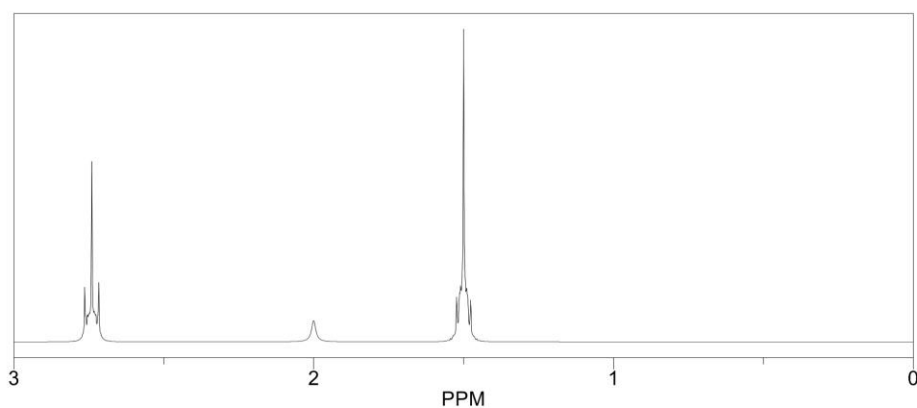


A Highly Active Cobalt Catalyst for the General and Selective Hydrogenation of Aromatic Heterocycles

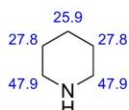
ChemNMR ^1H Estimation



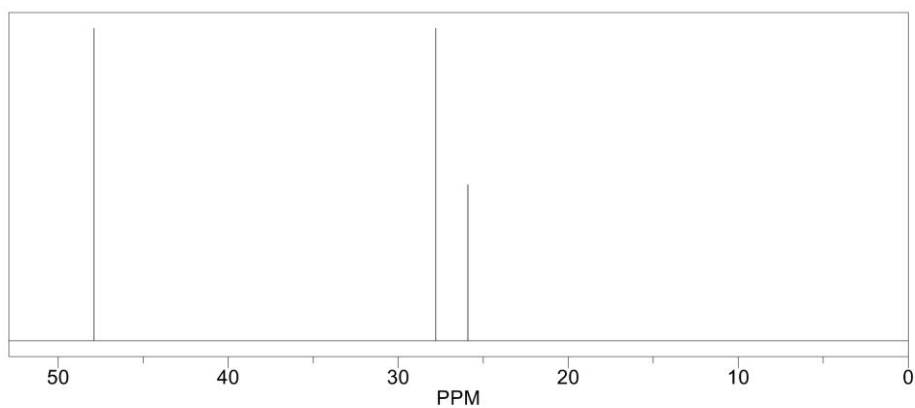
Estimation quality is indicated by color: good, medium, rough



ChemNMR ^{13}C Estimation

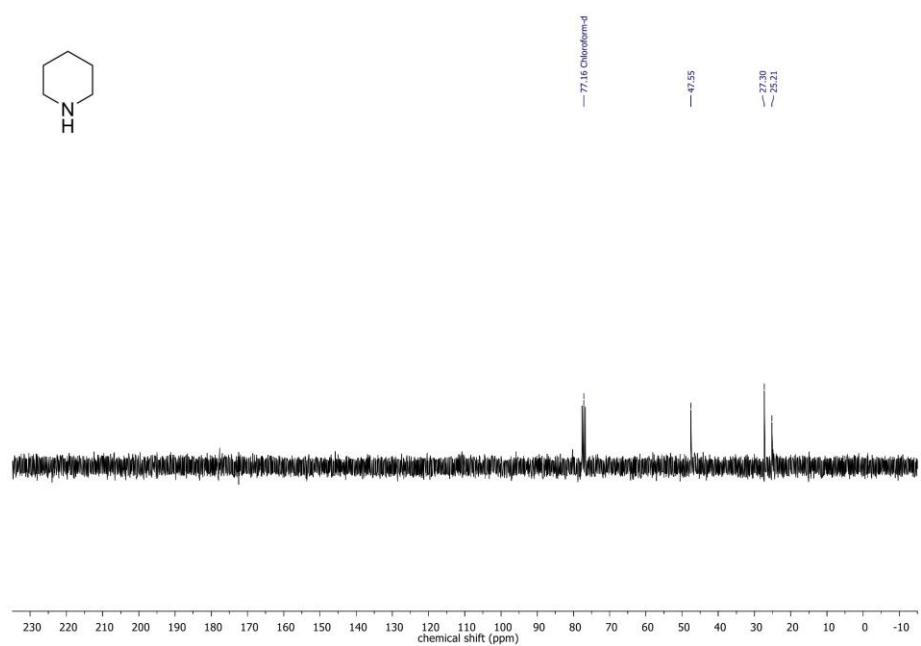
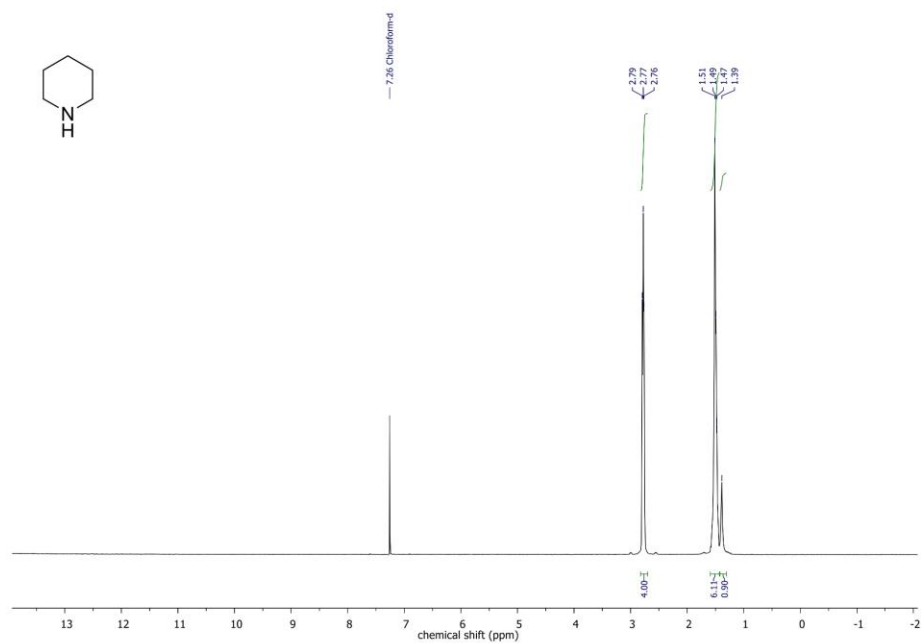


Estimation quality is indicated by color: good, medium, rough



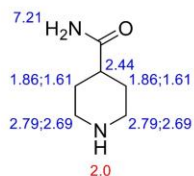
70

A Highly Active Cobalt Catalyst for the General and Selective Hydrogenation of Aromatic Heterocycles

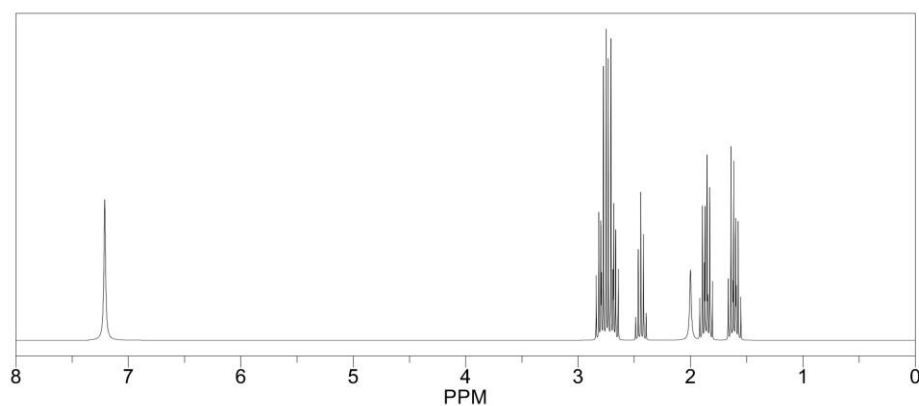


A Highly Active Cobalt Catalyst for the General and Selective Hydrogenation of Aromatic Heterocycles

ChemNMR ^1H Estimation



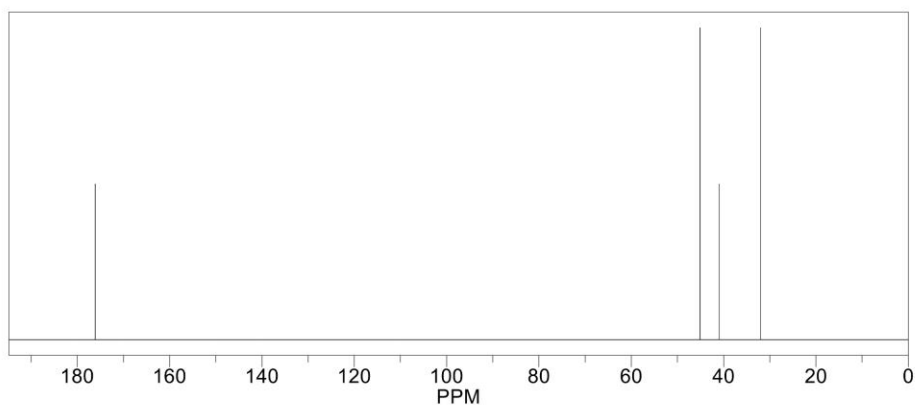
Estimation quality is indicated by color: good, medium, rough



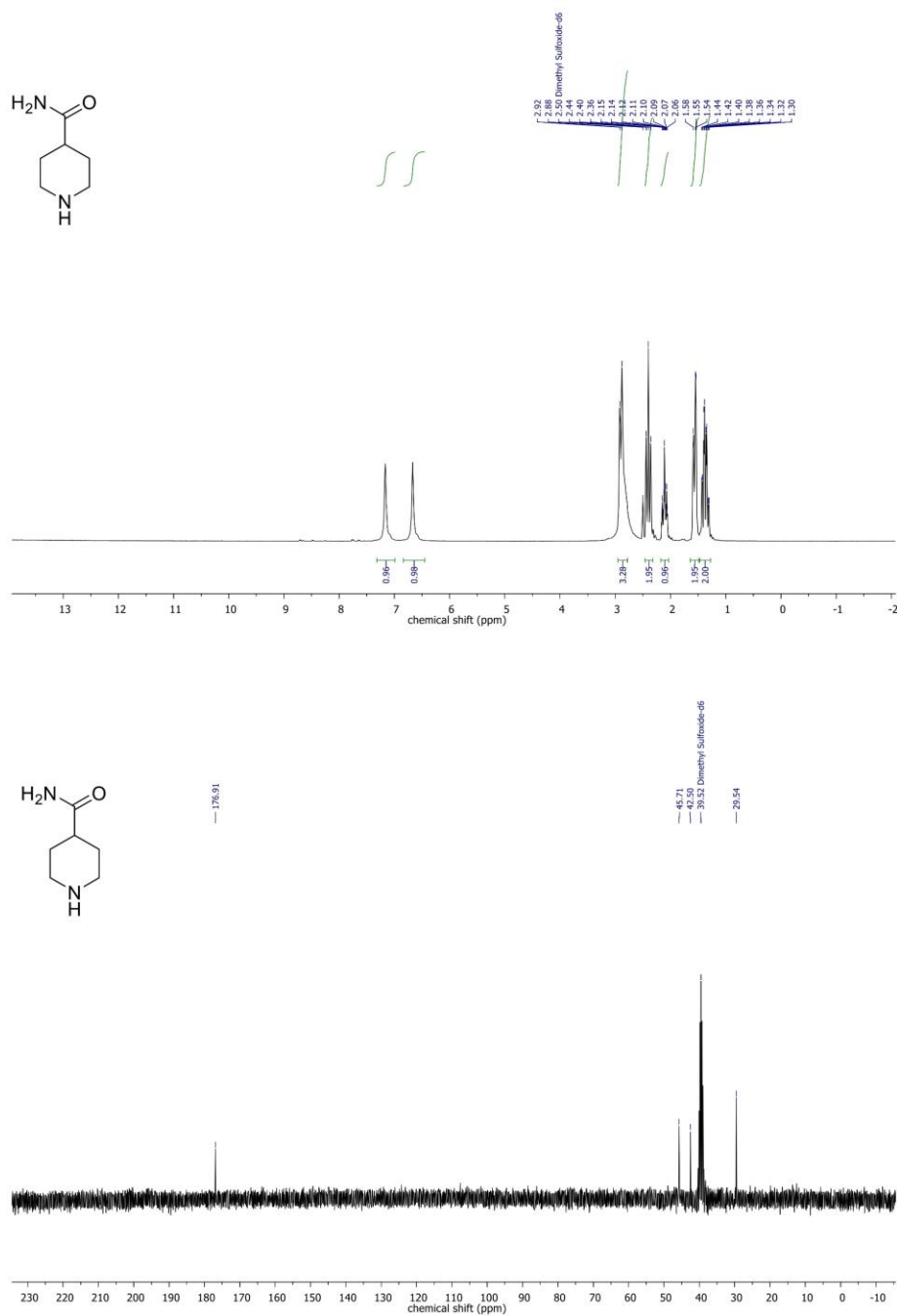
ChemNMR ^{13}C Estimation



Estimation quality is indicated by color: good, medium, rough



A Highly Active Cobalt Catalyst for the General and Selective Hydrogenation of Aromatic Heterocycles

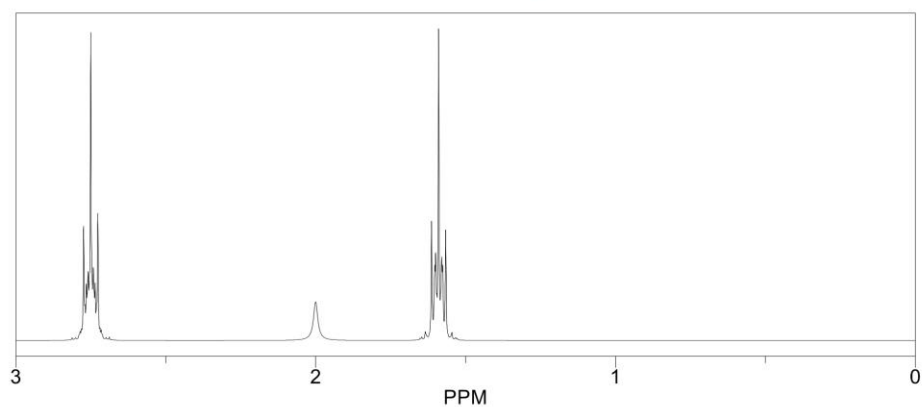


A Highly Active Cobalt Catalyst for the General and Selective Hydrogenation of Aromatic Heterocycles

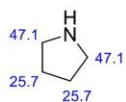
ChemNMR ^1H Estimation



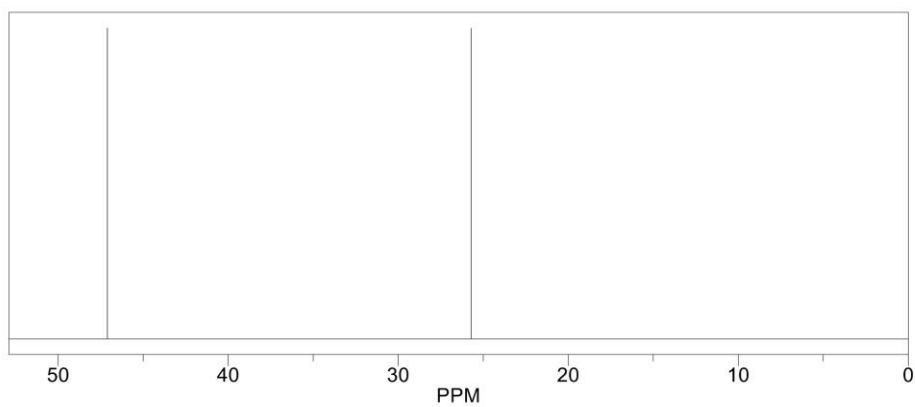
Estimation quality is indicated by color: good, medium, rough



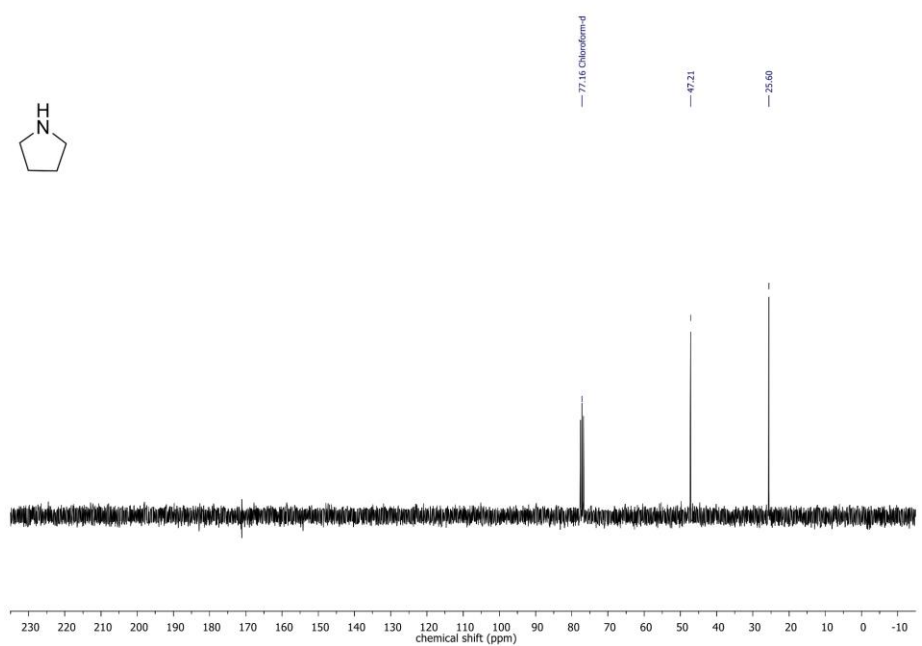
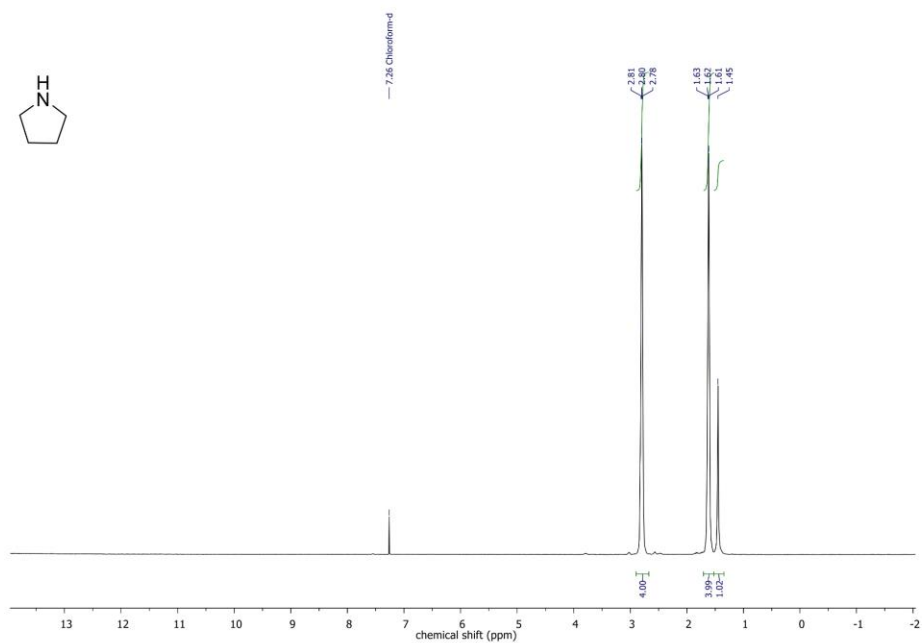
ChemNMR ^{13}C Estimation



Estimation quality is indicated by color: good, medium, rough

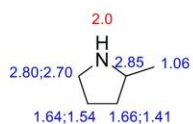


A Highly Active Cobalt Catalyst for the General and Selective Hydrogenation of Aromatic Heterocycles

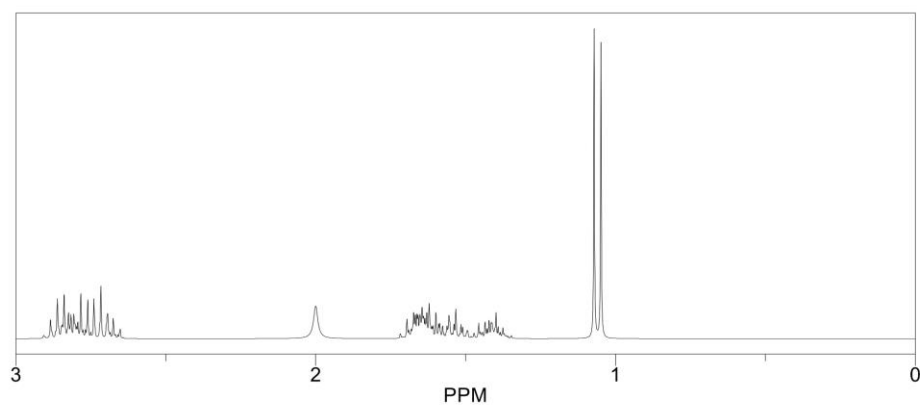


A Highly Active Cobalt Catalyst for the General and Selective Hydrogenation of Aromatic Heterocycles

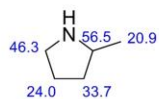
ChemNMR ^1H Estimation



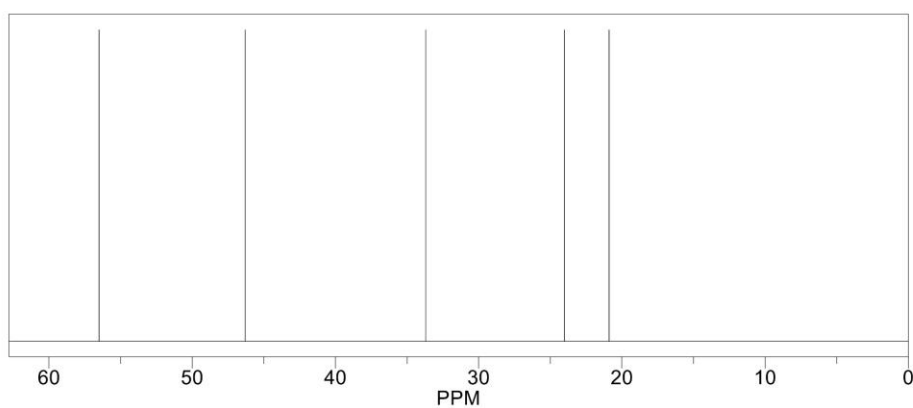
Estimation quality is indicated by color: good, medium, rough



ChemNMR ^{13}C Estimation



Estimation quality is indicated by color: good, medium, rough



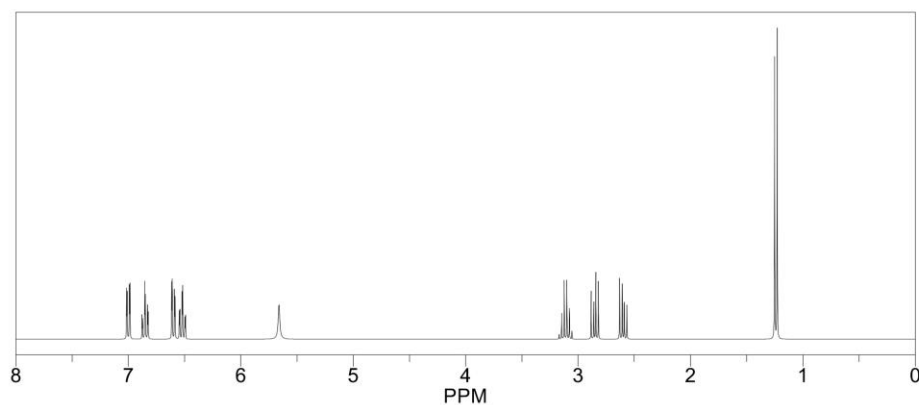


A Highly Active Cobalt Catalyst for the General and Selective Hydrogenation of Aromatic Heterocycles

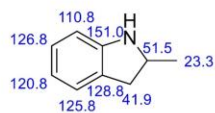
ChemNMR ^1H Estimation



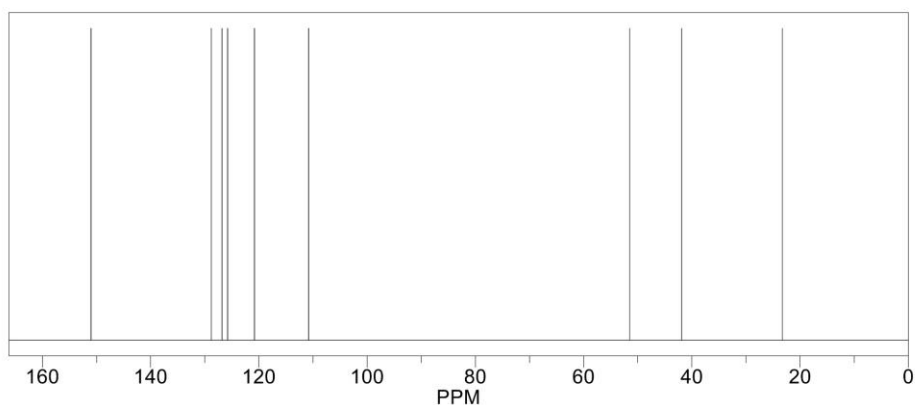
Estimation quality is indicated by color: good, medium, rough



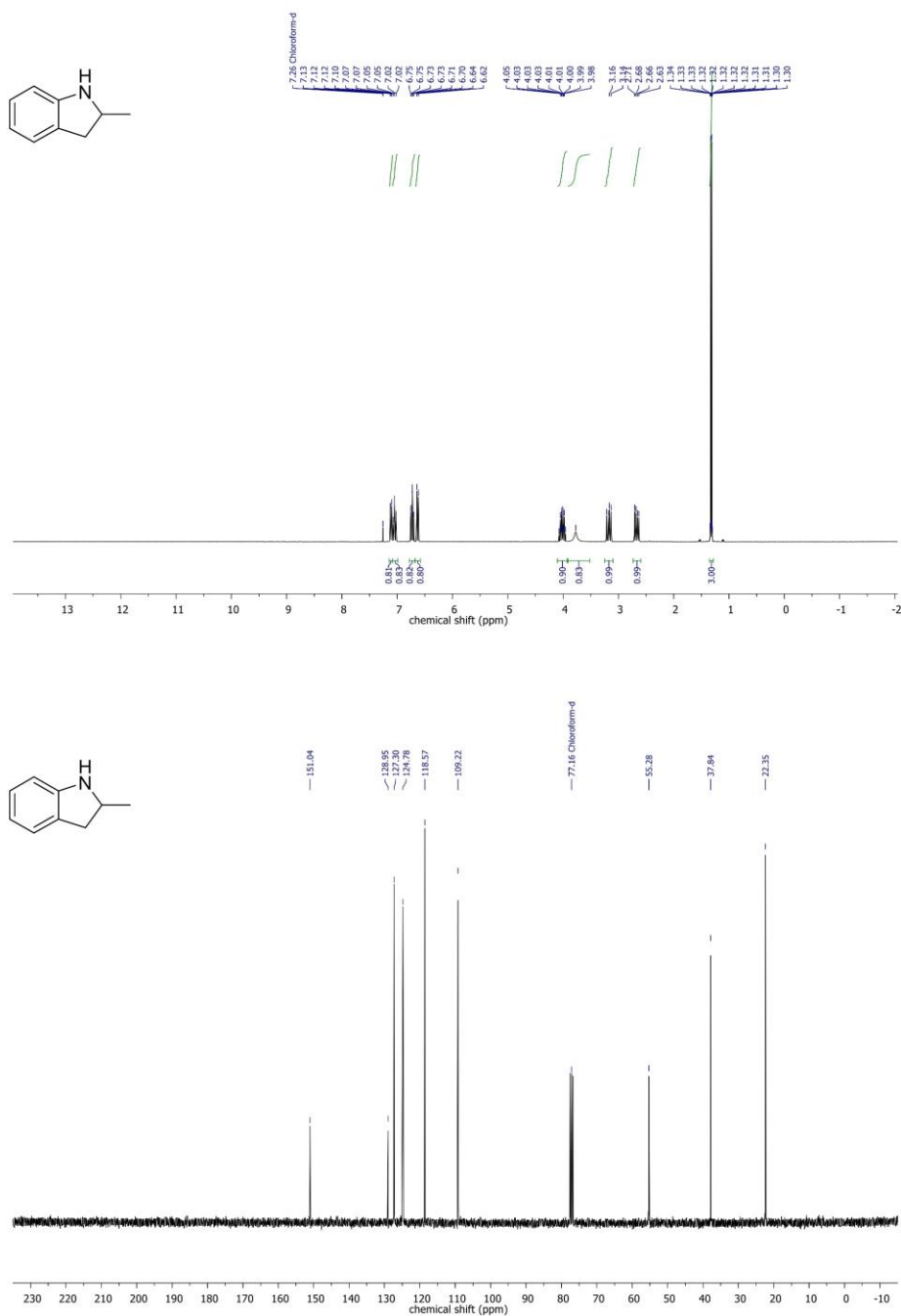
ChemNMR ^{13}C Estimation



Estimation quality is indicated by color: good, medium, rough

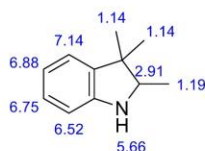


A Highly Active Cobalt Catalyst for the General and Selective Hydrogenation of Aromatic Heterocycles

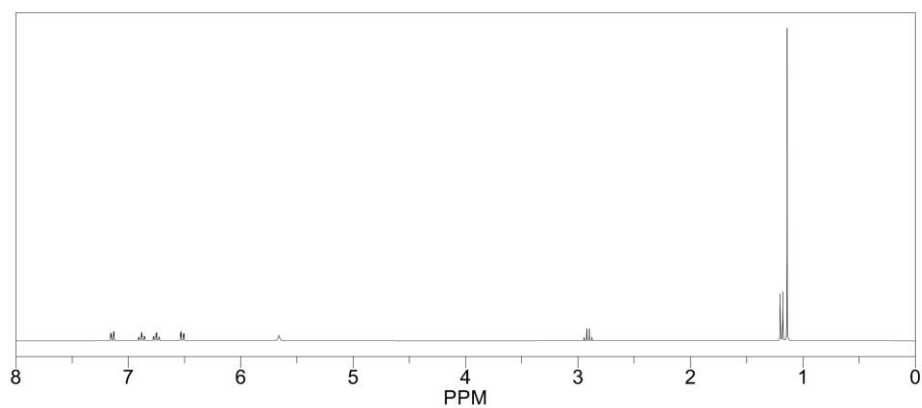


A Highly Active Cobalt Catalyst for the General and Selective Hydrogenation of Aromatic Heterocycles

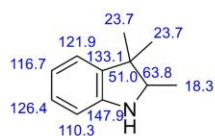
ChemNMR ^1H Estimation



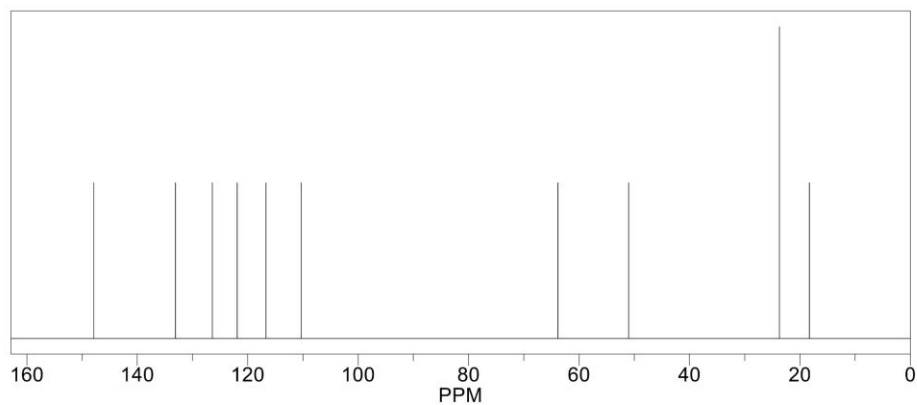
Estimation quality is indicated by color: good, medium, rough



ChemNMR ^{13}C Estimation



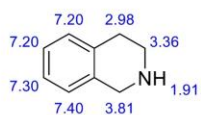
Estimation quality is indicated by color: good, medium, rough



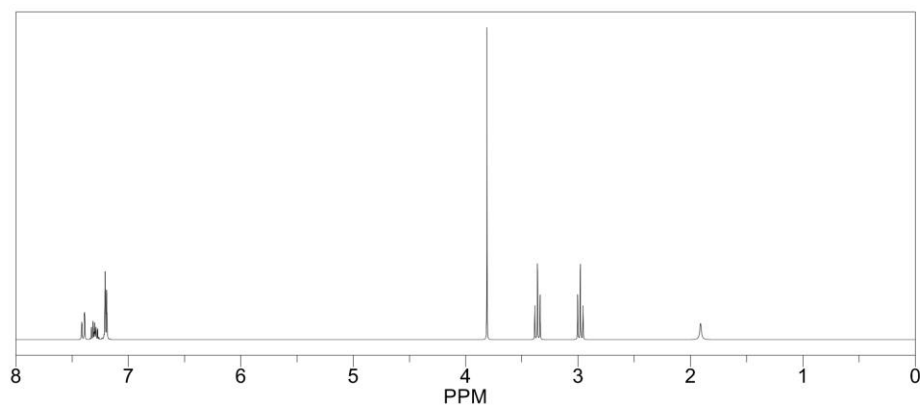


A Highly Active Cobalt Catalyst for the General and Selective Hydrogenation of Aromatic Heterocycles

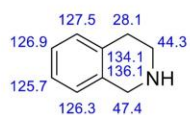
ChemNMR ^1H Estimation



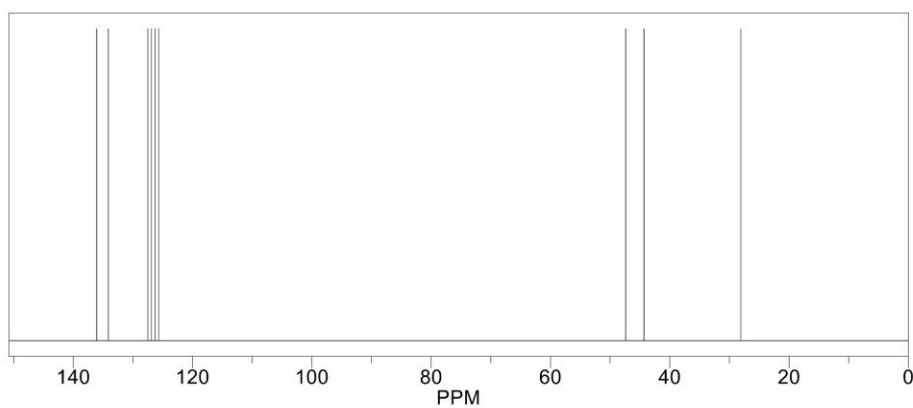
Estimation quality is indicated by color: good, medium, rough



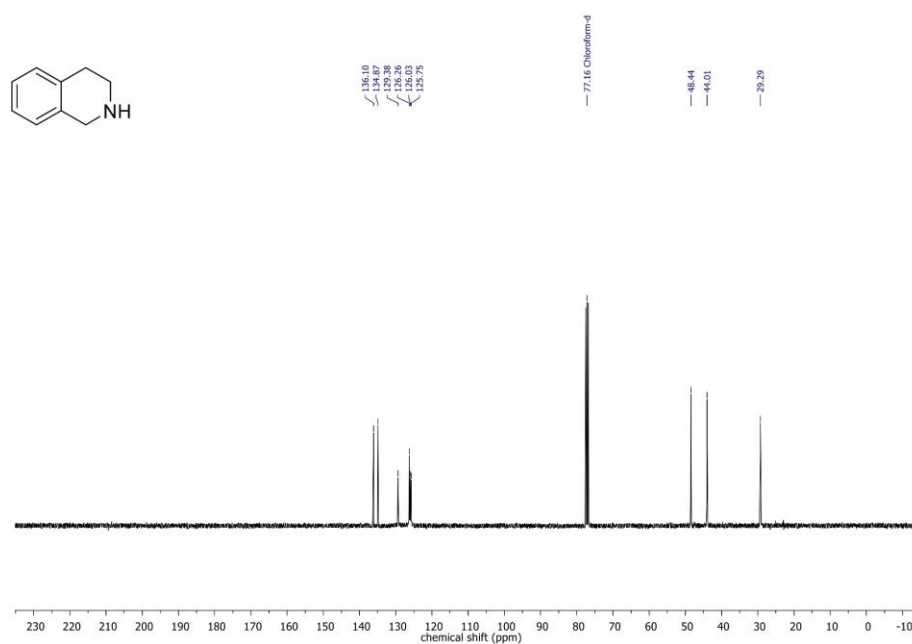
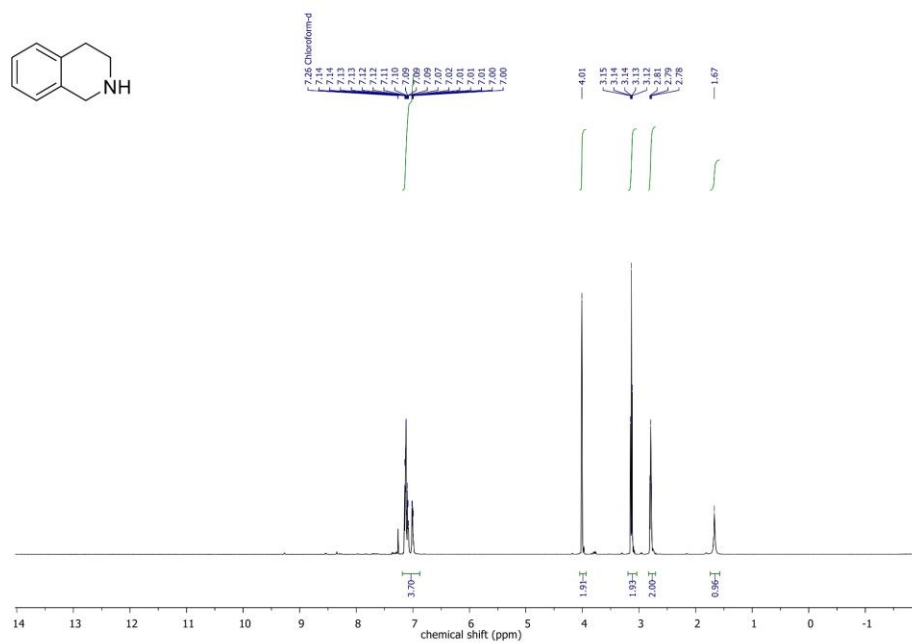
ChemNMR ^{13}C Estimation



Estimation quality is indicated by color: good, medium, rough

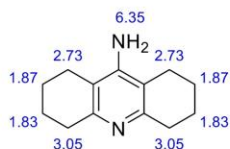


A Highly Active Cobalt Catalyst for the General and Selective Hydrogenation of Aromatic Heterocycles

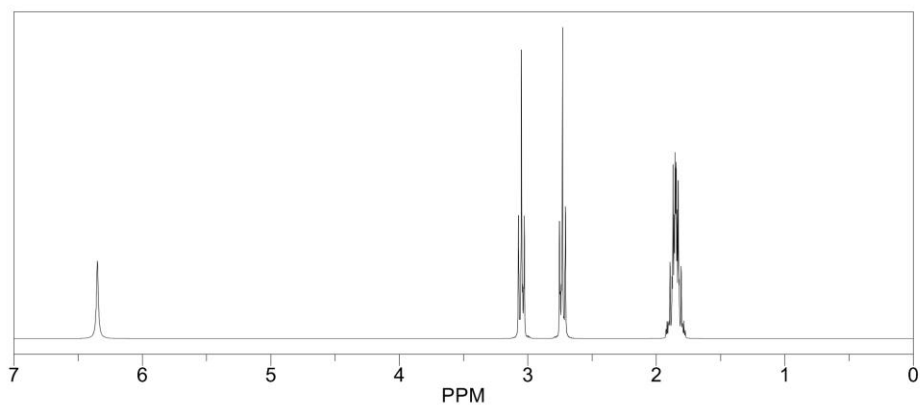


A Highly Active Cobalt Catalyst for the General and Selective Hydrogenation of Aromatic Heterocycles

ChemNMR ^1H Estimation



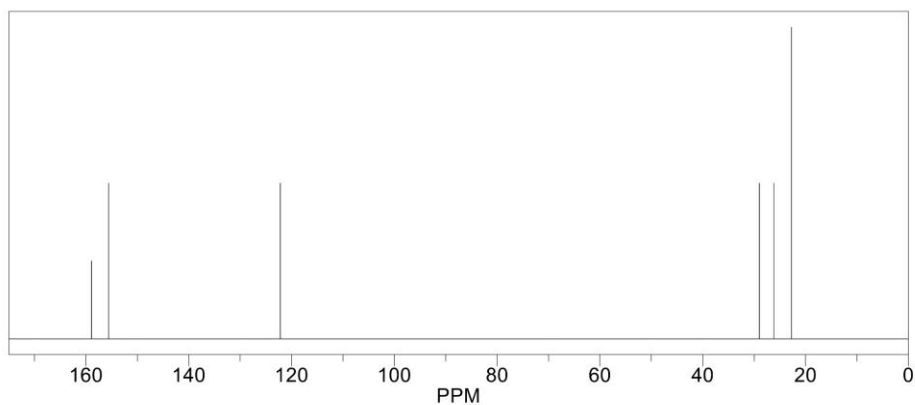
Estimation quality is indicated by color: good, medium, rough



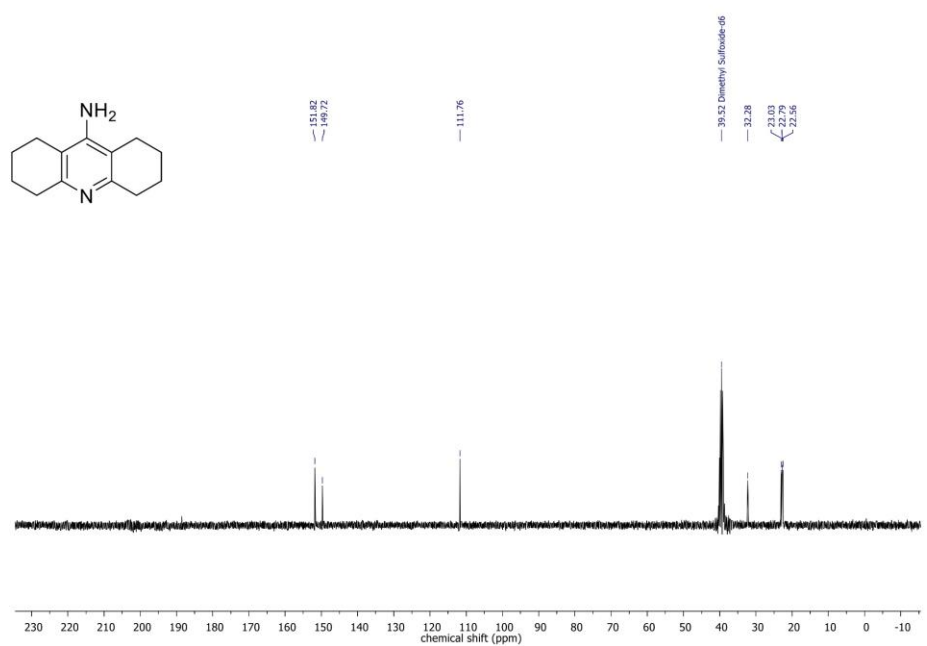
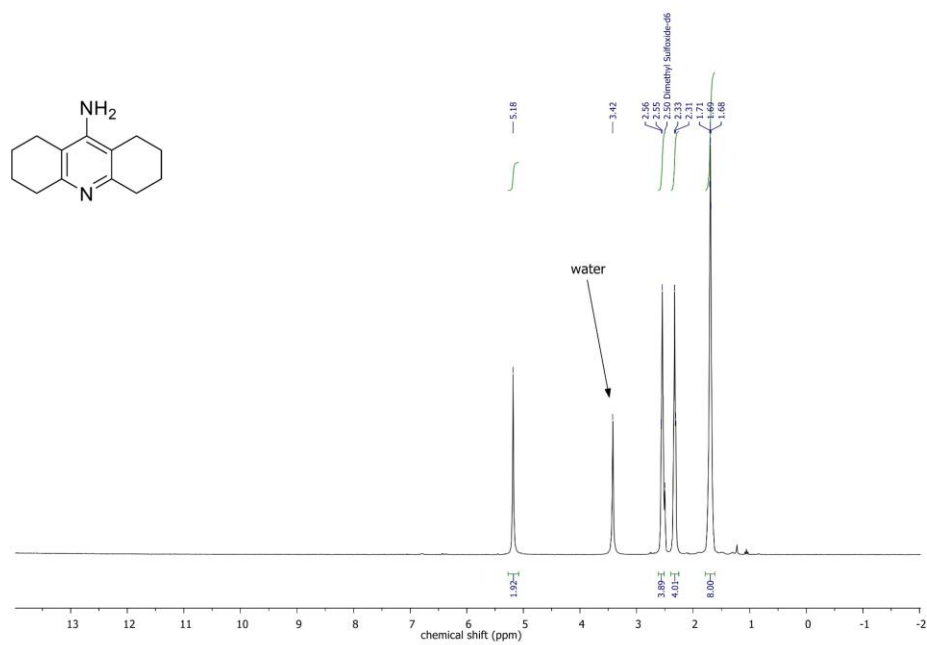
ChemNMR ^{13}C Estimation



Estimation quality is indicated by color: good, medium, rough

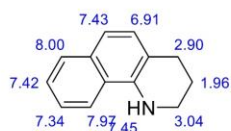


A Highly Active Cobalt Catalyst for the General and Selective Hydrogenation of Aromatic Heterocycles

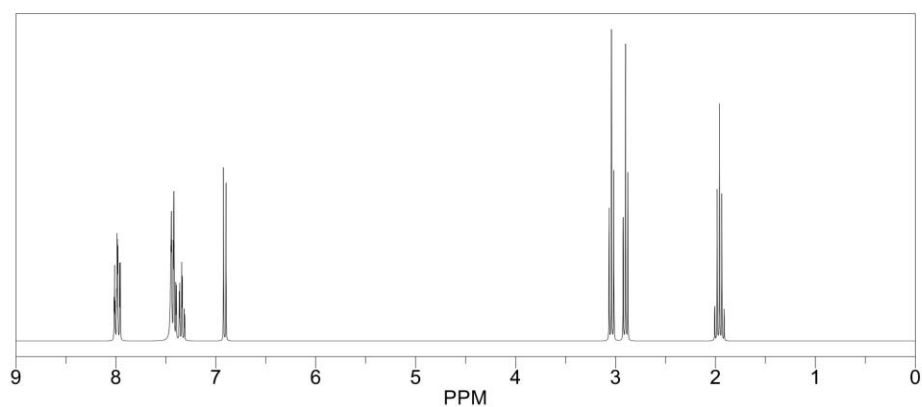


A Highly Active Cobalt Catalyst for the General and Selective Hydrogenation of Aromatic Heterocycles

ChemNMR ^1H Estimation



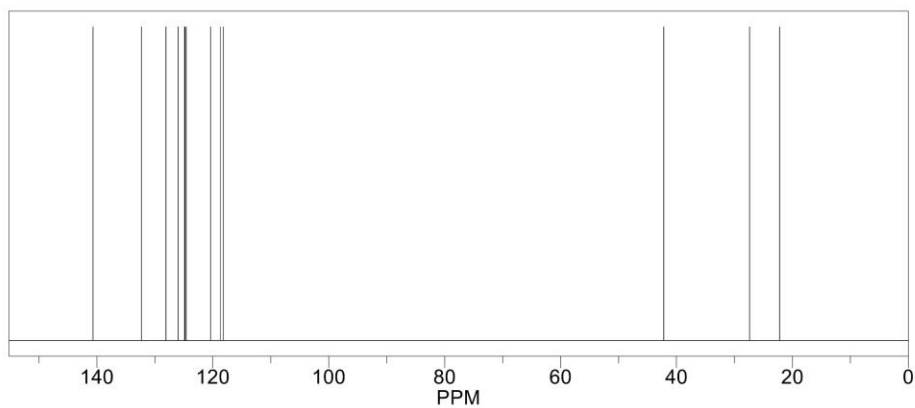
Estimation quality is indicated by color: good, medium, rough

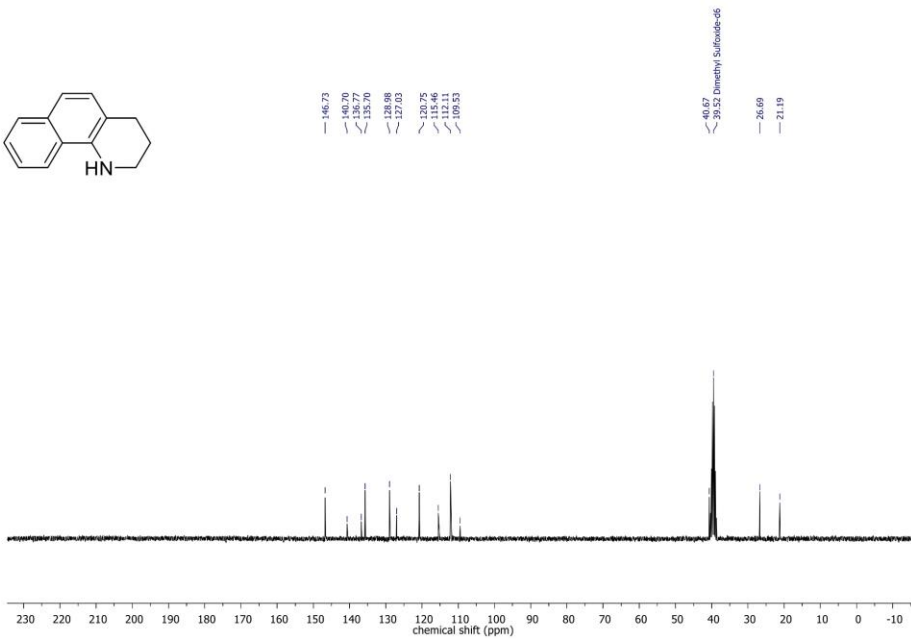


ChemNMR ^{13}C Estimation



Estimation quality is indicated by color: good, medium, rough



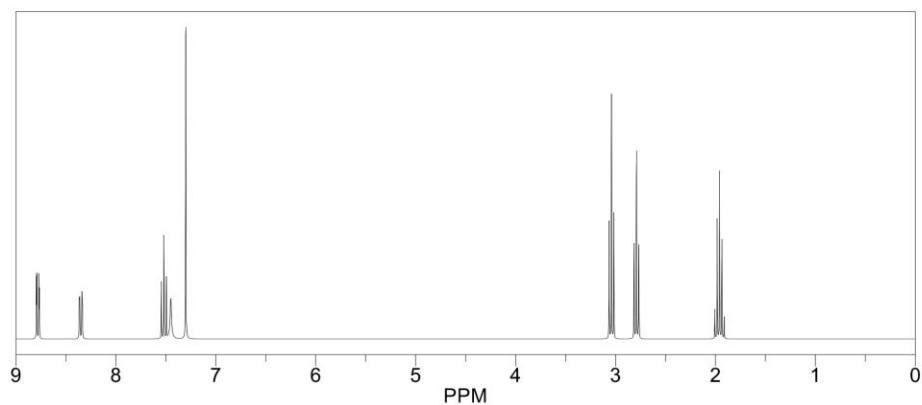


A Highly Active Cobalt Catalyst for the General and Selective Hydrogenation of Aromatic Heterocycles

ChemNMR ^1H Estimation



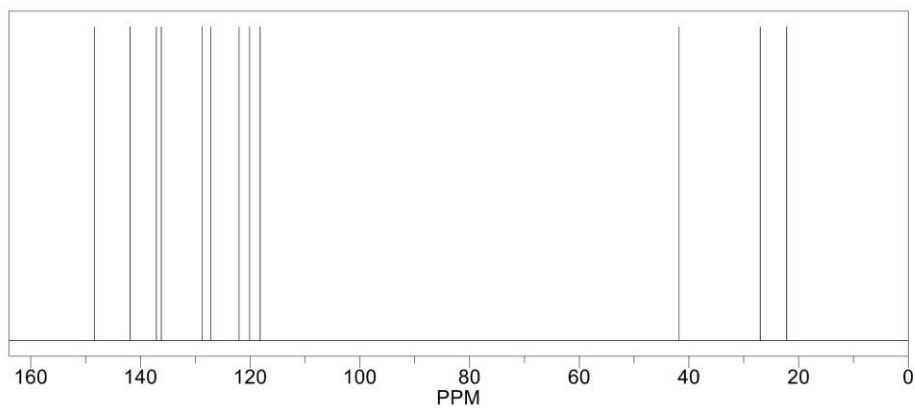
Estimation quality is indicated by color: good, medium, rough



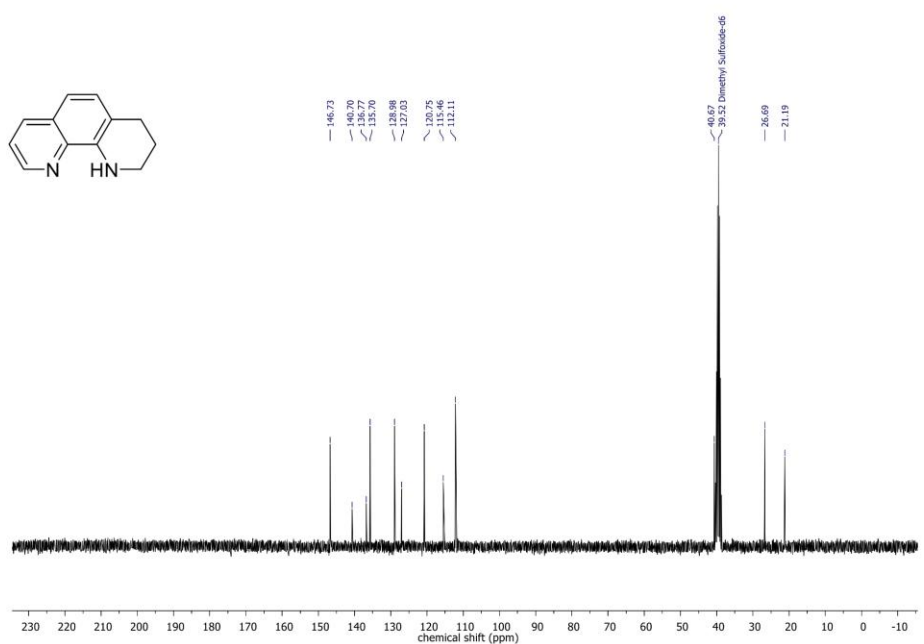
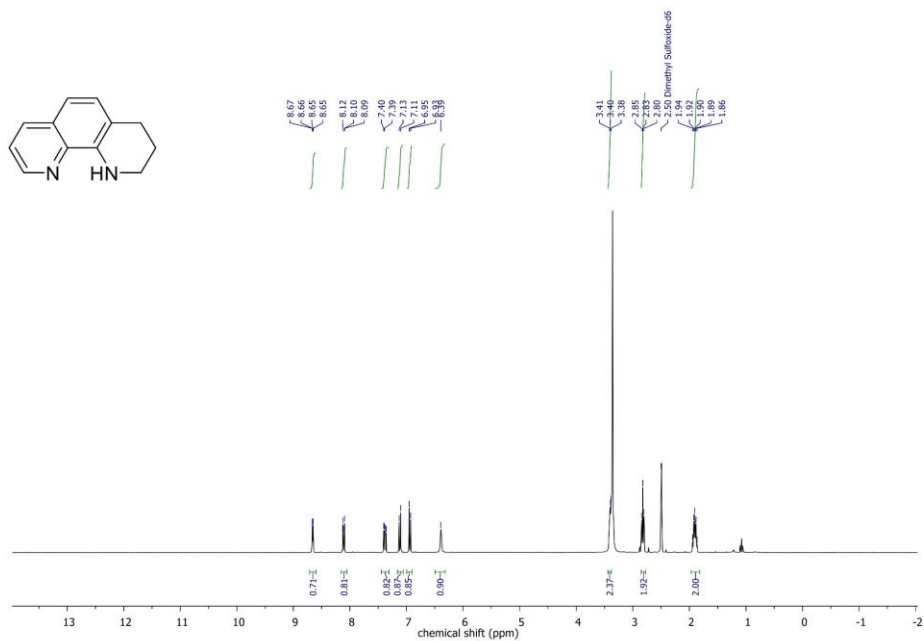
ChemNMR ^{13}C Estimation



Estimation quality is indicated by color: good, medium, rough

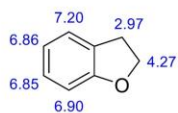


A Highly Active Cobalt Catalyst for the General and Selective Hydrogenation of Aromatic Heterocycles

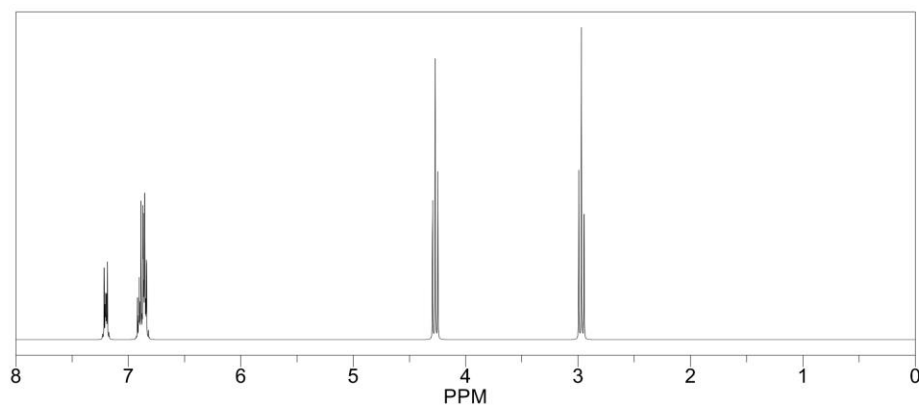


A Highly Active Cobalt Catalyst for the General and Selective Hydrogenation of Aromatic Heterocycles

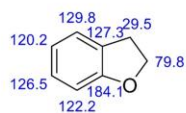
ChemNMR ^1H Estimation



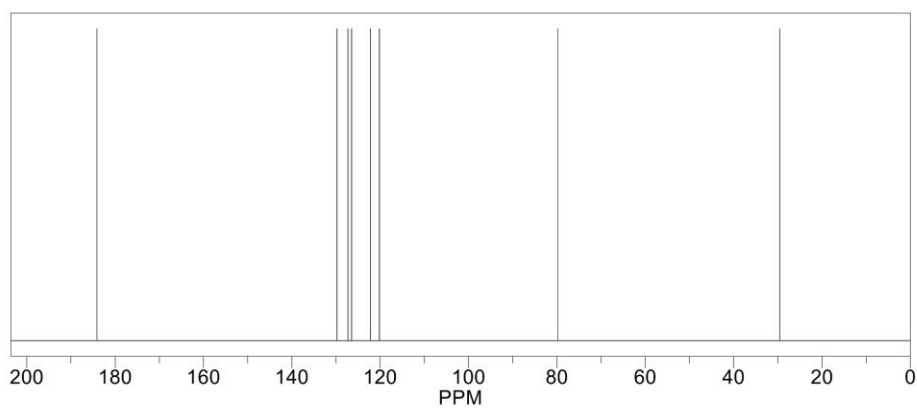
Estimation quality is indicated by color: good, medium, rough



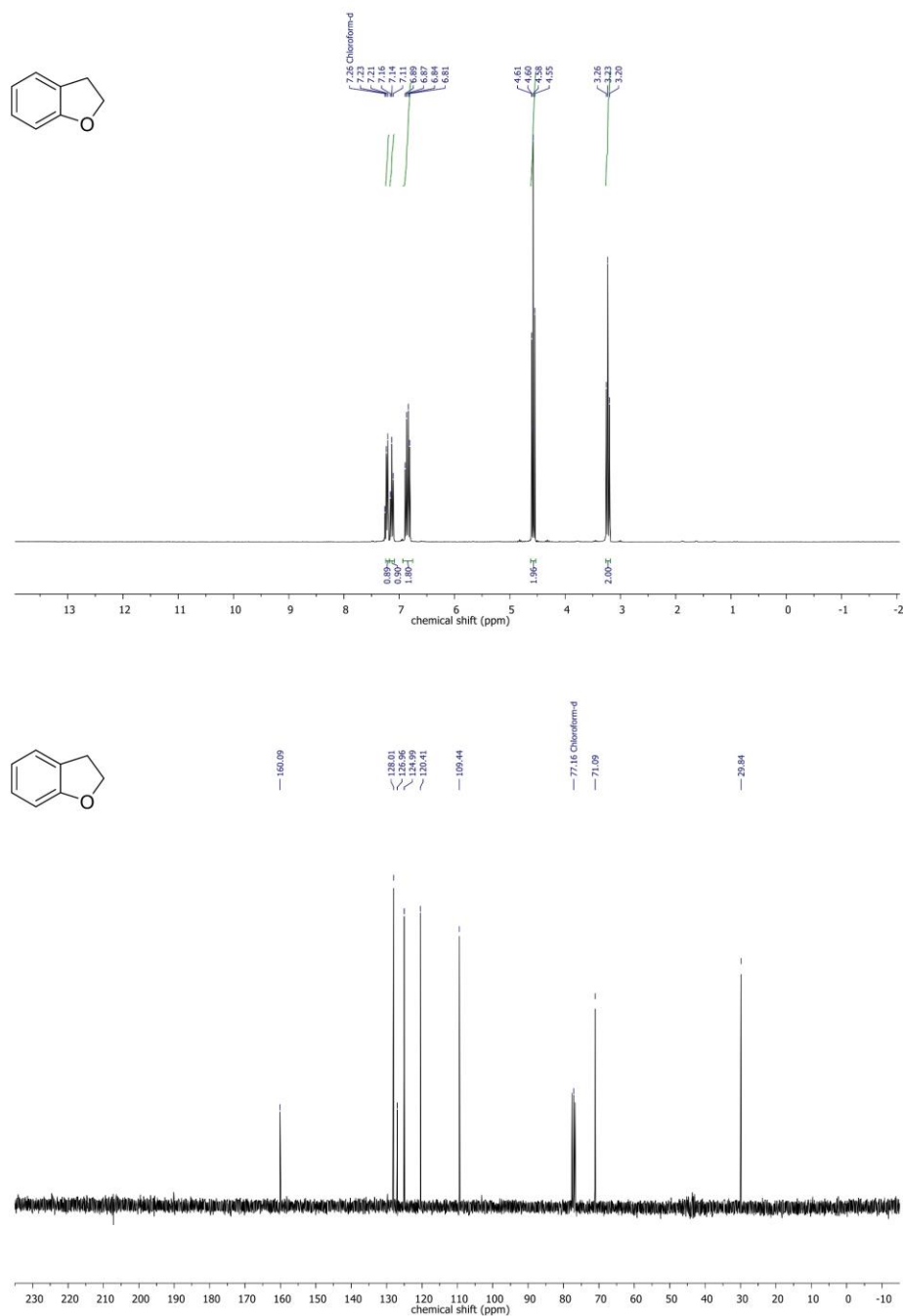
ChemNMR ^{13}C Estimation



Estimation quality is indicated by color: good, medium, rough

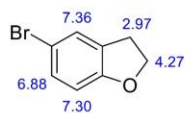


A Highly Active Cobalt Catalyst for the General and Selective Hydrogenation of Aromatic Heterocycles

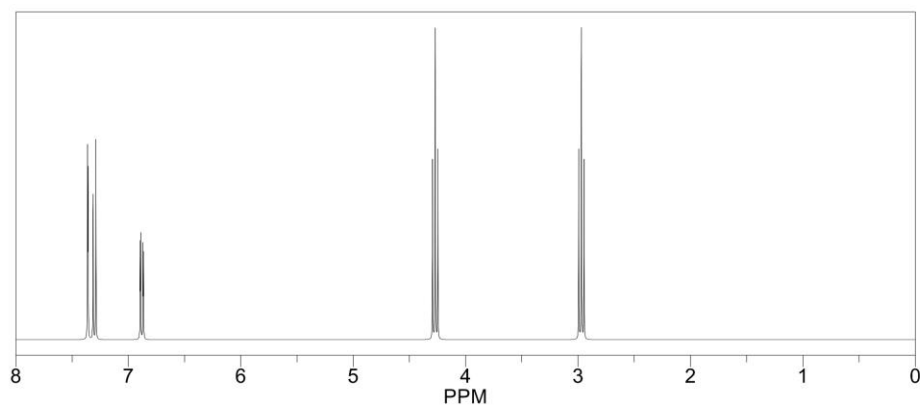


A Highly Active Cobalt Catalyst for the General and Selective Hydrogenation of Aromatic Heterocycles

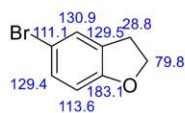
ChemNMR ^1H Estimation



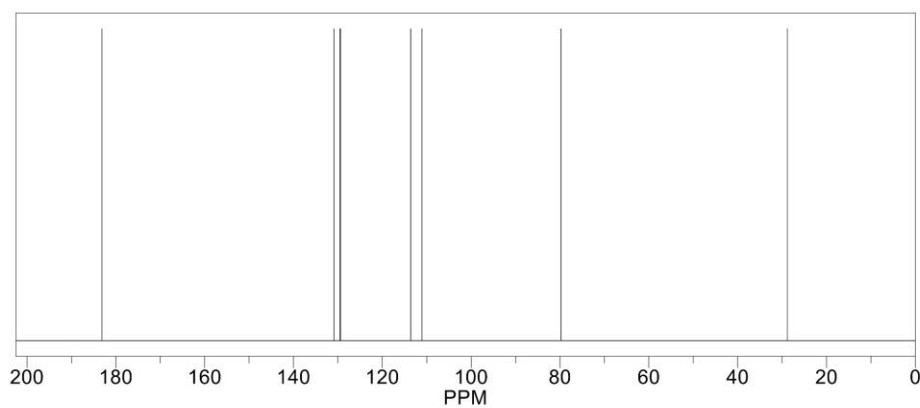
Estimation quality is indicated by color: good, medium, rough



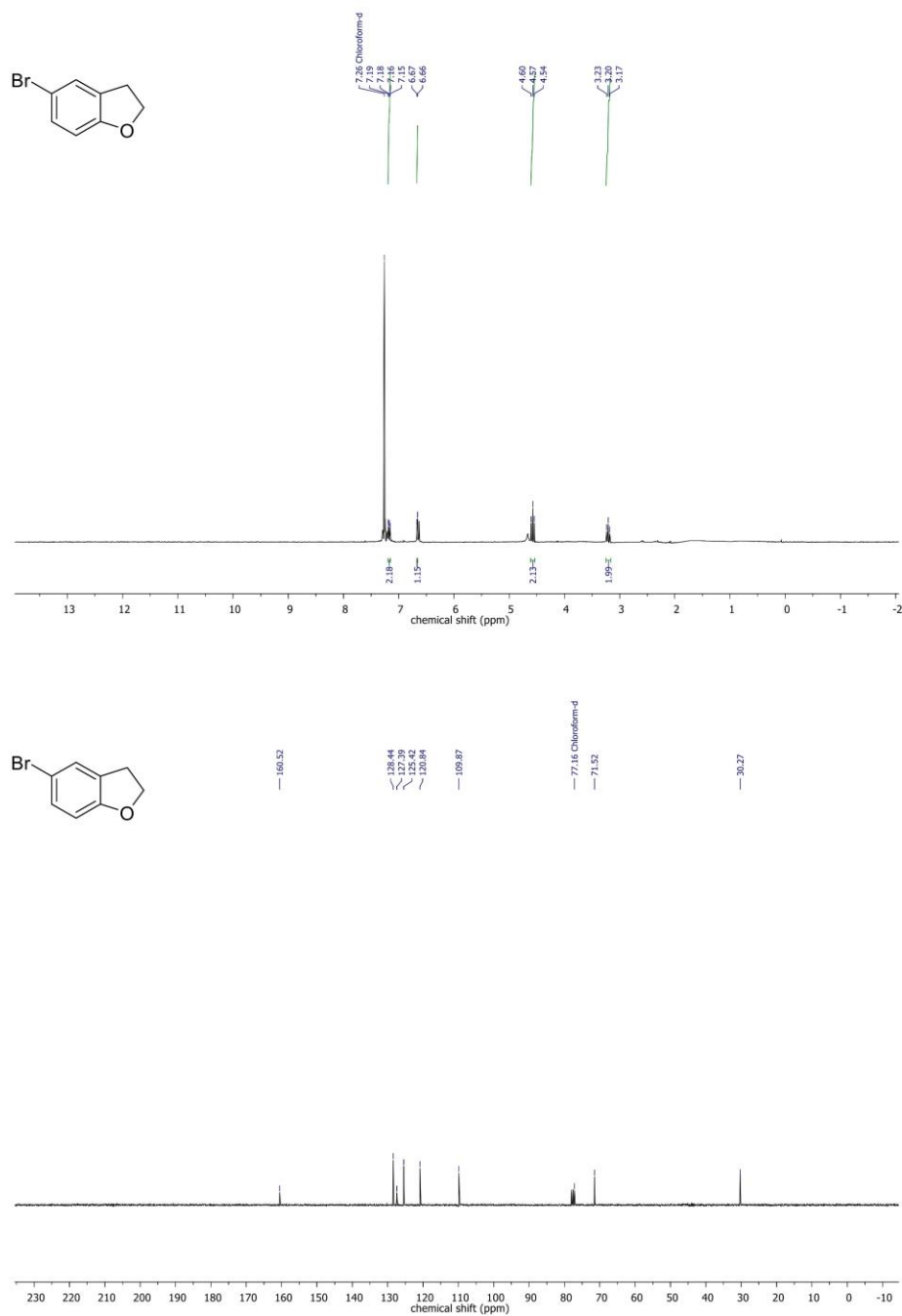
ChemNMR ^{13}C Estimation



Estimation quality is indicated by color: good, medium, rough



A Highly Active Cobalt Catalyst for the General and Selective Hydrogenation of Aromatic Heterocycles

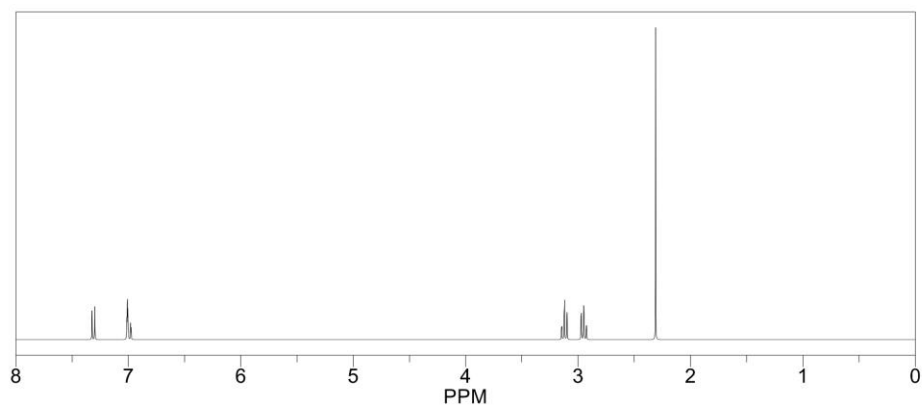


A Highly Active Cobalt Catalyst for the General and Selective Hydrogenation of Aromatic Heterocycles

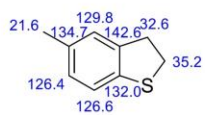
ChemNMR ^1H Estimation



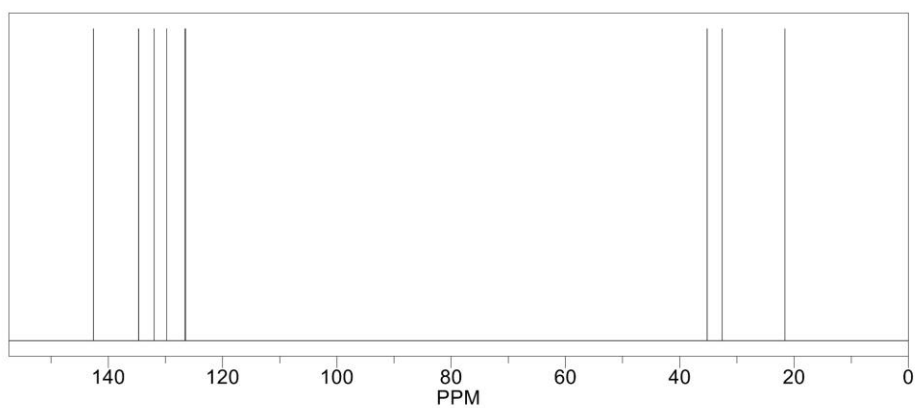
Estimation quality is indicated by color: good, medium, rough

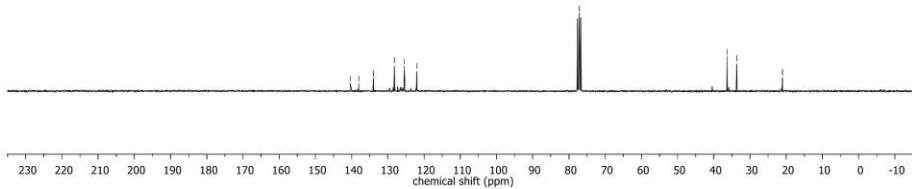
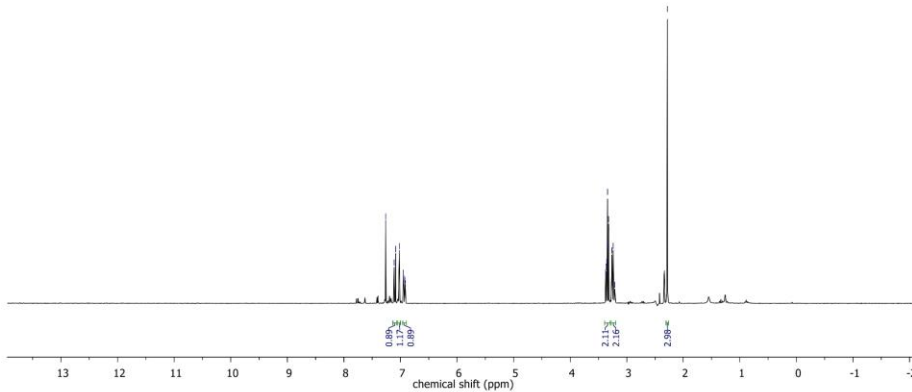


ChemNMR ^{13}C Estimation



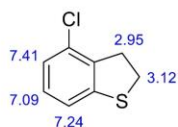
Estimation quality is indicated by color: good, medium, rough



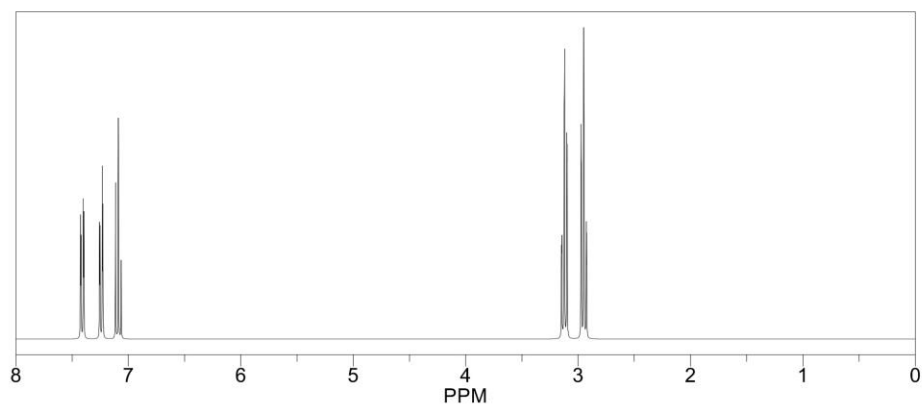


A Highly Active Cobalt Catalyst for the General and Selective Hydrogenation of Aromatic Heterocycles

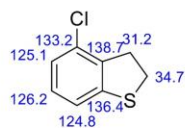
ChemNMR ^1H Estimation



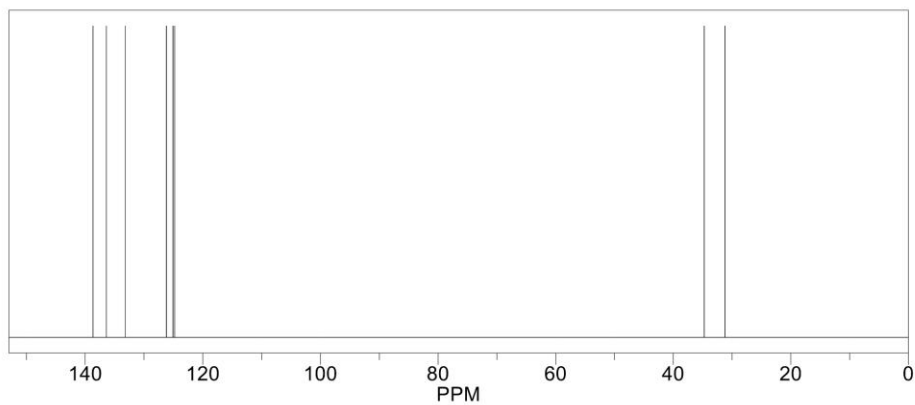
Estimation quality is indicated by color: good, medium, rough



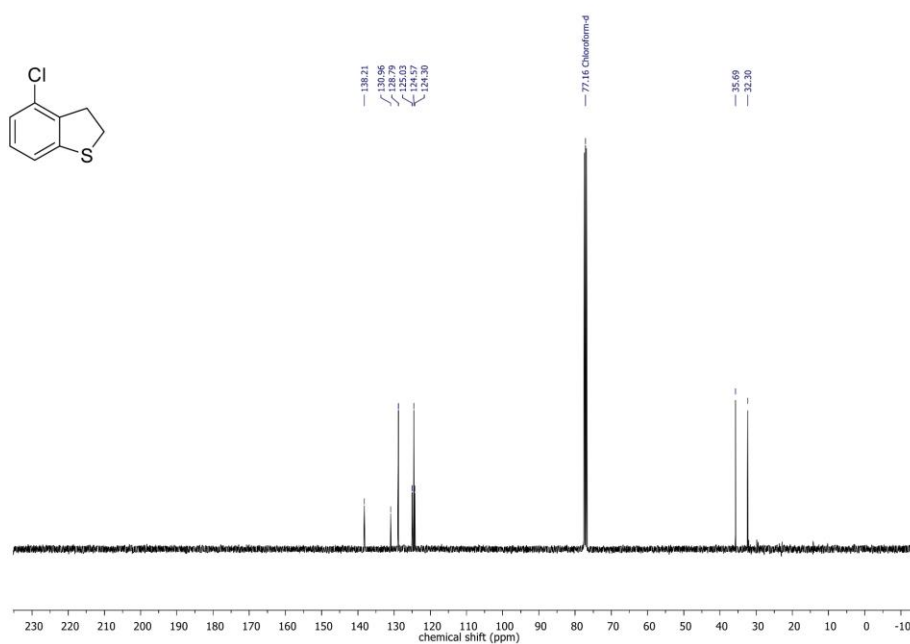
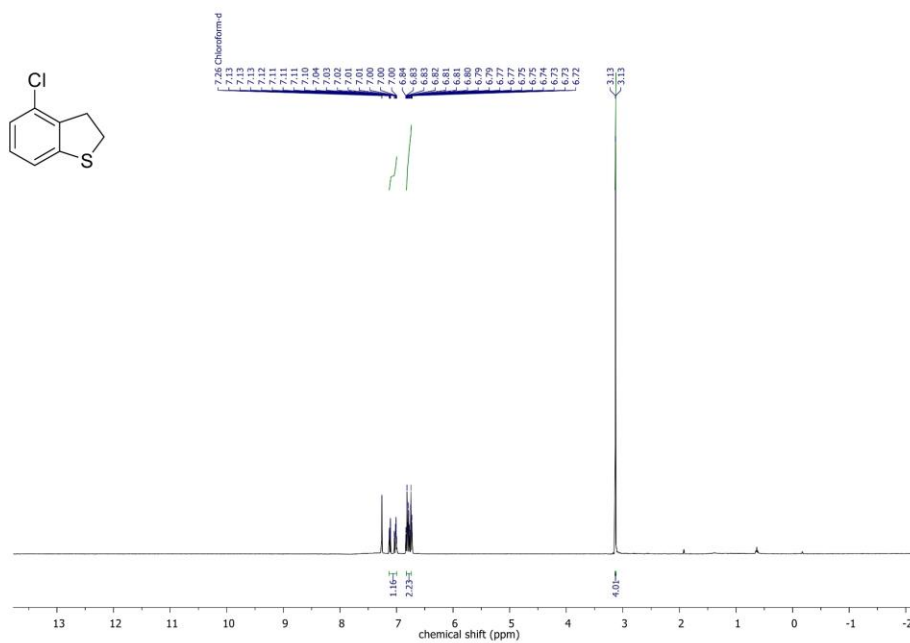
ChemNMR ^{13}C Estimation



Estimation quality is indicated by color: good, medium, rough



A Highly Active Cobalt Catalyst for the General and Selective Hydrogenation of Aromatic Heterocycles



7 References

- [1] P. Juhás, C. L. Farrow, X. Yang, K. R. Knox, S. J. L. Billinge, *Acta Crystallogr. A* **2015**, *71*, 562–568.
- [2] I. J. Bruno, J. C. Cole, P. R. Edgington, M. Kessler, C. F. Macrae, P. McCabe, J. Pearson, R. Taylor, *Acta. Crystallogr. B. Struct. Sci. Cryst. Eng. Mater.* **2002**, *58*, 389–397.
- [3] A. Khort, S. Roslyakov, P. Loginov, *Nano-Struct. Nano-Objects* **2021**, *26*, 100727.
- [4] J. A. Shriver, S. G. Westphal, *J. Chem. Educ.* **2006**, *83*, 1330–1332.
- [5] J. Lipp, R. Banerjee, M. F. Patwary, N. Patra, A. Dong, F. Girgsdies, S. R. Bare, J. R. Regalbuto, *Chem. Mater.* **2022**, *34*, 8091–8111.
- [6] S. J. L. Billinge, I. Levin, *Science* **2007**, *316*, 561–565.
- [7] H. G. Jiang, M. Rühle, E. J. Lavernia, *J. Mater. Res.* **1999**, *14*, 549–559.
- [8] F. H. Allen, O. Kennard, D. G. Watson, L. Brammer, A. G. Orpen, R. Taylor, *J. Chem. Soc., Perkin trans. II* **1987**, S1.
- [9] C. Didier, W. K. Pang, Z. Guo, S. Schmid, V. K. Peterson, *Chem. Mater.* **2020**, *32*, 2518–2531.
- [10] Z. Huang, P. Thomson, S. Di, *J. Phys. Chem. Solids* **2007**, *68*, 530–535.
- [11] J. Hervochon, V. Dorcet, K. Junge, M. Beller, C. Fischmeister, *Catal. Sci. Technol.* **2020**, *10*, 4820–4826.
- [12] K. Murugesan, V. G. Chandrashekar, C. Kreyenschulte, M. Beller, R. V. Jagadeesh, *Angew. Chem. Int. Ed.* **2020**, *132*, 17561–17565.
- [13] F. Chen, A.-E. Surkus, L. He, M.-M. Pohl, J. Radnik, C. Topf, K. Junge, M. Beller, *J. Am. Chem. Soc.* **2015**, *137*, 11718–11724.
- [14] V. M. Asaula, V. V. Buryanov, B. Y. Solod, D. M. Tryus, O. O. Pariiska, I. E. Kotenko, Y. M. Volovenko, D. M. Volochnyuk, S. V. Ryabukhin, S. V. Kolotilov, *Justus Liebigs Ann. Chem.* **2021**, *2021*, 6616–6625.
- [15] A. Sahin, O. Cakmak, I. Demirtas, S. Okten, A. Tutar, *Tetrahedron* **2008**, *64*, 10068–10074.
- [16] R. Adam, J. R. Cabrero-Antonino, A. Spannenberg, K. Junge, R. Jackstell, M. Beller, *Angew. Chem. Int. Ed.* **2017**, *129*, 3264–3268.
- [17] V. Papa, Y. Cao, A. Spannenberg, K. Junge, M. Beller, *Nat. Catal.* **2020**, *3*, 135–142.
- [18] Q. Xuan, Q. Song, *Org. Lett.* **2016**, *18*, 4250–4253.

- [19] R. J. Abraham, M. Reid, *J. Chem. Soc., Perkin trans. II* **2002**, 1081–1091.
- [20] F. Chen, W. Li, B. Sahoo, C. Kreyenschulte, G. Agostini, H. Lund, K. Junge, M. Beller, *Angew. Chem. Int. Ed.* **2018**, *57*, 14488–14492.
- [21] A. García-Abuín, D. Gómez-Díaz, J. M. Navaza, A. Rumbo, *AIChE J.* **2014**, *60*, 1098–1106.
- [22] M. R. Crimmin, M. Arrowsmith, A. G. M. Barrett, I. J. Casely, M. S. Hill, P. A. Procopiou, *J. Am. Chem. Soc.* **2009**, *131*, 9670–9685.
- [23] A. Kulkarni, W. Zhou, B. Török, *Org. Lett.* **2011**, *13*, 5124–5127.
- [24] T. Kappe, P. Roschger, B. Schuiki, W. Stadlbauer, *J. Heterocycl. Chem.* **2003**, *40*, 297–302.
- [25] A. Ratnamala, K. Lalitha, J. K. Reddy, V. D. Kumari, M. Subrahmanyam, *J. Mol. Catal. A Chem.* **2008**, *279*, 112–118.
- [26] Y. Li, C. Topf, X. Cui, K. Junge, M. Beller, *Angew. Chem. Int. Ed.* **2015**, *54*, 5196–5200.
- [27] P. G. Cozzi, L. Zoli, *Angew. Chem. Int. Ed.* **2008**, *47*, 4162–4166.
- [28] S. Chen, M. Wang, X. Jiang, *Chin. J. Chem.* **2018**, *36*, 921–924.
- [29] M. Konobe, WO2011065451 (A1), **2010**.

5 The Synthesis of Hydroquinolines from Nitroaldehydes and Ketones by Hydrogenation Sequences and Condensations

Christof Bauer, Fatemeh Zareh, Lisa Nüßlein, Johanna Frank, Maxime Boniface, Thomas Lunkenbein and Rhett Kempe

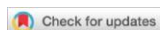
The Synthesis of Hydroquinolines from Nitroaldehydes and Ketones by Hydrogenation Sequences and Condensations

Chem. Eur. J. **2025**, e202500462

Copyright Wiley-VCH GmbH.

Reproduced with permission (<https://creativecommons.org/licenses/by/4.0/>).

DOI: <https://doi.org/10.1002/chem.202500462>



The Synthesis of Hydroquinolines from Nitroaldehydes and Ketones by Hydrogenation Sequences and Condensations

Christof Bauer^{†, [a]} Fatemeh Zareh^{†, [a]} Lisa Nüßlein,^[a] Johanna Frank,^[a] Maxime Boniface,^[b] Thomas Lunkenbein,^[b] and Rhett Kempe^{*[a]}

Catalytic reaction discovery or methodology development is preferably performed with homogeneous catalysts, but heterogeneous catalysts allow the design of complex multistep syntheses based on their reusability. We introduce here the catalytic synthesis of hydroquinolines starting from nitroaldehydes, ketones and hydrogen. The reaction is complex and proceeds via multiple selective hydrogenation and condensation steps. The nitroaldehyde is selectively hydrogenated

forming an aminoaldehyde, followed by a base-catalyzed Friedländer synthesis and selective quinoline hydrogenation. The starting materials are inexpensive, simple regarding their structure and diversely available, and the hydroquinoline motif is part of numerous biologically active compounds. A nano-structured earth-abundant metal catalyst mediates our reaction most efficiently.

Introduction

The discovery of catalytic reactions or methodology development is preferentially carried out with homogeneous catalysts.^[1] Homogeneous or molecular catalysts are easily modified to provide the activity and selectivity required to mediate novel chemical reactions. In addition, detailed (structural) characterization of active catalysts is easier in comparison to heterogeneous or enzyme catalysts.^[2] Heterogeneous catalysts, if reusable, can not only be used several times for the same reaction but also in different reactions sequentially.^[3] This quality might open perspectives to rationally design and mediate complex chemical reactions. We have introduced a complex condensation reaction where reusable noble metal catalysts were added and removed to mediate a multistep hydrogenation and dehydrogenation sequence^[4] and report here the direct synthesis of hydroquinolines starting from nitroaldehydes and ketones and (no break here)hydrogen (Figure 1). The starting materials of our reaction are inexpensive, simple regarding their structure and diversely available, and the hydroquinoline motif

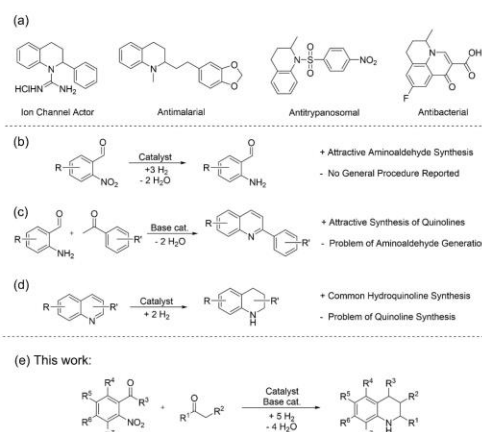


Figure 1. State of the art and reaction reported here. (a) Selection of bioactive molecules with a 1,2,3,4-tetrahydroquinoline motif. (b) Selective hydrogenation of 2-nitrobenzaldehyde to 2-aminobenzaldehyde. (c) Friedländer synthesis. (d) Selective hydrogenation of 2-phenylquinoline to 2-phenyl-1,2,3,4-tetrahydroquinoline. (e) The direct synthesis of tetrahydroquinolines.

[a] C. Bauer,[†] F. Zareh,[†] L. Nüßlein, J. Frank, Prof. Dr. R. Kempe
Inorganic Chemistry II – Catalyst Design
Sustainable Chemistry Centre
University of Bayreuth
95440 Bayreuth (Germany)
E-mail: kempe@uni-bayreuth.de
Homepage: www.sustainable-chemistry-centre.uni-bayreuth.de

[b] Dr. M. Boniface, Dr. T. Lunkenbein
Fritz Haber Institute of the Max Planck Society
Department of Inorganic Chemistry
14195 Berlin (Germany)

[†] These authors contribute equally.

Supporting information for this article is available on the WWW under <https://doi.org/10.1002/chem.202500462>

© 2025 The Author(s). Chemistry – A European Journal published by Wiley-VCH GmbH. This is an open access article under the terms of the Creative Commons Attribution License, which permits use, distribution and reproduction in any medium, provided the original work is properly cited.

is important, figures prominently among pharmaceuticals (Figure 1a) and its synthesis is intensively investigated.^[5] Our reaction proceeds via multiple selective hydrogenation and condensation steps. The nitroaldehyde is selectively hydrogenated to an aminoaldehyde^[6] (Figure 1b) followed by a base-catalyzed Friedländer synthesis^[7] (Figure 1c) forming a quinoline and a final selective quinoline hydrogenation step^[8] (Figure 1d). A novel reusable nickel catalyst mediates all hydrogenation steps selectively. The reaction has a broad scope, an attractive functional group tolerance and upscaling has been demonstrated.

The Synthesis of Hydroquinolines from Nitroaldehydes and Ketones by Hydrogenation Sequences and Condensations

Chemistry—A European Journal

Research Article
doi.org/10.1002/chem.202500462

Chemistry
Europe
European Chemical
Societies Publishing

Results and Discussion

Catalyst Synthesis and Characterization

The synthesis of our catalyst is shown in Figure 2a. The catalyst support material N-SiC (a porous N-doped and Si-coated carbon) was synthesized according to a procedure published previously (Supporting Information 2.1).^[9] Cross-linking of the commercially available polycarbosilane precursor SMP-10 and acrylonitrile using azobis(isobutyronitrile), pyrolysis and the removal of the Si-rich phase by base treatment are the N-SiC synthesis steps. The N-SiC support material was wet impregnated with a solution of $\text{Ni}(\text{NO}_3)_2 \cdot 6 \text{H}_2\text{O}$ in water, followed by pyrolysis (700 °C) under nitrogen flow and reduction (550 °C) under forming gas ($\text{N}_2:\text{H}_2$, 90:10) to form the Ni/N-SiC catalyst (Figure 2b and Supporting Information 2.2). Inductively coupled plasma optical emission spectrometry analysis of Ni/N-SiC showed no significant deviation from the theoretical nickel content of 4.0 wt% (Supporting Information 3.1). Elemental analysis revealed that Ni/N-SiC consists of 83.3% C, 5.7% N and 7.0% Si in addition to nickel (Supporting Information 3.2). Scanning electron microscopy in combination with energy dispersive X-ray spectroscopy (SEM-EDX) confirmed the homogeneous distribution of nickel over N-SiC (Supporting Information 3.3) and verified a smooth wet impregnation process.

Scanning transmission electron microscopy (STEM) in combination with high-angle annular dark-field (HAADF) imaging analysis revealed a homogeneous distribution of nanoparticles over the support material (Figure 2b–c) and an average particle size of 8.5 nm (Figure 2d). The presence of nickel nanoparticles was confirmed using HAADF-STEM in combination with EDX element maps (Figure 2e–h). High resolution transmission electron microscopy in combination with electron energy loss spectroscopy (EELS) with a line scan over one nickel nanoparticle was performed next (Supporting Information 3.5). The resulting EELS spectrum and the calculated $\text{Ni}(\text{L}_3) : \text{Ni}(\text{L}_2)$ intensity ratio of 1.38 fit to the literature value consistent with metallic Ni.^[10] In addition, no oxygen was detected in the STEM-EELS measurements. We propose that Ni/N-SiC consist of metallic nickel nanoparticles supported by N-SiC. Fast Fourier transformation of a single nickel nanoparticle (Supporting Information 3.6) indicates cubic nickel. (no break here)X-ray photoelectron spectroscopy (XPS) was performed to study the surface of the cubic nickel nanoparticles (Supporting Information 3.7). The spectra were measured before and after Pt sputtering. The pre-sputtering spectrum shows the presence of metallic nickel (49%) and nickel oxide (51%), while after sputtering, the metallic nickel content increases to 89% and the nickel oxide content decreases to 11%. We assume that the nickel nanoparticles are surrounded by a very thin layer of

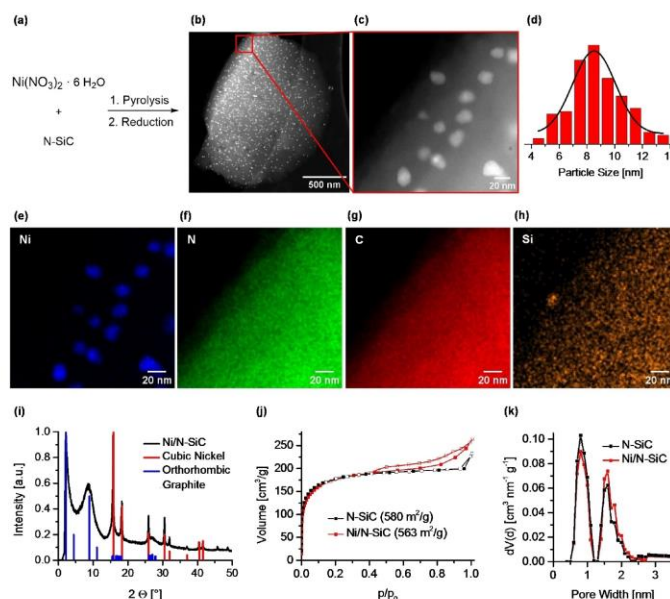


Figure 2. Synthesis and characterization of the Ni/N-SiC catalyst. (a) Synthesis of the Ni/N-SiC catalyst: Wet impregnation of N-SiC with aqueous solution of $\text{Ni}(\text{NO}_3)_2 \cdot 6 \text{H}_2\text{O}$, pyrolysis and reduction. (b) HAADF-STEM analysis suggests the presence of homogeneously distributed nanoparticles. (c) Close-up of the HAADF-STEM. (d) Nanoparticle distribution with an average particle size of 8.5 nm (150 particles counted). (e–h) HAADF-STEM images of Ni/N-SiC with representative EDX element maps of nickel (e), nitrogen (f), carbon (g) and silicon (h). (i) PXRD of the Ni/N-SiC catalyst (black). The reflexes match those of cubic nickel (red, reference code: 00-004-0850). (j) Surface characterization and (k) pore size distribution of the catalyst via Ar physisorption measurements (calculation model: Ar at -186.15°C on carbon: cylindric pores, non-local density functional theory equilibrium model). The specific surface area showed a slight decrease from 580 m^2/g of the support material to 563 m^2/g of the catalyst.

The Synthesis of Hydroquinolines from Nitroaldehydes and Ketones by Hydrogenation Sequences and Condensations

Chemistry—A European Journal

Research Article
doi.org/10.1002/chem.202500462

Chemistry
Europe
European Chemical
Societies Publishing

nickel oxide. Powder X-ray diffraction (PXRD) of Ni/N-SiC (Figure 2i) confirms cubic nickel (red) and orthorhombic graphite (blue). The specific surface area was determined by argon physisorption measurements (Figure 2j), which showed a slight decrease of the surface area from 580 m²/g of the N-SiC support to 563 m²/g of the catalyst. The pore size distribution of Ni/N-SiC (Figure 2k) shows a predominance of micropores.

Optimization of Reaction Conditions

The reaction of 2-nitrobenzaldehyde with acetophenone to form 2-phenyl-1,2,3,4-tetrahydroquinoline was chosen to determine suitable reaction conditions. The reaction is complex and consists of three steps: the hydrogenation of nitrobenzaldehydes to aminobenzaldehydes (A), the *Friedländer* synthesis (B) and the hydrogenation of quinolines to 1,2,3,4-tetrahydroquinolines (C). A screening of different solvents revealed that 3 mL ethanol is the best solvent for all three steps (Table S2–S3). Several types of bases were investigated, with LiOH being the best base used in a catalytic amount (Table S4–S5). The amount of base seems to have an optimum. More base accelerates the condensation steps but slows down the final hydrogenation step. Investigation of the H₂ pressure, if needed, and time and temperature revealed that the best conditions for step A are 40 °C at 3.0 MPa hydrogen pressure for 20 h (Table S6–S7). The best yield for step B was obtained at 60 °C for 20 h (Table S8), and 120 °C with 5.0 MPa hydrogen pressure for 48 h (Table S9–S10) gave the best results for step C. Next, the pyrolysis temperature for the catalyst synthesis was varied and different commercially available support materials and nickel precursors were tested for the overall reaction (Table 1). Lowering the pyrolysis temperature below 700 °C reduced the yield obtained, as did pyrolysis temperatures above 700 °C. Different catalyst

lines (C). A screening of different solvents revealed that 3 mL ethanol is the best solvent for all three steps (Table S2–S3). Several types of bases were investigated, with LiOH being the best base used in a catalytic amount (Table S4–S5). The amount of base seems to have an optimum. More base accelerates the condensation steps but slows down the final hydrogenation step. Investigation of the H₂ pressure, if needed, and time and temperature revealed that the best conditions for step A are 40 °C at 3.0 MPa hydrogen pressure for 20 h (Table S6–S7). The best yield for step B was obtained at 60 °C for 20 h (Table S8), and 120 °C with 5.0 MPa hydrogen pressure for 48 h (Table S9–S10) gave the best results for step C. Next, the pyrolysis temperature for the catalyst synthesis was varied and different commercially available support materials and nickel precursors were tested for the overall reaction (Table 1). Lowering the pyrolysis temperature below 700 °C reduced the yield obtained, as did pyrolysis temperatures above 700 °C. Different catalyst

Table 1. Nickel catalyst screening.^[a]

<div> <p>Overall Reaction</p> <p>Step A: 2-nitrobenzaldehyde + 3 H₂ → 2-aminobenzaldehyde + 2 H₂O (catalyzed by Ni/N-SiC)</p> <p>Step B: 2-aminobenzaldehyde + acetophenone → 2-phenylquinoline + 2 H₂O (catalyzed by LiOH)</p> <p>Step C: 2-phenylquinoline + 2 H₂ → 2-phenyl-1,2,3,4-tetrahydroquinoline (catalyzed by Ni/N-SiC)</p> </div>				
Entry	Metal Source	Support Material	Pyrolysis Temperature [°C]	Yield [%]
1	Ni(NO ₃) ₂ ·6 H ₂ O	N-SiC	500	45
2	Ni(NO ₃) ₂ ·6 H ₂ O	N-SiC	600	48
3	Ni(NO ₃) ₂ ·6 H ₂ O	N-SiC	700	91
4	Ni(NO ₃) ₂ ·6 H ₂ O	N-SiC	800	28
5	Ni(NO ₃) ₂ ·6 H ₂ O	N-SiC	900	8
6	Ni(NO ₃) ₂ ·6 H ₂ O	Activated Carbon	700	6
7	Ni(NO ₃) ₂ ·6 H ₂ O	γ-Al ₂ O ₃	700	0
8	Ni(NO ₃) ₂ ·6 H ₂ O	TiO ₂	700	0
9	Ni(NO ₃) ₂ ·6 H ₂ O	SiO ₂	700	0
10	Ni(NO ₃) ₂ ·6 H ₂ O	CeO ₂	700	0
11	Ni(OAc) ₂ ·4 H ₂ O	N-SiC	700	4
12	Ni(acac) ₃ ·2 H ₂ O	N-SiC	700	51
13	Ni(II)stearate	N-SiC	700	12
14	NiCl ₂ ·6 H ₂ O	N-SiC	700	4
15	–	N-SiC	700	0

[a] Reaction conditions: Step A: 4 mol % Ni/N-SiC (0.02 mmol Ni, 1.17 mg Ni), 0.5 mmol 2-nitrobenzaldehyde, 0.5 mmol acetophenone, 3 mL ethanol, 3.0 MPa H₂, 40 °C for 20 h. Step B: Addition of 0.3 mmol LiOH then 60 °C for 20 h. Step C: 5.0 MPa H₂, 120 °C for 48 h. Yields were determined by GC using n-dodecane as an internal standard.

The Synthesis of Hydroquinolines from Nitroaldehydes and Ketones by Hydrogenation Sequences and Condensations

Chemistry—A European Journal

Research Article
doi.org/10.1002/chem.202500462

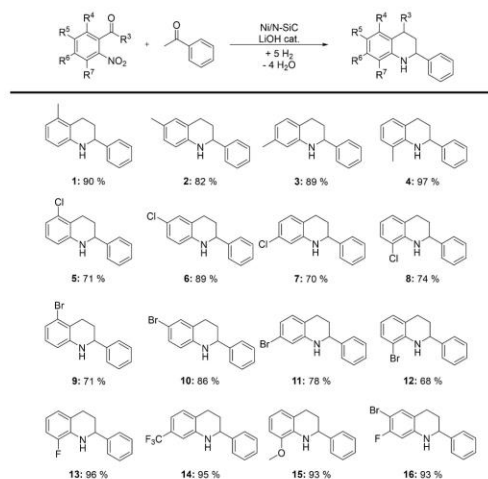
Chemistry
Europe
European Chemical
Societies Publishing

support materials, such as activated carbon, γ -Al₂O₃, TiO₂, SiO₂ and CeO₂, were investigated. They all showed no activity, except for activated carbon with a very low yield of 6%. The use of nickel nitrate as a metal precursor is important for the superior activity and selectivity of our catalyst. Only a little activity was observed for the metal precursors nickel acetate, nickel stearate and nickel chloride. An important issue is the smooth impregnation including the solubility of the nickel salt used. It is solely the nickel acetylacetonate precursor that shows a higher yield, with 51% of the product of interest. Variation of the catalyst metal loading revealed that a catalyst with 4.0 wt% nickel is optimal (Table S11) and 4.0 mol% Ni was identified as the catalyst loading for the three reaction steps (Table S12). Time conversion studies (Supporting Information 4.2) showed that step A is complete after 15 h under the optimal reaction conditions applied. The complete conversion of 2-aminobenzaldehyde with acetophenone to 2-phenylquinoline is achieved after 14 h in step B. The selective hydrogenation of 2-phenylquinoline to 2-phenyl-1,2,3,4-tetrahydroquinoline, step C, is the most demanding step of the overall reaction. A maximum yield of 91% was obtained after 42 h. In summary, the overall reaction can be carried out applying the following reaction conditions: Step A: 4.0 mol% Ni (4.0 wt% Ni), 0.5 mmol 2-nitrobenzaldehyde, 0.5 mmol acetophenone, 3 mL ethanol, 3.0 MPa H₂, 40 °C and 20 h reaction time. Step B: Addition of 0.6 eq LiOH and 20 h reaction time. Step C: 5.0 MPa H₂, 120 °C and 48 h reaction time. Starting the reaction with step B is challenging since there is no general amino aldehyde synthesis.

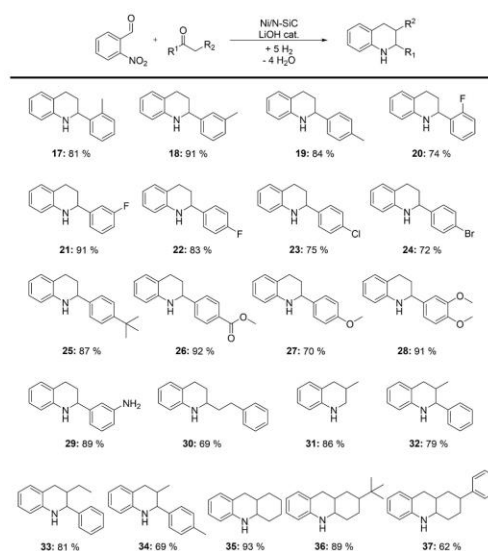
Substrate Scope

With the optimized reaction conditions in hand, we became interested in the applicability of our complex reaction. Aldehyde variations employing acetophenone are shown in Scheme 1. Firstly, we applied our protocol to synthesize products carrying electron-donating methyl substituents. The products desired were obtained in mostly very good yields and any position on the aryl ring of the 2-nitrobenzaldehyde derivatives could be addressed (Scheme 1, products 1–4). In addition, we can tolerate electron-withdrawing substituents and, again, any position on the aryl ring of the 2-nitrobenzaldehyde could be tolerated (Scheme 1, products 5–12), albeit lower product yields were obtained. Furthermore, 8-fluoro-2-phenyl-1,2,3,4-tetrahydroquinoline was synthesized in a 96% isolated yield (Scheme 1, product 13) and a CF₃ group was tolerated and an isolated yield of 95% was obtained (Scheme 1, product 14). Moreover, we successfully synthesized 8-methoxy-2-phenyl-1,2,3,4-tetrahydroquinoline in a 93% isolated yield (Scheme 1, product 15), and a product bearing two different functional groups was also introduced (Scheme 1, product 16).

We next investigated the ketone variation (Scheme 2). We used the same conditions and isolated 21 different products. Electron-donating methyl groups in the *para*-, *meta*- and *ortho*-positions of the 2-phenyl substituent of the 1,2,3,4-tetrahydroquinoline were well tolerated (Scheme 2, products 17–19).



Scheme 1. Direct synthesis of hydroquinolines with acetophenone and variation of the nitroaldehyde educts. Reaction conditions: Step A: 29.3 mg Ni/N-SiC catalyst (4 mol% Ni, 0.02 mmol Ni, 1.17 mg Ni), 0.5 mmol 2-nitrobenzaldehyde, 0.5 mmol acetophenone, 3 mL ethanol, 3.0 MPa H₂, 40 °C for 20 h. Step B: Addition of 0.3 mmol LiOH. Then 60 °C for 20 h. Step C: 5.0 MPa H₂, 120 °C for 48 h. Isolated yields are given.



Scheme 2. Direct synthesis of hydroquinolines with 2-nitrobenzaldehyde and a variation of the ketone educt. Reaction conditions: Step A: 29.3 mg Ni/N-SiC catalyst (4 mol% Ni, 0.02 mmol Ni, 1.17 mg Ni), 0.5 mmol 2-nitrobenzaldehyde, 0.5 mmol ketone, 3 mL ethanol, 3.0 MPa H₂, 40 °C for 20 h. Step B: Addition of 0.3 mmol LiOH. Then 60 °C for 20 h. Step C: 5.0 MPa H₂, 120 °C for 48 h. Isolated yields are given.

The Synthesis of Hydroquinolines from Nitroaldehydes and Ketones by Hydrogenation Sequences and Condensations

Chemistry—A European Journal

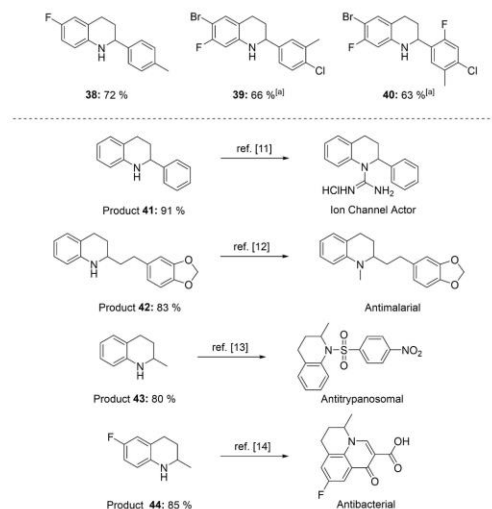
Research Article
doi.org/10.1002/chem.202500462

Chemistry
Europe
European Chemical
Societies Publishing

Similarly, it is possible to incorporate electron-withdrawing groups and products with fluoro substituents in the *para*-, *meta*- and *ortho*-positions of the 2-phenyl substituent which were synthesized (Scheme 2, products 20–22). The conversion of 2-fluoroacetophenone with 2-nitrobenzaldehyde was the most challenging and resulted in an isolated product yield of 74%. We assume that the combination of electron-withdrawing and steric hindrance is challenging. Chloro- (Scheme 2, product 23) and bromo-substituted (Scheme 2, product 24) products could be synthesized. Note that the difficulty of introducing halogen-substituted educts into the procedure due to the harsh conditions in step C did not occur in a large quantity. The *tert*-butyl group could be introduced, giving 2-(4-(*tert*-butyl)phenyl)-1,2,3,4-tetrahydroquinoline in an 87% yield (Scheme 2, product 25) and a 1,2,3,4-tetrahydroquinoline bearing an acetate group on the phenyl ring was also obtained in a very good yield (Scheme 2, product 26). Methoxy groups are tolerated and a dimethoxy derivative gives a higher yield (91%, product 28) than a monomethoxy derivative (70%, product 27). The synthesis protocol is also successful when an amine group is present (Scheme 2, product 29). We next investigated the synthesis of alkyl-substituted hydroquinolines: 2-phenethyl-1,2,3,4-tetrahydroquinoline (Scheme 2, product 30) and 3-methyl-1,2,3,4-tetrahydroquinoline (Scheme 2, product 31) were synthesized. The latter example shows that we can use two aldehydes in our catalytic synthesis. Furthermore, various 2,3-disubstituted products, including three-cyclic products, were synthesized (Scheme 2, products 32 to 37). Aldehyde and ketone can be varied simultaneously and we obtained 6-fluoro-2-(*para*-tolyl)-1,2,3,4-tetrahydroquinoline in a 72% yield (Scheme 3, product 38). Moreover, 1,2,3,4-tetrahydroquinoline with up to four different substituents was synthesized (Scheme 3, product 39 and 40).

Our hydroquinoline synthesis is also interesting in terms of applications (synthesis of biologically active ingredients [of drug molecules], Scheme 3). Our benchmark substrate, product 41, can be easily converted into an ion channel inhibitor in one step.^[11] 2-(2-(benzo[d][1,3]dioxol-5-yl)ethyl)-1,2,3,4-tetrahydroquinoline (Product 42), which we synthesized in an 83% isolated yield, can be easily converted to galipinine.^[12] Alkaloids from *Galipea officinalis* have long been known for their medicinal effects and galipinine acts as an antiparasitic and cytotoxic agent against malaria. Product 43, synthesized from 2-nitrobenzaldehyde and acetone in an 80% yield, can be converted into the active ingredient of an antiparasitic drug.^[13] The synthesized 6-fluoro-2-methyl-1,2,3,4-tetrahydroquinoline (Product 44, 85% yield) can be converted to flumequine, which has antimicrobial activity, can be used as an antibacterial agent and was first synthesized in 1972.^[14]

An upscaling of the benchmark reaction was performed using 10 mmol of 2-nitrobenzaldehyde and 10 mmol of acetophenone. An isolated yield of 86% of 2-phenyl-1,2,3,4-tetrahydroquinoline was observed (Supporting Information 4.3). Examinations of the catalyst after the direct synthesis of hydroquinolines by TEM showed no agglomeration or growth of the nickel nanoparticles of the catalyst used. Moreover, the particle size distribution remains constant, with an average



Scheme 3. Highly functionalized 1,2,3,4-tetrahydroquinolines varying both aldehyde and ketone sides and applications of synthesized substrates as precursors for drug molecules. Reaction conditions: Step A: 29.3 mg Ni/N-SiC catalyst (4 mol % Ni, 0.02 mmol Ni, 1.17 mg Ni), 0.5 mmol aldehyde, 0.5 mmol ketone, 3 mL ethanol, 3.0 MPa H₂, 40 °C for 20 h. Step B: Addition of 0.3 mmol LiOH. Then 60 °C, for 20 h. Step C: 5.0 MPa H₂, 120 °C for 48 h. [a] Step B: 1.5 mmol LiOH. Isolated yields are given.

particle diameter of 8.5 nm (Supporting Information 4.5.1). A hot filtration test was subsequently conducted. The separated solution showed no activity and the formation of other products was not observed (Supporting Information 4.5.2). Investigation of leaching via ICP-OES suggested negligible leaching and reusability test indicated very good reusability.

Conclusions

In summary, we report a complex catalytic reaction mediated by a reusable earth-abundant metal catalyst and a simple base (catalyst). The reaction was designed to permit the conversion of inexpensive, structurally simple and diversely available starting materials (nitroaldehydes, ketones and hydrogen) into an important class of N-heterocyclic compounds, namely, hydroquinolines.

Acknowledgements

We thank the SFB 1585 Project A02, 492723217 for financial support. M.B. and T.L. acknowledge the Federal Ministry of Education and Research in the framework of the Catlab project (03EW0015A). In addition, the authors thank F. Baier for XPS measurements, Dr. U. Lacher for HRMS analysis and Dr. C. Denner for SEM-EDX measurements and the Bavarian Polymer Institute (University of Bayreuth, KeyLab Electron and Optical

The Synthesis of Hydroquinolines from Nitroaldehydes and Ketones by Hydrogenation Sequences and Condensations

Chemistry—A European Journal

Research Article
doi.org/10.1002/chem.202500462



Microscopy) for assistance with TEM and SEM-EDX measurements. Open Access funding enabled and organized by Projekt DEAL.

Conflict of Interests

The authors declare no conflict of interest.

Data Availability Statement

The data that support the findings of this study are available in the supplementary material of this article.

Keywords: condensation/synthesis · heterogeneous catalysis · hydrogenation · hydroquinolines · nickel

- [1] a) T. Zhang, Z. Zhang, G. Kang, T. Sheng, J. Yan, Y. Yang, Y. Ouyang, J. Yu, *Science* **2024**, *384*, 793–798; b) J.-J. Chen, J.-H. Fang, X.-Y. Du, J.-Y. Zhang, J.-Q. Bian, F.-L. Wang, C. Luan, W.-L. Liu, J.-R. Liu, X.-Y. Dong, et al., *Nature* **2023**, *618*, 294–300; c) C. Chen, G. C. Fu, *Nature* **2023**, *618*, 301–307; d) B. Ramadoss, Y. Jin, S. Asako, L. Ilies, *Science* **2022**, *375*, 658–663; e) F. Le Vaillant, A. Mateos Calbet, S. González-Pelayo, E. J. Reijerse, S. Ni, J. Busch, J. Cornella, *Nature* **2022**, *604*, 677–683; f) T. Dietel, F. Lukas, W. P. Kretschmer, R. Kempe, *Science* **2022**, *375*, 1021–1024.
- [2] B. Cornils, W. A. Herrmann, J.-H. Xu, H.-W. Zanthoff, *Catalysis from A to Z*, Wiley-VCH, **2020**.
- [3] a) R. V. Jagadeesh, K. Murugesan, A. S. Alshammari, H. Neumann, M.-M. Pohl, J. Radnik, M. Beller, *Science* **2017**, *358*, 326–332; b) F. A. West-erhaus, R. V. Jagadeesh, G. Wienhöfer, M.-M. Pohl, J. Radnik, A.-E. Surkus, J. Rabeah, K. Junge, H. Junge, M. Nielsen, et al., *Nat. Chem.* **2013**, *5*, 537–543; c) R. V. Jagadeesh, A.-E. Surkus, H. Junge, M.-M. Pohl, J. Radnik, J. Rabeah, H. Huan, V. Schünemann, A. Brückner, M. Beller, *Science* **2013**, *342*, 1073–1076; d) G. Hahn, P. Kunas, N. de Jonge, R. Kempe, *Nat. Catal.* **2019**, *2*, 71–77; e) J.-L. Sun, H. Jiang, P. H. Dixneuf, M. Zhang, *J. Am. Chem. Soc.* **2024**, *146*, 11289–11298; f) H. Hua, C. Ci, P. H. Dixneuf, M. Zhang, *J. Am. Chem. Soc.* **2025**, *147*, 6572–6582.
- [4] D. Forberg, T. Schwob, R. Kempe, *Nat. Commun.* **2018**, *9*, 1751.
- [5] a) J. J. Melder, M. L. Heldner, R. Kugler, L. A. Ziegenhagen, F. Rominger, M. Rudolph, A. S. K. Hashmi, *J. Am. Chem. Soc.* **2024**, *146*, 14521–14527; b) G. J. Sherborne, P. Kemmitt, C. Prentice, E. Zysman-Colman, A. D. Smith, C. Fallan, *Angew. Chem. Int. Ed.* **2023**, *62*, e202207829; c) P. Rojo, M. Molinari, A. Cabré, C. García-Mateos, A. Riera, X. Verdager, *Angew. Chem. Int. Ed.* **2022**, *61*, e202204300; d) S. Guo, Y. Wu, C. Wang, Y. Gao, M. Li, B. Zhang, C. Liu, *Nat. Commun.* **2022**, *13*, 5297; e) X. Xu, X. Zheng, X. Xu, *ACS Catal.* **2021**, *11*, 14995–15003; f) Z. Han, G. Liu, X. Yang, X.-Q. Dong, X. Zhang, *ACS Catal.* **2021**, *11*, 7281–7291; g) X. Feng, Y. Song, W. Lin, *J. Am. Chem. Soc.* **2021**, *143*, 8184–8192; h) L. Qi, J. Chen, B. Zhang, R. Nie, Z. Qi, T. Kobayashi, Z. Bao, Q. Yang, Q. Ren, Q. Sun, et al., *ACS Catal.* **2020**, *10*, 5707–5714; i) V. Papa, Y. Cao, A. Spannenberg, K. Junge, M. Beller, *Nat. Catal.* **2020**, *3*, 135–142; j) J. Zhang, Z. An, Y. Zhu, X. Shu, H. Song, Y. Jiang, W. Wang, X. Xiang, L. Xu, J. He, *ACS Catal.* **2019**, *9*, 11438–11446.
- [6] D. Formenti, F. Ferretti, F. K. Scharnagl, M. Beller, *Chem. Rev.* **2019**, *119*, 2611–2680.
- [7] a) P. Friedlaender, *Ber. Dtsch. Chem. Ges.* **1882**, *15*, 2572–2575; b) P. Friedländer, C. F. Gohring, *Ber. Dtsch. Chem. Ges.* **1883**, *16*, 1833–1839.
- [8] a) H. Adkins, H. I. Cramer, *J. Am. Chem. Soc.* **1930**, *52*, 4349–4358; b) H. Adkins, H. R. Billica, *J. Am. Chem. Soc.* **1948**, *70*, 695–698; c) J. E. Shaw, P. R. Stapp, *J. Heterocycl. Chem.* **1987**, *24*, 1477–1483; d) P. Ryabchuk, G. Agostini, M.-M. Pohl, H. Lund, A. Agapova, H. Junge, K. Junge, M. Beller, *Sci. Adv.* **2018**, *4*, eaat0761.
- [9] a) L. F. B. Ribeiro, O. Flores, P. Furtat, C. Gervais, R. Kempe, R. A. F. Machado, G. Motz, *J. Mater. Chem. A* **2017**, *5*, 720–729; b) C. Bäuml, C. Bauer, R. Kempe, *ChemSusChem* **2020**, *13*, 3110–3114; c) T. Schöner, S. L. J. Thomä, L. Kaiser, M. Zobel, R. Kempe, *Chem. Eur. J.* **2020**, *26*, 1609–1614; d) M. Elfinger, T. Schöner, S. L. J. Thomä, R. Stäglich, M. Drechsler, M. Zobel, J. Senker, R. Kempe, *ChemSusChem* **2021**, *14*, 2360–2366.
- [10] G. Evmenenko, T. T. Fister, D. B. Buchholz, F. C. Castro, Q. Li, J. Wu, V. P. David, P. Fenter, M. J. Bedzyk, *Phys. Chem. Chem. Phys.* **2017**, *19*, 20029–20039.
- [11] M. C. Maillard, M. E. Perlman, O. Amitay, D. Baxter, D. Berlove, S. Connaughton, J. B. Fischer, J. Q. Guo, L. Y. Hu, R. N. McBurney, et al., *J. Med. Chem.* **1998**, *41*, 3048–3061.
- [12] a) I. Jacquemond-Collet, F. Benoit-Vical, A. Valentín, E. Stanislas, M. Mallié, I. Fourasté, *Planta Med.* **2002**, *68*, 68–69; b) J. H. Rakotoson, N. Fabre, I. Jacquemond-Collet, S. Hannedouche, I. Fourasté, C. Moulis, *Planta Med.* **1998**, *64*, 762–763.
- [13] R. J. Pagliaro, S. Lusvardi, A. B. Pierini, R. Brun, M. R. Mazzieri, *Bioorg. Med. Chem.* **2010**, *18*, 142–150.
- [14] a) F. Chen, A.-E. Surkus, L. He, M.-M. Pohl, J. Radnik, C. Topf, K. Junge, M. Beller, *J. Am. Chem. Soc.* **2015**, *137*, 11718–11724; b) J. F. S. P. M. V. S. A. Gerster, J. F. S. P. M. U. Gerster, DE2264163 (A1), **1972**; c) J. Bálint, G. Egri, E. Fogassy, Z. Böcskei, K. Simon, A. Gajáry, A. Friesz, *Tetrahedron: Asymmetry* **1999**, *10*, 1079–1087.

Manuscript received: February 5, 2025

Accepted manuscript online: March 12, 2025

Version of record online: April 2, 2025

Chemistry–A European Journal

Supporting Information

The Synthesis of Hydroquinolines from Nitroaldehydes and Ketones by Hydrogenation Sequences and Condensations

Christof Bauer, Fatemeh Zareh, Lisa Nüßlein, Johanna Frank, Maxime Boniface,
Thomas Lunkenbein, and Rhett Kempe*

Table of Contents

1	General Considerations	4
2	Experimental Procedures	6
2.1	Synthesis of the Support Material N-SiC	6
2.2	Catalyst Synthesis	6
2.3	Catalytic Procedures	7
2.3.1	Synthesis of Hydroquinolines from Nitroaldehydes and Ketones – General Procedure	7
3	Characterization of the Catalyst	8
3.1	ICP-OES	8
3.2	CHN Analysis	8
3.3	SEM-EDX	9
3.4	HAADF-STEM with EDX	10
3.5	HR-TEM with EELS	11
3.6	HR-TEM with FFT	12
3.7	XPS	13
4	Catalytic Studies	14
4.1	Screening of Reaction Parameters	14
4.2	Time-Conversion-Plot	22
4.3	Upscaling of the Reaction	23
4.4	Reusability	24
4.5	Evaluation of the Used Catalyst	25
4.5.1	TEM Measurements	25
4.5.2	Hot Filtration Test	26
4.5.3	Leaching Test	27
5	Characterization of Isolated Products	28
6	NMR Spectra	51

The Synthesis of Hydroquinolines from Nitroaldehydes and Ketones by Hydrogenation Sequences and Condensations

7	References.....	95
---	-----------------	----

1 General Considerations

All air- and moisture sensitive reactions were performed under dry argon or nitrogen atmosphere using standard Schlenk and glove box techniques. Dried solvents were obtained from a solvent purification system (activated alumina cartridges) or purchased from commercial sources. Deuterated solvents were dried via molecular sieves. All chemicals were acquired from commercial sources with purity over 95 % and used without further purification.

Pyrolysis of the catalyst was performed under nitrogen atmosphere in a ChemBET Pulsar TPR/TPD instrument from Quantachrome.

Transmission electron microscopy (TEM) was carried out by using a JEOL JEM-2200FS. For the sample preparation, the samples were suspended in chloroform and sonicated for 5 min. For analysis, the suspension was dropcast on LC200-Cu grids. High-angle annular dark-field scanning transmission electron microscopy (HAADF-STEM) and electron energy loss spectroscopy (EELS) measurements were performed using a JEM-ARM200F (JEOL, 200 kV), equipped with a HAADF detector with a collection angle (inner and outer) of 68 - 280 mrad and a Quantum Gatan image filter (GIF). EELS was acquired with a convergence angle of 20.8 mrad, a collection angle of 32 mrad, and a dispersion of 0.1 eV. STEM energy dispersive X-ray (STEM-EDX) measurements were performed on a FEI Talos operated at 300 kV equipped with a SuperX system offering a high solid angle and thus superior collection efficiency.

Scanning electron microscopy (SEM) and coupled energy dispersive X-ray spectroscopy (EDX) measurements were carried out by using a Zeiss Ultra plus device. The acceleration voltage was 20 kV. The detection was carried out with an in-lens backscatter detector. For a conductive surface, the samples were sputtered with platinum (layer thickness: 1.3 μm) with the Sputter Coater 208HR from Cressington.

Pore characterizations were carried out via argon physisorption measurements using a 3P Micro 100 Surface Area and Pore Size Analyzer device. The pore size distribution was computed via DFT calculations (calculation model: Ar at -186.15 °C: slit pore, MDFT equilibrium model). The specific surface area was calculated by using p/p_0 values from 0.005-0.1 (BET).

Powder X-ray diffraction (PXRD) data was collected at room temperature on a STOE STADI P Mythen2 4K diffractometer (Ge(111) monochromator; Ag $K\alpha_1$ radiation, $\lambda = 0.5594 \text{ \AA}$), optimized for PDF data collection using four Dectris MYTHEN2 R 1K detectors in Debye-

The Synthesis of Hydroquinolines from Nitroaldehydes and Ketones by Hydrogenation Sequences and Condensations

Scherrer geometry.^[1] Samples were measured in 0.5 mm glass capillaries (Hilgenberg special-purpose glass).

The nickel content was determined by Inductively Coupled Plasma Optical Emission Spectrometry (ICP-OES). The fusion of the catalyst was carried out in a CEM MARS 6 microwave, for the ICP-OES measurements a SPECTRO ARCOS (Spectro Ametek) was used.

X-ray photoelectron spectroscopy (XPS) was performed using a Physical Electronics Phi 5000 Versa Probe III instrument. As X-ray source a monochromatic Al K α with a spot size of 100 μ m (21.1 W) was used. The kinetic pass energy of the photoelectrons was determined with a hemispheric analyzer (45°) set to pass energy of 13 eV for high-resolution spectra.

Elemental analyses were carried out on an Elementar UNICUBE® device.

GC analyses were carried out on an Agilent 6890N GC system equipped with a HP-5 column (30 m x 0.32 mm x 0.25 μ m).

For column chromatography, silica gel 60 (M = 60.09 g/mol, 0.063 - 0.200 mm particle size) from Macherey-Nagel was used. For plate chromatography, silica gel 60 (M = 60.09 g/mol, 15 μ m particle size) from Merck was used.

NMR measurements were performed using a Varian INOVA 300 (300 MHz for ^1H , 75 MHz for ^{13}C) and a Varian INOVA 400 (400 MHz for ^1H , 100 MHz for ^{13}C) instrument at 296 K. Chemical shifts are reported in ppm relative to the residual solvent signal (CDCl_3 : 7,26 ppm (^1H), 77,16 ppm (^{13}C); DMSO-d_6 : 2.50 ppm (^1H), 39.51 ppm (^{13}C)), coupling constants (J) are reported in Hz. Corresponding water peaks from the DMSO-d_6 exchanges are marked in the spectra.

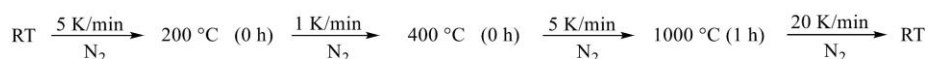
Unknown substrates or substrates with incomplete spectroscopic literature data were additionally analyzed via liquid chromatography-high resolution mass spectra (LC-HRMS). LC-HRMS were obtained from a Thermo Fisher scientific Q-Exactive instrument with a hybrid quadrupole orbitrap analyzer in ESI+ mode.

The hydrogenation experiments were carried out in a 10 mL glass vial with Parr Instrument stainless steel autoclaves N-MT5 300 mL equipped with heating mantles and temperature controller.

2 Experimental Procedures

2.1 Synthesis of the Support Material N-SiC

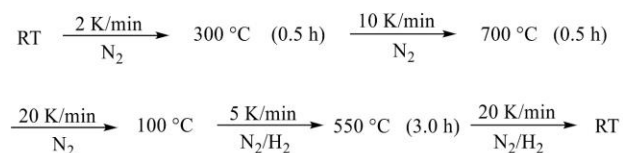
The applied support material was modified according to a known literature procedure.^[2] 0.200 g StarPCSTM SMP-10, 0.988 mL (0.800 g, 15.08 mmol) acrylonitrile (AN) and 0.075 g (0.46 mmol) azobis(isobutyronitrile) (AIBN) were dissolved in 4 mL dimethylformamide (DMF). After polymerization and crosslinking for 16 h at 75 °C, the solvent was removed under reduced pressure, the obtained greenbody was pyrolyzed using following program:



The mass loss after pyrolysis was 45 %. After ball milling for 40 minutes, 500 mg of the ceramic support material were washed by stirring in an aqueous solution of 6.7 mL NaOH ($c = 1 \text{ mol/L}$) and 5 mL MeOH at 90 °C for 24 h under aerobic conditions. Afterwards the material was washed until neutrality and dried at room temperature to obtain the final N-SiC ceramic.

2.2 Catalyst Synthesis

To an aqueous solution (20 mL H₂O) of Ni(NO₃)₂ · 6 H₂O (0.681 mmol, 198.06 mg, 4.0 wt%) 1000 mg support N-SiC were added and the suspension was stirred at 105 °C. After evaporation of the solvent, the active catalyst material is generated by pyrolysis under nitrogen atmosphere at 700 °C followed by reduction at 550 °C (N₂ : H₂ 90 : 10) with the following heating program:



2.3 Catalytic Procedures

2.3.1 Synthesis of Hydroquinolines from Nitroaldehydes and Ketones – General Procedure

For step A a 10 mL glass reaction vial was charged with a magnetic stirring bar, 0.5 mmol nitroaldehyde, 0.5 mmol ketone, 3 mL EtOH and 29.3 mg catalyst (4.0 mol% Ni, 4 wt% Ni, 0.02 mmol Ni, 1.17 mg Ni). The vial was placed in a 300 mL high-pressure autoclave (Parr Instruments). The autoclave was flushed three times with 2.0 MPa hydrogen. Afterwards, 3.0 MPa hydrogen was applied, and the reaction was stirred at 40 °C for 20 h. After completion of the reaction time, the hydrogen was released and subsequently started with step B. To the reaction mixture 7.2 mg LiOH (0.3 mmol, 0.6 eq) were added. After, the reaction mixture was stirred in the autoclave at 60 °C for 20 h to give the corresponding quinoline. Followed by step C the autoclave was flushed again three times with 2.0 MPa hydrogen and pressured with 5.0 MPa hydrogen at 120 °C for 48 h to selectively hydrogenate the quinoline to the corresponding 1,2,3,4-tetrahydroquinoline. At the end of the reaction time, the autoclave was cooled down to room temperature and the hydrogen was released. The catalyst was removed by filtration and the solvent was evaporated via rotary evaporation and high vacuum. If needed, purification via column or plate chromatography was applied. The corresponding product yield was analyzed by ^1H and ^{13}C NMR spectroscopy.

3 Characterization of the Catalyst

3.1 ICP-OES

Theoretical Ni content: 4.00 wt%

Measured Ni content: 3.96 wt%

There is no difference between theoretical and measured nickel loading. The small difference in the values (0.04 wt%, 1.0 % deviation) is due to measurement errors. Since the difference of theoretical and measured contents are insignificant, we continued to use the theoretical value of 4.00 wt% Ni loading on our catalyst.

3.2 CHN Analysis

Table S 1: CHN analysis of the support material N-SiC and the Ni/N-SiC catalyst.

Entry	Material	C [%]	H [%]	N [%]	Si [%]
1	N-SiC	82.7	0.1	6.7	10.5
2	Ni/N-SiC (4 wt% Ni)	83.3	0.0	5.7	7.0

The silicon content was calculated as the difference of the abovementioned elements (C, H, N) and the Ni content to 100 %. Theoretical and measured Ni content via ICP-OES in brackets.

3.3 SEM-EDX

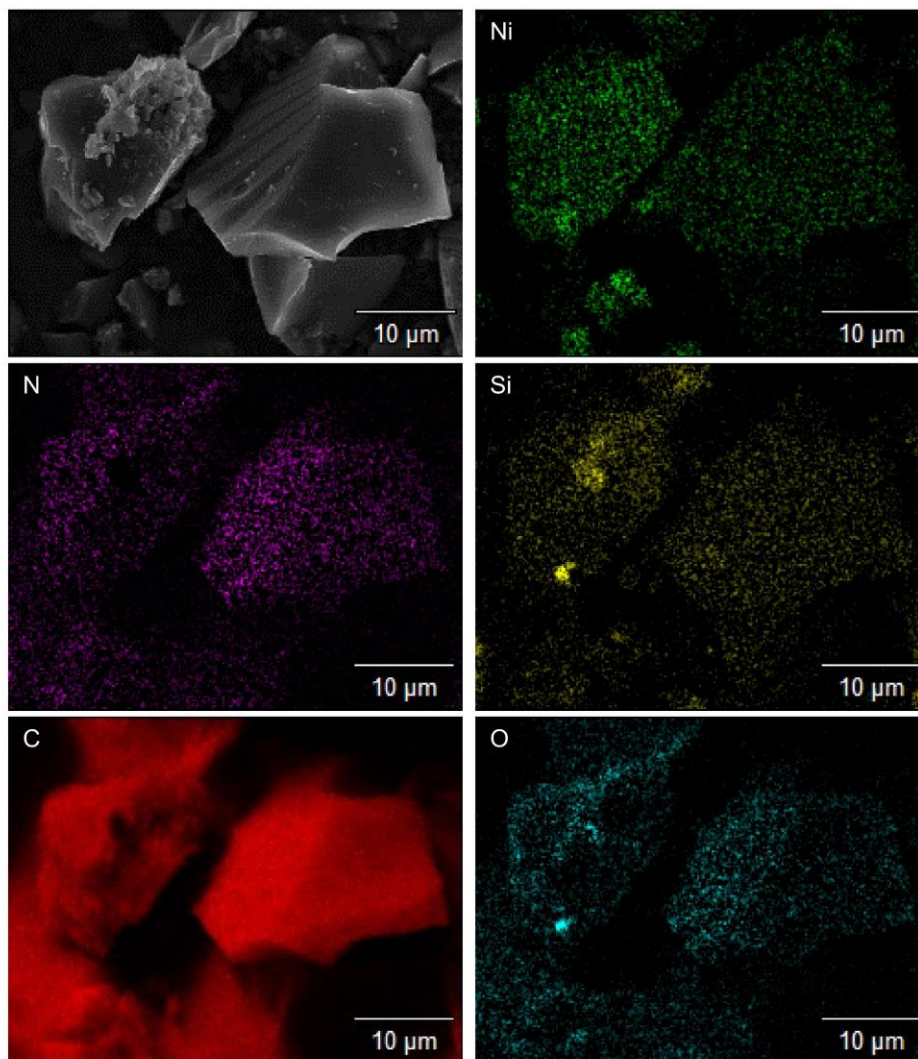


Figure S 1: Scanning electron microscopy (SEM) in combination with energy dispersive X-ray (EDX) mapping of the catalyst Ni/N-SiC. The measurements show a homogeneous distribution of the nickel nanoparticles over the entire material which indicates a smooth impregnation process. The distribution of N, Si, C and O verifies a homogeneous surface of the support material.

3.4 HAADF-STEM with EDX

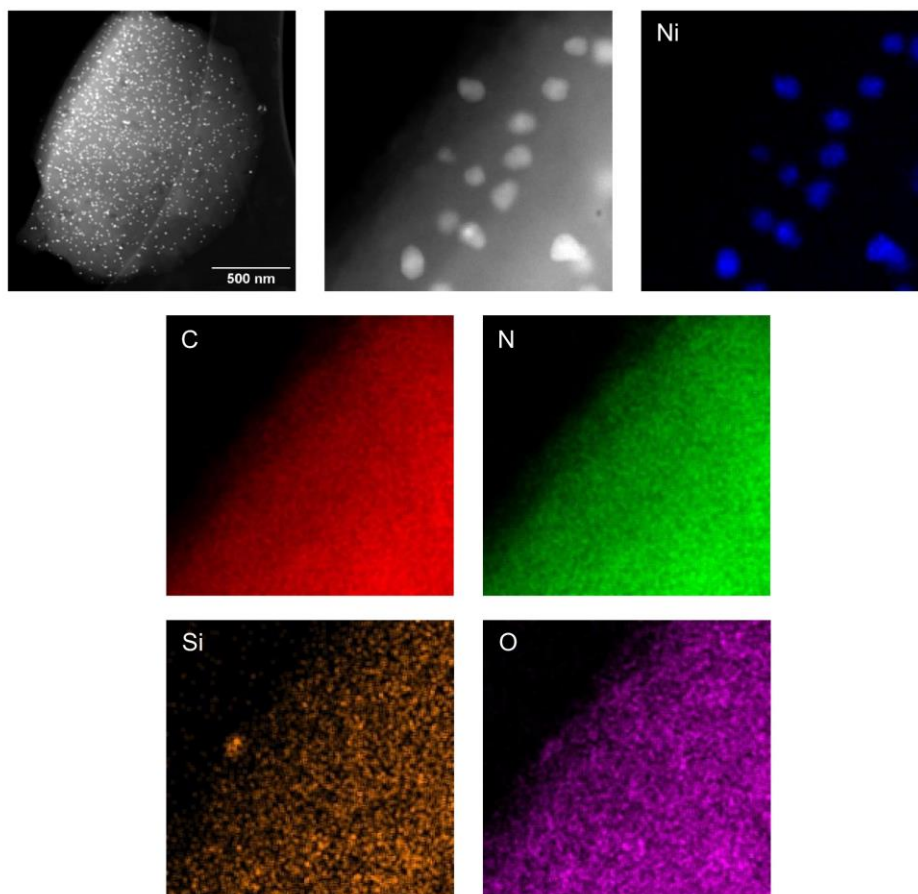


Figure S 2: Characterization of the Ni nanoparticles by high-angle annular dark-field scanning TEM (HAADF-STEM) analysis combined with energy-dispersed X-ray (EDX) element mapping. The support material N-SiC (N: green, Si: orange, C: red) is covered with homogeneously dispersed Ni (Ni: blue) nanoparticles. The nanoparticles are embedded in the nitrogen, silicon doped carbon layer of the N-SiC support. Oxygen (O: violet) is also present because of the sample preparation at ambient air.

3.5 HR-TEM with EELS

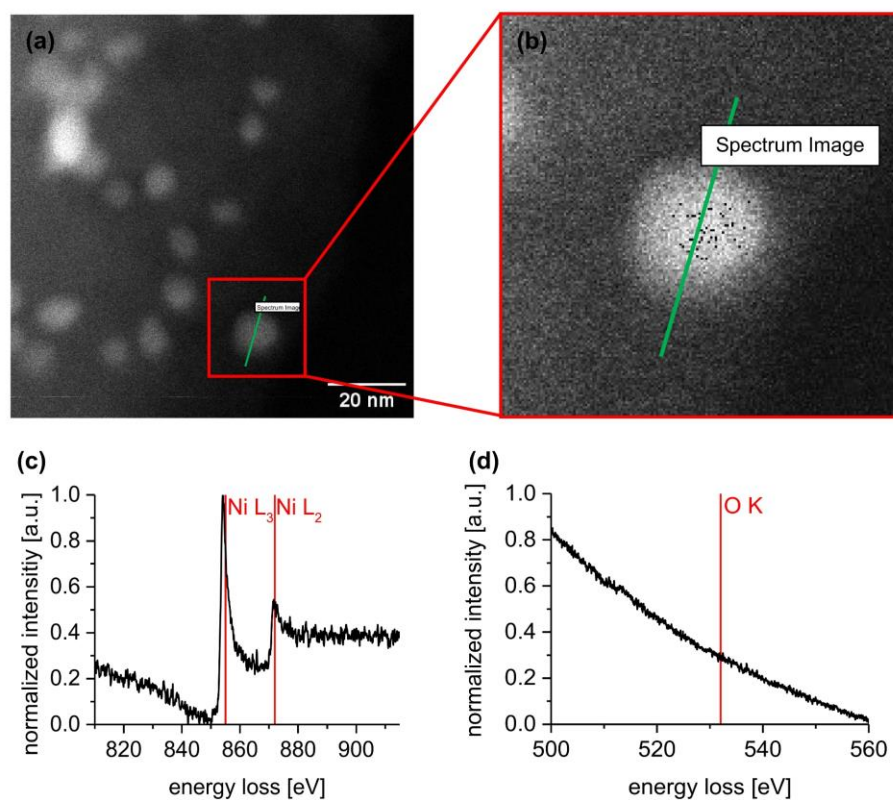


Figure S 3: (a) HR-TEM (high resolution transmission electron microscopy) with a line scan over one nickel nanoparticle and (b) the detailed image of the scanned particle. (c) The resulting EELS spectrum of the nickel area. The EELS spectrum fits to the literature measurements of Ni^0 . The calculated $\text{Ni}(\text{L}_3) : \text{Ni}(\text{L}_2)$ intensity ratio of 1.38 (Ni^0 reference: 1.41, Ni^{2+} reference: 1.84) agrees with the literature value.^[3] (d) The measured EELS spectrum of the oxygen area. There is no oxygen edge detected. This confirms that there is no nickel oxide species on the catalyst.

3.6 HR-TEM with FFT

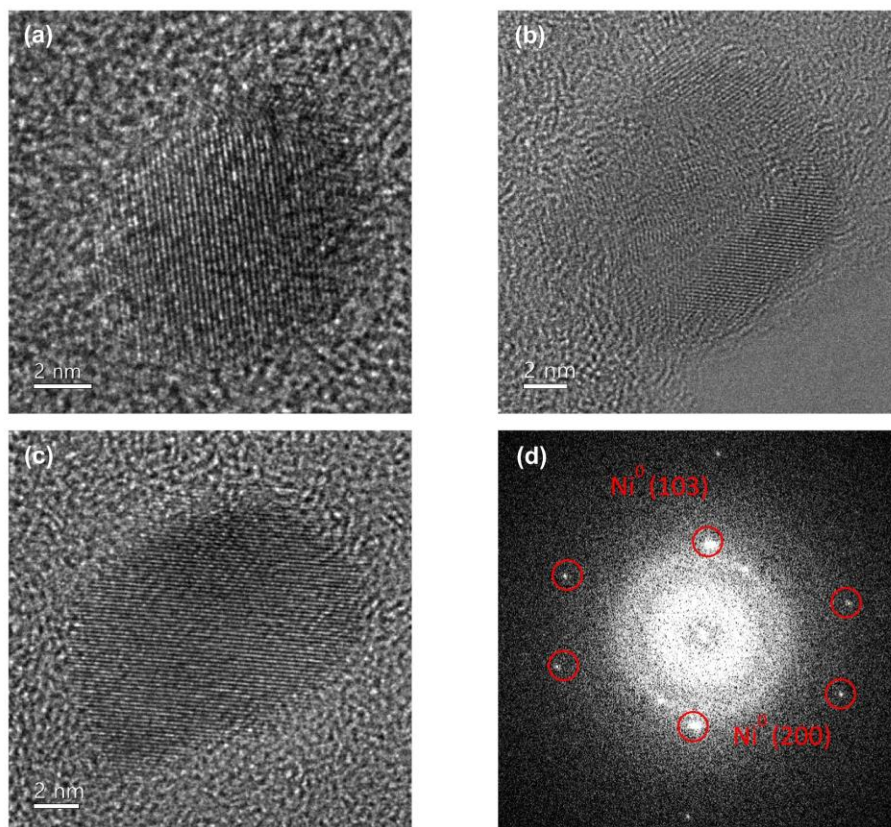


Figure S 4: (a)-(c) HR-TEM images of different nickel nanoparticles. One can see very clearly the lattice spacings in the nanoparticles. (d) FFT of the nanoparticle depicted in (c). The examination of the diffraction spots revealed two miller planes (200 and 103) consistent with those of cubic nickel.

3.7 XPS

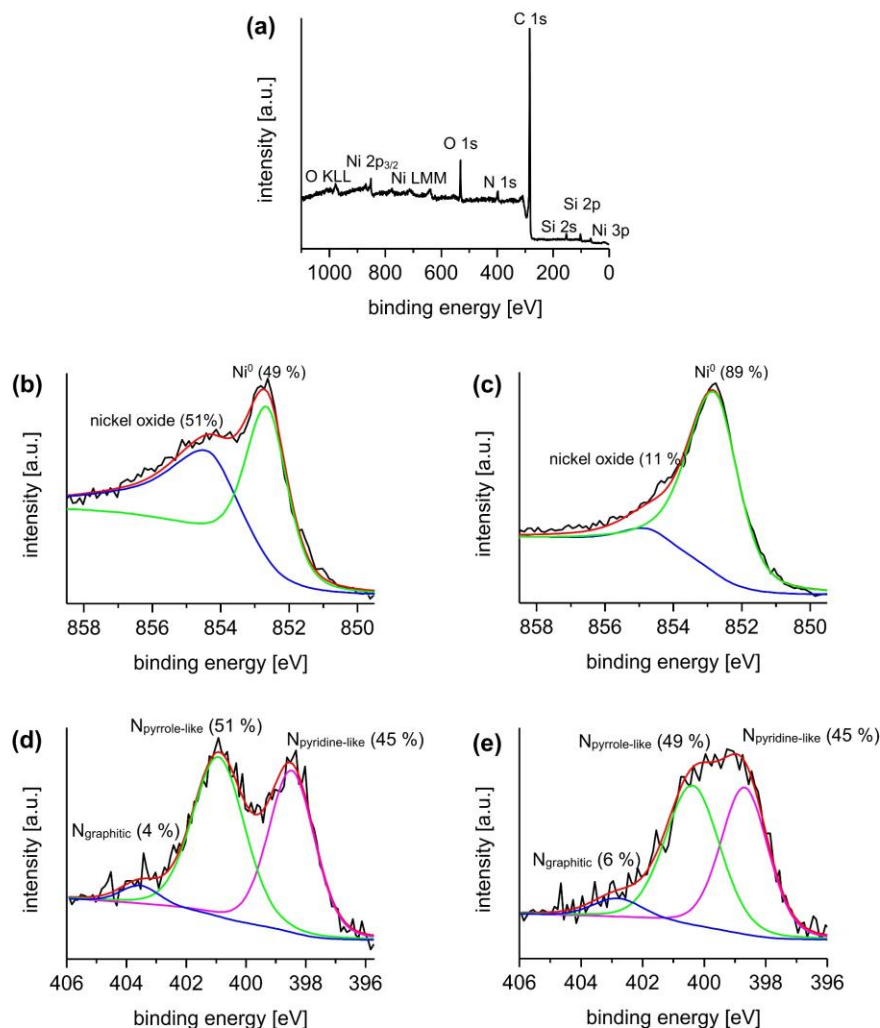


Figure S 5: X-ray photoelectron spectra (XPS) of the surface area of the catalyst Ni/N-SiC. (a) XPS survey of Ni/N-SiC. The catalyst contains Si, O, C, N and Ni at the surface. (b) Analysis of the Ni 2p_{3/2} area pre-Pt sputtering with an asymmetric fit. It shows Ni⁰ (49 %) and nickel oxide (51 %) on the surface. (c) Analysis of the Ni 2p_{3/2} area post-Pt sputtering with an asymmetric fit. It shows Ni⁰ (89 %) and nickel oxide (11 %). (d) Analysis of the nitrogen area pre-Pt sputtering suggests different binding models of nitrogen within the catalyst (graphitic: 4 %, pyrrole-like: 51 %, pyridine-like: 45 %). (e) Analysis of the nitrogen area post-Pt sputtering suggests different binding models of nitrogen (graphitic: 6 %, pyrrole-like: 49 %, pyridine-like: 45 %).

4 Catalytic Studies

4.1 Screening of Reaction Parameters

Table S 2: Reaction parameters – solvent.

Entry	Solvent	Yield [%]
1	Ethanol	91
2	Methanol	65
3	Water	48
4	Dimethylformamide	0
5	2-Methyltetrahydrofuran	0
6	Toluene	0
7	Methylcyclohexane	0
8	Diglyme	0
9	1,4-Dioxane	34
10	Triethylamine	0

Reaction conditions: Step A: 29.3 mg Ni/N-SiC catalyst, 4 mol% Ni (4.0 wt% Ni, 0.02 mmol Ni, 1.17 mg Ni), 0.5 mmol 2-nitrobenzaldehyde, 0.5 mmol acetophenone, 3 mL solvent, 3.0 MPa H₂, 40 °C, 20 h. Step B: Addition of 0.3 mmol LiOH. Then 60 °C, 20 h. Step C: 5.0 MPa H₂, 120 °C, 48 h. Yields were determined by GC using *n*-dodecane as an internal standard.

The Synthesis of Hydroquinolines from Nitroaldehydes and Ketones by Hydrogenation Sequences and Condensations

Table S 3: Reaction parameters – amount of ethanol.

<p>Reaction scheme: 2-nitrobenzaldehyde (I) + acetophenone (II) $\xrightarrow[\text{-2 H}_2\text{O}]{\text{Step A: catalyst + 3 H}_2}$ 2-amino-3-phenylpropanal (III) + acetophenone (II) $\xrightarrow[\text{-2 H}_2\text{O}]{\text{Step B: LiOH}}$ 2-phenyl-1,2,3,4-tetrahydroquinoline (IV) $\xrightarrow[\text{+ 2 H}_2]{\text{Step C: catalyst}}$ 2-phenyl-1,2,3,4-tetrahydroquinoline (V)</p>		
Entry	Ethanol [mL]	Yield [%]
1	1	26
2	2	63
3	3	91
4	4	86
5	5	81

Reaction conditions: Step A: 29.3 mg Ni/N-SiC catalyst, 4 mol% Ni (4.0 wt% Ni, 0.02 mmol Ni, 1.17 mg Ni), 0.5 mmol 2-nitrobenzaldehyde, 0.5 mmol acetophenone, ethanol, 3.0 MPa H₂, 40 °C, 20 h. Step B: Addition of 0.3 mmol LiOH. Then 60 °C, 20 h. Step C: 5.0 MPa H₂, 120 °C, 48 h. Yields were determined by GC using *n*-dodecane as an internal standard.

The Synthesis of Hydroquinolines from Nitroaldehydes and Ketones by Hydrogenation Sequences and Condensations

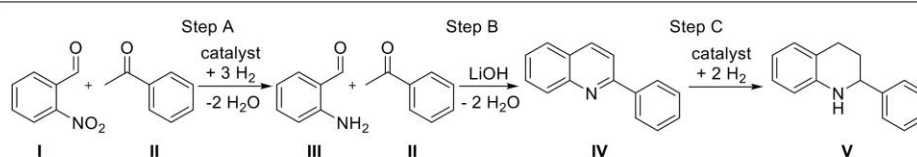
Table S 4: Reaction parameters – base.

Entry	Base	Yield [%]
1	LiOH	91
2	NaOH	79
3	KOH	84
4	KO ^t Bu	0
5	Na-HMDS	0
6	Amberlyst 21	47
7	Amberlyst 26	54
8	CaO	0
9	MgO	0
10	K ₂ CO ₃	0
11	Na ₂ CO ₃	0
12	CaCO ₃	0
13	BaCO ₃	0
14	SrCO ₃	0

Reaction conditions: Step A: 29.3 mg Ni/N-SiC catalyst, 4 mol% Ni (4.0 wt% Ni, 0.02 mmol Ni, 1.17 mg Ni), 0.5 mmol 2-nitrobenzaldehyde, 0.5 mmol acetophenone, 3 mL ethanol, 3.0 MPa H₂, 40 °C, 20 h. Step B: Addition of 0.3 mmol base. Then 60 °C, 20 h. Step C: 5.0 MPa H₂, 120 °C, 48 h. Yields were determined by GC using *n*-dodecane as an internal standard.

The Synthesis of Hydroquinolines from Nitroaldehydes and Ketones by Hydrogenation Sequences and Condensations

Table S 5: Reaction parameters – amount of base.



Entry	LiOH [mmol]	LiOH [eq]	Yield [%]
1	0.00	0.0	0
2	0.05	0.1	28
3	0.10	0.2	30
4	0.15	0.3	35
5	0.20	0.4	36
6	0.25	0.5	49
7	0.30	0.6	91
8	0.35	0.7	61
9	0.40	0.8	45
10	0.45	0.9	39
11	0.50	1.0	34
12	0.75	1.5	31

Reaction conditions: Step A: 29.3 mg Ni/N-SiC catalyst, 4 mol% Ni (4.0 wt% Ni, 0.02 mmol Ni, 1.17 mg Ni), 0.5 mmol 2-nitrobenzaldehyde, 0.5 mmol acetophenone, 3 mL ethanol, 3.0 MPa H₂, 40 °C, 20 h. Step B: Addition of LiOH. Then 60 °C, 20 h. Step C: 5.0 MPa H₂, 120 °C, 48 h. Yields were determined by GC using *n*-dodecane as an internal standard.

The Synthesis of Hydroquinolines from Nitroaldehydes and Ketones by Hydrogenation Sequences and Condensations

Table S 6: Reaction parameters – reaction temperature for step A.

Step A

O=Cc1ccccc1 + O=Cc1ccccc1
 $\xrightarrow[\text{-2 H}_2\text{O}]{\text{catalyst + 3 H}_2}$
Nc1ccccc1C(=O)c2ccccc2 + O=Cc1ccccc1

I II III II

Entry	Temperature [°C]	Yield [%]
1	30	66
2	40	> 99
3	50	93
4	60	90
5	70	15

Reaction conditions: Step A: 29.3 mg Ni/N-SiC catalyst, 4 mol% Ni (4.0 wt%, 0.02 mmol Ni, 1.17 mg Ni), 0.5 mmol 2-nitrobenzaldehyde, 0.5 mmol acetophenone, 3 mL ethanol, 3.0 MPa H₂, 20 h, at desired temperature. Yields were determined by GC using *n*-dodecane as an internal standard.

Table S 7: Reaction parameters – H₂ pressure for step A.

Step A

O=Cc1ccccc1 + O=Cc1ccccc1
 $\xrightarrow[\text{-2 H}_2\text{O}]{\text{catalyst + 3 H}_2}$
Nc1ccccc1C(=O)c2ccccc2 + O=Cc1ccccc1

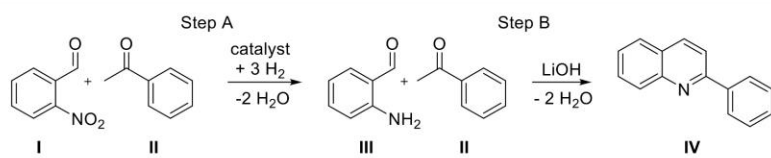
I II III II

Entry	H ₂ Pressure [MPa]	Yield [%]
1	1.0	65
2	2.0	82
3	3.0	> 99
4	4.0	> 99
5	5.0	> 99

Reaction conditions: 29.3 mg Ni/N-SiC catalyst, 4 mol% Ni (4.0 wt%, 0.02 mmol Ni, 1.17 mg Ni), 0.5 mmol 2-nitrobenzaldehyde, 0.5 mmol acetophenone, 3 mL ethanol, H₂, 40 °C, 20 h. Yields were determined by GC using *n*-dodecane as an internal standard.

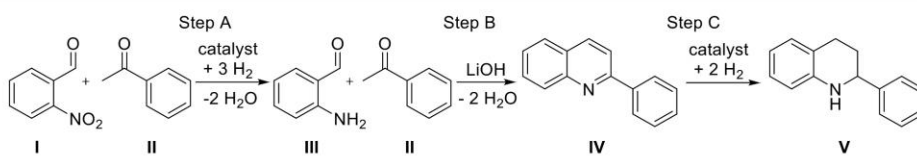
The Synthesis of Hydroquinolines from Nitroaldehydes and Ketones by Hydrogenation Sequences and Condensations

Table S 8: Reaction parameters – reaction temperature for step B.

		
Entry	Temperature [°C]	Yield [%]
1	30	61
2	40	83
3	50	95
4	60	> 99
5	70	> 99
6	80	> 99
7	90	> 99
8	100	> 99

Reaction conditions: Step A: 29.3 mg Ni/N-SiC catalyst, 4 mol% Ni (4.0 wt% Ni, 0.02 mmol Ni, 1.17 mg Ni), 0.5 mmol 2-nitrobenzaldehyde, 0.5 mmol acetophenone, 3 mL ethanol, 3.0 MPa H₂, 40 °C, 20 h. Step B: Addition of 0.3 mmol LiOH. Then 20 h reaction time at desired temperature. Yields were determined by GC using *n*-dodecane as an internal standard.

Table S 9: Reaction parameters – reaction temperature for step C.

		
Entry	Temperature [°C]	Yield [%]
6	80	64
7	90	68
8	100	73
9	110	86
10	120	91
11	130	71

Reaction conditions: Step A: 29.3 mg Ni/N-SiC catalyst, 4 mol% Ni (4.0 wt% Ni, 0.02 mmol Ni, 1.17 mg Ni), 0.5 mmol 2-nitrobenzaldehyde, 0.5 mmol acetophenone, 3 mL ethanol, 3.0 MPa H₂, 40 °C, 20 h. Step B: Addition of 0.3 mmol LiOH. Then 60 °C, 20 h. Step C: 5.0 MPa H₂, 48 h reaction time at desired temperature. Yields were determined by GC using *n*-dodecane as an internal standard.

The Synthesis of Hydroquinolines from Nitroaldehydes and Ketones by Hydrogenation Sequences and Condensations

Table S 10: Reaction parameters – H₂ pressure for step C.

Entry	H ₂ Pressure [MPa]	Yield [%]
1	2.0	22
2	3.0	32
3	4.0	34
4	5.0	91
5	6.0	48

Reaction conditions: Step A: 29.3 mg Ni/N-SiC catalyst, 4 mol% Ni (4.0 wt% Ni, 0.02 mmol Ni, 1.17 mg Ni), 0.5 mmol 2-nitrobenzaldehyde, 0.5 mmol acetophenone, 3 mL ethanol, 3.0 MPa H₂, 40 °C, 20 h. Step B: Addition of 0.3 mmol LiOH. Then 60 °C, 20 h. Step C: H₂, 120 °C, 48 h reaction time. Yields were determined by GC using *n*-dodecane as an internal standard.

Table S 11: Reaction parameters – metal loading.

Entry	Metal loading [wt% Ni]	Yield [%]
1	1.0	11
2	2.0	23
3	3.0	36
4	4.0	91
5	5.0	16

Reaction conditions: Step A: Ni/N-SiC catalyst, 4 mol% Ni (0.02 mmol Ni, 1.17 mg Ni), 0.5 mmol 2-nitrobenzaldehyde, 0.5 mmol acetophenone, 3 mL ethanol, 3.0 MPa H₂, 40 °C, 20 h. Step B: Addition of 0.3 mmol LiOH. Then 60 °C, 20 h. Step C: 5.0 MPa H₂, 120 °C, 48 h. Yields were determined by GC using *n*-dodecane as an internal standard.

The Synthesis of Hydroquinolines from Nitroaldehydes and Ketones by Hydrogenation Sequences and Condensations

Table S 12: Reaction parameters – catalyst loading to substrate ratio.

Reaction scheme: 2-nitrobenzaldehyde (I) + acetophenone (II) $\xrightarrow[\text{-2 H}_2\text{O}]{\text{Step A: catalyst + 3 H}_2}$ 2-amino-3-phenylpropanal (III) + acetophenone (II) $\xrightarrow[\text{-2 H}_2\text{O}]{\text{Step B: LiOH}}$ 2-phenyl-1,2,3,4-tetrahydroquinoline (IV) $\xrightarrow[\text{+ 2 H}_2]{\text{Step C: catalyst}}$ 2-phenyl-1,2,3,4-tetrahydroquinoline (V)

Entry	Catalyst loading [mol% Ni]	Yield [%]
1	0.0	0
2	1.0	30
3	2.0	58
4	3.0	73
5	4.0	91
6	5.0	84

Reaction conditions: Step A: Ni/N-SiC catalyst (4 wt% Ni), 0.5 mmol 2-nitrobenzaldehyde, 0.5 mmol acetophenone, 3 mL ethanol, 3.0 MPa H₂, 40 °C, 20 h. Step B: Addition of 0.3 mmol LiOH. Then 60 °C, 20 h. Step C: 5.0 MPa H₂, 120 °C, 48 h. Yields were determined by GC using *n*-dodecane as an internal standard.

4.2 Time-Conversion-Plot

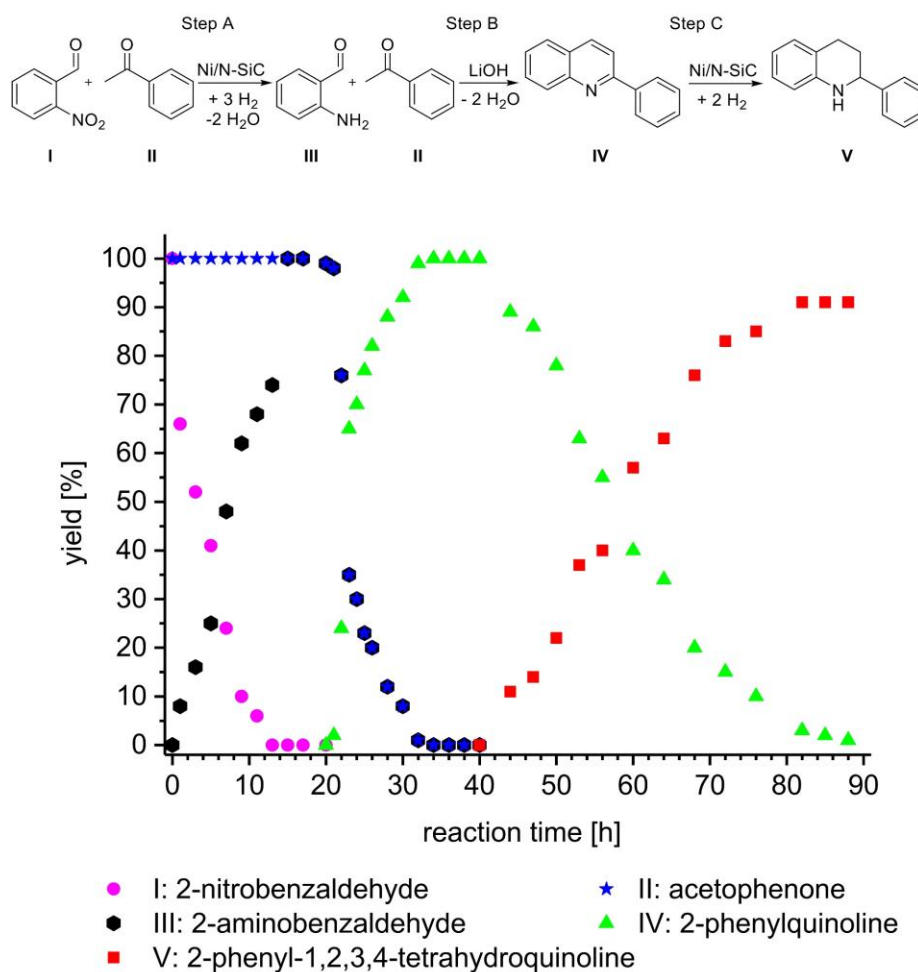


Figure S 6: Time-Conversion-Plot of the direct synthesis of 2-phenyl-1,2,3,4-tetrahydroquinoline (V). The reaction progress was observed at different time intervals during each step. Reaction conditions: Step A: 29.3 mg Ni/N-SiC catalyst (4.0 wt% Ni, 0.02 mmol Ni, 1.17 mg Ni), 0.5 mmol 2-nitrobenzaldehyde, 0.5 mmol acetophenone, 3 mL ethanol, 3.0 MPa H₂, 40 °C. Step B: Addition of 0.3 mmol LiOH. Then 60 °C. Step C: 5.0 MPa H₂, 120 °C. Yields were determined by GC using *n*-dodecane as an internal standard.

4.3 Upscaling of the Reaction

The benchmark reaction which is the synthesis of 2-phenyl-1,2,3,4-tetrahydroquinoline from 2-nitrobenzaldehyde and acetophenone was used to carry out an upscaling experiment. For the reaction, 586.0 mg Ni/N-SiC catalyst (4.0 mol% Ni, 4 wt% Ni, 0.02 mmol Ni, 1.17 mg Ni), 10 mmol 2-nitrobenzaldehyde, 10 mmol acetophenone and 60 mL EtOH were stirred in a 100 mL glass vial equipped with a magnetic stirring bar. The vial was placed in a 300 mL high-pressure autoclave (Parr Instruments) and the autoclave was flushed three times with 2.0 MPa hydrogen. After pressuring the autoclave with the desired 3.0 MPa hydrogen pressure, the reaction was stirred for 20 h at 40 °C. After completion of the reaction time, the hydrogen was released and subsequently started with step B. To the reaction mixture 144 mg LiOH (6.0 mmol, 0.6 eq) were added. After, the reaction mixture was stirred in the autoclave at 60 °C for 20 h to give the corresponding 2-phenylquinoline. Followed by step C the autoclave was flushed again three times with 2.0 MPa hydrogen and pressured with 5.0 MPa hydrogen at 120 °C for 48 h to selectively hydrogenate the 2-phenylquinoline to the corresponding 2-phenyl-1,2,3,4-tetrahydroquinoline. The autoclave was cooled to room temperature and the hydrogen was released. The reaction mixture was separated from the catalyst and the yield of 2-phenyl-1,2,3,4-tetrahydroquinoline was isolated. Yield: 86 % (1799 mg) as an oil.

4.4 Reusability

The hydrogenation of 2-nitrobenzaldehyde to 2-aminobenzaldehyde was chosen to investigate the recyclability of the Ni/N-SiC catalyst. A 10 mL reaction vial was charged with a magnetic stirring bar, 0.5 mmol 2-nitrobenzaldehyde, 3 mL EtOH and 29.3 mg catalyst (4.0 mol% Ni, 4 wt% Ni, 0.02 mmol Ni, 1.17 mg Ni). The vial was placed in a high-pressure autoclave (Parr Instruments) and the autoclave was flushed three times with 2.0 MPa hydrogen. The autoclave was pressured with 3.0 MPa hydrogen and the reaction was carried out for 20 h at 30 °C to obtain 70 % yield. After 20 h the autoclave was opened and there the catalyst was washed three times with ethanol via centrifugation. Therefore, the catalyst could be completely recovered. The yield of 2-aminobenzaldehyde was determined by GC using *n*-dodecane as an internal standard (Figure S 7). The Ni/N-SiC catalyst demonstrates reusability without any loss of activity.

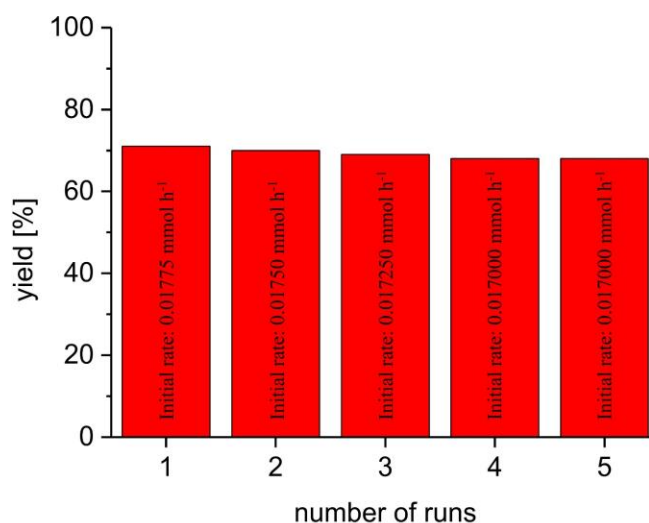


Figure S 7: Results and the initial rates of the recycling experiments. There is no decrease in catalytic activity in five consecutive runs in the hydrogenation of 2-nitrobenzaldehyde to 2-aminobenzaldehyde.

4.5 Evaluation of the Used Catalyst

4.5.1 TEM Measurements

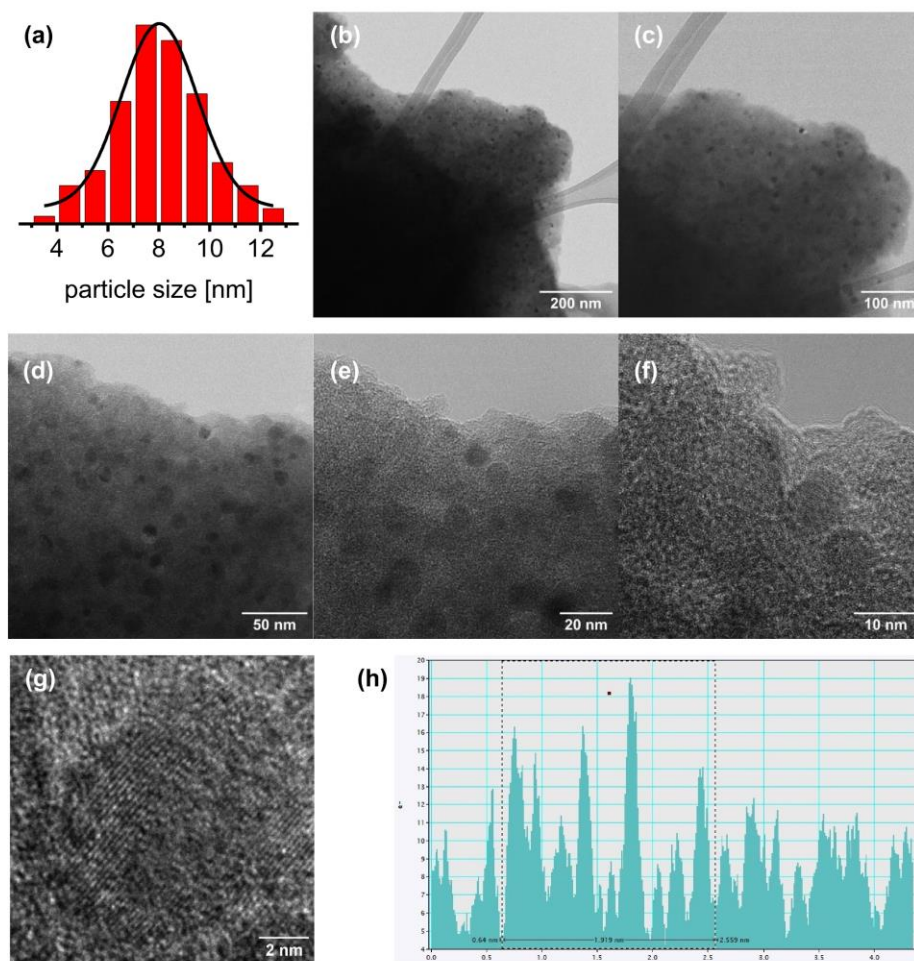


Figure S 8: TEM characterization of the used Ni/N-SiC catalyst. (a) Particle size distribution of the nanoparticles after catalysis. The distribution is homogeneous with an average diameter of 8.0 nm, close to the same average diameter as before catalysis (8.5 nm). (b) – (e) There is no agglomeration or growing of nanoparticles in the Ni/N-SiC catalyst after catalysis. (f) HR-TEM measurement of the catalyst. The particles are in good shape with the particles before catalysis. (g) One can see the lattice spacing of nickel. (h) Line profile of the particle in (g). The average lattice spacing found is 1.74 Å and is in good accordance with the d(200) spacing of 1.76 Å of cubic nickel (reference code: 00-004-0850).

The Ni/N-SiC catalyst was investigated with TEM measurements after the catalysis (Figure S 8). The general procedure for the catalytic reaction was applied (Section 2.3.1). For step A the vial was charged with a magnetic stirring bar, 0.5 mmol 2-nitrobenzaldehyde, 0.5 mmol acetophenone, 3 mL EtOH and 29.3 mg catalyst (4.0 mol% Ni, 4 wt% Ni, 0.02 mmol Ni, 1.17 mg Ni). The vial was placed in a 300 mL high-pressure autoclave (Parr Instruments). The autoclave was flushed three times with 2.0 MPa hydrogen. Afterwards, 3.0 MPa hydrogen was applied, and the reaction was stirred at 40 °C for 20 h. After completion of the reaction time, the hydrogen was released and subsequently started with step B. To the reaction mixture 7.2 mg LiOH (0.3 mmol, 0.6 eq) were added. After, the reaction mixture was stirred in the autoclave at 60 °C for 20 h to give the corresponding quinoline. Followed by step C the autoclave was flushed again three times with 2.0 MPa hydrogen and pressured with 3.0 MPa hydrogen at 120 °C for 48 h to selectively hydrogenate the quinoline to the corresponding 1,2,3,4-tetrahydroquinoline. At the end of the reaction time, the autoclave was cooled down to room temperature and the hydrogen was released. The catalyst was removed by centrifugation and the organic phase was separated. After, the catalyst was washed three times with ethanol and dried in vacuo. The catalyst was characterized via TEM measurements.

4.5.2 Hot Filtration Test

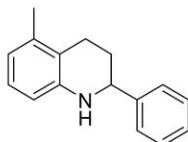
To demonstrate the catalyst stability a hot filtration test was performed. Therefore, a 10 mL reaction vial was charged with a magnetic stirring bar, 0.5 mmol 2-nitrobenzaldehyde, 3 mL EtOH and 29.3 mg catalyst (4.0 mol% Ni, 4 wt% Ni, 0.02 mmol Ni, 1.17 mg Ni). The vial was placed in a 300 mL high pressure autoclave (Parr Instruments) and the autoclave was flushed three times with 2.0 MPa hydrogen. Afterwards, 3.0 MPa hydrogen was applied, and the reaction was stirred at the desired 40 °C. When 15 % yield of 2-aminobenzaldehyde were generated (after 3 h reaction time), the hot catalytic mixture was filtered to remove the catalyst. Afterwards, 0.5 mmol 2-nitrobenzaldehyde were added to the filtrate and the mixture was stirred at the catalytic conditions mentioned above. The filtrate did not show any activity and the desired product 2-aminobenzaldehyde was not generated. No other product was to be seen either. The yield of 2-aminobenzaldehyde was determined by GC using *n*-dodecane as an internal standard.

4.5.3 Leaching Test

A leaching test was performed to demonstrate that our catalyst does not form homogeneous nickel species. For step A the vial was charged with a magnetic stirring bar, 0.5 mmol 2-nitrobenzaldehyde, 0.5 mmol acetophenone, 3 mL EtOH and 29.3 mg catalyst (4.0 mol% Ni, 4 wt% Ni, 0.02 mmol Ni, 1.17 mg Ni). The vial was placed in a 300 mL high-pressure autoclave (Parr Instruments). The autoclave was flushed three times with 2.0 MPa hydrogen. Afterwards, 3.0 MPa hydrogen was applied, and the reaction was stirred at 40 °C for 20 h. After completion of the reaction time, the hydrogen was released and subsequently started with step B. To the reaction mixture 7.2 mg LiOH (0.3 mmol, 0.6 eq) were added. After, the reaction mixture was stirred in the autoclave at 60 °C for 20 h. Followed by step C, the autoclave was flushed again three times with 2.0 MPa hydrogen and pressured with 3.0 MPa hydrogen at 120 °C for 48 h. Upon completion of the reaction time, the autoclave was cooled to room temperature and the hydrogen was released. The reaction mixture was separated from the catalyst and the leaching amount of the Ni/N-SiC catalyst was determined via ICP-OES. The measured nickel amount of the used Ni/N-SiC catalyst was 3.94 wt%. The slightly different values (0.06 wt%, 1.5 % deviation) from the original 4.0 wt% nickel loading is negligible. Since the difference between the initial nickel loading and the measured nickel loading is insignificant, it can be said that our catalyst is not leaching at all.

5 Characterization of Isolated Products

5-Methyl-2-phenyl-1,2,3,4-tetrahydroquinoline (1)



MW ($C_{16}H_{17}N$) = 223.32 g/mol (M)

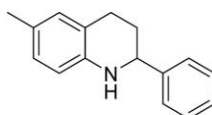
1H NMR (400 MHz, DMSO- d_6 , 296 K): δ = 7.48 – 7.35 (m, 4H), 7.35 – 7.28 (m, 1H), 6.86 (t, J = 7.7 Hz, 1H), 6.56 (d, J = 8.0 Hz, 1H), 6.43 (d, J = 7.2 Hz, 1H), 5.96 (s, 1H), 4.38 (dd, J = 8.6, 3.0 Hz, 1H), 2.75 – 2.62 (m, 1H), 2.58 – 2.51 (m, 1H), 2.15 (s, 3H), 2.09 (dt, J = 14.1, 4.4 Hz, 1H), 1.97 – 1.86 (m, 1H) ppm.

^{13}C NMR (100 MHz, DMSO- d_6 , 296 K): δ = 145.49, 145.23, 135.75, 128.21, 126.84, 126.47, 125.87, 118.19, 117.45, 112.02, 54.17, 30.67, 22.73, 19.17 ppm.

Yield: 90 % (100 mg) as an oil. The product was purified via column chromatography (*n*-pentane : EtOAc, 10:2).

The spectroscopic data match those reported in literature.^[4] (CAS Number: 2912523-66-9)

6-Methyl-2-phenyl-1,2,3,4-tetrahydroquinoline (2)



MW ($C_{16}H_{17}N$) = 223.32 g/mol (M)

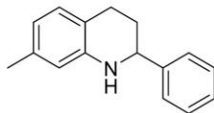
1H NMR (400 MHz, DMSO- d_6 , 296 K): δ = 7.41 – 7.29 (m, 4H), 7.25 (ddd, J = 6.5, 4.0, 1.9 Hz, 1H), 6.69 (d, J = 2.3 Hz, 1H), 6.50 (d, J = 7.9 Hz, 1H), 5.81 (s, 1H), 4.36 (d, J = 7.1 Hz, 1H), 2.80 – 2.70 (m, 1H), 2.55 – 2.51 (m, 1H), 2.13 (s, 3H), 2.01 – 1.92 (m, 1H), 1.87 – 1.75 (m, 1H) ppm.

^{13}C NMR (100 MHz, DMSO- d_6 , 296 K): δ = 145.42, 143.05, 129.21, 128.20, 126.99, 126.82, 126.43, 123.71, 119.52, 113.73, 54.63, 30.46, 25.41, 20.16 ppm.

Yield: 82 % (92 mg) as an oil. The product was purified via plate chromatography (*n*-pentane : EtOAc, 30:1).

The spectroscopic data match those reported in literature.^[4] (CAS Number: 876491-83-7)

7-Methyl-2-phenyl-1,2,3,4-tetrahydroquinoline (3)



MW (C₁₆H₁₇N) = 223.32 g/mol (M)

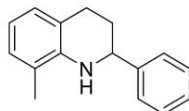
¹H NMR (400 MHz, DMSO-d₆, 296 K): δ = 7.41 – 7.17 (m, 5H), 6.73 (dd, *J* = 7.5, 4.0 Hz, 1H), 6.40 (d, *J* = 2.6 Hz, 1H), 6.27 (dd, *J* = 7.6, 2.6 Hz, 1H), 5.94 (s, 1H), 4.41 – 4.33 (m, 1H), 2.75 – 2.64 (m, 1H), 2.44 (dd, *J* = 9.3, 4.3 Hz, 1H), 2.12 (t, *J* = 5.2 Hz, 3H), 2.01 – 1.89 (m, 1H), 1.80 (dtd, *J* = 17.0, 8.6, 4.3 Hz, 1H) ppm.

¹³C NMR (100 MHz, DMSO-d₆, 296 K): δ = 145.44, 145.17, 135.22, 128.60, 128.24, 126.84, 126.41, 116.68, 116.43, 114.03, 54.43, 30.46, 24.93, 21.03 ppm.

Yield: 89 % (99 mg) as an oil. The product was purified via plate chromatography (*n*-pentane : EtOAc, 30:1).

The spectroscopic data match those reported in literature.^[5] (CAS Number: 876491-82-6)

8-Methyl-2-phenyl-1,2,3,4-tetrahydroquinoline (4)



MW (C₁₆H₁₇N) = 223.32 g/mol (M)

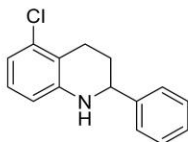
¹H NMR (400 MHz, DMSO-d₆, 296 K): δ = 7.38 – 7.29 (m, 4H), 7.24 (td, *J* = 6.1, 2.7 Hz, 1H), 6.77 (dd, *J* = 28.2, 7.4 Hz, 2H), 6.41 (t, *J* = 7.4 Hz, 1H), 5.24 (s, 1H), 4.52 (dt, *J* = 6.5, 3.2 Hz, 1H), 2.77 – 2.70 (m, 1H), 2.46 (t, *J* = 5.8 Hz, 1H), 2.08 (s, 3H), 2.03 – 1.95 (m, 1H), 1.89 – 1.80 (m, 1H) ppm.

¹³C NMR (100 MHz, DMSO-d₆, 296 K): δ = 145.79, 142.85, 128.19, 127.76, 126.68, 126.62, 126.21, 120.78, 119.44, 115.29, 54.54, 29.83, 25.15, 17.50 ppm.

Yield: 94 % (105 mg) as an oil. The product was purified via column chromatography (*n*-pentane : EtOAc, 7:1).

The spectroscopic data match those reported in literature.^[6] (CAS Number: 876491-80-4)

5-Chloro-2-phenyl-1,2,3,4-tetrahydroquinoline (5)



MW ($C_{15}H_{14}ClN$) = 243.73 g/mol (M)

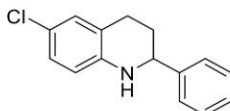
1H NMR (400 MHz, DMSO- d_6 , 296 K): δ = 7.39 – 7.29 (m, 4H), 7.29 – 7.22 (m, 1H), 6.87 – 6.84 (m, 1H), 6.58 (dd, J = 8.0, 1.0 Hz, 1H), 6.44 (td, J = 7.3, 1.2 Hz, 1H), 6.02 (s, 1H), 4.40 (dd, J = 4.9, 1.7 Hz, 1H), 2.82 – 2.72 (m, 1H), 2.54 (dd, J = 11.0, 5.6 Hz, 1H), 2.02 – 1.94 (m, 1H), 1.84 (ddd, J = 13.0, 8.9, 4.4 Hz, 1H) ppm.

^{13}C NMR (100 MHz, DMSO- d_6 , 296 K): δ = 145.36, 128.70, 128.33, 128.23, 126.88, 126.47, 126.43, 119.47, 115.39, 113.55, 54.45, 30.24, 25.38 ppm.

Yield: 71 % (87 mg) as an oil. The product was purified via column chromatography (*n*-pentane : EtOAc, 10:1).

The spectroscopic data match those reported in literature.^[7] (CAS Number: 2793403-68-4)

6-Chloro-2-phenyl-1,2,3,4-tetrahydroquinoline (6)



MW ($C_{15}H_{14}ClN$) = 243.73 g/mol (M)

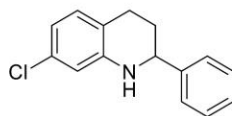
1H NMR (400 MHz, DMSO- d_6 , 296 K): δ = 7.39 – 7.32 (m, 4H), 7.29 – 7.21 (m, 1H), 6.89 – 6.85 (m, 1H), 6.60 (d, J = 7.9 Hz, 1H), 6.49 – 6.41 (m, 1H), 6.03 (s, 1H), 4.41 (d, J = 6.5 Hz, 1H), 2.75 (dd, J = 9.8, 5.5 Hz, 1H), 2.55 (t, J = 5.3 Hz, 1H), 1.98 (dd, J = 11.3, 5.2 Hz, 1H), 1.90 – 1.77 (m, 1H) ppm.

^{13}C NMR (100 MHz, DMSO- d_6 , 296 K): δ = 145.37, 144.87, 128.70, 128.23, 126.87, 126.47, 126.42, 119.48, 115.41, 113.56, 54.47, 30.26, 25.37 ppm.

Yield: 89 % (108 mg) as an oil. The product was purified via column chromatography (*n*-pentane : EtOAc, 10:2).

The spectroscopic data match those reported in literature.^[8] (CAS Number: 1206880-24-1)

7-Chloro-2-phenyl-1,2,3,4-tetrahydroquinoline (7)



MW (C₁₅H₁₄ClN) = 243.73 g/mol (M)

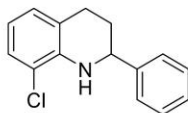
¹H NMR (400 MHz, DMSO-d₆, 296 K): δ = 7.45 – 7.18 (m, 5H), 6.87 (d, J = 7.6 Hz, 1H), 6.62 (dd, J = 15.5, 5.1 Hz, 1H), 6.49 – 6.41 (m, 1H), 6.03 (s, 1H), 4.42 (t, J = 5.2 Hz, 1H), 2.84 – 2.65 (m, 1H), 2.60 – 2.50 (m, 1H), 2.04 – 1.93 (m, 1H), 1.89 – 1.75 (m, 1H) ppm.

¹³C NMR (100 MHz, DMSO-d₆, 296 K): δ = 145.37, 144.73, 130.74, 130.08, 128.32, 128.23, 127.04, 126.87, 126.43, 119.49, 118.35, 113.56, 54.48, 30.26, 25.38 ppm.

Yield: 70 % (85 mg) as an oil. The product was purified via column chromatography (*n*-pentane : EtOAc, 10:2).

The spectroscopic data match those reported in literature.^[9] (CAS Number: 2642399-25-3)

8-Chloro-2-phenyl-1,2,3,4-tetrahydroquinoline (8)



MW (C₁₅H₁₄ClN) = 243.73 g/mol (M)

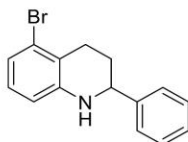
¹H NMR (400 MHz, DMSO-d₆, 296 K): δ = 7.38 – 7.21 (m, 5H), 7.10 (d, J = 7.9 Hz, 1H), 6.88 (d, J = 7.4 Hz, 1H), 6.50 (t, J = 7.7 Hz, 1H), 5.71 (s, 1H), 4.64 – 4.58 (m, 1H), 2.79 – 2.67 (m, 1H), 2.46 (dd, J = 9.8, 6.5 Hz, 1H), 2.04 – 1.87 (m, 2H) ppm.

¹³C NMR (100 MHz, DMSO-d₆, 296 K): δ = 145.00, 140.63, 128.30, 127.55, 126.83, 126.79, 126.05, 122.05, 116.73, 115.79, 53.84, 28.78, 24.44 ppm.

Yield: 74 % (90 mg) as an oil. The product was purified via column chromatography (*n*-pentane : EtOAc, 10:2).

The spectroscopic data match those reported in literature.^[7] (CAS Number: 2793403-77-5)

5-Bromo-2-phenyl-1,2,3,4-tetrahydroquinoline (9)



MW ($C_{15}H_{14}BrN$) = 288.19 g/mol (M)

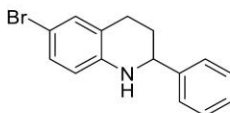
1H NMR (400 MHz, DMSO- d_6 , 296 K): δ = 7.42 – 7.29 (m, 4H), 7.25 (ddt, J = 7.3, 5.7, 2.2 Hz, 1H), 6.86 (d, J = 6.2 Hz, 1H), 6.59 (dd, J = 8.0, 1.0 Hz, 1H), 6.45 (td, J = 7.3, 1.2 Hz, 1H), 6.03 (s, 1H), 4.43 – 4.35 (m, 1H), 2.84 – 2.71 (m, 1H), 2.54 (dd, J = 10.8, 5.5 Hz, 1H), 2.04 – 1.93 (m, 1H), 1.89 – 1.76 (m, 1H) ppm.

^{13}C NMR (100 MHz, DMSO- d_6 , 296 K): δ = 145.37, 145.29, 128.71, 128.24, 126.88, 126.48, 126.43, 119.48, 115.41, 113.56, 54.47, 30.26, 25.37 ppm.

Yield: 71 % (102 mg) as an oil. The product was purified via column chromatography (n -pentane : EtOAc, 15:1).

The spectroscopic data match those reported in literature.^[10] (CAS Number: 957211-73-3)

6-Bromo-2-phenyl-1,2,3,4-tetrahydroquinoline (10)



MW ($C_{15}H_{14}BrN$) = 288.19 g/mol (M)

1H NMR (400 MHz, DMSO- d_6 , 296 K): δ = 7.35 (t, J = 3.4 Hz, 4H), 7.26 (dd, J = 8.7, 4.0 Hz, 1H), 6.85 (d, J = 7.0 Hz, 1H), 6.58 (d, J = 7.7 Hz, 1H), 6.44 (t, J = 7.1 Hz, 1H), 6.02 (s, 1H), 4.40 (d, J = 6.8 Hz, 1H), 2.82 – 2.70 (m, 1H), 2.54 (t, J = 5.2 Hz, 1H), 2.02 – 1.93 (m, 1H), 1.88 – 1.75 (m, 1H) ppm.

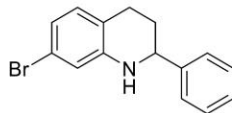
^{13}C NMR (100 MHz, DMSO- d_6 , 296 K): δ = 145.37, 145.29, 128.71, 128.23, 126.88, 126.47, 126.43, 119.48, 115.40, 113.55, 54.46, 30.25, 25.37 ppm.

HRMS (ESI $^+$) Calculated for $C_{15}H_{14}BrN$: 288.03751; found: 288.03824.

Yield: 86 % (124 mg) as an oil. The product was purified via column chromatography (n -pentane : EtOAc, 15:1).

The spectroscopic data is insufficient reported in literature.^[11] (CAS Number: 2247450-56-0)

7-Bromo-2-phenyl-1,2,3,4-tetrahydroquinoline (11)



MW ($C_{15}H_{14}BrN$) = 288.19 g/mol (M)

1H NMR (400 MHz, DMSO- d_6 , 296 K): δ = 7.41 – 7.29 (m, 4H), 7.28 – 7.21 (m, 1H), 6.86 (d, J = 6.5 Hz, 1H), 6.61 – 6.54 (m, 1H), 6.45 (td, J = 7.3, 1.1 Hz, 1H), 6.02 (s, 1H), 4.40 (dd, J = 8.2, 3.4 Hz, 1H), 2.82 – 2.70 (m, 1H), 2.54 (dd, J = 10.8, 5.3 Hz, 1H), 2.02 – 1.93 (m, 1H), 1.83 (ddd, J = 12.7, 8.8, 4.7 Hz, 1H) ppm.

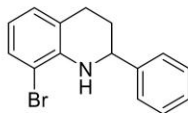
^{13}C NMR (100 MHz, DMSO- d_6 , 296 K): δ = 145.38, 145.31, 128.73, 128.25, 126.90, 126.50, 126.44, 119.51, 115.43, 113.58, 54.48, 30.27, 25.38 ppm.

HRMS (ESI $^+$) Calculated for $C_{15}H_{14}BrN$: 288.03751; found: 288.09561.

Yield: 78 % (112 mg) as an oil. The product was purified via column chromatography (*n*-pentane : EtOAc, 15:1).

The spectroscopic data is insufficient reported in literature.^[11] (CAS Number: 2322842-03-3)

8-Bromo-2-phenyl-1,2,3,4-tetrahydroquinoline (12)



MW ($C_{15}H_{14}BrN$) = 288.19 g/mol (M)

1H NMR (400 MHz, DMSO- d_6 , 296 K): δ = 7.44 – 7.31 (m, 4H), 7.30 – 7.20 (m, 1H), 6.86 (d, J = 6.8 Hz, 1H), 6.59 (dd, J = 8.0, 1.0 Hz, 1H), 6.45 (td, J = 7.3, 1.1 Hz, 1H), 6.03 (s, 1H), 4.45 – 4.35 (m, 1H), 2.82 – 2.72 (m, 1H), 2.54 (dd, J = 10.8, 5.3 Hz, 1H), 2.03 – 1.94 (m, 1H), 1.88 – 1.77 (m, 1H) ppm.

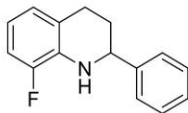
^{13}C NMR (100 MHz, DMSO- d_6 , 296 K): δ = 145.38, 145.30, 128.71, 128.24, 126.88, 126.48, 126.43, 119.49, 115.39, 113.56, 54.46, 30.25, 25.37 ppm.

HRMS (ESI $^+$) Calculated for $C_{15}H_{14}BrN$: 288.03751; found: 288.04372.

Yield: 68 % (98 mg) as an oil. The product was purified via plate chromatography (*n*-pentane : EtOAc, 30:1).

The spectroscopic data is insufficient reported in literature.

8-Fluoro-2-phenyl-1,2,3,4-tetrahydroquinoline (13)



MW ($C_{15}H_{14}FN$) = 227.28 g/mol (M)

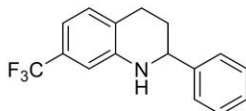
1H NMR (400 MHz, DMSO- d_6 , 296 K): δ = 7.35 (dd, J = 5.5, 3.2 Hz, 4H), 7.32 – 7.23 (m, 1H), 6.89 (dd, J = 11.5, 8.2 Hz, 1H), 6.76 (d, J = 7.2 Hz, 1H), 6.54 – 6.40 (m, 1H), 5.89 (s, 1H), 4.53 (dd, J = 6.4, 3.2 Hz, 1H), 2.83 – 2.72 (m, 1H), 2.53 (dd, J = 4.5, 2.8 Hz, 1H), 2.06 – 1.87 (m, 2H) ppm.

^{13}C NMR (100 MHz, DMSO- d_6 , 296 K): δ = 151.25, 148.89, 145.11, 133.24, 133.12, 128.21, 126.78, 126.20, 124.30, 122.71, 114.57, 112.33, 53.46, 29.31, 24.31 ppm.

Yield: 96 % (109 mg) as an oil. The product was purified via column chromatography (n -pentane : EtOAc, 10:1).

The spectroscopic data match those reported in literature.^[7] (CAS Number: 2891730-99-5)

2-Phenyl-7-(trifluoromethyl)-1,2,3,4-tetrahydroquinoline (14)



MW ($C_{16}H_{14}F_3N$) = 277.29 g/mol (M)

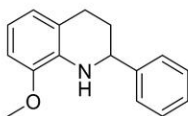
1H NMR (400 MHz, DMSO- d_6 , 296 K): δ = 7.35 (d, J = 4.3 Hz, 4H), 7.27 (dt, J = 8.5, 4.2 Hz, 1H), 7.06 (d, J = 7.8 Hz, 1H), 6.90 (s, 1H), 6.72 (d, J = 7.8 Hz, 1H), 6.58 (s, 1H), 4.48 (d, J = 6.0 Hz, 1H), 2.87 – 2.75 (m, 1H), 2.59 (dt, J = 16.5, 5.1 Hz, 1H), 2.01 (ddd, J = 14.8, 9.5, 5.0 Hz, 1H), 1.89 – 1.78 (m, 1H) ppm.

^{13}C NMR (100 MHz, DMSO- d_6 , 296 K): δ = 145.75, 144.65, 129.35, 128.36, 127.66, 127.35, 127.08, 126.38, 126.04, 123.75, 123.34, 111.03, 109.10, 54.18, 29.44, 25.18 ppm.

Yield: 95 % (132 mg) as an oil. The product was purified via column chromatography (n -pentane : EtOAc, 10:1).

The spectroscopic data match those reported in literature.^[12] (CAS Number: 2098241-71-3)

8-Methoxy-2-phenyl-1,2,3,4-tetrahydroquinoline (15)



MW ($C_{16}H_{17}NO$) = 239.32 g/mol (M)

1H NMR (400 MHz, DMSO- d_6 , 296 K): δ = 7.32 (dd, J = 6.6, 2.7 Hz, 4H), 7.29 – 7.20 (m, 1H), 6.67 (d, J = 7.9 Hz, 1H), 6.56 (d, J = 7.5 Hz, 1H), 6.48 (t, J = 7.7 Hz, 1H), 4.99 (s, 1H), 4.51 – 4.41 (m, 1H), 3.75 (s, 3H), 2.82 – 2.70 (m, 1H), 2.54 (t, J = 5.7 Hz, 1H), 1.99 (dd, J = 10.7, 5.7 Hz, 1H), 1.89 (ddd, J = 16.3, 8.0, 4.3 Hz, 1H) ppm.

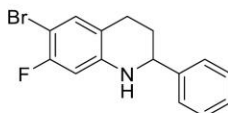
^{13}C NMR (100 MHz, DMSO- d_6 , 296 K): δ = 145.61, 145.28, 134.14, 128.25, 126.85, 126.23, 121.16, 119.77, 115.12, 115.10, 107.87, 55.24, 53.98, 29.65, 24.79 ppm.

HRMS (ESI $^+$) Calculated for $C_{16}H_{17}NO$: 240.13715; found: 240.13829.

Yield: 93 % (111 mg) as an oil. The product was purified via column chromatography (n -pentane : EtOAc, 7:1).

Spectroscopic data is insufficient reported in the literature.^[13] (CAS Number: 872273-99-9)

6-Bromo-7-fluoro-2-phenyl-1,2,3,4-tetrahydroquinoline (16)



MW ($C_{15}H_{13}BrFN$) = 306.18 g/mol (M)

1H NMR (400 MHz, DMSO- d_6 , 296 K): δ = 7.34 (dd, J = 8.6, 4.5 Hz, 4H), 7.30 – 7.23 (m, 1H), 6.89 – 6.82 (m, 1H), 6.39 (s, 1H), 6.22 (td, J = 8.6, 2.6 Hz, 1H), 4.41 (ddd, J = 8.2, 3.4, 1.6 Hz, 1H), 2.77 – 2.66 (m, 1H), 2.52 (dd, J = 8.4, 3.4 Hz, 1H), 2.04 – 1.93 (m, 1H), 1.88 – 1.75 (m, 1H) ppm.

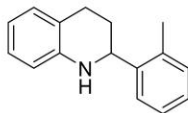
^{13}C NMR (100 MHz, DMSO- d_6 , 296 K): δ = 162.79, 160.43, 146.81, 146.70, 144.81, 129.82, 129.72, 128.31, 127.02, 126.41, 115.51, 115.49, 54.16, 30.01, 24.68 ppm.

HRMS (ESI $^+$) Calculated for $C_{15}H_{13}BrFN$: 307.02564; found: 307.05951.

Yield: 93 % (142 mg) as an oil. The product was purified via plate chromatography (n -pentane : EtOAc, 30:1).

The spectroscopic data is insufficient reported in literature.

2-(2-Methylphenyl)-1,2,3,4-tetrahydroquinoline (17)



MW ($C_{16}H_{17}N$) = 223.32 g/mol (M)

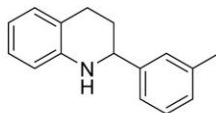
1H NMR (400 MHz, DMSO- d_6 , 296 K): δ = 7.48 – 7.35 (m, 1H), 7.25 – 7.12 (m, 3H), 6.88 (t, J = 7.3 Hz, 2H), 6.59 (d, J = 7.9 Hz, 1H), 6.46 (dd, J = 10.3, 4.2 Hz, 1H), 5.89 (s, 1H), 4.60 (d, J = 8.0 Hz, 1H), 2.88 – 2.74 (m, 1H), 2.66 – 2.53 (m, 1H), 2.34 (s, 3H), 1.97 (dd, J = 8.7, 4.5 Hz, 1H), 1.73 (dtd, J = 14.4, 9.8, 4.9 Hz, 1H) ppm.

^{13}C NMR (100 MHz, DMSO- d_6 , 296 K): δ = 145.71, 143.01, 134.33, 130.21, 128.68, 126.53, 126.45, 126.04, 125.87, 119.44, 115.31, 113.52, 50.92, 28.34, 25.57, 18.64, 18.62 ppm.

Yield: 81 % (90 mg) as an oil. The product was purified via column chromatography (*n*-pentane : EtOAc, 10:1).

The spectroscopic data match those reported in literature.^[14] (CAS Number: 123612-58-8)

2-(3-Methylphenyl)-1,2,3,4-tetrahydroquinoline (18)



MW ($C_{16}H_{17}N$) = 223.32 g/mol (M)

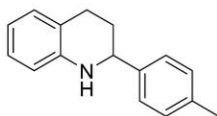
1H NMR (400 MHz, DMSO- d_6 , 296 K): δ = 7.19 (dt, J = 19.2, 7.7 Hz, 3H), 7.07 (d, J = 7.3 Hz, 1H), 6.92 – 6.83 (m, 2H), 6.60 (dd, J = 8.0, 1.0 Hz, 1H), 6.45 (td, J = 7.3, 1.2 Hz, 1H), 5.98 (s, 1H), 4.38 – 4.33 (m, 1H), 2.83 – 2.72 (m, 1H), 2.54 (dt, J = 17.0, 5.5 Hz, 1H), 2.30 (s, 3H), 1.97 (ddd, J = 13.3, 8.7, 4.7 Hz, 1H), 1.87 – 1.76 (m, 1H) ppm.

^{13}C NMR (100 MHz, DMSO- d_6 , 296 K): δ = 145.40, 145.23, 137.23, 128.68, 128.13, 127.51, 127.01, 126.45, 123.59, 119.50, 115.37, 113.56, 54.57, 30.36, 25.55, 21.13 ppm.

Yield: 91 % (102 mg) as an oil. The product was purified via column chromatography (*n*-pentane : EtOAc, 20:1).

The spectroscopic data match those reported in literature.^[15] (CAS Number: 1495968-76-7)

2-(4-Methylphenyl)-1,2,3,4-tetrahydroquinoline (19)



MW ($C_{16}H_{17}N$) = 223.32 g/mol (M)

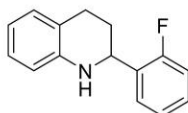
1H NMR (400 MHz, DMSO- d_6 , 296 K): δ = 7.23 (d, J = 8.0 Hz, 2H), 7.14 (d, J = 8.1 Hz, 2H), 6.86 (dd, J = 14.5, 7.4 Hz, 2H), 6.58 (d, J = 8.0 Hz, 1H), 6.44 (td, J = 7.3, 1.2 Hz, 1H), 5.96 (s, 1H), 4.35 (d, J = 7.0 Hz, 1H), 2.81 – 2.69 (m, 1H), 2.59 – 2.50 (m, 1H), 2.28 (s, 3H), 1.95 (dd, J = 12.9, 3.7 Hz, 1H), 1.86 – 1.73 (m, 1H) ppm.

^{13}C NMR (100 MHz, DMSO- d_6 , 296 K): δ = 145.42, 142.27, 135.87, 128.77, 128.70, 126.45, 126.33, 119.49, 115.34, 113.54, 54.21, 30.28, 25.41, 20.70 ppm.

Yield: 84 % (94 mg) as an oil. The product was purified via column chromatography (*n*-pentane : EtOAc, 7:1).

The spectroscopic data match those reported in literature.^[16] (CAS Number: 123612-59-9)

2-(2-Fluorophenyl)-1,2,3,4-tetrahydroquinoline (20)



MW ($C_{15}H_{14}FN$) = 227.28 g/mol (M)

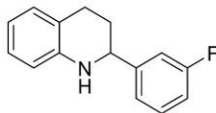
1H NMR (400 MHz, DMSO- d_6 , 296 K): δ = 7.42 – 7.16 (m, 4H), 6.87 (dd, J = 14.6, 7.5 Hz, 2H), 6.59 (dd, J = 7.9, 3.2 Hz, 1H), 6.46 (dd, J = 16.1, 7.7 Hz, 1H), 6.03 (d, J = 12.9 Hz, 1H), 4.77 – 4.67 (m, 1H), 4.40 (d, J = 7.0 Hz, 1H), 2.76 (ddd, J = 16.5, 11.1, 6.4 Hz, 1H), 2.60 – 2.50 (m, 1H), 2.06 – 1.93 (m, 1H), 1.84 (ddd, J = 17.5, 8.3, 4.5 Hz, 1H) ppm.

^{13}C NMR (100 MHz, DMSO- d_6 , 296 K): δ = 145.34, 128.68, 128.21, 126.85, 126.58, 126.45, 126.40, 124.29, 119.47, 115.60, 115.39, 113.54, 54.45, 47.75, 25.34 ppm.

Yield: 74 % (84 mg) as an oil. The product was purified via column chromatography (*n*-pentane : EtOAc, 15:1).

The spectroscopic data match those reported in literature.^[17] (CAS Number: 897931-78-1)

2-(3-Fluorophenyl)-1,2,3,4-tetrahydroquinoline (21)



MW ($C_{15}H_{14}FN$) = 227.28 g/mol (M)

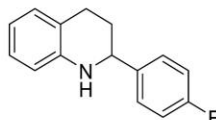
1H NMR (400 MHz, DMSO- d_6 , 296 K): δ = 7.48 – 7.27 (m, 4H), 7.25 (ddd, J = 5.7, 4.0, 2.3 Hz, 1H), 6.86 (d, J = 6.5 Hz, 1H), 6.59 (dd, J = 8.0, 1.0 Hz, 1H), 6.45 (td, J = 7.3, 1.2 Hz, 1H), 6.02 (s, 1H), 4.40 (ddd, J = 8.3, 3.3, 1.7 Hz, 1H), 2.81 – 2.72 (m, 1H), 2.54 (dd, J = 10.8, 5.4 Hz, 1H), 2.03 – 1.94 (m, 1H), 1.88 – 1.78 (m, 1H) ppm.

^{13}C NMR (100 MHz, DMSO- d_6 , 296 K): δ = 145.38, 145.30, 128.72, 128.55, 128.24, 126.88, 126.56, 126.48, 126.43, 119.49, 115.41, 113.56, 54.47, 30.26, 25.38 ppm.

Yield: 91 % (103 mg) as an oil. The product was purified via column chromatography (*n*-pentane : EtOAc, 7:1).

The spectroscopic data match those reported in literature.^[7] (CAS Number: 221910-33-4)

2-(4-Fluorophenyl)-1,2,3,4-tetrahydroquinoline (22)



MW ($C_{15}H_{14}FN$) = 227.28 g/mol (M)

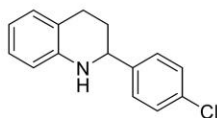
1H NMR (400 MHz, DMSO- d_6 , 296 K): δ = 7.34 (dd, J = 7.2, 1.8 Hz, 3H), 7.29 – 7.22 (m, 1H), 6.92 – 6.82 (m, 2H), 6.59 (dd, J = 8.0, 1.0 Hz, 1H), 6.45 (td, J = 7.3, 1.2 Hz, 1H), 6.02 (s, 1H), 4.47 – 4.35 (m, 1H), 2.77 (ddd, J = 15.1, 9.6, 5.3 Hz, 1H), 2.54 (dd, J = 10.6, 5.2 Hz, 1H), 2.03 – 1.94 (m, 1H), 1.88 – 1.77 (m, 1H) ppm.

^{13}C NMR (100 MHz, DMSO- d_6 , 296 K): δ = 145.31, 128.72, 128.24, 126.88, 126.49, 126.44, 119.50, 119.45, 115.41, 113.57, 54.48, 30.26, 25.38 ppm.

Yield: 83 % (94 mg) as an oil. The product was purified via plate chromatography (*n*-pentane : EtOAc, 20:1).

The spectroscopic data match those reported in literature.^[18] (CAS Number: 1402568-43-7)

2-(4-Chlorophenyl)-1,2,3,4-tetrahydroquinoline (23)



MW ($C_{15}H_{14}ClN$) = 243.73 g/mol (M)

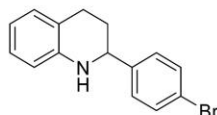
1H NMR (400 MHz, DMSO- d_6 , 296 K): δ = 7.27 (ddd, J = 20.5, 8.4, 2.3 Hz, 4H), 6.83 (dd, J = 14.3, 7.3 Hz, 2H), 6.55 (d, J = 8.0 Hz, 1H), 6.45 – 6.37 (m, 1H), 6.00 (d, J = 17.4 Hz, 1H), 4.40 – 4.31 (m, 1H), 2.78 – 2.63 (m, 1H), 2.46 (dd, J = 6.9, 3.1 Hz, 1H), 1.98 – 1.87 (m, 1H), 1.77 (ddd, J = 13.2, 9.0, 4.5 Hz, 1H) ppm.

^{13}C NMR (100 MHz, DMSO- d_6 , 296 K): δ = 145.29, 144.35, 131.26, 128.70, 128.22, 126.87, 126.42, 119.49, 115.41, 113.56, 54.48, 30.26, 25.37 ppm.

Yield: 75 % (91 mg) as an oil (diastereomeric mixture). The product was purified via column chromatography (n -pentane : EtOAc, 10:1).

The spectroscopic data match those reported in literature.^[17] (CAS Number: 78318-05-5)

2-(4-Bromophenyl)-1,2,3,4-tetrahydroquinoline (24)



MW ($C_{15}H_{14}BrN$) = 288.19 g/mol (M)

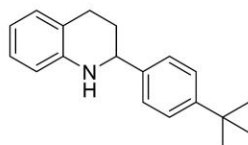
1H NMR (400 MHz, DMSO- d_6 , 296 K): δ = 7.40 – 7.29 (m, 4H), 7.28 – 7.22 (m, 1H), 6.87 (d, J = 5.6 Hz, 1H), 6.58 (d, J = 7.9 Hz, 1H), 6.44 (td, J = 7.3, 1.1 Hz, 1H), 6.02 (s, 1H), 4.40 (d, J = 6.8 Hz, 1H), 2.81 – 2.72 (m, 1H), 2.55 (t, J = 5.4 Hz, 1H), 2.01 – 1.95 (m, 1H), 1.83 (ddd, J = 12.8, 8.1, 4.4 Hz, 1H) ppm.

^{13}C NMR (100 MHz, DMSO- d_6 , 296 K): δ = 145.38, 145.30, 128.71, 128.24, 126.88, 126.48, 126.43, 119.48, 115.39, 113.55, 54.46, 30.25, 25.36 ppm.

Yield: 72 % (104 mg) as an oil (diastereomeric mixture). The product was purified via column chromatography (n -pentane : EtOAc, 15:1).

The spectroscopic data match those reported in literature.^[17] (CAS Number: 1494687-58-9)

2-(4-(*tert*-butyl)phenyl)-1,2,3,4-tetrahydroquinoline (25)



MW (C₁₉H₂₃N) = 265.40 g/mol (M)

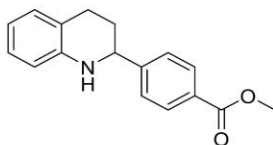
¹H NMR (400 MHz, DMSO-d₆, 296 K): δ = 7.36 (d, *J* = 8.2 Hz, 2H), 7.29 (d, *J* = 8.3 Hz, 2H), 6.86 (d, *J* = 7.9 Hz, 2H), 6.57 (d, *J* = 7.8 Hz, 1H), 6.44 (t, *J* = 7.3 Hz, 1H), 5.96 (s, 1H), 4.35 (dd, *J* = 8.3, 2.3 Hz, 1H), 2.84 – 2.73 (m, 1H), 2.56 (dt, *J* = 16.2, 4.9 Hz, 1H), 2.02 – 1.92 (m, 1H), 1.87 – 1.75 (m, 1H), 1.28 (s, 9H) ppm.

¹³C NMR (100 MHz, DMSO-d₆, 296 K): δ = 149.27, 145.47, 142.17, 128.68, 126.41, 126.21, 124.96, 119.45, 115.35, 113.54, 54.38, 34.17, 31.21, 30.31, 25.69 ppm.

Yield: 87 % (115 mg) as an oil. The product was purified via column chromatography (*n*-pentane : EtOAc, 20:1).

The spectroscopic data match those reported in literature.^[8] (CAS Number: 1483366-75-1)

Methyl-4-(1,2,3,4-tetrahydroquinolin-2-yl)benzoate (26)



MW (C₁₇H₁₇NO₂) = 267.33 g/mol (M)

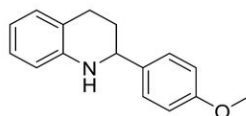
¹H NMR (400 MHz, DMSO-d₆, 296 K): δ = 7.96 (dd, *J* = 5.5, 2.7 Hz, 2H), 7.57 – 7.49 (m, 2H), 6.91 (dd, *J* = 11.9, 7.4 Hz, 2H), 6.63 (d, *J* = 7.9 Hz, 1H), 6.50 (dd, *J* = 10.3, 4.2 Hz, 1H), 6.17 (s, 1H), 4.54 (s, 1H), 3.01 – 2.67 (m, 2H), 2.04 (dd, *J* = 6.8, 4.3 Hz, 1H), 1.91 – 1.86 (m, 1H) ppm.

¹³C NMR (100 MHz, DMSO-d₆, 296 K): δ = 165.63, 150.98, 145.01, 129.50, 129.18, 128.74, 126.71, 126.56, 119.49, 115.61, 113.63, 60.60, 54.10, 29.92, 25.02 ppm.

Yield: 92 % (123 mg) as an oil. The product was purified via column chromatography (*n*-pentane : EtOAc, 10:3). There are ethyl acetate residues in the spectra.

The spectroscopic data match those reported in literature.^[18] (CAS Number: 2170087-20-2)

2-(4-Methoxyphenyl)-1,2,3,4-tetrahydroquinoline (27)



MW ($C_{16}H_{17}NO$) = 239.32 g/mol (M)

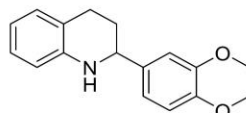
1H NMR (400 MHz, DMSO- d_6 , 296 K): δ = 7.27 (d, J = 8.3 Hz, 2H), 6.93 – 6.82 (m, 4H), 6.57 (d, J = 7.9 Hz, 1H), 6.44 (t, J = 7.3 Hz, 1H), 5.92 (s, 1H), 4.34 (d, J = 6.5 Hz, 1H), 3.74 (d, J = 1.1 Hz, 3H), 2.82 – 2.71 (m, 1H), 2.59 – 2.51 (m, 1H), 1.99 – 1.90 (m, 1H), 1.80 (ddd, J = 17.0, 8.4, 4.5 Hz, 1H) ppm.

^{13}C NMR (100 MHz, DMSO- d_6 , 296 K): δ = 158.23, 145.42, 137.14, 128.66, 127.45, 126.39, 119.46, 115.32, 113.59, 113.52, 55.02, 53.92, 30.38, 25.50 ppm.

Yield: 70 % (84 mg) as an oil. The product was purified via column chromatography (*n*-pentane : EtOAc, 10:1).

The spectroscopic data match those reported in literature.^[18] (CAS Number: 221910-30-1)

2-(3,4-Dimethoxyphenyl)-1,2,3,4-tetrahydroquinoline (28)



MW ($C_{17}H_{19}NO_2$) = 269.34 g/mol (M)

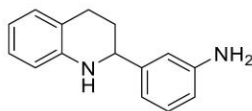
1H NMR (400 MHz, DMSO- d_6 , 296 K): δ = 6.99 – 6.83 (m, 5H), 6.58 (d, J = 8.0 Hz, 1H), 6.44 (t, J = 7.3 Hz, 1H), 5.92 (s, 1H), 4.32 (d, J = 7.4 Hz, 1H), 3.73 (d, J = 3.9 Hz, 6H), 2.83 – 2.74 (m, 1H), 2.60 – 2.53 (m, 1H), 1.96 (dd, J = 9.2, 3.1 Hz, 1H), 1.87 – 1.79 (m, 1H) ppm.

^{13}C NMR (100 MHz, DMSO- d_6 , 296 K): δ = 148.65, 147.79, 145.46, 137.64, 128.67, 126.40, 119.53, 118.36, 115.40, 113.60, 111.66, 110.25, 55.57, 55.42, 54.36, 30.49, 25.74 ppm.

Yield: 91 % (123 mg) as white crystals. The product was purified via column chromatography (*n*-pentane : EtOAc, 10:3).

The spectroscopic data match those reported in literature.^[19] (CAS Number: 1498916-68-9)

3-(1,2,3,4-Tetrahydroquinolin-2-yl)aniline (29)



MW ($C_{15}H_{16}N_2$) = 224.31 g/mol (M)

1H NMR (400 MHz, DMSO- d_6 , 296 K): δ = 6.97 (t, J = 7.7 Hz, 1H), 6.92 – 6.80 (m, 2H), 6.58 (dd, J = 7.2, 5.0 Hz, 2H), 6.54 – 6.38 (m, 3H), 5.90 (s, 1H), 5.01 (s, 2H), 4.23 (d, J = 6.8 Hz, 1H), 2.75 (td, J = 9.7, 4.8 Hz, 1H), 2.61 – 2.52 (m, 1H), 1.92 (d, J = 3.5 Hz, 1H), 1.78 (td, J = 8.2, 3.9 Hz, 1H) ppm.

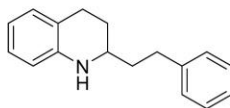
^{13}C NMR (100 MHz, DMSO- d_6 , 296 K): δ = 148.60, 145.99, 145.50, 128.65, 126.41, 119.50, 115.17, 114.06, 113.44, 112.59, 111.87, 54.87, 30.41, 25.63 ppm.

HRMS (ESI $^+$) Calculated for $C_{15}H_{16}N_2$: 225.13762; found: 225.13863.

Yield: 89 % (100 mg) as an oil. The product was purified via column chromatography (*n*-pentane : EtOAc, 10:5). There are ethyl acetate residues in the spectra.

The spectroscopic data is insufficient reported in literature.

2-Phenethyl-1,2,3,4-tetrahydroquinoline (30)



MW ($C_{17}H_{19}N$) = 237.35 g/mol (M)

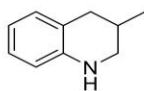
1H NMR (400 MHz, DMSO- d_6 , 296 K): δ = 7.27 (dt, J = 14.3, 7.0 Hz, 4H), 7.17 (t, J = 7.0 Hz, 1H), 6.82 (d, J = 7.4 Hz, 2H), 6.50 (d, J = 7.9 Hz, 1H), 6.39 (t, J = 7.3 Hz, 1H), 5.58 (s, 1H), 3.17 (d, J = 5.8 Hz, 1H), 2.76 – 2.61 (m, 4H), 1.94 – 1.87 (m, 1H), 1.79 – 1.66 (m, 2H), 1.54 – 1.47 (m, 1H) ppm.

^{13}C NMR (100 MHz, DMSO- d_6 , 296 K): δ = 145.23, 142.20, 128.69, 128.30, 126.32, 125.73, 125.67, 119.77, 115.15, 113.46, 50.09, 37.89, 31.21, 27.22, 25.80 ppm.

Yield: 69 % (82 mg) as an oil. The product was purified via column chromatography (*n*-pentane : EtOAc, 10:3).

The spectroscopic data match those reported in literature.^[20] (CAS Number: 101583-63-5)

3-Methyl-1,2,3,4-tetrahydroquinoline (31)



MW (C₁₀H₁₃N) = 147.22 g/mol (M)

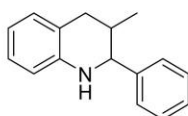
¹H NMR (400 MHz, DMSO-d₆, 296 K): δ = 6.91 – 6.71 (m, 2H), 6.50 – 6.29 (m, 2H), 5.62 (s, 1H), 3.16 (ddd, J = 11.2, 5.7, 3.6 Hz, 1H), 2.74 (t, J = 10.3 Hz, 1H), 2.70 – 2.62 (m, 1H), 2.30 (dd, J = 15.8, 10.0 Hz, 1H), 1.86 (qd, J = 10.1, 3.8 Hz, 1H), 0.96 (d, J = 6.6 Hz, 3H) ppm.

¹³C NMR (100 MHz, DMSO-d₆, 296 K): δ = 144.88, 128.97, 126.34, 119.43, 115.02, 113.01, 47.67, 39.52, 35.14, 26.38, 18.88 ppm.

Yield: 86 % (63 mg) as an oil. The product was purified via column chromatography (*n*-pentane : EtOAc, 10:1).

The spectroscopic data match those reported in literature.^[21] (CAS Number: 20668-20-6)

3-Methyl-2-phenyl-1,2,3,4-tetrahydroquinoline (32)



MW (C₁₆H₁₇N) = 223.32 g/mol (M)

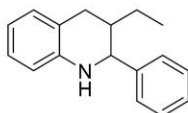
¹H NMR (400 MHz, DMSO-d₆, 296 K): δ = 7.25 – 7.03 (m, 5H), 6.91 – 6.85 (m, 2H), 6.59 (d, J = 8.0 Hz, 1H), 6.45 (t, J = 7.2 Hz, 1H), 6.07 (s, 1H), 4.40 (s, 1H), 2.83 (dd, J = 16.0, 4.8 Hz, 1H), 2.42 – 2.24 (m, 1H), 2.16 – 2.10 (m, 1H), 0.69 (d, J = 6.8 Hz, 3H) ppm.

¹³C NMR (100 MHz, DMSO-d₆, 296 K): δ = 144.88, 140.13, 129.09, 128.34, 127.01, 126.47, 118.58, 115.31, 113.17, 57.64, 32.71, 31.02, 15.29 ppm.

Yield: 79 % (88 mg) as an oil. The product was purified via column chromatography (*n*-pentane : EtOAc, 10:1).

The spectroscopic data match those reported in literature.^[21] (CAS Number: 24005-26-3)

3-Ethyl-2-phenyl-1,2,3,4-tetrahydroquinoline (33)



MW (C₁₇H₁₉N) = 237.35 g/mol (M)

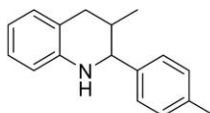
¹H NMR (400 MHz, DMSO-d₆, 296 K): δ = 8.28 (s, 1H), 8.01 – 7.93 (m, 2H), 7.71 (ddd, J = 8.3, 6.9, 1.4 Hz, 1H), 7.62 – 7.40 (m, 6H), 3.35 (s, 1H), 3.19 – 3.09 (m, 1H), 2.77 (q, J = 7.5 Hz, 2H), 2.62 (t, J = 6.3 Hz, 1H), 1.81 – 1.72 (m, 1H), 1.13 (t, J = 7.5 Hz, 3H) ppm.

¹³C NMR (100 MHz, DMSO-d₆, 296 K): δ = 159.86, 145.78, 140.55, 134.97, 134.89, 128.70, 128.06, 127.24, 126.47, 119.78, 114.97, 113.29, 40.78, 26.72, 25.44, 21.57, 14.56 ppm.

Yield: 81 % (96 mg) as an oil (diastereomeric mixture). The product was purified via column chromatography (*n*-pentane : EtOAc, 10:1).

The spectroscopic data match those reported in literature.^[22] (CAS Number: 2690326-14-6)

3-Methyl-2-(*para*-tolyl)-1,2,3,4-tetrahydroquinoline (34)



MW (C₁₇H₁₉N) = 237.35 g/mol (M)

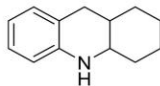
¹H NMR (400 MHz, DMSO-d₆, 296 K): δ = 7.21 – 7.07 (m, 4H), 6.91 – 6.83 (m, 2H), 6.59 (d, J = 8.0 Hz, 1H), 6.45 (t, J = 7.2 Hz, 1H), 6.07 (s, 1H), 4.40 (s, 1H), 2.83 (dd, J = 15.9, 4.6 Hz, 1H), 2.33 (dd, J = 16.2, 7.4 Hz, 1H), 2.28 (s, 3H), 2.14 (dd, J = 9.6, 5.6 Hz, 1H), 0.69 (d, J = 6.8 Hz, 3H) ppm.

¹³C NMR (100 MHz, DMSO-d₆, 296 K): δ = 144.88, 140.13, 135.63, 129.09, 128.34, 127.01, 126.47, 118.58, 115.31, 113.17, 57.64, 32.71, 31.02, 20.67, 15.29 ppm.

Yield: 69 % (82 mg) as an oil. The product was purified via column chromatography (*n*-pentane : EtOAc, 10:1).

The spectroscopic data match those reported in literature.^[23] (CAS Number: 1378900-79-8)

1,2,3,4,4a,9,9a,10-Octahydroacridine (35)



MW ($C_{13}H_{17}N$) = 187.29 g/mol (M)

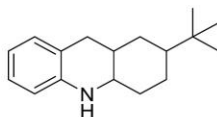
1H NMR (400 MHz, DMSO- d_6 , 296 K): δ = 6.77 – 6.70 (m, 2H), 6.37 (d, J = 7.8 Hz, 1H), 6.30 (t, J = 7.3 Hz, 1H), 5.39 (s, 1H), 3.34 – 3.31 (m, 1H), 2.72 (dd, J = 16.2, 5.4 Hz, 1H), 2.35 (dd, J = 16.3, 4.0 Hz, 1H), 1.79 (s, 1H), 1.63 (d, J = 12.6 Hz, 1H), 1.48 (dd, J = 29.1, 9.6 Hz, 3H), 1.26 (t, J = 7.7 Hz, 4H) ppm.

^{13}C NMR (100 MHz, DMSO- d_6 , 296 K): δ = 144.50, 129.14, 126.18, 117.76, 114.73, 112.74, 49.05, 32.20, 30.73, 26.92, 24.29, 24.18, 20.43 ppm.

Yield: 93 % (87 mg) as white crystals. The product was purified via column chromatography (n -pentane : EtOAc, 15:1).

The spectroscopic data match those reported in literature.^[24] (CAS Number: 92039-20-8)

2-(*Tert*-butyl)-1,2,3,4,4a,9,9a,10-octahydroacridine (36)



MW ($C_{17}H_{25}N$) = 243.39 g/mol (M)

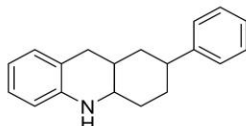
1H NMR (400 MHz, DMSO- d_6 , 296 K): δ = (d, J = 7.4 Hz, 2H), 6.43 (d, J = 7.7 Hz, 1H), 6.37 (td, J = 7.3, 1.1 Hz, 1H), 5.32 (s, 1H), 3.39 (d, J = 2.7 Hz, 1H), 2.95 (dd, J = 16.1, 5.7 Hz, 1H), 2.30 (d, J = 16.0 Hz, 1H), 1.90 – 1.76 (m, 2H), 1.53 – 1.38 (m, 2H), 1.29 (d, J = 4.1 Hz, 1H), 1.23 (s, 1H), 1.10 (t, J = 12.0 Hz, 1H), 0.97 (d, J = 12.2 Hz, 1H), 0.79 (s, 9H) ppm.

^{13}C NMR (100 MHz, DMSO- d_6 , 296 K): δ = 144.71, 129.21, 126.14, 117.62, 114.87, 112.80, 48.04, 47.45, 39.94, 33.64, 33.37, 32.20, 31.31, 27.47, 20.16 ppm.

Yield: 89 % (108 mg) as white/yellow crystals. The product was purified via column chromatography (n -pentane : EtOAc, 15:1).

The spectroscopic data match those reported in literature.^[25] (CAS Number: 113146-51-3)

2-Phenyl-1,2,3,4,4a,9,9a,10-octahydroacridine (37)



MW (C₁₉H₂₁N) = 263.38 g/mol (M)

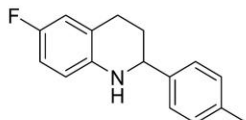
¹H NMR (400 MHz, DMSO-d₆, 296 K): δ = 7.35 – 7.05 (m, 5H), 6.89 – 6.75 (m, 2H), 6.49 (d, J = 8.0 Hz, 1H), 6.38 (t, J = 7.3 Hz, 1H), 5.47 (s, 1H), 3.49 (s, 1H), 2.98 (dd, J = 16.2, 5.0 Hz, 1H), 2.71 – 2.58 (m, 1H), 2.33 (d, J = 16.4 Hz, 1H), 2.01 (s, 1H), 1.92 (d, J = 12.7 Hz, 1H), 1.80 – 1.62 (m, 2H), 1.52 (d, J = 12.0 Hz, 1H), 1.41 (t, J = 9.4 Hz, 2H) ppm.

¹³C NMR (100 MHz, DMSO-d₆, 296 K): δ = 147.16, 144.64, 129.22, 128.26, 126.53, 126.24, 125.77, 117.49, 115.00, 112.89, 47.80, 43.05, 34.11, 33.33, 32.93, 31.00, 27.00 ppm.

Yield: 62 % (82 mg) as white crystals. The product was purified via column chromatography (*n*-pentane : EtOAc, 10:1).

The spectroscopic data match those reported in literature.^[26] (CAS Number: 2108737-33-1)

6-Fluoro-2-(*para*-tolyl)-1,2,3,4-tetrahydroquinoline (38)



MW (C₁₆H₁₆FN) = 241.31 g/mol (M)

¹H NMR (400 MHz, DMSO-d₆, 296 K): δ = 7.23 (d, *J* = 8.0 Hz, 2H), 7.14 (d, *J* = 7.9 Hz, 2H), 6.85 (m, 1H), 6.57 (d, *J* = 8.0 Hz, 1H), 6.47 – 6.40 (m, 1H), 5.96 (s, 1H), 4.35 (d, *J* = 7.7 Hz, 1H), 2.75 (ddd, *J* = 15.1, 9.6, 5.3 Hz, 1H), 2.54 (t, *J* = 5.3 Hz, 1H), 2.28 (s, 3H), 1.95 (dd, *J* = 12.5, 3.5 Hz, 1H), 1.85 – 1.75 (m, 1H) ppm.

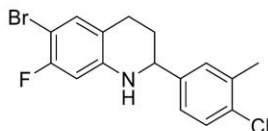
¹³C NMR (100 MHz, DMSO-d₆, 296 K): δ = 145.40, 142.26, 135.86, 128.76, 128.69, 126.44, 126.31, 119.47, 115.33, 113.51, 54.20, 30.26, 25.39, 20.70 ppm.

HRMS (ESI⁺) Calculated for C₁₆H₁₆FN: 242.13395; found: 242.13281.

Yield: 72 % (87 mg) as an oil. The product was purified via plate chromatography (*n*-pentane : EtOAc, 30:1).

The spectroscopic data is insufficient reported in literature.

6-Bromo-2-(4-chloro-3-methylphenyl)-7-fluoro-1,2,3,4-tetrahydroquinoline (39)



MW (C₁₆H₁₄BrClFN) = 354.65 g/mol (M)

¹H NMR (400 MHz, DMSO-d₆, 296 K): δ = 7.36 (d, *J* = 8.2 Hz, 1H), 7.32 (s, 1H), 7.17 (d, *J* = 8.1 Hz, 1H), 6.84 (t, *J* = 7.5 Hz, 1H), 6.36 (s, 1H), 6.21 (td, *J* = 8.8, 2.6 Hz, 1H), 4.38 (d, *J* = 6.4 Hz, 1H), 2.76 – 2.65 (m, 1H), 2.46 (t, *J* = 5.3 Hz, 1H), 2.31 (s, 3H), 2.00 – 1.90 (m, 1H), 1.84 – 1.72 (m, 1H) ppm.

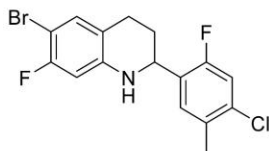
¹³C NMR (100 MHz, DMSO-d₆, 296 K): δ = 160.42, 146.59, 143.85, 135.19, 131.66, 129.83, 129.22, 128.67, 125.70, 115.52, 101.44, 99.39, 53.52, 29.87, 24.62, 19.68 ppm.

HRMS (ESI⁺) Calculated for C₁₆H₁₄BrClFN: 353.14268; found: 353.06294.

Yield: 66 % (177 mg) as an oil. The product was purified via plate chromatography (*n*-pentane : EtOAc, 30:1).

The spectroscopic data is insufficient reported in literature.

6-bromo-2-(4-chloro-2-fluoro-5-methylphenyl)-7-fluoro-1,2,3,4-tetrahydroquinoline (40)



MW ($C_{16}H_{13}BrClF_2N$) = 372.64 g/mol (M)

1H NMR (400 MHz, DMSO- d_6 , 296 K): δ = 7.18 (d, J = 7.4 Hz, 1H), 6.86 (t, J = 7.5 Hz, 1H), 6.37 (dd, J = 11.7, 2.7 Hz, 1H), 6.35 (s, 1H), 6.23 (td, J = 8.6, 2.6 Hz, 1H), 4.66 (s, 1H), 2.77 – 2.66 (m, 1H), 2.52 (d, J = 5.6 Hz, 1H), 2.25 (s, 3H), 1.98 (dt, J = 15.3, 5.1 Hz, 1H), 1.88 – 1.75 (m, 1H) ppm.

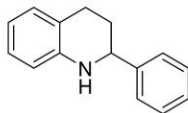
^{13}C NMR (100 MHz, DMSO- d_6 , 296 K): δ = 162.79, 158.84, 146.49, 133.24, 130.91, 129.74, 128.98, 128.33, 115.40, 114.90, 101.71, 99.15, 47.66, 28.19, 24.49, 20.45 ppm.

HRMS (ESI $^+$) Calculated for $C_{16}H_{13}BrClF_2N$: 370.99895; found: 371.04563.

Yield: 63 % (117 mg) as an oil. The product was purified via plate chromatography (n -pentane : EtOAc, 50:1).

The spectroscopic data is insufficient reported in literature.

2-Phenyl-1,2,3,4-tetrahydroquinoline (41)



MW ($C_{15}H_{15}N$) = 209.29 g/mol (M)

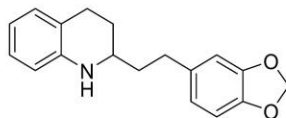
1H NMR (400 MHz, DMSO- d_6 , 296 K): δ = 7.37 – 7.25 (m, 4H), 7.20 (ddd, J = 5.7, 5.1, 2.2 Hz, 1H), 6.90 – 6.74 (m, 2H), 6.54 (d, J = 8.0 Hz, 1H), 6.40 (td, J = 7.3, 1.2 Hz, 1H), 5.97 (s, 1H), 4.40 – 4.30 (m, 1H), 2.76 – 2.66 (m, 1H), 2.47 – 2.42 (m, 1H), 1.98 – 1.89 (m, 1H), 1.84 – 1.72 (m, 1H) ppm.

^{13}C NMR (100 MHz, DMSO- d_6 , 296 K): δ = 145.37, 145.29, 128.71, 128.23, 126.87, 126.47, 126.42, 119.49, 115.40, 113.55, 54.46, 30.25, 25.36 ppm.

Yield: 91 % (95 mg) as an oil. The product was purified via column chromatography (n -pentane : EtOAc, 10:1).

The spectroscopic data match those reported in literature.^[21] (CAS Number: 24005-23-0)

2-(2-(Benzo[*d*][1,3]dioxol-5-yl)ethyl)-1,2,3,4-tetrahydroquinoline (42)



MW ($C_{18}H_{19}NO_2$) = 281.35 g/mol (M)

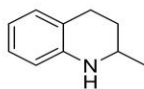
1H NMR (400 MHz, DMSO- d_6 , 296 K): δ = 6.69 (dd, J = 11.7, 8.4 Hz, 4H), 6.56 (d, J = 7.9 Hz, 1H), 6.37 (d, J = 7.9 Hz, 1H), 6.26 (t, J = 7.3 Hz, 1H), 5.82 (s, 2H), 5.41 (s, 1H), 3.01 (d, J = 6.3 Hz, 1H), 2.61 – 2.50 (m, 2H), 2.37 (d, J = 1.3 Hz, 2H), 1.80 – 1.71 (m, 1H), 1.55 (qd, J = 13.1, 6.6 Hz, 2H), 1.35 (ddd, J = 15.1, 9.6, 4.9 Hz, 1H) ppm.

^{13}C NMR (100 MHz, DMSO- d_6 , 296 K): δ = 147.18, 145.22, 145.14, 135.99, 128.67, 126.30, 120.97, 119.77, 115.15, 113.44, 108.74, 108.05, 100.56, 49.91, 38.05, 30.85, 27.22, 25.80 ppm.

Yield: 83 % (117 mg) as an oil. The product was purified via plate chromatography (n -pentane : EtOAc, 20:1).

The spectroscopic data match those reported in literature.^[21] (CAS Number: 375395-24-7)

2-Methyl-1,2,3,4-tetrahydroquinoline (43)



MW ($C_{10}H_{13}N$) = 147.22 g/mol (M)

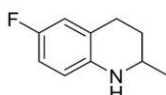
1H NMR (400 MHz, DMSO- d_6 , 296 K): δ = 6.82 (t, J = 7.2 Hz, 2H), 6.45 – 6.35 (m, 2H), 5.50 (s, 1H), 3.33 – 3.23 (m, 1H), 2.71 (ddd, J = 16.4, 11.3, 5.5 Hz, 1H), 2.60 (dt, J = 16.2, 4.5 Hz, 1H), 1.88 – 1.76 (m, 1H), 1.41 (dtdd, J = 13.0, 11.4, 5.2, 1.7 Hz, 1H), 1.12 (dd, J = 6.3, 1.9 Hz, 3H) ppm.

^{13}C NMR (100 MHz, DMSO- d_6 , 296 K): δ = 145.38, 128.69, 126.27, 119.54, 115.14, 113.28, 46.16, 29.70, 26.09, 22.17 ppm.

Yield: 80 % (59 mg) as an oil. The product was purified via column chromatography (*n*-pentane : EtOAc, 10:1).

The spectroscopic data match those reported in literature.^[21] (CAS Number: 1780-19-4)

6-Fluoro-2-methyl-1,2,3,4-tetrahydroquinoline (44)



MW ($C_{10}H_{12}FN$) = 165.21 g/mol (M)

1H NMR (400 MHz, DMSO- d_6 , 296 K): δ = 6.73 – 6.55 (m, 2H), 6.42 (dd, J = 9.6, 5.1 Hz, 1H), 5.46 (s, 1H), 3.28 – 3.18 (m, 1H), 2.72 (ddd, J = 16.8, 11.4, 5.7 Hz, 1H), 2.66 – 2.54 (m, 1H), 1.86 – 1.75 (m, 1H), 1.38 (dddd, J = 12.7, 11.4, 9.8, 5.4 Hz, 1H), 1.11 (d, J = 6.2 Hz, 3H) ppm.

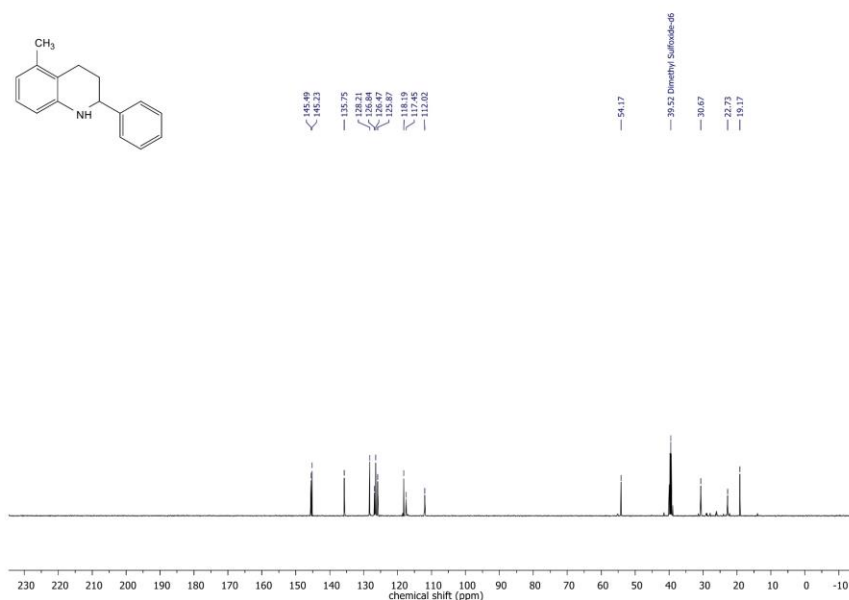
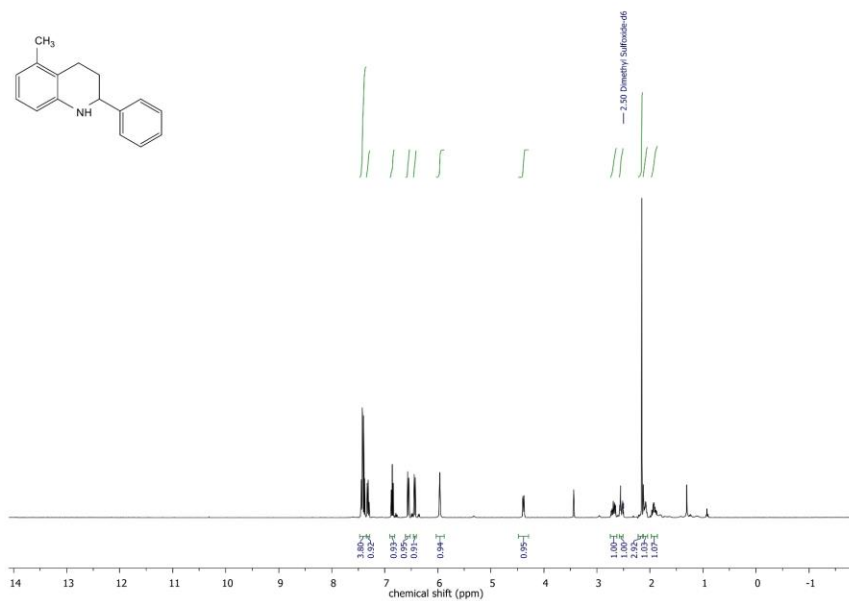
^{13}C NMR (100 MHz, DMSO- d_6 , 296 K): δ = 154.98, 141.99, 120.97, 114.79, 113.92, 112.80, 46.23, 29.39, 26.12, 22.06 ppm.

Yield: 85 % (70 mg) as an oil. The product was purified via column chromatography (*n*-pentane : EtOAc, 15:1).

The spectroscopic data match those reported in literature.^[21] (CAS Number: 42835-89-2)

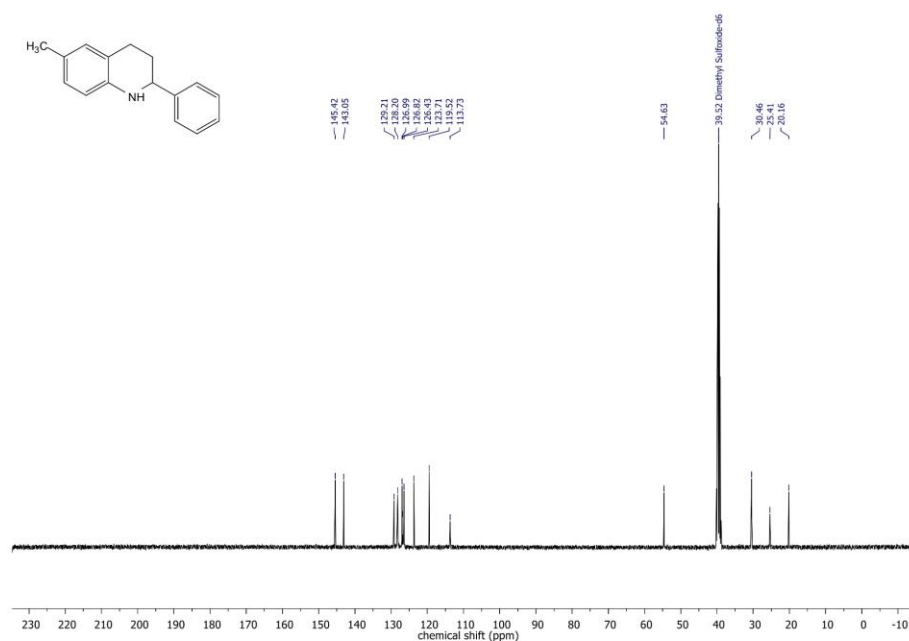
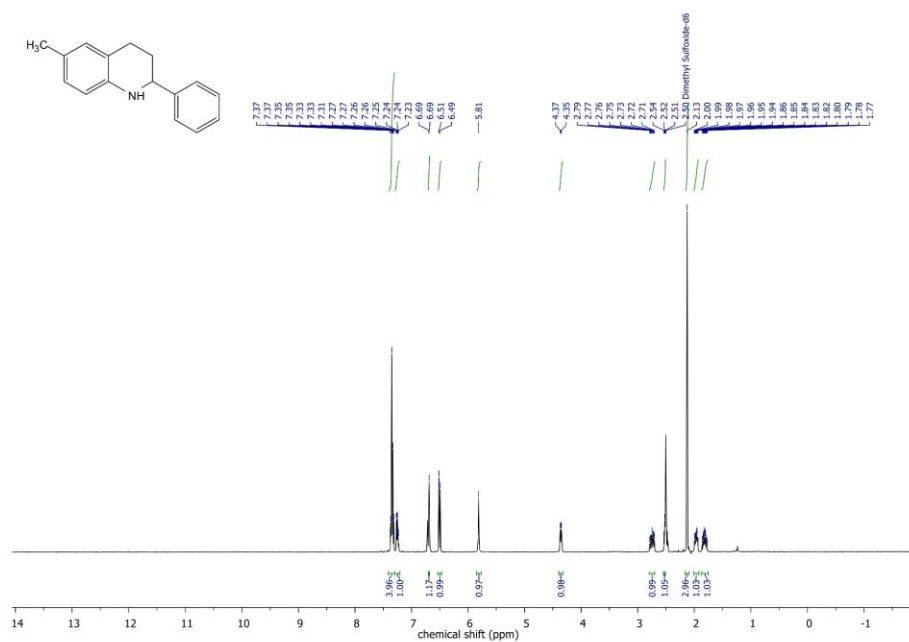
6 NMR Spectra

5-Methyl-2-phenyl-1,2,3,4-tetrahydroquinoline (1)



The Synthesis of Hydroquinolines from Nitroaldehydes and Ketones by Hydrogenation Sequences and Condensations

6-Methyl-2-phenyl-1,2,3,4-tetrahydroquinoline (2)

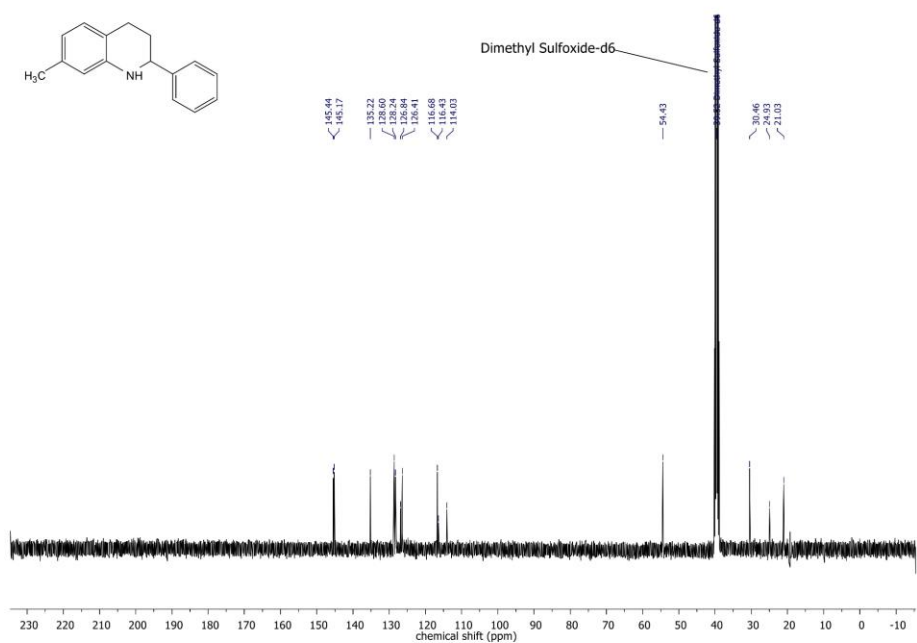


Chemical structure of 1-(4-methylphenyl)-2-phenylethan-1-one (Chalcone derivative):

Cc1ccc(cc1)C(=O)Cc2ccccc2

¹H NMR spectrum (DMSO-d₆) showing chemical shifts (ppm) and integration values:

Chemical Shift (ppm)	Integration
7.35, 7.33, 7.31, 7.27, 7.26, 7.25, 7.24	5.10
6.74, 6.73, 6.72, 6.60, 6.59, 6.28, 6.27, 6.25	0.99, 0.99, 0.99, 0.99, 0.99, 0.99, 0.99
4.39, 4.38, 4.37, 4.36	0.99
2.72, 2.70, 2.68, 2.66, 2.65	1.00, 1.08, 1.12, 1.13



The figure displays the chemical structure of 1-(2-methylphenyl)-2-phenylethan-1-amine and its corresponding ¹H and ¹³C NMR spectra.

Chemical Structure: 1-(2-methylphenyl)-2-phenylethan-1-amine. SMILES: Cc1cccc(NC1Cc2ccccc2)c1

¹H NMR Spectrum (400 MHz, DMSO-d₆):

- Chemical shift (ppm): 7.35, 7.34, 7.33, 7.32, 7.31, 7.30, 7.29, 7.28, 7.27, 7.26, 7.25, 7.24, 7.23, 7.22, 6.82, 6.80, 6.79, 6.78, 6.77, 6.43, 6.40, 5.24, 4.53, 4.52, 4.51, 4.50, 2.78, 2.76, 2.75, 2.74, 2.72, 2.70, 2.50, 2.48, 2.46, 2.44, 2.43, 2.03, 2.01, 1.99, 1.98, 1.97, 1.95, 1.87, 1.86, 1.85, 1.84, 1.83, 1.82, 1.81.
- Integration values: 4.04, 1.03, 2.06, 1.02, 1.01, 1.05, 1.06, 1.00, 1.12, 1.10.
- Peak assignments: Aromatic protons (7.35-7.22 ppm), NH (6.82-6.77 ppm), CH₂ (5.24 ppm), CH (4.53-4.50 ppm), CH₃ (2.78-2.70 ppm), and solvent (2.50 ppm).

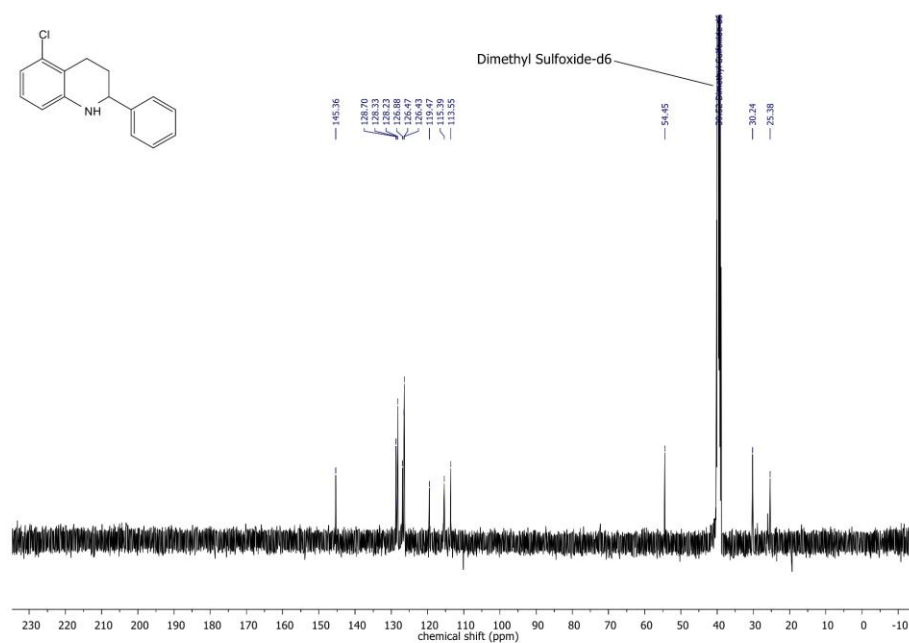
¹³C NMR Spectrum (100 MHz, DMSO-d₆):

- Chemical shift (ppm): 145.79, 142.85, 128.19, 127.66, 127.46, 126.62, 126.21, 125.81, 119.44, 115.29, 54.54, 39.52, 29.83, 25.15, 17.50.
- Peak assignments: Aromatic carbons (145.79-115.29 ppm), CH₂ (54.54 ppm), CH₃ (39.52 ppm), and solvent (29.83, 25.15, 17.50 ppm).

Chemical structure: 1-(2-chlorophenyl)-1,2,3,4-tetrahydroquinoline

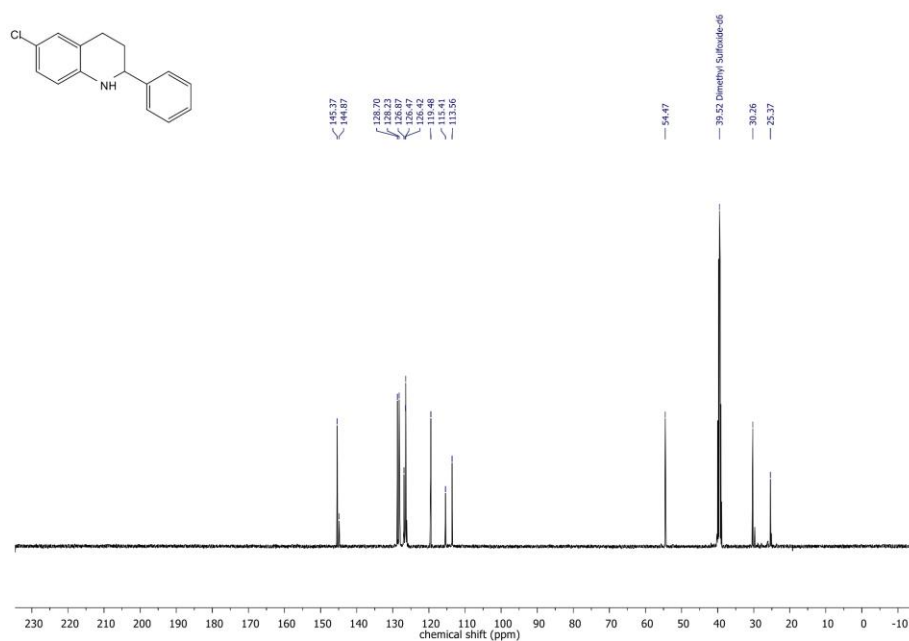
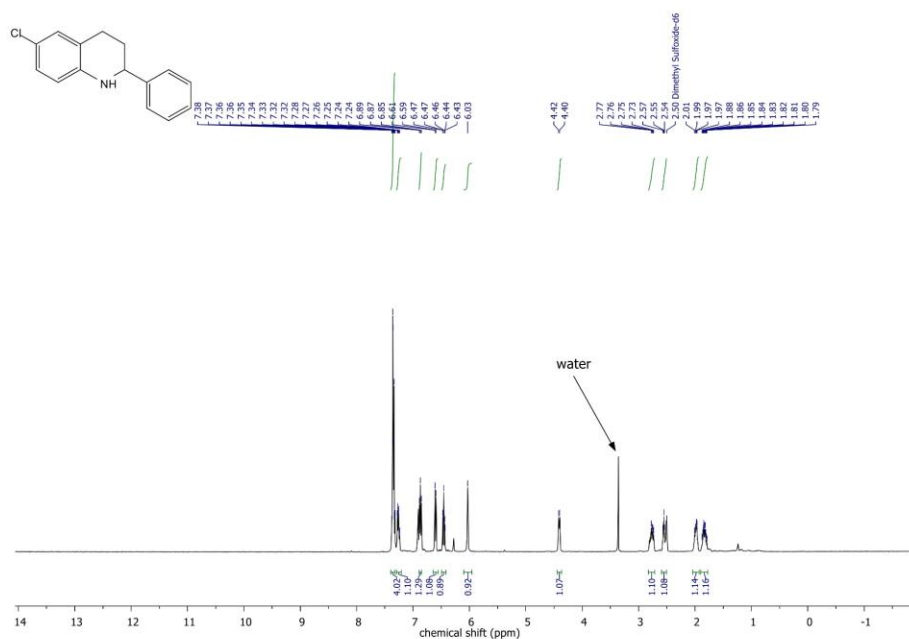
¹H NMR spectrum (DMSO-d₆) showing chemical shifts (ppm) and integration values:

Chemical Shift (ppm)	Integration
7.33	4.03
7.29	1.09
7.28	1.14
7.27	1.11
7.26	1.00
7.25	1.02
7.24	1.02
7.23	0.85
7.22	
7.21	
7.20	
7.19	
7.18	
7.17	
7.16	
7.15	
7.14	
7.13	
7.12	
7.11	
7.10	
7.09	
7.08	
7.07	
7.06	
7.05	
7.04	
7.03	
7.02	
7.01	
7.00	
6.99	
6.98	
6.97	
6.96	
6.95	
6.94	
6.93	
6.92	
6.91	
6.90	
6.89	
6.88	
6.87	
6.86	
6.85	
6.84	
6.83	
6.82	
6.81	
6.80	
6.79	
6.78	
6.77	
6.76	
6.75	
6.74	
6.73	
6.72	
6.71	
6.70	
6.69	
6.68	
6.67	
6.66	
6.65	
6.64	
6.63	
6.62	
6.61	
6.60	
6.59	
6.58	
6.57	
6.56	
6.55	
6.54	
6.53	
6.52	
6.51	
6.50	
6.49	
6.48	
6.47	
6.46	
6.45	
6.44	
6.43	
6.42	
6.41	
6.40	
6.39	
6.38	
6.37	
6.36	
6.35	
6.34	
6.33	
6.32	
6.31	
6.30	
6.29	
6.28	
6.27	
6.26	
6.25	
6.24	
6.23	
6.22	
6.21	
6.20	
6.19	
6.18	
6.17	
6.16	
6.15	
6.14	
6.13	
6.12	
6.11	
6.10	
6.09	
6.08	
6.07	
6.06	
6.05	
6.04	
6.03	
6.02	
6.01	
6.00	
5.99	
5.98	
5.97	
5.96	
5.95	
5.94	
5.93	
5.92	
5.91	
5.90	
5.89	
5.88	
5.87	
5.86	
5.85	
5.84	
5.83	
5.82	
5.81	
5.80	
5.79	
5.78	
5.77	
5.76	
5.75	
5.74	
5.73	
5.72	
5.71	
5.70	
5.69	
5.68	
5.67	
5.66	
5.65	
5.64	
5.63	
5.62	
5.61	
5.60	
5.59	
5.58	
5.57	
5.56	
5.55	
5.54	
5.53	
5.52	
5.51	
5.50	
5.49	
5.48	
5.47	
5.46	
5.45	
5.44	
5.43	
5.42	
5.41	
5.40	
5.39	
5.38	
5.37	
5.36	
5.35	
5.34	
5.33	
5.32	
5.31	
5.30	
5.29	
5.28	
5.27	
5.26	
5.25	
5.24	
5.23	
5.22	
5.21	
5.20	
5.19	
5.18	
5.17	
5.16	
5.15	
5.14	
5.13	
5.12	
5.11	
5.10	
5.09	
5.08	
5.07	
5.06	
5.05	
5.04	
5.03	
5	



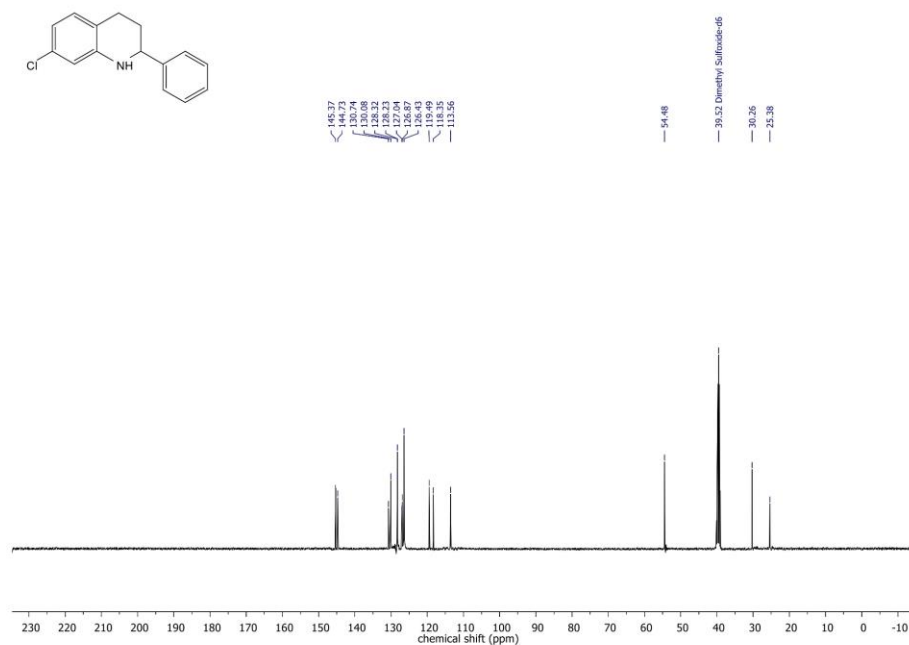
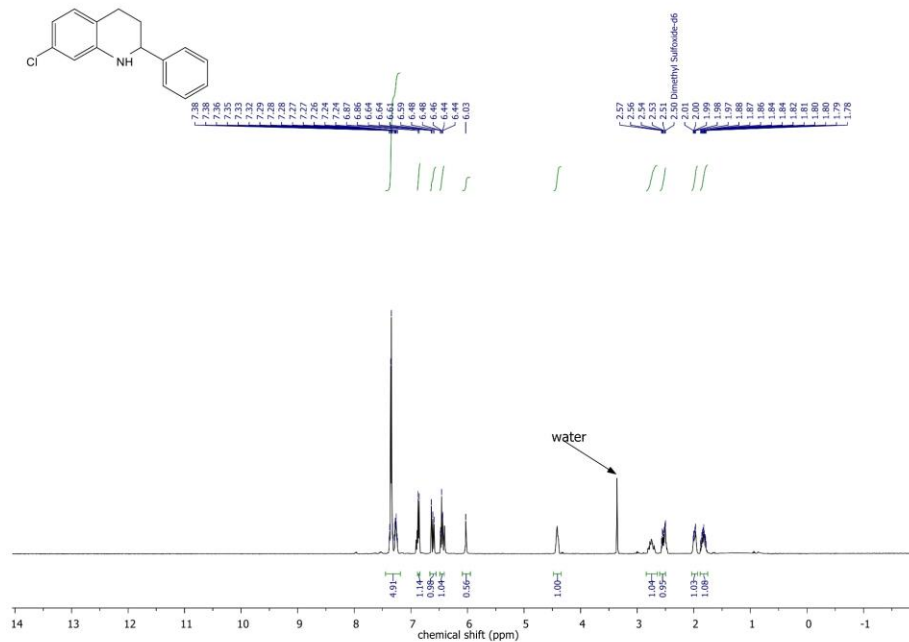
The Synthesis of Hydroquinolines from Nitroaldehydes and Ketones by Hydrogenation Sequences and Condensations

6-Chloro-2-phenyl-1,2,3,4-tetrahydroquinoline (6)



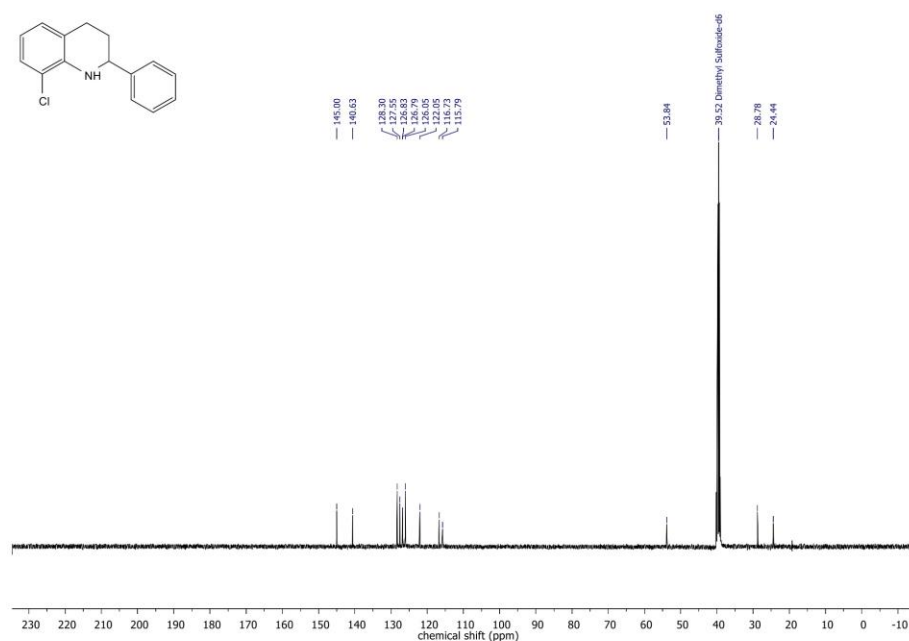
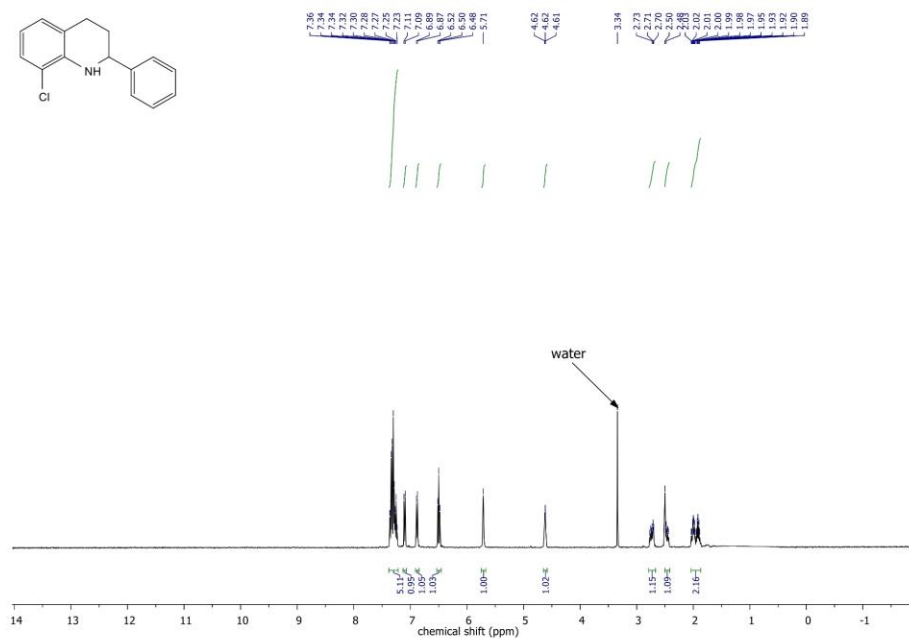
The Synthesis of Hydroquinolines from Nitroaldehydes and Ketones by Hydrogenation Sequences and Condensations

7-Chloro-2-phenyl-1,2,3,4-tetrahydroquinoline (7)



The Synthesis of Hydroquinolines from Nitroaldehydes and Ketones by Hydrogenation Sequences and Condensations

8-Chloro-2-phenyl-1,2,3,4-tetrahydroquinoline (8)

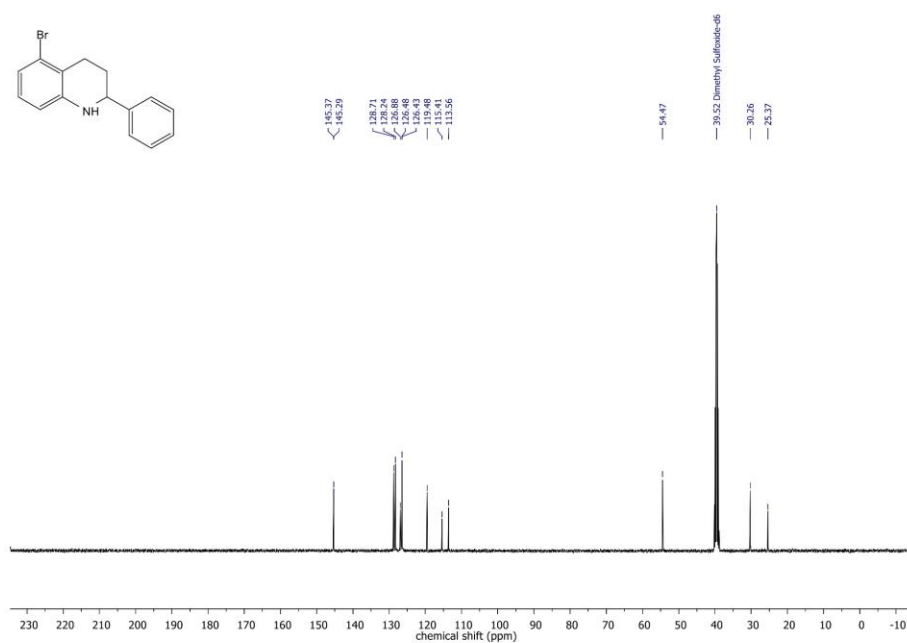


Chemical structure of 2-bromo-N-(2-phenyl-2-propyl)ethanamine:

BrCCN(CC1=CC=CC=C1)CC2=CC=CC=C2

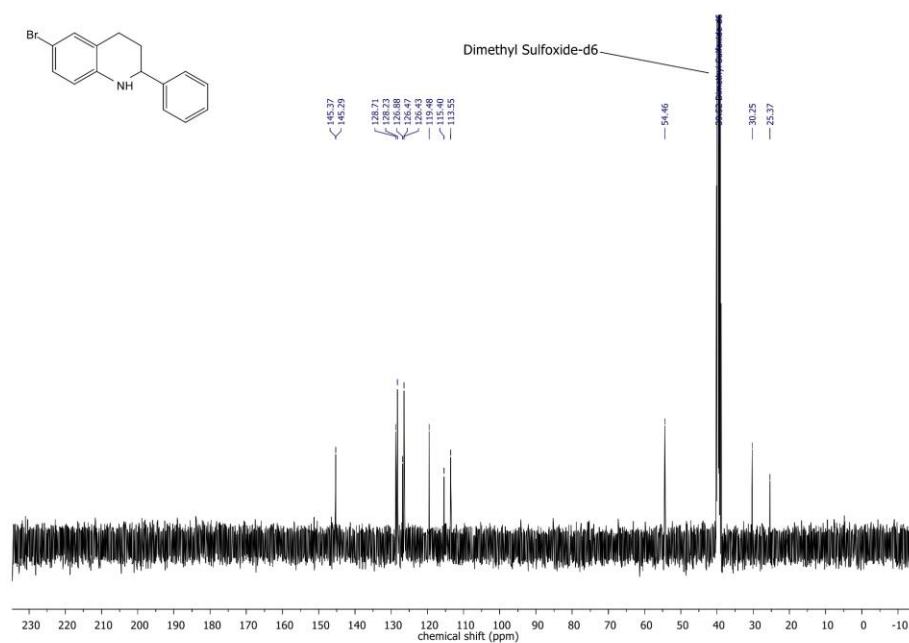
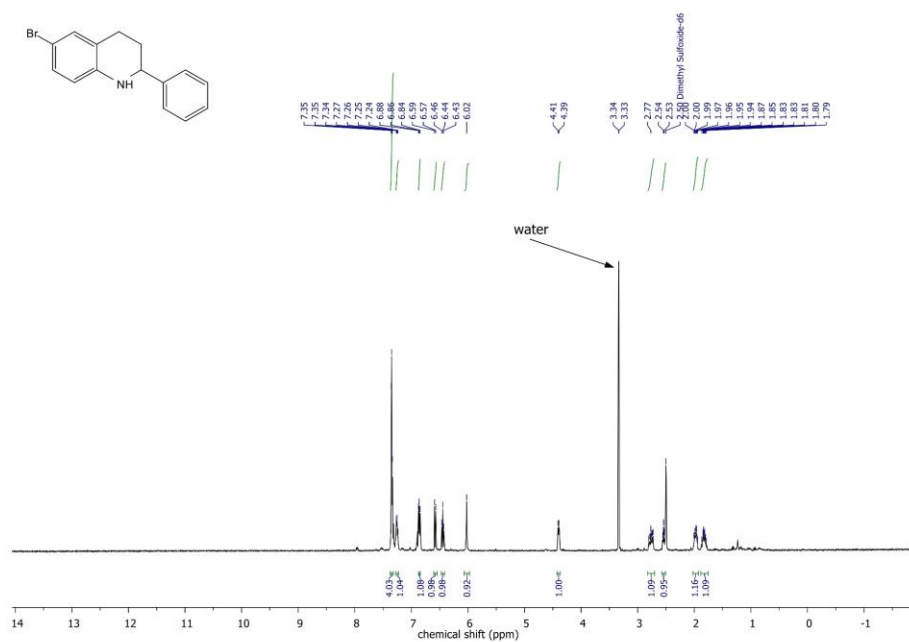
¹H NMR spectrum (DMSO-d₆) showing chemical shifts (ppm) and integration values:

Chemical Shift (ppm)	Integration
7.37, 7.34, 7.32, 7.28, 7.27, 7.26, 7.25, 7.25, 7.24, 7.23, 7.22, 7.20, 6.98, 6.95, 6.93, 6.63, 6.63	3.04, 0.98, 1.18, 0.96, 0.96, 0.94
4.53, 4.46, 4.46, 4.43, 4.43	0.96
3.34	0.99
2.77, 2.74, 2.72, 2.54, 2.50, 2.00, 1.99, 1.96, 1.92, 1.87, 1.86, 1.84, 1.83, 1.81, 1.80, 1.78	1.08, 1.02, 1.04



The Synthesis of Hydroquinolines from Nitroaldehydes and Ketones by Hydrogenation Sequences and Condensations

6-Bromo-2-phenyl-1,2,3,4-tetrahydroquinoline (10)

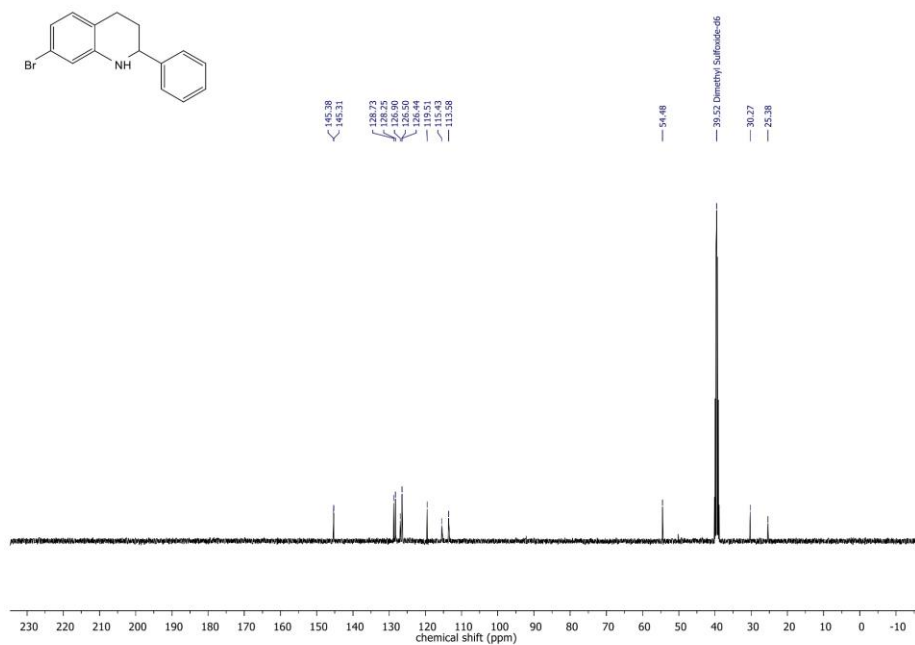


BrC1=CC=C2C(=C1)N(C2)CCc3ccccc3

Chemical structure: BrC1=CC=C2C(=C1)N(C2)CCc3ccccc3

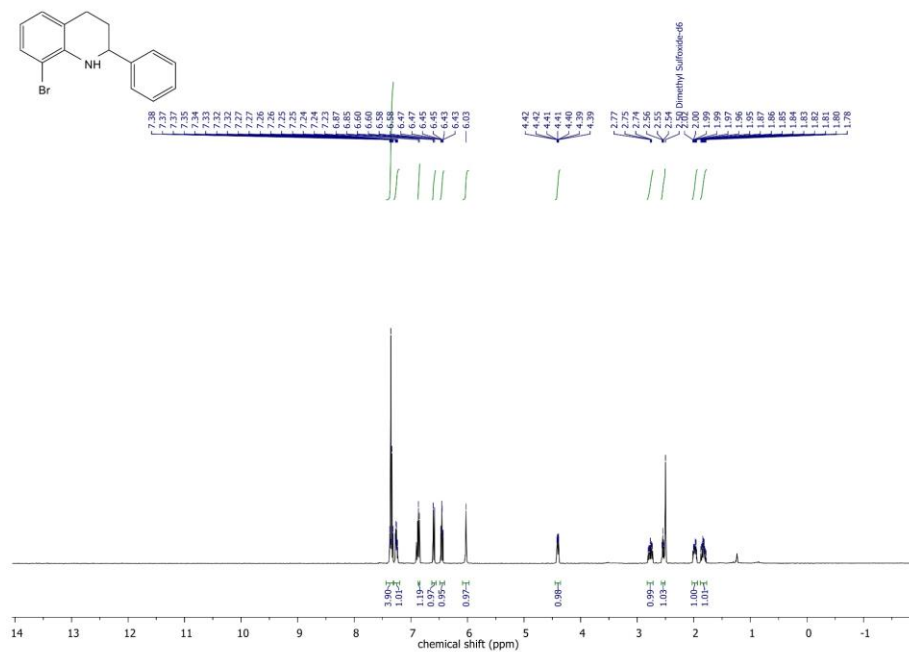
¹H NMR spectrum (DMSO-*d*₆) showing chemical shifts (ppm) and integration values:

Chemical Shift (ppm)	Integration
7.37	4.08
7.37	0.97
7.37	1.18
7.35	0.98
7.34	0.96
7.32	0.86
7.32	0.98
7.27	0.99
7.26	0.93
7.26	1.01
7.25	1.00
7.24	
7.24	
7.23	
7.23	
6.88	
6.86	
6.60	
6.58	
6.47	
6.46	
6.45	
6.43	
6.02	
4.41	0.98
4.39	
4.39	
3.36	0.99
2.77	0.99
2.77	0.93
2.55	1.01
2.53	1.00
2.50	
2.48	
1.98	
1.97	
1.95	
1.87	
1.86	
1.84	
1.83	
1.81	
1.79	



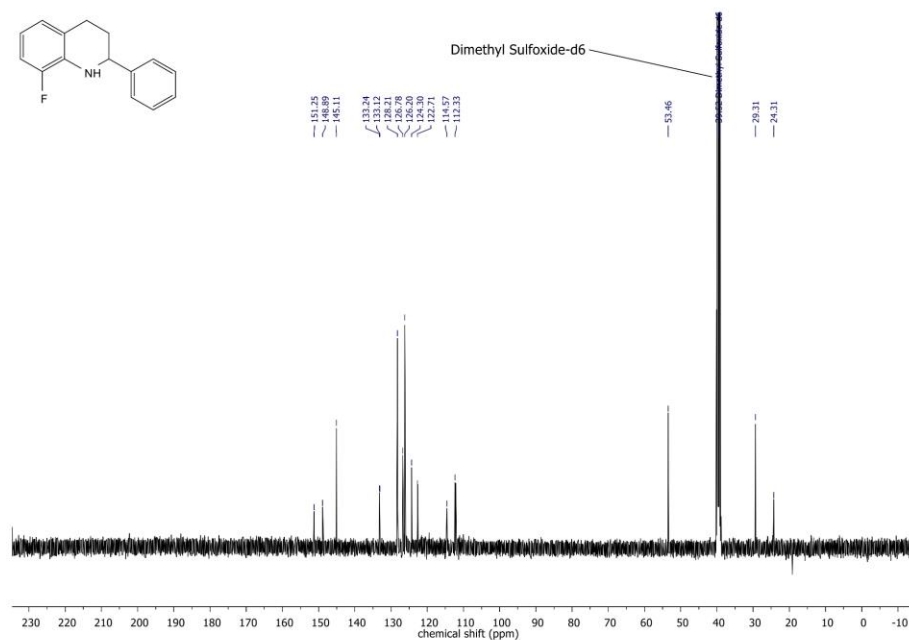
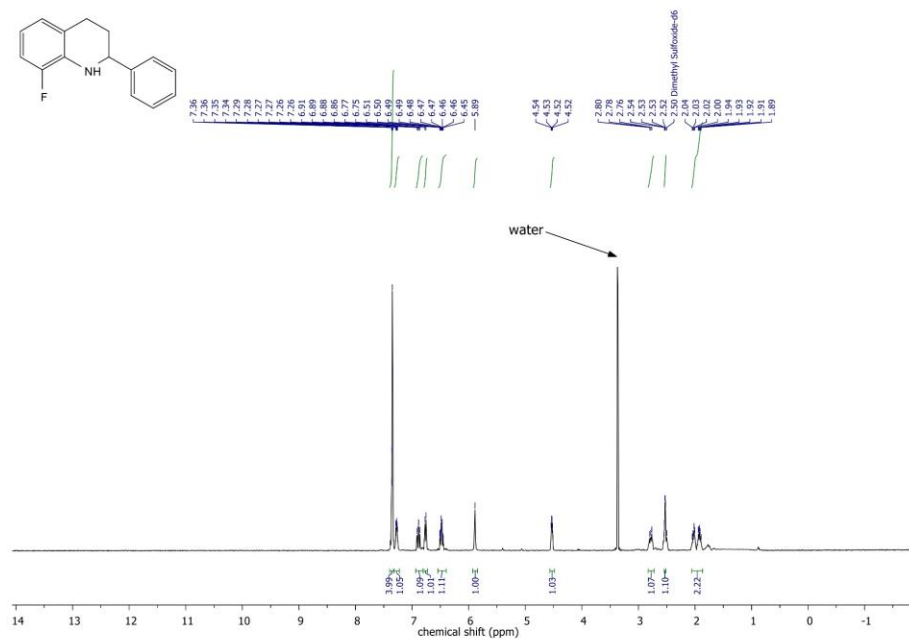
The Synthesis of Hydroquinolines from Nitroaldehydes and Ketones by Hydrogenation Sequences and Condensations

8-Bromo-2-phenyl-1,2,3,4-tetrahydroquinoline (12)



The Synthesis of Hydroquinolines from Nitroaldehydes and Ketones by Hydrogenation Sequences and Condensations

8-Fluoro-2-phenyl-1,2,3,4-tetrahydroquinoline (13)



¹H NMR Spectrum (DMSO-d₆)

Chemical structure: c1ccc(cc1)C2CN(Cc3cc(C(F)(F)F)ccc3)CC2

Chemical shift (ppm): 7.35, 7.30, 7.29, 7.28, 7.26, 7.25, 7.25, 7.05, 6.90, 6.87, 6.71, 6.58, 4.48, 4.47, 3.35, 2.81, 2.77, 2.61, 2.57, 2.56, 2.02, 2.01, 1.99, 1.97, 1.87, 1.85, 1.84, 1.83, 1.82, 1.81, 1.80, 1.79.

Integration values: 4.10, 1.00, 1.00, 1.00, 1.02, 0.97, 1.00, 1.00, 1.07, 1.06, 1.14.

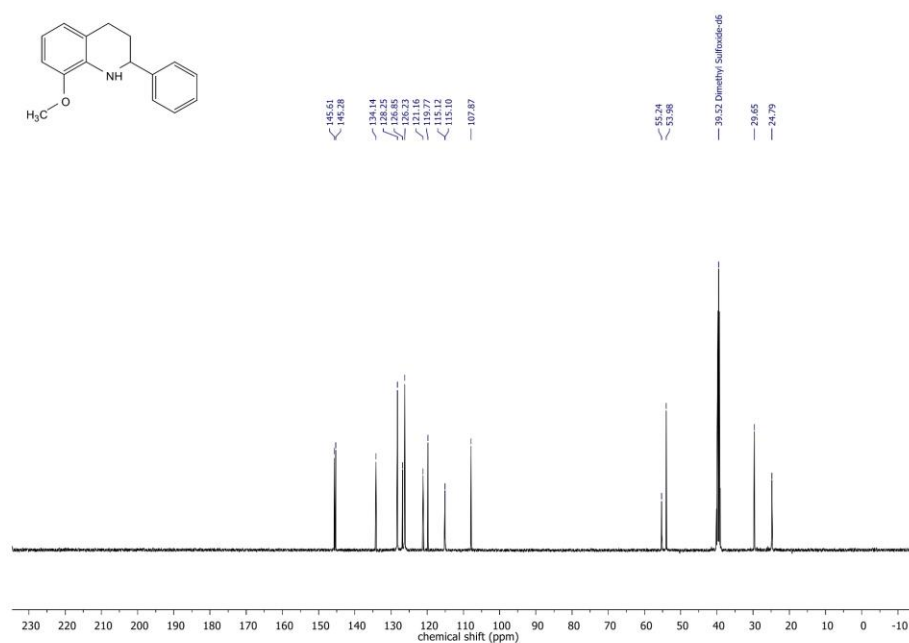
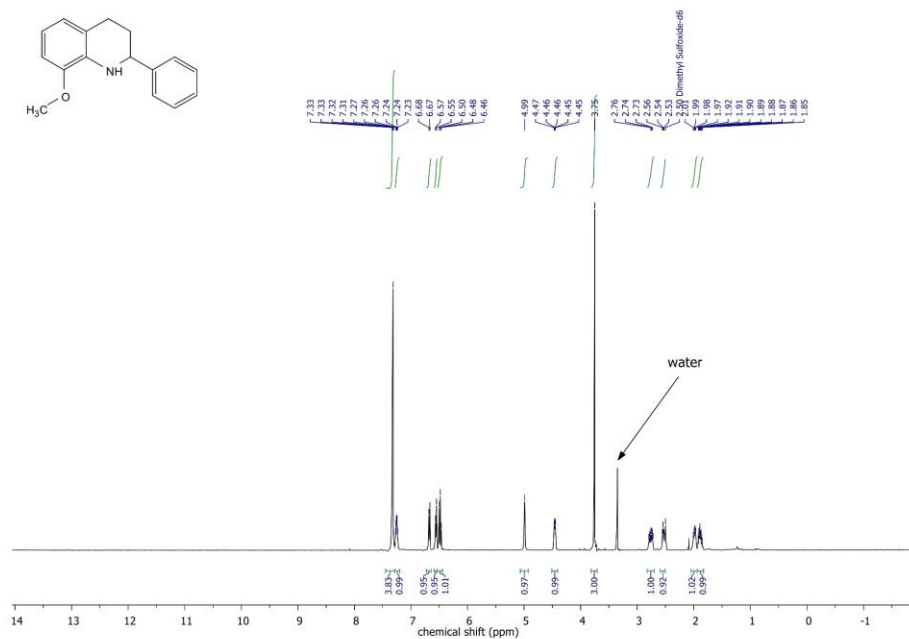
Water peak indicated at ~3.3 ppm.

¹³C NMR Spectrum (DMSO-d₆)

Chemical shift (ppm): 146.75, 146.61, 146.49, 128.36, 127.66, 127.55, 127.08, 126.38, 126.24, 123.75, 123.34, 123.13, 109.10, 54.18, 39.52, 29.44, 25.18.

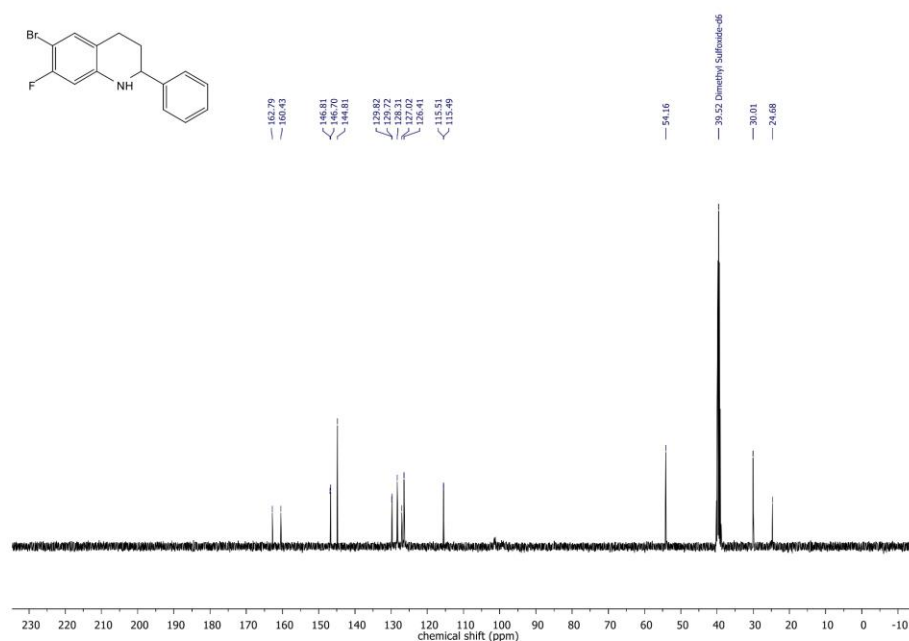
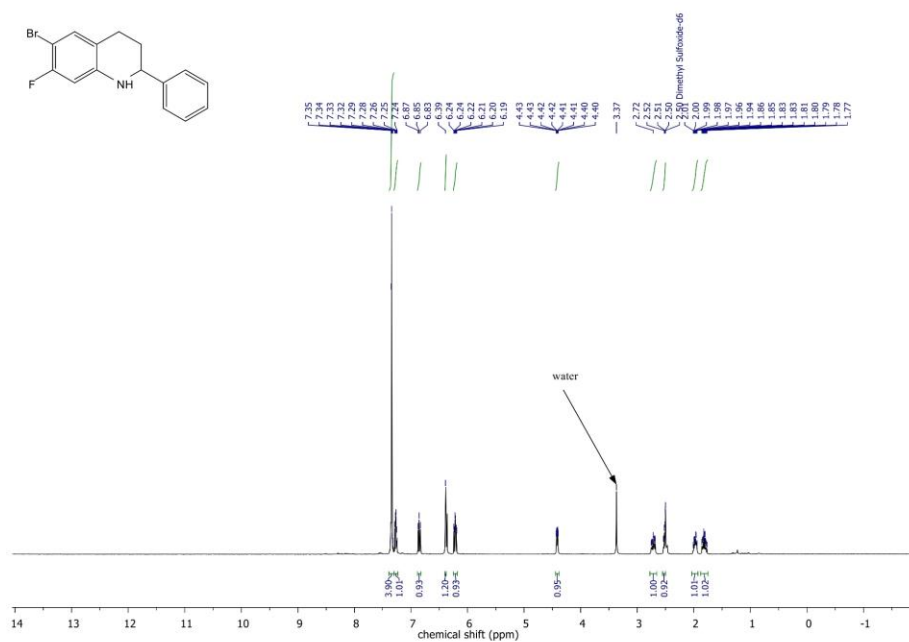
The Synthesis of Hydroquinolines from Nitroaldehydes and Ketones by Hydrogenation Sequences and Condensations

8-Methoxy-2-phenyl-1,2,3,4-tetrahydroquinoline (15)



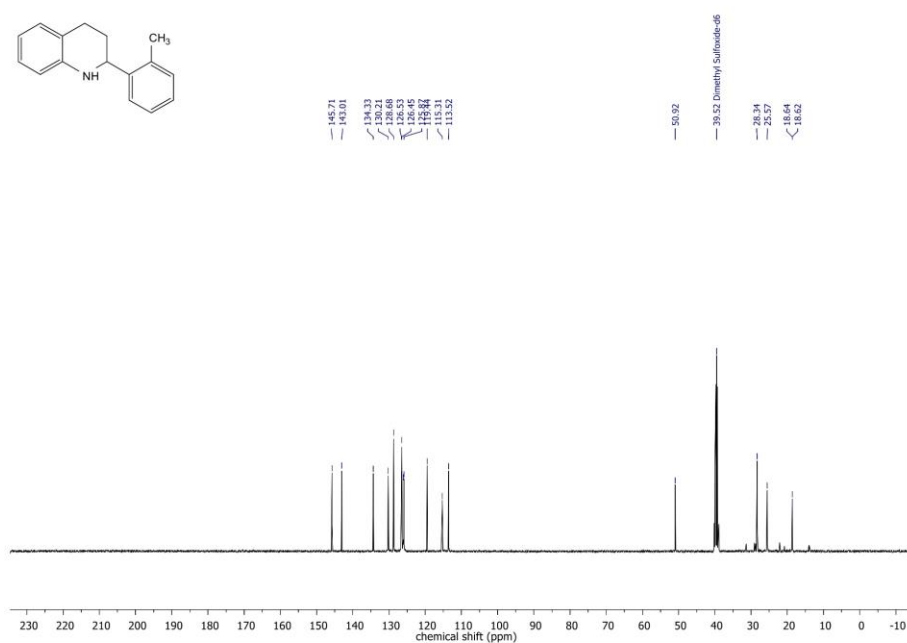
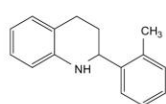
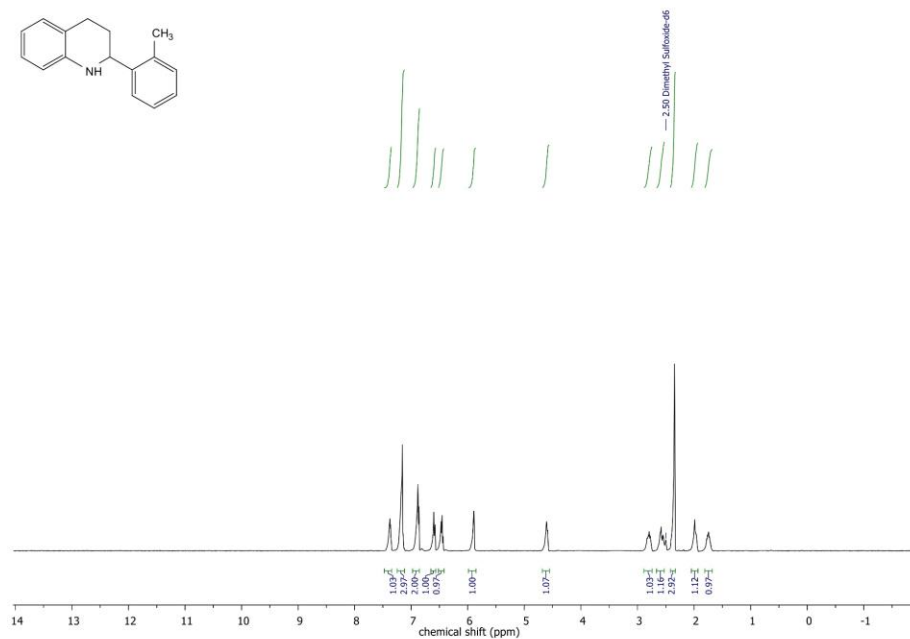
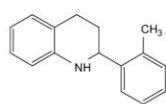
The Synthesis of Hydroquinolines from Nitroaldehydes and Ketones by Hydrogenation Sequences and Condensations

6-Bromo-7-fluoro-2-phenyl-1,2,3,4-tetrahydroquinoline (16)



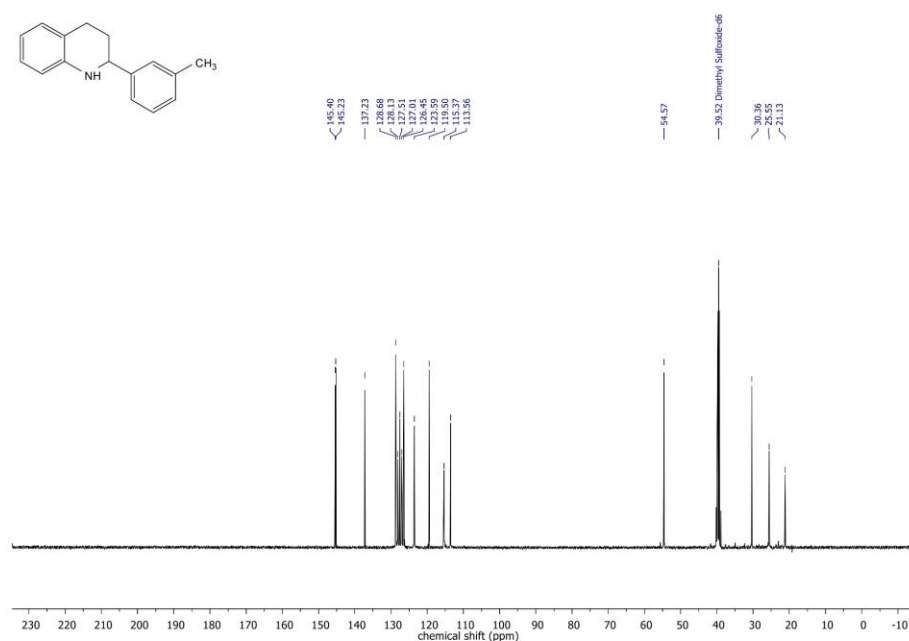
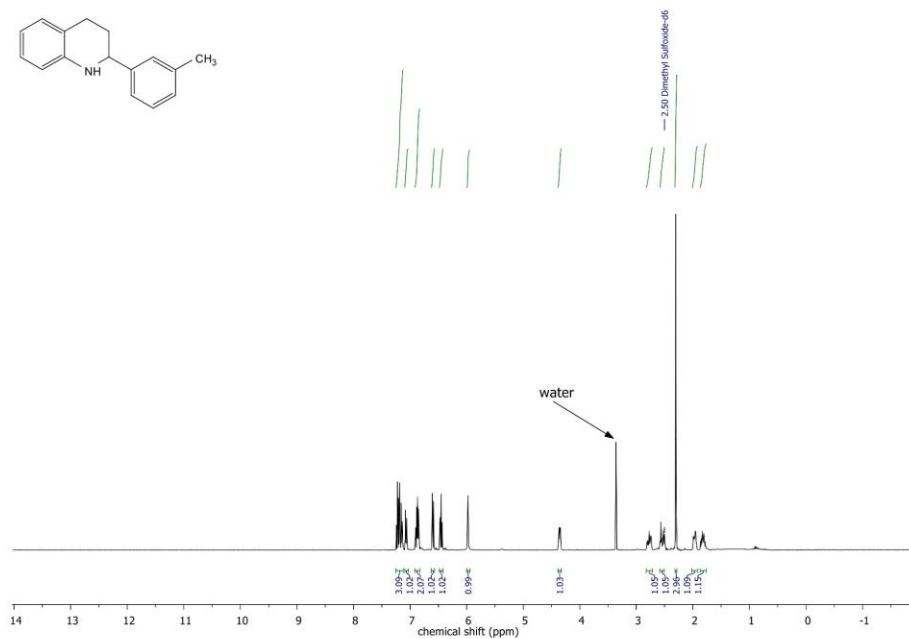
The Synthesis of Hydroquinolines from Nitroaldehydes and Ketones by Hydrogenation Sequences and Condensations

2-(2-Methylphenyl)-1,2,3,4-tetrahydroquinoline (17)



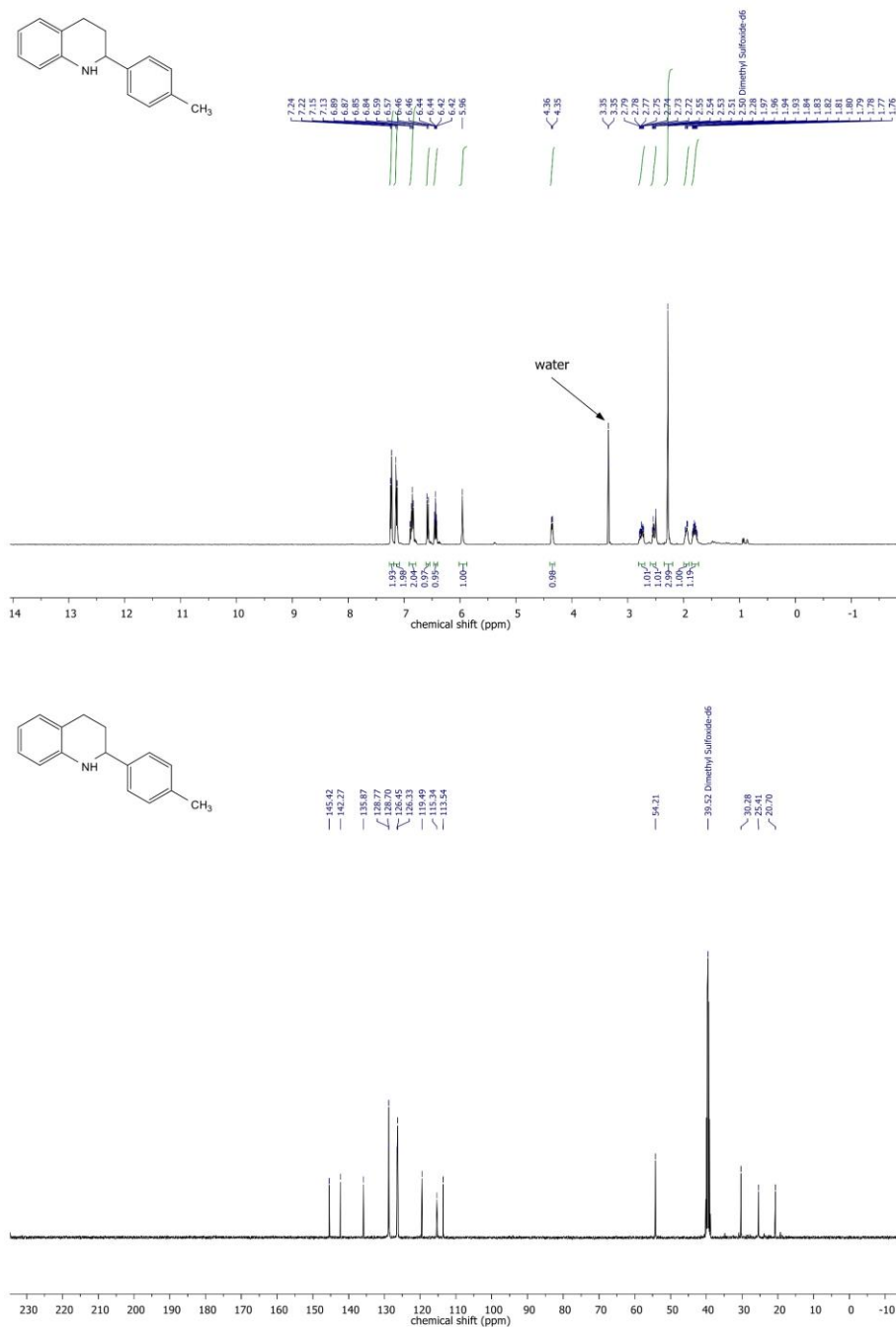
The Synthesis of Hydroquinolines from Nitroaldehydes and Ketones by Hydrogenation Sequences and Condensations

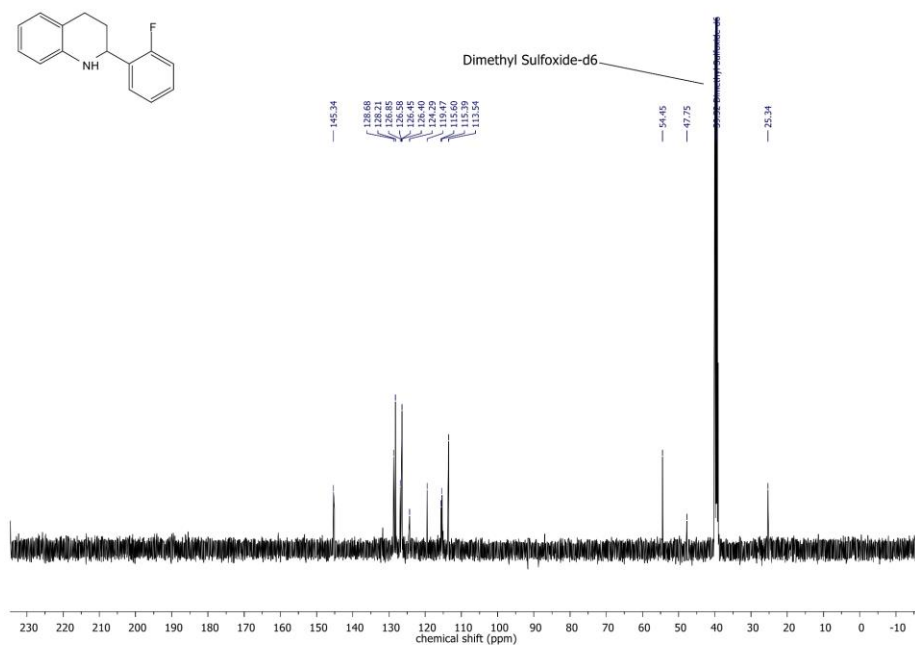
2-(3-Methylphenyl)-1,2,3,4-tetrahydroquinoline (18)



The Synthesis of Hydroquinolines from Nitroaldehydes and Ketones by Hydrogenation Sequences and Condensations

2-(4-Methylphenyl)-1,2,3,4-tetrahydroquinoline (19)



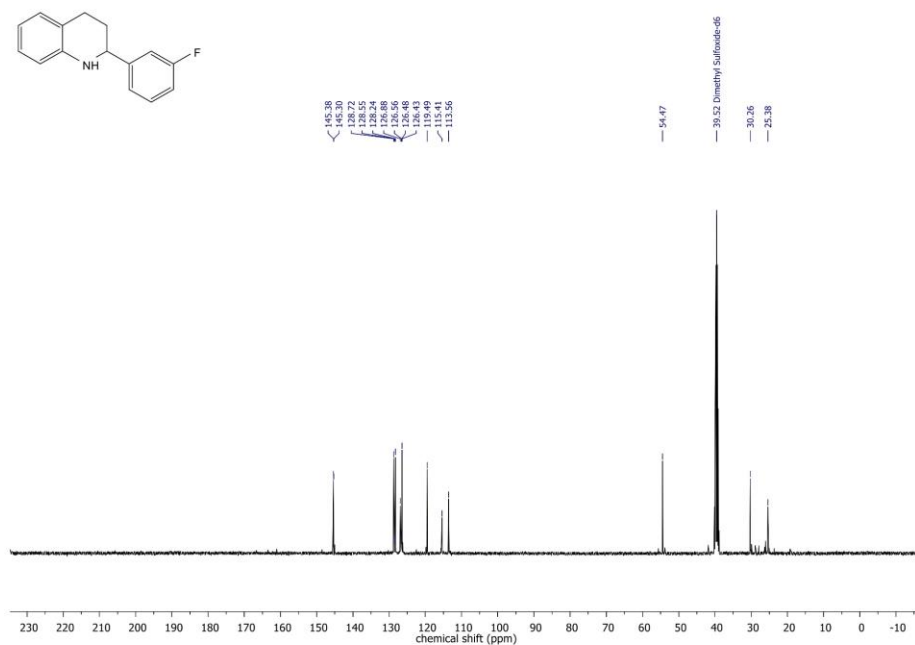
[illegible]

Chemical structure of 2-(4-fluorophenyl)-1,2,3,4-tetrahydro-1H-benz[h]quinoline is shown above the spectrum.

Chemical shifts (ppm) listed above the spectrum: 7.38, 7.37, 7.35, 7.34, 7.33, 7.32, 7.28, 7.27, 7.26, 7.25, 7.24, 7.24, 6.87, 6.85, 6.84, 6.60, 6.58, 6.47, 6.47, 6.45, 6.43, 6.42, 4.43, 4.41, 4.41, 4.40, 4.39, 4.39, 4.39, 3.35, 2.55, 2.54, 2.54, 2.50, 2.02, 2.02, 1.99, 1.99, 1.96, 1.95, 1.86, 1.85, 1.84, 1.82, 1.81, 1.78, 1.28.

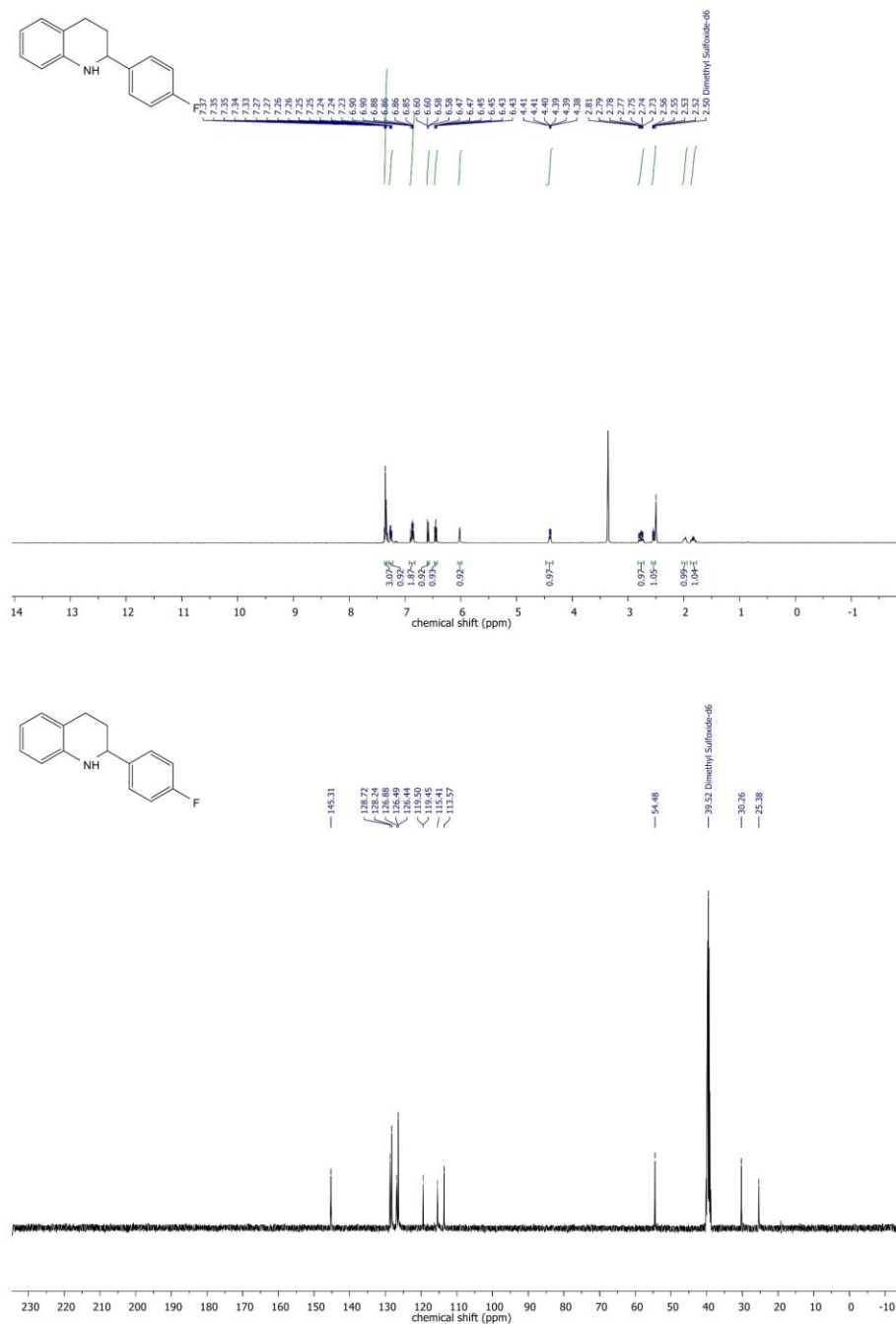
Integration values shown below the spectrum: 3.79, 3.79, 1.11, 0.98, 0.95, 1.00, 0.99, 1.00, 1.00, 1.03, 1.14.

A peak at 3.35 ppm is labeled "water".



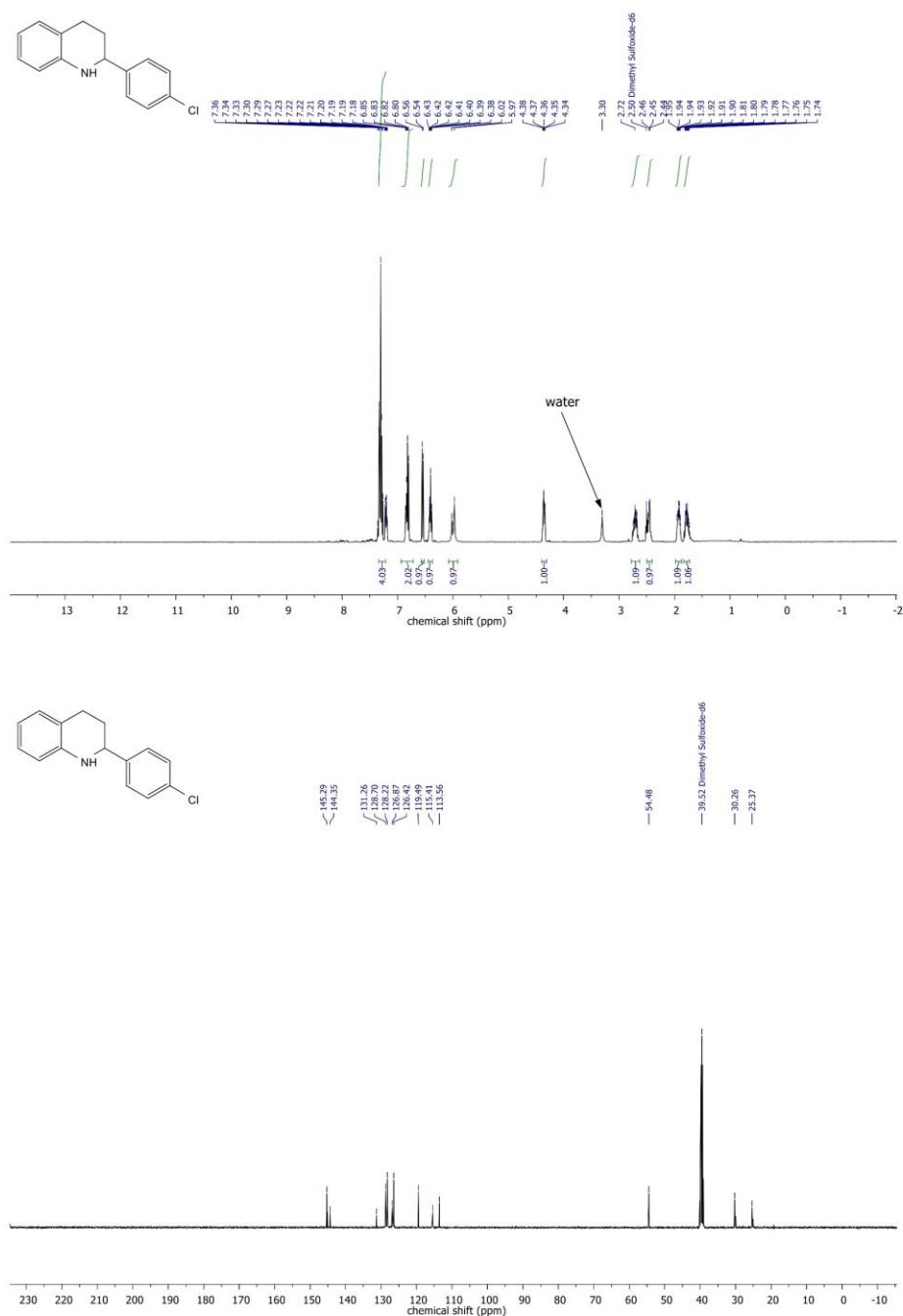
The Synthesis of Hydroquinolines from Nitroaldehydes and Ketones by Hydrogenation Sequences and Condensations

2-(4-Fluorophenyl)-1,2,3,4-tetrahydroquinoline (22)



The Synthesis of Hydroquinolines from Nitroaldehydes and Ketones by Hydrogenation Sequences and Condensations

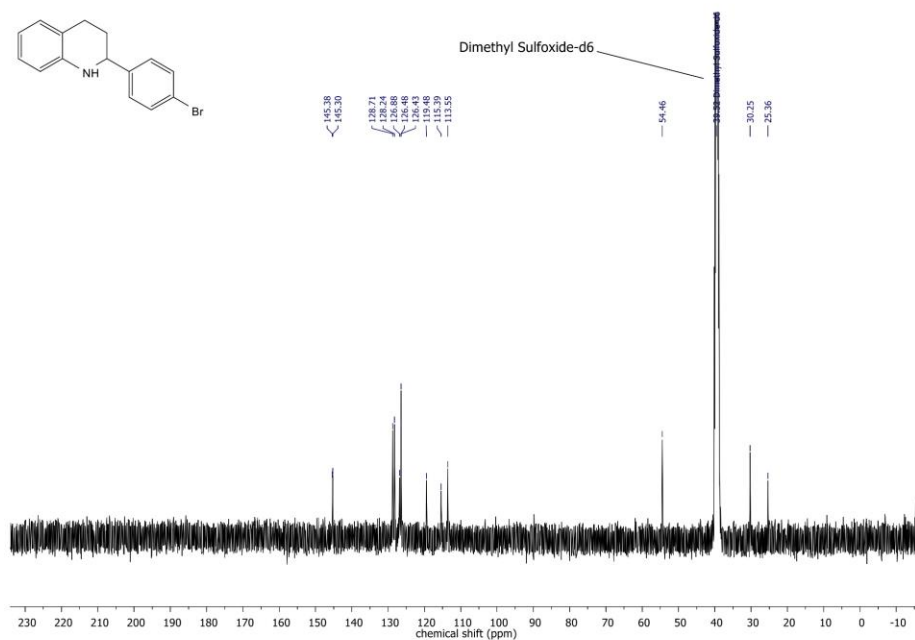
2-(4-Chlorophenyl)-1,2,3,4-tetrahydroquinoline (23)



Chemical structure: C1CCN(C1)c2ccc(cc2)Cc3ccccc3

¹H NMR spectrum (DMSO-d₆) showing chemical shifts (ppm) and integration values:

Chemical Shift (ppm)	Integration
7.37	0.91
7.35	1.05
7.34	1.07
7.33	0.93
7.32	0.95
7.30	0.90
7.27	
7.26	
7.24	
7.23	
7.22	
6.86	
6.59	
6.46	
6.45	
6.44	
6.43	
6.42	
6.41	
2.79	0.99
2.78	
2.77	
2.75	
2.74	
2.73	
2.58	1.15
2.55	0.96
2.50	0.99
2.00	0.98
1.97	
1.96	
1.87	
1.86	
1.84	
1.83	
1.81	
1.79	



The figure displays the chemical structure of 1-(4-(tert-butyl)phenyl)-1,2,3,4-tetrahydroquinoline and its corresponding ¹H and ¹³C NMR spectra.

Chemical Structure: CC1(C)CC2=CC=C(C=C2)C1Nc3ccccc3

¹H NMR Spectrum (400 MHz, DMSO-d₆):

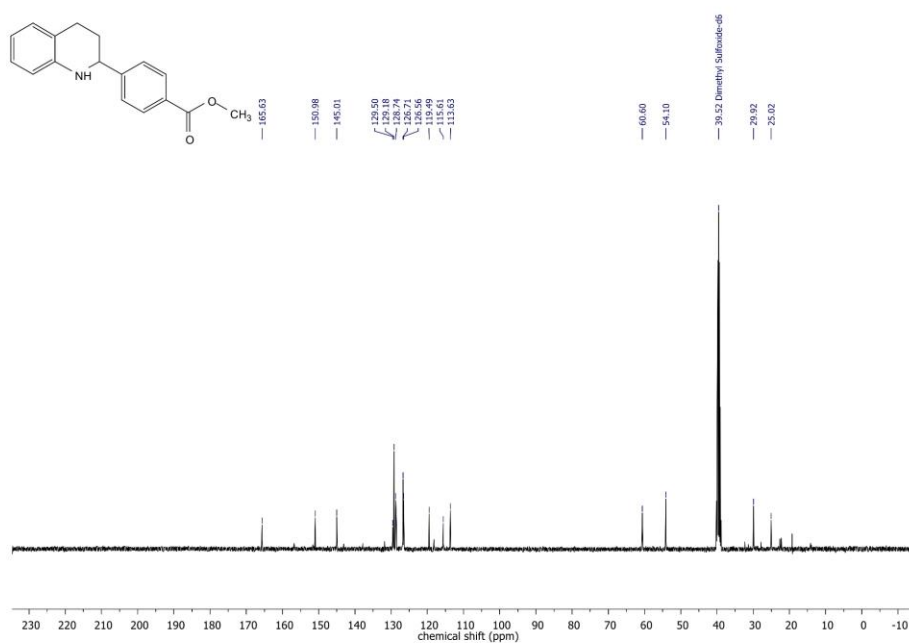
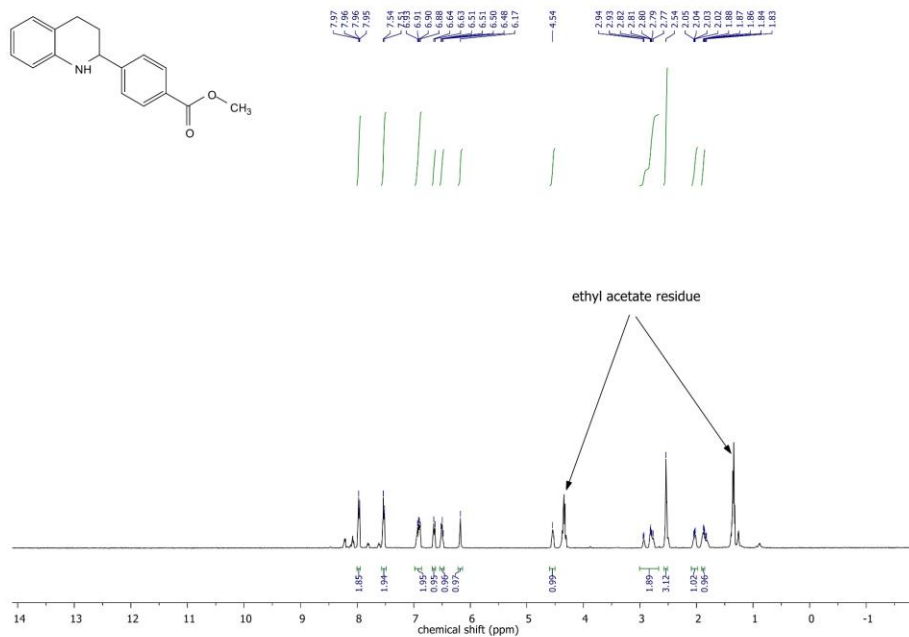
- Chemical shift range: 1 to 8 ppm.
- Key peaks and integrations:
 - ~7.2 ppm (m, 2H, integration 1.97)
 - ~7.1 ppm (m, 2H, integration 2.08)
 - ~6.8 ppm (m, 2H, integration 2.04)
 - ~6.6 ppm (m, 2H, integration 1.02)
 - ~6.5 ppm (m, 2H, integration 1.02)
 - ~6.4 ppm (m, 2H, integration 0.98)
 - ~4.3 ppm (m, 2H, integration 1.00)
 - ~3.3 ppm (m, 2H, integration 1.04)
 - ~2.9 ppm (m, 2H, integration 1.03)
 - ~2.5 ppm (m, 2H, integration 1.06)
 - ~2.4 ppm (m, 2H, integration 1.10)
 - ~1.3 ppm (s, 9H, integration 9.10)
- Water peak is indicated at ~3.3 ppm.

¹³C NMR Spectrum (100 MHz, DMSO-d₆):

- Chemical shift range: 25 to 150 ppm.
- Key peaks:
 - ~149.27, 145.47, 142.17 ppm (aromatic C-N)
 - ~128.68, 126.41, 126.21, 126.21, 119.45, 119.45, 113.35, 113.34 ppm (aromatic C-H)
 - ~54.38 ppm (CH₂-N)
 - ~39.52, 34.17, 32.11, 30.31, 25.69 ppm (tert-butyl methyls)

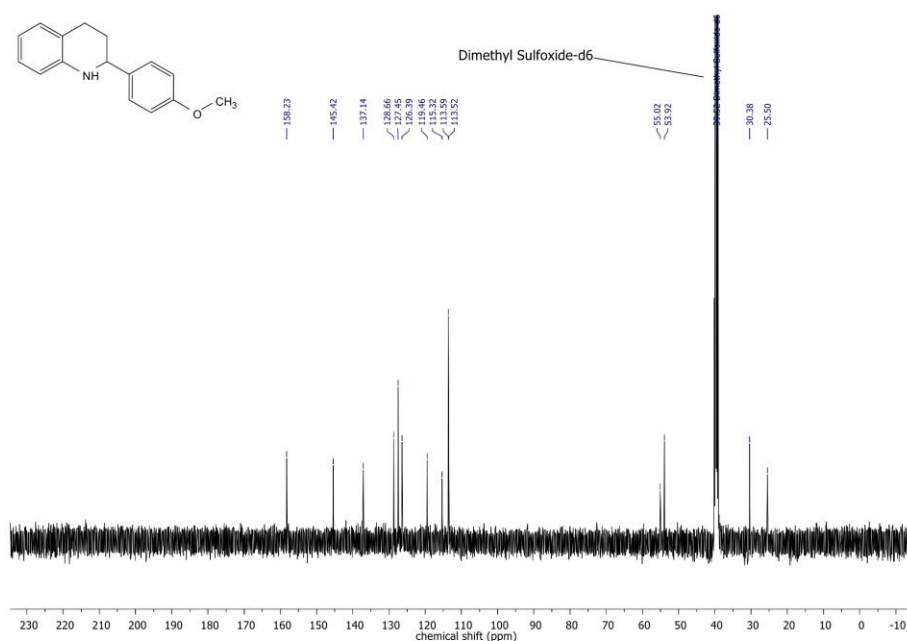
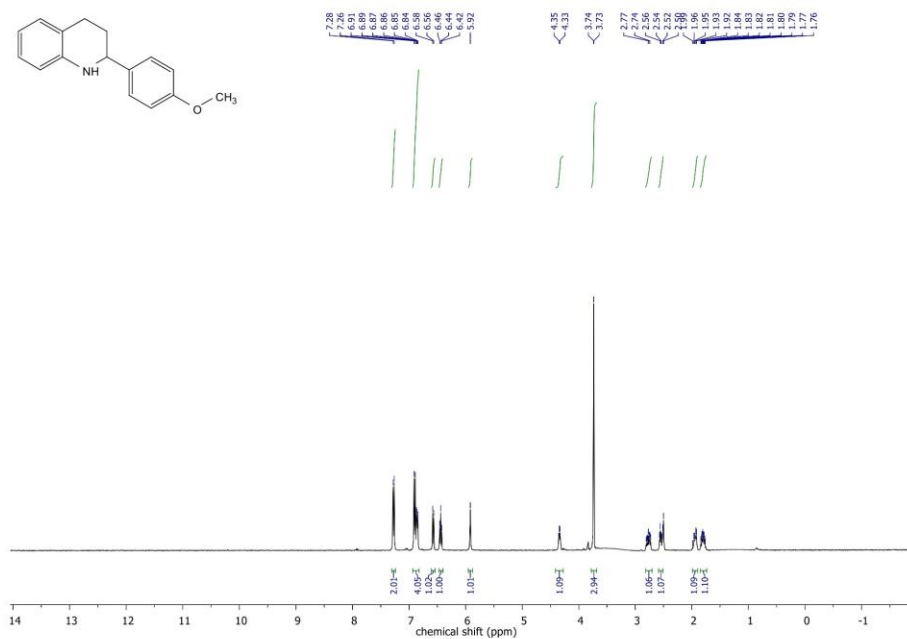
The Synthesis of Hydroquinolines from Nitroaldehydes and Ketones by Hydrogenation Sequences and Condensations

Methyl-4-(1,2,3,4-tetrahydroquinolin-2-yl)benzoate (26)



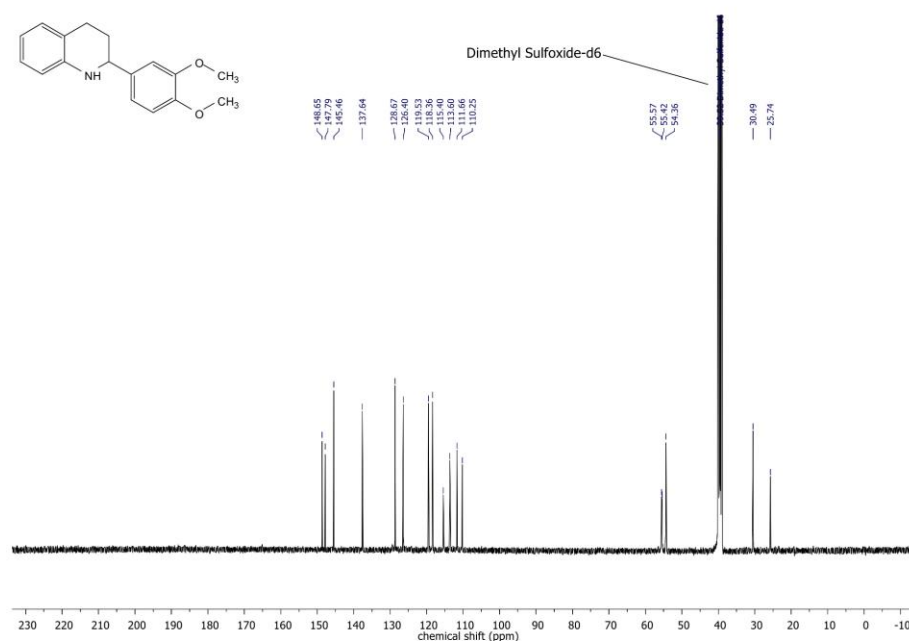
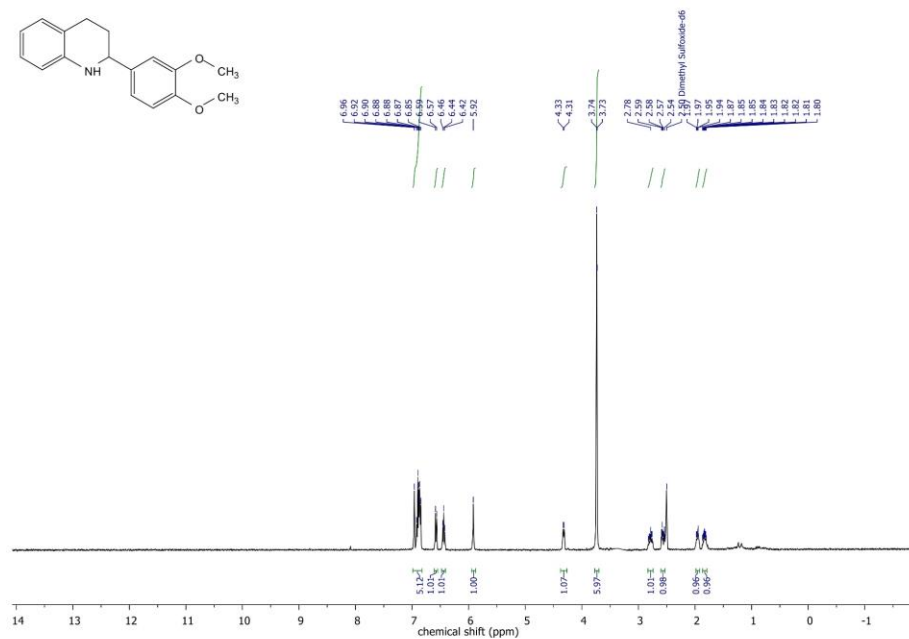
The Synthesis of Hydroquinolines from Nitroaldehydes and Ketones by Hydrogenation Sequences and Condensations

2-(4-Methoxyphenyl)-1,2,3,4-tetrahydroquinoline (27)



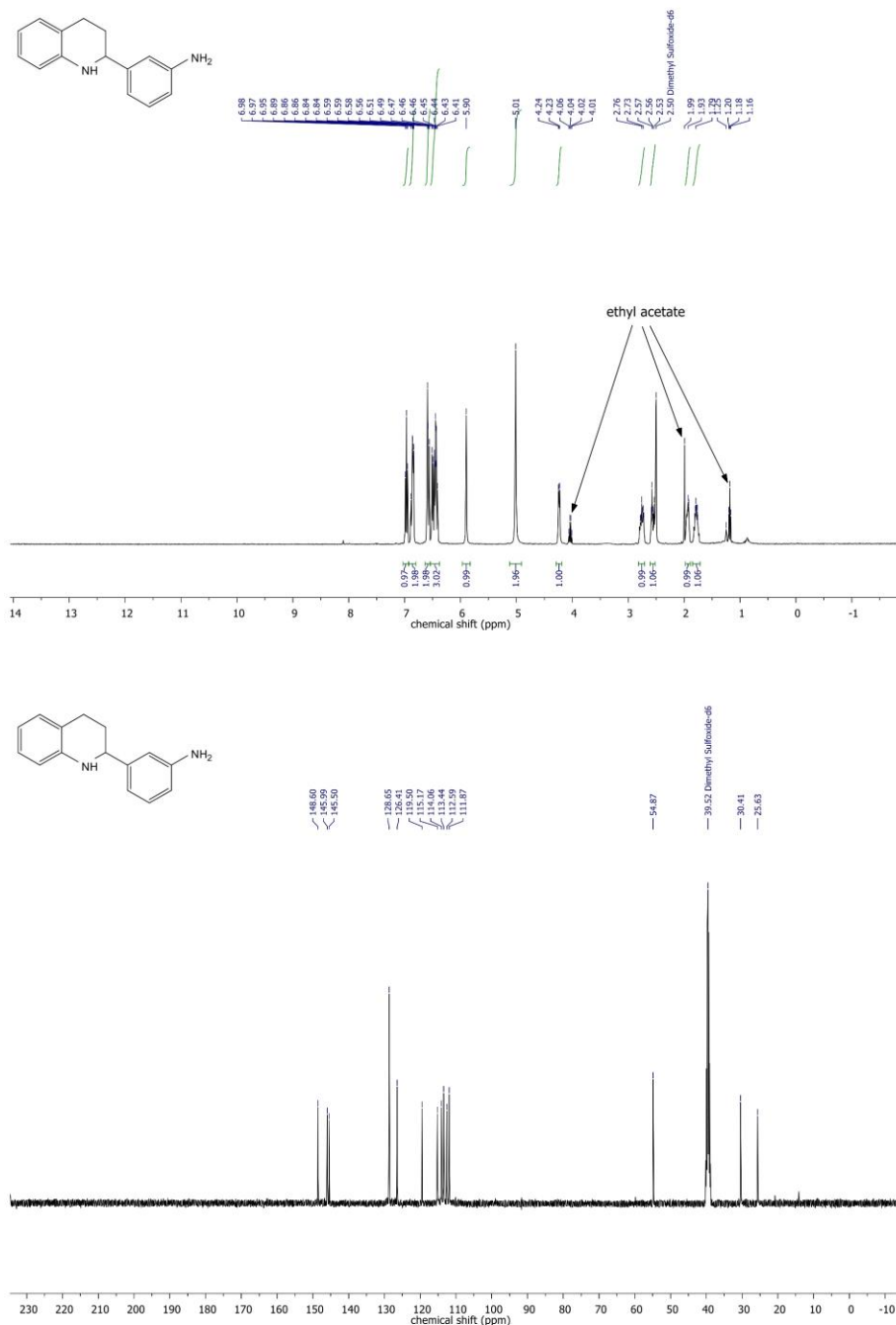
The Synthesis of Hydroquinolines from Nitroaldehydes and Ketones by Hydrogenation Sequences and Condensations

2-(3,4-Dimethoxyphenyl)-1,2,3,4-tetrahydroquinoline (28)



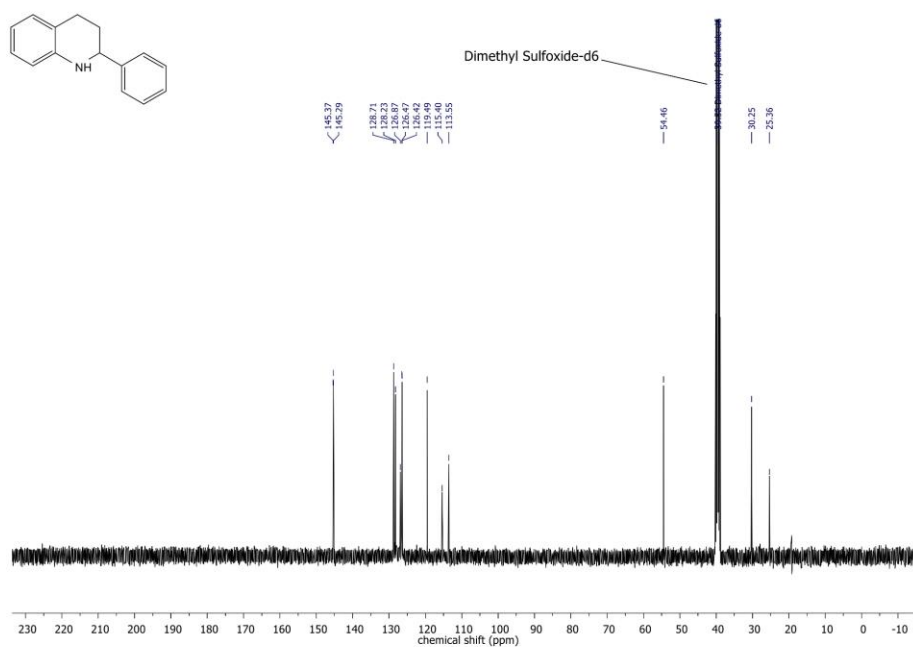
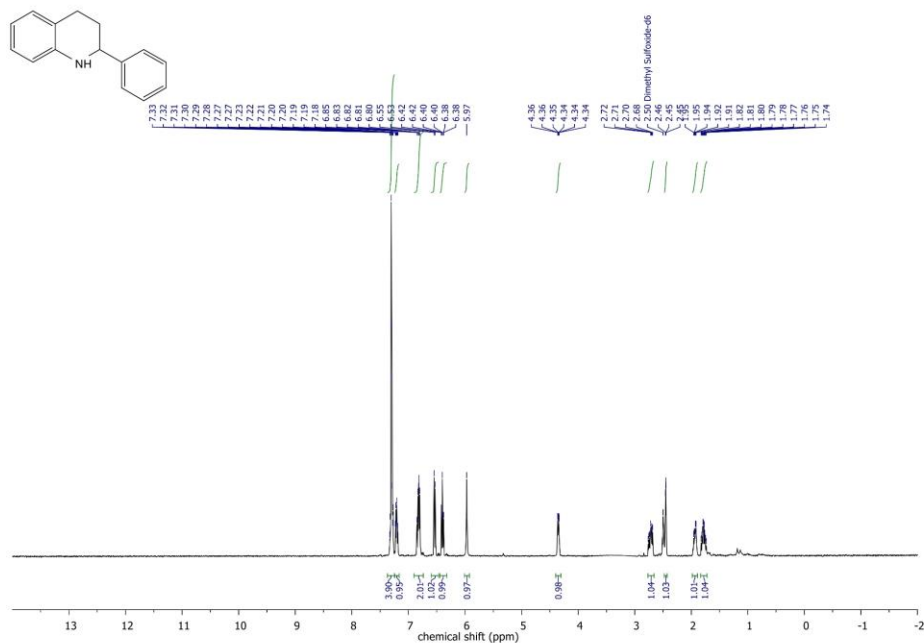
The Synthesis of Hydroquinolines from Nitroaldehydes and Ketones by Hydrogenation Sequences and Condensations

3-(1,2,3,4-Tetrahydroquinolin-2-yl)aniline (29)



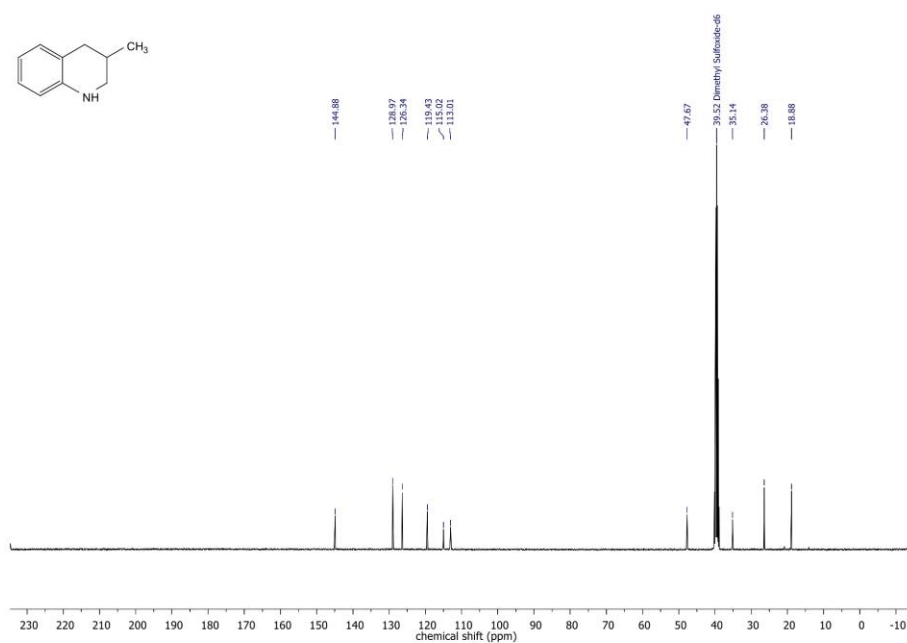
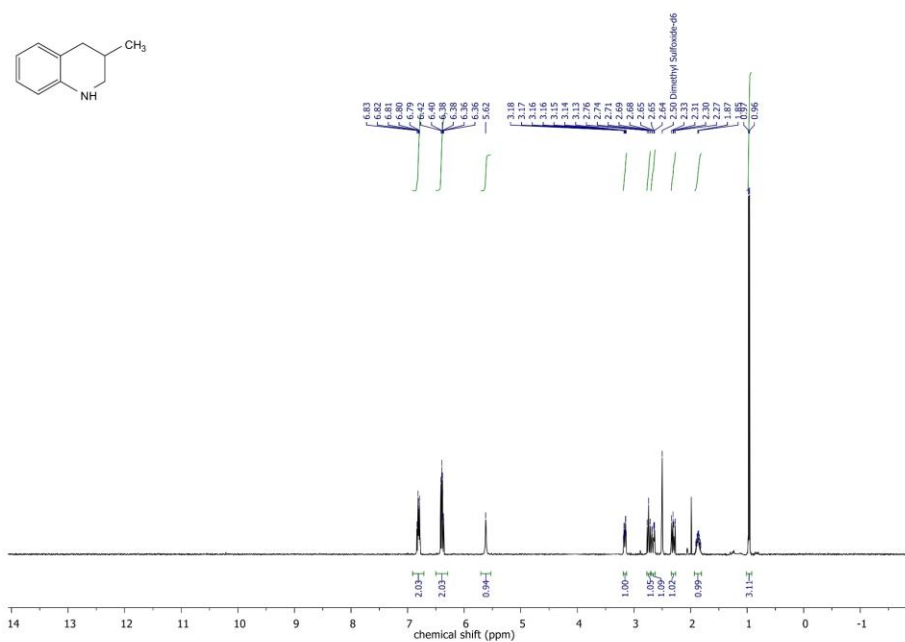
The Synthesis of Hydroquinolines from Nitroaldehydes and Ketones by Hydrogenation Sequences and Condensations

2-Phenethyl-1,2,3,4-tetrahydroquinoline (30)



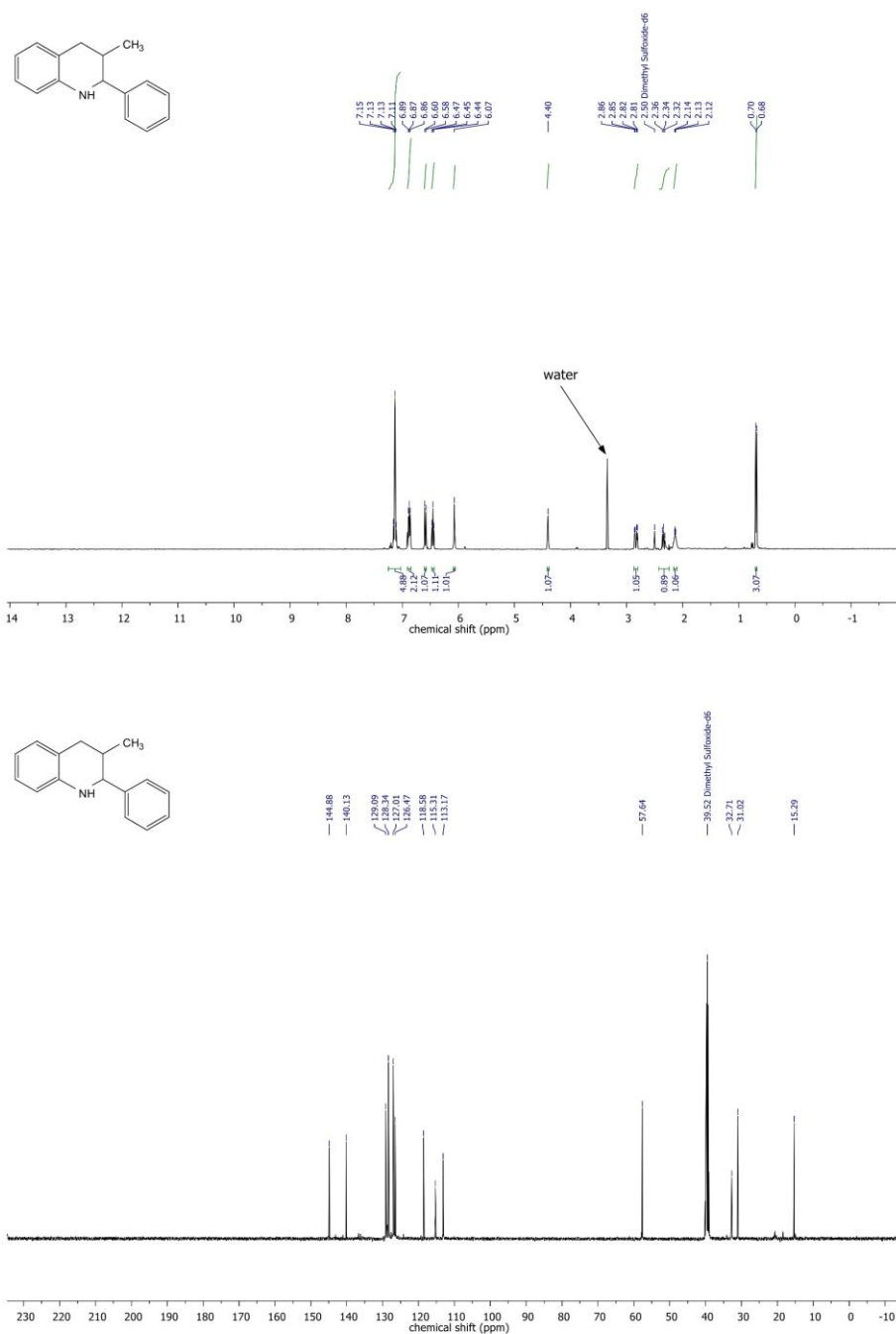
The Synthesis of Hydroquinolines from Nitroaldehydes and Ketones by Hydrogenation Sequences and Condensations

3-Methyl-1,2,3,4-tetrahydroquinoline (31)



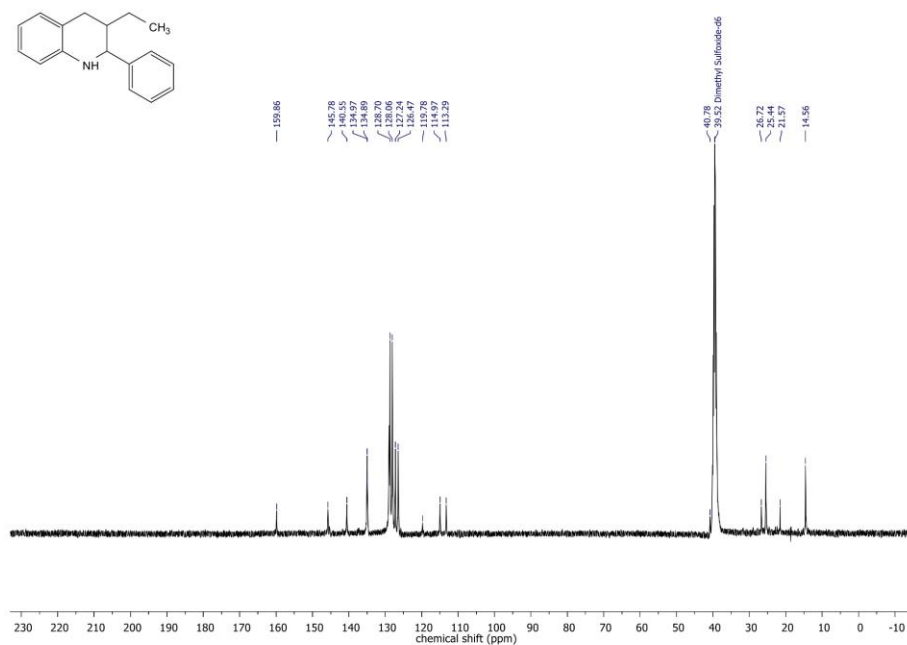
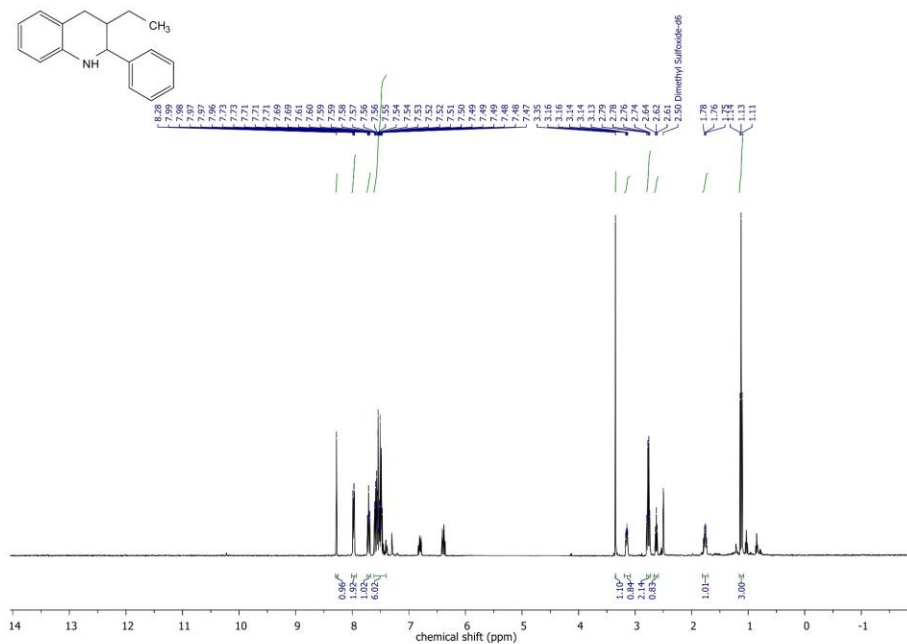
The Synthesis of Hydroquinolines from Nitroaldehydes and Ketones by Hydrogenation Sequences and Condensations

3-Methyl-2-phenyl-1,2,3,4-tetrahydroquinoline (32)

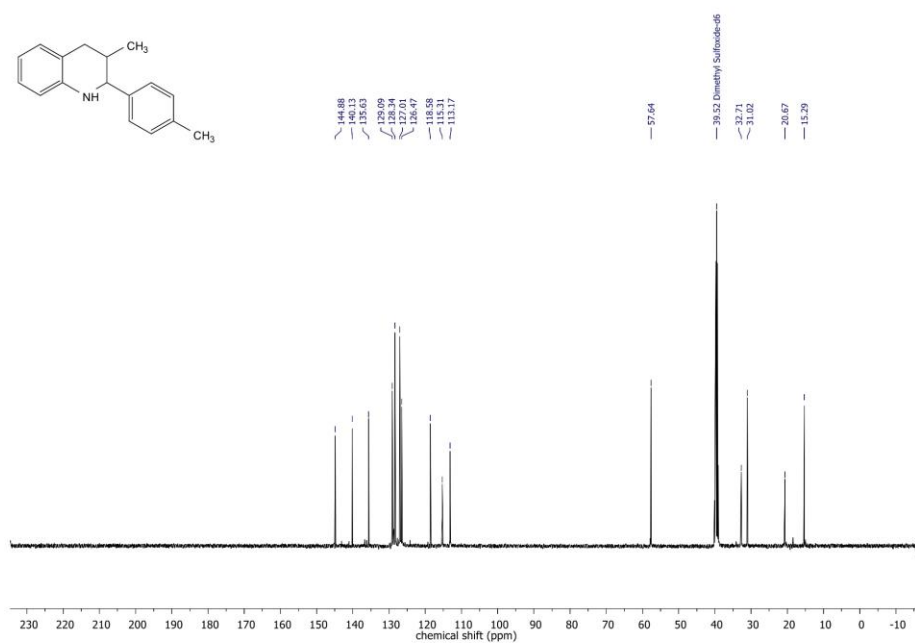


The Synthesis of Hydroquinolines from Nitroaldehydes and Ketones by Hydrogenation Sequences and Condensations

3-Ethyl-2-phenyl-1,2,3,4-tetrahydroquinoline (33)

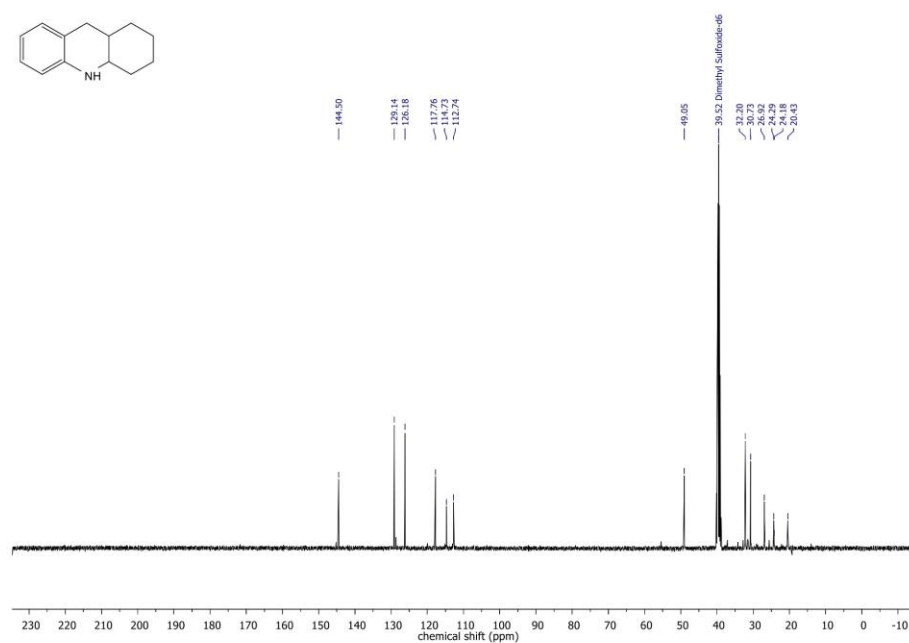
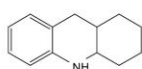
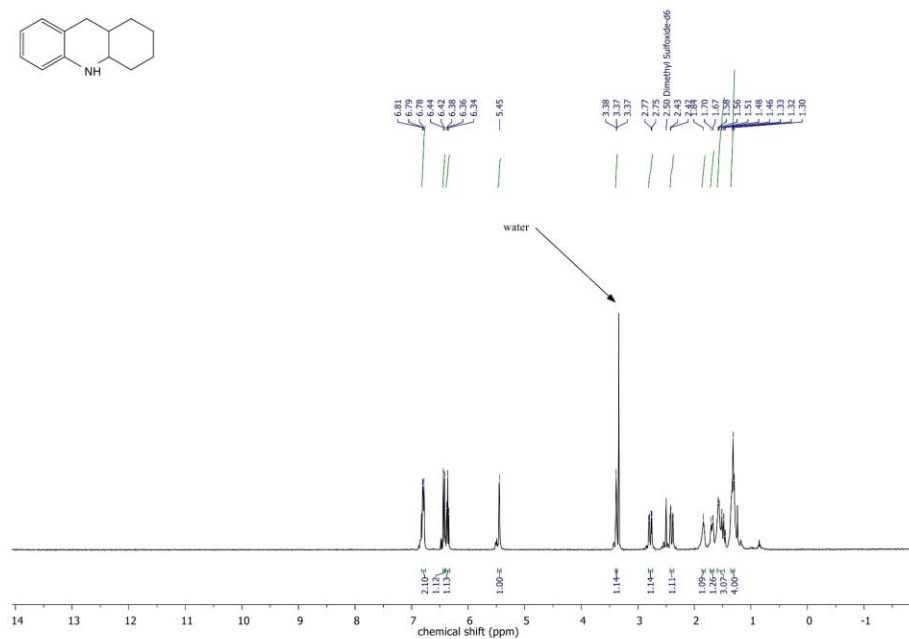
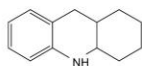


Chemical structure of 1-(4-methylphenyl)-2-methyl-1,2,3,4-tetrahydroquinoline is shown. The ^1H NMR spectrum (DMSO- d_6) displays peaks corresponding to the structure. The x-axis represents chemical shift (ppm) from 14 to -1. The spectrum shows aromatic and NH protons between 6.5 and 7.2 ppm, a methyl group on the ring at 4.60 ppm, and the p-tolyl group protons and methyl group between 2.2 and 2.9 ppm. Integration values are provided below the peaks.



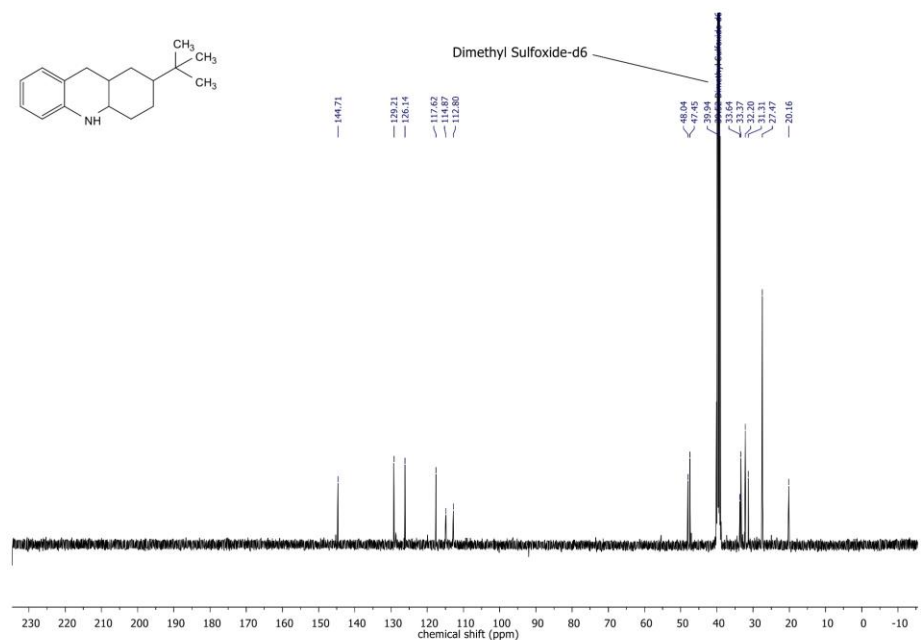
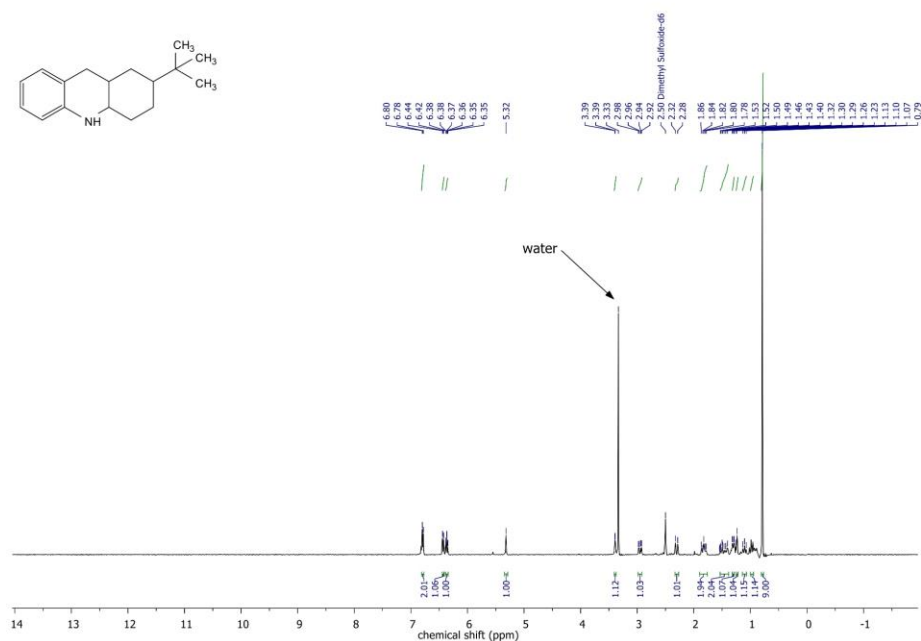
The Synthesis of Hydroquinolines from Nitroaldehydes and Ketones by Hydrogenation Sequences and Condensations

1,2,3,4,9a,10-Octahydroacridine (35)



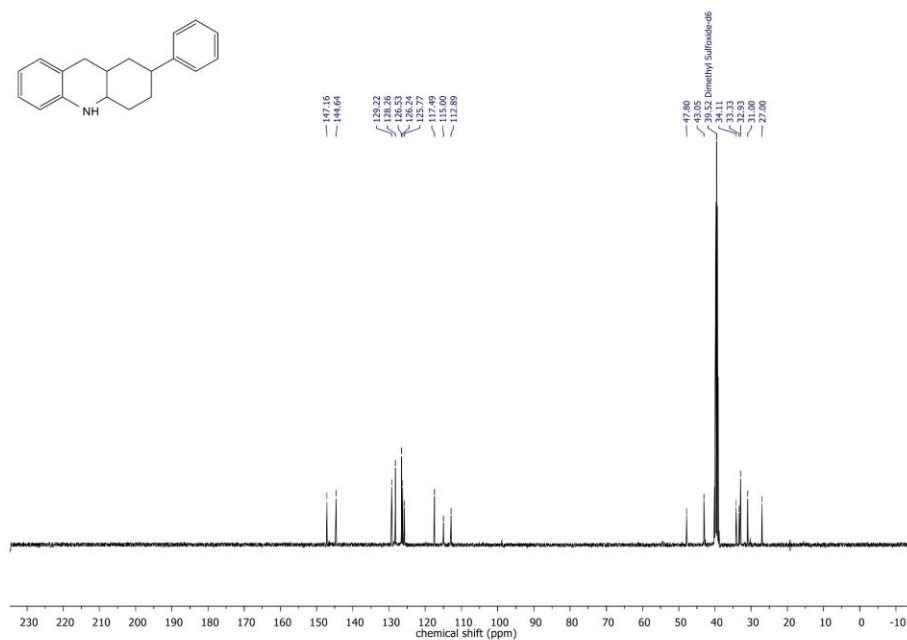
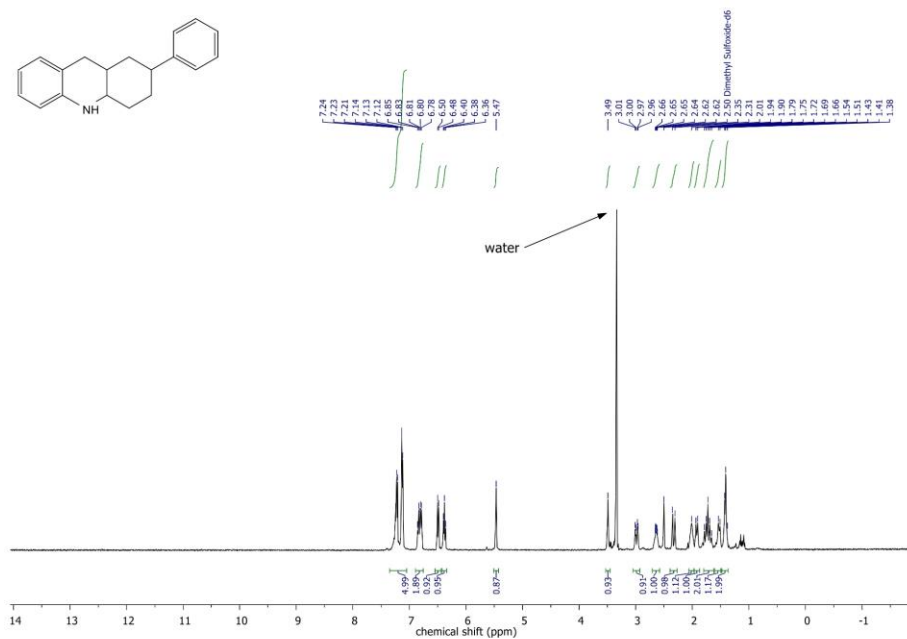
The Synthesis of Hydroquinolines from Nitroaldehydes and Ketones by Hydrogenation Sequences and Condensations

2-(*Tert*-butyl)-1,2,3,4,4a,9,9a,10-Octahydroacridine (36)



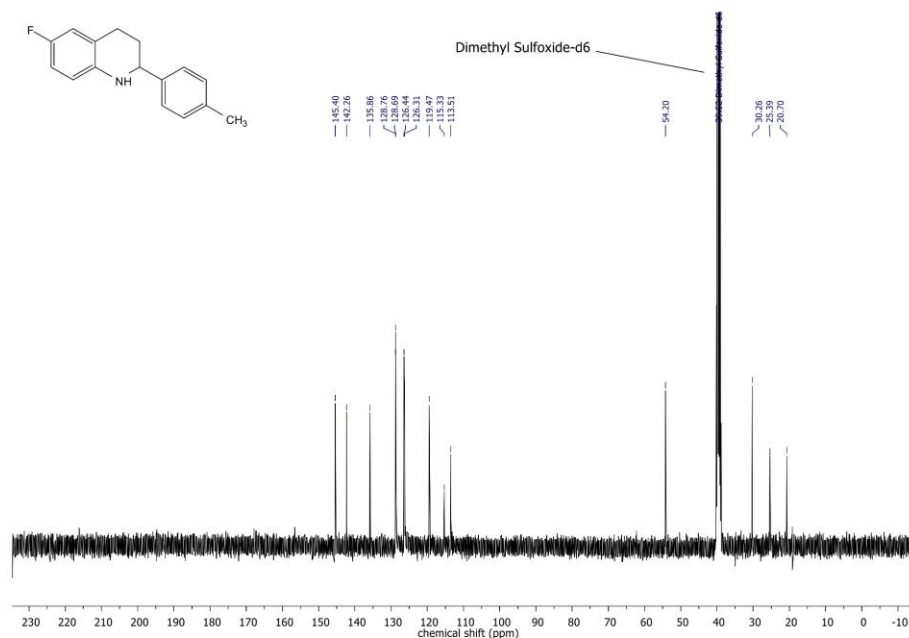
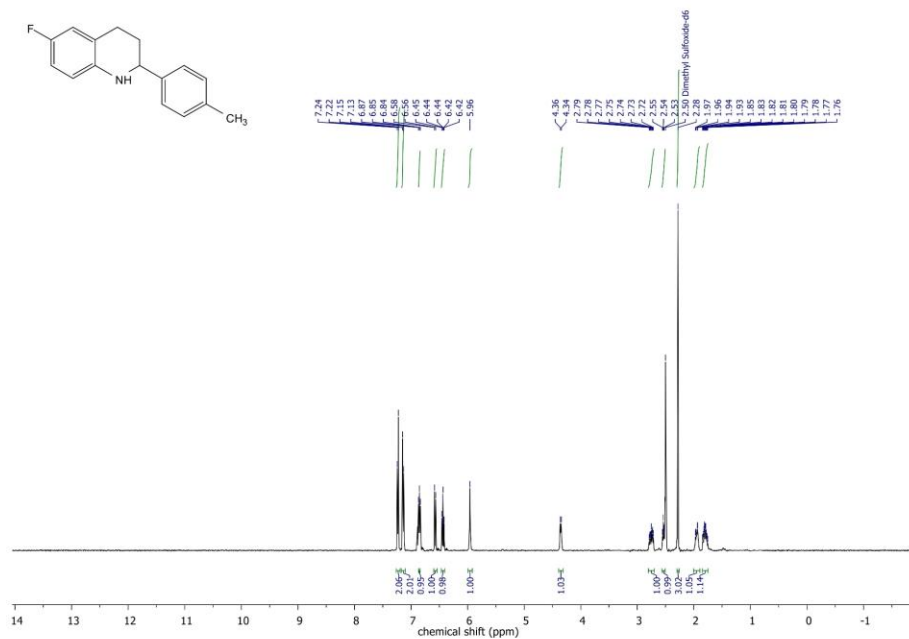
The Synthesis of Hydroquinolines from Nitroaldehydes and Ketones by Hydrogenation Sequences and Condensations

2-Phenyl-1,2,3,4,4a,9,9a,10-octahydroacridine (37)



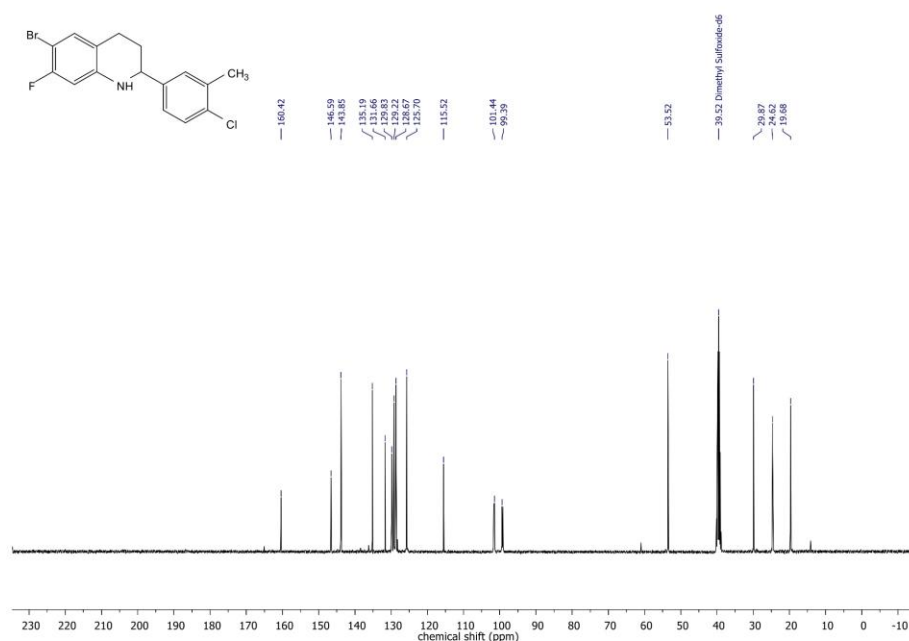
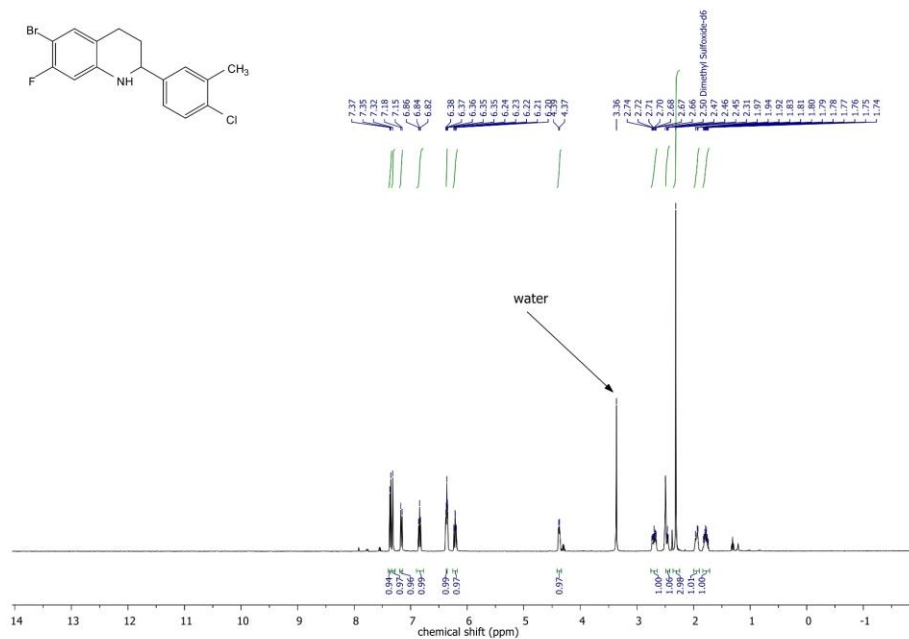
The Synthesis of Hydroquinolines from Nitroaldehydes and Ketones by Hydrogenation Sequences and Condensations

6-Fluoro-2-(*para*-tolyl)-1,2,3,4-tetrahydroquinoline (38)



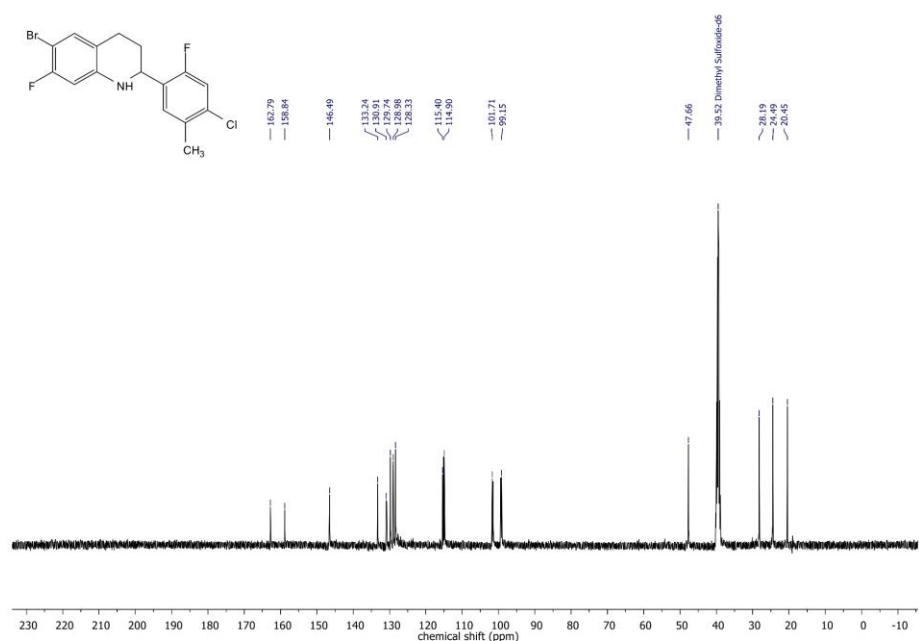
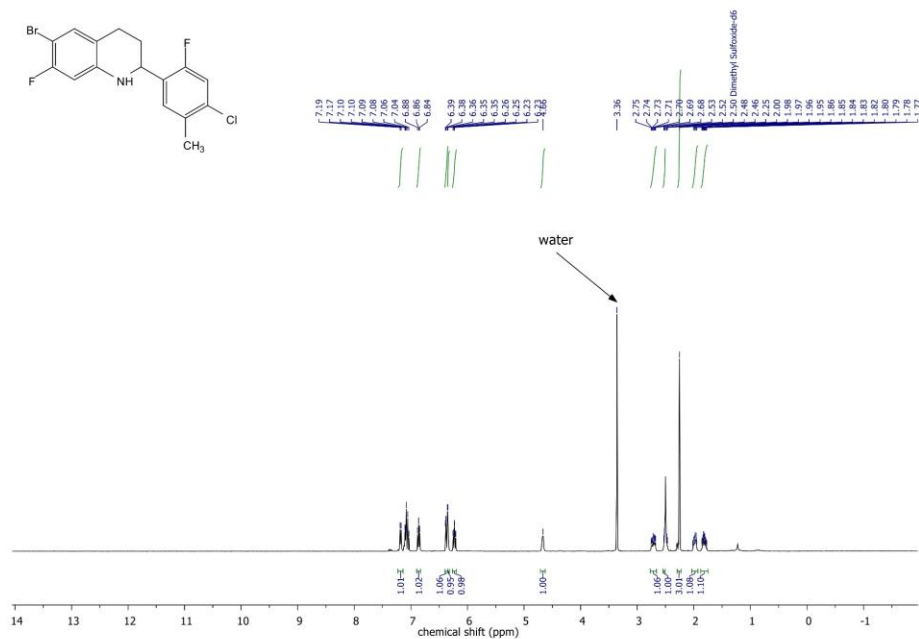
The Synthesis of Hydroquinolines from Nitroaldehydes and Ketones by Hydrogenation Sequences and Condensations

6-Bromo-2-(4-chloro-3-methylphenyl)-7-fluoro-1,2,3,4-tetrahydroquinoline (39)



The Synthesis of Hydroquinolines from Nitroaldehydes and Ketones by Hydrogenation Sequences and Condensations

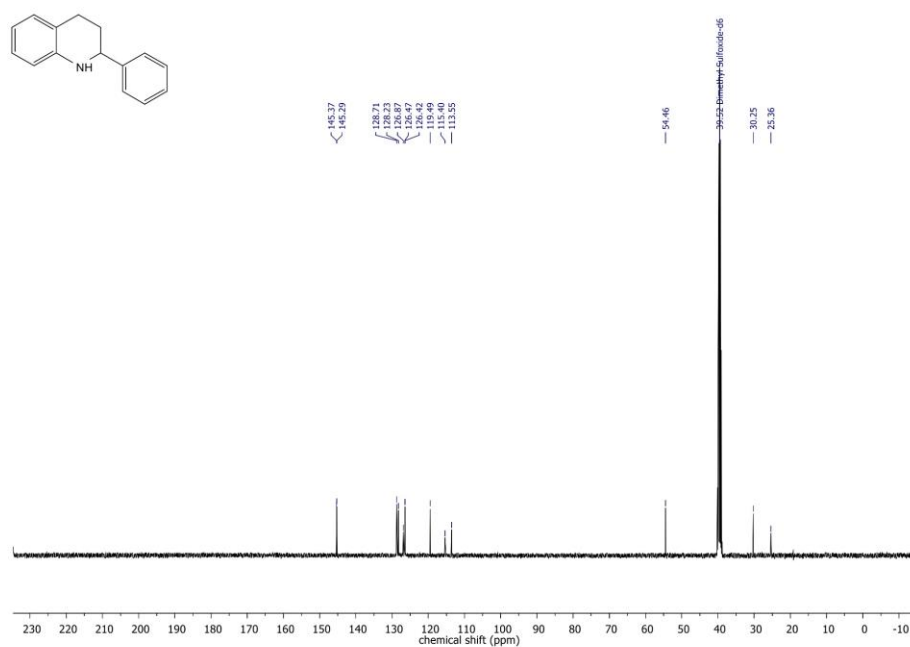
6-Bromo-2-(4-chloro-2-fluoro-5-methylphenyl)-7-fluoro-1,2,3,4-tetrahydroquinoline (40)



Chemical structure: Nc1ccc2c(c1)ccc(C2Cc3ccccc3)c3ccccc3

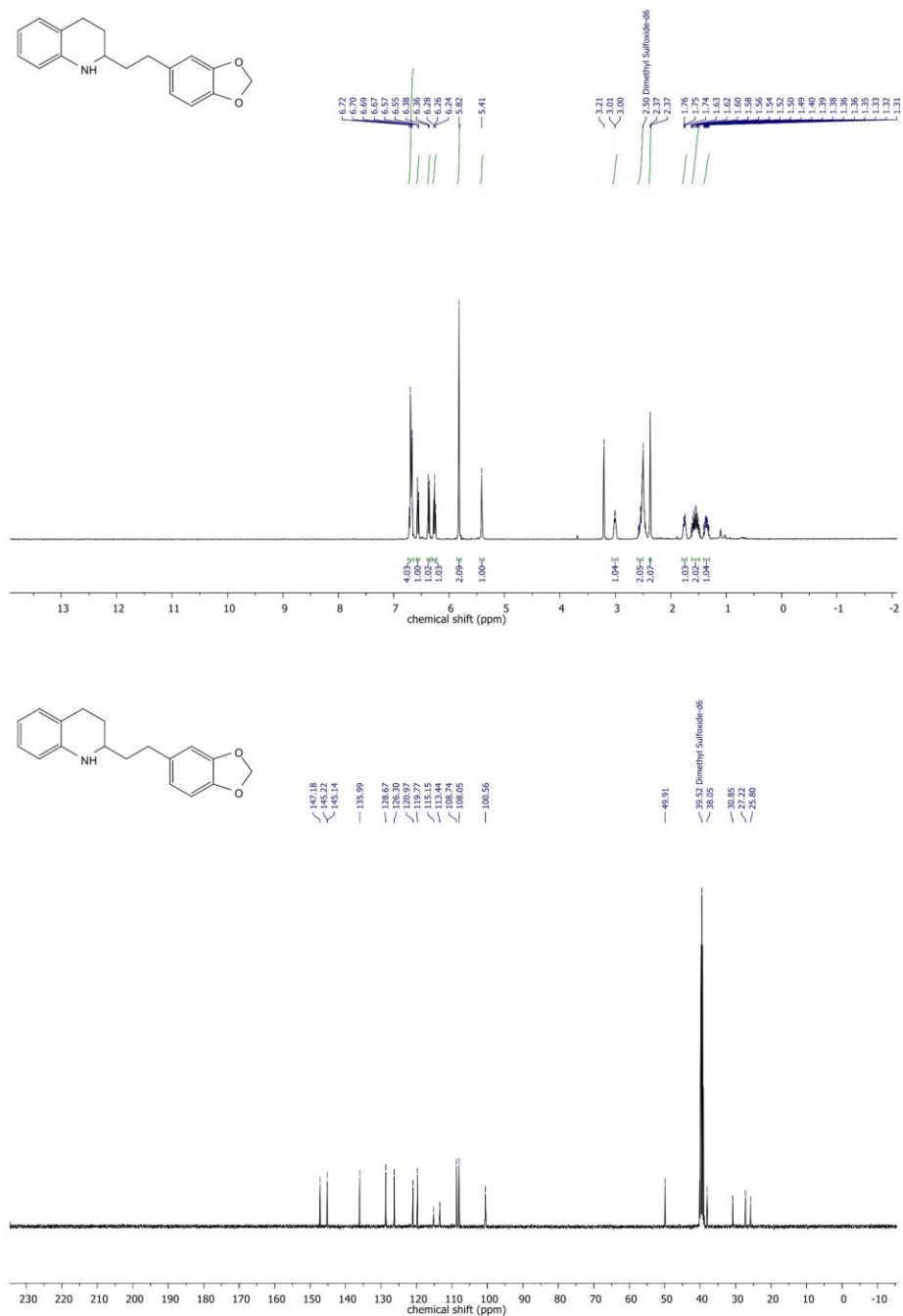
¹H NMR spectrum (DMSO-d₆) showing chemical shifts (ppm) and integration values:

Chemical Shift (ppm)	Integration
7.33	3.90
7.32	0.95
7.31	2.01
7.29	1.02
7.28	0.99
7.27	0.97
7.23	0.97
7.21	0.97
7.20	0.97
7.19	0.97
7.18	0.97
6.85	0.97
6.83	0.97
6.81	0.97
6.80	0.97
6.63	0.97
6.62	0.97
6.42	0.97
6.40	0.97
6.38	0.97
5.87	0.97
2.76	0.09
2.75	0.09
2.74	0.09
2.72	0.09
2.71	0.09
2.68	0.09
2.50	1.04
2.45	1.03
1.95	1.01
1.85	1.04
1.84	1.04
1.81	1.04
1.82	1.04
1.83	1.04
1.79	1.04
1.77	1.04
1.76	1.04
1.75	1.04
1.24	1.04



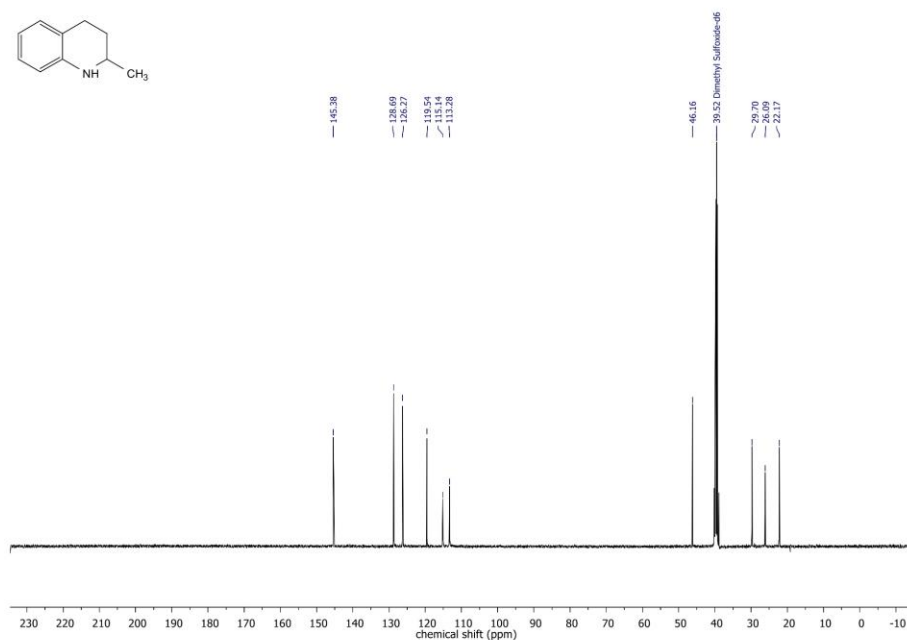
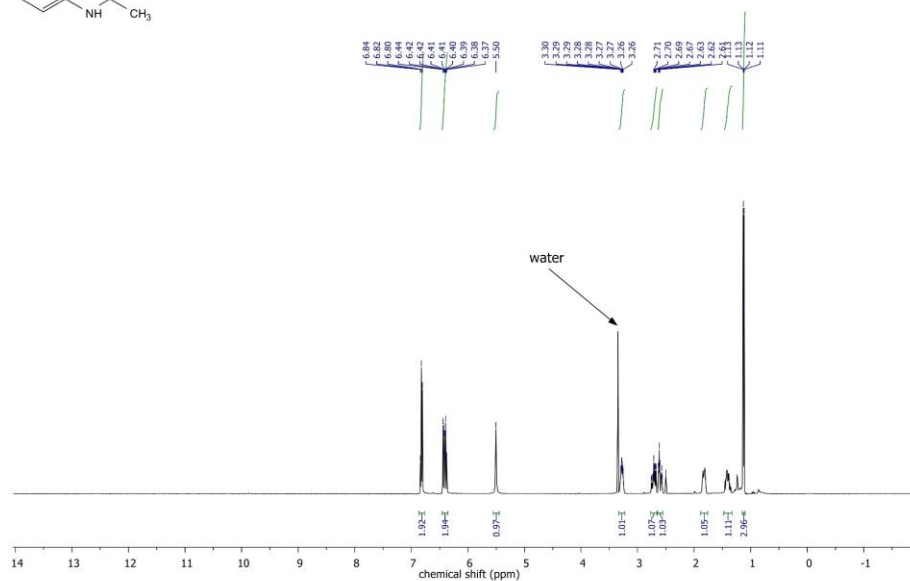
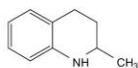
The Synthesis of Hydroquinolines from Nitroaldehydes and Ketones by Hydrogenation Sequences and Condensations

2-(2-(Benzo[d][1,3]dioxol-5-yl)ethyl)-1,2,3,4-tetrahydroquinoline (42)



The Synthesis of Hydroquinolines from Nitroaldehydes and Ketones by Hydrogenation Sequences and Condensations

2-Methyl-1,2,3,4-tetrahydroquinoline (43)



The Synthesis of Hydroquinolines from Nitroaldehydes and Ketones by Hydrogenation Sequences and Condensations

6-Fluoro-2-methyl-1,2,3,4-tetrahydroquinoline (44)



7 References

- [1] S. L. J. Thomae, N. Prinz, T. Hartmann, M. Teck, S. Correll, M. Zobel, *Rev. Sci. Instrum.* **2019**, *90*, 43905.
- [2] L. F. B. Ribeiro, O. Flores, P. Furtat, C. Gervais, R. Kempe, R. A. F. Machado, G. Motz, *J. Mater. Chem. A* **2017**, *5*, 720–729.
- [3] G. Evmenenko, T. T. Fister, D. B. Buchholz, F. C. Castro, Q. Li, J. Wu, V. P. Dravid, P. Fenter, M. J. Bedzyk, *Phys. Chem. Chem. Phys.* **2017**, *19*, 20029–20039.
- [4] B. Gao, Z. Han, W. Meng, X. Feng, H. Du, *J. Org. Chem.* **2023**, *88*, 3335–3339.
- [5] M. Ueda, S. Kawai, M. Hayashi, T. Naito, O. Miyata, *J. Org. Chem.* **2010**, *75*, 914–921.
- [6] N. Hofmann, L. Homberg, K. C. Hultsch, *Org. Lett.* **2020**, *22*, 7964–7970.
- [7] K. N. Asaba, T. Takahashi, M. Yamamoto, K. Takagaki, M. Nogami, R. Tsuji, H. Meguro, N. Ukegawa, WO2022138888 (A1), **2021**.
- [8] L. Ouyang, Y. Xia, J. Liao, R. Miao, X. Yang, R. Luo, *ACS Omega* **2021**, *6*, 10415–10427.
- [9] J. Chen, L. Qi, B. Zhang, M. Chen, T. Kobayashi, Z. Bao, Q. Yang, Q. Ren, W. Huang, Z. Zhang, *Catal. Sci. Technol.* **2021**, *11*, 4332–4341.
- [10] T. Rano, G. H. Kuo, M. E. Sieber, K. T. Demarest, P. Pelton, A. Wang, US2007265304 (A1), **2007**.
- [11] W. Xiong, S. Li, B. Fu, J. Wang, Q.-A. Wang, W. Yang, *Org. Lett.* **2019**, *21*, 4173–4176.
- [12] C. S. Lim, T. T. Quach, Y. Zhao, *Angew. Chem. Int. Ed.* **2017**, *56*, 7176–7180.
- [13] J. Tröger, St. Gerö, *J. Prakt. Chem.* **1926**, *113*, 293–308.
- [14] S. W. Goldstein, P. J. Dambek, *Synthesis* **1989**, *1989*, 221–222.
- [15] K. Matsuzaki, H. Uno, E. Tokunaga, N. Shibata, *ACS Catal.* **2018**, *8*, 6601–6605.
- [16] I. T. Alt, C. Guttroff, B. Plietker, *Angew. Chem. Int. Ed.* **2017**, *56*, 10582–10586.
- [17] X. Qiao, Z. Zhang, Z. Bao, B. Su, H. Xing, Q. Yang, Q. Ren, *RSC Adv.* **2014**, *4*, 42566–42568.
- [18] R. Mitra, H. Zhu, S. Grimme, J. Niemeyer, *Angew. Chem. Int. Ed.* **2017**, *56*, 11456–11459.

- [19] T. Felicetti, R. Cannalire, M. S. Burali, S. Massari, G. Manfroni, M. L. Barreca, O. Tabarrini, B. D. Schindler, S. Sabatini, G. W. Kaatz et al., *ChemMedChem* **2017**, *12*, 1293–1302.
- [20] S. C. Cosgrove, S. Hussain, N. J. Turner, S. P. Marsden, *ACS Catal.* **2018**, *8*, 5570–5573.
- [21] F. Chen, A.-E. Surkus, L. He, M.-M. Pohl, J. Radnik, C. Topf, K. Junge, M. Beller, *J. Am. Chem. Soc.* **2015**, *137*, 11718–11724.
- [22] N. Luo, H. Shui, Y. Zhong, J. Huang, R. Luo, *Synthesis* **2021**, *53*, 4516–4524.
- [23] X. Hu, X. Hu, CN112521333 (A), **2019**.
- [24] J. Wu, C. Wang, W. Tang, A. Pettman, J. Xiao, *Chem. Eur. J.* **2012**, *18*, 9525–9529.
- [25] A. Canas-Rodriguez, R. G. Canas, A. Mateo-Bernardo, *Tricyclic inhibitors of gastric acid secretion. Part, V*, **1987**.
- [26] H. Zhou, D. Pi, Q. Liu, R. He, P. Cui, CN106831565 (A), **2017**.

6 General Synthesis of Alkyl Amines via Borrowing Hydrogen and Reductive Amination

Matthias Elfinger, Christof Bauer, Jörg Schmauch, Michael Moritz, Christoph Wichmann, Christian Papp and Rhett Kempe

General Synthesis of Alkyl Amines via Borrowing Hydrogen and Reductive Amination

Adv. Synth. Catal. **2023**, 365, 4654-4661.

Copyright Wiley-VCH GmbH.

Reproduced with permission (<https://creativecommons.org/licenses/by/4.0/>).

DOI: <https://doi.org/10.1002/adsc.202301179>

General Synthesis of Alkyl Amines via Borrowing Hydrogen and Reductive Amination

Matthias Elfinger,^a Christof Bauer,^a Jörg Schmauch,^b Michael Moritz,^c
 Christoph Wichmann,^{c, d} Christian Papp,^c and Rhett Kempe^{a, *}


^a Inorganic Chemistry II – Catalyst Design, Sustainable Chemistry Centre
 University of Bayreuth
 95440 Bayreuth, Germany
 E-mail: kempe@uni-bayreuth.de


^b Department of Experimental Physics
 Saarland University, Campus D2 2
 66123 Saarbrücken, Germany

^c Department of Physical Chemistry II
 Friedrich-Alexander-University Erlangen-Nürnberg
 91058 Erlangen, Germany

^d Department of Physical and Theoretical Chemistry
 Free University of Berlin
 14195 Berlin, Germany

Manuscript received: October 16, 2023; Revised manuscript received: October 30, 2023;
 Version of record online: November 21, 2023

 Supporting information for this article is available on the WWW under <https://doi.org/10.1002/adsc.202301179>

 © 2023 The Authors. Advanced Synthesis & Catalysis published by Wiley-VCH GmbH. This is an open access article under the terms of the Creative Commons Attribution License, which permits use, distribution and reproduction in any medium, provided the original work is properly cited.

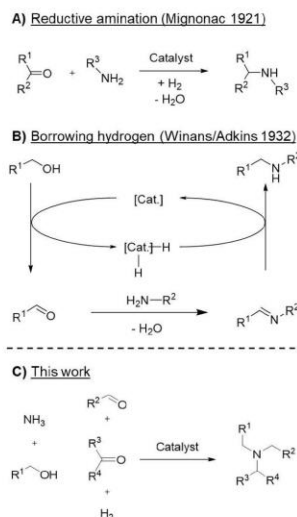
Abstract: Amines are a very important class of compounds and the selective synthesis of differently substituted primary, secondary and tertiary alkyl amines is challenging. Here we present the synthesis of primary, secondary, and tertiary alkyl amines from ammonia and alcohols, aldehydes, ketones and hydrogen by combining borrowing hydrogen or hydrogen autotransfer and reductive amination with hydrogen. The key is a nanostructured, bimetallic Co/Sc catalyst able to mediate both reactions or concepts efficiently. We observe a broad product scope, a very good functional group tolerance, upscaling is easily accomplished and our catalyst is reusable.

Keywords: amines; borrowing hydrogen; cobalt; reductive amination; scandium

Introduction

Amines are one of the most important classes of chemical compounds and are present in many bulk and fine chemicals,^[1] drugs,^[2] agro chemicals and materials.^[3] The selective synthesis of differently substituted primary, secondary and tertiary alkyl amines is especially challenging since the alkylated product amine is a better nucleophile and more reactive than the amine or ammonia starting material. Two broadly applied and green or sustainable and selective methods have been developed a century ago namely

the reductive amination^[4] (Scheme 1A) introduced by Mignonac in 1921^[5] and the borrowing hydrogen^[6] or the hydrogen auto-transfer^[7] (BH HA) concepts^[8] (Scheme 1B) introduced by Winans and Adkins in 1932.^[9] Both methods have strengths and weaknesses in comparison to each other. The BH HA approach is highly selective in the first alkylation step while an already alkylated primary or secondary amine is challenging to be modified. The reductive amination is rather unselective in the primary alkylation step if ammonia is employed but selective and efficient regarding the introduction of an already alkylated



Scheme 1. Combination of reductive amination employing hydrogen (A) and borrowing hydrogen (B) permits the general synthesis of alkyl amines (C).

amine. We concluded that a catalyst mediating both reactions would permit to use the one or the other reaction or concept if they are strong and could give rise to a general catalytic access to primary, secondary, and tertiary alkyl amines. We have introduced the first Co^[10] and Cr^[11] catalyst for BH HA and highly efficient and selective nanostructured catalysts for the synthesis of primary amines via reductive amination employing hydrogen.^[12,13] A nanostructured Co catalyst for the synthesis of alkyl amines via BH HA has been introduced by Beller and Jagadeesh and coworkers recently.^[14] No potential use of that catalyst in reductive amination employing hydrogen has been reported. Furthermore, nanostructured Co catalysts for the general synthesis of primary alkyl amines via reductive amination from carbonyl compounds and ammonia employing hydrogen as the reducing agent have been disclosed.^[15,15] Here, the potential use as catalysts in BH HA based amine alkylation has not been disclosed. Furthermore, Beller and Jagadeesh and coworkers introduced a general alkyl amine synthesis namely the nickel mediated hydrogenative coupling of nitriles and amines recently.^[16] We report here on the synthesis of primary, secondary, and tertiary alkyl amines from ammonia and alcohols, aldehydes, and ketones with hydrogen as a reducing agent for the amination step (Scheme 1C). The key is a nanostructured, bimetallic Co/Sc catalyst able to mediate BH HA and reductive amination with hydrogen efficiently. Our catalyst is based on 3d metals with a

high abundance in the earth's crust with Sc being more abundant than Co.^[17] Our catalyst is easy to synthesize and based on a N-doped and Si-doped porous carbon support developed by us.^[18] While numerous catalysts that mediate reductive amination employing hydrogen or borrowing hydrogen-based amine alkylation are known, the combination of both approaches seems not been reported yet. We observe a broad product scope, a very good functional group tolerance, upscaling is easily accomplished and our catalyst is reusable.

Results and Discussion

Catalyst Synthesis and Characterization

The synthesis of the catalyst support follows an already published procedure, based on the crosslinking of the commercially available polycarbosilane precursor SMP-10 and acrylonitrile applying azobisisobutyronitrile as an initiator.^[13,18] The resulting greenbody was pyrolyzed at 1000 °C under nitrogen atmosphere (see Supporting Information 2.1). By means of this process a microphase separated, silicon rich NC-material is created. To obtain the final N-SiC support material, an activation step is required. By treatment with 1 M NaOH at 85 °C overnight, a significant percentage of the Si rich domains are washed out and thus creating free C-N-H_x groups.^[13] The metal nanoparticles could be introduced via wet impregnation of the N-SiC support and the two metal salts Co(NO₃)₂·6 H₂O and Sc(NO₃)₃·5 H₂O in water, pyrolysis (700 °C, N₂) and subsequent reduction (550 °C, N₂/H₂). The measured metal content, identified via inductively coupled plasma optical emission spectroscopy (ICP-OES) analysis, showed no significant deviation from the theoretical metal content of 2 wt% for Sc and Co. Scanning transmission electron microscopy in combination with high-angle annular dark-field imaging (HAADF-STEM) analysis (Figure 1A and B) revealed homogeneously distributed Co nanoparticles with an average particle size of 13.9 nm. In combination with electron energy loss spectroscopy (EELS, Figure 1C), the STEM analysis could also show that the scandium particles are smaller by orders of magnitude than the cobalt ones with the former finely distributed over the support material. Scanning electron microscopy (SEM) in combination with energy dispersive X-ray spectroscopy (EDX) also confirmed the homogeneously distributed cobalt nanoparticles and revealed, that the remaining silicon, which was not removed from the support material, is allocated in the same way as the scandium particles (see Supporting Information Figure S2). To further explore the nature of our catalyst material, X-ray Photoelectron Spectroscopy (XPS) was performed. The spectra of the support without metal particles (black) and the metal particles on the support (green) are shown in Figure 2. In Figure 2A, a wide

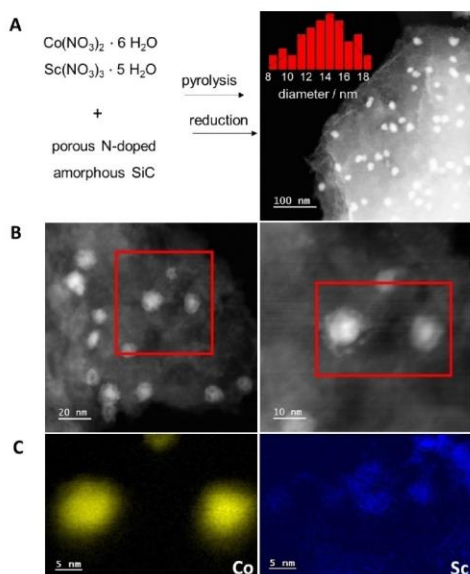


Figure 1. Synthesis and characterization of the Co catalyst: (A) Synthesis of the crosslinked material, followed by pyrolysis and NaOH treatment to obtain the support material; wet impregnation, pyrolysis and reduction led to the active Co/Sc catalyst. (B) HAADF-STEM analysis of the nanoparticles combined with STEM-EELS analysis (C) revealed the size difference of cobalt and scandium particles with the latter being significantly smaller and finely distributed over the support material.

scan with the expected signals for both, the support material (Si 2p, N 1s, C 1s, O 1s) and the supported catalyst particles (Si 2p, C 1s, O 1s, Sc 2p, Co 2p) and carbon and oxygen impurities, are shown. Additional ghost signals, originating from Ga L α radiation and shifted by 155.7 eV, are marked with a “*”. In Figure 2B, the Co 2p $_{3/2}$ region is shown. For the support, as expected, no signals are visible. For the supported Sc/Co catalyst, a broad signal arises at 780 eV. Two binding energies at 780.6 and 786.4 eV for Co oxides and their shake-ups, respectively, are indicated.^[19] The splitting is characteristic for Co₂O₃ and/or Co(OH)₂. Additionally, a third energy at 777.3 eV for metallic Co is indicated.^[17,20] The binding energies suggest that the surface Co is oxidized. The Sc 2s region is shown in Figure 2C. A single species with a binding energy of 501.1 eV is found, indicating oxidized Sc when considering the literature binding energy for metallic Sc of 499 eV.^[18] Comparing the corrected signal areas of the Co 2p and the Sc 2s region, the amount of Sc detected by XPS is 10 times higher than that of Co (9.6 : 1.3 at%, Sc : Co), albeit

the same concentration is expected from ICP-OES results. Because of the high surface sensitivity of XPS and additional information from microscopy; we conclude that Sc is finely dispersed on the outer layer, while Co is present as or inside of bigger particles. We assume that the close proximity of the Co and Sc oxide centres are beneficial for the combination of (de)hydrogenation and condensation steps needed in both catalytic reactions - reductive amination and BH HA.

Optimization of the Reaction Conditions

To determine the optimal reaction conditions, the BH HA reaction of benzyl alcohol with gaseous ammonia has been selected as a benchmark for all screenings (see Supporting Information 2.4). The solvent screening revealed that toluene was the most suitable. The toluene amount was set to 2.0 mL since this delivered the maximum yield of benzyl amine. Furthermore, potassium hydroxide in equimolar amounts as well as a temperature of 160 °C were determined. The ammonia pressure was kept at 20 bar. For the comparison to other catalysts, the rare earth metal was varied (Table 1). It could be shown that the selectivity of the catalyst is higher the smaller the used rare earth metal is, which led us to Sc as the most active. Neither Co nor Sc as monometallic catalysts could deliver the

Table 1. Catalyst Screening.^[a]

$\text{C}_6\text{H}_5\text{CH}_2\text{OH} + \text{NH}_3 \xrightarrow[\text{-H}_2\text{O}]{\text{Catalyst, Ar}} \text{C}_6\text{H}_5\text{CH}_2\text{NH}_2$			
Entry	Metal(s)	Support	Yield/%
1	Co/La	N-SiC	5
2	Co/Gd	N-SiC	9
3	Co/Lu	N-SiC	54
4	Co/Sc	N-SiC	99
5	Fe/Sc	N-SiC	7
6	Ni/Sc	N-SiC	33
7 ^[b]	Fe	N-SiC	0
8 ^[b]	Ni	N-SiC	12
9 ^[b]	Co	N-SiC	16
10 ^[b]	Sc	N-SiC	32
11	Co/Sc	Activated C	67
12	Co/Sc	Al ₂ O ₃	2
13	Co/Sc	TiO ₂	0
14	Co/Sc	SiO ₂	0
15	–	N-SiC	0

^[a] Reaction conditions: 1.5 mol% Co/Fe/Ni, 0.85 mol% La, 0.74 mol% Gd, 0.66 mol% Lu, 0.49 mol% Sc, pyrolyzed at 700 °C, 0.5 mmol benzyl alcohol, 2.0 mL toluene, 0.5 mmol KOH, 160 °C, 44 h, 20 bar NH₃. Yields were determined by GC using *n*-dodecane as an internal standard.

^[b] 1.5 mol% Fe/Ni/Co/Sc.

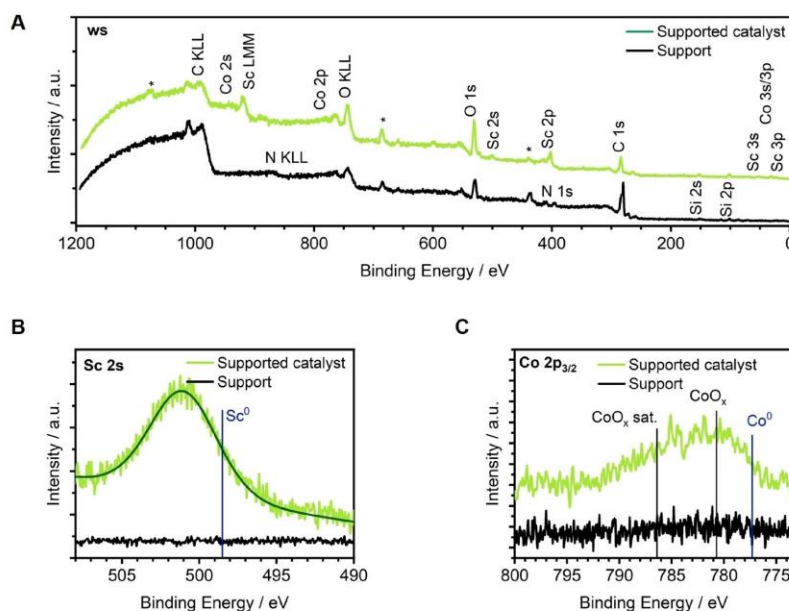


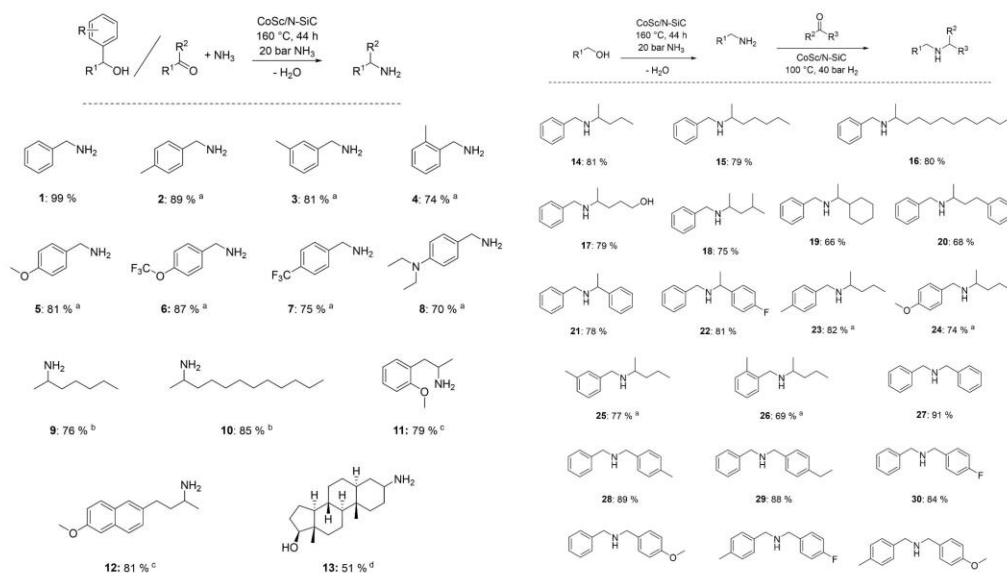
Figure 2. XPS spectra: (A) wide scan (ghost peaks from Ga $L\alpha$ excitation (*)), (B) Co 2p, (C) Sc 2s.

outstanding activity of the bimetallic material. The variation of the support material revealed that only activated carbon could show a decent activity while Al_2O_3 , TiO_2 , SiO_2 and N-SiC without a metal loading indicated little to no conversion of benzyl alcohol. The superiority of the N-SiC material as a catalyst support is based on its unique structure with free C–N–H_x functionalities and an Si coating.^[13]

Substrate Scope

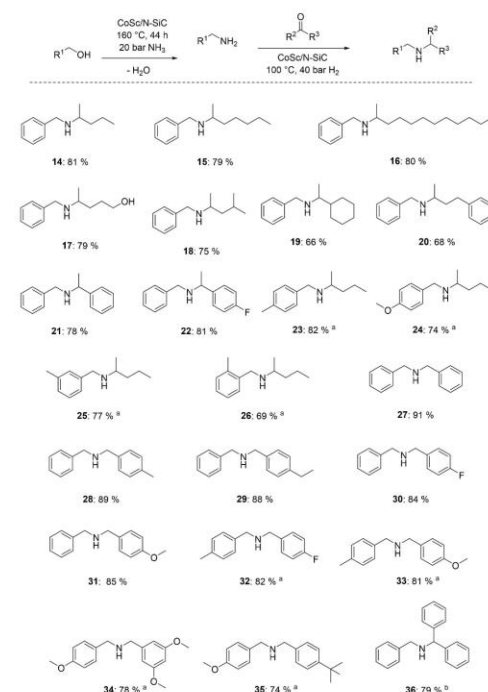
After the optimized reaction conditions have been determined, we became interested in the applicability of our catalyst system and investigated the substrate scope. The product yields are given for the isolated corresponding hydrochloride salts of the synthesized amines. For better clarity, we split the substrate scope in three parts, one for primary, secondary, and tertiary amines each. First, we wanted to show that the catalyst permits the synthesis of different primary amines (Scheme 2). We discovered that as soon as the aromatic ring of the benzyl alcohol derivate was substituted, we had to raise the reaction temperature from 160 to 180 °C. With that done, several electron donating substituents in various ring positions (products 2–5) as well as electron withdrawing substituents (6, 7) could be tolerated. Unfortunately, there is too

much steric hindrance to the reaction if the CF_3 group is placed in the ortho position. NO_2 , CN and CONR_2 groups were also not tolerated due to numerous side reactions. A second amine function within the alcohol did not pose any problem (8). To further show the applicability of our catalyst we synthesized two completely aliphatic amines (products 9 and 10) from ketones like we did in our previous work with a single metal Co/N-SiC catalyst employed in the reductive amination.^[13] The conversion of three biologically active molecules (11–13) could also be accomplished. As it can be seen, the bimetallic CoSc/N-SiC catalyst could also mediate the reductive amination of these ketones with aqueous ammonia. Next, we explored the synthesis of secondary amines. Since we already showed above that the catalyst can permit the reductive amination of carbonyl compounds, we combined borrowing hydrogen and reductive amination as a consecutive reaction to give rise to more complex amine structures. The same catalyst is reused for the second step and beside neutralization, 0.8 mmol carbonyl compound was added (Scheme 3). The reductive amination part then proceeds at 100 °C and 40 bars of hydrogen pressure. Under these conditions, short, medium and long aliphatic moieties could be introduced (Scheme 3, substrates 14–16). The presence of a terminal hydroxy group on the carbonyl compound



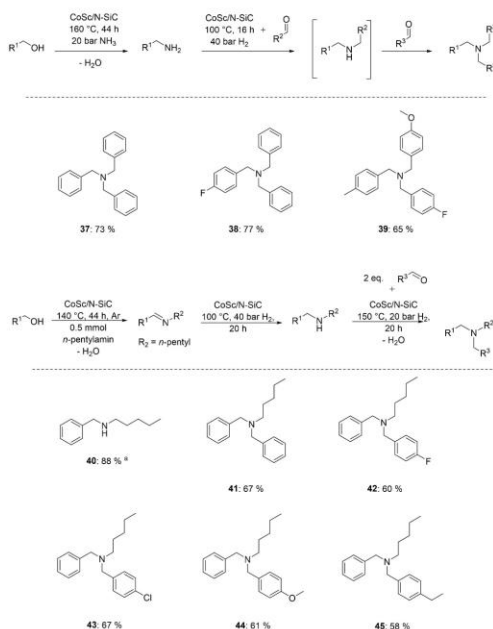
Scheme 2. Synthesis of primary amines employing a Co/Sc-catalyst. Isolated yields of the converted hydrochloride salts. Reaction conditions: 1.5 mol% Co, 0.49 mol% Sc, 0.5 mmol alcohol, 2.0 mL toluene, 0.5 mmol KOH, 160 °C, 44 h, 20 bar NH_3 . [a] 180 °C. [b] 0.5 mmol ketone, 50 °C, 20 h, 10 bar H_2 , 3.5 mL aq. NH_3 32%. [c] 0.5 mmol ketone, 60 °C, 20 h, 15 bar H_2 , 3.5 mL aq. NH_3 32%. [d] 0.25 mmol ketone, 65 °C, 20 h, 15 bar H_2 , 3.2 mL aq. NH_3 32%, 0.3 mL EtOH.

did not present any difficulties for our catalyst (17). Even double branched (18) or alicyclic ketones (19) could be tolerated in good to median yields. Combining an aliphatic part with a terminal aromatic ring led to substrate 20. Furthermore, acetophenone and its fluoro-substituted derivative could be employed in the reductive amination step due to dehalogenation under these harsh conditions could thus be compensated. When varying the benzyl alcohol side of the amine (23–26), the temperature had to be raised to 180 °C again. Hence, a methyl group in all ring positions as well as a methoxy group could be tolerated. Moving forward, we switched the carbonyl compound of the reductive amination step from ketones to aldehydes. Besides dibenzyl amine (27), its methyl- (28), ethyl- (29), fluoro- (30) and methoxy-substituted (31) derivatives could be synthesized with very good yields. Varying both sides was also possible at 180 °C for the first step and gave rise to multiple products (32–35) with small to more bulkier substituents. Lastly, the addition of benzophenone as an educt



Scheme 3. One pot synthesis of secondary amines employing a Co/Sc-catalyst. Isolated yields of the converted hydrochloride salts. Reaction conditions for first step: 1.5 mol% Co, 0.49 mol% Sc, 0.5 mmol alcohol, 2.0 mL toluene, 0.5 mmol KOH, 160 °C, 44 h, 20 bar NH_3 . [a] 180 °C. Reaction conditions for second step: 1.5 mol% Co, 0.49 mol% Sc, 0.8 mmol carbonyl compound, 2.0 mL toluene, 100 °C, 20 h, 40 bar H_2 , 0.05 mL 32% HCl. [b] 150 °C.

could also be accomplished by increasing the temperature of the second step from 100 to 150 °C (36). To complete our work, we studied the synthesis of (differently substituted) tertiary amines, which presented a major challenge overall. For the synthesis of tertiary amines with three benzylic alkyl substituents (Scheme 4, upper half), we extended our consecutive synthesis by a third step, which involves the addition of 1.0 mmol of a further aldehyde as well as an increase in temperature to 140 °C. The addition of 0.05 mL concentrated hydrochloric acid was necessary since it supports the tertiary imine formation of the secondary amine with the aldehyde. Utilizing this three-step synthesis protocol we were able to synthesize three tertiary amines with one, two and three different moieties in good to very good yields (37–39). Next, we established a workaround approach (Scheme 4, lower half). For the borrowing hydrogen



Scheme 4. One pot synthesis of tertiary amines employing a Co/Sc-catalyst. Isolated yields of the converted hydrochloride salts. Substrates 37–39: Reaction conditions for first step: 1.5 mol% Co, 0.49 mol% Sc, 0.5 mmol alcohol, 2.0 mL toluene, 0.5 mmol KOH, 160 °C, 44 h, 20 bar NH_3 . Reaction conditions for second step: 1.5 mol% Co, 0.49 mol% Sc, 0.8 mmol aldehyde, 2.0 mL toluene, 100 °C, 20 h, 40 bar H_2 , 0.05 mL 32% HCl. Reaction conditions for third step: 1.5 mol% Co, 0.49 mol% Sc, 1.0 mmol aldehyde, 2.0 mL toluene, 140 °C, 20 h, 40 bar H_2 , 0.05 mL 32% HCl. Substrates 40–45: Reaction conditions for first step: 2.0 mol% Co, 0.65 mol% Sc, 0.5 mmol alcohol, 0.5 mmol *n*-pentylamine, 2.0 mL toluene, 0.5 mmol KOH, 140 °C, 44 h, Ar atmosphere. Reaction conditions for second step: 2.0 mol% Co, 0.65 mol% Sc, 2.0 mL toluene, 100 °C, 20 h, 40 bar H_2 . Reaction conditions for third step: 2.0 mol% Co, 0.65 mol% Sc, 1.0 mmol aldehyde, 2.0 mL toluene, 150 °C, 20 h, 20 bar H_2 , 0.05 mL 32% HCl. [a] Product isolated after second step.

step we switched the gaseous ammonia with *n*-pentylamine. By increasing the catalyst loading to 2.0 mol% Co and lowering the temperature to 140 °C under argon atmosphere, the catalyst was able to generate the imine, but not to hydrogenate it further to the corresponding amine. Thus, we had to implement an extra hydrogenation step by applying 40 bars of hydrogen pressure at 100 °C for 20 h, which led to the desired product (**40**). By then adding 1.0 mmol aldehyde and 0.05 mL of concentrated hydrochloric acid as well as slightly adjusting the reaction con-

ditions (150 °C, 20 bar H_2), five more tertiary amines could be isolated (**41–45**) with products **39** and **42–45** not yet known to literature. Unfortunately, the synthesis of tertiary alkyl amines carrying one branched alkyl substituent (resulting from a ketone educt) failed due to steric overloading. For the synthesis of such secondary alkyl amines, see Scheme 3. Although our reaction protocol alone confirms the reusability of our bimetallic catalyst system, we investigated it further for five consecutive runs of the first reaction step - the borrowing hydrogen reaction of our model substrate benzyl alcohol. Five consecutive runs without any loss of activity could be accomplished (see Supporting Information 2.4.3). Furthermore, we confirmed the upscaling capabilities of our catalyst by carrying out the above reaction and the consecutive reductive amination to give rise to product **14** (Scheme 3) again - but this time with ten times the amount of all compounds involved. This led to 76% yield of the isolated product (see Supporting Information 2.4.4). Finally, a hot filtration test was performed and the filtrate did not show any catalytic activity (see Supporting Information 2.4.5). In addition, competition experiments have been conducted for BH HA and the reductive amination (see Supporting Information 2.4.6).

Conclusion

In conclusion, we report on the synthesis of primary, secondary, and tertiary alkyl amines combining the borrowing hydrogen or hydrogen auto-transfer concept and the concept of reductive amination employing hydrogen. We use green or sustainable starting materials namely ammonia and alcohols or aldehydes and ketones and hydrogen for our amine synthesis. The key is a nanostructured, bimetallic Co/Sc catalyst able to mediate both reactions or concepts. Both metals are of high abundance in the Earth's crust with Sc being the more abundant 3d metal. We observe a broad product scope with five examples not known to literature yet, a very good functional group tolerance, upscaling is easily accomplished and our catalyst is reusable.

Experimental Section

Synthesis of the Support Material

For the preparation of the N-SiC support material 0.200 g SMP-10 (StarPCS™), 0.987 mL (0.800 g, 15.08 mmol) acrylonitrile and 45 mg (0.28 mmol) azobis(isobutyronitrile) were dissolved in 4 mL dimethylformamide and crosslinked for 16 h at 75 °C. After solvent removal under reduced pressure, the obtained greenbody was pyrolyzed at 1000 °C under nitrogen flow. After ball mining for 40 min, 0.400 g of the ceramic were washed by stirring in solution of 5.3 mL aq. NaOH (1 M) and 4 mL MeOH at 85 °C for 24 h. Afterwards the material was washed until neutrality and dried at room temperature.

RESEARCH ARTICLE

asc.wiley-vch.de



Synthesis of the Catalyst

1000 mg N-SiC were impregnated with 98.75 mg $\text{Co}(\text{NO}_3)_2 \cdot 6 \text{H}_2\text{O}$ and 143 mg $\text{Sc}(\text{NO}_3)_3 \cdot 5 \text{H}_2\text{O}$ in 20 mL H_2O and stirred at 110°C until the solvent was completely removed. Afterwards, the material was pyrolyzed at 700°C under nitrogen atmosphere and reduced at 550°C under forming gas (90:10, $\text{N}_2:\text{H}_2$).

Catalytic Procedures

The first step of the catalytic reaction (borrowing hydrogen/hydrogen autotransfer) of benzyl alcohol and its derivatives was carried out after the procedure described in the following: A magnetic stirring bar, 0.5 mmol alcohol, 2.0 mL toluene (freeze pumped), 0.5 mmol KOH (28 mg) and 28.8 mg of cobalt/scandium-catalyst (2.0 wt% Co, 1.5 mol% Co, 0.58 mg Co, 2.0 wt% Sc, 0.49 mol% Sc, 0.58 mg Sc) were placed directly into a 130 mL high pressure autoclave (Parr Instruments) and flushed with argon for 10 seconds. The autoclave was placed in a liquid nitrogen bath for 5 min whereafter gaseous ammonia was condensed inside for 5 s. The autoclave was then heated to the desired temperature and the reaction was stirred for 44 h. After cooling to room temperature and release of the ammonia pressure, the autoclave was opened and 0.8 mmol of the carbonyl compound as well as one drop of concentrated hydrochloric acid for the neutralization of the remaining ammonia was added. The autoclave was then flushed three times with 10 bars of H_2 , pressurized with 40 bars of H_2 and heated to 100°C for 20 h. In case of the synthesis of tertiary amines, the autoclave was opened again after cooldown and pressure release and 1.0 mmol of aldehyde as well as one drop of concentrated hydrochloric acid were added. The autoclave was flushed again three times with 10 bars of H_2 , pressurized with 20 bars of H_2 and heated to 140°C . To obtain the amine hydrochloride salts, the remaining solution was filtrated into a round bottom flask to remove the catalyst. After the addition of 30 mL of diethyl ether and 0.5 mL HCl in ether (2 M) the precipitate was filtrated, dried under reduced pressure and the resulting solid was then further analyzed by NMR spectroscopy. This was carried out after every step from which the product should be obtained for characterization. For the synthesis of amines with a non-branched aliphatic moiety a slightly different method was used. For the first step, a magnetic stirring bar, 0.5 mmol benzyl alcohol or its derivatives and 0.5 mmol of *n*-pentylamine together with 0.5 mmol of KOH (28 mg), 2 mL of freeze pumped toluene and 38.4 mg of cobalt/scandium-catalyst (2.0 wt% Co, 2.0 mol% Co, 0.77 mg Co, 2.0 wt% Sc, 0.65 mol% Sc, 0.77 mg Sc) were placed inside a pressure tube and flushed with argon. The tube was heated to 140°C for 44 h. After cooling, the whole content was transferred to an autoclave, flushed with 10 bars of H_2 three times and pressurized with 40 bars of H_2 to hydrogenate the remaining double bond. After cooldown, 1.0 mmol of aldehyde as well as one drop of concentrated hydrochloric acid were added. The autoclave was flushed with 10 bars of H_2 three times, pressurized with 20 bars of H_2 and heated to 150°C for 20 h. To obtain the amine hydrochloride salts, the remaining solution was filtrated into a round bottom flask to remove the catalyst. After the addition of 30 mL of diethyl ether and 0.5 mL HCl in ether (2 M) the precipitate was filtrated, dried under reduced

pressure and the resulting solid was then further analyzed by NMR spectroscopy.

Acknowledgements

R. Kempe thanks the DFG for financial support: KE 756/34-1. M. Moritz, C. Wichmann and C. Papp acknowledge the SFB 1452 CLINT from the DFG for financial support and we thank C. Denner for SEM/EDX measurements. J. Schmauch thanks the Leibniz Institute for New Materials, Saarbrücken, for the access to the Jeol ARM200 STEM. Open Access funding enabled and organized by Projekt DEAL.

References

- [1] H.-J. Arpe, *Industrial organic chemistry*, Wiley-VCH, Weinheim, 2010.
- [2] R. Vardanyan, V. Hruby, *Synthesis of best-seller drugs*, Academic Press, London, 2016.
- [3] S. A. Lawrence, *Amines. Synthesis, properties, and applications*, Cambridge University Press, Cambridge, 2004.
- [4] a) T. Irrgang, R. Kempe, *Chem. Rev.* **2020**, *120*, 9583; b) K. Murugesan, T. Senthamarai, V. G. Chandrashekhar, K. Natte, P. C. J. Kamer, M. Beller, R. V. Jagadeesh, *Chem. Soc. Rev.* **2020**, *49*, 6273.
- [5] G. Mignonac, *Compt. Rend.* **1921**, *172*, 223–226.
- [6] A. J. A. Watson, J. M. J. Williams, *Science* **2010**, *329*, 635.
- [7] G. Guillena, D. J. Ramón, M. Yus, *Chem. Rev.* **2010**, *110*, 1611.
- [8] a) A. Corma, J. Navas, M. J. Sabater, *Chem. Rev.* **2018**, *118*, 1410; b) T. Irrgang, R. Kempe, *Chem. Rev.* **2019**, *119*, 2524.
- [9] C. F. Winans, H. Adkins, *J. Am. Chem. Soc.* **1932**, *54*, 306.
- [10] S. Rösler, M. Ertl, T. Irrgang, R. Kempe, *Angew. Chem. Int. Ed.* **2015**, *54*, 15046.
- [11] F. Kallmeier, R. Fertig, T. Irrgang, R. Kempe, *Angew. Chem. Int. Ed.* **2020**, *59*, 11789.
- [12] a) G. Hahn, P. Kunnas, N. de Jonge, R. Kempe, *Nat. Catal.* **2019**, *2*, 71; b) C. Bäuml, C. Bauer, R. Kempe, *ChemSusChem* **2020**, *13*, 3110.
- [13] M. Elfinger, T. Schöner, S. L. J. Thomä, R. Stäglich, M. Drechsler, M. Zobel, J. Senker, R. Kempe, *ChemSusChem* **2021**, *14*, 2360.
- [14] a) Z. Ma, B. Zhou, X. Li, R. G. Kadam, M. B. Gawande, M. Petr, R. Zbořil, M. Beller, R. V. Jagadeesh, *Chem. Sci.* **2022**, *13*, 111.
- [15] a) R. V. Jagadeesh, K. Murugesan, A. S. Alshammari, H. Neumann, M.-M. Pohl, J. Radnik, M. Beller, *Science* **2017**, *358*, 326–332; b) B. Zheng, J. Xu, J. Song, H. Wu, X. Mei, K. Zhang, W. Han, W. Wu, M. He, B. Han, *Chem. Sci.* **2022**, *13*, 9047; c) M. Sheng, S. Fujita, S. Yamaguchi, J. Yamasaki, K. Nakajima, S. Yamazoe, T. Mizugaki, T. Mitsudome, *JACS Au* **2021**, *1*, 501; d) K. Kato, D. Deng, Y. Kita, K. Kamata, M. Hara, *Catal. Sci.*

RESEARCH ARTICLE

asc.wiley-vch.de



- Technol.* **2022**, *12*, 5425; e) T. Senthamarai, V. G. Chandrashekar, M. B. Gawande, N. V. Kalevaru, R. Zboril, P. C. J. Kamer, R. V. Jagadeesh, M. Beller, *Chem. Sci.* **2020**, *11*, 2973–2981.
- [16] V. G. Chandrashekar, W. Baumann, M. Beller, R. V. Jagadeesh, *Science* **2022**, *376*, 1433.
- [17] U. S. Geological Survey Fact Sheet, **2002**, 087–02.
- [18] L. F. B. Ribeiro, O. Flores, P. Furtat, C. Gervais, R. Kempe, R. A. F. Machado, G. Motz, *J. Mater. Chem. A* **2017**, *5*, 720.
- [19] B. J. Tan, K. J. Klabunde, P. M. A. Sherwood, *J. Am. Chem. Soc.* **1991**, *113*, 855.
- [20] J. F. Moulder, J. Chastain (Eds.) *Handbook of X-ray photoelectron spectroscopy. A reference book of standard spectra for identification and interpretation of XPS data*, Perkin-Elmer Corporation, Eden Prairie, Minn., **1992**.



Supporting Information

General Synthesis of Alkyl Amines via Borrowing Hydrogen and Reductive Amination

Matthias Elfinger, Christof Bauer, Jörg Schmauch, Michael Moritz, Christoph Wichmann, Christian Papp, and Rhett Kempe* © 2023 The Authors. Advanced Synthesis & Catalysis published by Wiley-VCH GmbH. This is an open access article under the terms of the Creative Commons Attribution License, which permits use, distribution and reproduction in any medium, provided the original work is properly cited.

SUPPORTING INFORMATION

Table of Contents

1 General considerations	3
2. Experimental procedures	4
2.1 Synthesis of the support material	4
2.2. Synthesis of the catalyst	4
2.3 Catalytic procedures.....	4
2.4 Catalytic studies	6
2.4.1 Screening of reaction parameters for the Borrowing Hydrogen/Hydrogen Autotransfer step	6
2.4.2 Screening of reaction parameters for the Reductive Amination step	7
2.4.3 Reusability	9
2.4.5 Hot filtration test	10
2.4.6 Competition experiments.....	10
3. Characterization of the catalyst	12
3.1 ICP-OES	12
3.2 SEM/EDX	12
3.3 Argon physisorption.....	13
4. Characterization of the isolated products.....	14
5. NMR and IR spectra.....	37
6 References	138
Author Contributions	140

SUPPORTING INFORMATION

1 General considerations

All air- and moisture sensitive reactions were performed under dry argon or nitrogen atmosphere using standard Schlenk and glove box techniques. All dried solvents were obtained from a solvent purification system (activated alumina cartridges) or purchased from Acros. Deuterated solvents were dried via molecular sieves. All chemicals were acquired from commercial sources with purity over 95 % and used without further purification. The precursor SMP-10 was purchased from Starfire Systems, New York, USA. Pyrolysis of the support material was carried out under nitrogen atmosphere in a high temperature furnace (Gero, Berlin, Germany). Pyrolysis and reduction of the catalyst were performed under nitrogen or forming gas (90/10) atmosphere in a ChemBET Pulsar TPR/TPD instrument from Quantachrome. For the STEM investigations a JEOL JEM-ARM 200F with cold FEG emission gun was used equipped with a CEOS Cs corrector, a HAADF detector and a GATAN EELS spectrometer. The EELS mapping was carried out with a collecting semi-angle of 120 mrad and a dispersion of 1 eV/ch.

IR spectra were collected on a JASCO FT/IR-6100 apparatus in a measuring range from 4000-400 cm^{-1} .

Pore characterizations were carried out via argon sorption measurements using a 3P Micro 100 Surface Area and Pore Size Analyzer device. The pore size distribution was computed via DFT calculations (calculation model: Ar at -186.15 °C on cylindrical pore, MDFT equilibrium model). The specific surface area was calculated by using p/p_0 values from 0.005-0.1 (BET). The cobalt and scandium contents were determined by ICP-OES. The fusion of the catalyst was carried out in a Berghof SpeedWave 4 microwave, for the ICP-OES measurement a Varian Vista Pro was used.

X-ray photoelectron spectroscopy measurements were conducted in a dedicated instrument described in detail elsewhere.^[1] The instrument is equipped with a non-monochromatized Specs XR 50 NAP dual Al/Mg anode for X-ray generation. The spectra in this work were attained in Mg mode. A modified Omicron EA 125 hemispherical analyzer was used. The catalyst particles were glued onto vacuum copper tape and introduced to the vacuum right after opening. The data was signal to 101.9 eV.^[2] For the fitting of non-metallic signals, a Gaussian-Lorentzian function was chosen (GL(30) as implemented in Casa XPS). For quantification, the intensities of the respective regions were divided by theoretically derived sensitivity factors.^[3]

NMR measurements were performed using a Varian INOVA 300 (300 MHz for ^1H , 75 MHz for ^{13}C) or a Bruker Avance III HD 500 (500 MHz for ^1H , 125.7 MHz for ^{13}C , 376 MHz for ^{19}F) instruments at 296 K. Chemical shifts are reported in ppm relative to the residual solvent signal (DMSO- d_6 : 2.50 ppm (^1H), 39.51 ppm (^{13}C)), coupling constants (J) are reported in Hz. Estimated ^1H and ^{13}C NMR spectra were simulated (DMSO- d_6 , 300 MHz) using ChemDraw Professional Version 21.0.0.28.

GC analyses were carried out on an Agilent 6850 GC system equipped with an Optima 17 column (30 m x 0.32 mm x 0.25 μm).

Unknown substrates with incomplete spectroscopic literature data were additionally analyzed via liquid chromatography high resolution mass spectra (LC-HRMS). LC-HRMS were obtained from a Thermo Fisher scientific Q-Exactive instrument with a hybrid quadrupole orbitrap analyzer in ESI+ mode.

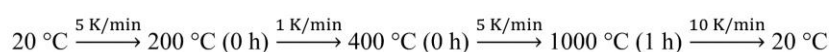
The hydrogenation as well as ammonia experiments were carried out with Parr Instrument stainless steel autoclaves N-MT5 250 mL and 130 mL respectively equipped with heating mantle and temperature controller.

SUPPORTING INFORMATION

2. Experimental procedures

2.1 Synthesis of the support material

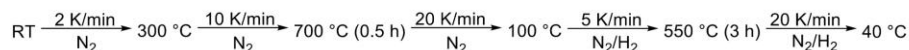
For the preparation of the N-SiC support material a known literature method was modified.^[4] 200 mg SMP-10 (StarPCS™), 0.987 mL (0.800 g, 15.08 mmol) acrylonitrile and 45 mg (0.28 mmol) azobis(isobutyronitrile) were dissolved in 4 mL dimethylformamide and crosslinked for 16 h at 75 °C. After solvent removal under reduced pressure, the obtained greenbody was pyrolyzed using the following program:



After ball mining for 40 minutes, 400 mg of the ceramic were washed by stirring in solution of 5.3 mL aq. NaOH (1 M) and 4 mL MeOH at 85 °C for 24 h. Afterwards the material was washed until neutrality and dried at room temperature.

2.2. Synthesis of the catalyst

1000 mg N-SiC were impregnated with 98,75 mg $\text{Co}(\text{NO}_3)_2 \cdot 6\text{H}_2\text{O}$ and 143 mg $\text{Sc}(\text{NO}_3)_3 \cdot 5\text{H}_2\text{O}$ in 20 mL H_2O and stirred at 110 °C until the solvent was completely removed. Afterwards, the material was pyrolyzed and reduced using the following program:



2.3 Catalytic procedures

The first step of the catalytic reaction (borrowing hydrogen/hydrogen autotransfer) of benzyl alcohol and its derivatives was carried out after the procedure described in the following: A magnetic stirring bar, 0.5 mmol alcohol, 2.0 mL toluene (freeze pumped), 0.5 mmol KOH (28 mg) and 28.8 mg of cobalt/scandium-catalyst (2.0 wt% Co, 1.5 mol% Co, 0.58 mg Co, 2.0 wt% Sc, 0.49 mol% Sc, 0.58 mg Sc) were placed directly into a 130 mL high pressure autoclave (Parr Instruments) and flushed with argon for 10 seconds. The autoclave was placed in a liquid nitrogen bath for 5 minutes whereafter gaseous ammonia was condensed inside for 5 seconds. The autoclave was then heated to the desired temperature (160 °C for benzyl alcohol and 180 °C for derivatives) and the reaction was stirred for 44 h. After cooling to room temperature and release of the ammonia pressure, the autoclave was opened and 0.8 mmol of the carbonyl compound as well as one drop of concentrated hydrochloric acid for the neutralization of the remaining ammonia was added. The autoclave was then flushed three times with 10 bars of hydrogen, pressurized with 40 bars of hydrogen and heated to 100 °C for 20 h. In case of the synthesis of tertiary amines, the autoclave was opened again after cooldown and pressure release and 1.0 mmol of aldehyde as well as one drop of concentrated hydrochloric acid were added. The autoclave was flushed again three times with 10 bars of hydrogen, pressurized with 20 bars of hydrogen and heated to 140 °C. To obtain the amine hydrochloride salts, the remaining solution was filtrated into a round bottom flask to remove the catalyst. After the addition of 30 mL of diethyl ether and 0.5 mL HCl in ether (2 M) the

WILEY-VCH

SUPPORTING INFORMATION

precipitate was filtrated, dried under reduced pressure and the resulting solid was then further analyzed by NMR spectroscopy. This was carried out after every step from which the product should be obtained for characterization.


For the synthesis of amines with a non-branched aliphatic moiety (substrates numbers **40-45**), a slightly different method was used. For the first step, a magnetic stirring bar, 0.5 mmol benzyl alcohol or its derivatives and 0.5 mmol of *n*-pentylamine together with 0.5 mmol of KOH (28 mg), 2 mL of freeze pumped toluene and 38.4 mg of cobalt/scandium-catalyst (2.0 wt% Co, 2.0 mol% Co, 0.77 mg Co, 2.0 wt% Sc, 0.65 mol% Sc, 0.77 mg Sc) were placed inside a pressure tube and flushed with argon. The tube was heated to 140 °C for 44 h. After cooling, the whole content was transferred to an autoclave (130 mL, Parr Instruments), flushed with 10 bars of hydrogen three times and pressurized with 40 bars of hydrogen to hydrogenate the remaining double bond. After cooldown, 1.0 mmol of aldehyde as well as one drop of concentrated hydrochloric acid were added. The autoclave was flushed with 10 bars of hydrogen three times, pressurized with 20 bars of hydrogen and heated to 150 °C for 20 h. To obtain the amine hydrochloride salts, the remaining solution was filtrated into a round bottom flask to remove the catalyst. After the addition of 30 mL of diethyl ether and 0.5 mL HCl in ether (2 M) the precipitate was filtrated, dried under reduced pressure and the resulting solid was then further analyzed by NMR spectroscopy.

SUPPORTING INFORMATION

2.4 Catalytic studies


2.4.1 Screening of reaction parameters for the Borrowing Hydrogen/Hydrogen Autotransfer step

Solvent screening of the model substrate benzyl alcohol

	
Solvent	Yield / %
Xylene	52
THF	28
Toluene	99


Reaction conditions: 0.5 mmol benzyl alcohol, 1.5 mol% cobalt; 0.49 mol% scandium, 2.0 mL solvent, 0.5 mmol KOH, 160 °C, 44 h, 20 bar NH₃. Yields determined by GC using *n*-dodecane as an internal standard.

Screening of the toluene amount

	
Volume toluene / mL	Yield / %
0.5	94
1	95
2	99
5	77

Reaction conditions: 0.5 mmol benzyl alcohol, 1.5 mol% cobalt; 0.49 mol% scandium, 0.5 mmol KOH, 160 °C, 44 h, 20 bar NH₃. Yields determined by GC using *n*-dodecane as an internal standard.


Base screening

	
Base	Yield / %
KOtBu	64
NaOH	4
KOH	99
Amberlyst A-26	9

Reaction conditions: 0.5 mmol benzyl alcohol, 1.5 mol% cobalt; 0.49 mol% scandium, 2 mL toluene, 0.5 mmol base, 160 °C, 44 h, 20 bar NH₃. Yields determined by GC using *n*-dodecane as an internal standard.

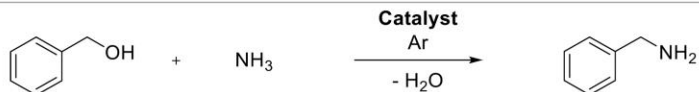
SUPPORTING INFORMATION

Screening of the KOH amount

	
KOH amount / eq.	Yield / %
0	-
0.5	59
1	99
2	99

Reaction conditions: 0.5 mmol benzyl alcohol, 1.5 mol% cobalt; 0.49 mol% scandium, 2 mL toluene, 160 °C, 44 h, 20 bar NH₃. Yields determined by GC using *n*-dodecane as an internal standard.

Screening of the reaction temperature

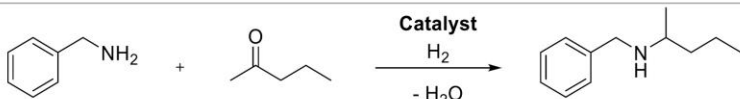
	
Temperature / °C	Yield / %
120	-
140	78
160	99

Reaction conditions: 0.5 mmol benzyl alcohol, 1.5 mol% cobalt; 0.49 mol% scandium, 0.5 mmol KOH, 2 mL toluene, 44 h, 20 bar NH₃. Yields determined by GC using *n*-dodecane as an internal standard.

2.4.2 Screening of reaction parameters for the Reductive Amination step

The only parameters varied here are temperature, hydrogen pressure and reaction time since all other parameters are predetermined due to the consecutive nature of the reaction. As a model substrate, the reductive amination of 2-pentanone with benzyl amine was used.

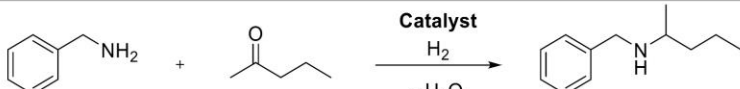
Screening of the reaction temperature

	
Temperature / °C	Yield / %
60	35
80	71
90	91
100	99

Reaction conditions: 1.5 mol% Co (2.24 wt% Co, 0.0075 mmol Co, 0.44 mg Co), 0.5 mmol benzyl amine; 0.8 mmol 2-pentanone, 20 h, 40 bar H₂, 2 mL toluene; yields were determined by GC using *n*-dodecane as an internal standard.

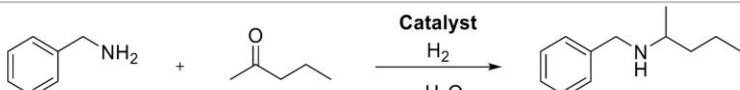
SUPPORTING INFORMATION

Screening of the hydrogen pressure

	
H ₂ pressure / °bar	Yield / %
20	53
30	84
40	99

Reaction conditions: 1.5 mol% Co (2.24 wt% Co, 0.0075 mmol Co, 0.44 mg Co), 0.5 mmol benzyl amine; 0.8 mmol 2-pentanone, 100 °C, 20 h, 2 mL toluene; yields were determined by GC using *n*-dodecane as an internal standard.

Screening of the reaction time

	
Reaction time / h	Yield / %
16	92
20	99

Reaction conditions: 1.5 mol% Co (2.24 wt% Co, 0.0075 mmol Co, 0.44 mg Co), 0.5 mmol benzyl amine; 0.8 mmol 2-pentanone, 100 °C, 40 bar H₂, 2 mL toluene; yields were determined by GC using *n*-dodecane as an internal standard.

SUPPORTING INFORMATION

2.4.3 Reusability

The reusability of the catalyst was investigated using the borrowing hydrogen reaction of benzyl alcohol with gaseous ammonia. The reaction was carried out for 24 h under the optimized reaction conditions to obtain 60 % yield of benzyl amine, which was determined by GC using *n*-dodecane as an internal standard. After each run, the reaction mixture was centrifuged and separated from the catalyst using Pasteur pipettes. The catalyst was washed two times with toluene and used directly for the subsequent run. The procedure was carried out 5 times without a significant loss of activity (Fig. S1). The turnover number (TON) for each run is given in the figure below. It was calculated via the mmol amount of obtained product divided by the mmol amount of metal in the catalyst used.

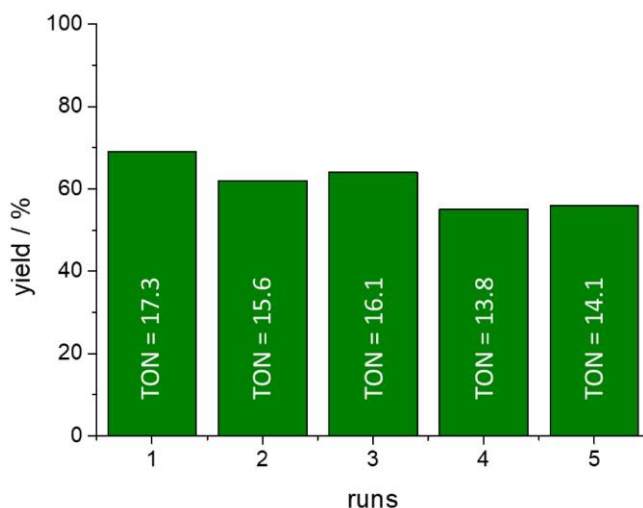


Figure S1: Reusability of the CoSc/N-SiC catalyst for 5 consecutive runs. Reaction conditions for approximately 60 % yield: 1.5 mol% Co, 0.49 mol% Sc, 0.5 mmol benzyl alcohol; 20 h, 20 bar NH_3 ; yields were determined by GC using *n*-dodecane as an internal standard. The turnover number for each run is given in the respective column.

SUPPORTING INFORMATION

2.4.4 Up-scaling

The borrowing hydrogen reaction of benzyl alcohol to benzyl amine and subsequent reductive amination with 2-pentanone to the corresponding amine was performed as up-scaling experiment. For the reaction, 288 mg CoSC/N-SiC (1.5 mol% Co, 0.49 mol% Sc), 5 mmol benzyl alcohol (320 μ l), 5 mmol KOH (280 mg) and 20 mL toluene were put into a 250 mL high pressure autoclave (Parr Instruments) and pressurized with 20 bar NH_3 via condensation. The reaction was carried out under the optimized reaction conditions (160 $^\circ\text{C}$, 44 h). After 44 h, the autoclave was cooled to room temperature, opened and 10 drops of aq. HCl (32 %) as well as 8 mmol 2-pentanone were added. The autoclave was then closed again, pressurized with 40 bar H_2 and heated to 100 $^\circ\text{C}$ for 24 h. The yield of *N*-(1-Methylbutyl)-benzenemethanamine was 76 % and determined by GC using *n*-dodecane as an internal standard.

2.4.5 Hot filtration test

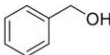
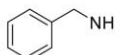
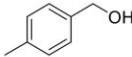
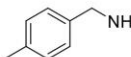
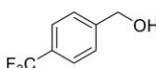
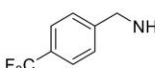
To assess the heterogeneity of the catalyst, a hot filtration test was performed. For this, a magnetic stirring bar, 0.5 mmol benzyl alcohol, 2.0 mL toluene (freeze pumped), 0.5 mmol KOH (28 mg) and 28.8 mg of cobalt/scandium-catalyst (2.0 wt% Co, 1.5 mol% Co, 0.58 mg Co, 2.0 wt% Sc, 0.49 mol% Sc, 0.58 mg Sc) were placed directly into a 130 mL high pressure autoclave (Parr Instruments) and flushed with argon for 10 seconds. The autoclave was placed in a liquid nitrogen bath for 5 minutes whereafter gaseous ammonia was condensed inside for 5 seconds. The autoclave was then heated to 160 $^\circ\text{C}$ and the reaction was stirred for 18 h to obtain 30 % yield of benzylamine. After cooling to approx. 80 $^\circ\text{C}$, the reaction mixture was filtrated hot to remove the catalyst and re-added to the autoclave. After the addition of 0.5 mmol of benzyl alcohol, the reaction was carried out again, following the procedure above. After 44 h, no further formation of benzylamine could be observed. The yield of the product was monitored via GC using *n*-dodecane as an internal standard.

2.4.6 Competition experiments

To check the selectivity of the catalyst, two different competition experiments were conducted. First, the borrowing hydrogen step was carried out as described above (section 2.3) with the exception, that 0.5 mmol benzyl alcohol were switched for a combination of benzyl alcohol, 4-methyl-benzyl alcohol and 4-trifluoromethyl-benzyl alcohol (0.167 mmol each). After the reaction time was over, the resulting solution was analyzed via GC with *n*-dodecane as an internal standard. The results are shown in Table S9.

SUPPORTING INFORMATION

Table S9: Borrowing hydrogen competition experiment.

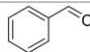
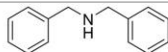
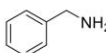
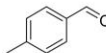
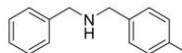
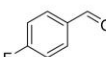
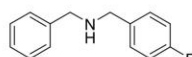
0.167 mmol					1	
0.167 mmol		+	NH ₃	$\xrightarrow[\text{-H}_2\text{O}]{\text{CoSc/N-SiC, Ar}}$		2
0.167 mmol						3
Product		Yield / %				
1		43				
2		27				
3		14				

Reaction conditions: 1.5 mol% Co, 0.49 mol% Sc, 2.0 mL toluene, 0.5 mmol KOH, 160 °C, 44 h, 20 bar NH₃. Yields were determined by GC using *n*-dodecane as an internal standard.

It can be seen that at 160 °C the selectivity of the catalyst is highest towards the formation of benzylamine and lowest towards the formation of 4-trifluoromethyl-benzyl amine. The remaining 15 % of product could be determined as various coupling products of the various benzyl amines with the intermediate aldehyde products.

To check the selectivity of the catalyst in the reductive amination step, 0.5 mmol of benzyl amine were used and 0.167 mmol each of benzaldehyde, 4-methyl-benzaldehyde and 4-fluoro-benzaldehyde were added. The reaction was carried out as described at point 2.3. GC analyses revealed the results in Table S10.

Table S10: Reductive amination competition experiment.

	0.167 mmol				1	
	+	0.167 mmol		$\xrightarrow[\text{-H}_2\text{O}]{\text{CoSc/N-SiC, Ar}}$		2
		0.167 mmol				3
Product		Yield / %				
1		56				
2		34				
3		4				

Reaction conditions: 1.5 mol% Co, 0.49 mol% Sc, 2.0 mL Toluene, 100 °C, 20 h, 40 bar H₂. Yields were determined by GC using *n*-dodecane as an internal standard.

The selectivity of the catalyst is highest towards the formation of product **1** and lowest towards the formation of product **3**. The remaining 5 % of product are the hydrogenated aldehydes.

SUPPORTING INFORMATION

3. Characterization of the catalyst

3.1 ICP-OES

The elemental amounts were determined via a microwave digestion in a MARS 6 from CEM followed by ICP-OES analysis in a SPECTRO ARCOS device from Spectro.

Theoretical Co content:	2.00 wt%
Measured Co content:	2.06 wt%
Theoretical Sc content:	2.00 wt%
Measured Sc content:	2.09 wt%

Since the differences of theoretical and measured contents are insignificant and most likely caused by measuring errors, we continued to use the theoretical values.

3.2 SEM/EDX

SEM/EDX measurements were performed to determine the distribution of the individual elements of the support material. As shown in Figure S3, all studied elements can be described as homogeneously distributed.

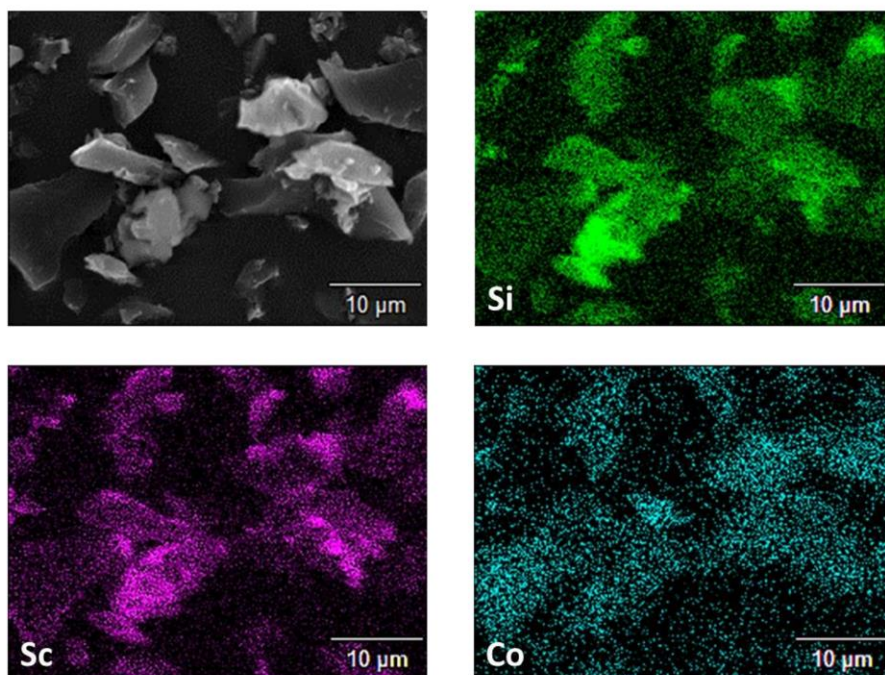


Figure S2: Scanning electron microscopy (SEM) in combination with energy dispersive X-ray (EDX) mapping. The measurements show the distribution of the elements on the sample surface.

SUPPORTING INFORMATION

3.3 Argon physisorption

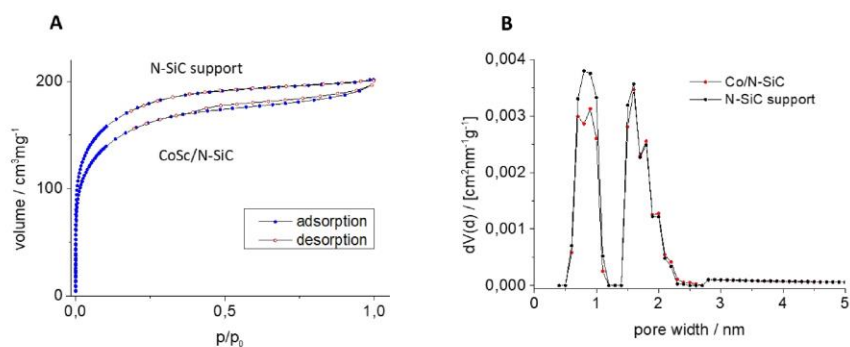
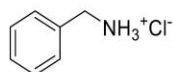


Figure S3: **A** Surface characterization and **B** pore size distribution of the catalyst and activated N-SiC support via argon physisorption measurements. Calculation model: Ar at 87 K on carbon (cylindr. pores, NLDFE equilibrium model). The specific surface showed a slight decline from 545 m²/g of the activated support material to 468 m²/g of the catalyst.

SUPPORTING INFORMATION

4. Characterization of the isolated products

Phenylmethanaminium chloride (1)



MW = 143.61 g/mol

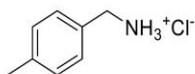
¹H NMR (300 MHz, DMSO-D₆): δ = 8.70 (s, 3 H), 7.56-7.36 (m, 5 H), 4.01 (q, *J* = 5.8 Hz, 2 H) ppm

¹³C NMR (75 MHz, DMSO-D₆): δ = 134.6, 129.5, 129.0, 128.8, 42.5 ppm

Yield: 99 % (71 mg) as a white solid.

The spectroscopic data match those reported in literature.^[5] (CAS Number: 3287-99-8)

p-tolylmethanaminium chloride (2)



MW = 157.64 g/mol

¹H NMR (300 MHz, DMSO-D₆): δ = 8.54 (s, 3 H), 7.40 (d, *J* = 7.8 Hz, 2 H), 7.24 (d, *J* = 7.8 Hz, 2 H), 4.04-3.91 (m, 2 H), 2.32 (s, 3 H) ppm

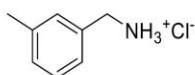
¹³C NMR (75 MHz, DMSO-D₆): δ = 138.2, 131.5, 129.6, 129.4, 42.4, 21.2 ppm

Yield: 89 % (70 mg) as a white solid.

The spectroscopic data match those reported in literature.^[6] (CAS Number: 26177-45-7)

SUPPORTING INFORMATION

m-tolylmethanaminium chloride (3)



MW = 157.64 g/mol

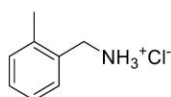
¹H NMR (300 MHz, DMSO-*D*₆): δ = 8.59 (s, 3 H), 7.33-7.29 (m, 3 H), 7.18 (d, *J* = 6.9 Hz, 2 H), 3.95 (s, 2 H), 2.31 (s, 3 H) ppm

¹³C NMR (75 MHz, DMSO-*D*₆): δ = 138.1, 134.5, 130.0, 129.4, 128.9, 126.5, 42.5, 21.4.

Yield: 81 % (64 mg) as a white solid.

The spectroscopic data match those reported in literature.^[6] (CAS Number: 42365-50-4)

o-tolylmethanaminium chloride (4)



MW = 157.64 g/mol

¹H NMR (300 MHz, DMSO-*D*₆): δ = 8.58 (s, 3 H), 7.42-7.40 (m, 1 H), 7.24-7.18 (m, 3 H), 3.95 (q, *J* = 5.5 Hz, 2 H), 2.32 (s, 3 H) ppm

¹³C NMR (75 MHz, DMSO-*D*₆): δ = 136.7, 132.4, 130.3, 129.2, 128.4, 126.0, 39.4, 18.9 ppm

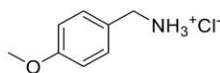
Yield: 74 % (58 mg) as a white solid.

The spectroscopic data match those reported in literature.^[6] (CAS Number: 14865-38-4)

WILEY-VCH

SUPPORTING INFORMATION

(4-Methoxyphenyl)methanaminium chloride (5)



MW = 173.64 g/mol

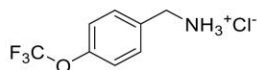
¹H NMR (300 MHz, DMSO-D₆): δ = 8.51 (s, 3 H), 7.47 (m, 2 H), 6.98 (m, 2 H), 4.01-3.88 (m, 2 H), 3.79-3.77 (s, 3 H) ppm

¹³C NMR (75 MHz, DMSO-D₆): δ = 159.8, 131.0, 126.5, 114.4, 55.7, 42.1 ppm

Yield: 81 % (70 mg) as a white solid.

The spectroscopic data match those reported in literature.^[6] (CAS Number: 14865-38-4)

(4-Trifluoromethoxy)methanaminium chloride (6)



MW = 227.61 g/mol

¹H NMR (500 MHz, DMSO-D₆): δ = 8.67 (s, 3 H), 7.68 (d, *J* = 8.5 Hz, 2 H), 7.42 (d, *J* = 8.3 Hz, 2 H), 4.05 (s, 2 H) ppm

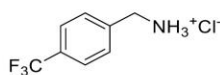
¹³C NMR (126 MHz, DMSO-D₆): δ = 148.7, 134.2, 131.7, 123.6, 121.6, 119.5, 117.4, 41.7 ppm

¹⁹F NMR (376 MHz, DMSO-D₆): δ = -59.9 ppm

Yield: 87 % (99 mg) as a white solid.

The spectroscopic data match those reported in literature.^[7] (CAS Number: 403841-98-5)

SUPPORTING INFORMATION

(4-Trifluoromethyl)methanaminium chloride (7)

MW = 211.61 g/mol

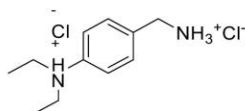
¹H NMR (500 MHz, DMSO- D_6): δ = 8.63 (s, 3 H), 7.70 (dd, J_1 = 8.2 Hz, J_2 = 23.9 Hz, 4 H), 4.06 (s, 2 H) ppm

¹³C NMR (126 MHz, DMSO- D_6): δ = 138.9, 129.8, 125.4, 125.3, 122.8, 41.56 ppm

¹⁹F NMR (376 MHz, DMSO- D_6): δ = -61.1 ppm

Yield: 87 % (99 mg) as a white solid.

The spectroscopic data match those reported in literature.^[8] (CAS Number: 3047-99-2)

(4-Diethylamino)methanaminium chloride (8)

MW = 214.74 g/mol

¹H NMR (300 MHz, DMSO- D_6): δ = 13.20 (s, 1 H), 8.76 (s, 2 H), 7.89-7.77 (m, 3 H), 4.03 (s, 2 H), 3.50 (s, 4 H), 0.99 (t, J = 7.1 Hz, 6 H) ppm

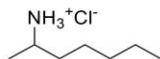
¹³C NMR (75 MHz, DMSO- D_6): δ = 137.9, 135.9, 132.0, 130.7, 130.4, 123.2, 52.2, 41.4, 9.94 ppm

Yield: 70 % (88 mg) as a white solid.

Not all the protons of the amino group are visible due to the exchange of deuterium with the NMR solvent. The spectroscopic data match those reported in literature.^[9] (CAS Number: 104566-33-8)

SUPPORTING INFORMATION

Heptan-2-aminium chloride (9)



MW = 151.68 g/mol

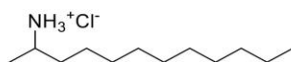
¹H NMR (300 MHz, DMSO-D₆): δ = 8.10 (s, 3 H), 3.07-3.02 (m, 1 H), 1.59-1.52 (m, 1 H), 1.39-1.32 (m, 1 H), 1.26-1.20 (m, 6 H), 0.82 (t, *J* = 7.0 Hz, 3 H) ppm

¹³C NMR (75 MHz, DMSO-D₆): δ = 47.1, 34.4, 31.4, 24.8, 22.3, 18.5, 14.3 ppm

Yield: 76 % (58 mg) as a white solid.

The spectroscopic data match those reported in literature.^[10] (CAS Number: 6159-35-9)

Dodecan-2-aminium chloride (10)



MW = 221.81 g/mol

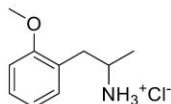
¹H NMR (300 MHz, DMSO-D₆): δ = 8.54 (s, 3 H), 3.21 (s, 1 H), 1.74 (s, 1 H), 1.49-1.21 (m, 20 H), 0.91-0.87 (m, 3 H) ppm

¹³C NMR (75 MHz, DMSO-D₆): δ = 61.9, 31.8, 29.5, 29.5, 29.3, 29.3, 29.2, 22.6, 18.4, 14.5 ppm

Yield: 85 % (94 mg) as a white solid.

Not all the protons of the amino group are visible due to the exchange of deuterium with the NMR solvent. The spectroscopic data match those reported in literature.^[6] (CAS Number: 205746-45-8)

SUPPORTING INFORMATION

1-(2-methoxyphenyl)propan-2-aminium chloride (11)

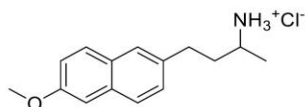
MW = 201.69 g/mol

¹H NMR (500 MHz, DMSO-*D*₆): δ = 8.29 (s, 3H), 7.23 (dd, *J* = 10.8, 4.8 Hz, 1H), 7.15 (dd, *J* = 7.4, 1.5 Hz, 1H), 6.98 (d, *J* = 8.2 Hz, 1H), 6.89 (t, *J* = 7.4 Hz, 1H), 3.77 (s, 3H), 3.37 (s, 1H), 3.01 (dd, *J* = 13.1, 5.1 Hz, 1H), 2.70 (dd, *J* = 13.0, 9.3 Hz, 1H), 1.08 (d, *J* = 6.5 Hz, 3H) ppm

¹³C NMR (126 MHz, DMSO-*D*₆): δ = 157.7, 131.3, 128.8, 125.0, 120.8, 111.3, 55.7, 47.1, 35.3, 18.1 ppm

Yield: 79 % (80 mg) as a white solid.

The spectroscopic data match those reported in literature.^[6] (CAS Number: 72739-03-8)

Nabumetone-NH₃⁺Cl⁻ (12)

MW = 265.78 g/mol

¹H NMR (500 MHz, DMSO-*D*₆): δ = 8.17 (s, 3 H), 7.71 (dd, *J*₁ = 8.7 Hz, *J*₂ = 3.1 Hz, 2 H), 7.59 (s, 1 H), 7.30 (dd, *J*₁ = 8.4 Hz, *J*₂ = 1.7 Hz, 1 H), (d, *J* = 2.5 Hz, 1 H), (dd, *J*₁ = 8.9 Hz, *J*₂ = 2.6 Hz, 1 H), 3.8 (s, 3 H), 3.1 (s, 1 H), 2.77-2.71 (m, 2 H), 2.00-1.94 (m, 1 H), 1.80-1.76 (m, 1 H), 1.22 (d, *J* = 6.5 Hz, 3 H) ppm

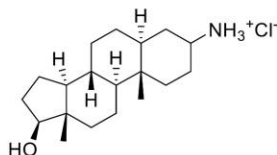
¹³C NMR (126 MHz, DMSO-*D*₆): δ = 157.2, 136.5, 133.2, 129.2, 129.0, 128.0, 127.3, 126.4, 119.0, 106.2, 55.5, 46.8, 36.2, 31.2, 19.6, 18.5 ppm

Yield: 81 % (107 mg) as a white solid.

The spectroscopic data match those reported in literature.^[6] (CAS Number: 2247686-16-2)

WILEY-VCH

SUPPORTING INFORMATION

Stanolone-NH₃⁺Cl⁻ (13)

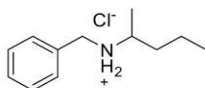
MW = 327.94 g/mol

¹H NMR (500 MHz, MeOH-D₄): δ = 7.84 (s, 3 H), 3.55-3.48 (m, 2 H), 1.95-1.15 (m, 20 H), 1.02-0.84 (m, 6 H), 0.7 (s, 3 H) ppm

¹³C NMR (126 MHz, MeOH-D₄): δ = 81.0, 54.2, 53.9, 50.9, 50.8, 50.3, 44.7, 42.6, 38.9, 36.5, 36.3, 35.7, 35.4, 35.3, 35.1, 32.5, 31.3, 31.2, 31.1, 30.6, 29.2, 28.0, 27.8, 26.1, 25.8, 23.9, 22.8, 22.8, 20.4, 20.0, 11.1, 10.3, 10.2 ppm

Yield: 51 % (42 mg) as a white solid (diastereomeric mixture).

Not all the protons of the amino group are visible due to the exchange of deuterium with the NMR solvent. The spectroscopic data match those reported in literature.^[11] (CAS Number: 2365462-75-3)

N-(1-methylbutyl)-benzenemethanamine hydrochloride (14)

MW = 213.75 g/mol

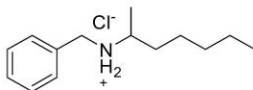
¹H NMR (300 MHz, DMSO-D₆): δ = 9.29 (s, 2 H), 7.64-7.62 (m, 2 H), 7.45-7.40 (m, 3 H), 4.13 (q, *J* = 13.2 Hz, 2 H), 3.08 (s, 1 H), 1.82-1.79 (m, 1 H), 1.53-1.50 (m, 1 H), 1.40-1.38 (m, 1 H), 1.29-1.24 (m, 4 H), 0.9 (t, *J* = 7.3 Hz, 3 H) ppm

¹³C NMR (75 MHz, DMSO-D₆): δ = 132.8, 130.5, 129.2, 129.1, 53.3, 47.4, 34.5, 18.7, 15.9, 14.2 ppm

Yield: 81 % (87 mg) as a white solid.

The spectroscopic data match those reported in literature.^[12] (CAS Number: 2103392-27-2)

SUPPORTING INFORMATION

***N*-(1-methylhexyl)-benzenemethanamine hydrochloride (15)**

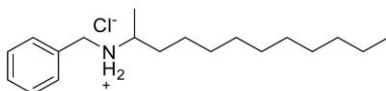
MW = 241.80 g/mol

¹H NMR (300 MHz, DMSO-*D*₆): δ = 9.44 (d, *J* = 43.5 Hz, 2H), 7.70 – 7.59 (m, 2H), 7.46 – 7.34 (m, 3H), 4.11 (s, 2H), 3.05 (s, 1H), 1.90 – 1.77 (m, 1H), 1.59 – 1.45 (m, 1H), 1.35 – 1.18 (m, 9H), 0.86 (t, *J* = 6.8 Hz, 3H).

¹³C NMR (75 MHz, DMSO-*D*₆): δ = 132.8, 130.6, 129.2, 129.0, 53.4, 47.4, 32.3, 31.4, 25.0, 22.4, 15.9, 14.3 ppm

Yield: 79 % (96 mg) as a white solid.

The spectroscopic data match those reported in literature.^[13] (CAS Number: 92330-45-5)

***N*-(1-methylundecyl)-benzenemethanamine hydrochloride (16)**

MW = 311.94 g/mol

¹H NMR (300 MHz, DMSO-*D*₆): δ = 9.44 (s, 1 H), 9.30 (s, 1 H), 7.67-7.64 (m, 2 H), 7.48-7.41 (m, 3 H), 4.17-4.12 (m, 2 H), 3.08 (s, 1 H), 1.91-1.79 (m, 1 H), 1.57-1.42 (m, 1 H), 1.33-1.26 (m, 19 H), 0.88 (m, 3 H) ppm

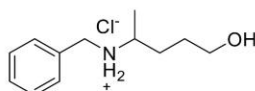
¹³C NMR (75 MHz, DMSO-*D*₆): δ = 132.2, 130.0, 128.7, 128.5, 52.9, 46.8, 31.8, 31.2, 28.9, 28.6, 24.7, 22.0, 15.4, 13.9 ppm

Yield: 79 % (123 mg) as a white solid.

The spectroscopic data match those reported in literature.^[13] (CAS Number: 1427378-88-8)

SUPPORTING INFORMATION

4-[(Phenylmethyl)amino]-1-pentanol hydrochloride (17)



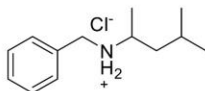
MW = 229.75 g/mol

¹H NMR (300 MHz, DMSO-D₆): δ = 9.51 (s, 1 H), 9.36 (s, 1 H), 7.66-7.63 (m, 2 H), 7.40-7.37 (m, 3 H), 4.90 (s, 2 H), 4.11 (s, 2 H), 3.43-3.38 (t, *J* = 6.2 Hz, 2 H), 1.98-1.88 (m, 1 H), 1.65-1.54 (d, *J* = 6.5 Hz, 3 H) ppm

¹³C NMR (75 MHz, DMSO-D₆): δ = 132.7, 130.5, 129.1, 128.9, 60.8, 53.7, 47.6, 29.5, 28.80, 16.1 ppm

Yield: 75 % (86 mg) as a white solid.

No spectroscopic data in the literature but known substrate. (CAS Number: 1514217-60-7)

N-(1,3-dimethylbutyl)-benzenemethanamine hydrochloride (18)

MW = 227.78 g/mol

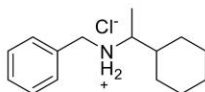
¹H NMR (300 MHz, DMSO-D₆): δ = 9.40 (s, 2 H), 7.68-7.65 (m, 2 H), 7.46-7.41 (m, 3 H), 4.15 (s, 2 H), 3.16-3.09 (m, 1 H), 1.31 (d, *J* = 6.5 Hz, 3 H), 1.70-1.65 (m, 2 H), 1.52-1.46 (m, 1 H), 0.91 (d, *J* = 9 Hz, 3 H), 0.81 (d, *J* = 9 Hz, 3 H) ppm

¹³C NMR (75 MHz, DMSO-D₆): δ = 132.8, 130.6, 129.2, 129.0, 51.9, 47.3, 24.5, 24.0, 21.4, 16.2 ppm

Yield: 75 % (85 mg) as a white solid.

The spectroscopic data match those reported in literature.^[14] (CAS Number: 2375135-37-6)

SUPPORTING INFORMATION

***N*-(1-cyclohexylethyl)-benzenemethanamine hydrochloride (19)**

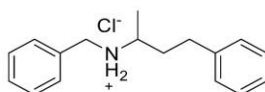
MW = 253.81 g/mol

¹H NMR (300 MHz, DMSO-*D*₆): δ = 9.57 (s, 1 H), 9.10 (s, 1 H), 7.71-7.68 (m, 2 H), 7.47-7.42 (m, 3 H), 4.19-4.12 (m, 2 H), 2.92 (s, 1 H), 1.82-1.53 (m, 6 H), 1.24-1.02 (m, 8 H), ppm

¹³C NMR (75 MHz, DMSO-*D*₆): δ = 132.5, 130.8, 129.3, 129.0, 57.5, 48.0, 29.7, 26.3, 26.2, 25.8, 12.1 ppm

Yield: 66 % (84 mg) as a white solid.

The spectroscopic data match those reported in literature.^[15] (CAS Number: 177721-69-6)

***α*-methyl-*N*-(phenylmethyl)-benzenepropanamine hydrochloride (20)**

MW = 275.82 g/mol

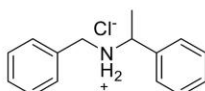
¹H NMR (300 MHz, DMSO-*D*₆): δ = 9.49 (d, *J* = 7.8 Hz, 2 H), 7.66-7.22 (m, 10 H), 4.156 (s, 2 H), 3.10 (s, 1 H), 2.76-2.57 (m, 2 H), 2.24-2.19 (m, 1 H), 1.89-1.85 (m, 1 H), 1.39 (d, *J* = 6.5 Hz, 3 H) ppm

¹³C NMR (75 MHz, DMSO-*D*₆): δ = 140.7, 132.2, 130.1, 128.7, 128.5, 128.4, 128.2, 126.0, 52.5, 46.8, 33.7, 30.8, 15.4 ppm

Yield: 68 % (94 mg) as a white solid.

The spectroscopic data match those reported in literature.^[16] (CAS Number: 1158736-70-9)

SUPPORTING INFORMATION

 α -methyl-*N*-(phenylmethyl)-benzenemethanamine hydrochloride (21)

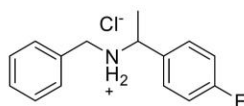
MW = 247.77 g/mol

^1H NMR (300 MHz, DMSO- D_6): δ = 10.48 (s, 1 H), 9.90 (s, 1 H), 7.69-7.39 (m, 10 H), 4.35 (s, 1 H), 3.99 (s, 1 H), 3.80 (s, 1 H), 1.68 (d, J = 6.4 Hz, 3 H) ppm

^{13}C NMR (75 MHz, DMSO- D_6): δ = 137.8, 132.4, 130.6, 129.4, 129.3, 129.2, 129.0, 128.5, 57.7, 48.8, 20.3 ppm

Yield: 78 % (97 mg) as a white solid.

The spectroscopic data match those reported in literature.^[17] (CAS Number: 49746-32-9)

4-fluoro- α -methyl-*N*-(phenylmethyl)-benzenepropanamine hydrochloride (22)

MW = 265.76 g/mol

^1H NMR (300 MHz, DMSO- D_6): δ = 10.42 (s, 1 H), 9.92 (s, 1 H), 7.77-7.72 (m, 2 H), 7.56-7.53 (m, 2 H), 7.42-7.28 (m, 5 H), 4.40 (s, 1 H), 4.00 (s, 1 H), 3.80 (s, 1 H), 1.67 (d, J = 6.5 Hz, 3 H) ppm

^{13}C NMR (75 MHz, DMSO- D_6): δ = 162.6 (d, $J_{\text{C-F}}$ = 245.1 Hz), 134.0, 134.0, 132.4, 130.9 (d, $J_{\text{C-F}}$ = 8.4 Hz), 130.6, 129.2, 129.0, 116.2 (d, $J_{\text{C-F}}$ = 8.4 Hz), 57.0, 48.7, 20.2 ppm

^{19}F NMR (376 MHz, DMSO- D_6): δ = -113.1 ppm

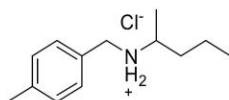
Yield: 81 % (108 mg) as a white solid.

The spectroscopic data match those reported in literature.^[18] (CAS Number: 820245-52-1)

WILEY-VCH

SUPPORTING INFORMATION

4-methyl-*N*-(1-methylbutyl)-benzenemethanamine hydrochloride (23)



MW = 227.78 g/mol

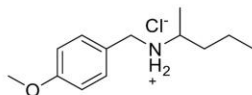
¹H NMR (300 MHz, DMSO-*D*₆): δ = 9.52 (s, 1 H), 9.38 (s, 1 H), 7.55 (d, *J* = 8.0 Hz, 2 H), 7.24 (d, *J* = 7.8 Hz, 2 H), 4.08 (s, 2 H), 3.04 (s, 1 H), 2.33 (s, 3 H), 1.87-1.77 (m, 1 H), 1.57-1.21 (m, 6 H), 0.88 (t, *J* = 7.3 Hz, 3 H) ppm

¹³C NMR (75 MHz, DMSO-*D*₆): δ = 138.6, 130.6, 129.6, 129.5, 52.9, 47.0, 34.4, 21.3, 18.7, 15.8, 14.2 ppm

Yield: 82 % (93 mg) as a white solid.

No spectroscopic data in the literature but known substrate. (CAS Number: 1020964-62-8)

4-methoxy-*N*-(1-methylbutyl)-benzenemethanamine hydrochloride (24)



MW = 243.78 g/mol

¹H NMR (300 MHz, DMSO-*D*₆): δ = 9.27 (s, 2 H), 7.59-7.56 (m, 2 H), 7.01-6.98 (m, 2 H), 4.08 (s, 2 H), 3.79 (s, 3 H), 3.06 (s, 1 H), 1.87-1.77 (m, 1 H), 1.56-1.21 (m, 6 H), 0.90 (t, *J* = 0.89 Hz, 3 H) ppm

¹³C NMR (75 MHz, DMSO-*D*₆): δ = 132.1, 124.5, 114.4, 55.7, 52.9, 46.8, 34.5, 18.7, 15.9, 14.2 ppm

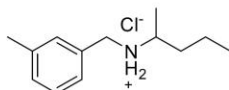
Yield: 81 % (84 mg) as a white solid.

No spectroscopic data in the literature but known substrate. (CAS Number: 1019472-43-5)

WILEY-VCH

SUPPORTING INFORMATION

3-methyl-*N*-(1-methylbutyl)-benzenemethanamine hydrochloride (25)



MW = 227.78 g/mol

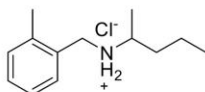
¹H NMR (300 MHz, DMSO-*D*₆): δ = 9.32 (s, 2 H), 7.47-7.22 (m, 4 H), 4.10 (s, 2 H), 3.09 (s, 1 H), 2.35 (s, 3 H), 1.87-1.78 (m, 1 H), 1.57-1.21 (m, 6 H), 0.90 (t, *J* = 6.8 Hz, 3 H) ppm

¹³C NMR (75 MHz, DMSO-*D*₆): δ = 138.3, 132.6, 131.1, 129.8, 129.0, 127.6, 53.3, 47.4, 34.5, 31.2, 21.4, 18.7, 16.0, 14.2 ppm

Yield: 77 % (88 mg) as a white solid.

No spectroscopic data in the literature but known substrate. (CAS Number: 1019491-23-6)

2-methyl-*N*-(1-methylbutyl)-benzenemethanamine hydrochloride (26)



MW = 227.78 g/mol

¹H NMR (300 MHz, DMSO-*D*₆): δ = 9.37 (d, *J* = 9.5 Hz, 2 H), 7.65-7.62 (m, 1 H), 7.30-7.22 (m, 3 H), 4.10 (t, *J* = 6.8 Hz, 2 H), 3.23 (s, 1 H), 2.40 (s, 3 H), 1.87-1.78 (m, 1 H), 1.57-1.21 (m, 6 H), 0.90 (t, *J* = 7.2 Hz, 3 H) ppm

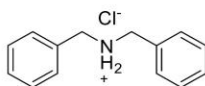
¹³C NMR (75 MHz, DMSO-*D*₆): δ = 138.0, 131.4, 131.3, 130.8, 129.3, 126.4, 54.3, 44.7, 19.7, 18.9, 15.9, 14.2 ppm

Yield: 69 % (79 mg) as a white solid.

No spectroscopic data in the literature but known substrate. (CAS Number: 1019545-40-4)

SUPPORTING INFORMATION

***N*-(phenylmethyl)-benzenemethanamine hydrochloride (27)**



MW = 233.74 g/mol

¹H NMR (300 MHz, DMSO-*D*₆): δ = 10.06 (s, 1 H), 7.63-7.41 (m, 10 H), 4.14-4.11 (m, 4 H) ppm

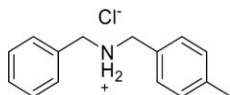
¹³C NMR (75 MHz, DMSO-*D*₆): δ = 132.4, 130.7, 129.3, 129.0, 50.0 ppm

¹⁹F NMR (376 MHz, DMSO-*D*₆): δ = -113.1 ppm

Yield: 91 % (106 mg) as a white solid.

The spectroscopic data match those reported in literature.^[19] (CAS Number: 20455-68-9)

4-methyl-*N*-(phenylmethyl)-benzenemethanamine hydrochloride (28)



MW = 247.77 g/mol

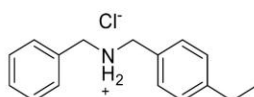
¹H NMR (300 MHz, DMSO-*D*₆): δ = 9.91 (s, 1 H), 7.62-7.24 (m, 9 H), 4.18-4.07 (m, 4 H), 2.34 (s, 3 H) ppm

¹³C NMR (75 MHz, DMSO-*D*₆): δ = 138.8, 138.2, 131.9, 131.4, 130.1, 129.1, 129.1, 129.0, 128.8, 128.5, 128.5, 126.8, 49.4, 49.3, 20.7 ppm

Yield: 89 % (110 mg) as a white solid.

The spectroscopic data match those reported in literature.^[17] (CAS Number: 1158274-26-0)

SUPPORTING INFORMATION

4-ethyl-*N*-(phenylmethyl)-benzenemethanamine hydrochloride (29)

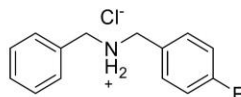
MW = 261.79 g/mol

¹H NMR (300 MHz, DMSO-*D*₆): δ = 9.93 (s, 1 H), 7.63-7.27 (m, 9 H), 4.13-4.09 (m, 4 H), 2.64 (q, *J* = 6.2 Hz, 2 H), 1.20 (t, *J* = 7.0 Hz, 3 H) ppm

¹³C NMR (75 MHz, DMSO-*D*₆): δ = 144.5, 131.9, 130.1, 129.1, 128.8, 128.5, 127.9, 127.8, 49.5, 49.3, 27.9, 15.6 ppm

Yield: 88 % (115 mg) as a white solid.

No spectroscopic data in the literature but known substrate. (CAS Number: 1158454-56-8)

4-fluor-*N*-(phenylmethyl)-benzenemethanamine hydrochloride (30)

MW = 251.73 g/mol

¹H NMR (300 MHz, DMSO-*D*₆): δ = 9.97 (s, 1 H), 7.70-7.60 (m, 4 H), 7.46-7.43 (m, 3 H), 7.31-7.26 (m, 2 H), 4.15 (q, *J* = 6.8 Hz, 4 H) ppm.

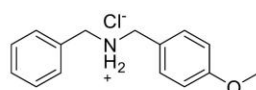
¹³C NMR (75 MHz, DMSO-*D*₆): δ = 162.8 (d, *J* = 245.1 Hz), 133.2, 132.4, 130.6, 129.3, 129.0, 116.0, 115.7, 50.1, 49.4 ppm.

¹⁹F NMR (376 MHz, DMSO-*D*₆): δ = -113.1 (dq, *J*₁ = 8.9 Hz, *J*₂ = 5.5 Hz) ppm

Yield: 84 % (106 mg) as a white solid.

The spectroscopic data match those reported in literature.^[17] (CAS Number: 55097-55-7)

SUPPORTING INFORMATION

4-methoxy-*N*-(phenylmethyl)-benzenemethanamine hydrochloride (31)

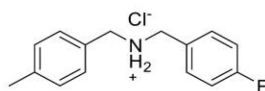
MW = 263.77 g/mol

¹H NMR (300 MHz, DMSO-*D*₆): δ = 9.81 (s, 1 H), 7.61-7.43 (m, 7 H), 7.01-6.98 (m, 2 H), 4.18-4.08 (m, 4 H), 3.80 (s, 3 H) ppm

¹³C NMR (75 MHz, DMSO-*D*₆): δ = 159.65, 133.04, 132.02, 131.82, 131.29, 130.17, 128.83, 128.73, 128.58, 123.67, 121.64, 113.91, 55.21, 49.35, 49.15 ppm

Yield: 85 % (106 mg) as a white solid.

Not all the protons of the amino group are visible due to the exchange of deuterium with the NMR solvent. The spectroscopic data match those reported in literature.^[17] (CAS Number: 58405-57-5)

4-fluoro-*N*-[(4-methyl)phenylmethyl]-benzenemethanamine hydrochloride (32)

MW = 265.76 g/mol

¹H NMR (300 MHz, DMSO-*D*₆): δ = 10.06 (s, 1 H), 7.73-7.68 (m, 2 H), 7.52 (d, *J* = 7.8 Hz, 2 H), 7.26-7.16 (m, 4 H), 4.11 (d, *J* = 6.8 Hz, 3 H) ppm

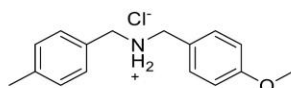
¹³C NMR (75 MHz, DMSO-*D*₆): δ = 163.6, 160.4, 137.8, 132.2, 132.1, 129.7, 128.7, 128.6, 128.4, 127.8, 115.0, 114.7, 49.0, 48.4, 20.3 ppm

¹⁹F NMR (376 MHz, DMSO-*D*₆): δ = -113.1 (m) ppm

Yield: 82 % (118 mg) as a white solid.

Not all the protons of the amino group are visible due to the exchange of deuterium with the NMR solvent. The spectroscopic data match those reported in literature.^[20] (CAS Number: 774554-55-1)

SUPPORTING INFORMATION

4-methoxy-*N*-[(4-methyl]phenylmethyl)-benzenemethanamine hydrochloride (33)

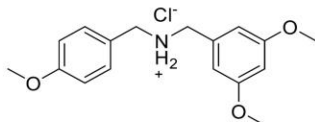
MW = 277.79 g/mol

¹H NMR (300 MHz, DMSO-*D*₆): δ = 10.00 (s, 1 H), 7.63-7.50 (m, 4 H), 7.22 (d, *J* = 7.8 Hz, 2 H), 6.99-6.94 (m, 2 H), 4.15 (s, 2 H), 4.06 (s, 2 H), 3.80 (s, 3 H), 2.34 (s, 3 H) ppm

¹³C NMR (75 MHz, DMSO-*D*₆): δ = 159.4, 137.7, 132.5, 131.3, 130.8, 129.7, 128.7, 128.6, 128.5, 123.4, 113.7, 113.6, 55.2, 54.9, 48.8, 20.3 ppm

Yield: 81 % (112 mg) as a white solid.

Not all the protons of the amino group are visible due to the exchange of deuterium with the NMR solvent. The spectroscopic data match those reported in literature.^[21] (CAS Number: 1158430-76-2)

3,5-dimethoxy-*N*-[(4-methoxy]phenylmethyl)-benzenemethanamine hydrochloride (34)

MW = 323.82 g/mol

¹H NMR (300 MHz, DMSO-*D*₆): δ = 9.85 (s, 1 H), 7.54-7.51 (m, 2 H), 7.01-6.98 (m, 2 H), 6.84 (d, *J* = 6.8 Hz, 2 H), 6.54-6.53 (t, *J* = 6.6 Hz, 1 H), 4.04 (s, 4 H), 3.80-3.77 (m, 9 H) ppm

¹³C NMR (75 MHz, DMSO-*D*₆): δ = 160.4, 159.6, 134.0, 131.8, 123.6, 113.8, 107.8, 100.5, 55.4, 55.3, 55.1, 49.3, 49.0 ppm

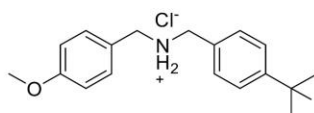
Yield: 78 % (126 mg) as a white solid.

The spectroscopic data match those reported in literature.^[22] (CAS Number: 356093-54-4)

WILEY-VCH

SUPPORTING INFORMATION

4-tertbutyl-N-[(4-methoxy]phenylmethyl)-benzenemethanamine hydrochloride (35)



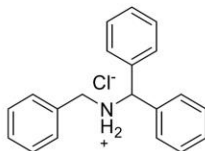
MW = 319.87 g/mol

¹H NMR (300 MHz, DMSO-D₆): δ = 9.75 (s, 1 H), 7.52-7.41 (m, 6 H), 6.99-6.93 (m, 2 H), 4.15-4.00 (m, 4 H), 3.76 (s, 3 H), 1.27 (s, 9 H) ppm

¹³C NMR (75 MHz, DMSO-D₆): δ = 160.1, 151.8, 132.2, 130.4, 129.5, 125.8, 124.1, 114.4, 55.7, 49.7, 49.5, 34.9, 31.5 ppm

Yield: 74 % (123 mg) as a white solid.

The spectroscopic data match those reported in literature.^[23] (CAS Number: 2245774-03-0)

α-phenyl-N-(phenylmethyl)-benzenepropanamine hydrochloride (36)

MW = 309.84 g/mol

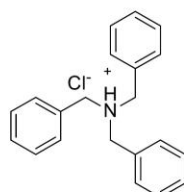
¹H NMR (300 MHz, DMSO-D₆): δ = 10.62 (s, 2 H), 7.72 (d, *J* = 7.4 Hz, 4 H), 7.46-7.31 (m, 11 H), 5.46 (s, 1 H), 4.09-4.00 (m, 2 H) ppm

¹³C NMR (75 MHz, DMSO-D₆): δ = 137.2, 131.7, 131.0, 129.4, 129.1, 129.0, 128.5, 65.1, 49.8 ppm

Yield: 79 % (122 mg) as a white solid.

Not all the protons of the amino group are visible due to the exchange of deuterium with the NMR solvent. The spectroscopic data match those reported in literature.^[17] (CAS Number: 23934-60-3)

SUPPORTING INFORMATION

***N,N*-bis(phenylmethyl)-benzenemethanamine hydrochloride (37)**

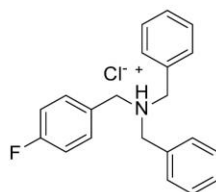
MW = 323.86 g/mol

¹H NMR (300 MHz, CDCl₃): δ = 11.53 (s, 1 H), 7.62-7.61 (m, 6 H), 7.43-7.42 (m, 9 H) 4.20-4.19 (d, *J* = 7.5 Hz, 6 H) ppm

¹³C NMR (75 MHz, CDCl₃): δ = 131.4, 129.9, 129.4, 128.8, 56.0 ppm

Yield: 73 % (118 mg) as a white solid.

The spectroscopic data match those reported in literature.^[24] (CAS Number: 7673-07-6)

4-fluoro-*N,N*-bis(phenylmethyl)-benzenemethanamine hydrochloride (38)

MW = 341.85 g/mol

¹H NMR (300 MHz, DMSO-*d*₆): δ = 11.82 (s, 1 H), 7.67 (d, *J* = 32 Hz, 6 H), 7.41 (s, 6 H), 7.23 (t, *J* = 7.8 Hz, 2 H), 4.25-4.22 (m, 6 H) ppm

¹³C NMR (75 MHz, DMSO-*d*₆): δ = 163.0 (d, *J* = 246.5 Hz), 134.5, 134.3, 131.9, 130.5, 129.8, 129.1, 126.8, 126.8, 116.1, 115.8, 56.7, 56.0 ppm

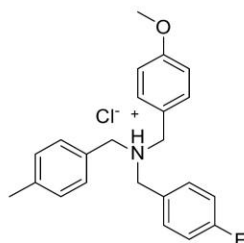
¹⁹F NMR (376 MHz, DMSO-*d*₆): δ = -112.2 ppm

Yield: 77 % (132 mg) as a white solid.

The spectroscopic data match those reported in literature.^[25] (CAS Number: 359445-99-1)

WILEY-VCH

SUPPORTING INFORMATION

***N*-(4-fluorobenzyl)-*N*-(4-methoxybenzyl)-1-(*p*-tolyl)methanamine hydrochloride (39)**

MW = 385.91 g/mol

¹H NMR (300 MHz, DMSO-*D*₆): δ = 11.30 (s, 1 H), 7.68-6.95 (m, 12 H), 4.22-4.13 (m, 6 H), 3.77 (s, 3 H), 2.3 (s, 3 H) ppm

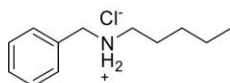
¹³C NMR (75 MHz, DMSO-*D*₆): δ = 164.6, 160.9 (d, *J* = 72.8 Hz), 139.3, 134.3, 134.3, 134.2, 133.5, 131.9, 131.8, 129.8, 127.4, 126.8, 122.0, 116.2, 115.9, 114.5, 56.5, 56.1, 55.7, 55.4, 21.3 ppm

¹⁹F NMR (376 MHz, DMSO-*D*₆): δ = -112.2 ppm

HRMS (ESI⁺) Calculated for C₂₃H₂₅OFN: 350.1915; found: 350.1904

Yield: 65 % (125 mg) as a colorless oil.

Unknown substrate with incomplete spectroscopic literature data was additionally analyzed via LC-HRMS.

***N*-pentyl-benzenemethanamine hydrochloride (40)**

MW = 199.72 g/mol

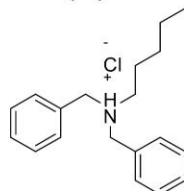
¹H NMR (300 MHz, DMSO-*D*₆): δ = 9.46 (s, 2H), 7.63 – 7.54 (m, 2H), 7.45 – 7.36 (m, 3H), 4.09 (s, 2H), 2.80 (dd, *J* = 18.0, 9.9 Hz, 2H), 1.70 – 1.54 (m, 2H), 1.26 (d, *J* = 4.0 Hz, 2H), 0.88 – 0.83 (m, 3H) ppm

¹³C NMR (75 MHz, DMSO-*D*₆): δ = 132.6, 130.6, 129.3, 129.0, 50.2, 46.8, 28.6, 25.3, 22.1, 14.2 ppm

Yield: 88 % (89 mg) as a white solid.

The spectroscopic data match those reported in literature.^[17] (CAS Number: 90389-36-9)

SUPPORTING INFORMATION

***N,N*-dibenzylpentan-1-aminium chloride (41)**

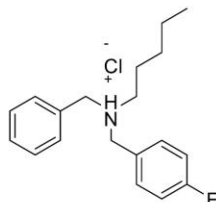
MW = 303.87 g/mol

¹H NMR (300 MHz, DMSO-*D*₆): δ = 11.60 (s, 1 H), 7.76-7.41 (m, 10 H), 4.33-4.12 (m, 4 H), 2.85-2.81 (m, 2 H), 1.78-1.73 (m, 2 H), 1.29-1.09 (m, 4 H), 0.81 (m, 3 H) ppm

¹³C NMR (75 MHz, DMSO-*D*₆): δ = 131.9, 130.6, 129.8, 129.2, 56.4, 51.3, 28.7, 22.5, 21.9, 14.1 ppm

Yield: 67 % (102 mg) as a colorless oil.

Not all the protons of the amino group are visible due to the exchange of deuterium with the NMR solvent. The spectroscopic data match those reported in literature.^[25] (CAS Number: 79865-95-5)

***N*-benzyl-*N*-(4-fluorobenzyl)pentan-1-aminium chloride (42)**

MW = 321.86 g/mol

¹H NMR (300 MHz, DMSO-*D*₆): δ = 11.55 (s, 1 H), 7.79-7.68 (m, 4 H), 7.42-7.40 (m, 2 H), 7.25 (td, *J*₁ = 8.8 Hz, *J*₂ = 1.7 Hz, 3 H), 4.30-4.24 (m, 4 H), 2.80-2.77 (m, 2 H), 1.73-1.69 (m, 2 H), 1.18-1.04 (m, 4 H), 0.78-0.75 (m, 3 H) ppm

¹³C NMR (75 MHz, DMSO-*D*₆): δ = 164.2, 161.8, 134.3, 134.2, 130.6, 129.7, 129.1, 126.9, 126.9, 116.1, 115.9, 56.3, 55.6, 51.2, 28.7, 22.5, 21.9, 14.1 ppm

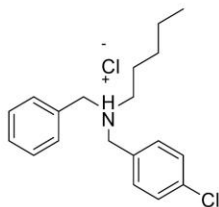
¹⁹F NMR (376 MHz, DMSO-*D*₆): δ = -112.1 (m) ppm

HRMS (ESI⁺) Calculated for C₁₉H₂₅FN: 286.1966; found: 286.1954

Yield: 60 % (96 mg) as a colorless oil.

Not all the protons of the amino group are visible due to the exchange of deuterium with the NMR solvent. Unknown substrate with incomplete spectroscopic literature data was additionally analyzed via LC-HRMS.

SUPPORTING INFORMATION

***N*-benzyl-*N*-(4-chlorobenzyl)pentan-1-aminium chloride (43)**

MW = 338.32 g/mol

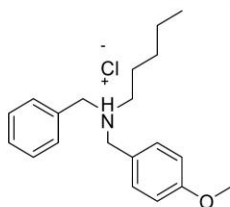
¹H NMR (300 MHz, DMSO-*D*₆): δ = 11.72 (s, 1 H), 7.78-7.46 (m, 9 H), 4.34-4.28 (m, 4 H), 2.96-2.82 (m, 2 H), 1.81-1.73 (m, 2 H), 1.25-1.09 (m, 4 H), 0.87-0.79 (m, 3 H) ppm

¹³C NMR (75 MHz, DMSO-*D*₆): δ = 134.1, 133.3, 131.3, 130.0, 129.1, 129.0, 128.6, 128.6, 55.0, 50.8, 28.1, 22.0, 21.4, 13.5 ppm

HRMS (ESI⁺) Calculated for C₁₉H₂₅ClN: 302.1670; found: 302.1658

Yield: 67 % (105 mg) as a colorless oil.

Not all the protons of the amino group are visible due to the exchange of deuterium with the NMR solvent. Unknown substrate with incomplete spectroscopic literature data was additionally analyzed via LC-HRMS.

***N*-benzyl-*N*-(4-methoxybenzyl)pentan-1-aminium chloride (44)**

MW = 333.90 g/mol

¹H NMR (300 MHz, DMSO-*D*₆): δ = 11.45 (d, *J* = 60.4 Hz, 1H), 7.73 (s, 1H), 7.63 (d, *J* = 8.2 Hz, 3H), 7.41 (s, 1H), 6.96 (d, *J* = 8.3 Hz, 4H), 4.21 (dd, *J* = 18.0, 6.8 Hz, 4H), 3.76 (s, 3H), 2.76 (s, 2H), 1.71 (s, 2H), 1.14 (d, *J* = 6.7 Hz, 2H), 1.06 (d, *J* = 6.5 Hz, 2H), 0.77 (dd, *J* = 9.3, 4.8 Hz, 3H) ppm

¹³C NMR (75 MHz, DMSO-*D*₆): δ = 159.8, 132.9, 131.3, 130.3, 129.2, 128.7, 121.8, 114.0, 55.2, 55.1, 50.4, 50.0, 28.3, 22.1, 21.5, 13.6 ppm

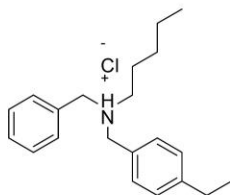
HRMS (ESI⁺) Calculated for C₂₀H₂₈NO: 298.2165; found: 298.2153

Yield: 61 % (97 mg) as a colorless oil.

Unknown substrate with incomplete spectroscopic literature data was additionally analyzed via LC-HRMS.

SUPPORTING INFORMATION

***N*-benzyl-*N*-(4-ethylbenzyl)pentan-1-aminium chloride (45)**



MW = 331.91 g/mol

¹H NMR (300 MHz, DMSO-*D*₆): δ = 11.42 (s, 1 H), 7.76-7.17 (m, 9 H), 4.31-4.17 (m, 4 H), 2.83-2.80 (m, 2 H), 2.67-2.60 (m, 4 H), 1.80-1.75 (m, 2 H), 1.22-1.09 (m, 5 H), 0.80 (t, *J* = 7.1 Hz, 3 H) ppm

¹³C NMR (75 MHz, DMSO-*D*₆): δ = 145.5, 131.9, 130.7, 129.2, 128.6, 128.5, 127.8, 127.8, 56.1, 51.1, 28.7, 28.4, 22.6, 21.9, 15.8, 14.1 ppm

HRMS (ESI⁺) Calculated for C₂₁H₃₀N: 296.2373; found: 296.2361

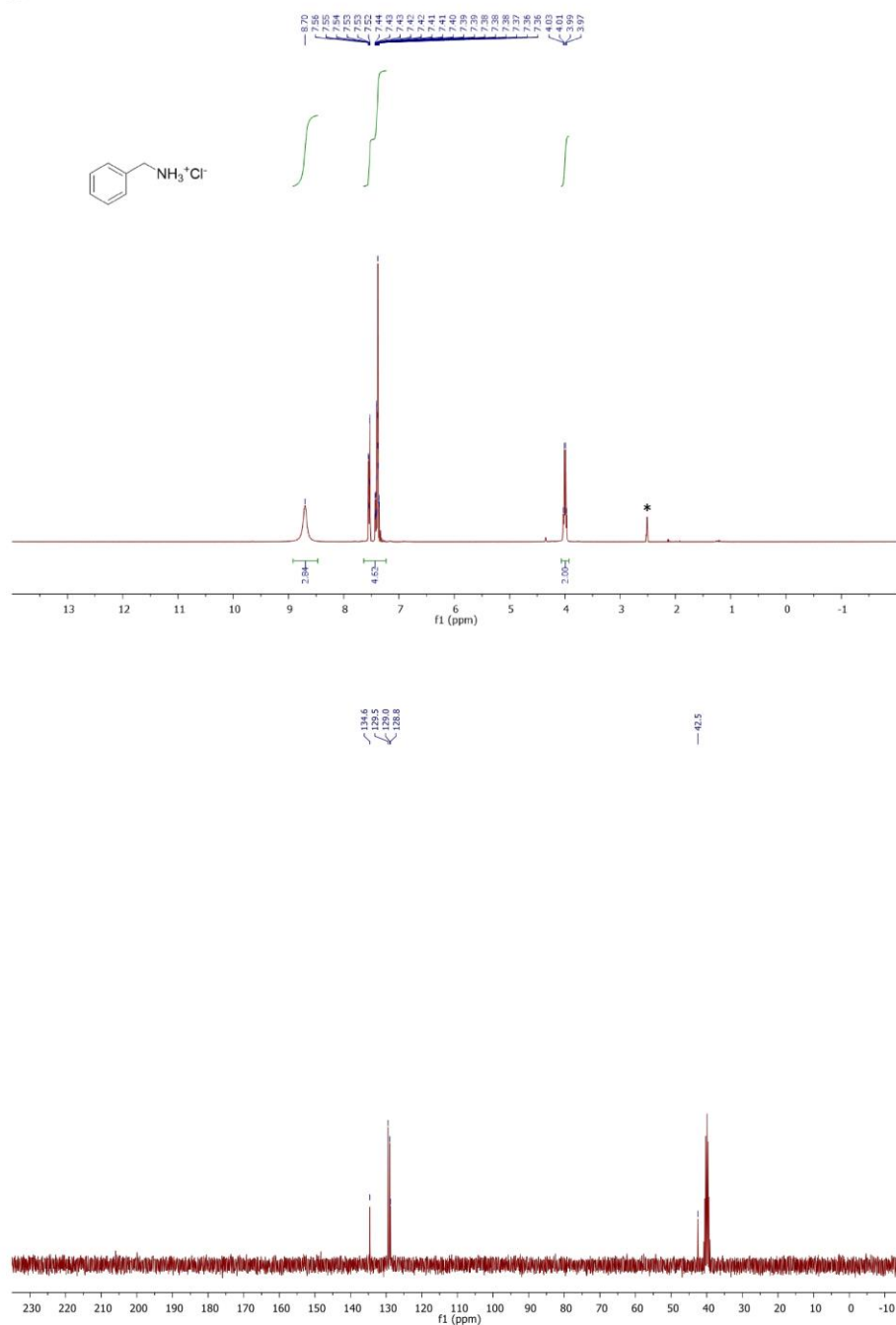
Yield: 58 % (91 mg) as a colorless oil.

Unknown substrate with incomplete spectroscopic literature data was additionally analyzed via LC-HRMS.

SUPPORTING INFORMATION

5. NMR and IR spectra

1:

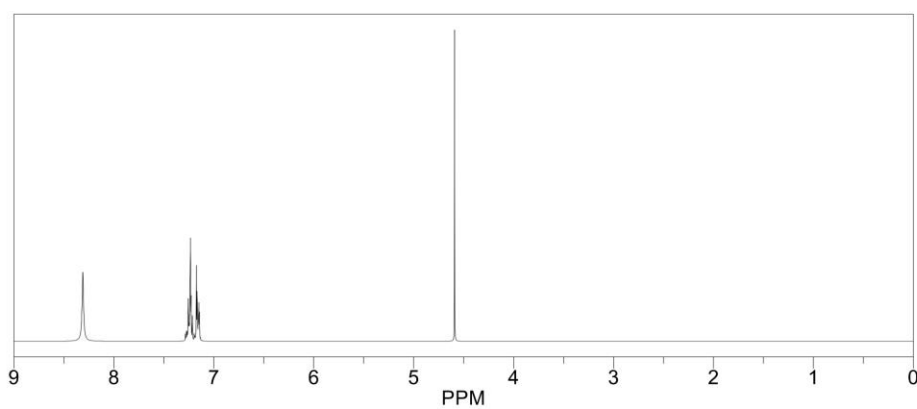


SUPPORTING INFORMATION

ChemNMR ^1H Estimation



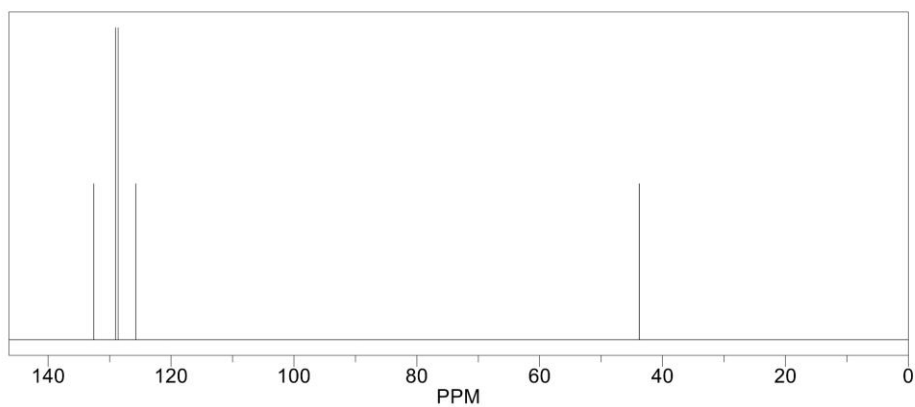
Estimation quality is indicated by color: good, medium, rough



ChemNMR ^{13}C Estimation



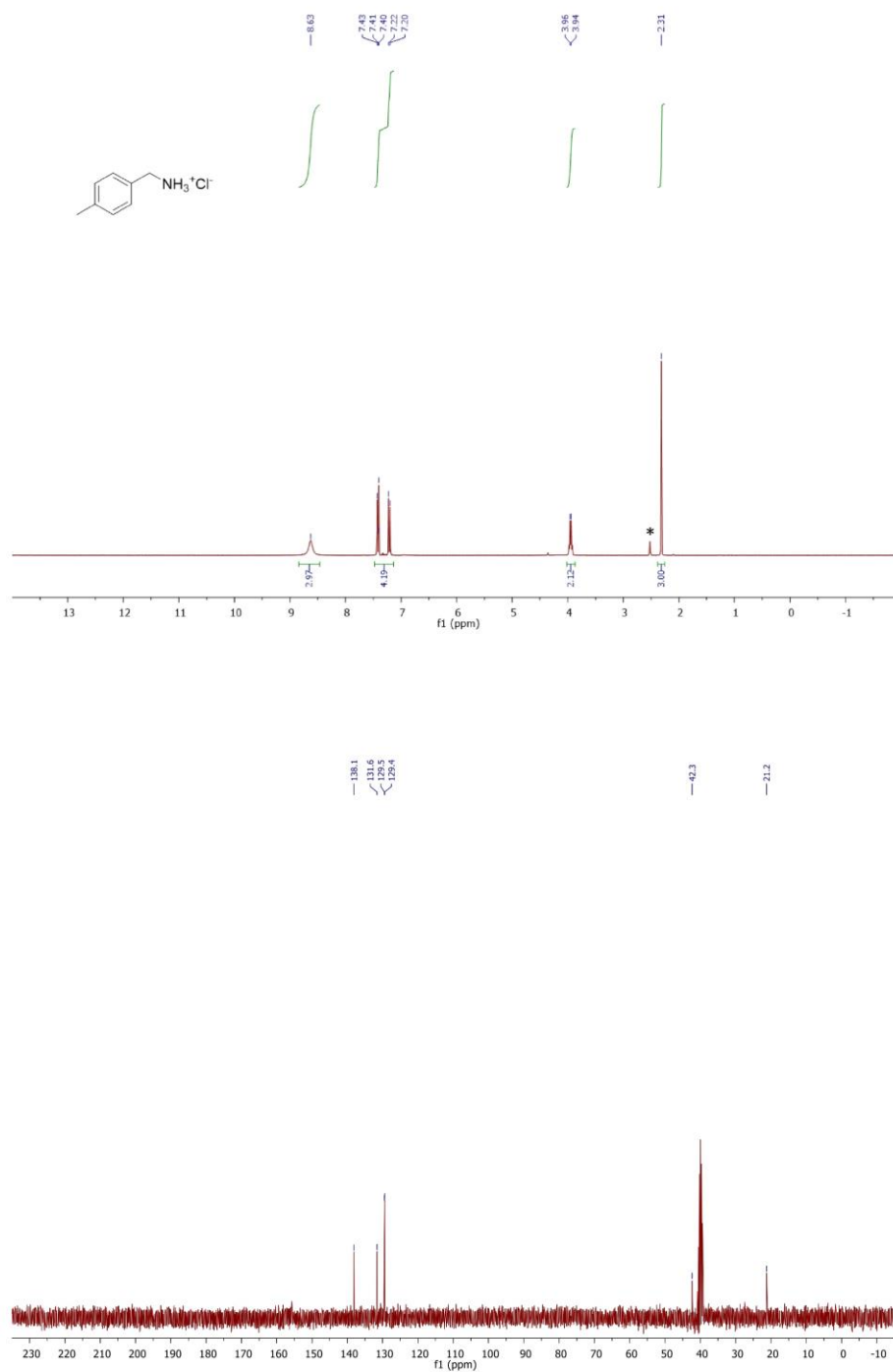
Estimation quality is indicated by color: good, medium, rough



WILEY-VCH

SUPPORTING INFORMATION

2:

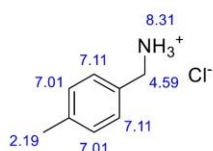


39

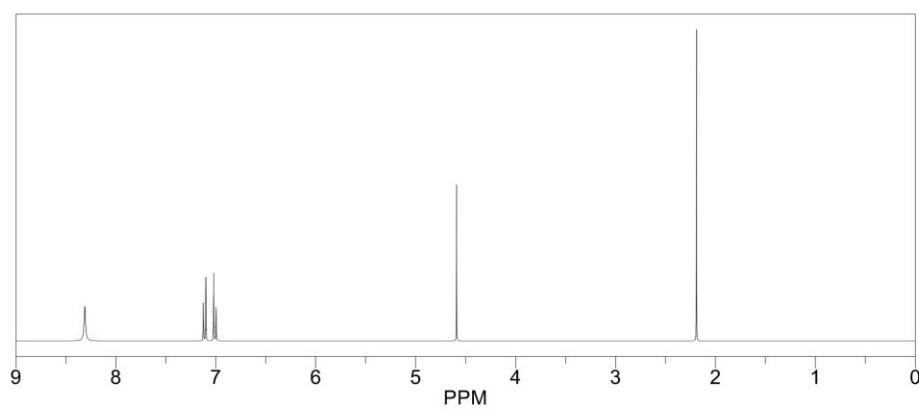
WILEY-VCH

SUPPORTING INFORMATION

ChemNMR ^1H Estimation



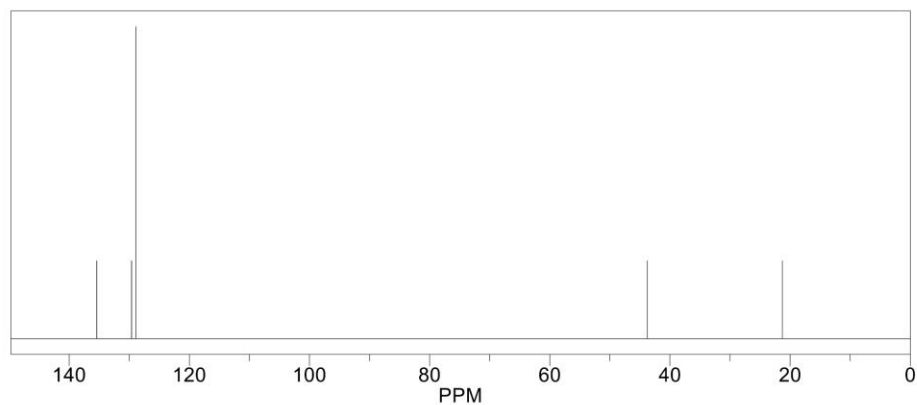
Estimation quality is indicated by color: good, medium, rough



ChemNMR ^{13}C Estimation



Estimation quality is indicated by color: good, medium, rough

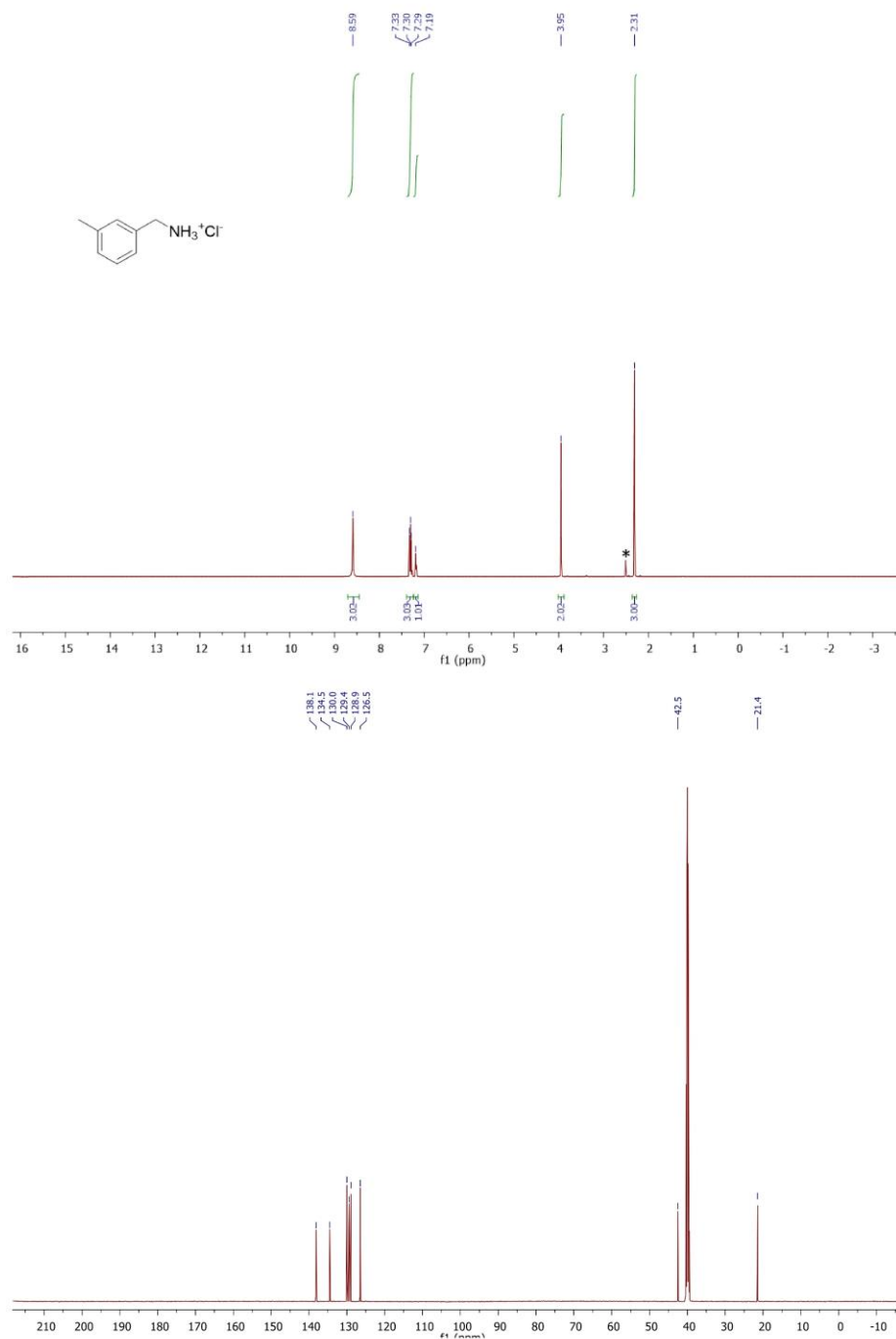


40

WILEY-VCH

SUPPORTING INFORMATION

3:



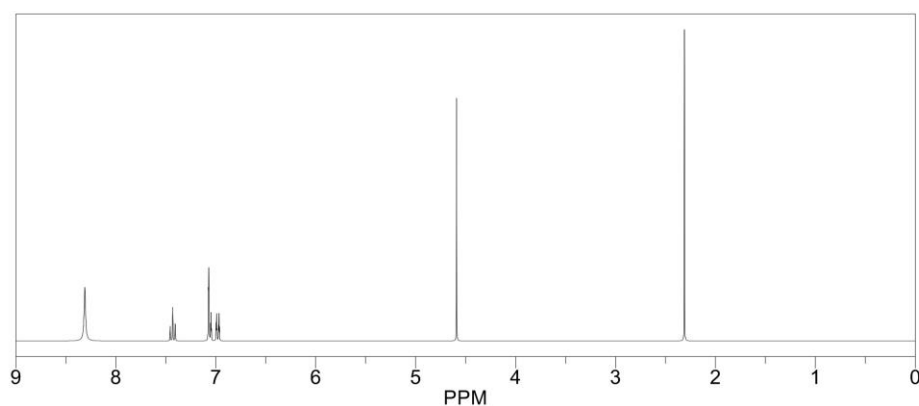
WILEY-VCH

SUPPORTING INFORMATION

ChemNMR ^1H Estimation



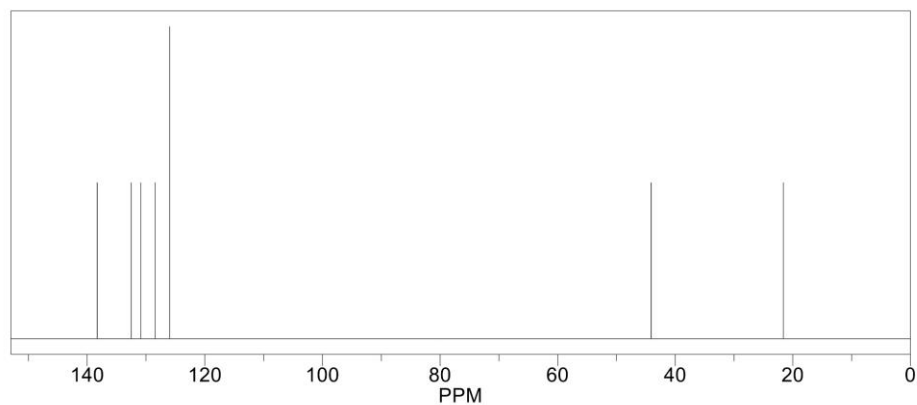
Estimation quality is indicated by color: good, medium, rough



ChemNMR ^{13}C Estimation



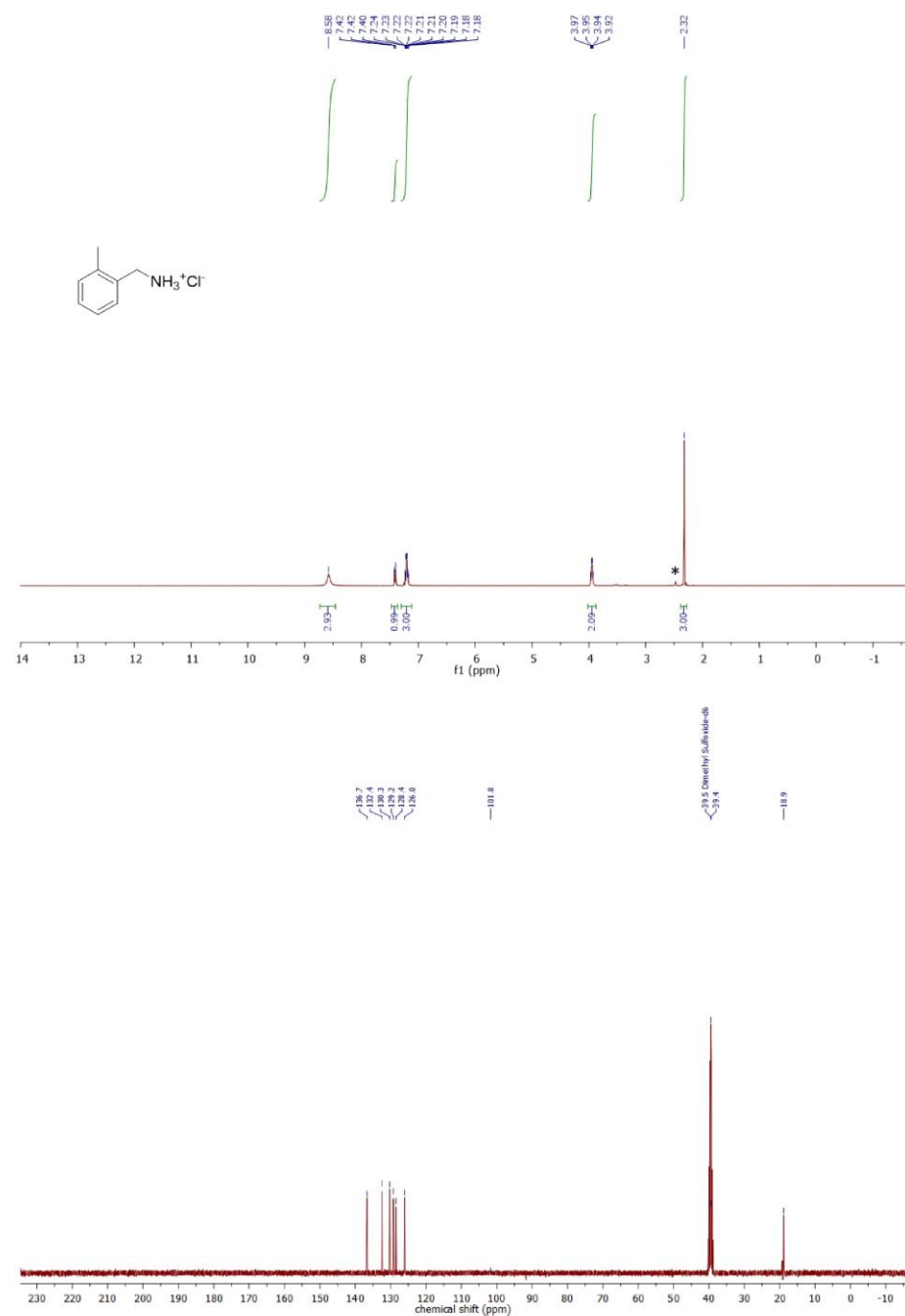
Estimation quality is indicated by color: good, medium, rough



WILEY-VCH

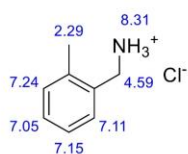
SUPPORTING INFORMATION

4:

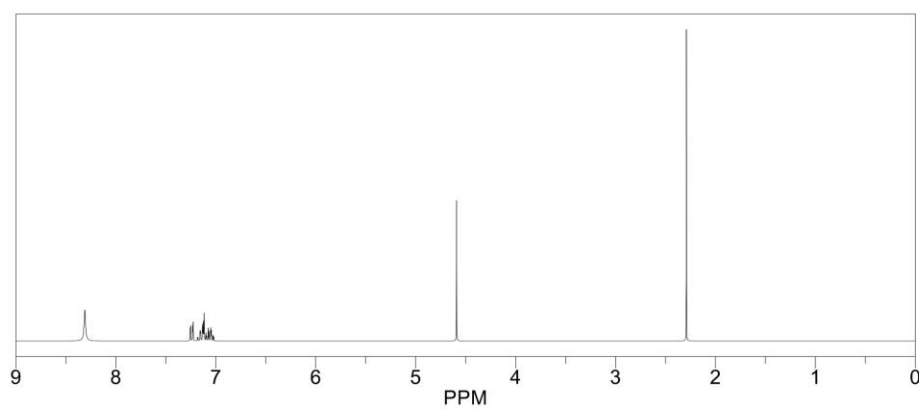


SUPPORTING INFORMATION

ChemNMR ^1H Estimation



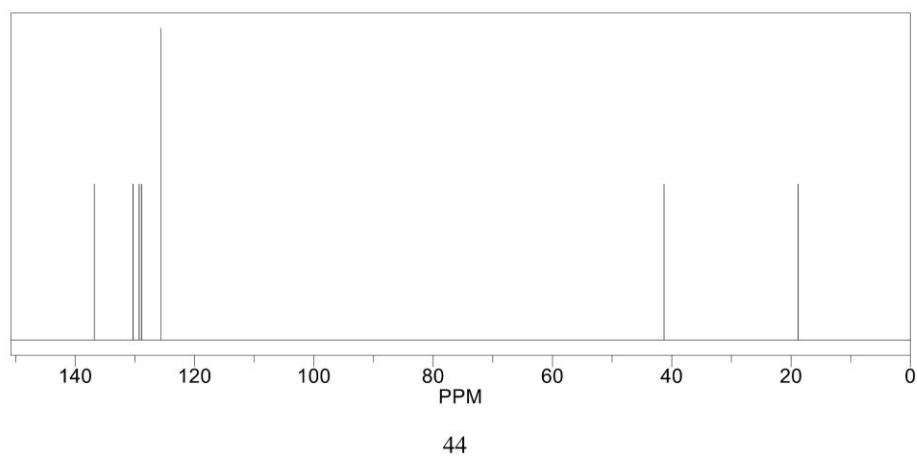
Estimation quality is indicated by color: good, medium, rough



ChemNMR ^{13}C Estimation



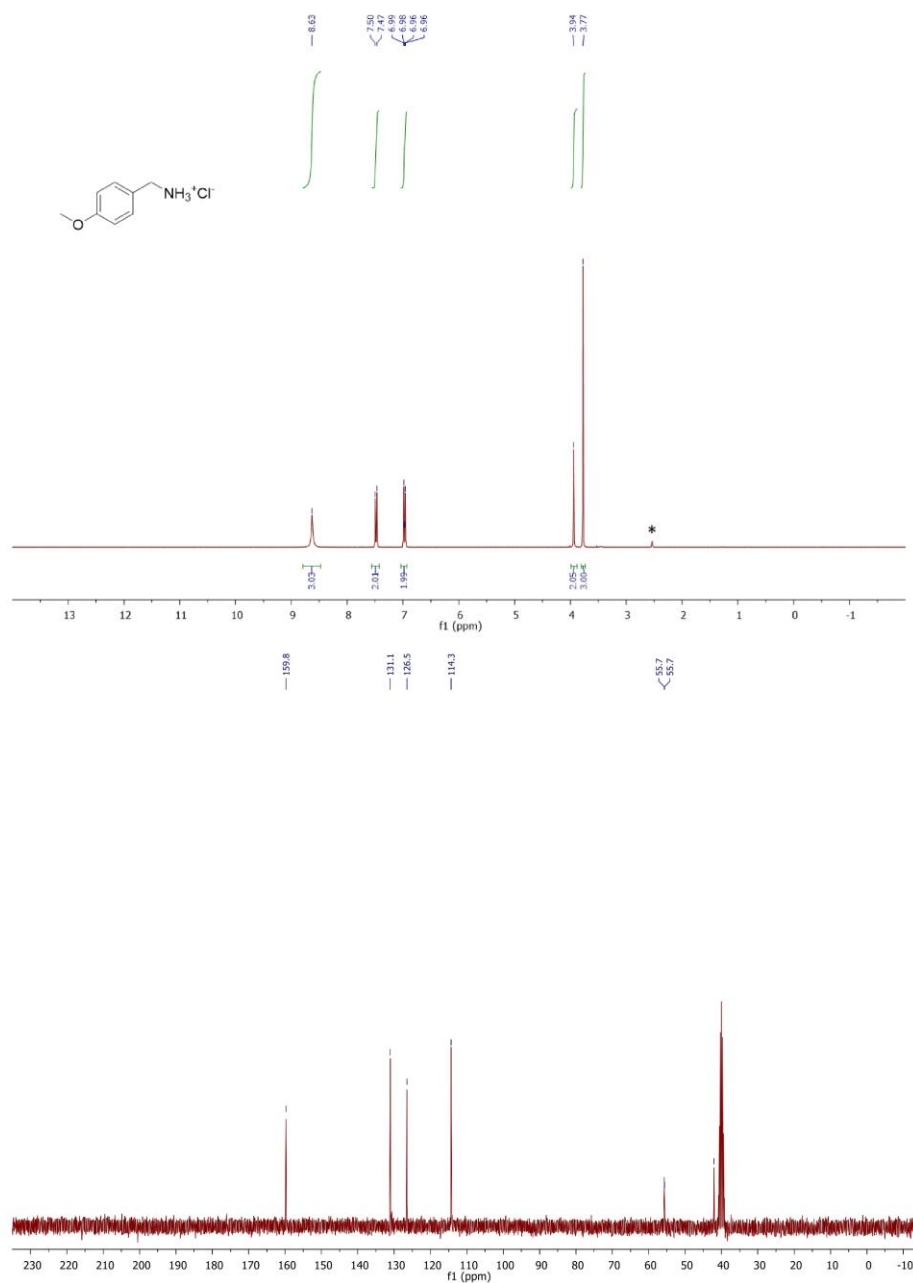
Estimation quality is indicated by color: good, medium, rough



WILEY-VCH

SUPPORTING INFORMATION

5:

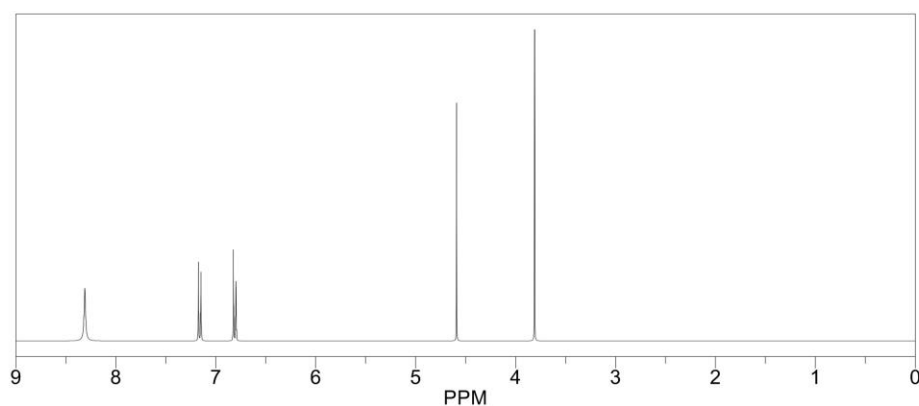


SUPPORTING INFORMATION

ChemNMR ^1H Estimation



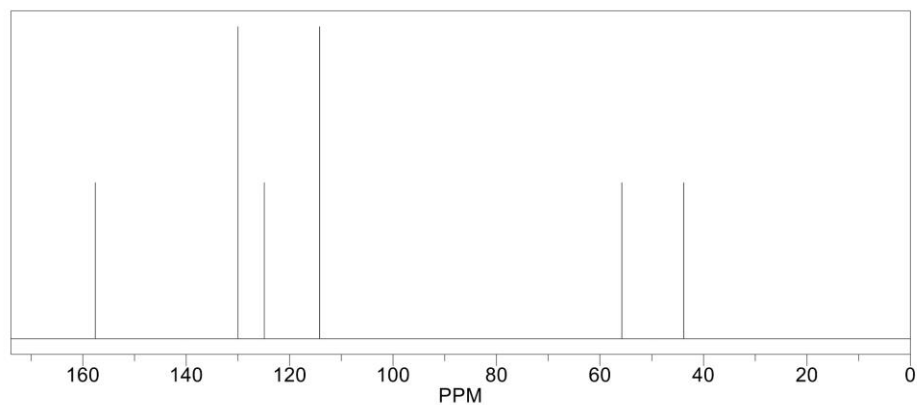
Estimation quality is indicated by color: good, medium, rough



ChemNMR ^{13}C Estimation



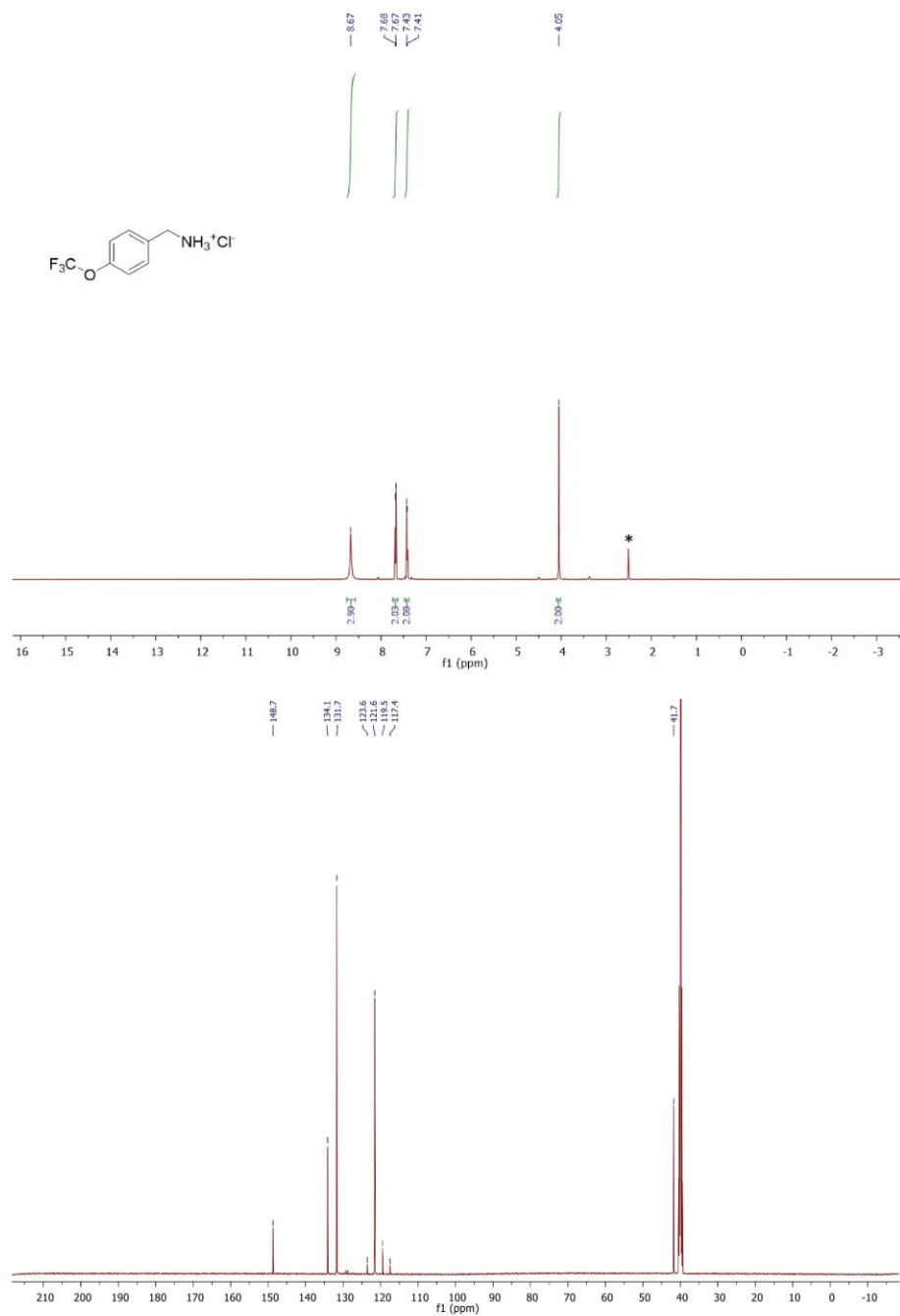
Estimation quality is indicated by color: good, medium, rough



WILEY-VCH

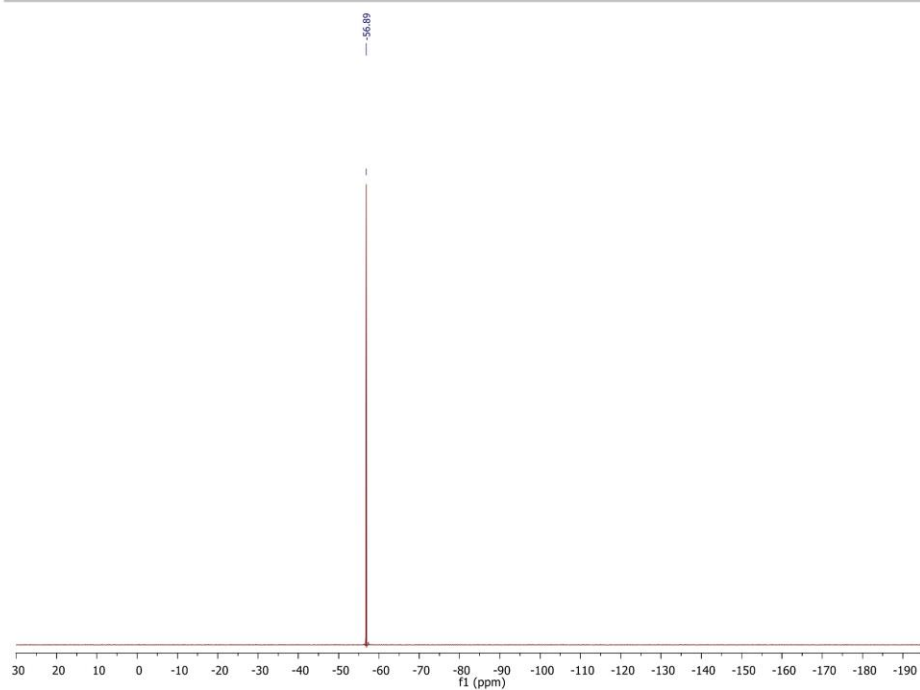
SUPPORTING INFORMATION

6:



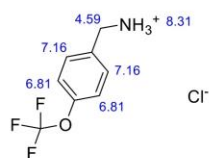
WILEY-VCH

SUPPORTING INFORMATION

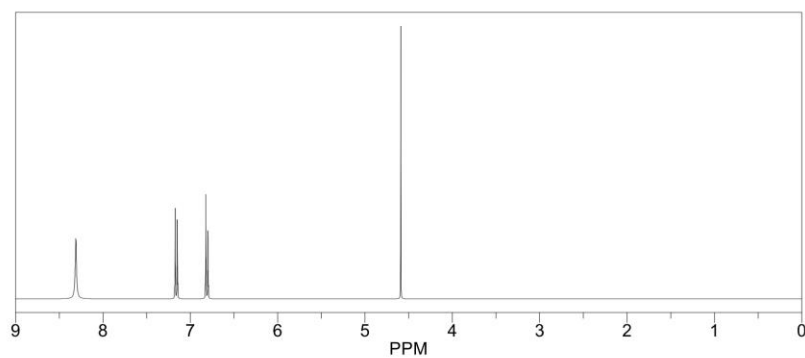


SUPPORTING INFORMATION

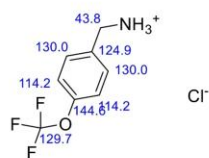
ChemNMR ^1H Estimation



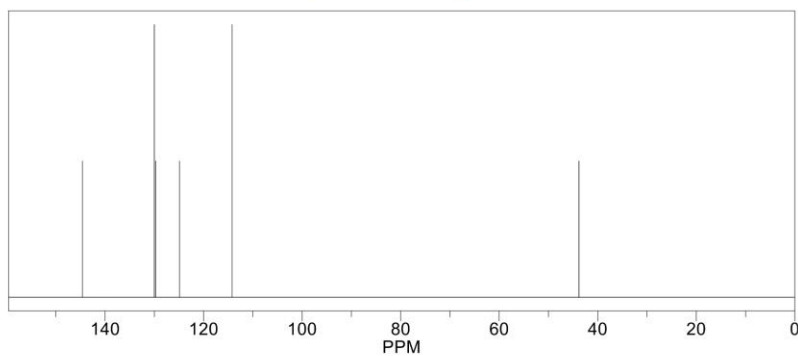
Estimation quality is indicated by color: good, medium, rough



ChemNMR ^{13}C Estimation



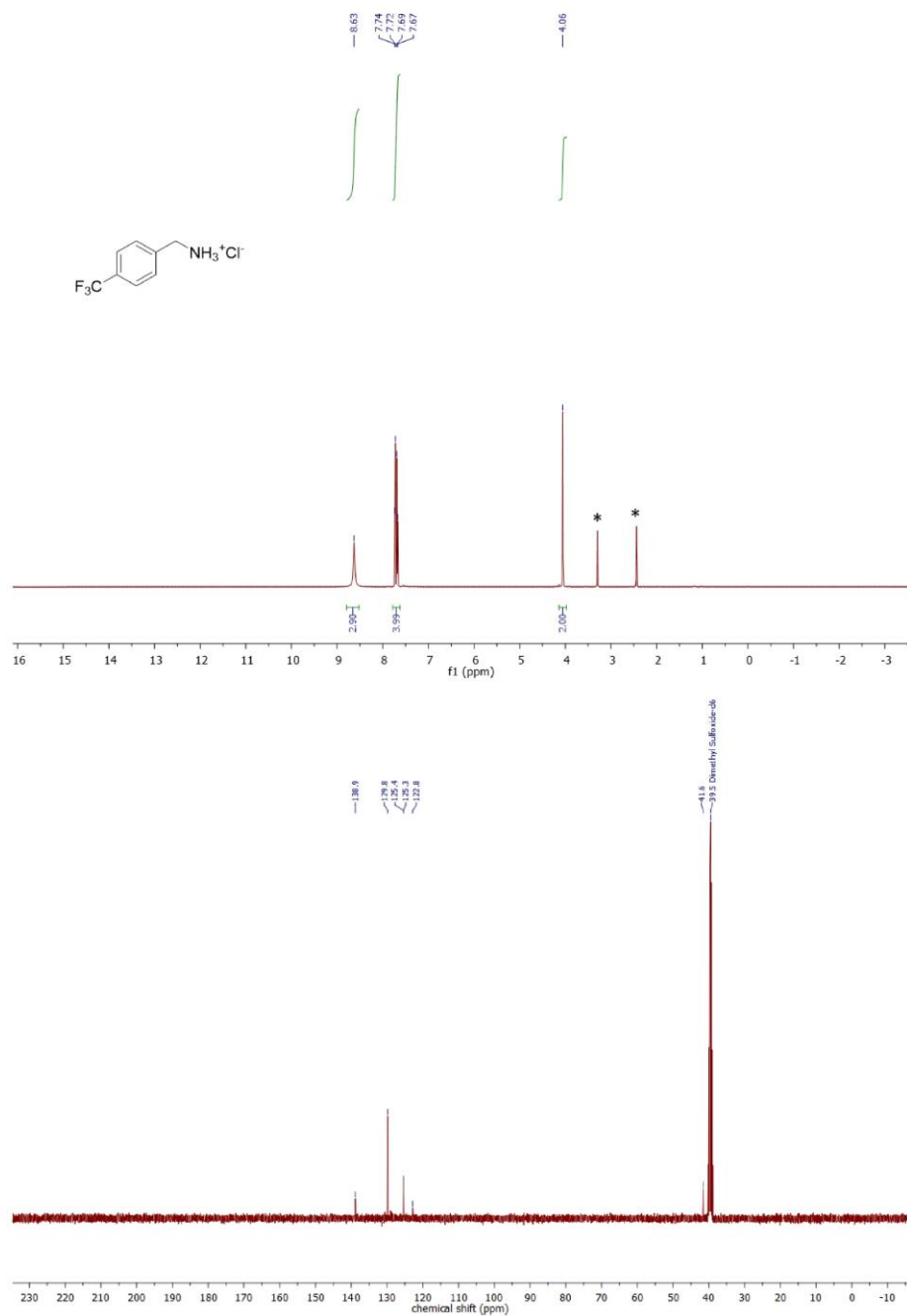
Estimation quality is indicated by color: good, medium, rough



WILEY-VCH

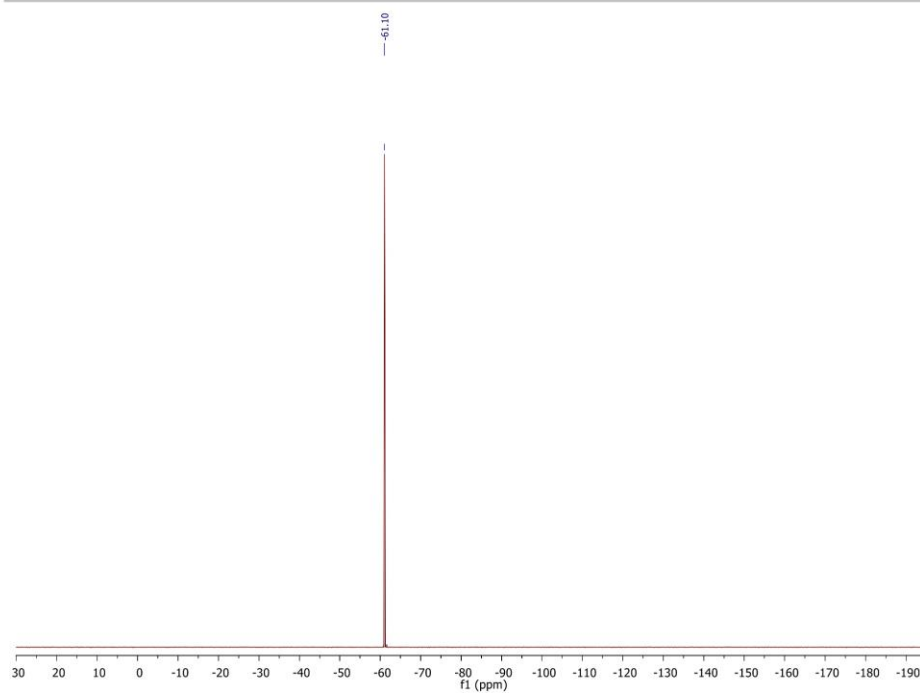
SUPPORTING INFORMATION

7:



WILEY-VCH

SUPPORTING INFORMATION

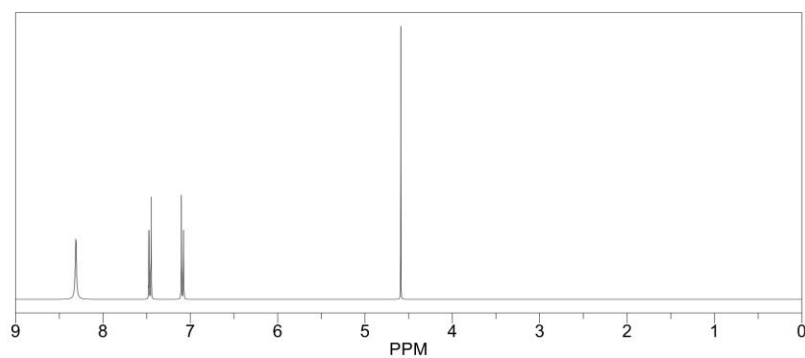


SUPPORTING INFORMATION

ChemNMR ^1H Estimation



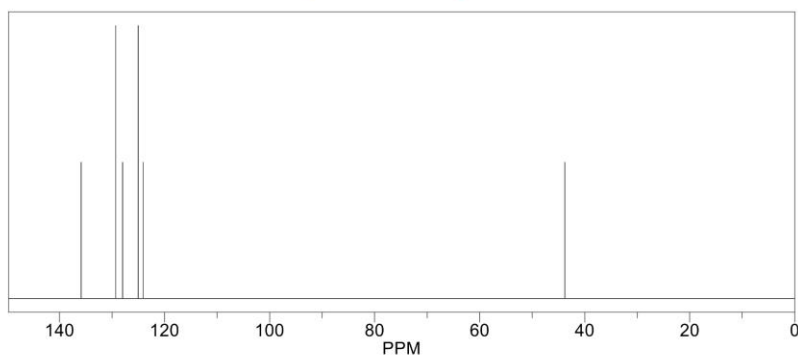
Estimation quality is indicated by color: good, medium, rough



ChemNMR ^{13}C Estimation



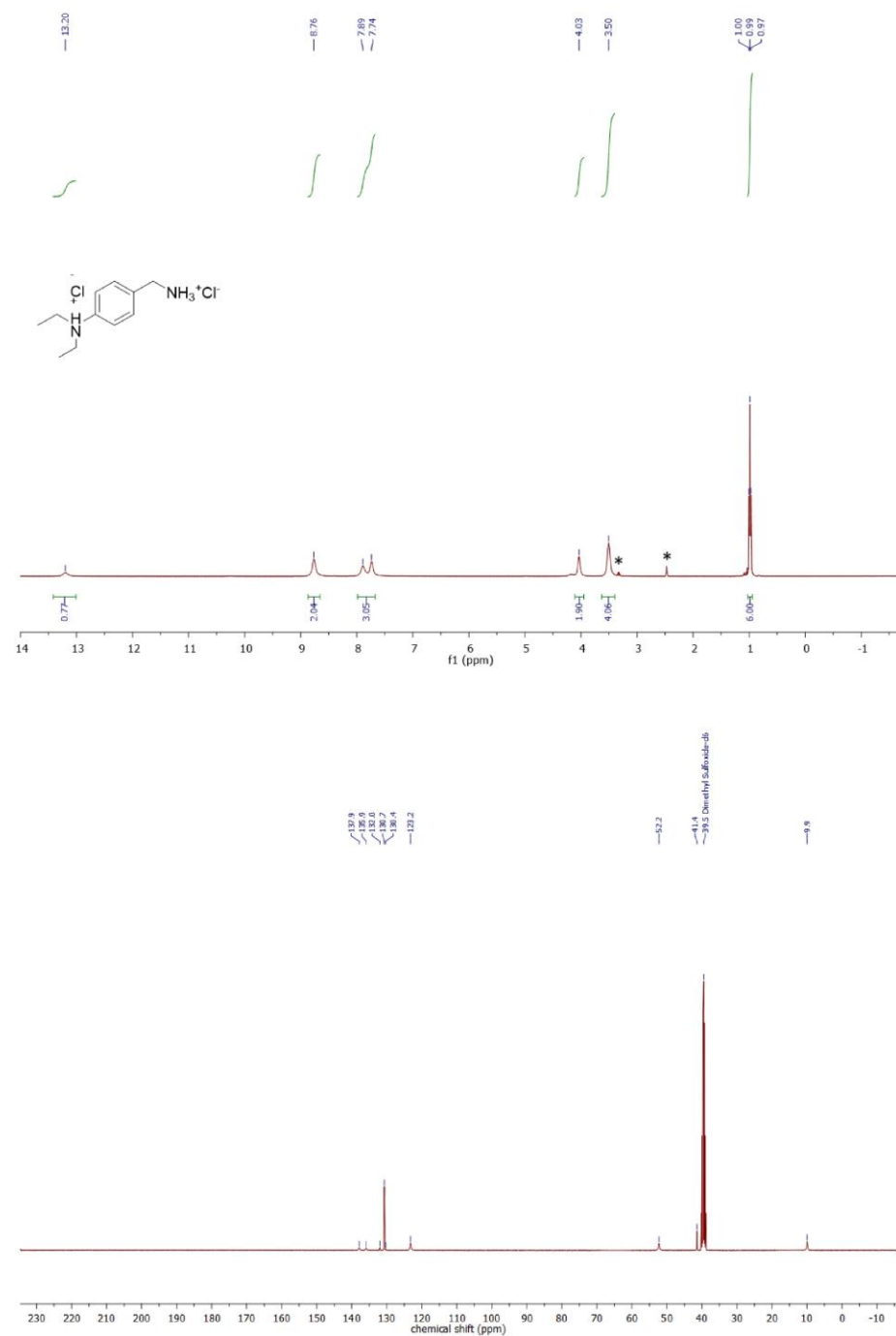
Estimation quality is indicated by color: good, medium, rough



WILEY-VCH

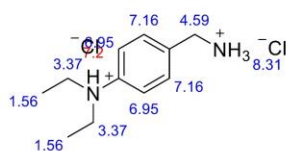
SUPPORTING INFORMATION

8:

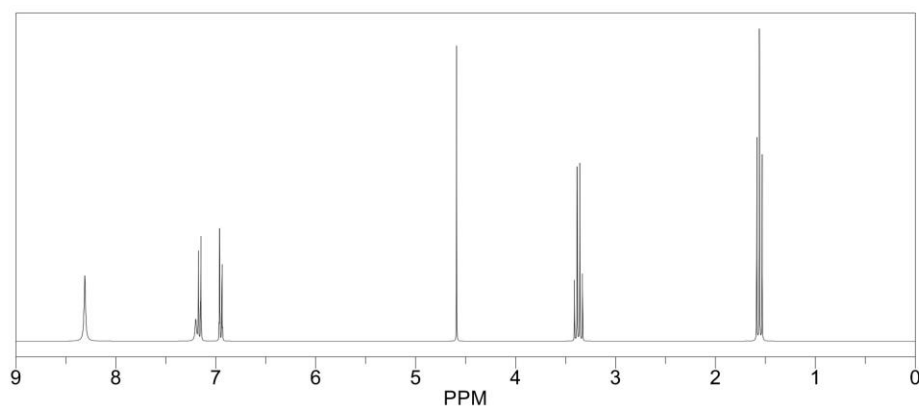


SUPPORTING INFORMATION

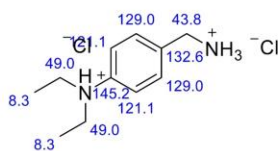
ChemNMR ^1H Estimation



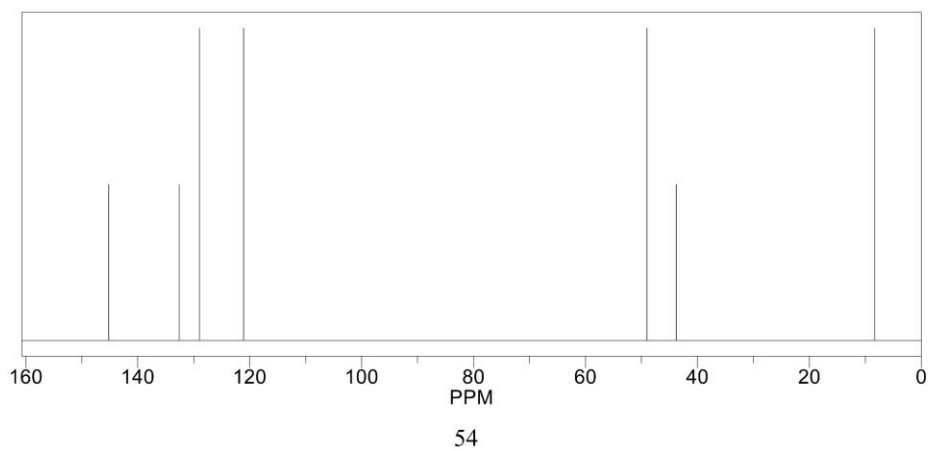
Estimation quality is indicated by color: good, medium, rough



ChemNMR ^{13}C Estimation



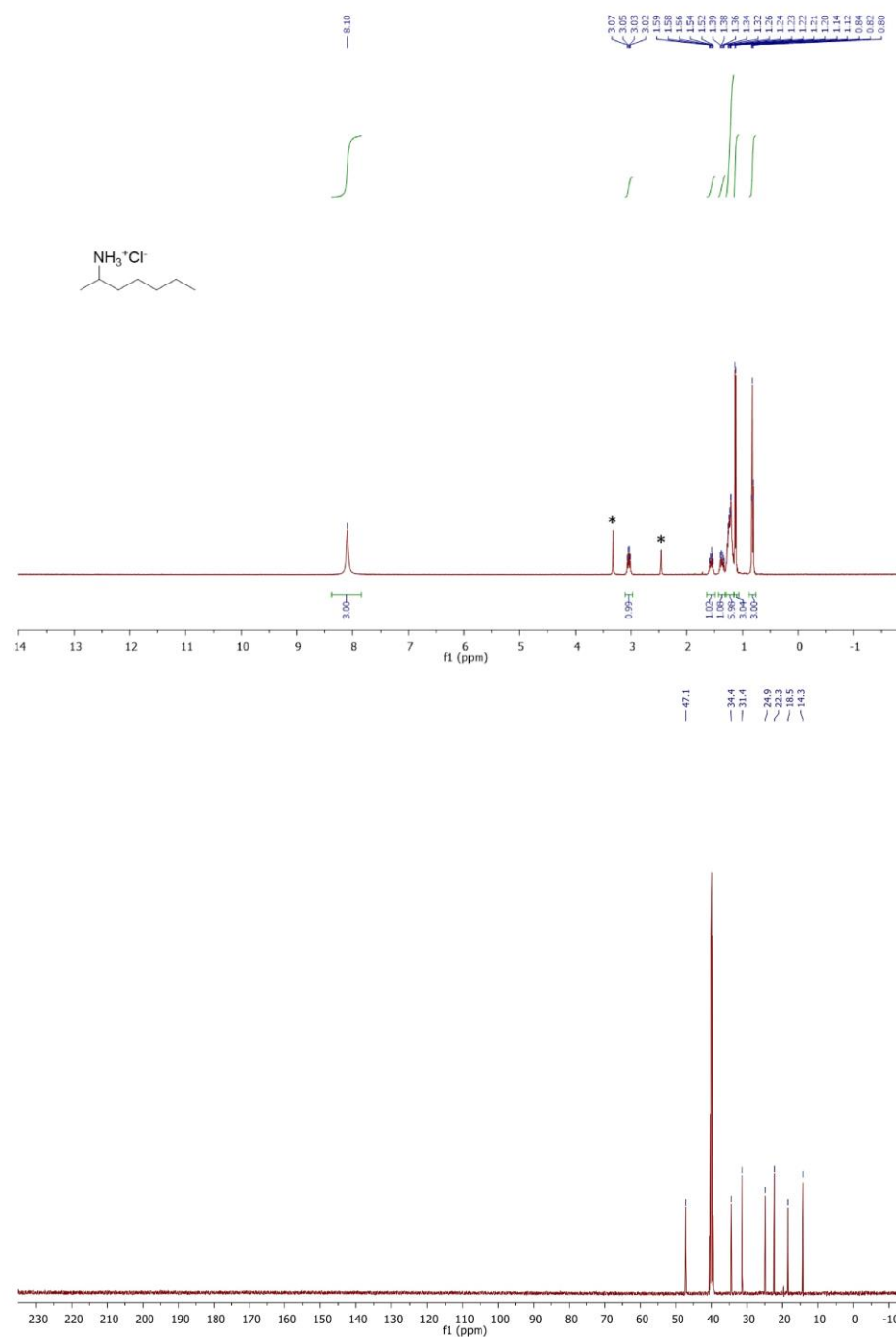
Estimation quality is indicated by color: good, medium, rough



WILEY-VCH

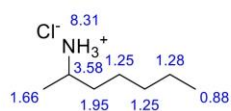
SUPPORTING INFORMATION

9:

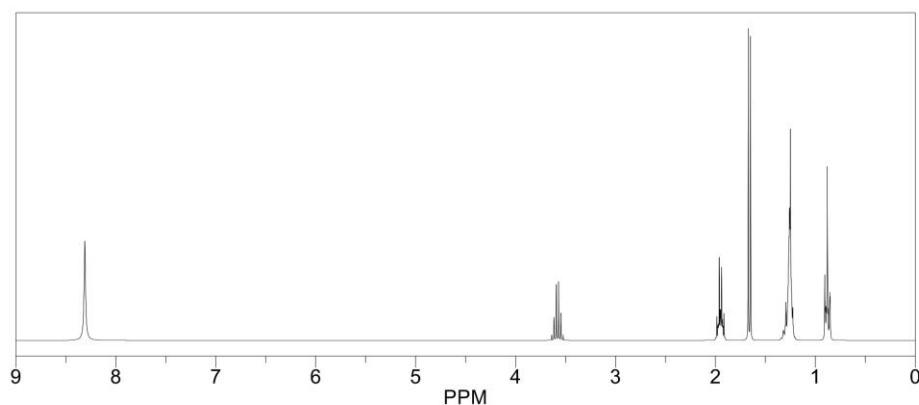


SUPPORTING INFORMATION

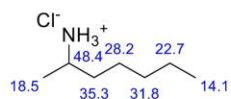
ChemNMR ^1H Estimation



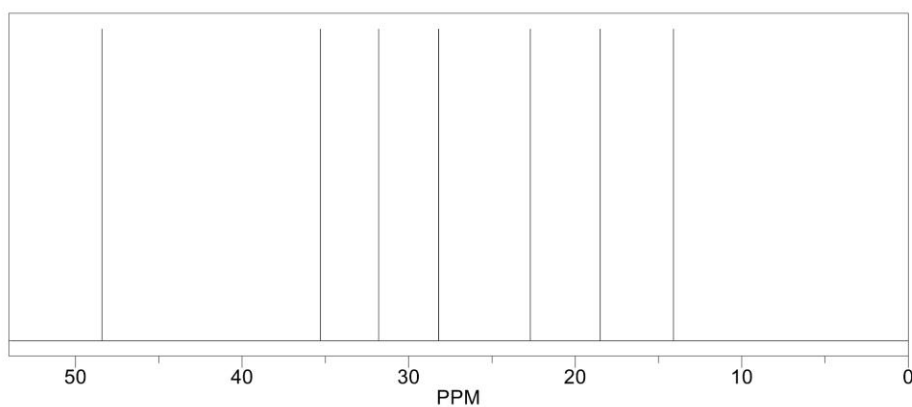
Estimation quality is indicated by color: good, medium, rough



ChemNMR ^{13}C Estimation



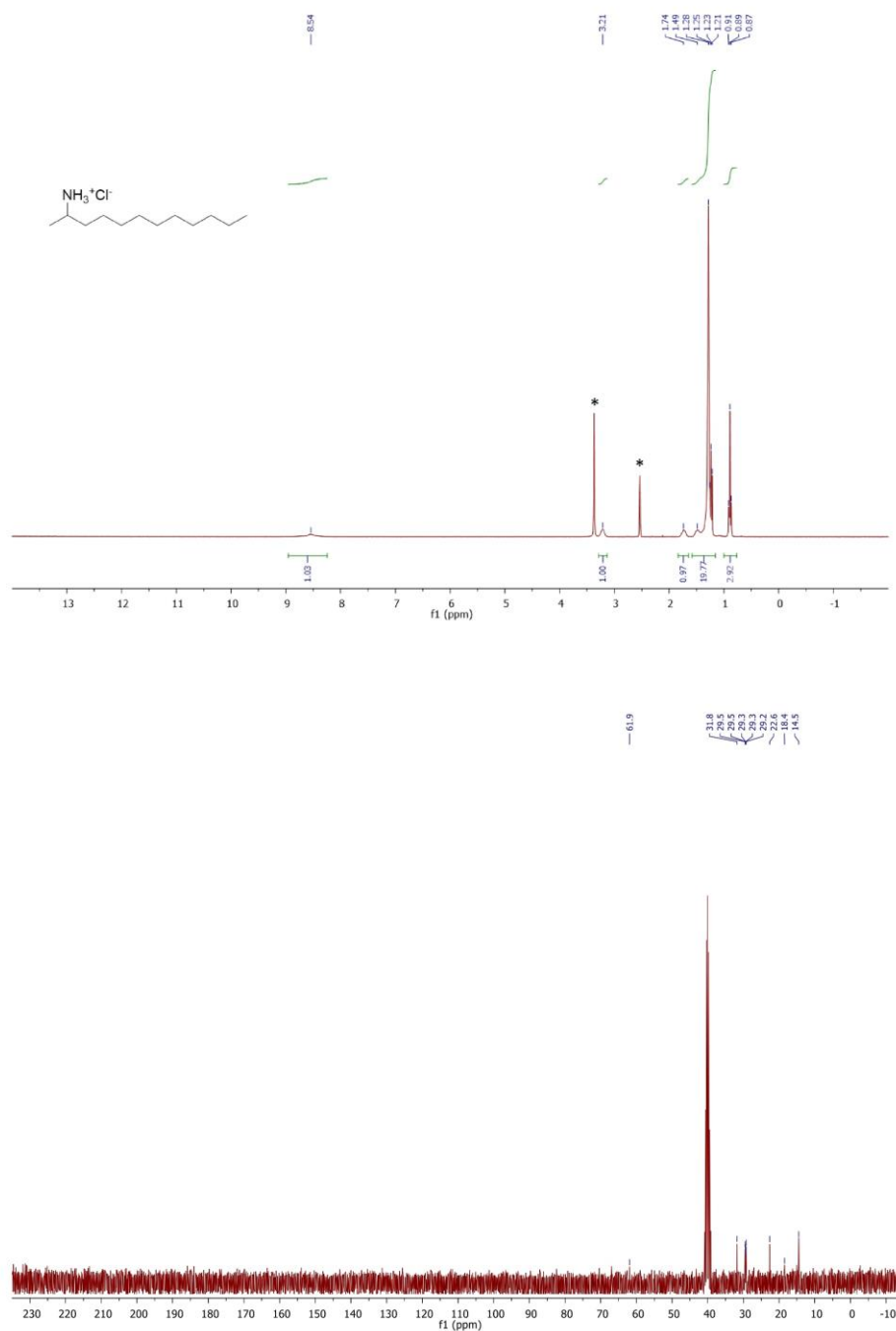
Estimation quality is indicated by color: good, medium, rough



WILEY-VCH

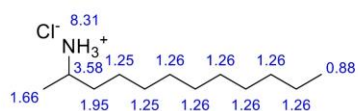
SUPPORTING INFORMATION

10:

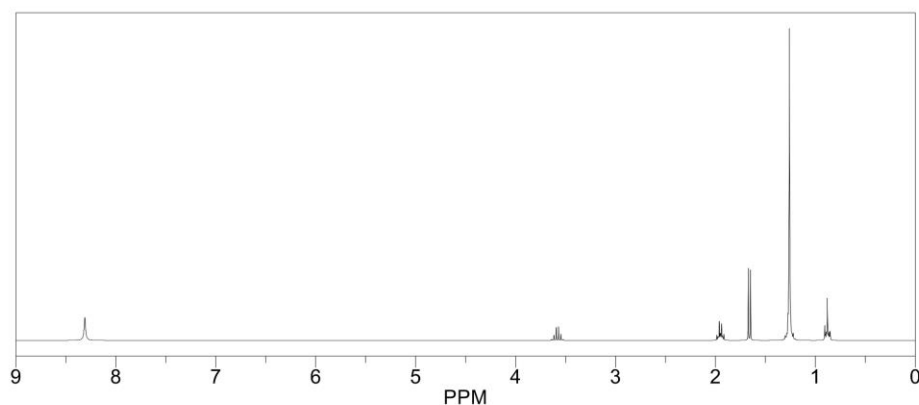


SUPPORTING INFORMATION

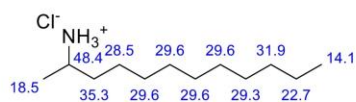
ChemNMR ^1H Estimation



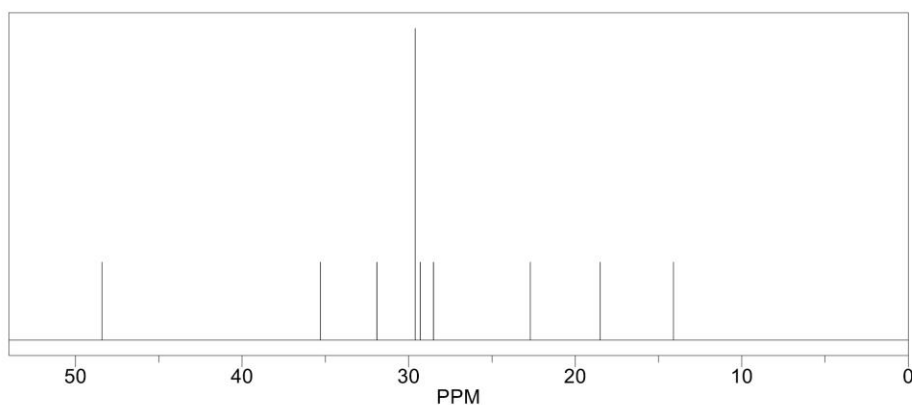
Estimation quality is indicated by color: good, medium, rough



ChemNMR ^{13}C Estimation

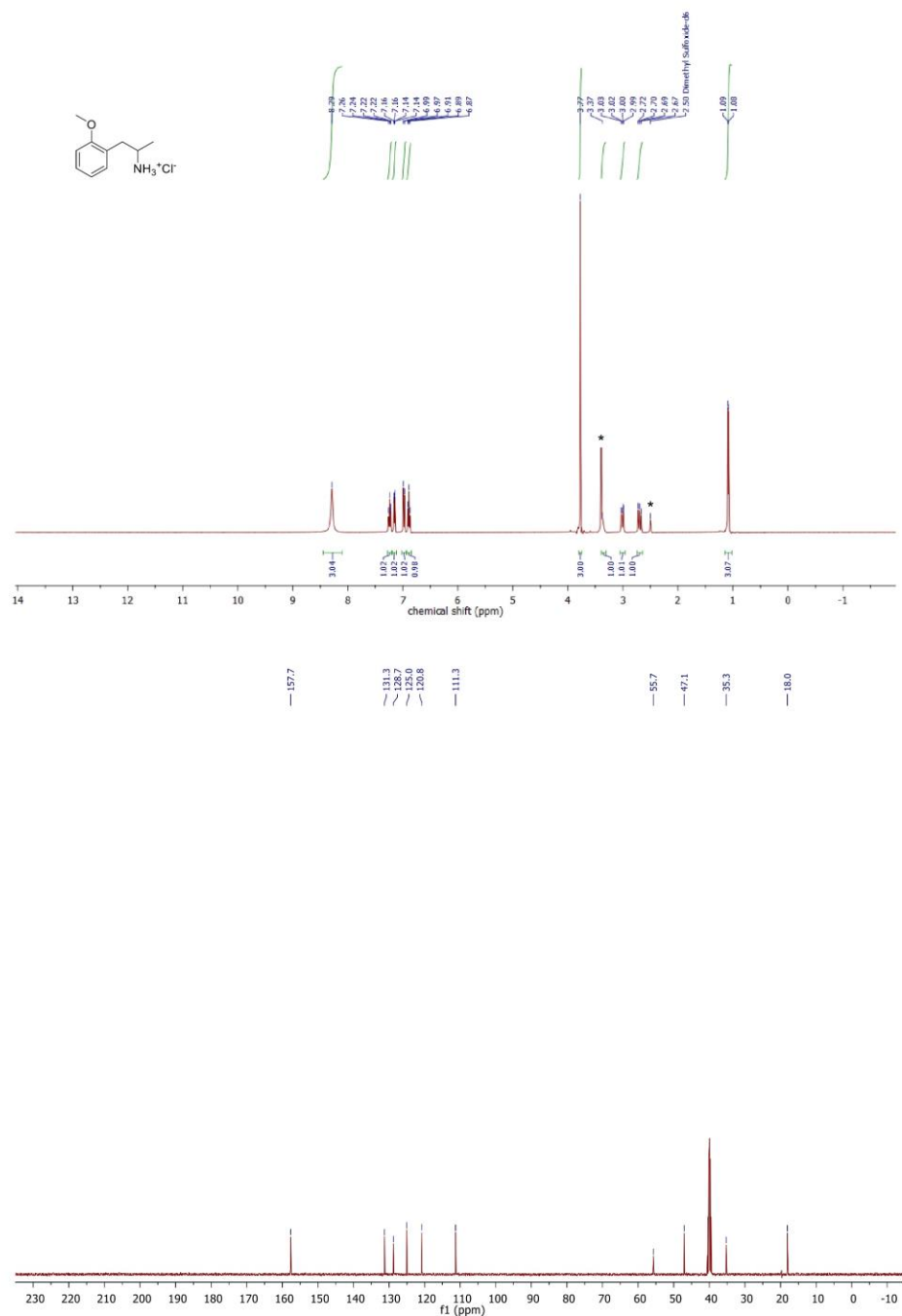


Estimation quality is indicated by color: good, medium, rough



SUPPORTING INFORMATION

11:

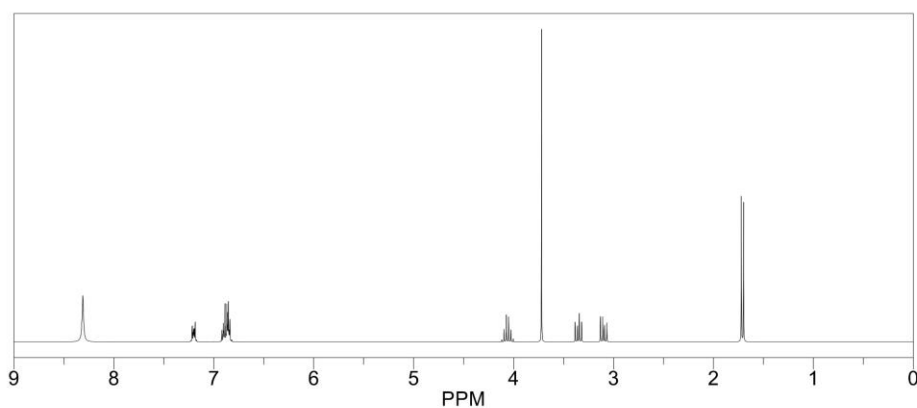


SUPPORTING INFORMATION

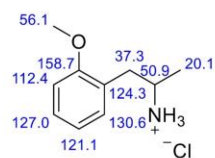
ChemNMR ^1H Estimation



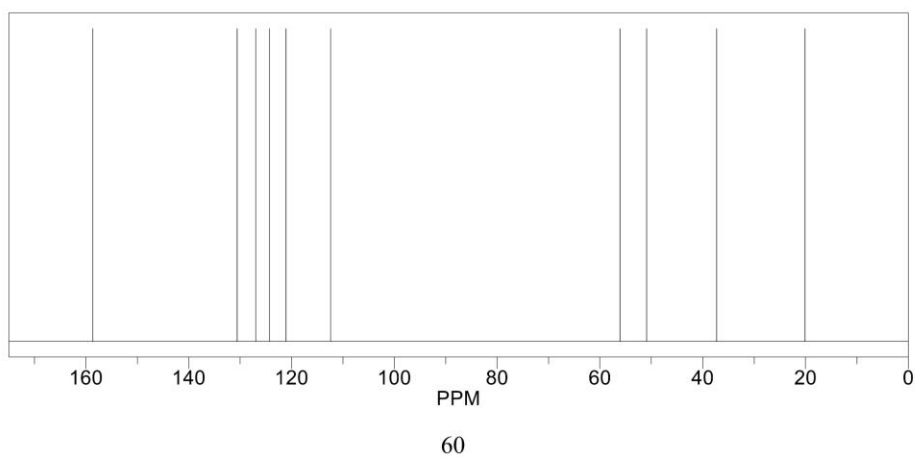
Estimation quality is indicated by color: good, medium, rough



ChemNMR ^{13}C Estimation



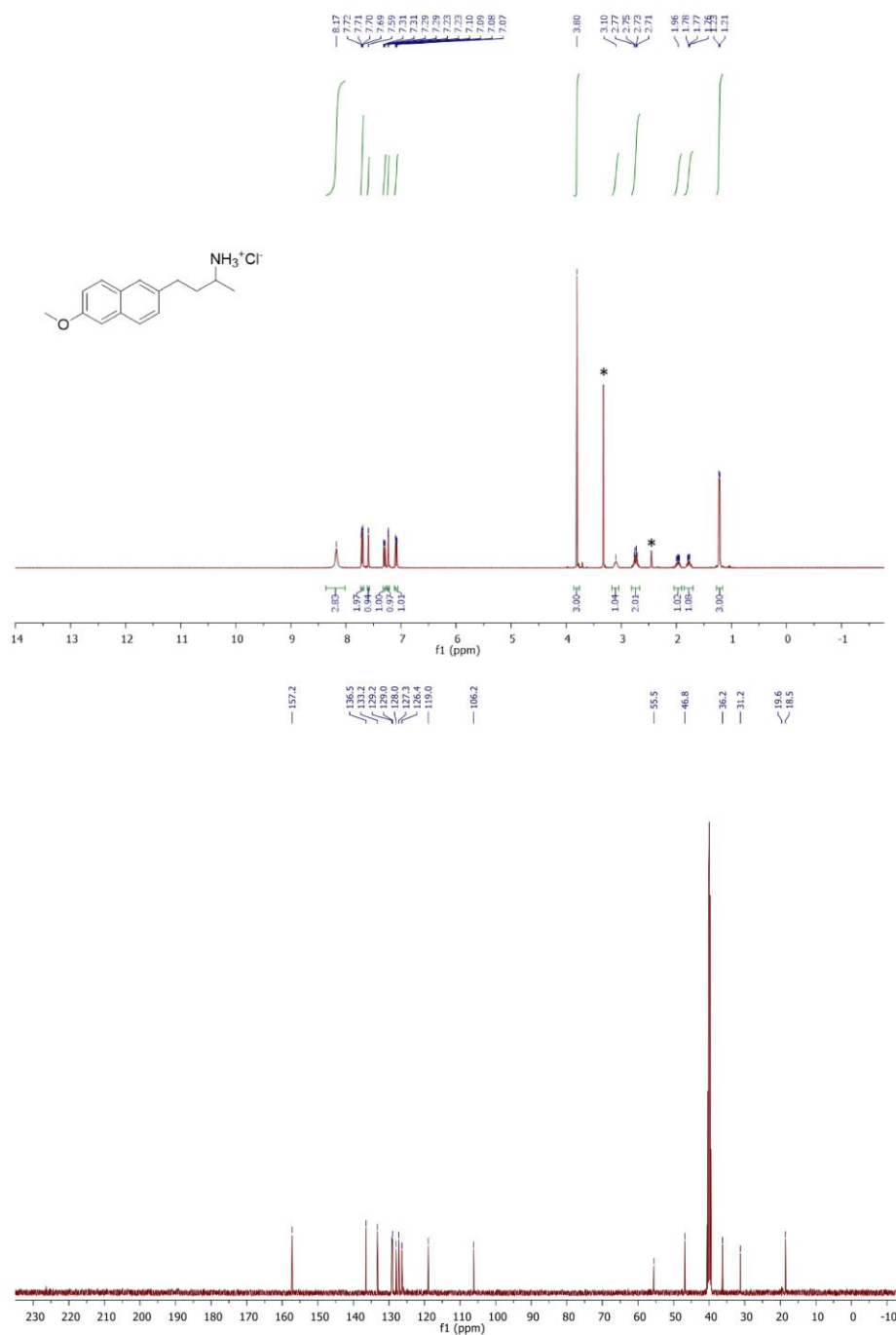
Estimation quality is indicated by color: good, medium, rough



WILEY-VCH

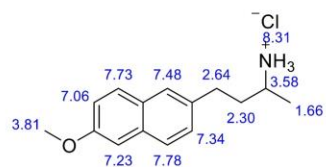
SUPPORTING INFORMATION

12:

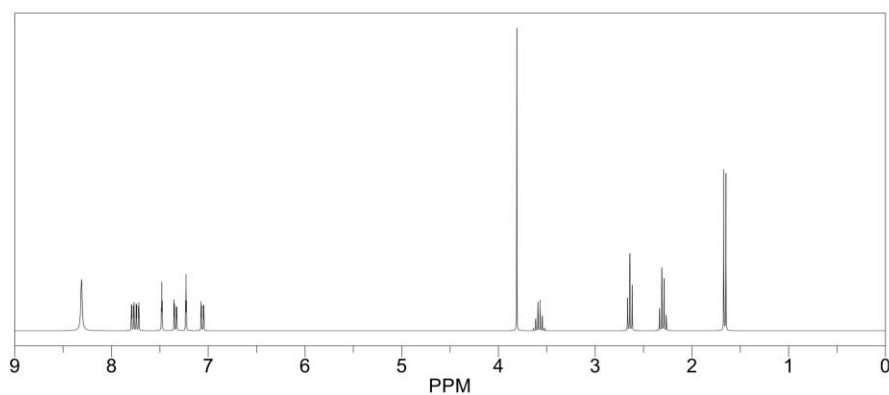


SUPPORTING INFORMATION

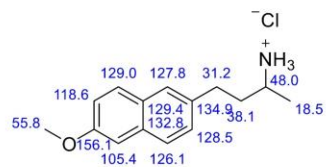
ChemNMR ^1H Estimation



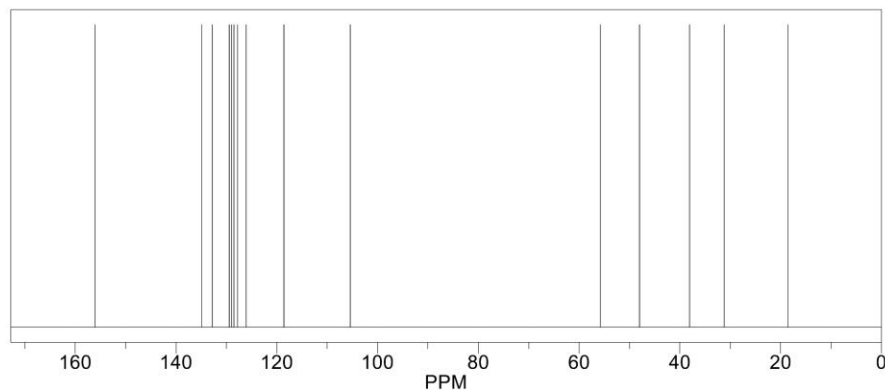
Estimation quality is indicated by color: good, medium, rough



ChemNMR ^{13}C Estimation



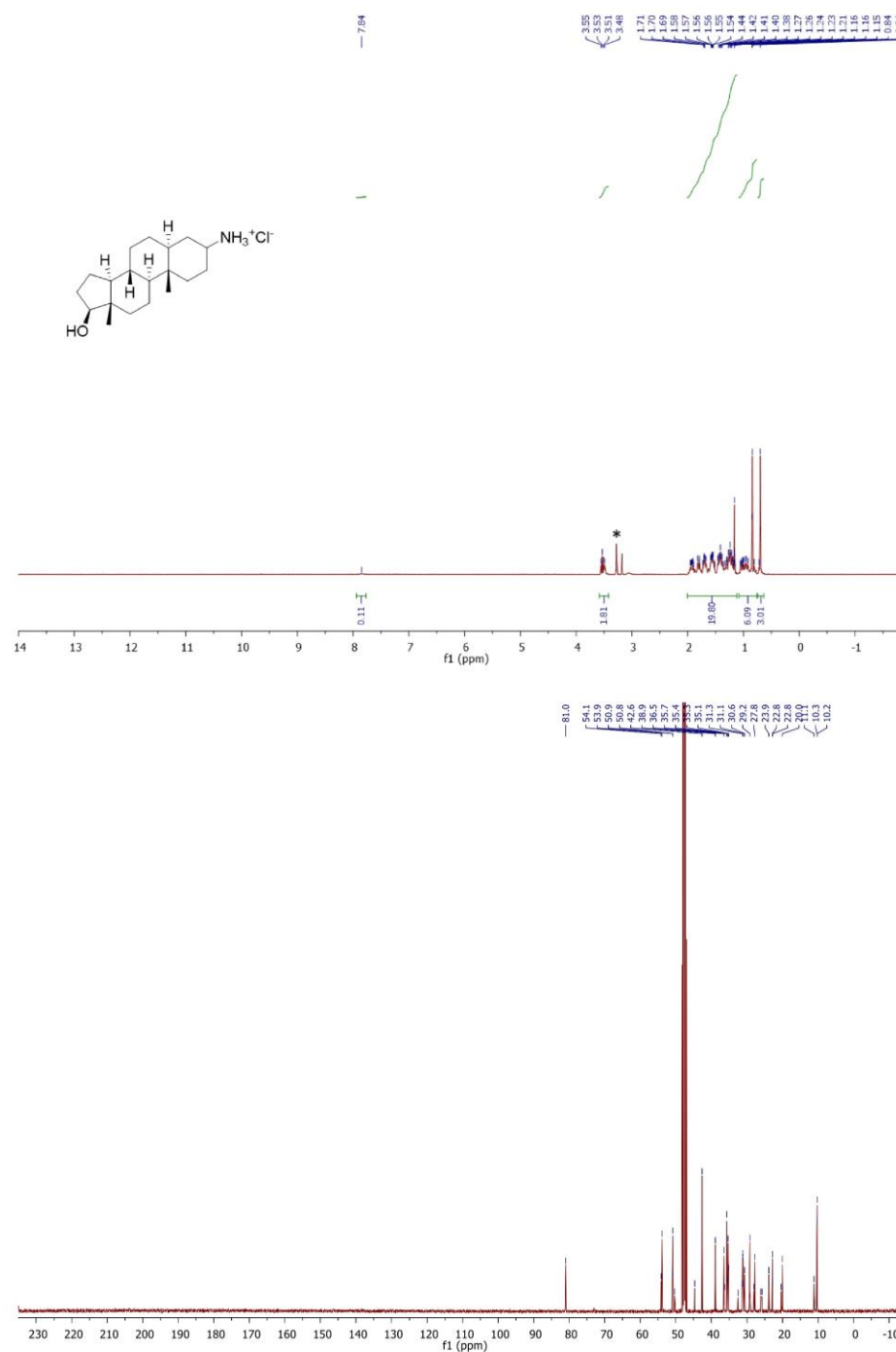
Estimation quality is indicated by color: good, medium, rough



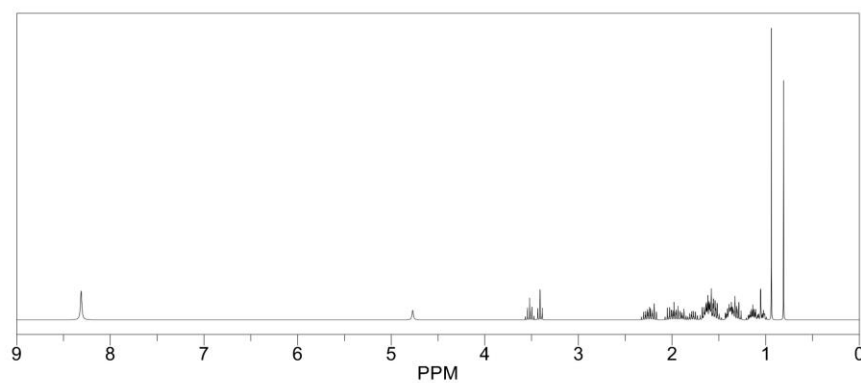
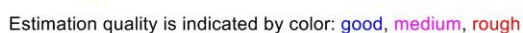
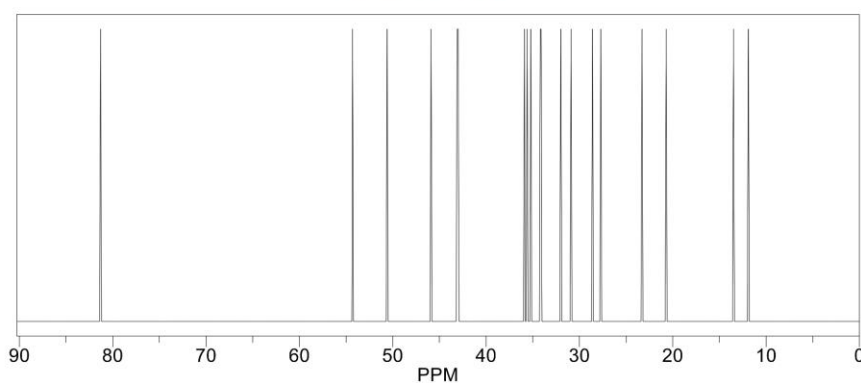
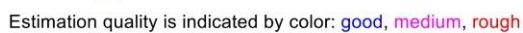
WILEY-VCH

SUPPORTING INFORMATION

13:



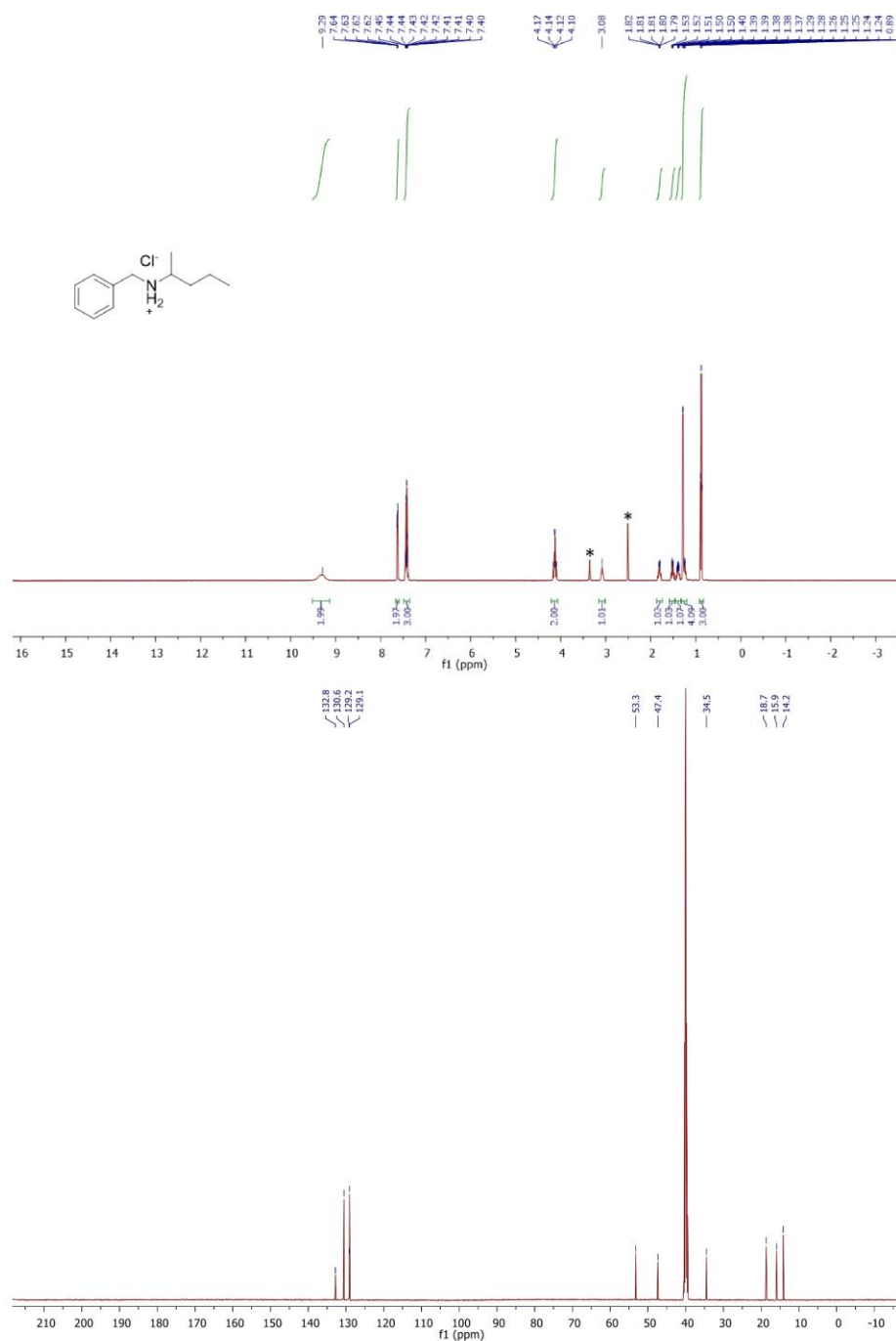
63

ChemNMR ¹H EstimationChemNMR ¹³C Estimation

WILEY-VCH

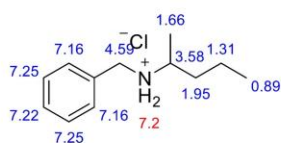
SUPPORTING INFORMATION

14:

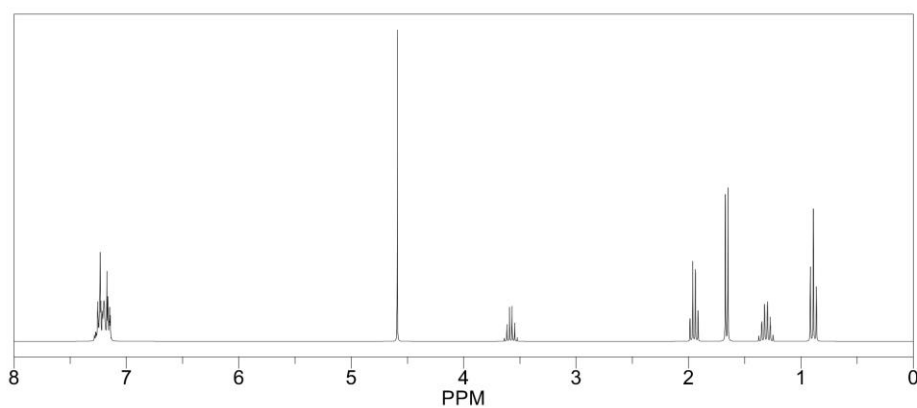


SUPPORTING INFORMATION

ChemNMR ^1H Estimation



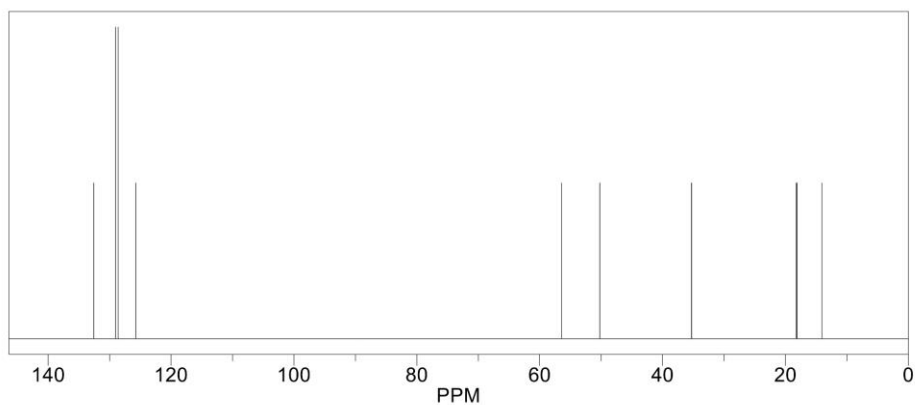
Estimation quality is indicated by color: good, medium, rough



ChemNMR ^{13}C Estimation



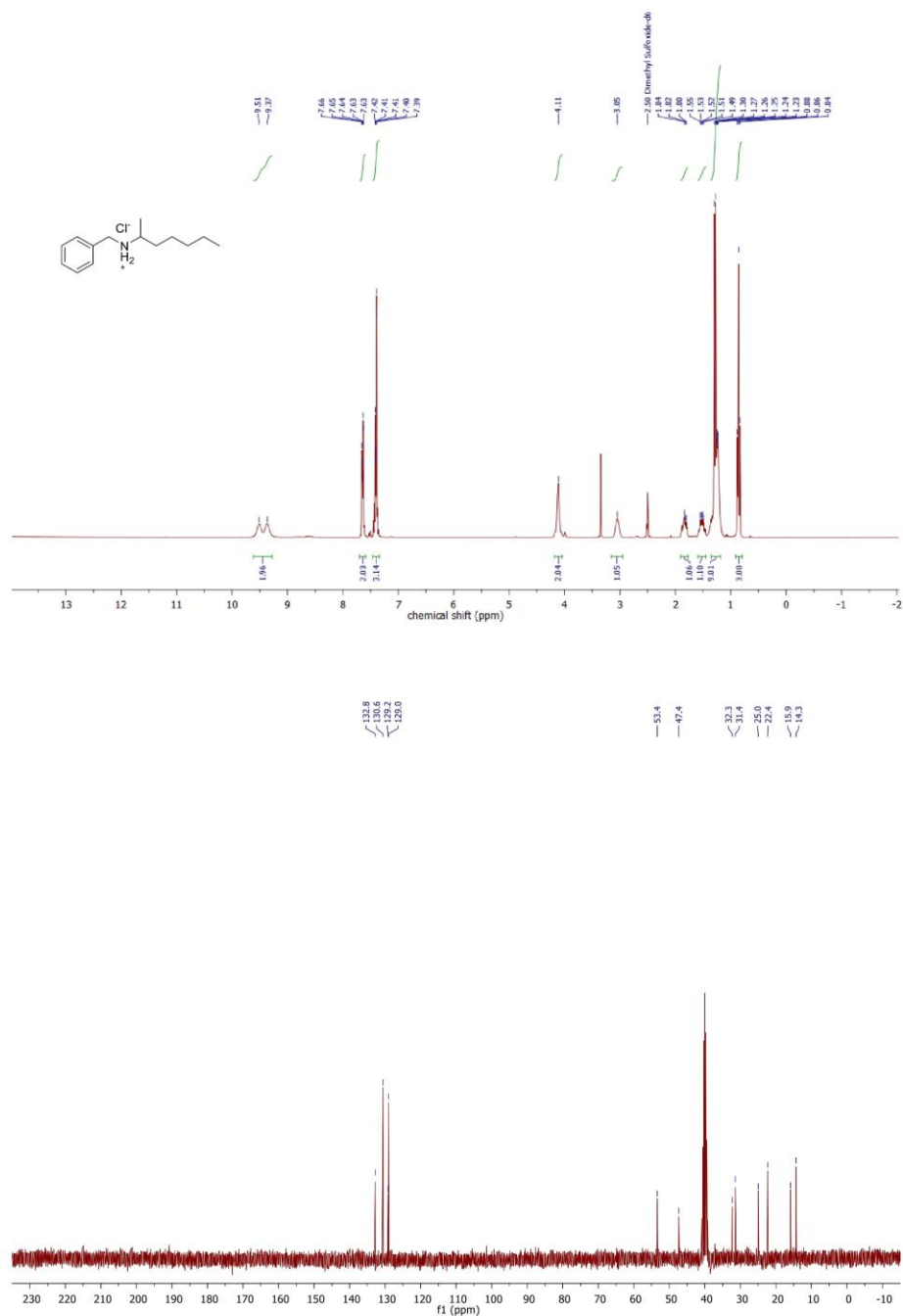
Estimation quality is indicated by color: good, medium, rough



WILEY-VCH

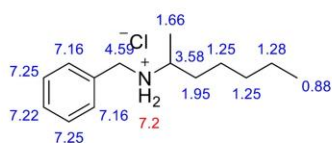
SUPPORTING INFORMATION

15:

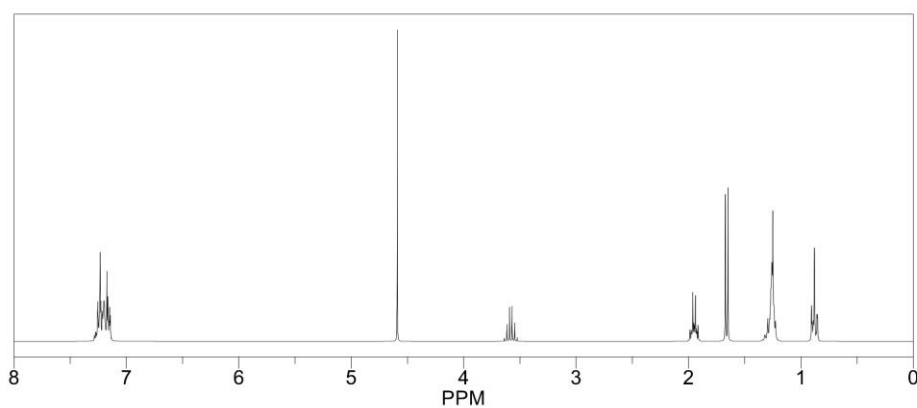


SUPPORTING INFORMATION

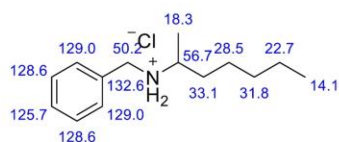
ChemNMR ^1H Estimation



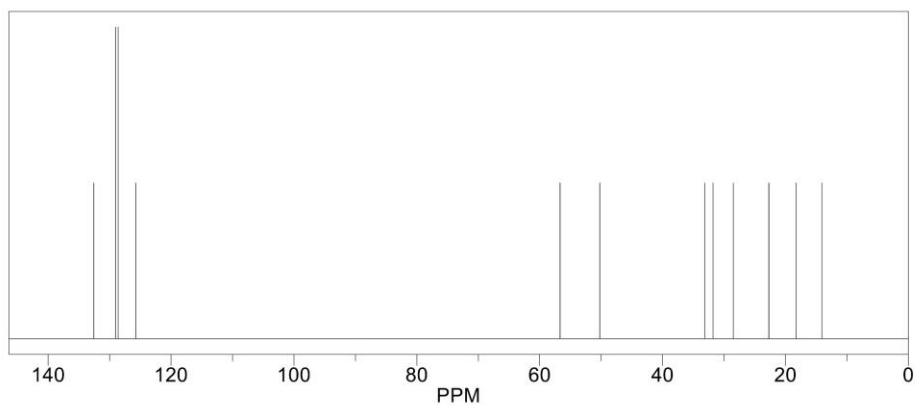
Estimation quality is indicated by color: good, medium, rough



ChemNMR ^{13}C Estimation



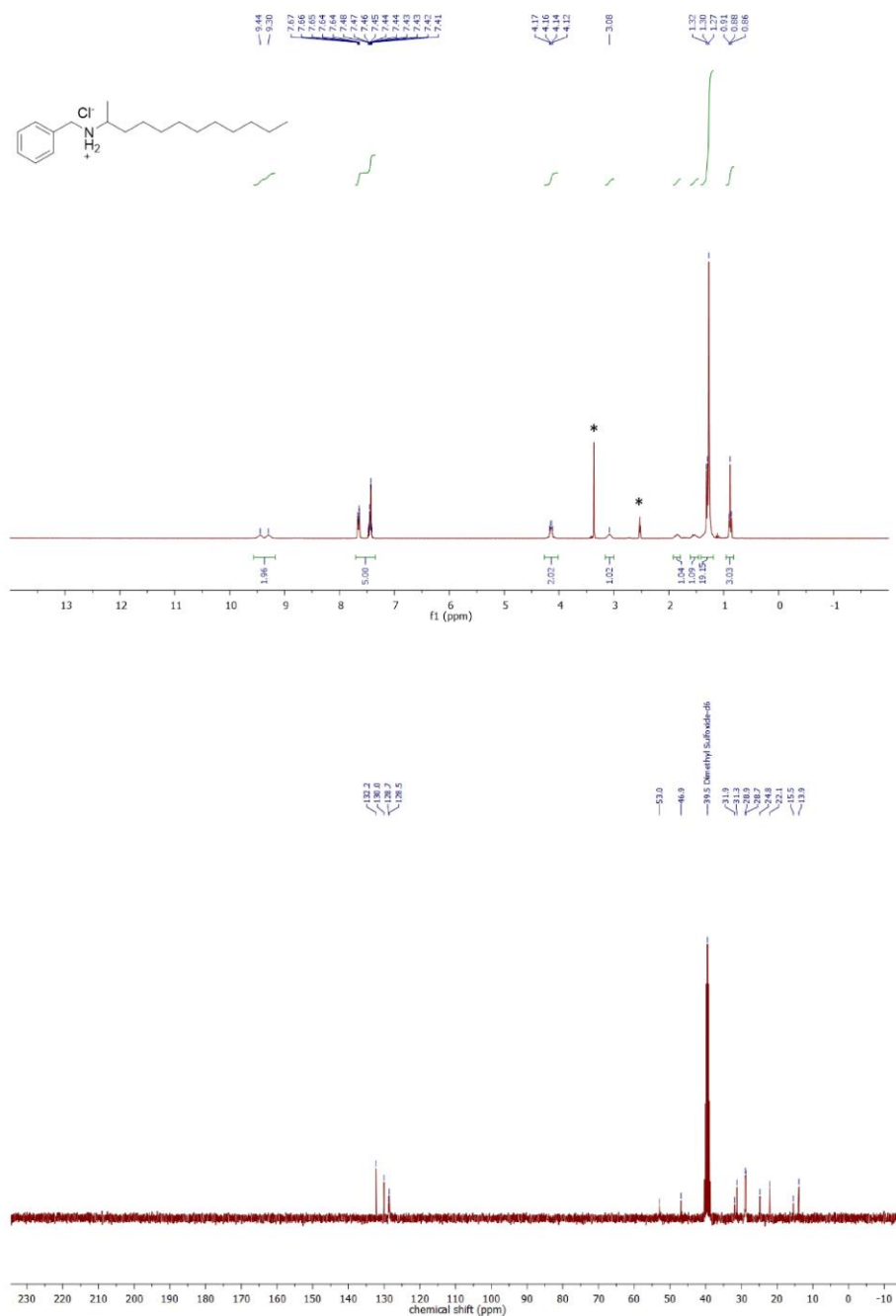
Estimation quality is indicated by color: good, medium, rough



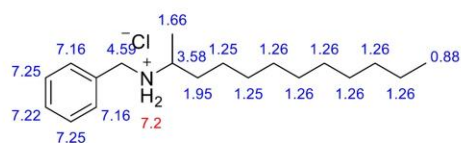
WILEY-VCH

SUPPORTING INFORMATION

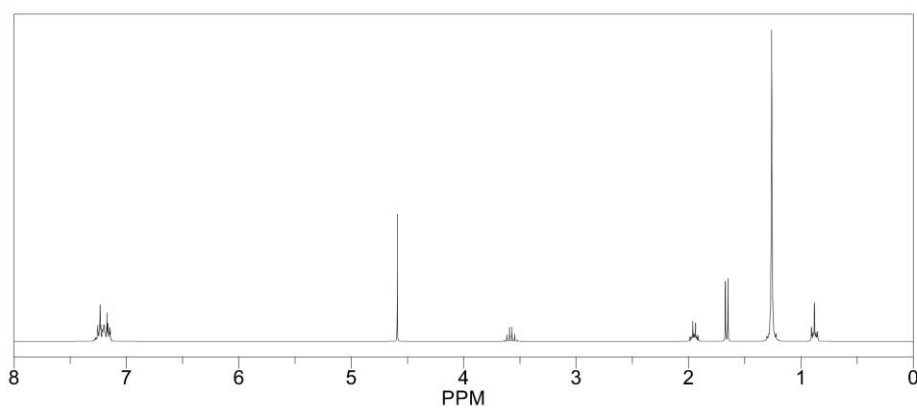
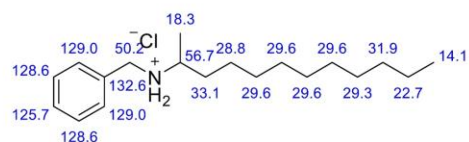
16:



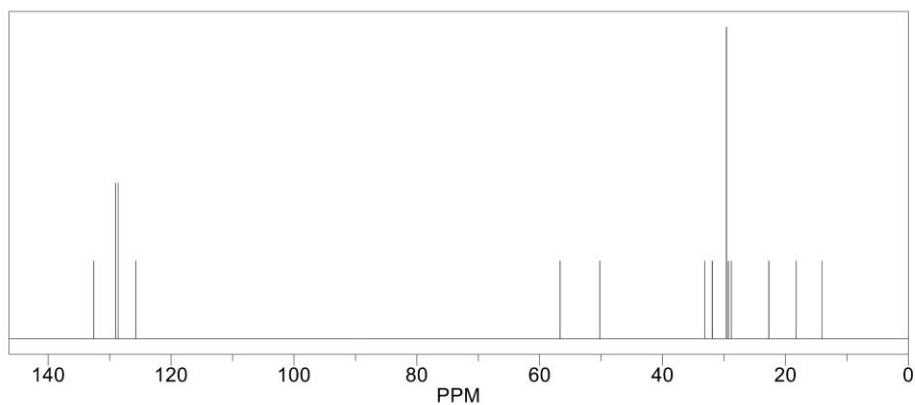
SUPPORTING INFORMATION

ChemNMR ^1H Estimation

Estimation quality is indicated by color: good, medium, rough

ChemNMR ^{13}C Estimation

Estimation quality is indicated by color: good, medium, rough

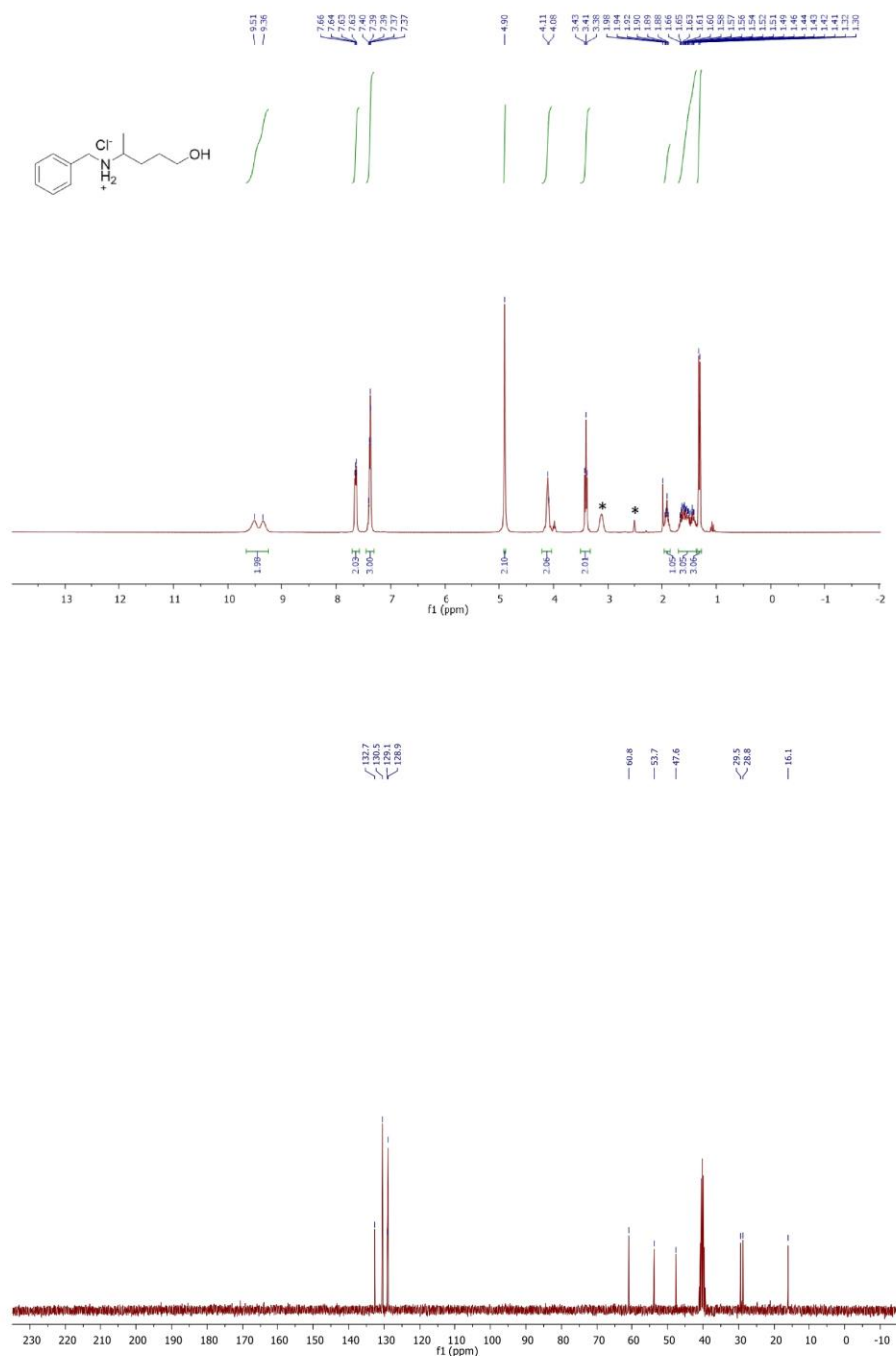


70

WILEY-VCH

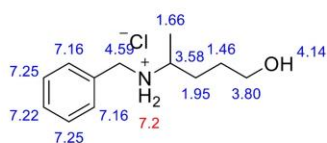
SUPPORTING INFORMATION

17:

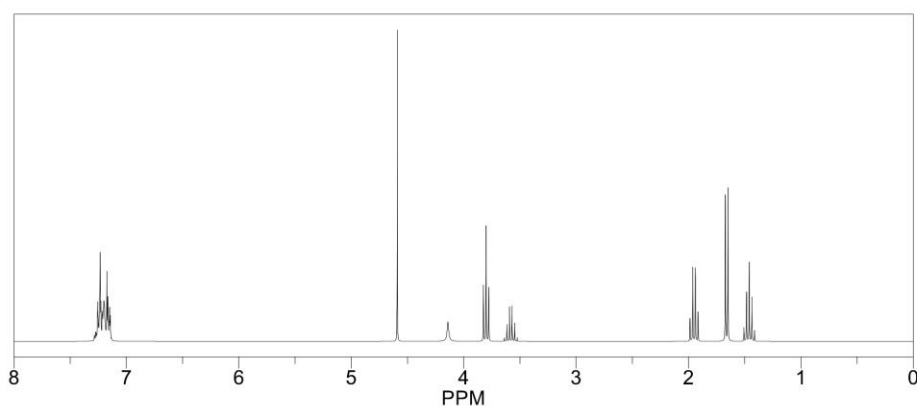


SUPPORTING INFORMATION

ChemNMR ^1H Estimation



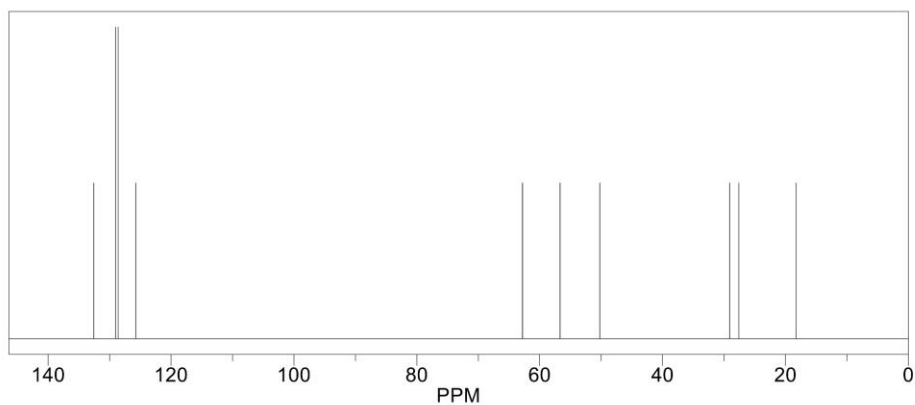
Estimation quality is indicated by color: good, medium, rough



ChemNMR ^{13}C Estimation



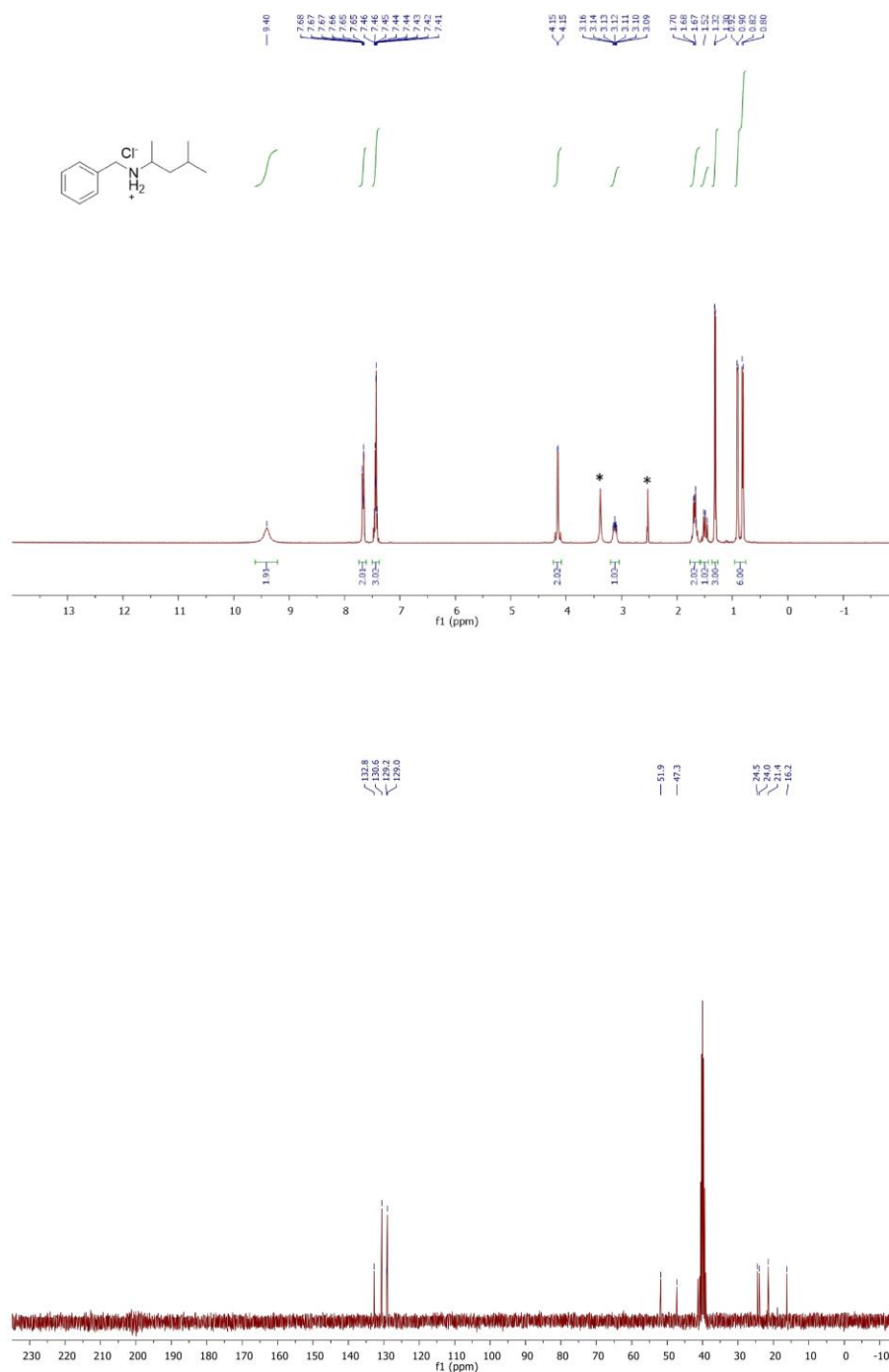
Estimation quality is indicated by color: good, medium, rough



WILEY-VCH

SUPPORTING INFORMATION

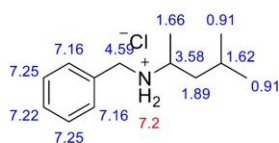
18:



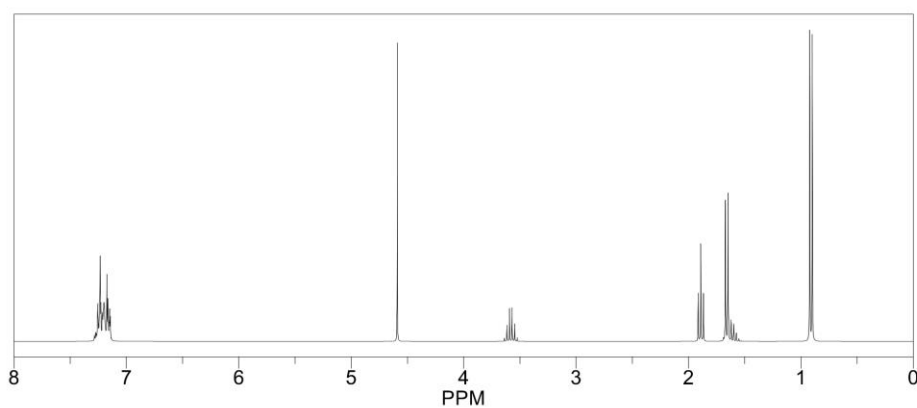
73

SUPPORTING INFORMATION

ChemNMR ^1H Estimation



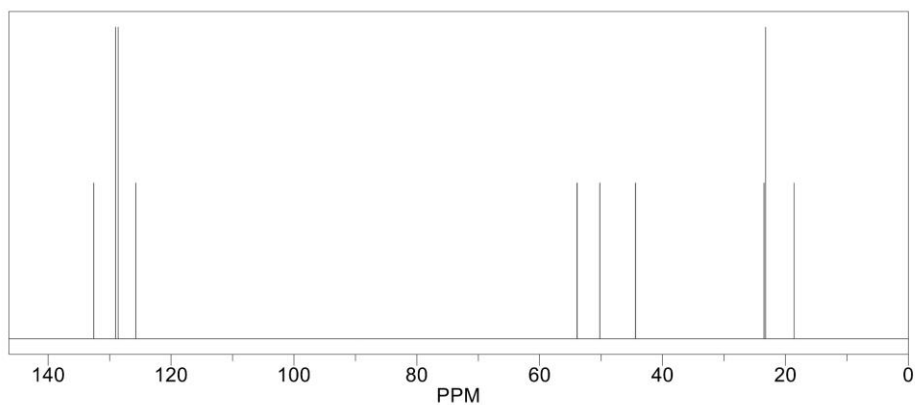
Estimation quality is indicated by color: good, medium, rough



ChemNMR ^{13}C Estimation



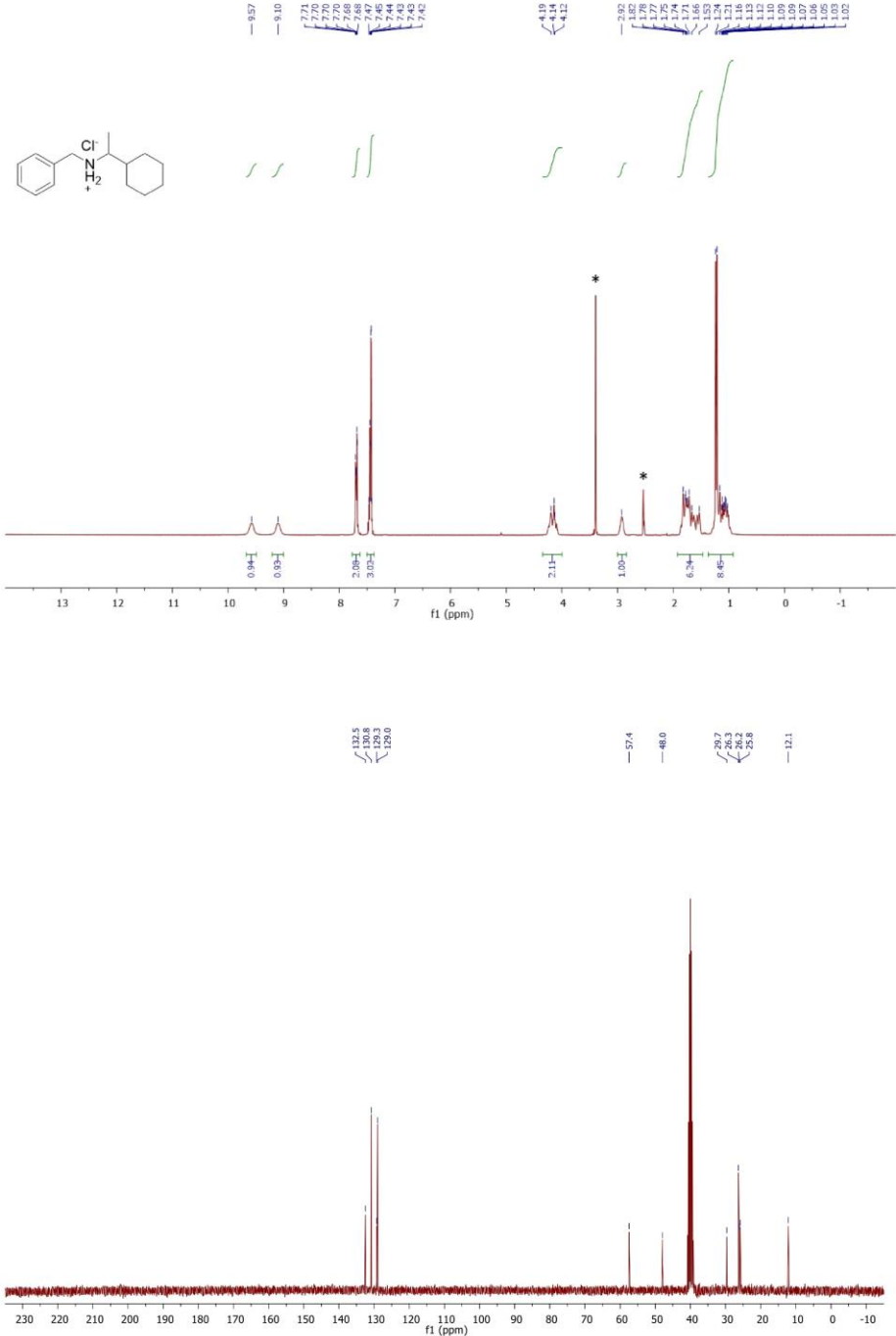
Estimation quality is indicated by color: good, medium, rough



WILEY-VCH

SUPPORTING INFORMATION

19:



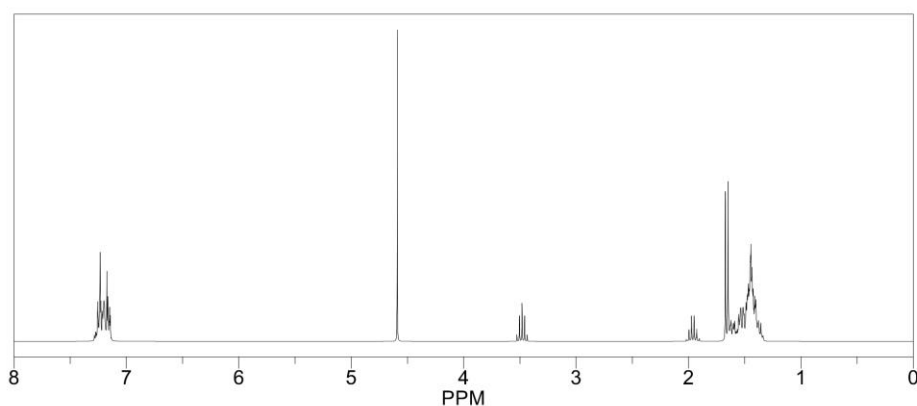
WILEY-VCH

SUPPORTING INFORMATION

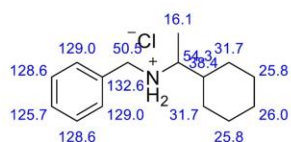
ChemNMR ^1H Estimation



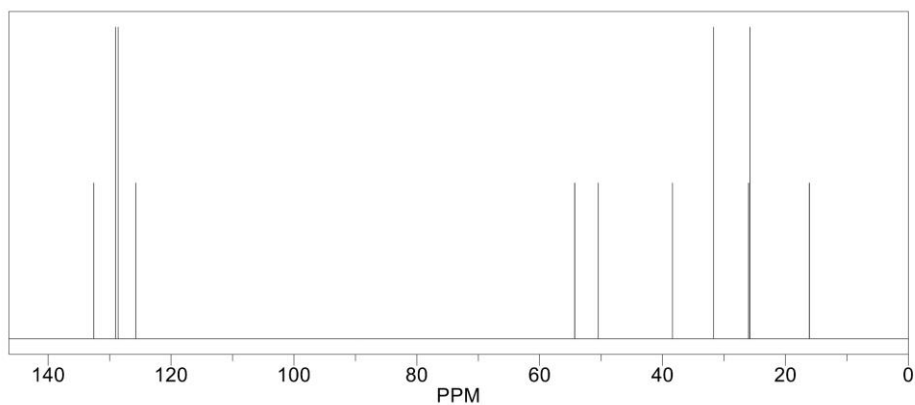
Estimation quality is indicated by color: good, medium, rough



ChemNMR ^{13}C Estimation



Estimation quality is indicated by color: good, medium, rough

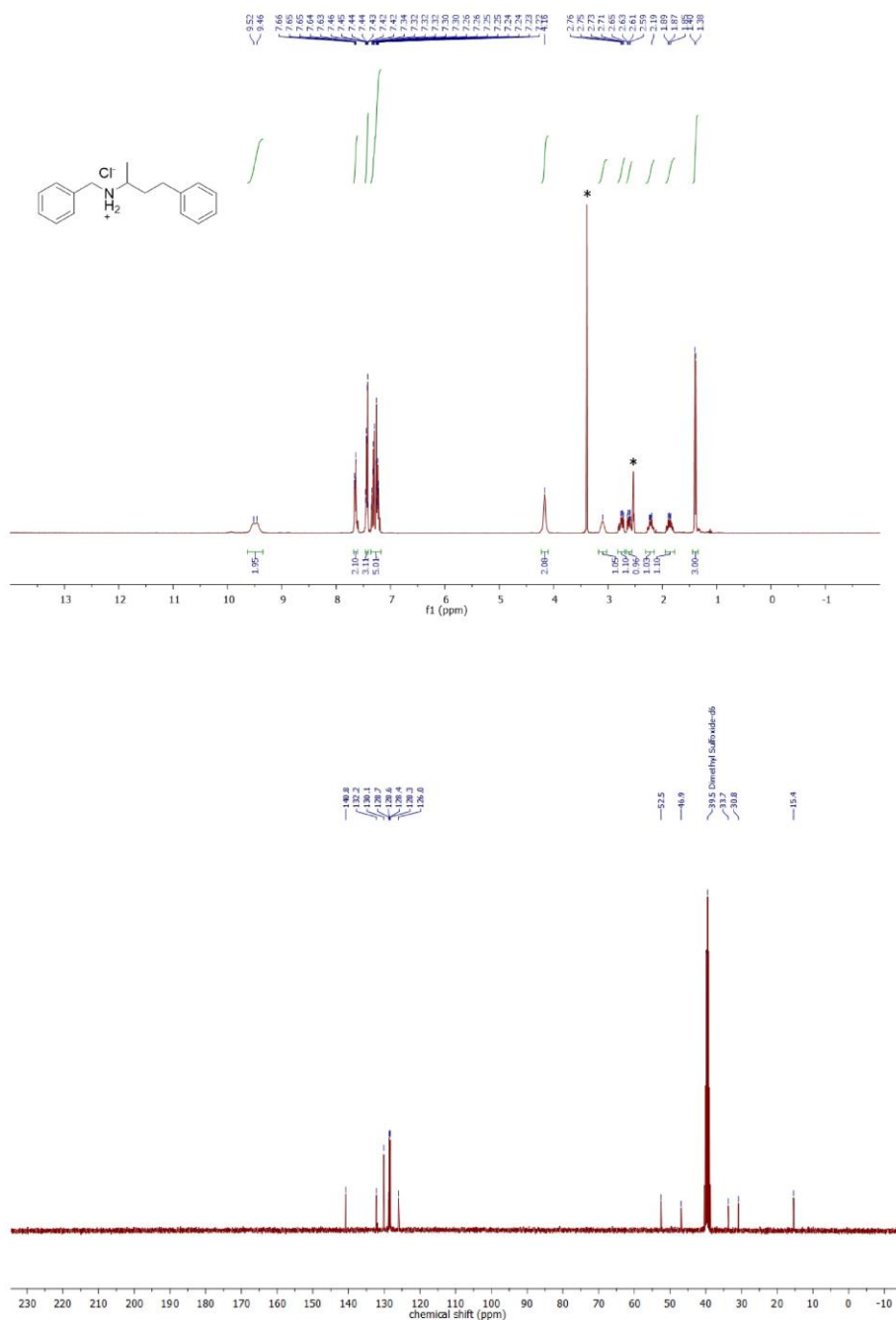


76

WILEY-VCH

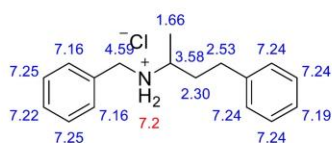
SUPPORTING INFORMATION

20:

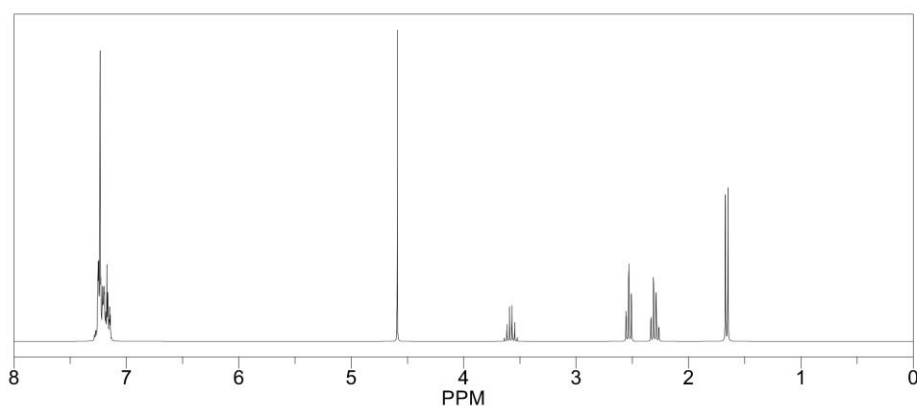


SUPPORTING INFORMATION

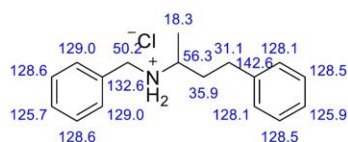
ChemNMR ^1H Estimation



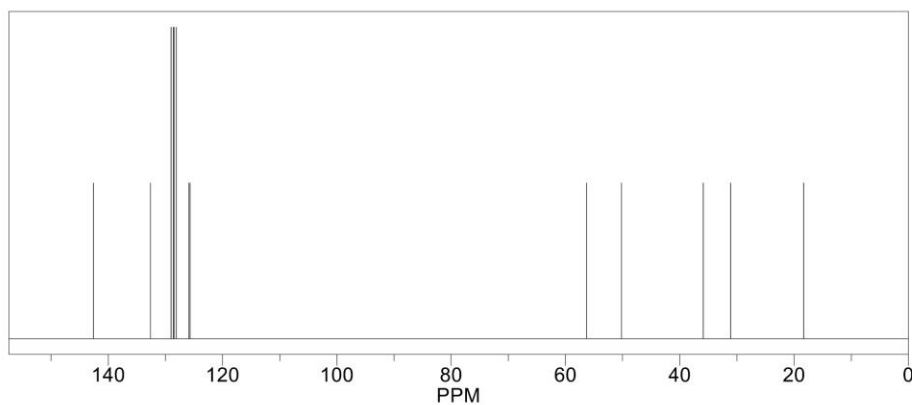
Estimation quality is indicated by color: good, medium, rough



ChemNMR ^{13}C Estimation



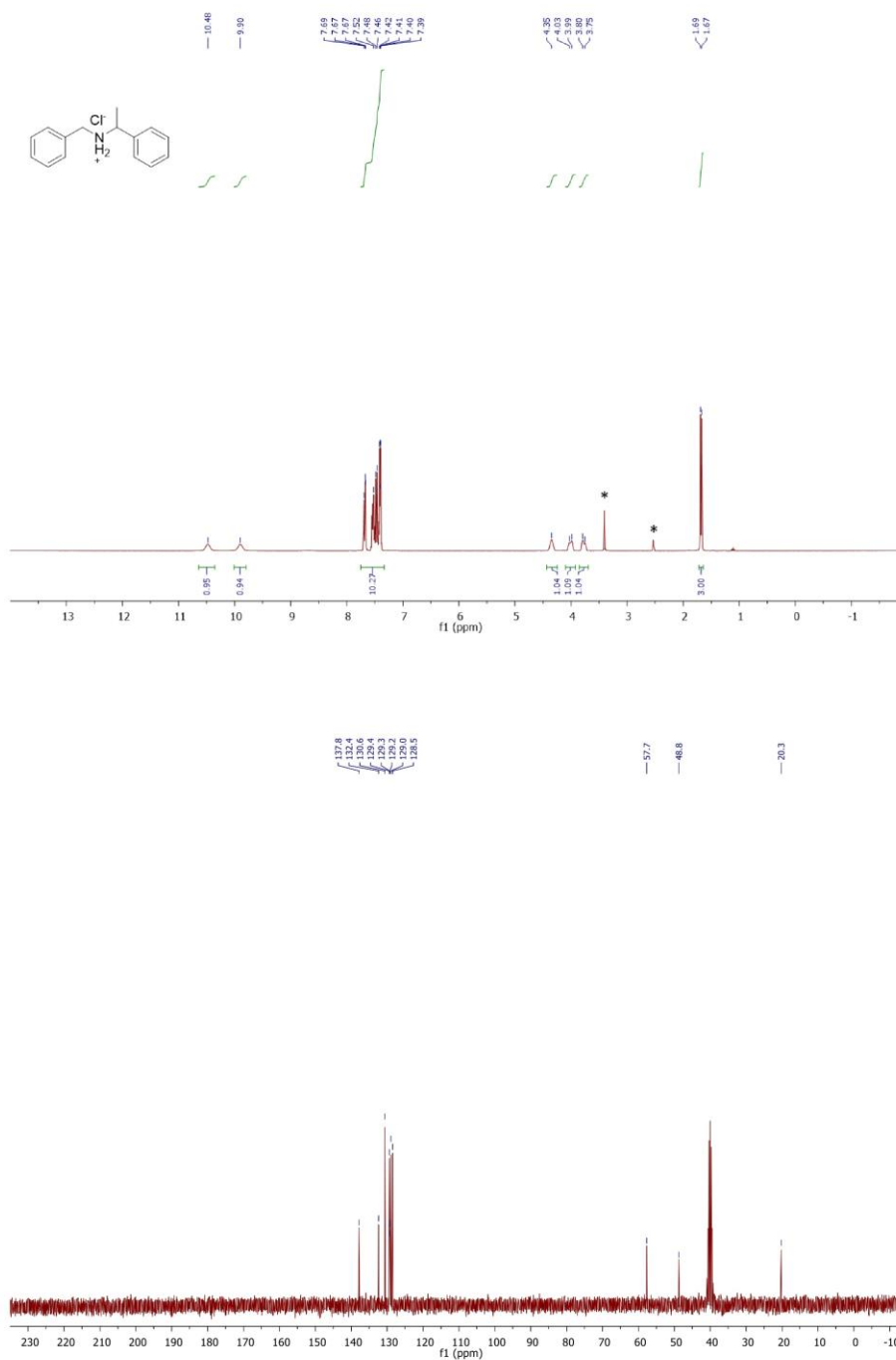
Estimation quality is indicated by color: good, medium, rough



WILEY-VCH

SUPPORTING INFORMATION

21:



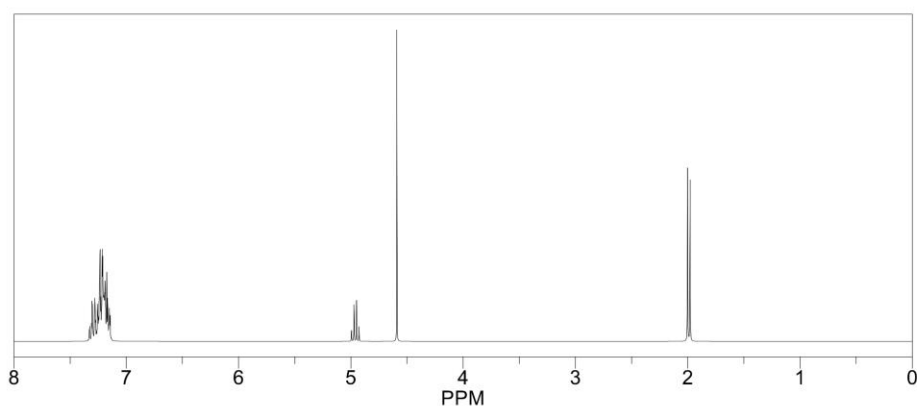
WILEY-VCH

SUPPORTING INFORMATION

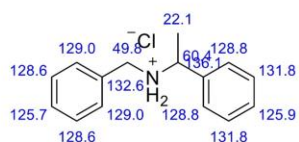
ChemNMR ^1H Estimation



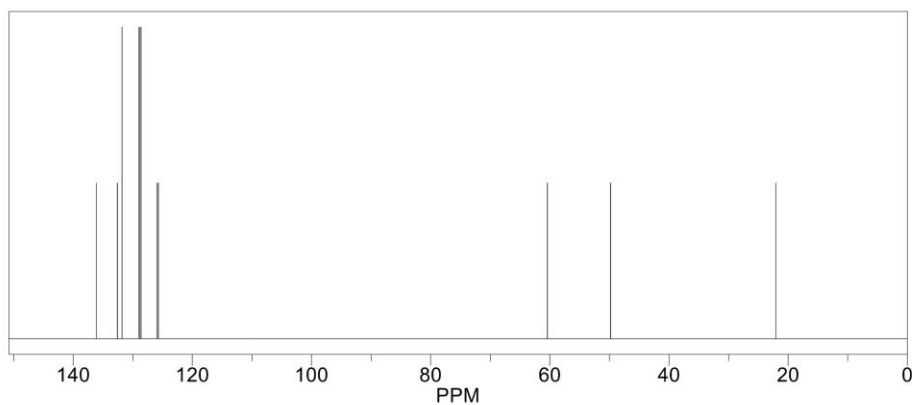
Estimation quality is indicated by color: good, medium, rough



ChemNMR ^{13}C Estimation



Estimation quality is indicated by color: good, medium, rough

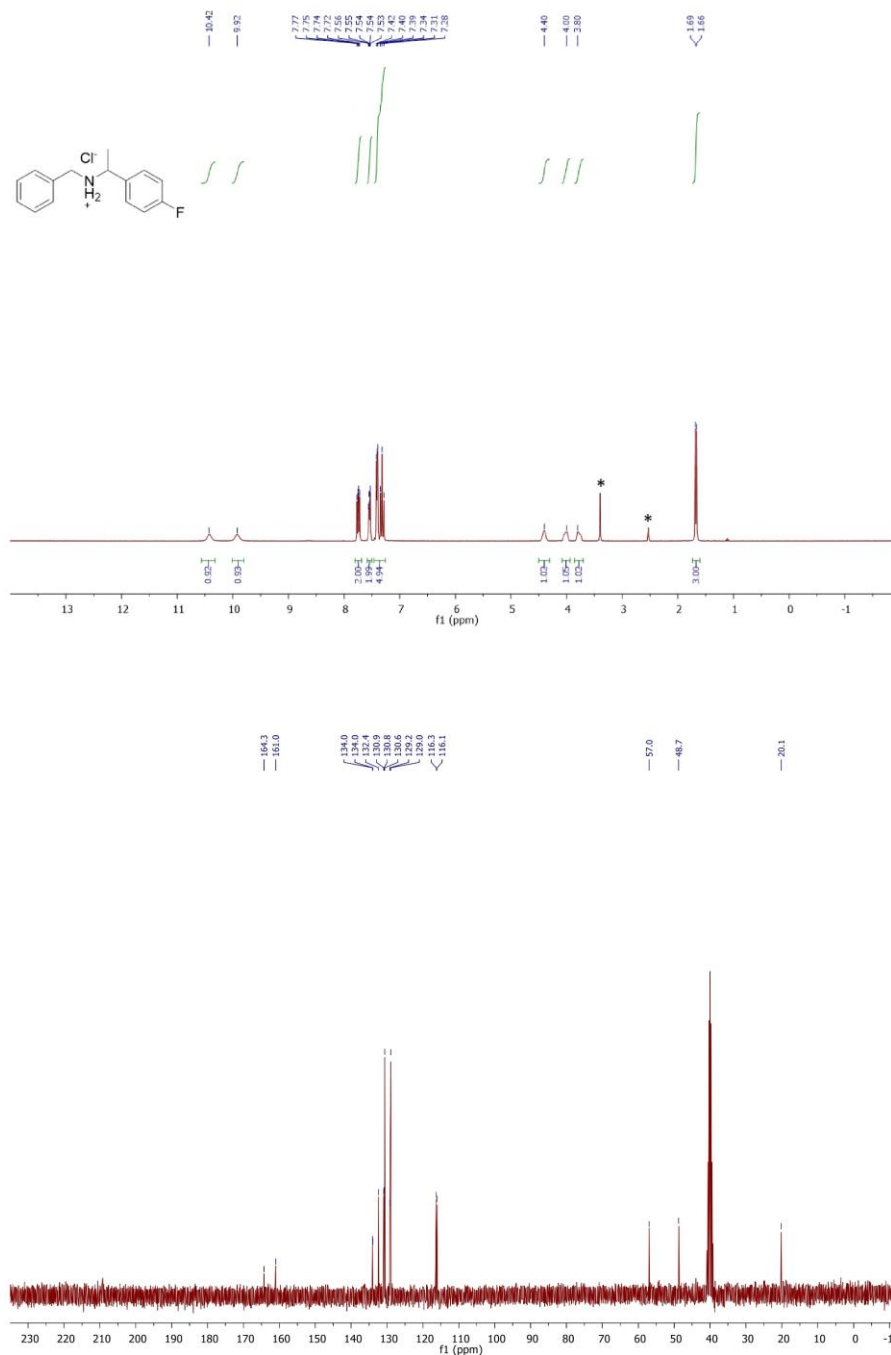


80

WILEY-VCH

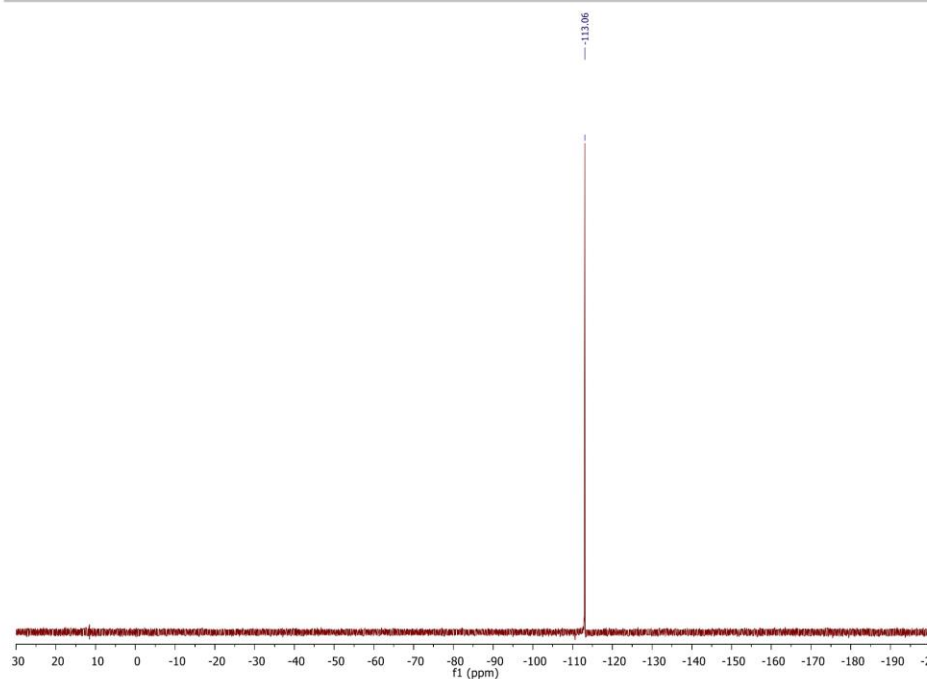
SUPPORTING INFORMATION

22:



WILEY-VCH

SUPPORTING INFORMATION

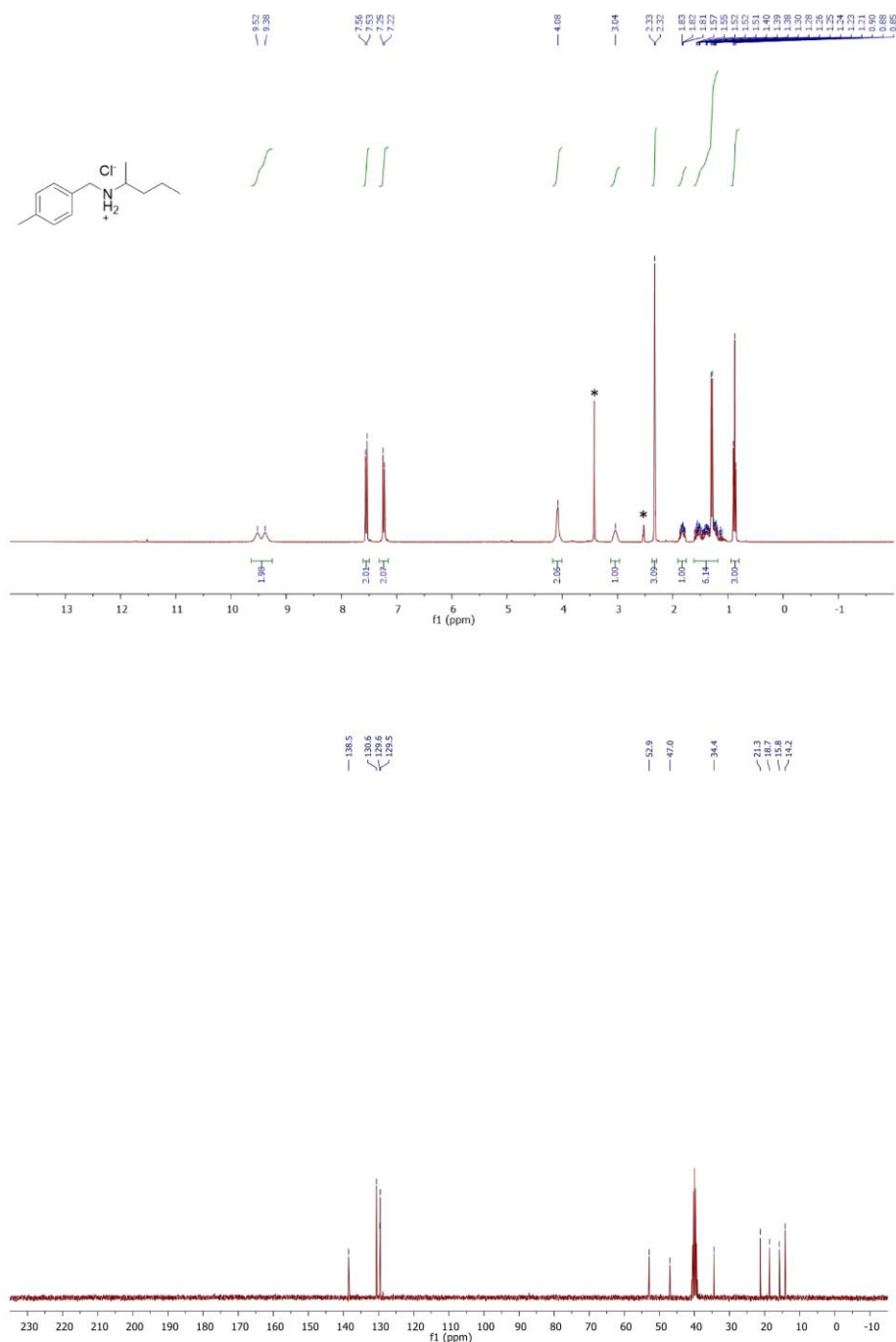


ChemNMR ¹H Estimation

WILEY-VCH

SUPPORTING INFORMATION

23:

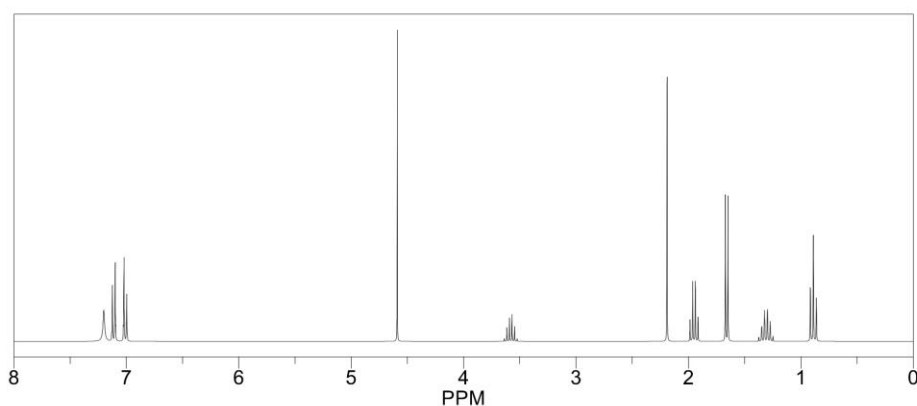


SUPPORTING INFORMATION

ChemNMR ^1H Estimation



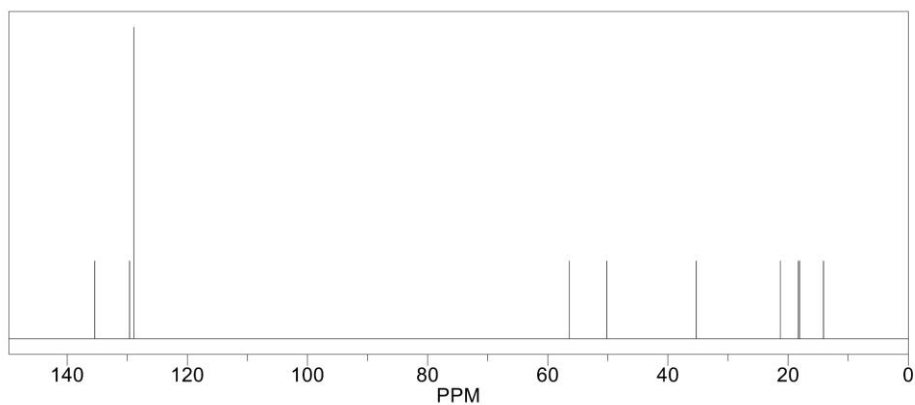
Estimation quality is indicated by color: good, medium, rough



ChemNMR ^{13}C Estimation

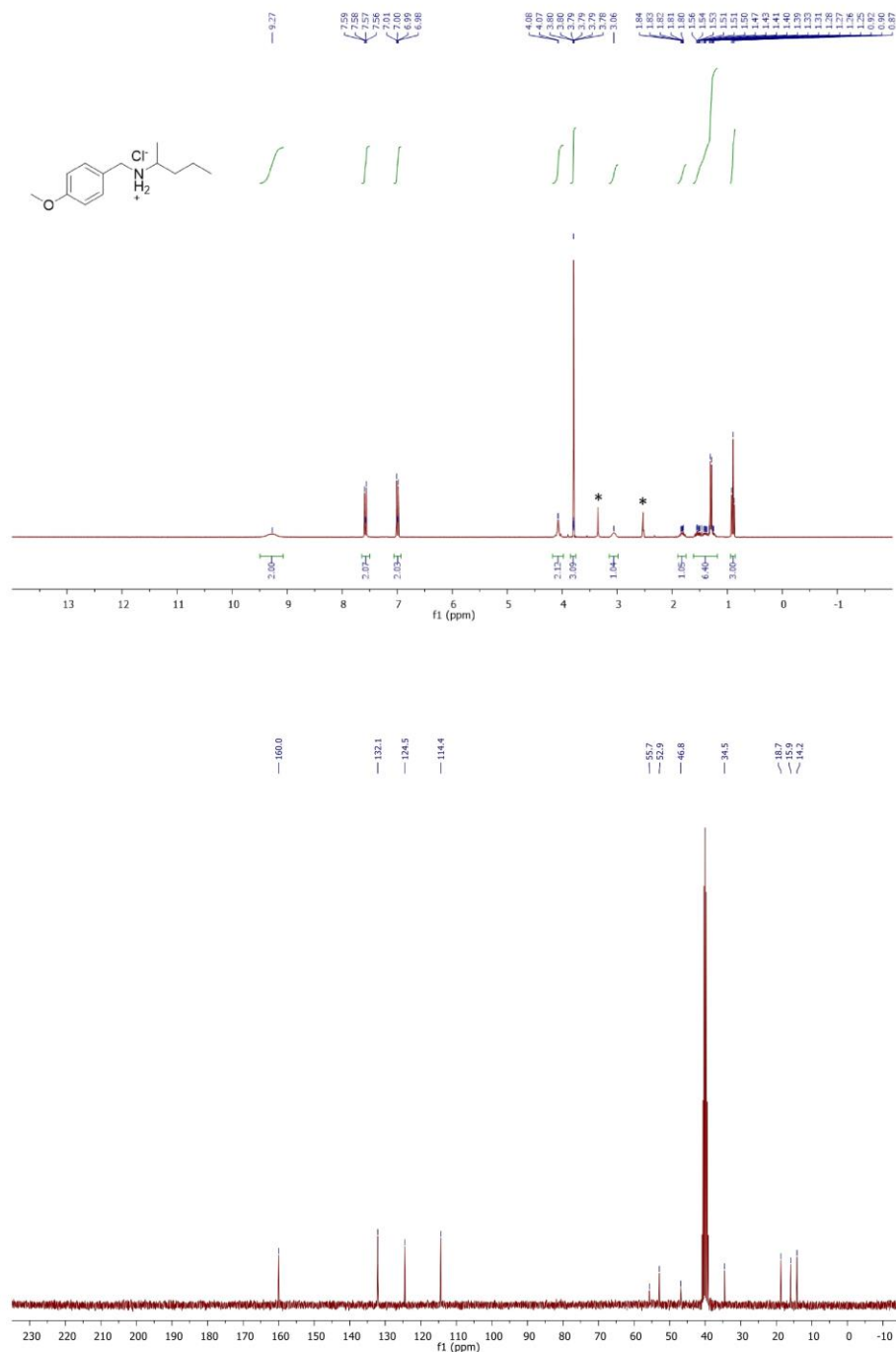


Estimation quality is indicated by color: good, medium, rough



SUPPORTING INFORMATION

24:

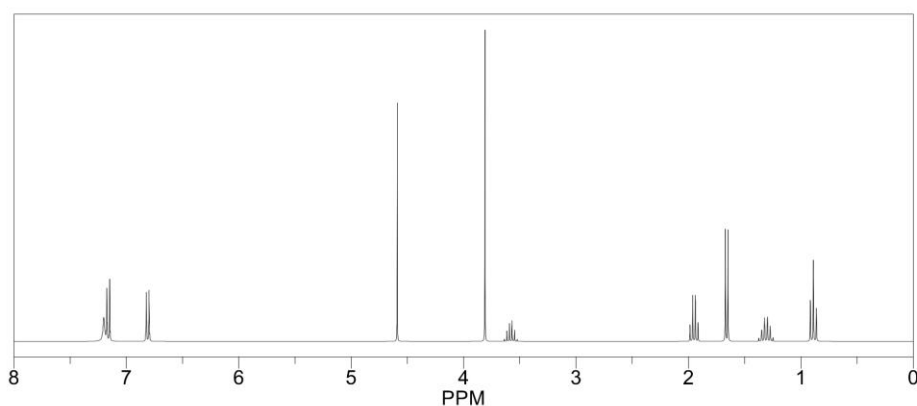


SUPPORTING INFORMATION

ChemNMR ^1H Estimation



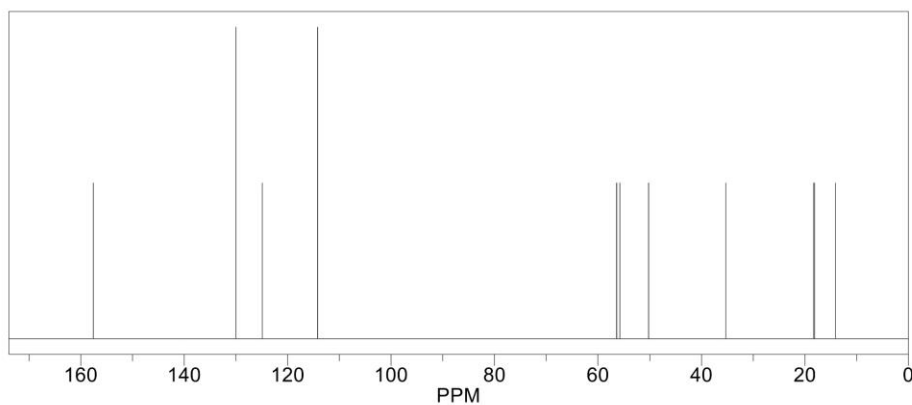
Estimation quality is indicated by color: good, medium, rough



ChemNMR ^{13}C Estimation



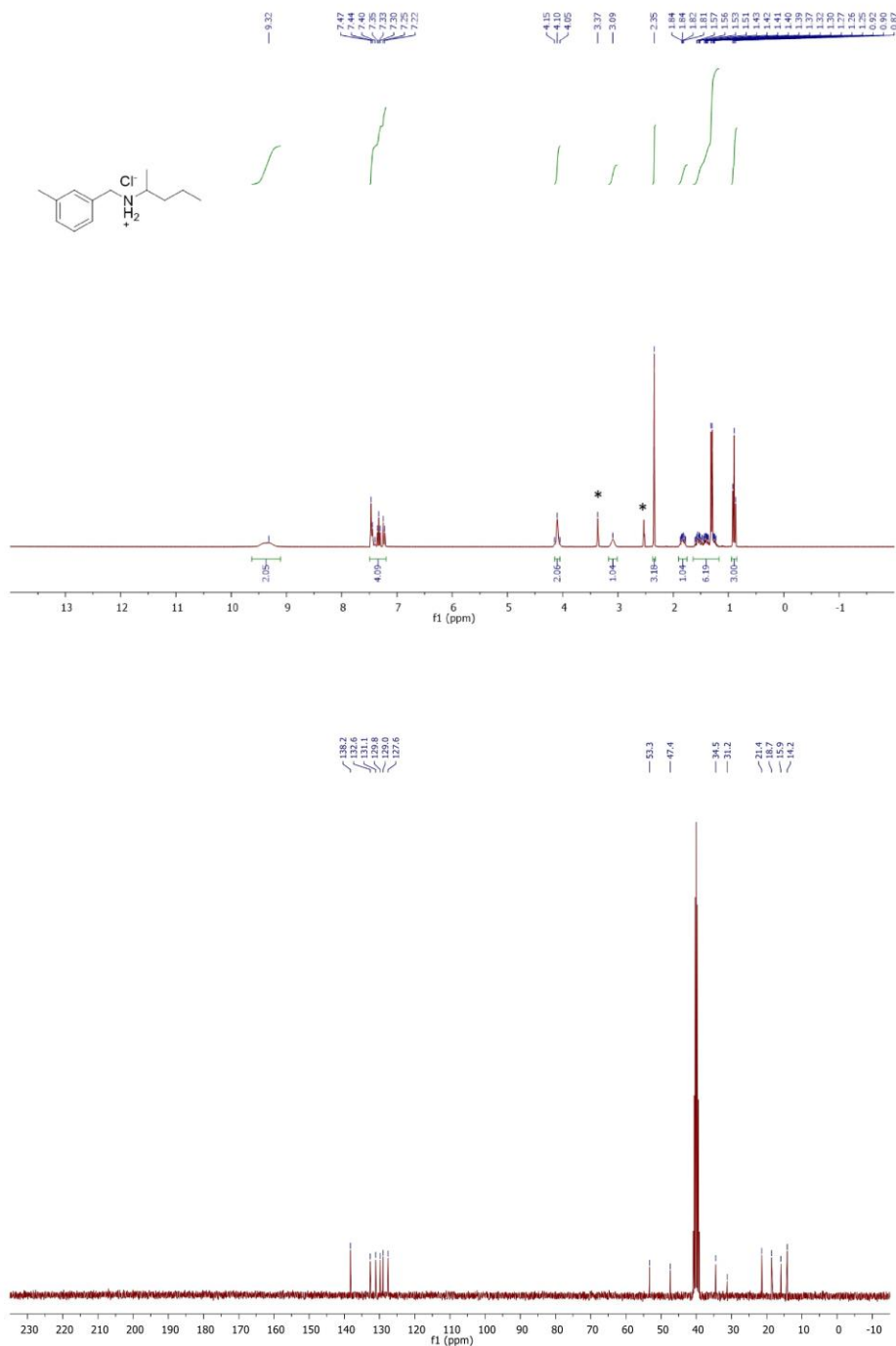
Estimation quality is indicated by color: good, medium, rough



WILEY-VCH

SUPPORTING INFORMATION

25:

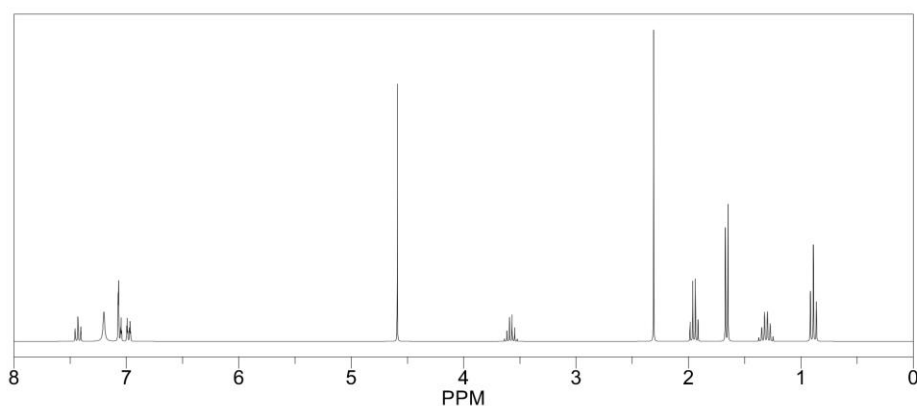


SUPPORTING INFORMATION

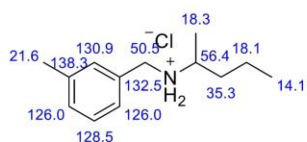
ChemNMR ^1H Estimation



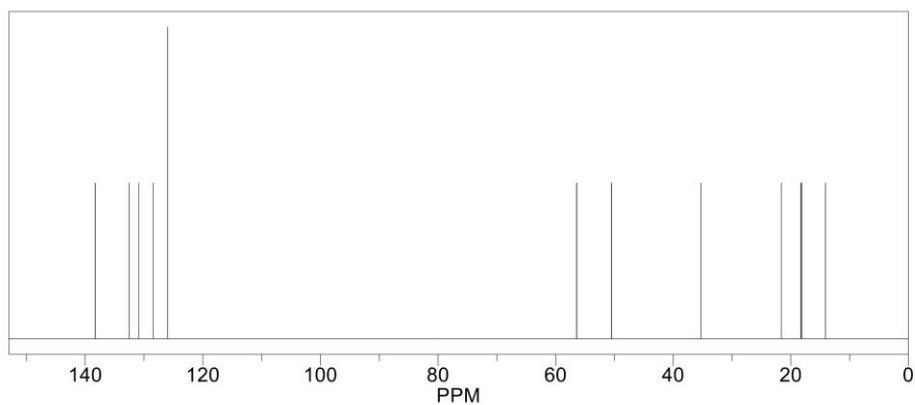
Estimation quality is indicated by color: good, medium, rough



ChemNMR ^{13}C Estimation



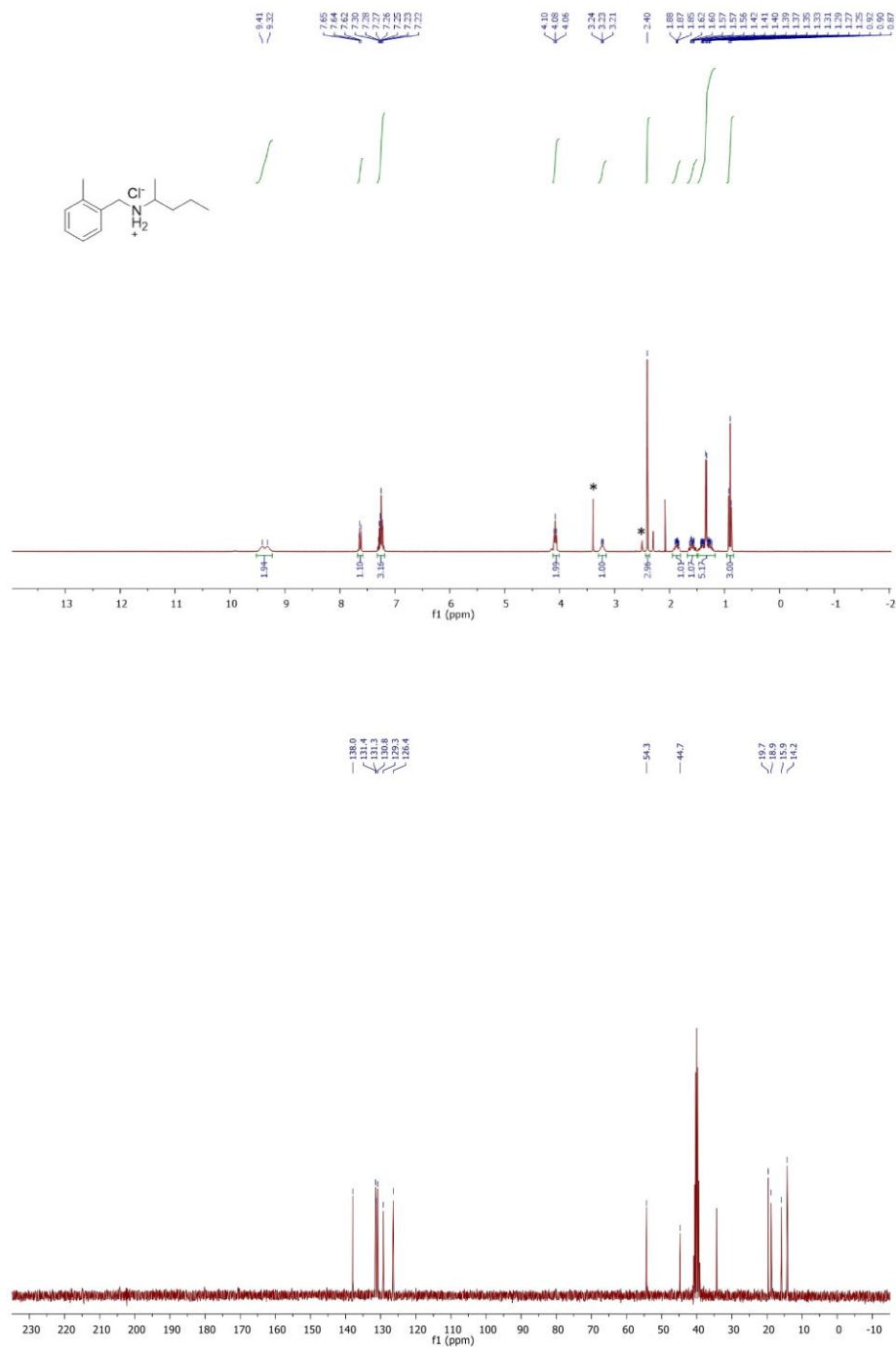
Estimation quality is indicated by color: good, medium, rough



WILEY-VCH

SUPPORTING INFORMATION

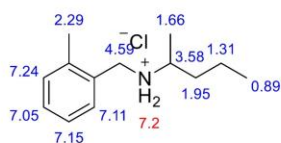
26:



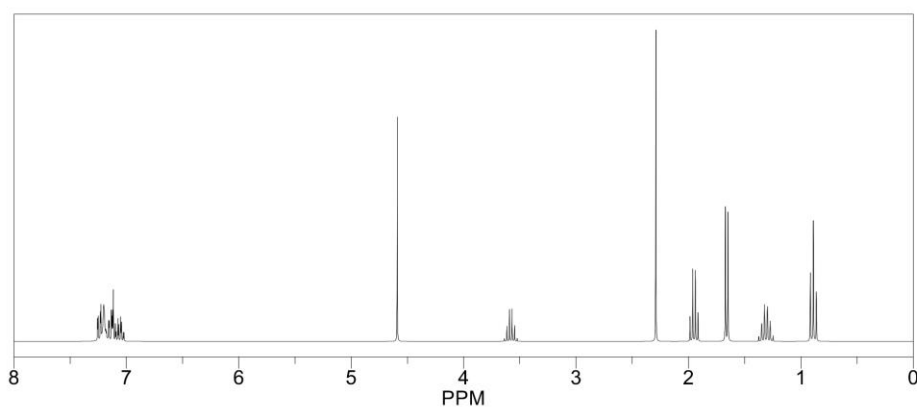
90

SUPPORTING INFORMATION

ChemNMR ^1H Estimation



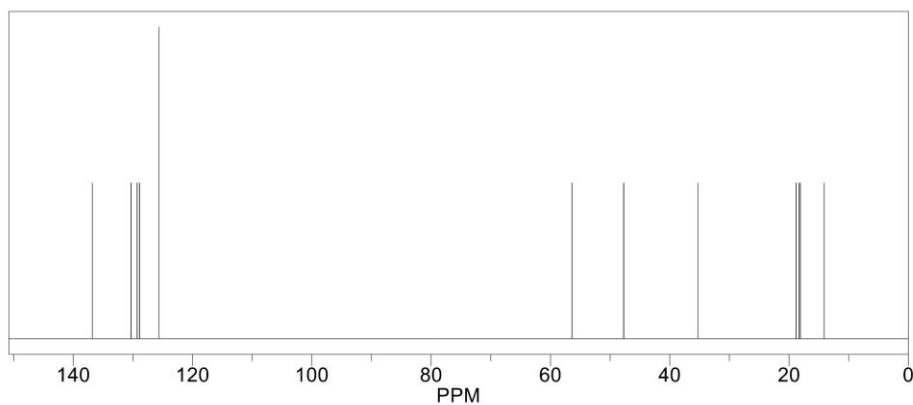
Estimation quality is indicated by color: good, medium, rough



ChemNMR ^{13}C Estimation



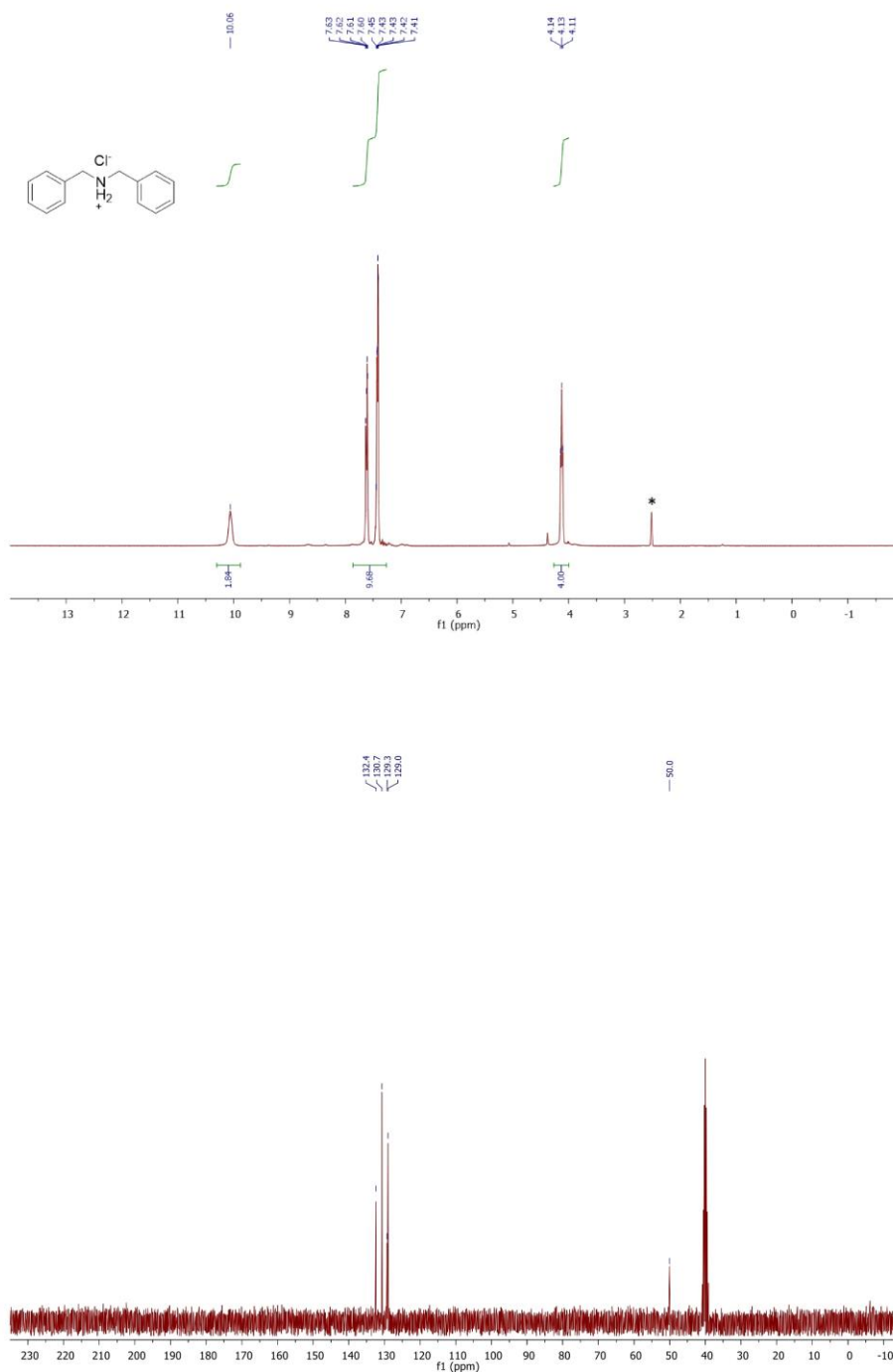
Estimation quality is indicated by color: good, medium, rough



WILEY-VCH

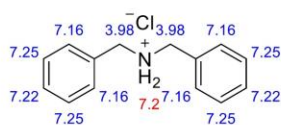
SUPPORTING INFORMATION

27:

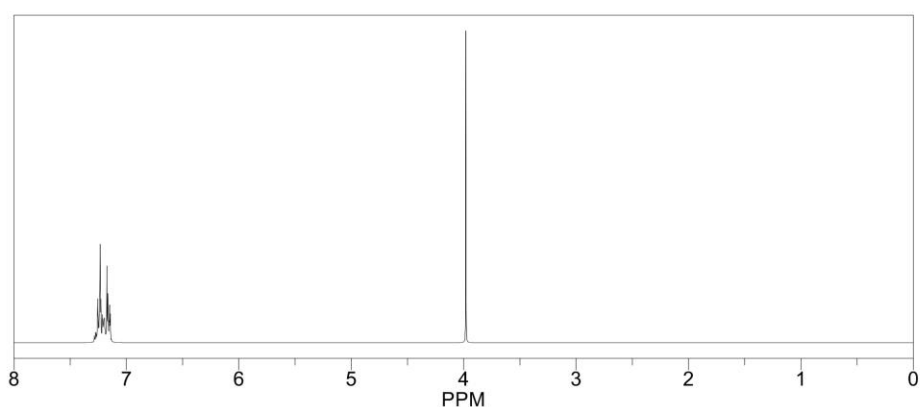


SUPPORTING INFORMATION

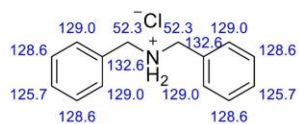
ChemNMR ^1H Estimation



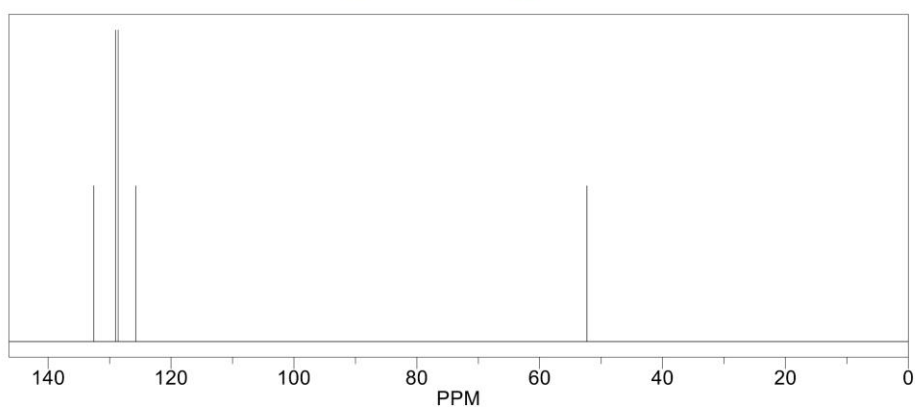
Estimation quality is indicated by color: good, medium, rough



ChemNMR ^{13}C Estimation



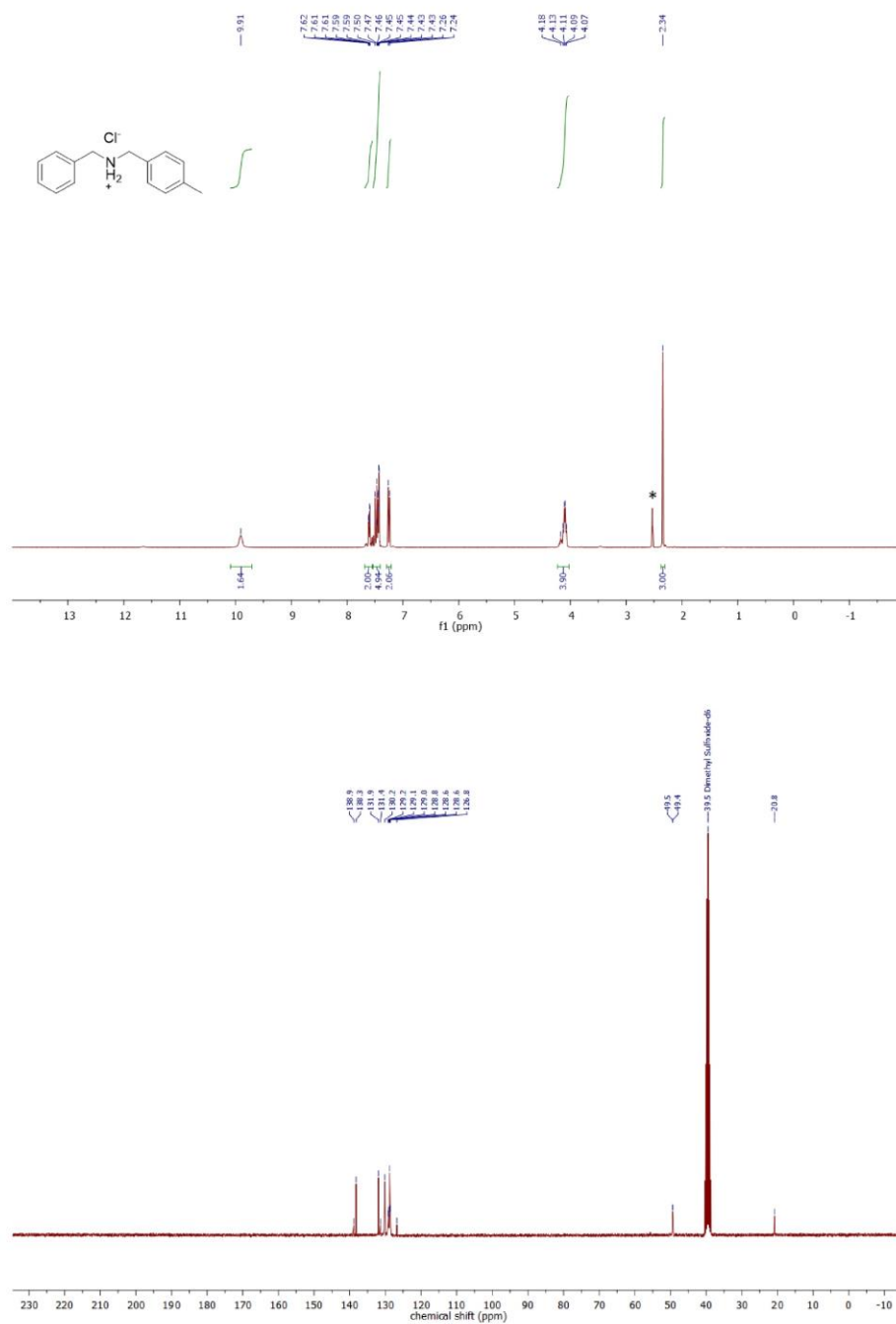
Estimation quality is indicated by color: good, medium, rough



WILEY-VCH

SUPPORTING INFORMATION

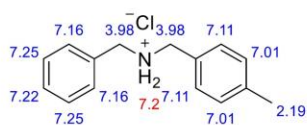
28:



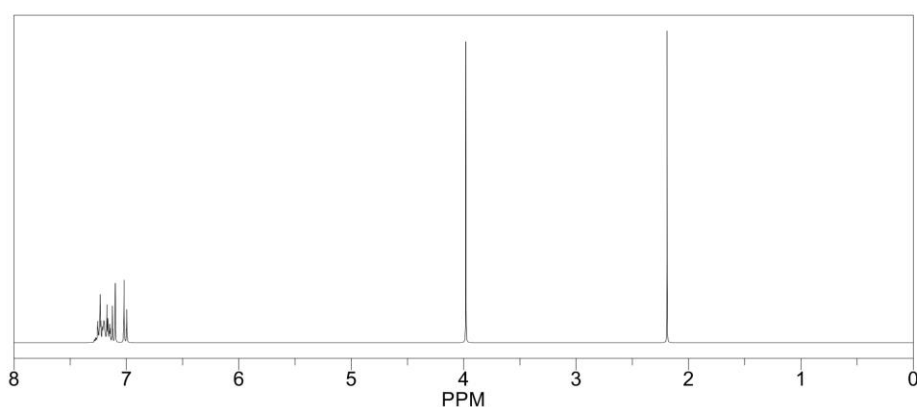
WILEY-VCH

SUPPORTING INFORMATION

ChemNMR ^1H Estimation



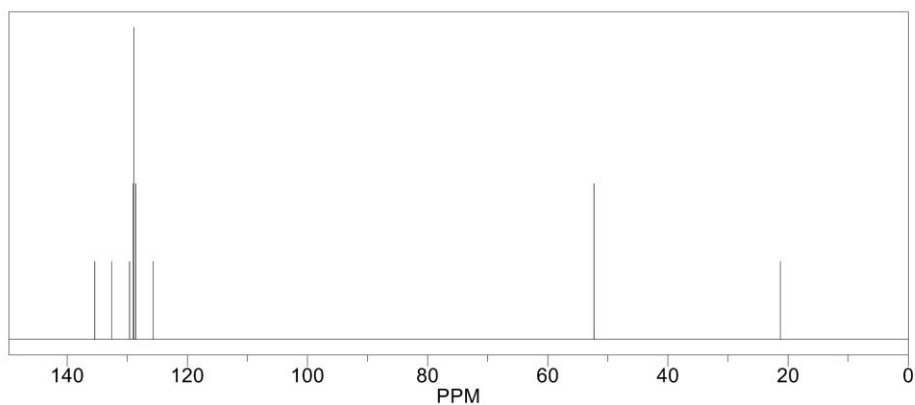
Estimation quality is indicated by color: good, medium, rough



ChemNMR ^{13}C Estimation



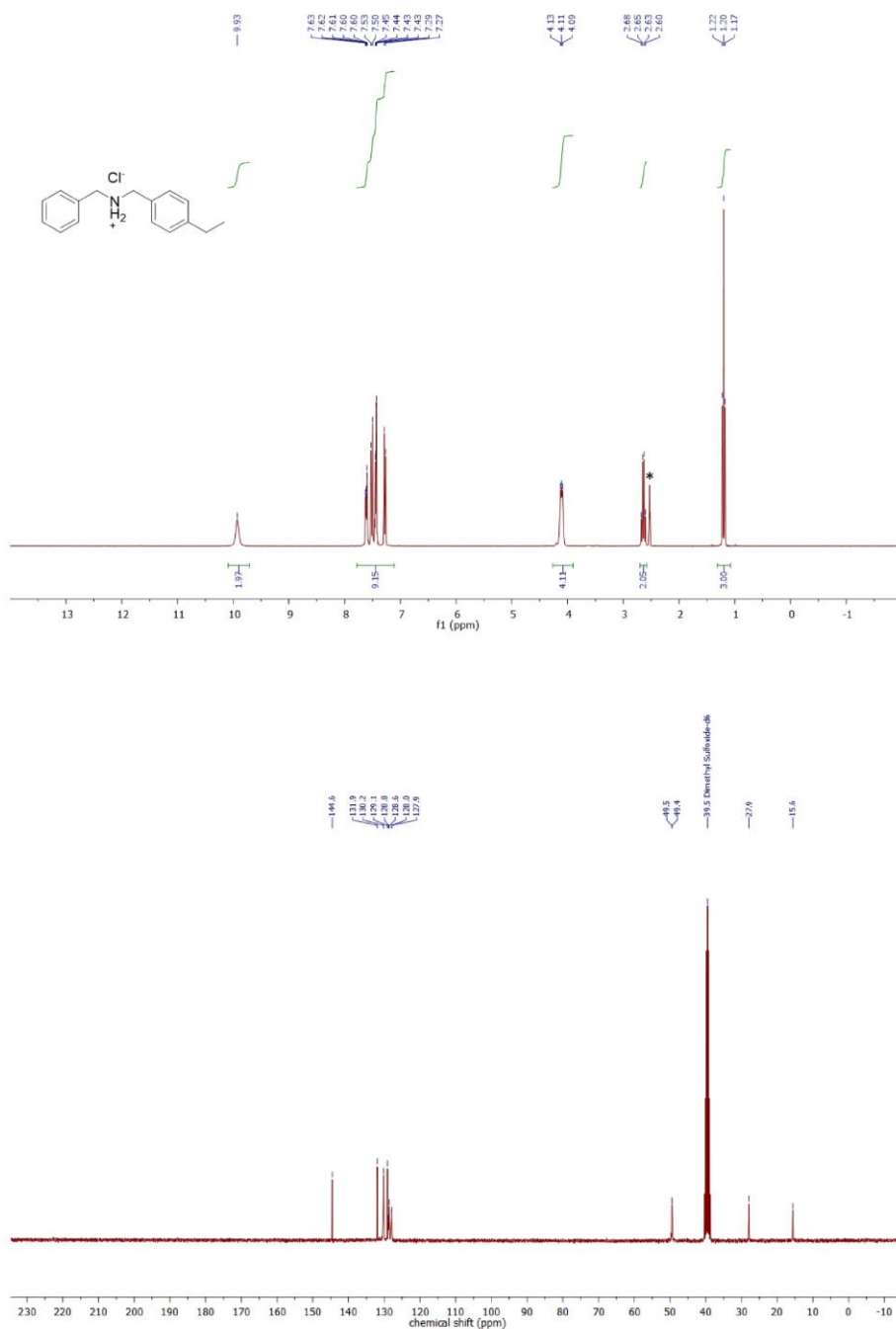
Estimation quality is indicated by color: good, medium, rough

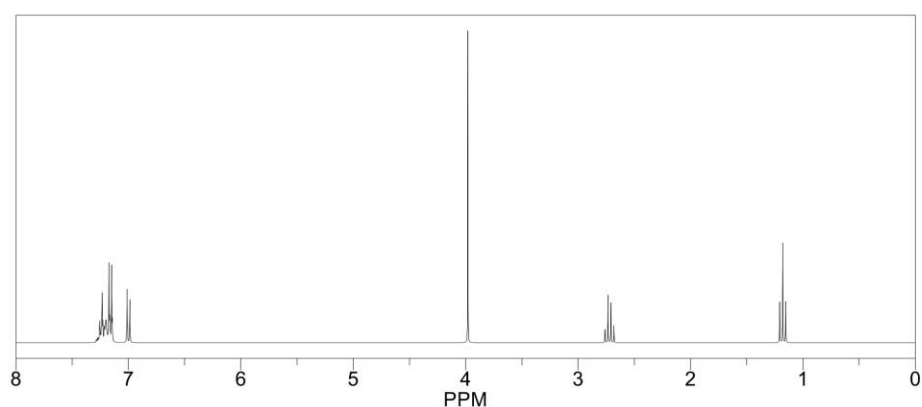
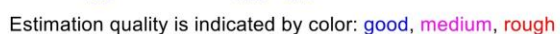
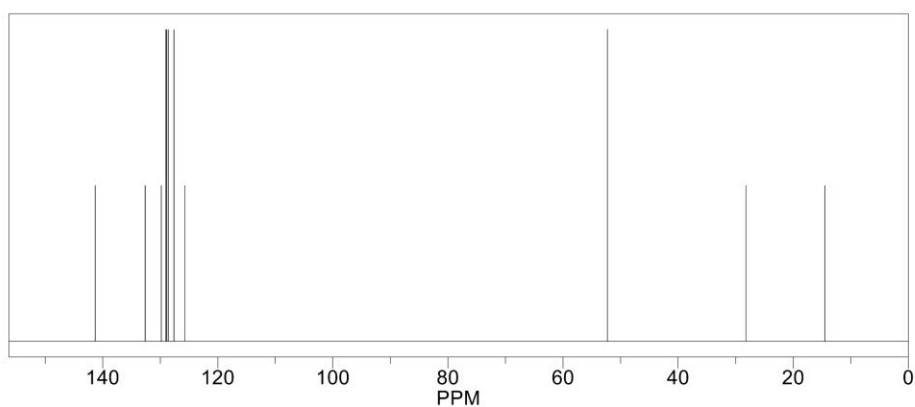
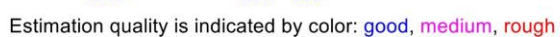


WILEY-VCH

SUPPORTING INFORMATION

29:

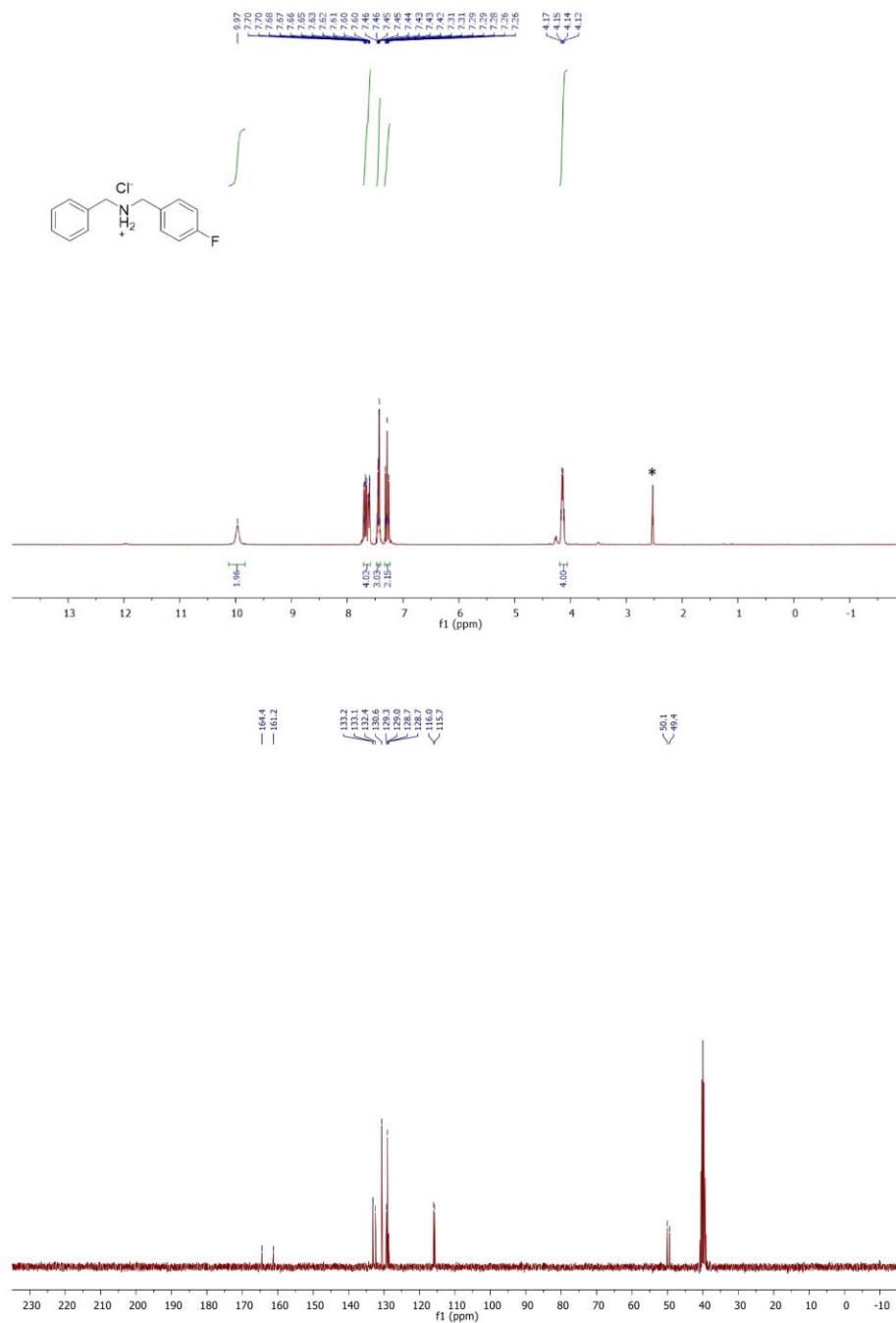


ChemNMR ¹H EstimationChemNMR ¹³C Estimation

WILEY-VCH

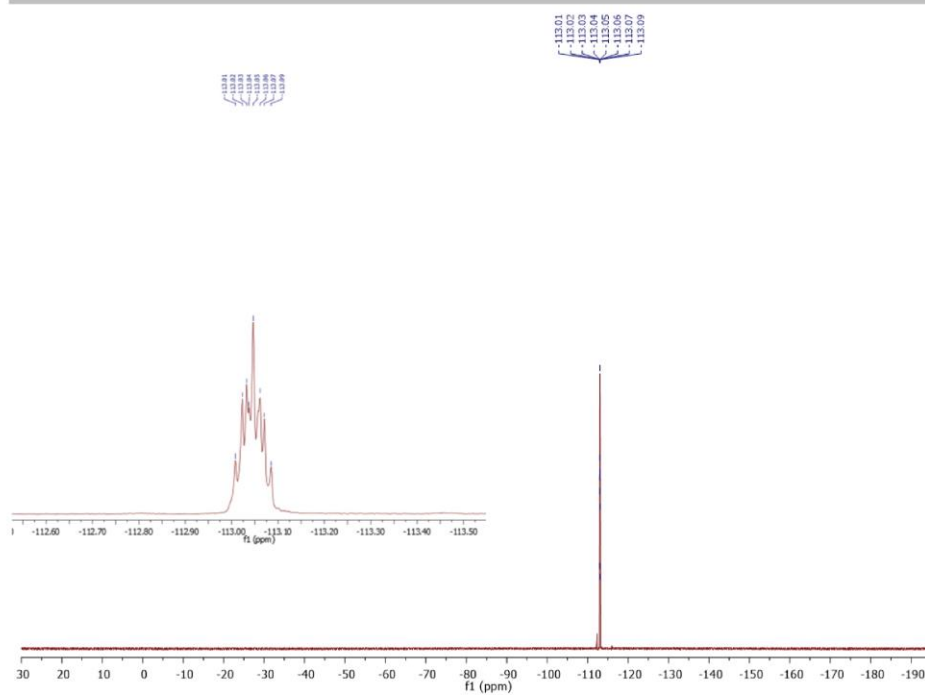
SUPPORTING INFORMATION

30:

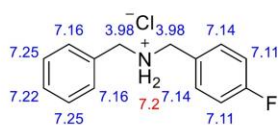


WILEY-VCH

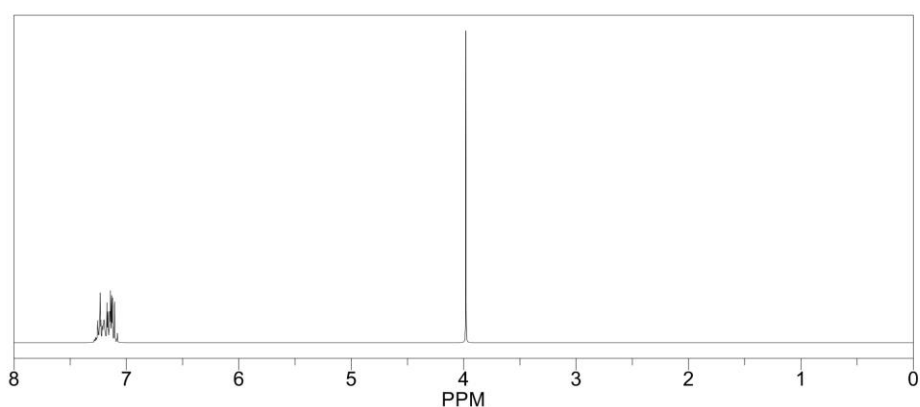
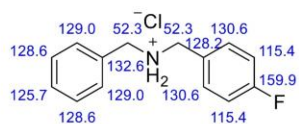
SUPPORTING INFORMATION



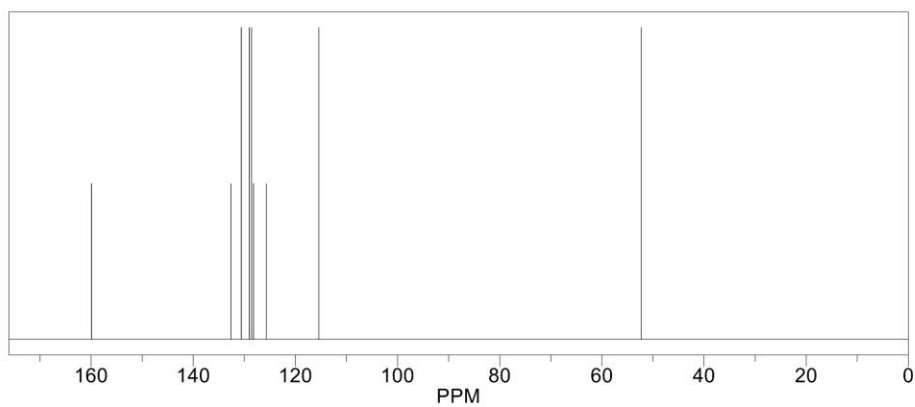
SUPPORTING INFORMATION

ChemNMR ^1H Estimation

Estimation quality is indicated by color: good, medium, rough

ChemNMR ^{13}C Estimation

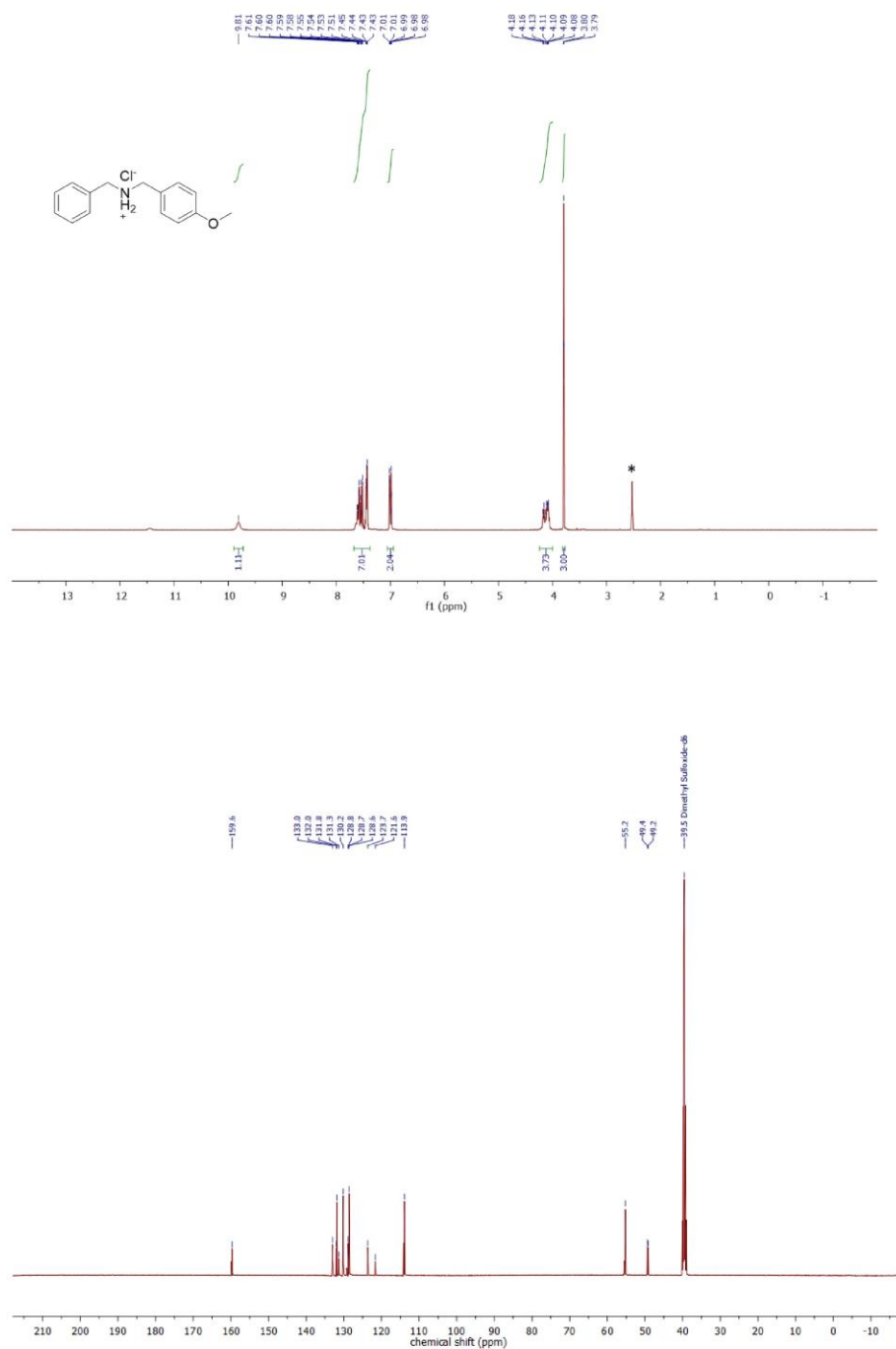
Estimation quality is indicated by color: good, medium, rough

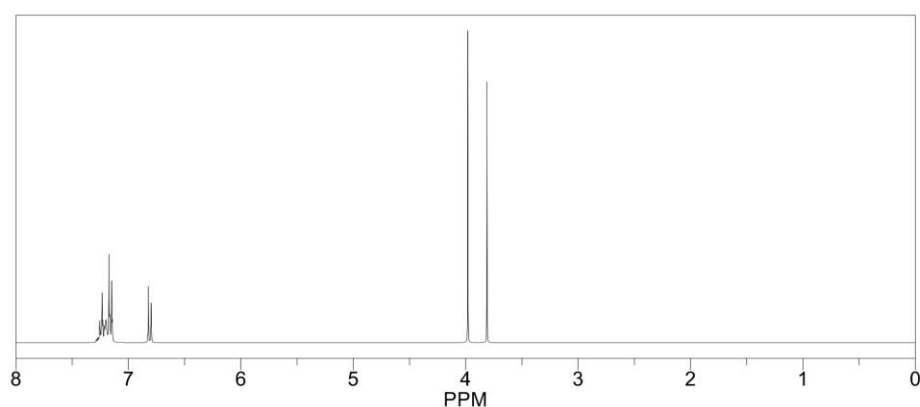
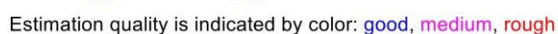
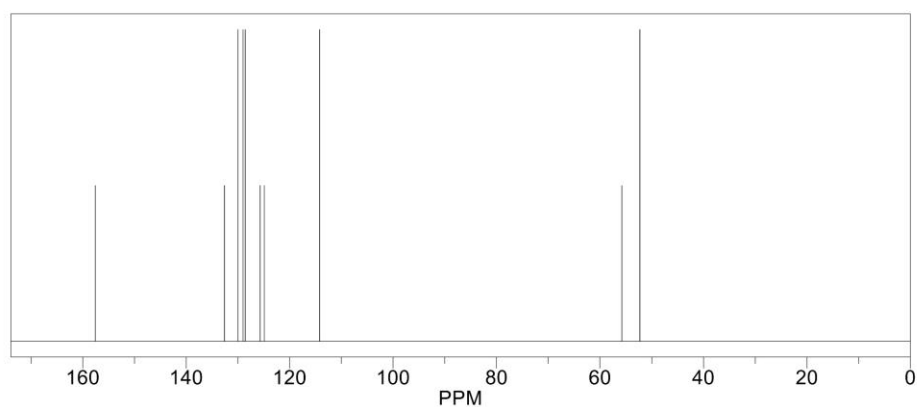
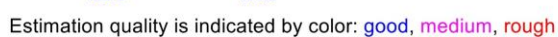


WILEY-VCH

SUPPORTING INFORMATION

31:

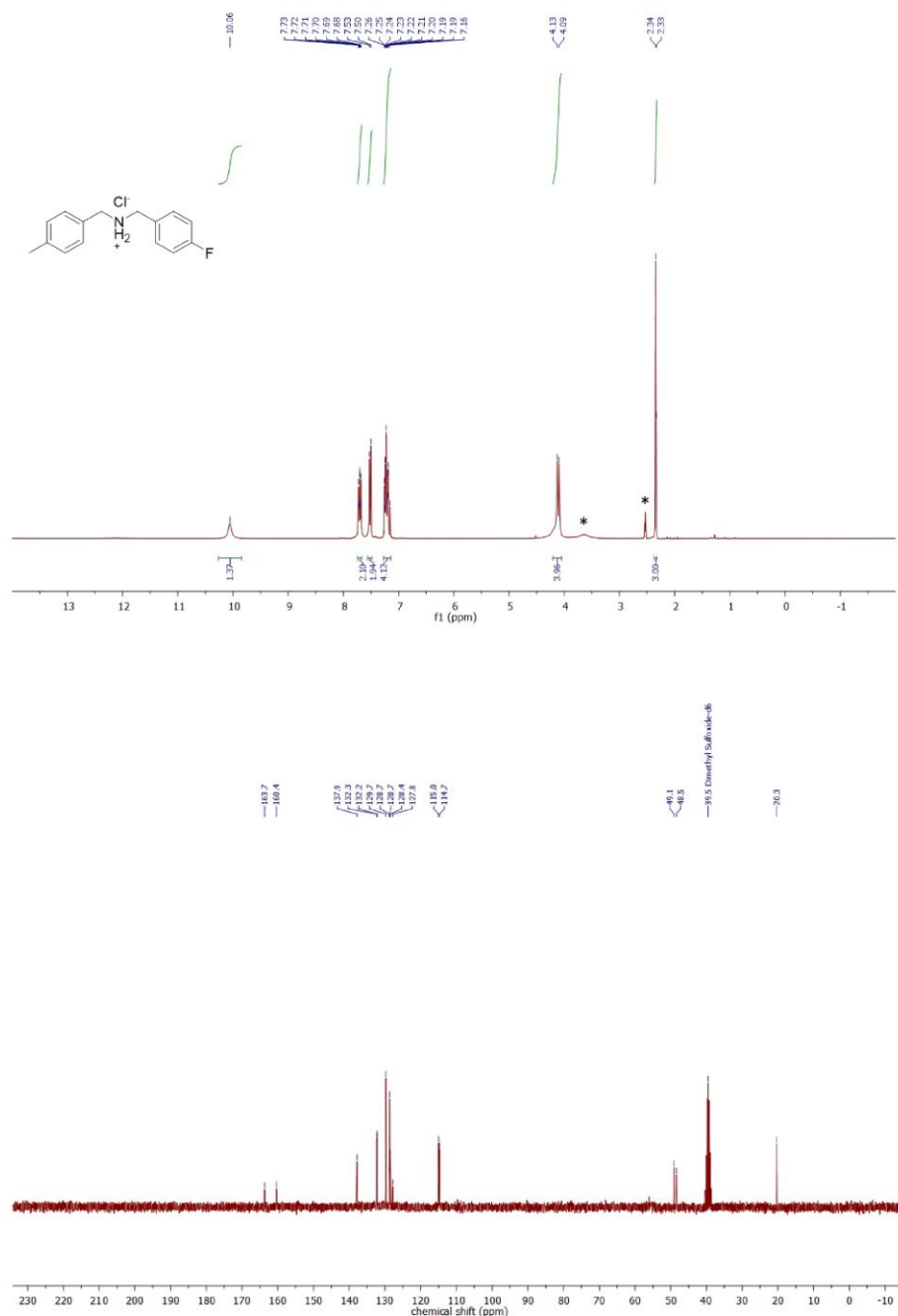


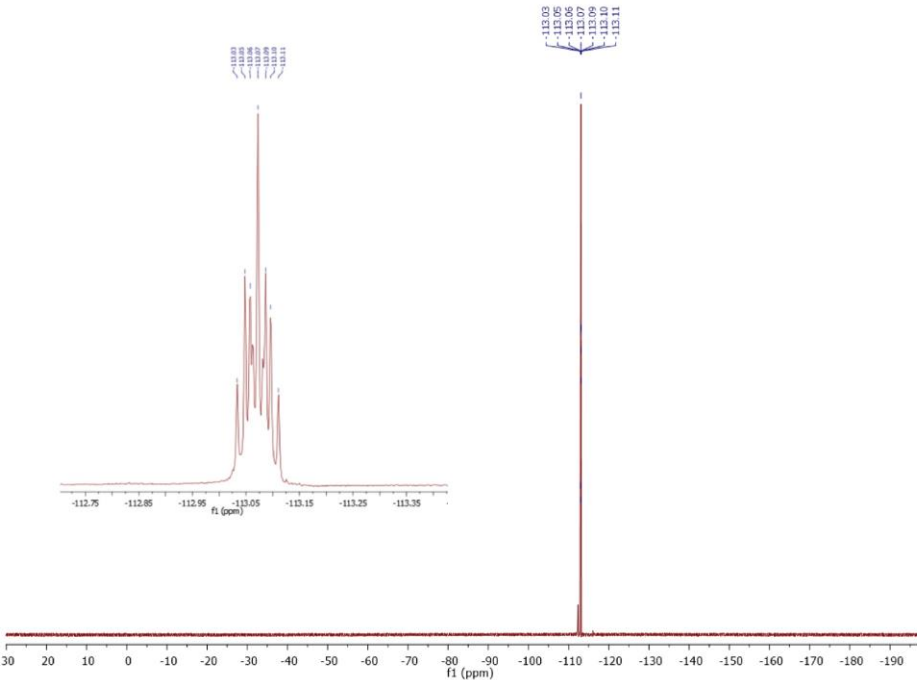
ChemNMR ¹H EstimationChemNMR ¹³C Estimation

WILEY-VCH

SUPPORTING INFORMATION

32:





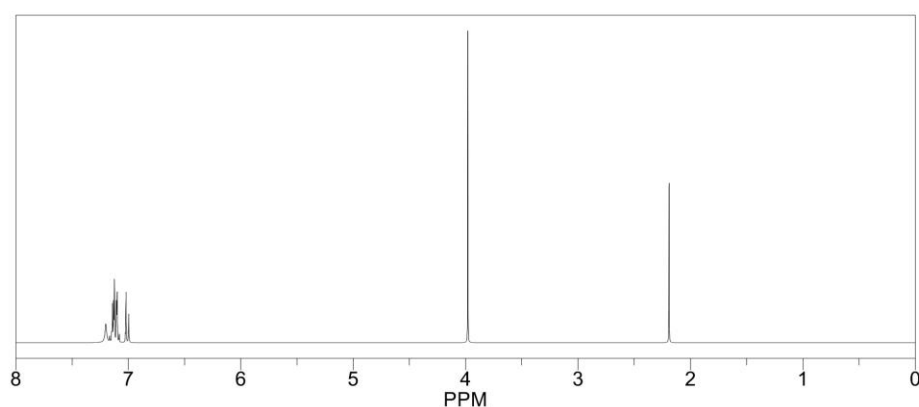
WILEY-VCH

SUPPORTING INFORMATION

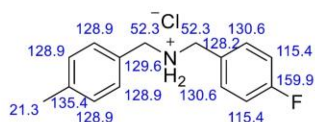
ChemNMR ^1H Estimation



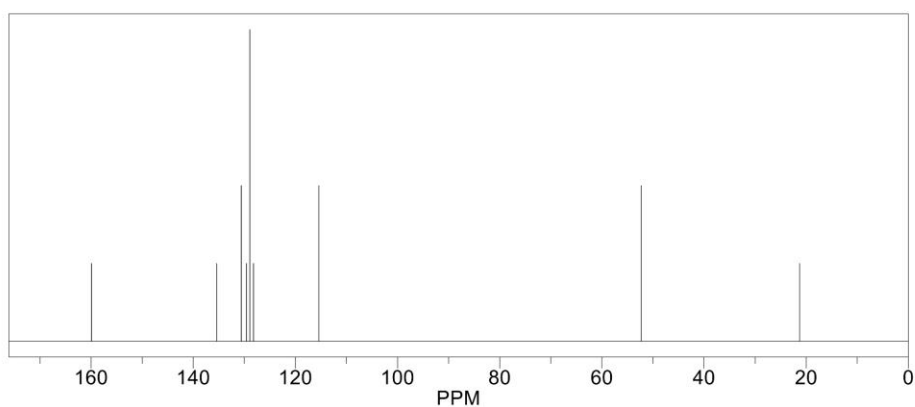
Estimation quality is indicated by color: good, medium, rough



ChemNMR ^{13}C Estimation



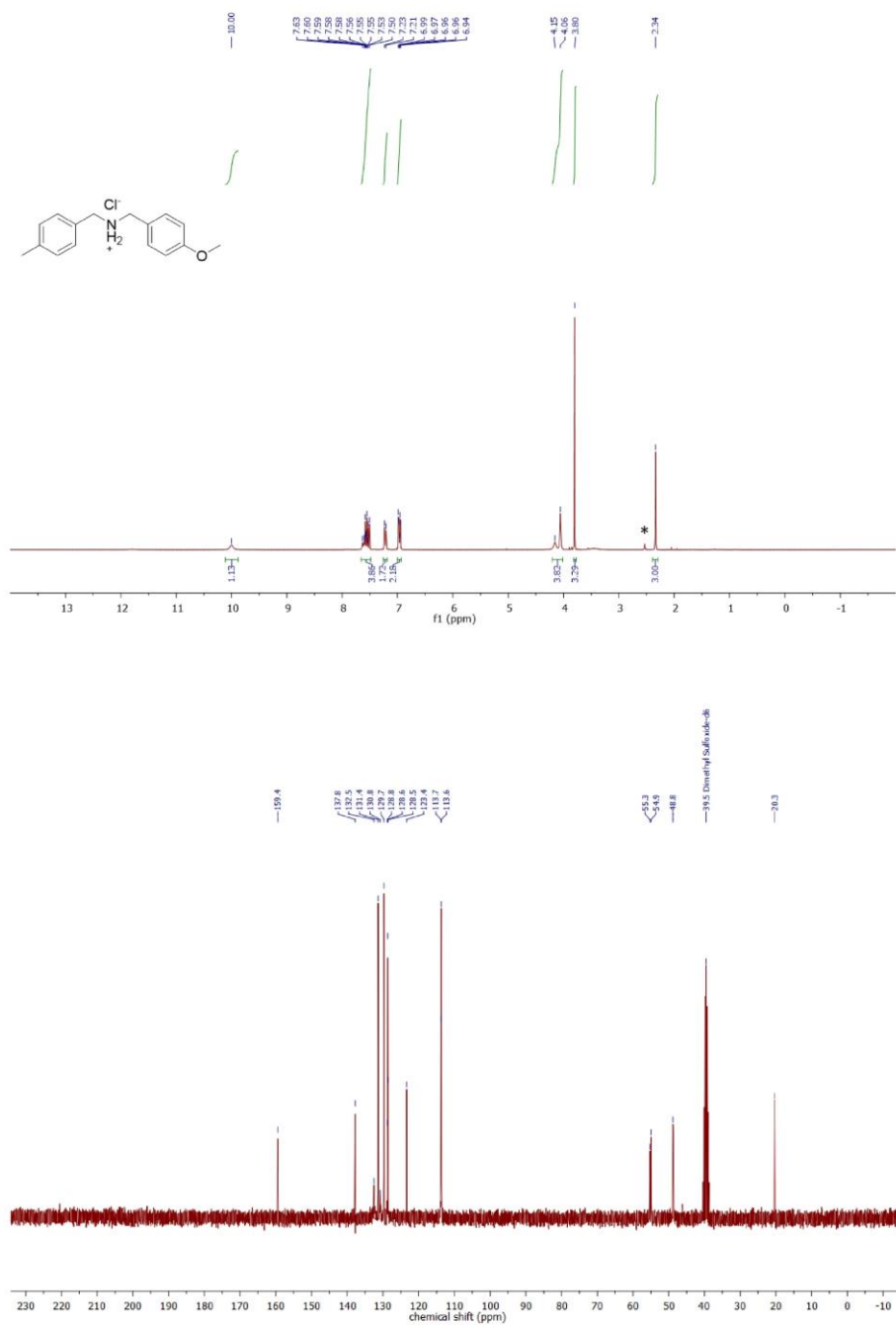
Estimation quality is indicated by color: good, medium, rough



WILEY-VCH

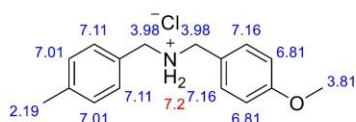
SUPPORTING INFORMATION

33:

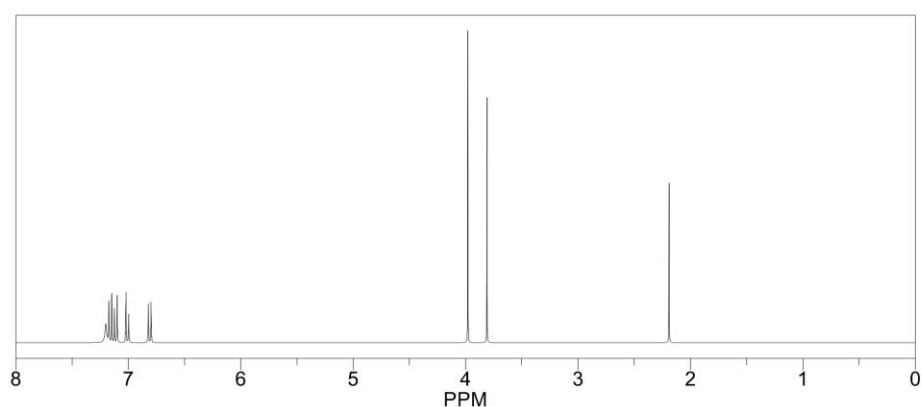


SUPPORTING INFORMATION

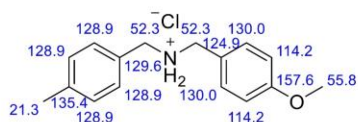
ChemNMR ^1H Estimation



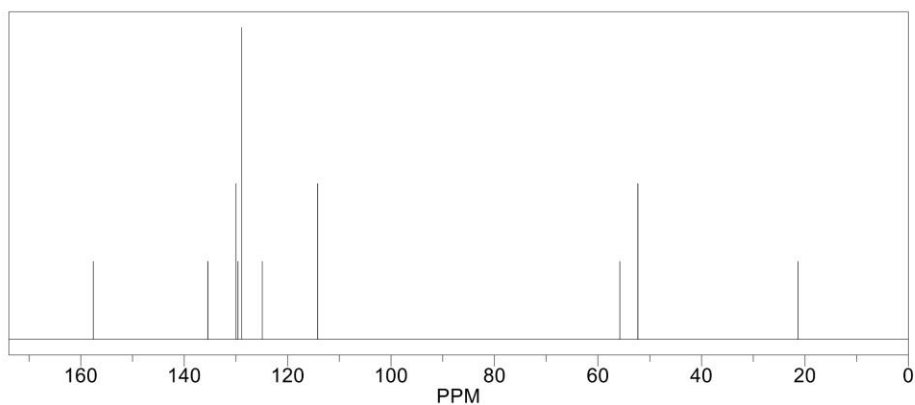
Estimation quality is indicated by color: good, medium, rough



ChemNMR ^{13}C Estimation



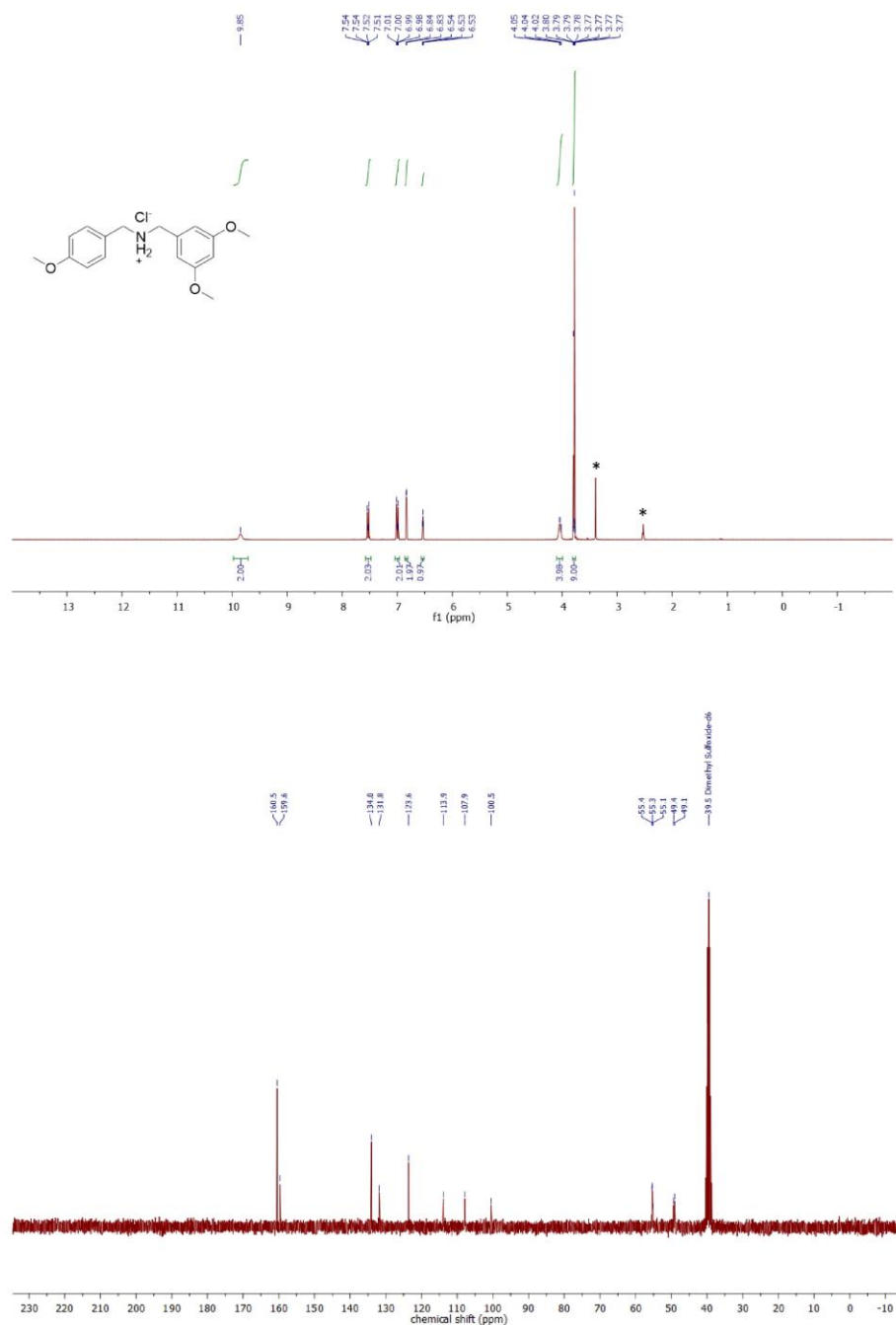
Estimation quality is indicated by color: good, medium, rough



WILEY-VCH

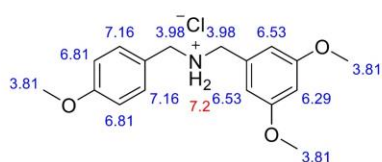
SUPPORTING INFORMATION

34:

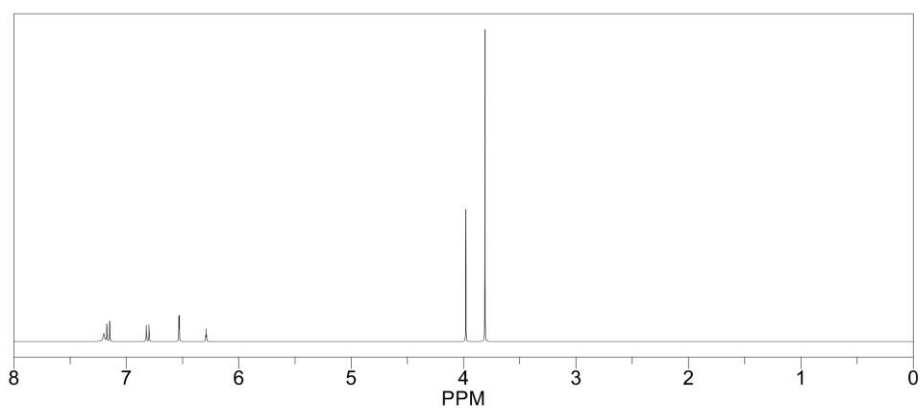


SUPPORTING INFORMATION

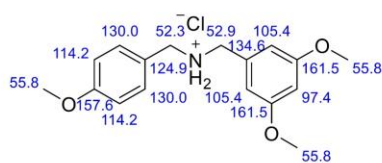
ChemNMR ^1H Estimation



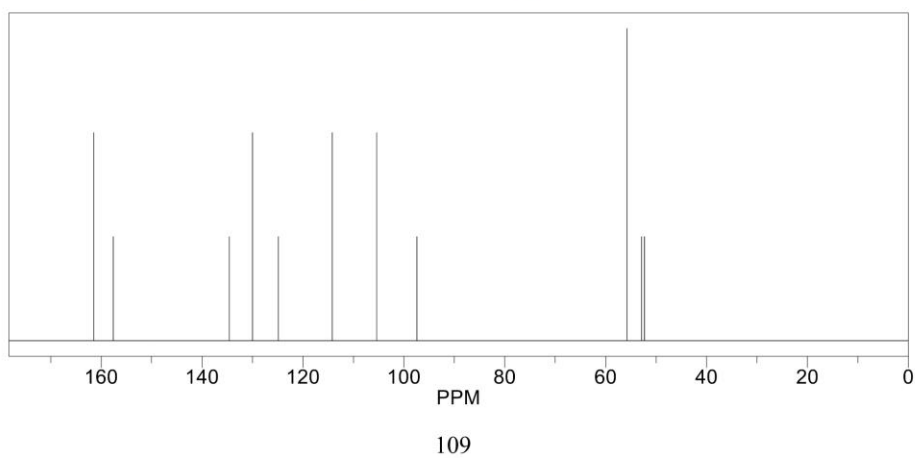
Estimation quality is indicated by color: good, medium, rough



ChemNMR ^{13}C Estimation



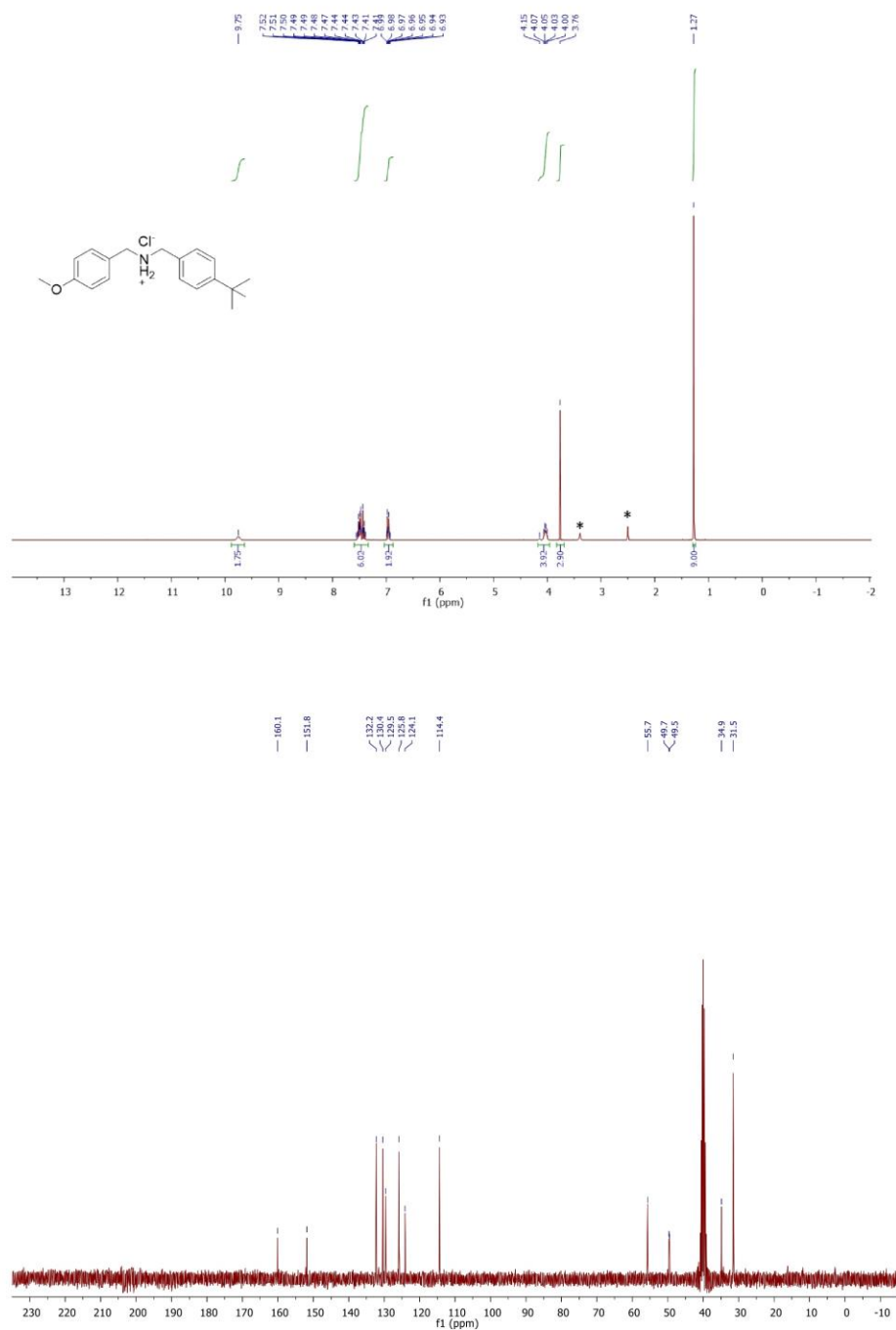
Estimation quality is indicated by color: good, medium, rough

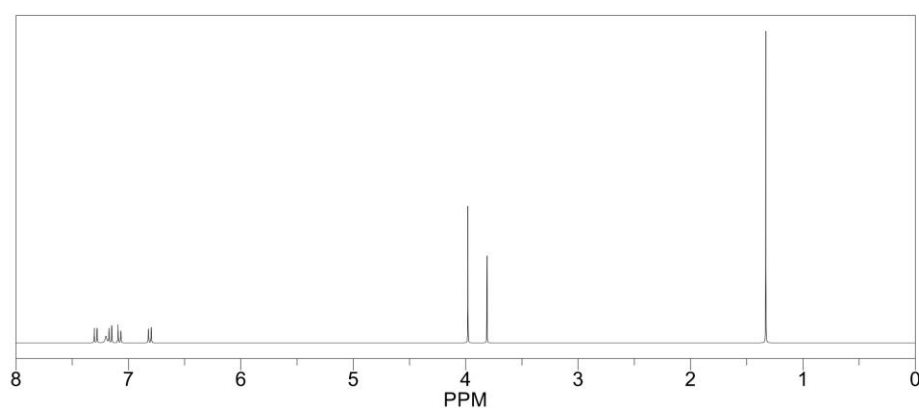
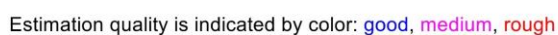


WILEY-VCH

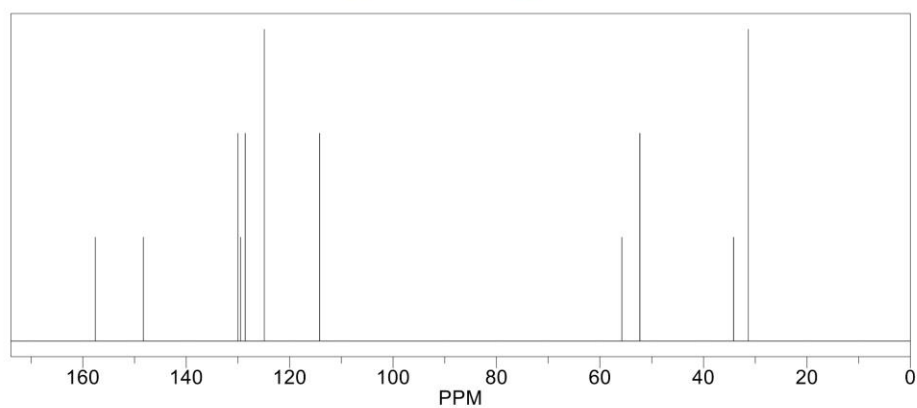
SUPPORTING INFORMATION

35:



ChemNMR ¹H Estimation

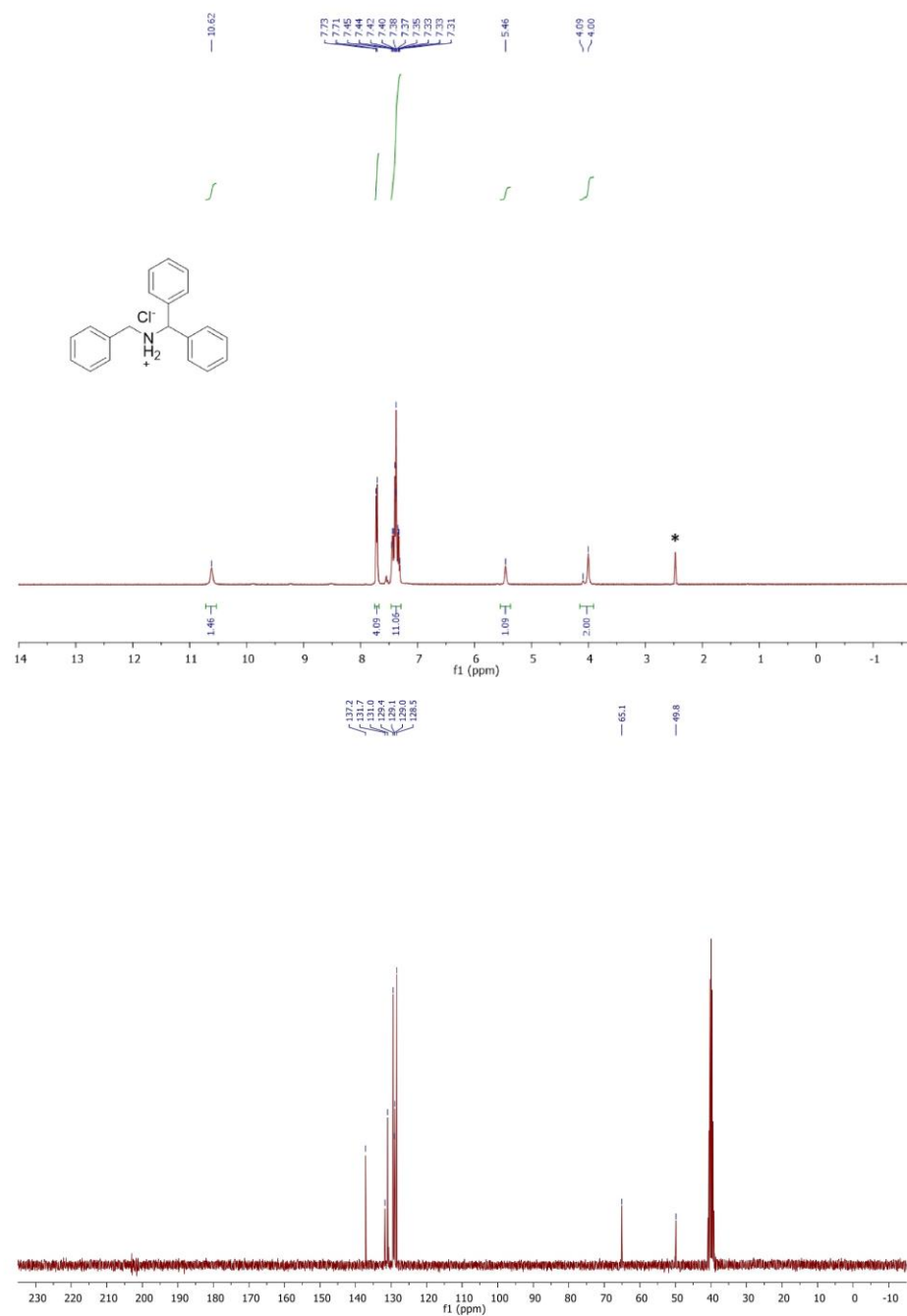
Estimation quality is indicated by color: **good**, **medium**, **rough**

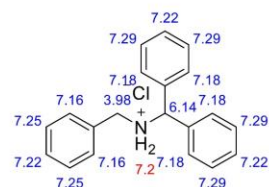


WILEY-VCH

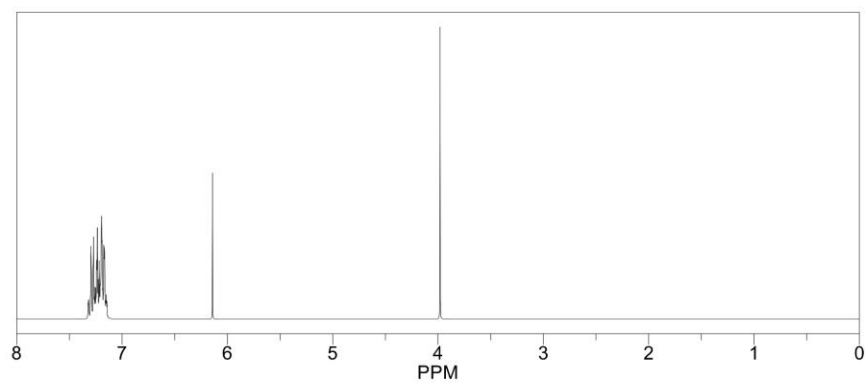
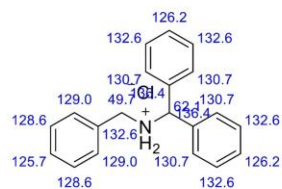
SUPPORTING INFORMATION

36:

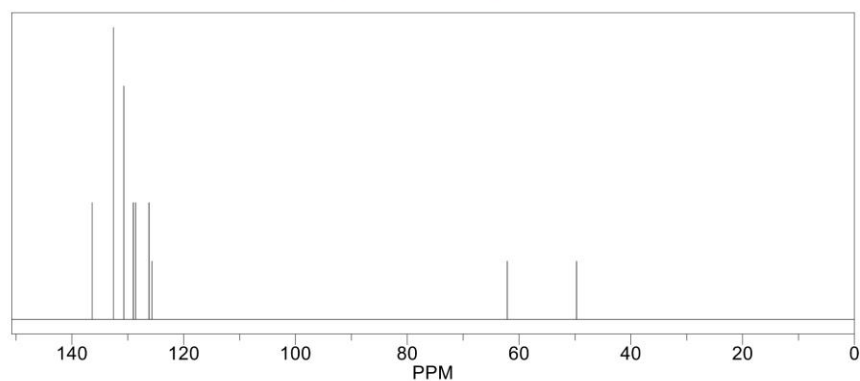


ChemNMR ¹H Estimation

Estimation quality is indicated by color: **good**, **medium**, **rough**

ChemNMR ¹³C Estimation

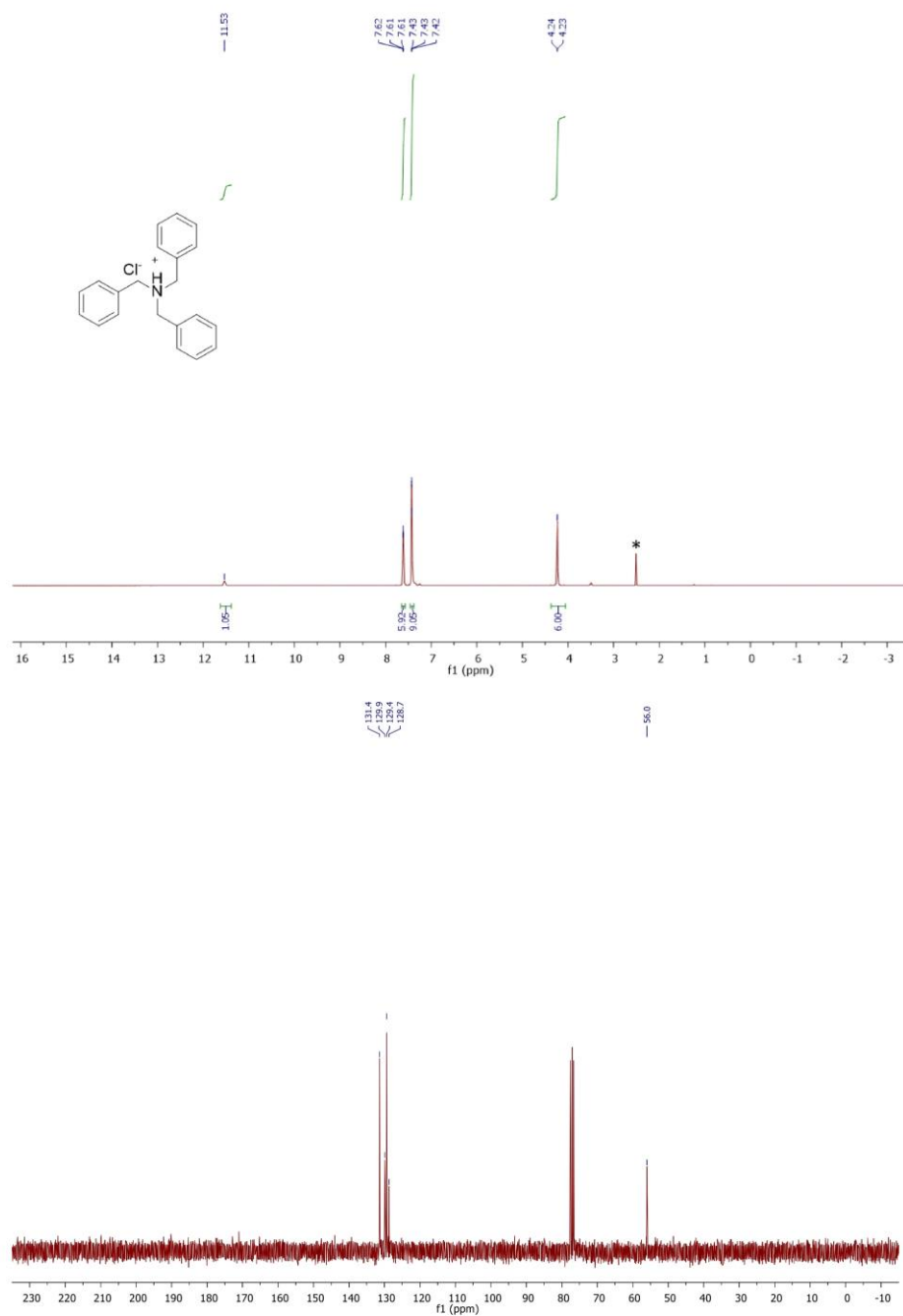
Estimation quality is indicated by color: **good**, **medium**, **rough**

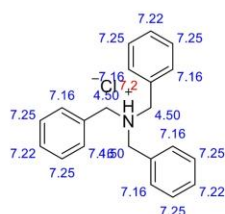


WILEY-VCH

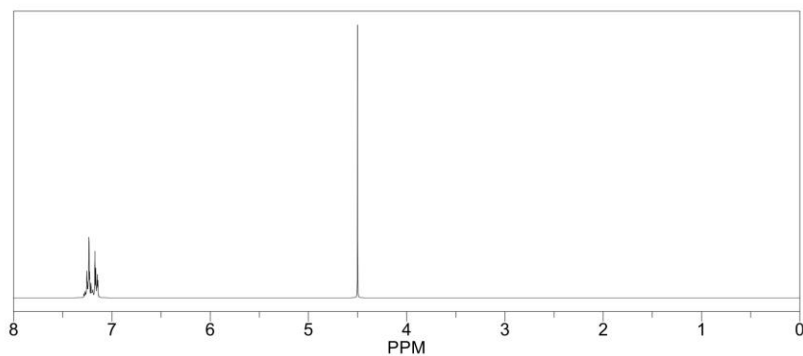
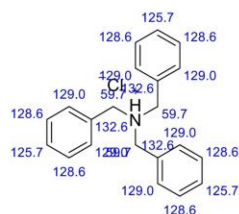
SUPPORTING INFORMATION

37:

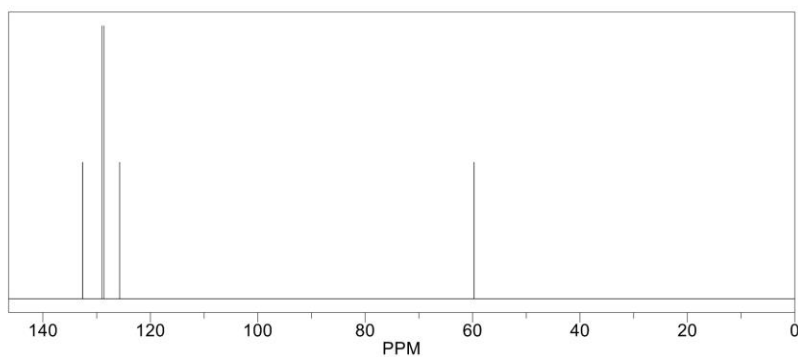


ChemNMR ¹H Estimation

Estimation quality is indicated by color: **good**, **medium**, **rough**

ChemNMR ¹³C Estimation

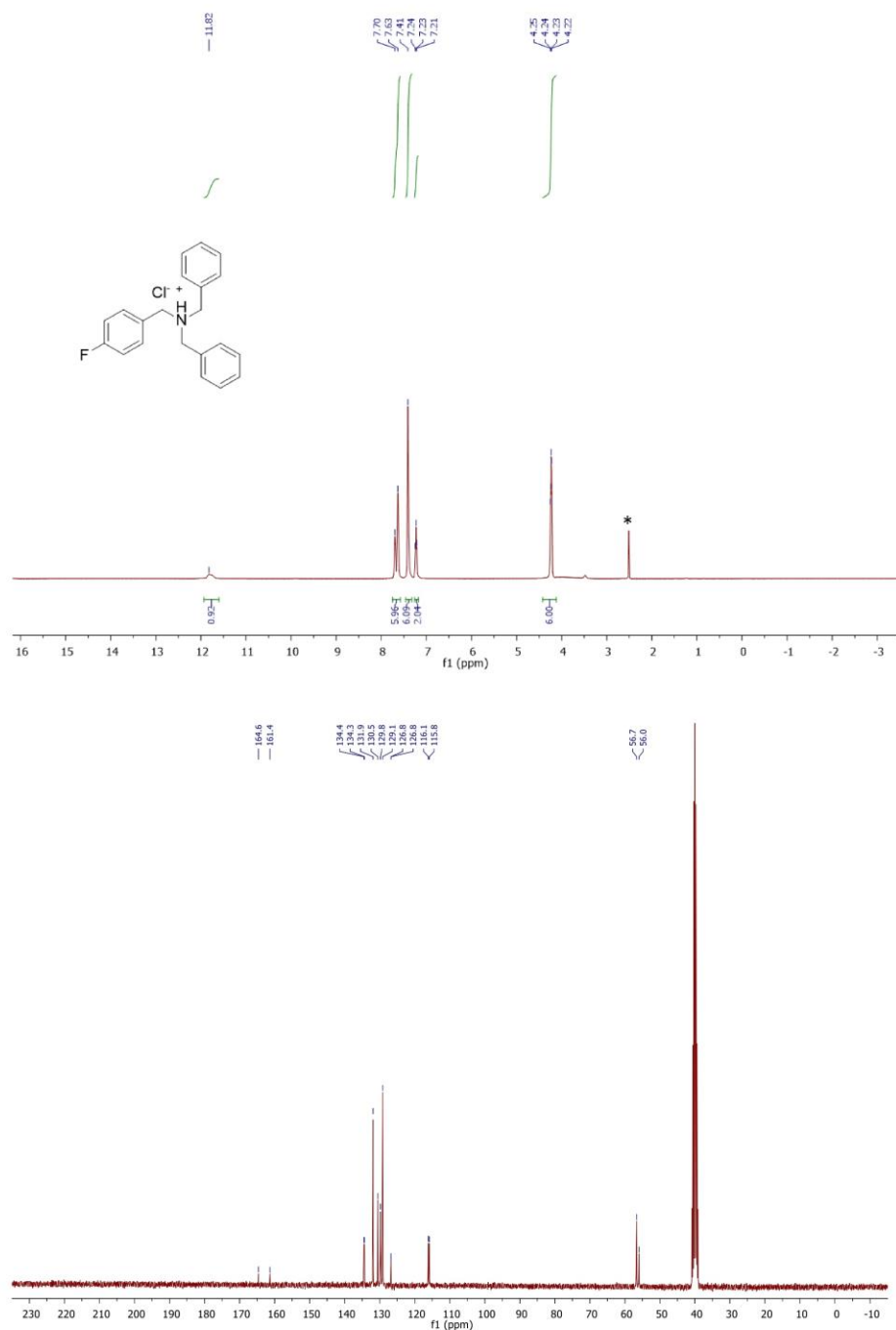
Estimation quality is indicated by color: **good**, **medium**, **rough**



WILEY-VCH

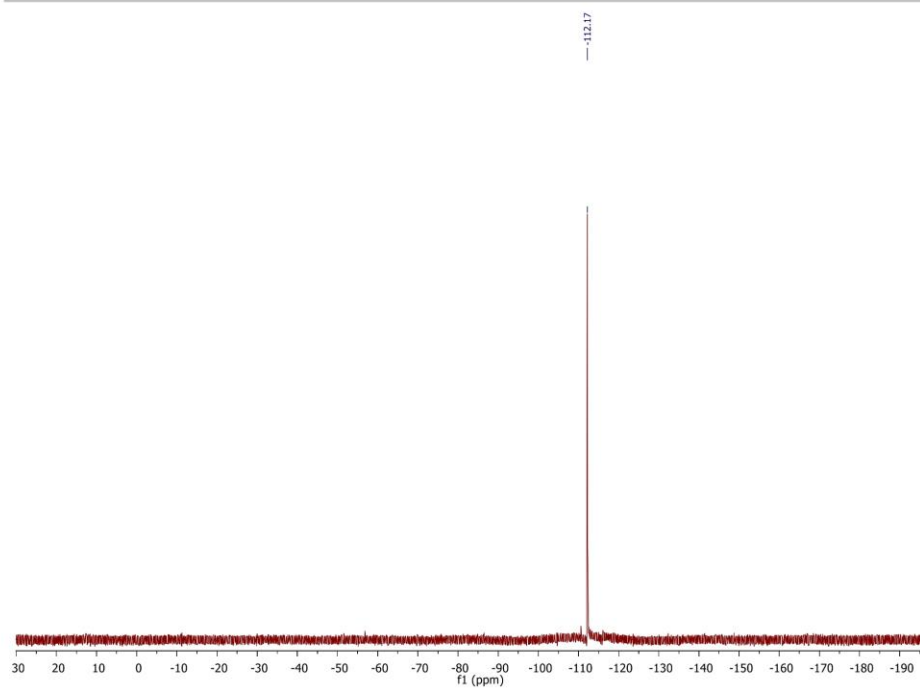
SUPPORTING INFORMATION

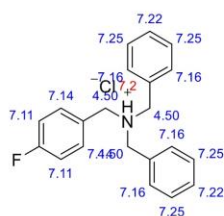
38:



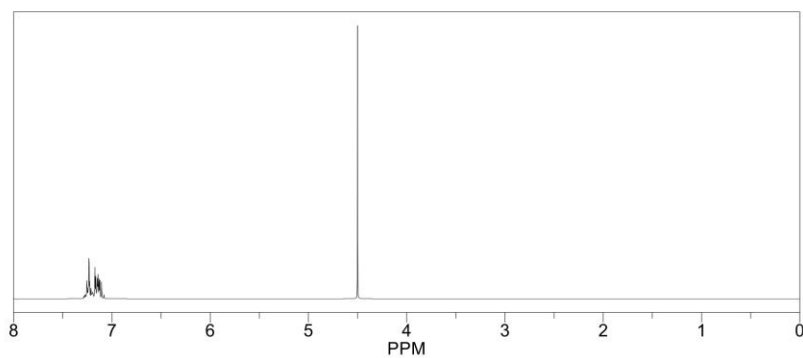
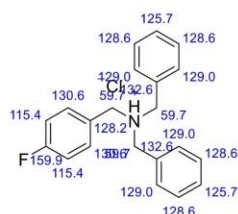
WILEY-VCH

SUPPORTING INFORMATION

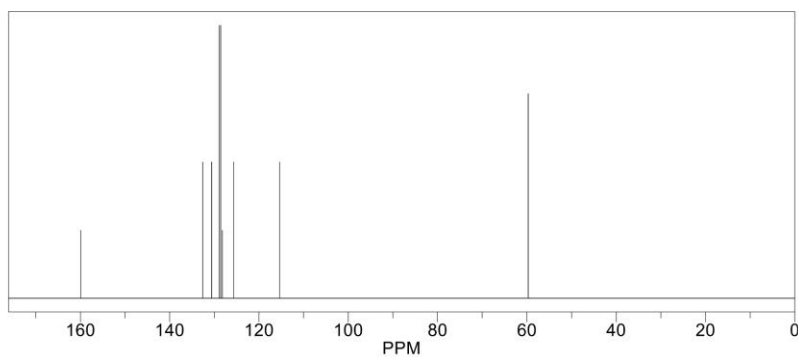


ChemNMR ¹H Estimation

Estimation quality is indicated by color: good, medium, rough

ChemNMR ¹³C Estimation

Estimation quality is indicated by color: **good**, **medium**, **rough**



WILEY-VCH

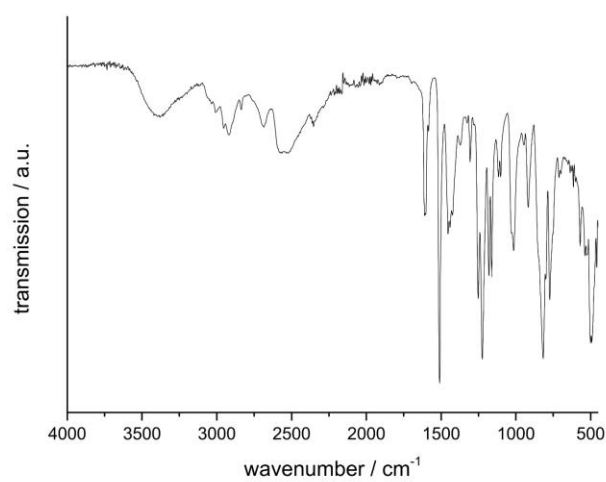
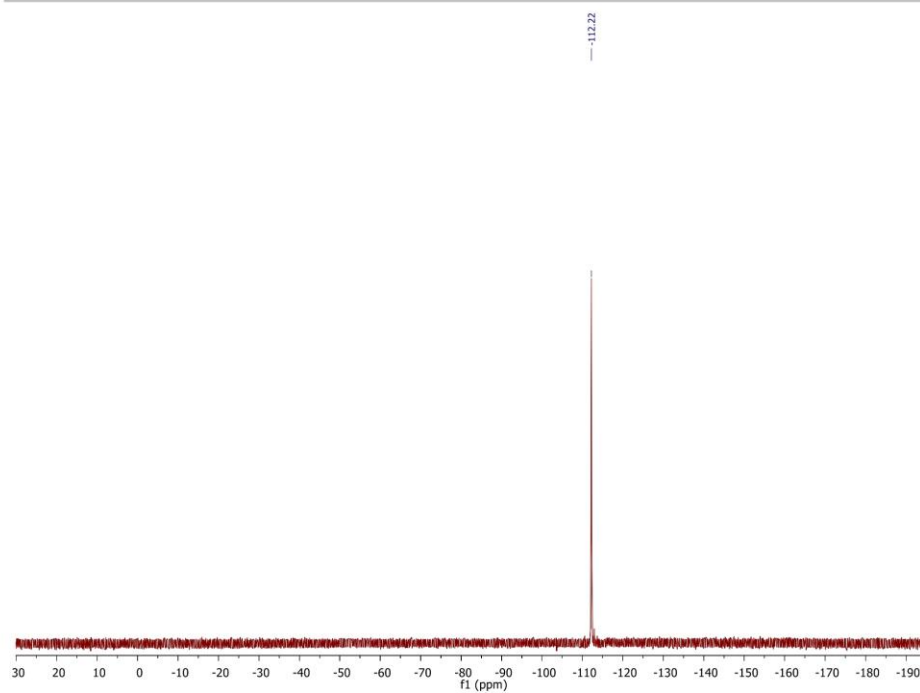
SUPPORTING INFORMATION

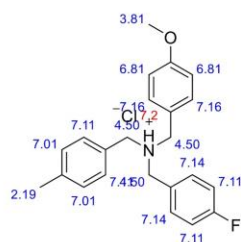
39:



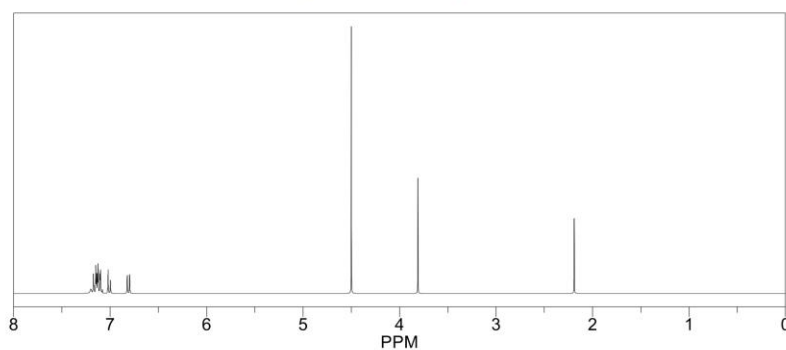
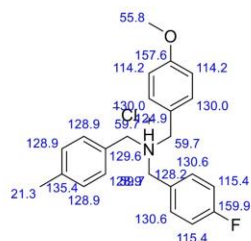
WILEY-VCH

SUPPORTING INFORMATION

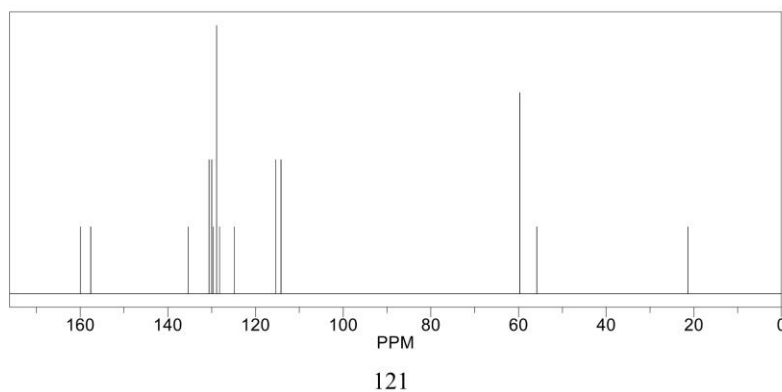


ChemNMR ¹H Estimation

Estimation quality is indicated by color: **good**, **medium**, **rough**

ChemNMR ¹³C Estimation

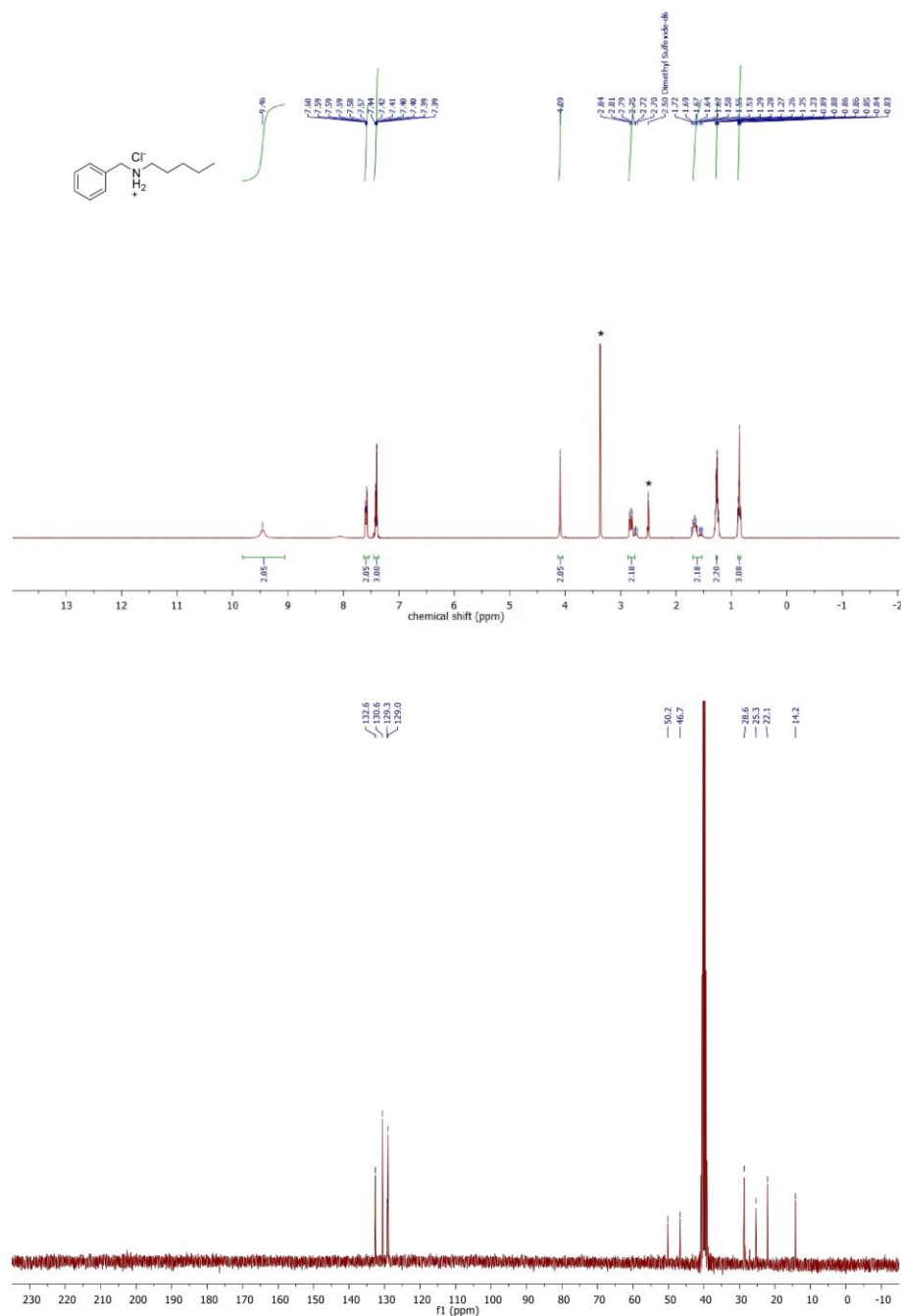
Estimation quality is indicated by color: good, medium, rough



WILEY-VCH

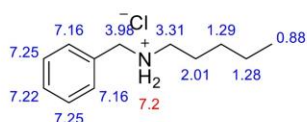
SUPPORTING INFORMATION

40:

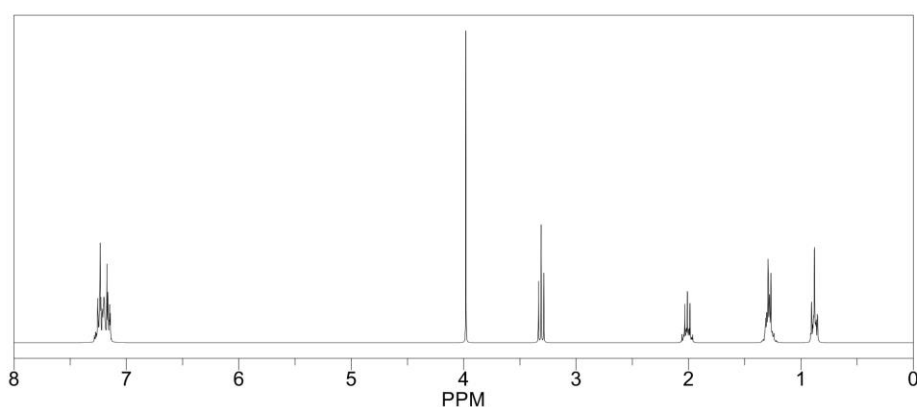


SUPPORTING INFORMATION

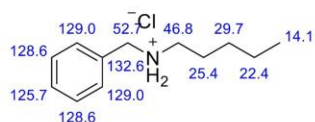
ChemNMR ^1H Estimation



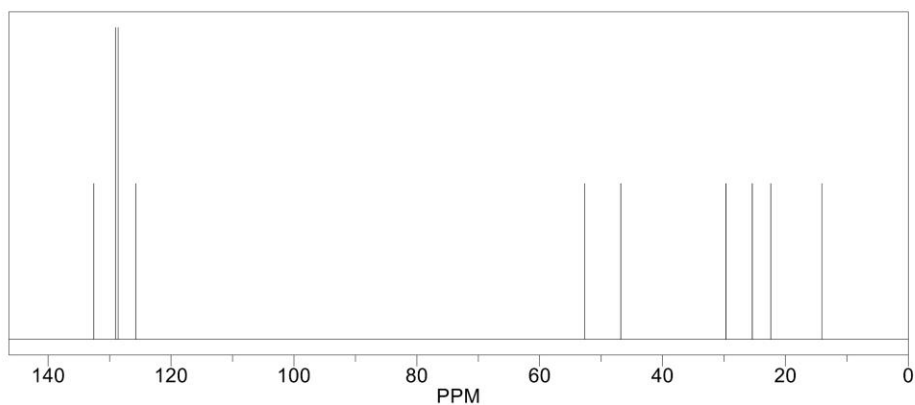
Estimation quality is indicated by color: good, medium, rough



ChemNMR ^{13}C Estimation



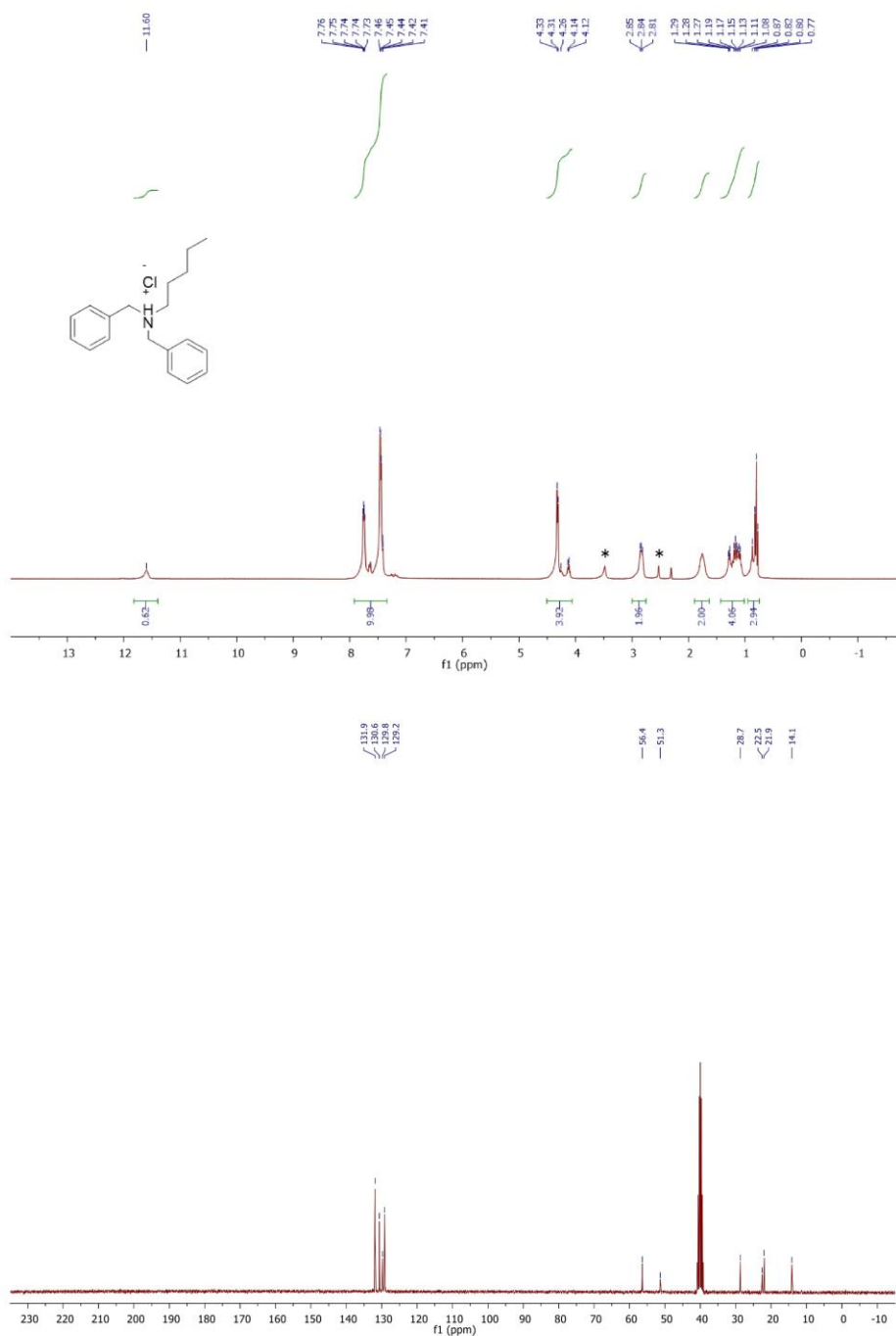
Estimation quality is indicated by color: good, medium, rough



WILEY-VCH

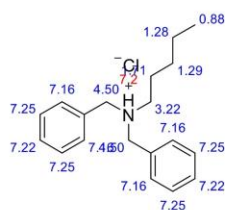
SUPPORTING INFORMATION

41:

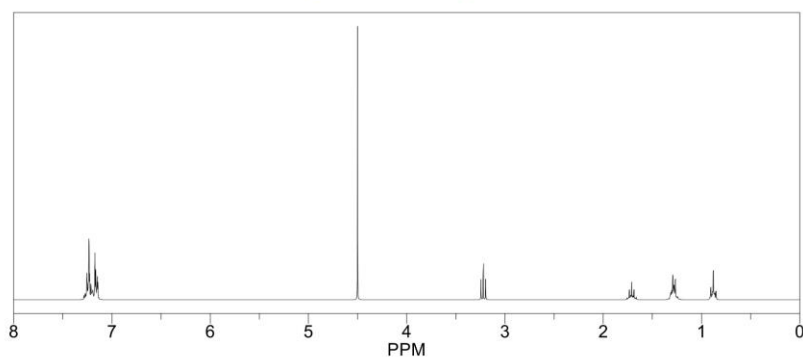


SUPPORTING INFORMATION

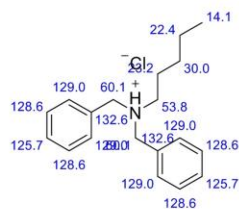
ChemNMR ^1H Estimation



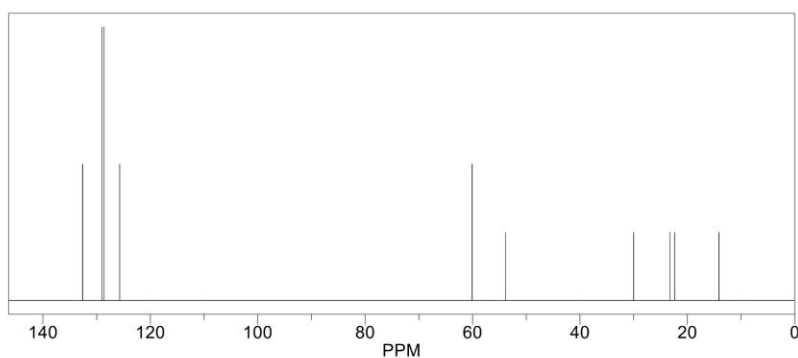
Estimation quality is indicated by color: good, medium, rough



ChemNMR ^{13}C Estimation



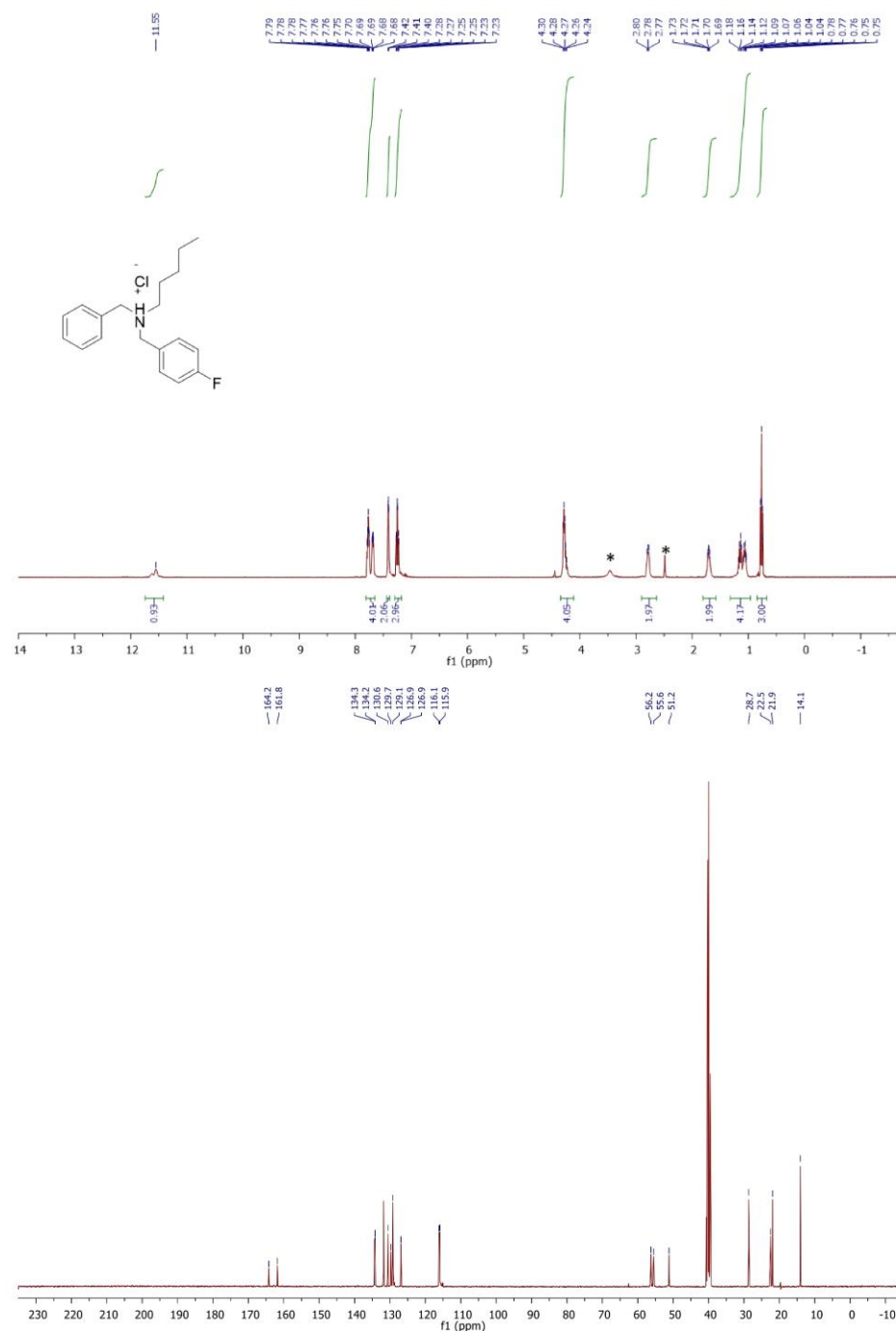
Estimation quality is indicated by color: good, medium, rough



WILEY-VCH

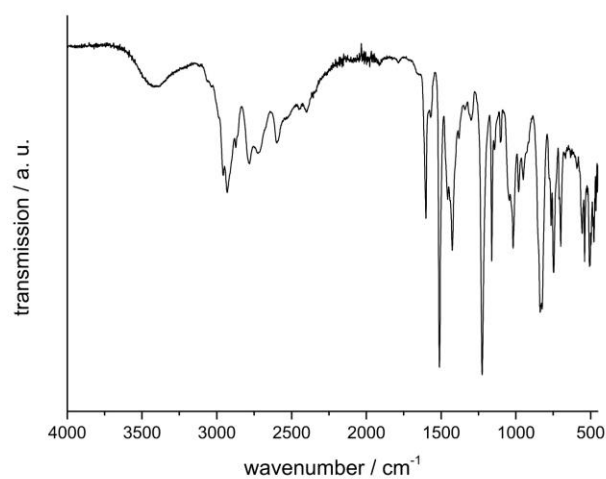
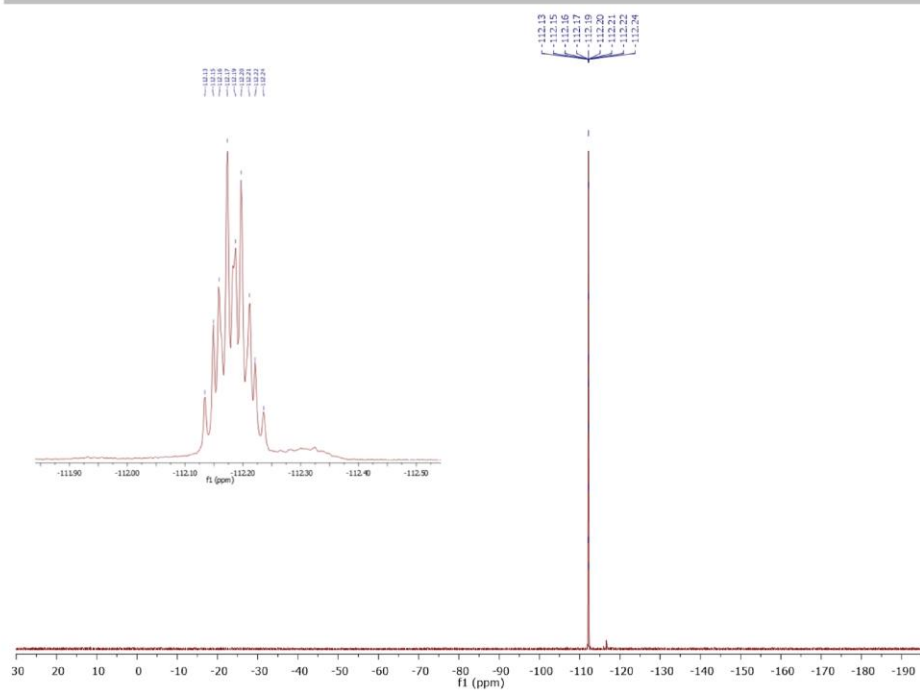
SUPPORTING INFORMATION

42:



WILEY-VCH

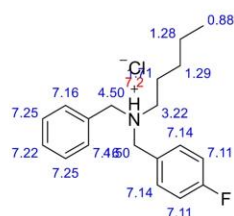
SUPPORTING INFORMATION



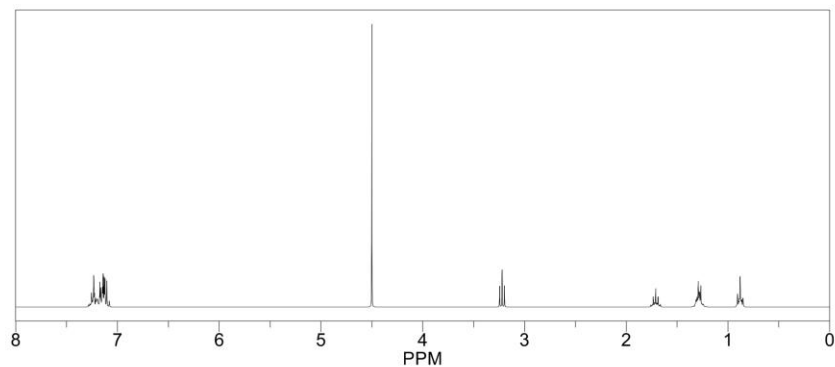
WILEY-VCH

SUPPORTING INFORMATION

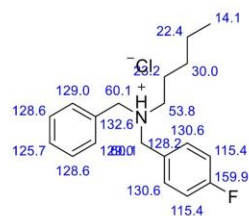
ChemNMR ^1H Estimation



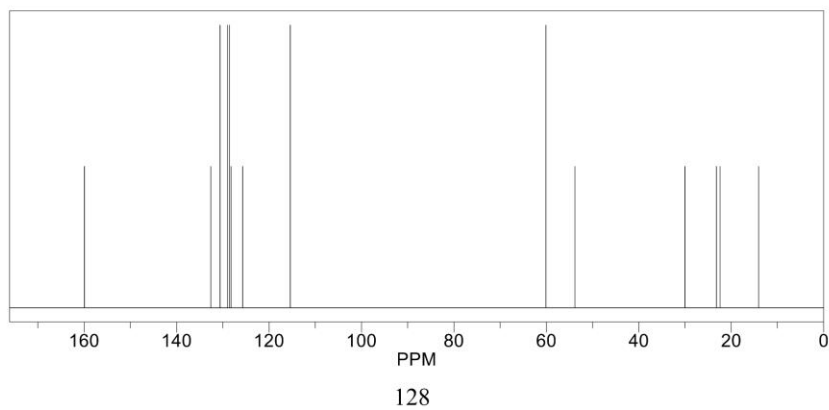
Estimation quality is indicated by color: good, medium, rough



ChemNMR ^{13}C Estimation

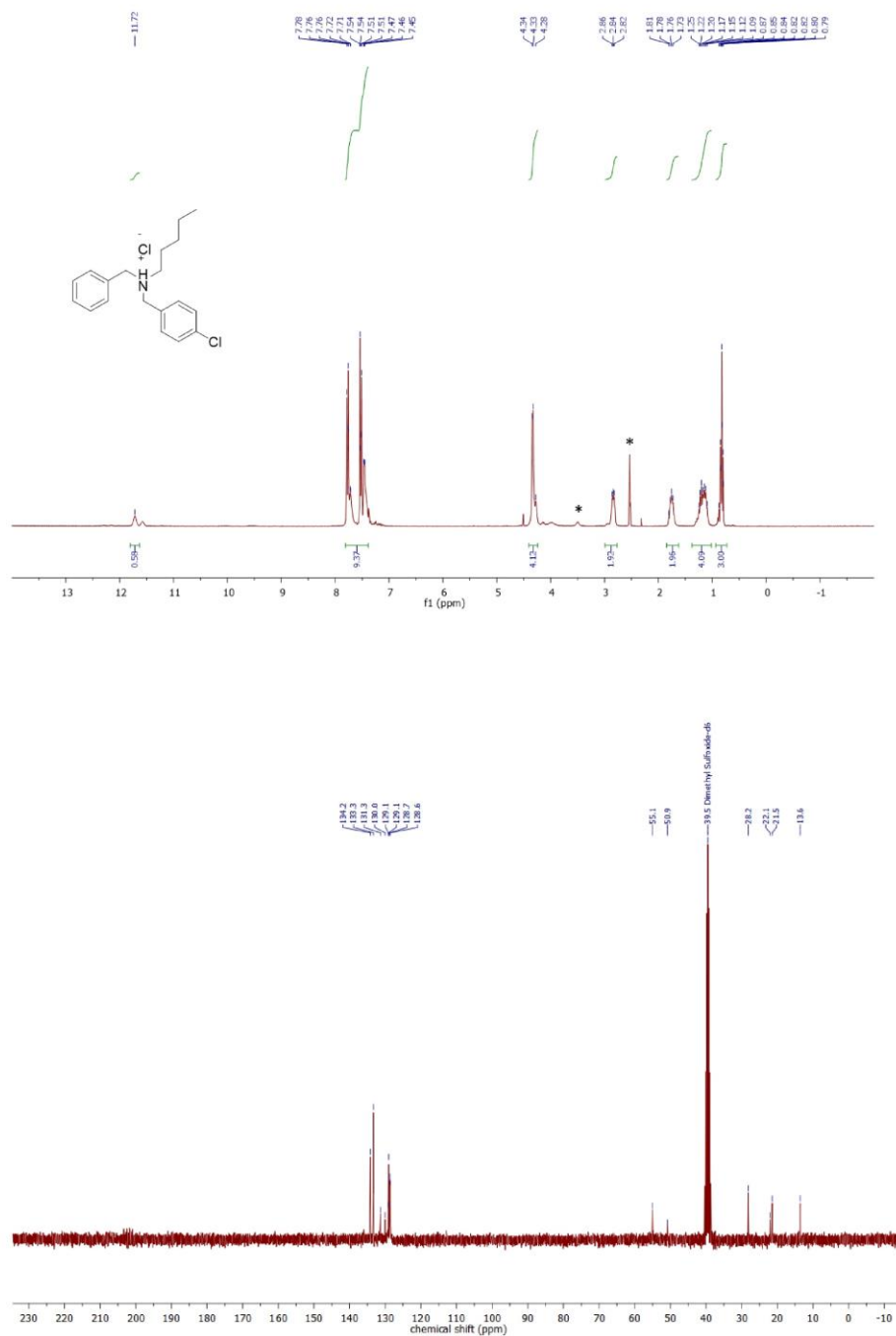


Estimation quality is indicated by color: good, medium, rough



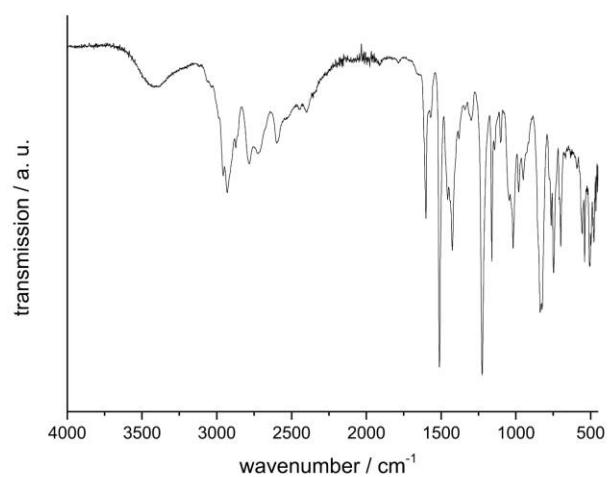
SUPPORTING INFORMATION

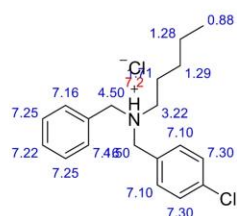
43:



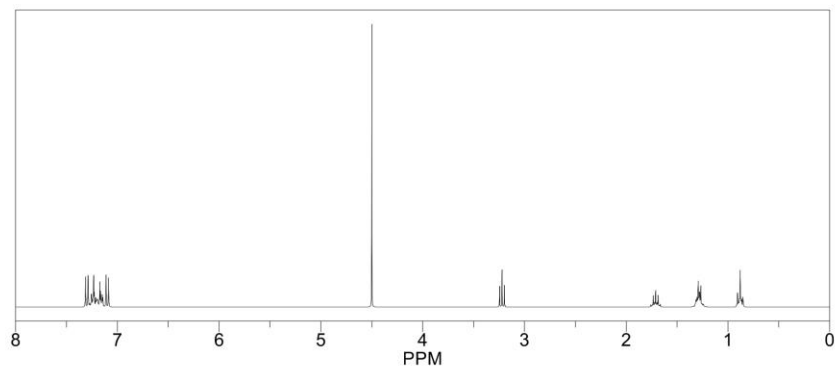
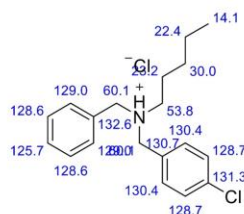
WILEY-VCH

SUPPORTING INFORMATION

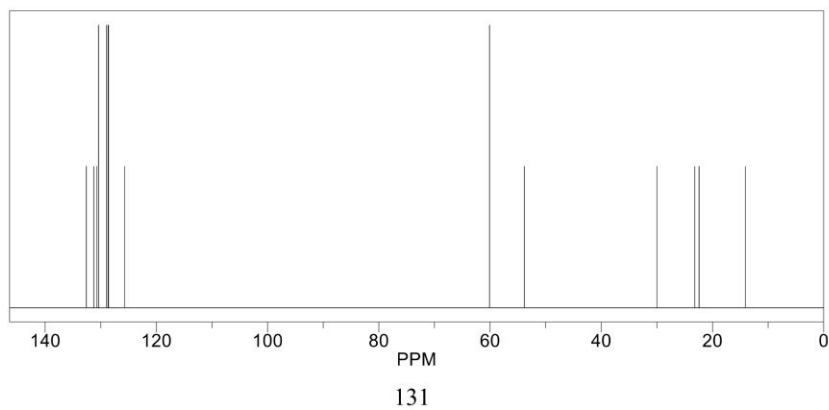


ChemNMR ¹H Estimation

Estimation quality is indicated by color: **good**, **medium**, **rough**

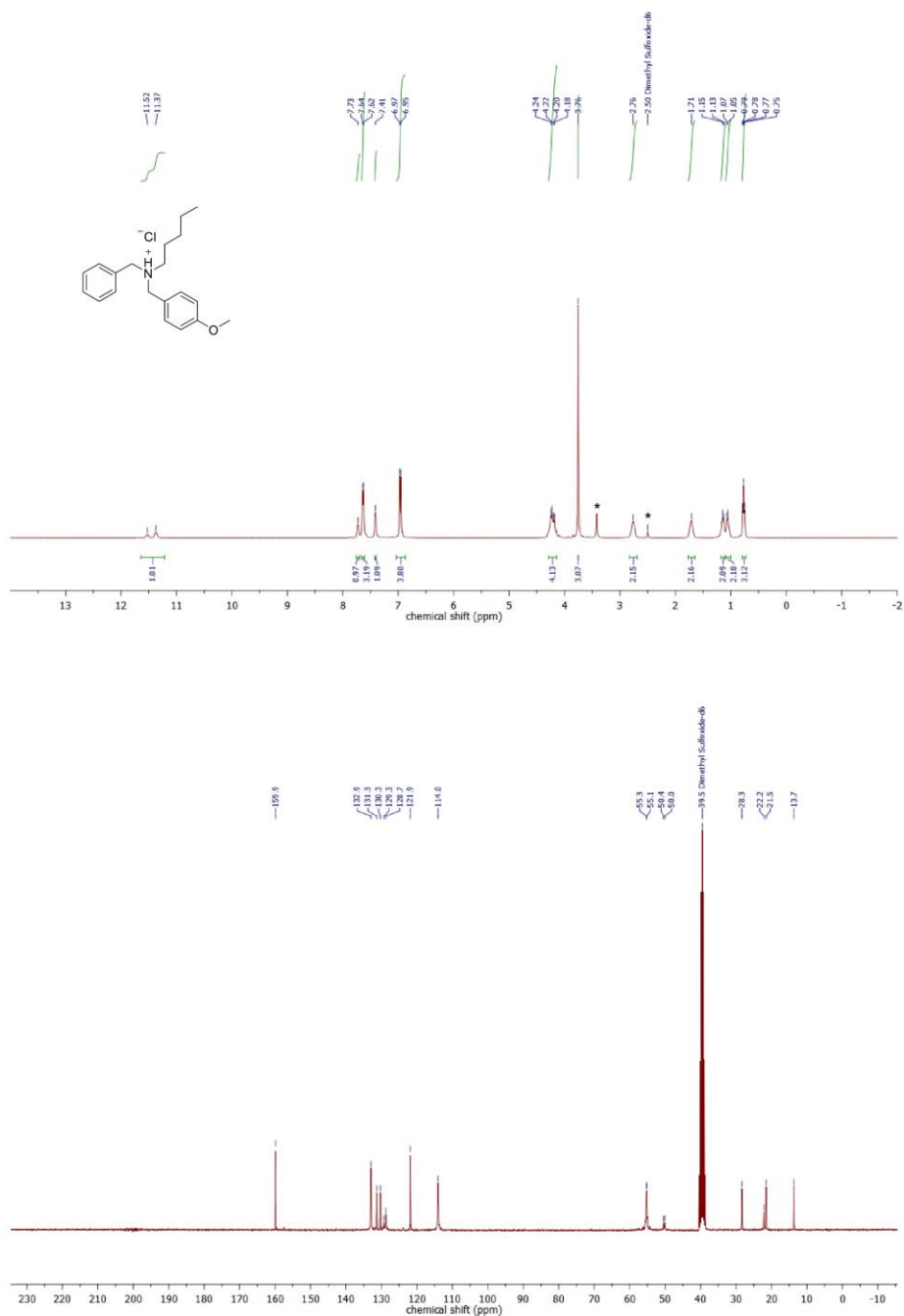
ChemNMR ¹³C Estimation

Estimation quality is indicated by color: **good**, **medium**, **rough**



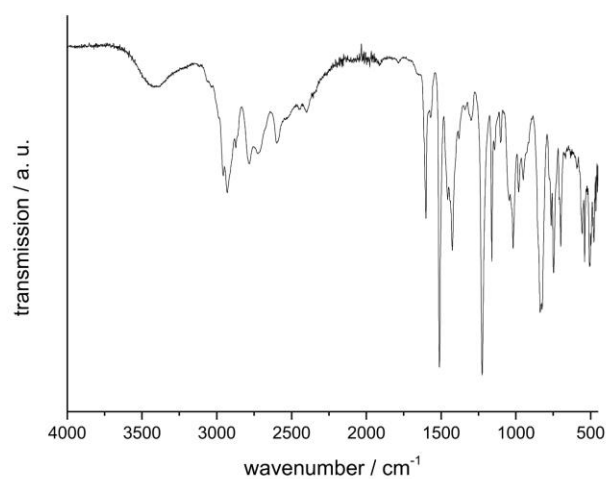
SUPPORTING INFORMATION

44:



WILEY-VCH

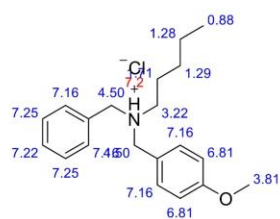
SUPPORTING INFORMATION



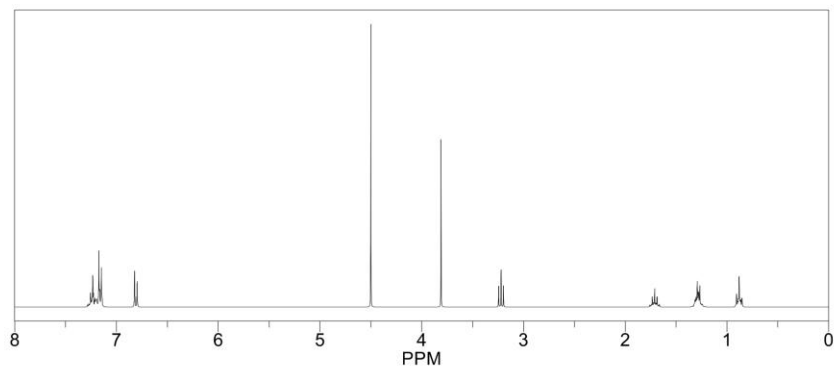
WILEY-VCH

SUPPORTING INFORMATION

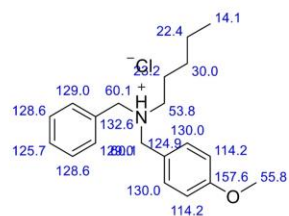
ChemNMR ^1H Estimation



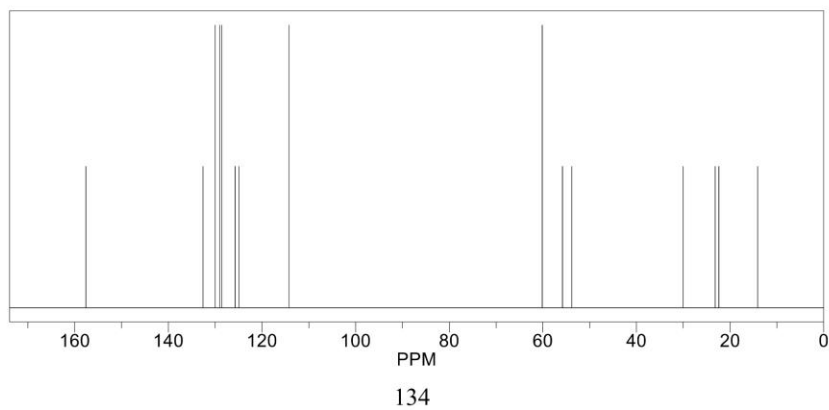
Estimation quality is indicated by color: good, medium, rough



ChemNMR ^{13}C Estimation

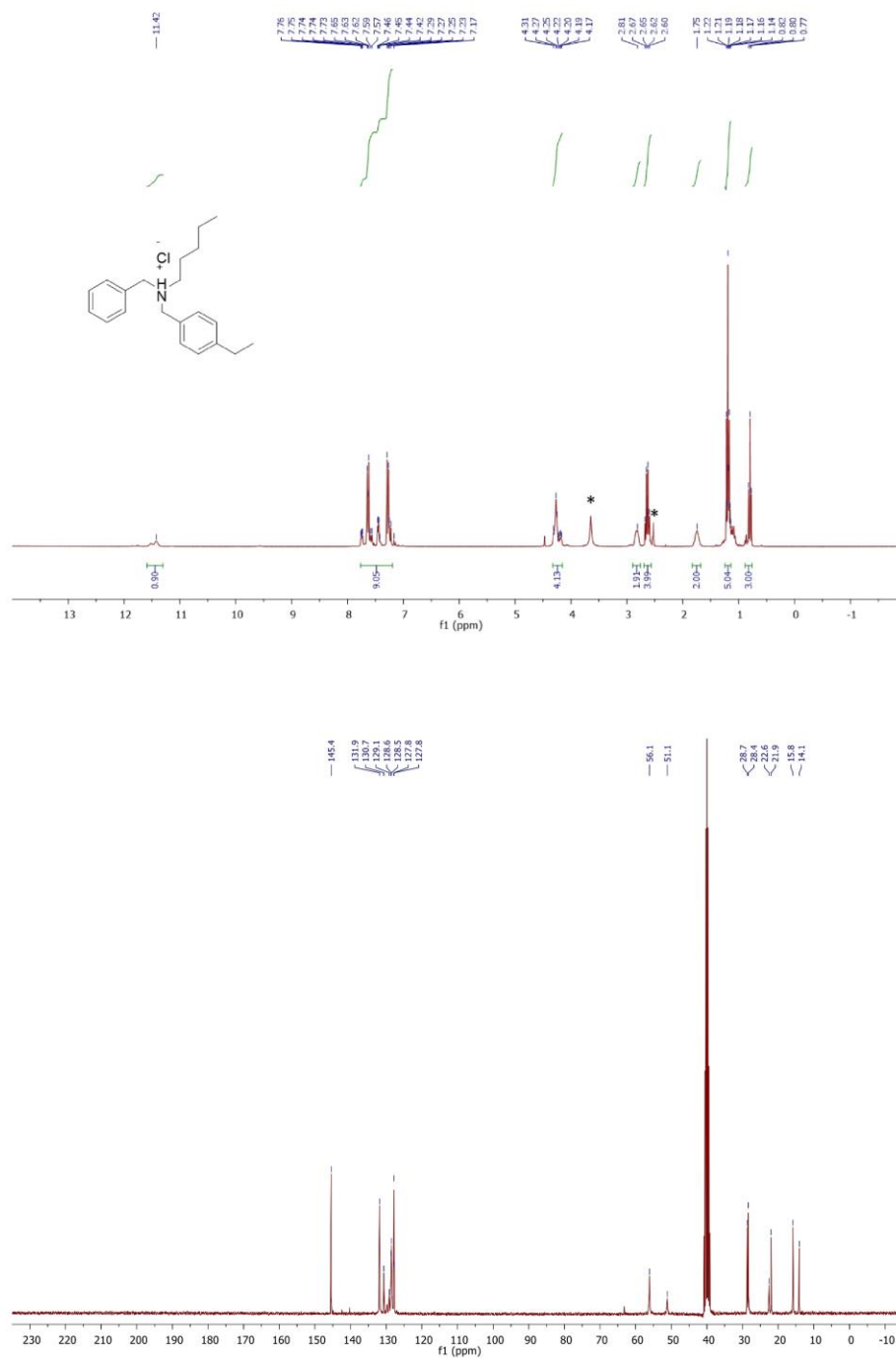


Estimation quality is indicated by color: good, medium, rough



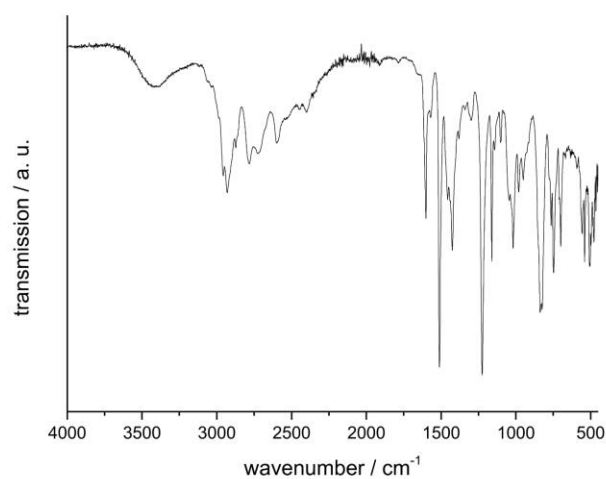
SUPPORTING INFORMATION

45:



WILEY-VCH

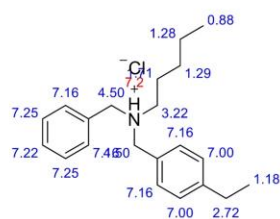
SUPPORTING INFORMATION



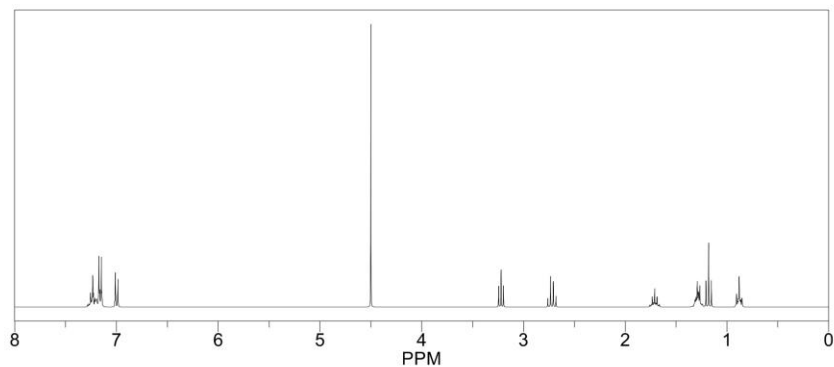
WILEY-VCH

SUPPORTING INFORMATION

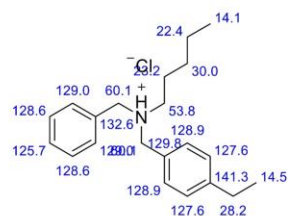
ChemNMR ^1H Estimation



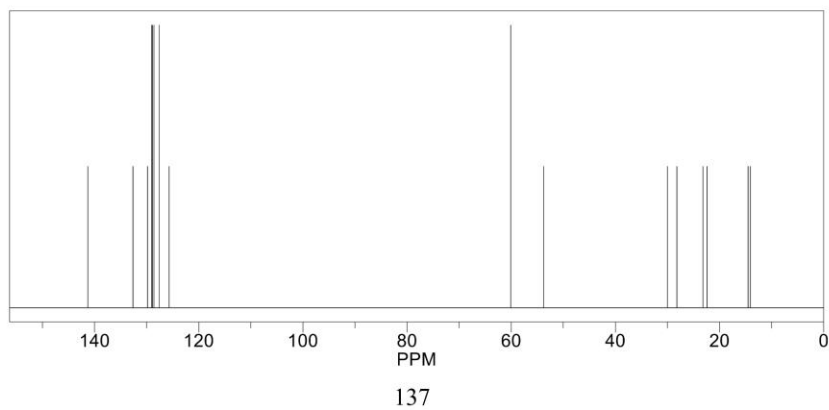
Estimation quality is indicated by color: good, medium, rough



ChemNMR ^{13}C Estimation



Estimation quality is indicated by color: good, medium, rough



SUPPORTING INFORMATION

6 References

- [1] J. Pantförder, S. Pöllmann, J. F. Zhu, D. Borgmann, R. Denecke, H.-P. Steinrück, *Rev. Sci. Instrum.* **2005**, 76.
- [2] A. Ermolieff, P. Bernard, S. Marthon, J. Da Camargo Costa, *J. Appl. Phys.* **1986**, 60, 3162–3166.
- [3] a) C. R. Brundle, B. V. Crist, *J. Vac. Sci. Technol.* **2020**, 38; b) W. S. M. Werner, W. Smekal, C. J. Powell, *Simulation of electron spectra for surface analysis (SESSA) version 2.2.0 user's guide*, National Institute of Standards and Technology (U.S.), Gaithersburg, MD, **2021**.
- [4] L. F. B. Ribeiro, O. Flores, P. Furtat, C. Gervais, R. Kempe, R. A. F. Machado, G. Motz, *J. Mater. Chem. A* **2017**, 5, 720–729.
- [5] C. Bäumler, C. Bauer, R. Kempe, *ChemSusChem* **2020**, 13, 3110–3114.
- [6] G. Hahn, P. Kunnas, N. de Jonge, R. Kempe, *Nat. Catal.* **2019**, 2, 71–77.
- [7] K. Murugesan, M. Beller, R. V. Jagadeesh, *Angew. Chem. Int. Ed.* **2019**, 58, 5064–5068.
- [8] K. Tokmic, B. J. Jackson, A. Salazar, T. J. Woods, A. R. Fout, *J. Am. Chem. Soc.* **2017**, 139, 13554–13561.
- [9] E. S. Reckzeh, G. Karageorgis, M. Schwalfenberg, J. Ceballos, J. Nowacki, M. C. M. Stroet, A. Binici, L. Knauer, S. Brand, A. Choidas et al., *Cell Chem. Biol.* **2019**, 26, 1214–1228.e25.
- [10] E. Rohrmann, H. A. Shonle, *J. Am. Chem. Soc.* **1944**, 66, 1516–1520.
- [11] R. V. Jagadeesh, K. Murugesan, A. S. Alshammari, H. Neumann, M.-M. Pohl, J. Radnik, M. Beller, *Science* **2017**, 358, 326–332.
- [12] M. S. Kwon, S. Kim, S. Park, W. Bosco, R. K. Chidrala, J. Park, *J. Org. Chem.* **2009**, 74, 2877–2879.
- [13] C. Wang, A. Pettman, J. Basca, J. Xiao, *Angew. Chem. Int. Ed.* **2010**, 49, 7548–7552.
- [14] S. Sato, T. Sakamoto, E. Miyazawa, Y. Kikugawa, *Tetrahedron* **2004**, 60, 7899–7906.
- [15] A. F. Abdel-Magid, K. G. Carson, B. D. Harris, C. A. Maryanoff, R. D. Shah, *J. Org. Chem.* **1996**, 61, 3849–3862.
- [16] Q. Lei, Y. Wei, D. Talwar, C. Wang, D. Xue, J. Xiao, *Chem. Eur. J.* **2013**, 19, 4021–4029.
- [17] R. Kempe, T. Schönauer, S. L. J. Thomä, L. Kaiser, M. Zobel, *Chem. Eur. J.* **2020**.
- [18] S. Liang, P. Monsen, G. B. Hammond, B. Xu, *Org. Chem. Front.* **2016**, 3, 505–509.
- [19] L. Xing, C. Cheng, R. Zhu, B. Zhang, X. Wang, Y. Hu, *Tetrahedron* **2008**, 64, 11783–11788.
- [20] T. Yan, B. L. Feringa, K. Barta, *ACS Catal.* **2016**, 6, 381–388.
- [21] K. Sarkar, K. Das, A. Kundu, D. Adhikari, B. Maji, *ACS Catal.* **2021**, 11, 2786–2794.
- [22] L. H. S. Smith, T. T. Nguyen, H. F. Sneddon, D. J. Procter, *Chem. Commun.* **2011**, 47, 10821–10823.

WILEY-VCH

SUPPORTING INFORMATION

- [23] S. Mizuta, K. Watanabe, N. Nishida, T. Hamada, T. Ishikawa, Y. Tanaka, H. Otaki, J. Yasuda, S. Urata, WO2018181892A1, **2018**.
- [24] M. Ruiz - Castañeda, A. M. Rodríguez, A. H. Aboo, B. R. Manzano, G. Espino, J. Xiao, F. A. Jalón, *Appl. Organometal. Chem.* **2020**, *34*.
- [25] P. Ye, Y. Shao, X. Ye, F. Zhang, R. Li, J. Sun, B. Xu, J. Chen, *Org. Lett.* **2020**, *22*, 1306–1310.

WILEY-VCH

SUPPORTING INFORMATION

Author Contributions

Matthias Elfinger carried out the catalyst synthesis, catalytic reactions and catalyst characterization. Jörg Schmauch carried out the STEM-EELS measurements. Michael Moritz measured the XPS samples, Michael Moritz, Christian Papp and Christoph Wichmann performed XPS data analysis and evaluation. Matthias Elfinger and Rhett Kempe co-wrote the manuscript. Christof Bauer revised the manuscript and supporting information and corrected the data and carried out the necessary experiments as well as co-wrote the manuscript.

7 List of Publications and Conference Contributions

7.1 Publications

1. C. Bäumlér, C. Bauer and Rhett Kempe, *ChemSusChem* **2020**, 13, 3110 – 3114.
“The Synthesis of Primary Amines through Reductive Amination Employing an Iron Catalyst”
2. C. Bauer, F. Müller, S. Keskin, M. Zobel and R. Kempe, *Chem. Eur. J.* **2023**, 29, e202300561.
“A Highly Active Cobalt Catalyst for the General and Selective Hydrogenation of Aromatic Heterocycles”
3. R. Loukrakpam, B. F. Gomes, M. Prokop, C. Bauer, M. Kutter, F. Baier, R. Kempe and C. Roth, *J. Power Sources* **2023**, 569, 232905.
“Challenges and limitations of accelerated stress testing in GDE half-cell set-ups”
4. M. Elfinger, C. Bauer, J. Schmauch, M. Moritz, C. Wichmann, C. Papp and R. Kempe, *Adv. Synth. Catal.* **2023**, 24, 4654 – 4661.
“General Synthesis of Alkyl Amines via Borrowing Hydrogen and Reductive Amination”
5. C. Bauer, F. Zareh, L. Nüßlein, J. Frank, M. Boniface, T. Lunkenbein and R. Kempe, *Chem. Eur. J.* **2025**, e202500462.
“The Synthesis of Hydroquinolines from Nitroaldehydes and Ketones by Hydrogenation Sequences and Condensations”

7.2 Conference Contributions

- 2022** “Linking Hydrogenation and *Friedländer* Synthesis“ – Invited Talk
30th Colloquy on Organometallic Chemistry for Catalysis, Poznań, Poland
- 2023** “A Highly Active Cobalt Catalyst for the General and Selective Hydrogenation of Aromatic Heterocycles” – Poster Presentation
31st Colloquy on Organometallic Chemistry for Catalysis, Bayreuth, Germany
- 2024** “Polymer Derived Ceramics in Catalysis” – Participation
3rd Symposium on Materials Chemistry for New Properties and Functions, Tokyo, Japan

8 Acknowledgement/Danksagung

8.1 Acknowledgement

My deepest gratitude goes to my academic advisor, Prof. Dr. Rhett Kempe, who gave me the opportunity to conduct research on this highly interesting and future-oriented topic under excellent working conditions. I am grateful for the many constructive scientific as well as non-scientific discussions and last but not least for the trust he placed in me by granting me the greatest possible scientific freedom during this dissertation.

I would like to express my heartfelt thanks to Dr. Christine Denner for the smooth integration into her research group, the excellent supervision and her friendly support at every stage of my doctoral studies. In particular, I am thankful for the numerous REM-EDX measurements and the daily morning coffee breaks.

My sincere thanks also go to my lab colleagues who accompanied me (at various stages) throughout my doctoral studies: Dr. Christoph Bäumler, Dr. Mara Klarner, Dr. Matthias Elfinger, Dr. Barbara Klausfelder, Dr. Timon Schönauer, Christoph Maier, Sandra Bieger, Marie Bergmann, Franziska Kreft, Fatemeh Zareh – you have positively shaped my time at the chair with your collegial and supportive working atmosphere in the lab, the many scientific discussions, and not least our friendly interactions. Furthermore, I would like to thank Alexander Goller, Patrick Wolff, Fabian Lukas, André Dickert, Christian Heber, Christoph Unger, Jannis Lipp, Paula Simon, Martin Schlagbauer, Felix Leowsky-Künstler, Johannes Porschke, Tobias Schwarz, Hendrik Kempf, Max Leinert, Tobias Seifert, Niko Sila, Dr. Torsten Irrgang and Dr. Winfried Kretschmer for the unforgettable time at the Sustainable Chemistry Centre. In addition to coffee breaks, many after-work beers, and numerous BBQ events, the sailing excursions organized by the chair will always stay with me.

I would like to thank all of my interns, especially Lisa Nüßlein and Johanna Frank, who not only provided great support during their theses and daily lab work but also became very dear to me.

A big thank you goes to Tina Fell, Heidi Maisel, Anna-Maria Dietl, Sandra Keller and Dana Dopheide for all their technical and organizational help throughout my doctoral studies.

I am grateful for the excellent collaboration with Prof. Dr. Christina Roth, Dr. Rameshwori Loukrakpam and Sven Hörnig as part of our joint project within the SFB 1585 MultiTrans. I greatly appreciated the open communication, the willingness to discuss, and the constructive

working atmosphere. I would like to thank my collaboration partners, Dr. Sercan Keskin at INM – Leibniz Institute for New Materials in Saarbrücken, as well as Prof. Dr. Mirjam Zobel and Felix Müller from the Institute of Crystallography at RWTH Aachen, for the constructive cooperation. I am also grateful to PD Dr. Thomas Lunkenbein and Dr. Maxime Boniface for hosting me at the Fritz Haber Institute of the Max Planck Society in Berlin and for the fruitful measurements I was able to conduct there. For various measurements, I would like to thank Dr. Tanja Feller, Dr. Ulrike Lacher, Alexander Berger and Felix Baier.

A very special thank you goes to Prof. Dr. Kazuhiko Maeda, who warmly welcomed me into his research group during my research stay at the Tokyo Institute of Technology. Many thanks to the entire group, especially Chomponoot Suppaso, Yura Jang and Xian Zhang, for the unforgettable trips in the Land of the Rising Sun.

I would like to thank the SFB 1585 of the German Research Foundation (DFG) and the EFR Green Hydrogen Scholarship of the German Academic Exchange Service (DAAD) for providing research funding, as well as for financing this dissertation and my research stay in Japan. I am also grateful to the Graduate School at the University of Bayreuth for the financial support of numerous training opportunities.

A special thanks go to my friends Anika, Lisa, Hania, Mirco, Johannes and Fabian, who enriched my time in Bayreuth.

I thank the alumni association “Chemiker Spass Gesellschaft”, CSG e.V., for the great time, the many friendships that were formed, and for the opportunity to lead and shape the organization. I would also like to thank my shooting friends at the club "Unteres Tor" in Bayreuth, who gave me a second home for my passion, olympic sport shooting.

Finally, I am endlessly grateful to my family – especially my parents, Klaus and Anita – for their incredible support. Thank you for your motivation, love, trust, and support in all aspects of my life.

8.2 Danksagung

Mein besonderer Dank gilt meinem akademischen Lehrer, Prof. Dr. Rhett Kempe, der mir die Möglichkeit gegeben hat, unter ausgezeichneten Arbeitsbedingungen an diesem sehr interessanten und zukunftssträchtigen Thema zu forschen. Ich bedanke mich für die vielen konstruktiven wissenschaftlichen, aber auch nicht-wissenschaftlichen Diskussionen und nicht zuletzt für das Vertrauen, mir die größtmögliche wissenschaftliche Freiheit während dieser Promotion zu gewähren.

Ich möchte mich sehr herzlich bei Dr. Christine Denner für die reibungslose Integration in ihre Arbeitsgruppe, die ausgezeichnete Betreuung und die freundschaftliche Unterstützung in jeder Phase meiner Promotion bedanken. Insbesondere bedanke ich mich für die zahlreichen REM-EDX-Messungen und die täglichen morgendlichen Kaffee-Runden.

Mein großer Dank gilt auch meinen Laborkolleginnen und -kollegen, die mich (teilweise) während meiner Doktorarbeit begleitet haben: Dr. Christoph Bäumler, Dr. Mara Klarner, Dr. Matthias Elfinger, Dr. Barbara Klausfelder, Dr. Timon Schönauer, Christoph Maier, Sandra Bieger, Marie Bergmann, Franziska Kreft, Fatemeh Zareh – ihr habt die Zeit am Lehrstuhl durch die kollegiale und unterstützende Arbeitsatmosphäre im Labor, durch zahlreiche wissenschaftliche Diskussionen und nicht zuletzt durch unseren freundschaftlichen Umgang positiv geprägt. Des Weiteren möchte ich mich bei Alexander Goller, Patrick Wolff, Fabian Lukas, André Dickert, Christian Heber, Christoph Unger, Jannis Lipp, Paula Simon, Martin Schlagbauer, Felix Leowsky-Künstler, Johannes Porschke, Tobias Schwarz, Hendrik Kempf, Max Leinert, Tobias Seifert, Niko Sila, Dr. Torsten Irrgang und Dr. Winfried Kretschmer für die unvergessliche Zeit am Sustainable Chemistry Centre bedanken. Neben den Kaffeepausen, vielen Feierabend-Bieren und zahlreichen Grillveranstaltungen wird mir vor allem das Lehrstuhl-Segeln für immer in Erinnerung bleiben.

Ich bedanke mich bei all meinen Praktikantinnen und Praktikanten, insbesondere bei Lisa Nüßlein und Johanna Frank, die mich nicht nur während ihrer Abschlussarbeiten tatkräftig bei der täglichen Laborarbeit unterstützt und neue Impulse gegeben haben, sondern mir auch sehr ans Herz gewachsen sind.

Ein großes Dankeschön geht an Tina Fell, Heidi Maisel, Anna-Maria Dietl, Sandra Keller und Dana Dopheide für jegliche technische und organisatorische Hilfe im Promotionsalltag.

Ich bin dankbar für die großartige Kooperation mit Prof. Dr. Christina Roth, Dr. Rameshwori Loukrakpam und Sven Hörnig im Rahmen unseres gemeinsamen Projekts im SFB 1585 MultiTrans. Die offene Kommunikation, Diskussionsbereitschaft und konstruktive Arbeitsatmosphäre habe ich sehr geschätzt. Ich bedanke mich bei meinen Kooperationspartnern Dr. Sercan Keskin am INM – Leibniz-Institut für Neue Materialien in Saarbrücken sowie bei Prof. Dr. Mirijam Zobel und Felix Müller vom Institut für Kristallographie an der RWTH Aachen für die konstruktive Zusammenarbeit. Ebenso danke ich PD Dr. Thomas Lunkenbein und Dr. Maxime Boniface für den Gastaufenthalt am Fritz-Haber-Institut der Max-Planck-Gesellschaft in Berlin und die lohnenden Messungen, die ich durchführen durfte. Für zahlreiche Auftragsmessungen bedanke ich mich bei Dr. Tanja Feller, Dr. Ulrike Lacher, Alexander Berger und Felix Baier.

Ein sehr großes Dankeschön geht an Prof. Dr. Kazuhiko Maeda, der mich in seiner Arbeitsgruppe während meines Forschungsaufenthalts am Tokyo Institute of Technology herzlich willkommen hieß. Vielen Dank an die gesamte Arbeitsgruppe, insbesondere an Chomponoot Suppaso, Yura Jang und Xian Zhang für die unvergesslichen Ausflüge im Land der aufgehenden Sonne.

Dem SFB 1585 der Deutschen Forschungsgemeinschaft und dem EFR-Zukunftsstipendium „Grüner Wasserstoff“ des Deutschen Akademischen Austauschdiensts danke ich für die Bereitstellung von Forschungsgeldern sowie die Finanzierung dieser Doktorarbeit und meines Forschungsaufenthalts in Japan. Für die finanzielle Unterstützung zahlreicher Fortbildungsmaßnahmen danke ich der Graduate School der Universität Bayreuth.

Ein besonderer Dank gilt meinen Freunden Anika, Lisa, Hania, Mirco, Johannes und Fabian, die die Zeit in Bayreuth sehr bereichert haben.

Ich danke der Chemiker Spass Gesellschaft, CSG e.V., für die großartige Zeit, die vielen entstandenen Freundschaften und dafür, dass ich den Verein führen und prägen durfte. Ebenfalls bedanke ich mich bei meinen Schützenbrüdern und -schwestern vom „Unteren Tor“ in Bayreuth, die mir eine zweite Heimat für meine Passion, das olympische Sportschießen, gegeben haben.

Nicht zuletzt bin ich meiner Familie – insbesondere meinen Eltern Klaus und Anita – unendlich dankbar für ihre unbeschreibliche Unterstützung. Danke für eure Motivation, Liebe, Vertrauen und Unterstützung in allen Belangen meines Lebens.

9 (Eidesstattliche) Versicherungen und Erklärungen

§ 9 Satz 2 Nr. 3 PromO BayNat

Hiermit versichere ich eidesstattlich, dass ich die Arbeit selbstständig verfasst und keine anderen als die von mir angegebenen Quellen und Hilfsmittel benutzt habe (vgl. Art. 97 Abs. 1 Satz 8 BayHIG).

§ 9 Satz 2 Nr. 3 PromO BayNat

Hiermit erkläre ich, dass ich die Dissertation nicht bereits zur Erlangung eines akademischen Grades eingereicht habe und dass ich bereits diese oder eine gleichartige Doktorprüfung endgültig nicht bestanden habe.

§ 9 Satz 2 Nr. 4 PromO BayNat

Hiermit erkläre ich, dass ich keine Hilfe von gewerblichen Promotionsberatern bzw. -vermittlern oder ähnlichen Dienstleistern in Anspruch genommen habe noch künftig in Anspruch nehmen werde.

§ 9 Satz 2 Nr. 7 PromO BayNat

Hiermit erkläre ich mein Einverständnis, dass die elektronische Fassung meiner Dissertation unter der Wahrung meiner Urheberrechte und des Datenschutzes einer gesonderten Überprüfung unterzogen werden kann.

§ 9 Satz 2 Nr. 8 PromO BayNat

Hiermit erkläre ich mein Einverständnis, dass bei Verdacht wissenschaftlichen Fehlverhaltens Ermittlungen durch universitätsinterne Organe der wissenschaftlichen Selbstkontrolle stattfinden können.